

THE DESIGN, SYNTHESIS, AND BIOLOGICAL EVALUATION OF STEROID-DERIVED
INHIBITORS OF THE SONIC HEDGEHOG SIGNALING PATHWAY

Lyndsay Leal

A DISSERTATION

in

Chemistry

Presented to the Faculties of the University of Pennsylvania

in

Partial Fulfillment of the Requirements for the

Degree of Doctor of Philosophy

2015

Supervisor of Dissertation

Jeffrey D. Winkler, Merriam Professor of Chemistry

Graduate Group Chairperson

Gary A. Molander, Hirschmann-Makineni Professor of Chemistry

Dissertation Committee

Amos B. Smith, III, Rhodes-Thompson Professor of Chemistry

Madeleine M. Joullié, Professor of Chemistry

Ronen Marmorstein, Professor of Biochemistry and Biophysics

THE DESIGN, SYNTHESIS, AND BIOLOGICAL EVALUATION OF STEROID-DERIVED
INHIBITORS OF THE SONIC HEDGEHOG SIGNALING PATHWAY

COPYRIGHT

2015

Lyndsay M. Leal

For my Grandfathers.

In Loving Memory of Charles Van Fleet and Andy Wood

ACKNOWLEDGMENT

I don't know if any words of wisdom can truly prepare someone for the journey of graduate school, and it is hard to put this process into words. It is far more than five years of schooling. This process is difficult, both mentally and emotionally, but I have learned more about who I am as a person than I had ever expected, and there are a few people that I would like to thank for helping me out along the way.

First, I would like to thank my advisor, Professor Jeffrey Winkler. I had no intention of coming to graduate school in Philadelphia, but from day one, I knew this was the place for me, and most of that is your doing. You have pushed me to become a better chemist, a better scientist, and an overall better thinker. Through all of the ebbs and flows of this process I could always count on your honesty and our candid conversations. I have the story to tell because you allowed me the freedom to explore, and for that I am truly grateful.

Choosing Penn as a place to spend these years has been a decision I will not regret. The people that I have met here have made a lasting impression. To my committee, Amos Smith, Madeleine Joullié, and Ronen Marmorstein, I want to say thank you for your words of encouragement, your scientific advice, and your time. Thank you for your kindness and continual support. To Sally Mallory, thank you for always being a stern voice of reason and for leaving me anonymous cat memes on my desk, they always made me smile. A special thanks to Chris Jeffrey who was extremely helpful during the job search process and has become a great friend.

No one really understands this process until they have gone through it and there are some really special friends that I have made along the way. Jason Melvin, thank you for being a mentor. You signed up to have me under your wing for a summer and you got stuck with me. To my postdoc, Christian Ventocilla, thank you for teaching me to be a chemist, without you I would have been lost. To Deidre Strahan and Andre Isaacs, thank you for being my cool older friends that showed me the way and kept me going on the bad days. To all of my friends in my incoming graduate class, especially Kaitlin and Bruno, thank you for being 2/3 of my musketeers. And to my labmates, old and new, and many other Penn friends, thank you for the coffee breaks, the happy hours, the lunches and every thing else that makes the days go by so fast.

To my mom and dad, I cannot put into words how much your support truly means. You have always been so proud of my accomplishments, no matter how small. I love you both and I thank you from the bottom of my heart for everything you have done to provide me the ability to succeed. Thank you to my grandparents for shaping me into the person I am today and keeping me focused on what is truly important in life.

Finally, my husband, Dan. You know me better than anyone else, and you still love me anyway. I wouldn't have made it through this process without you. You make me want to be a better person, to keep pushing, and to make you proud. Because of you I will never forget, "what is essential is invisible to the eye".

ABSTRACT

THE DESIGN, SYNTHESIS, AND BIOLOGICAL EVALUATION OF STEROID-DERIVED INHIBITORS OF THE SONIC HEDGEHOG SIGNALING PATHWAY

Lyndsay M. Leal

Jeffrey D. Winkler

The Sonic Hedgehog (SHH) signaling pathway is required during embryogenesis for cell differentiation and growth; however, medulloblastoma, a pediatric malignancy in the cerebellum, as well as glioblastoma multiforme (GBM), a malignant and invasive adult brain tumor, also require SHH signaling for growth. As SHH signaling remains inactive in healthy adult cells, this pathway provides an excellent target for chemotherapeutics. Cyclopamine, a naturally occurring alkaloid, inhibits the SHH pathway at the level of Smoothened (SMO) and has demonstrated reduced tumor growth in vivo. However, this alkaloid is metabolically unstable. Analysis of the hydrophobic core of cyclopamine revealed a similarity to the steroidal ABCD ring system. Using estrone as a hydrophobic surrogate, we have synthesized readily accessible and metabolically stable analogs to inhibit the SHH pathway. Using computational analysis in conjunction with high-throughput biological evaluation, we are continuing to design and synthesize novel antagonists of the SHH pathway in hopes to further understand the binding pocket of SMO. To this end, we have made significant progress towards elucidating which aspects of the molecules may be required for potency and have identified a new class of compounds that exhibit potency ten times that of cyclopamine.

TABLE OF CONTENTS

ABSTRACT.....	VI
LIST OF FIGURES	IX
LIST OF SCHEMES	XII
LIST OF ABBREVIATIONS	XIV
CHAPTER 1. THE SONIC HEDGEHOG PATHWAY.....	1
Section 1.1 Overview of the Sonic Hedgehog (SHH) Pathway	1
Section 1.2 The Inhibition of the Sonic Hedgehog Pathway.....	4
Section 1.3 Development of Steroid-Based Analogs	17
Section 1.4 Conclusions	26
Section 1.5 References.....	27
CHAPTER 2. ESTABLISHING AND VALIDATING A HIGH-THROUGHPUT BIOLOGICAL EVALUATION METHOD	33
Section 2.1 Summary of Previous Methods of Biological Evaluation	33
Section 2.2 Development of an In-House Dual Luciferase Reporter (DLR) Assay	36
Section 2.3 Control Experiments.....	47
Section 2.4 Summary of Biological Data from First Generation Analogs	49
Section 2.5 Experimental Details.....	50
Section 2.6 References.....	55
CHAPTER 3. COMPUTATIONAL ANALYSIS AND MOLECULAR MODELING	57
Section 3.1 Analysis of Seven Pass Transmembrane Smoothened	57
Section 3.2 Rigid Protein Molecular Modeling	64

Section 3.3 Flexible Protein Molecular Modeling.....	71
Section 3.4 Future Directions	83
Section 3.5 References.....	84
CHAPTER 4. DESIGN AND SYNTHESIS OF SECOND GENERATION ANALOGS.....	86
Section 4.1 Sulfonamides	86
Section 4.2 Aryl-Aryl Coupled Analogs	91
Section 4.3 Des-C Analogs and the Importance of Shape	98
Section 4.4 Androsterone Derived Oxetane Analog.....	102
Section 4.5 Establishing the Role of Oxygen.....	105
Section 4.6 Rigidity versus Flexibility.....	110
Section 4.7 Regenerating Rigidity without Oxygenation	114
Section 4.8 Second Generation Derivatives of Phenyl Allylic Alcohol.....	121
Section 4.9 Analyzing the Importance of the Nitrogen.....	126
Section 4.10 Access to Pyrrolidine Containing Derivatives	128
Section 4.11 Cross-Coupling Approach to Alkylidene Analog.....	134
Section 4.12 Conclusions	137
Section 4.13 References.....	139
Section 4.14 Experimental Details.....	142
APPENDICES	213
A.1 Chapter 2 Spectra.....	214
A.2 Chapter 4 Spectra.....	218
BIBLIOGRAPHY	416

LIST OF FIGURES

Figure 1.1 Proteins and Cellular Targets of the Sonic Hedgehog Pathway	2
Figure 1.2 Structures of the <i>Veratrum californicum</i> Alkaloids	5
Figure 1.3 Structural Analysis of Alkaloid Cyclopamine.....	6
Figure 1.4 Structures of biochemical probe derivatives	9
Figure 1.5 Infinity Pharmaceuticals: <i>D-homo-cyclopamine</i> Analogs	12
Figure 1.6 Structure of SHH Antagonist Cur61414	14
Figure 1.7 Structure of Benzimidazole Lead and SHH Antagonist GDC-0449	15
Figure 1.8 Compounds of Interest for Novartis	16
Figure 1.9 Eli Lilly Lead Compound LY2940680.....	17
Figure 1.10 Steroid Ring Nomenclature.....	18
Figure 1.11 Comparison of Cyclopamine, Estrone Analog, and Tomatidine	19
Figure 1.12 Proposed Two-Point Binding Model	20
Figure 1.13 Analogs to probe the Two-Point Binding Model.....	20
Figure 1.14 Envisioned Approach to F-Ring Saturated Derivatives.....	22
Figure 1.15 Relative Inhibition of <i>Gli-Luciferase</i> in SHH Light2 Cells	25
Figure 1.16 Inhibition of SHH-dependent Granule Neuron Precursor Growth.....	26
Figure 2.1 Activation of the SHH Signaling Pathway Results in Firefly Luminescence ..	34
Figure 2.2 Bioluminescent Reaction Catalyzed by Firefly Luciferase	38
Figure 2.3 Bioluminescent Reaction Catalyzed by Renilla Luciferase	39
Figure 2.4 IC ₅₀ Curves for Aromatic First Generation Analogs	40
Figure 2.5 IC ₅₀ Curves for Saturated First Generation Analogs.....	41
Figure 2.6 IC ₅₀ Curves for Aromatic F-Ring Analogs Using Shh-Light2 Cells	43
Figure 2.7 IC ₅₀ Curves for Saturated F-Ring Analogs Using Shh-Light2 Cells	44
Table 2.1 Statistical Analysis of Shh-Light2 DLR Assay	45
Figure 2.8 Des-B Analogs.....	46

Figure 2.9 Mechanism of Resazurin Oxidation	49
Figure 3.1 Overall Structure of Human SMO with Antagonist LY2940680	59
Figure 3.2 Ligand Interactions in Binding Pocket (LY2940680).....	60
Figure 3.3 Density Map of Cyclopamine Bound to Human SMO.....	61
Figure 3.4 Close Up View of Cyclopamine in Binding Pocket.....	62
Figure 3.5 Ligand Interactions in Binding Pocket (Cyclopamine)	63
Figure 3.6 Comparison of Cyclopamine and SANT1 Binding Pocket	64
Figure 3.7 Vina Predicted Binding Orientation of LY2940680 with SMO	66
Figure 3.8 Vina Predicted Binding Orientation of Cyclopamine with SMO	68
Figure 3.9 Vina Predicted Binding Orientation of Estrone Analog with SMO.....	69
Figure 3.10 Vina Predicted Binding Orientation of Oxetane with SMO.....	70
Figure 3.11 IFD Predicted Binding of Cyclopamine with SMO	73
Figure 3.12 IFD Ligand Interaction Diagram: Cyclopamine with SMO	74
Figure 3.13 IFD Predicted Binding of Estrone Analog with SMO.....	75
Figure 3.14 IFD Ligand Interaction Diagram of Estrone Analog with SMO.....	76
Figure 3.15 IFD Predicted Binding of Deoxy Estrone Analog with SMO	77
Figure 3.16 IFD Ligand Interaction Diagram of Deoxy Estrone Analog with SMO	77
Figure 3.17 IFD Predicted Binding of Oxetane Analog with SMO	78
Figure 3.18 IFD Ligand Interaction Diagram of Oxetane Analog with SMO	79
Figure 3.19 IFD Predicted Binding of Oxetane Analog with Mutant SMO	80
Figure 3.20 Correlation of IC ₅₀ from DLR Assay and IFD Docking Score.....	81
Figure 3.21 Correlation of logIC ₅₀ from DLR Assay and IFD Docking Score.....	82
Figure 4.1 Predicted Binding Orientation of IPI-926 with SMO.....	87
Figure 4.2 Schrodinger Ligand Interaction Diagram for Predicted Binding of IPI-926 with SMO.....	88
Figure 4.3 Proposed Binding Model: Alpha versus Beta Face	91
Figure 4.4 Depth of Pocket Hypothesis for Aryl-Aryl Coupled Analogs	92
Figure 4.5 Single Crystal X-Ray Structure of Compound 13	93

Figure 4.6 Biological Activity for Aryl-Aryl Coupled Analogs	97
Figure 4.7 Ligand Interaction Diagram for SANT-1 with SMO	98
Figure 4.8 Comparison of IPI926, LY2940680, and cyclopamine.....	99
Figure 4.9 Relative Shapes of Des-C Analogs in Comparison to Original Estrone Analog	101
Figure 4.10 Development of Androsterone Oxetane Analog	103
Figure 4.11 IFD Predicted Binding Affinity for Androsterone 33	105
Figure 4.12 Heteroatom Distances for Rigid and Flexible Analogs	111
Figure 4.13 IC ₅₀ Data for Flexible Linked Analogs.....	114
Figure 4.14 Retrosynthetic Design of Alkylidene Analogs	115
Figure 4.15 Biological Activities of Allylic Alcohols and Derivatives.....	120
Figure 4.16 Side by Side Comparison of Lead Analogs	125
Figure 4.17 Biological Activity of Flexible Pyrrolidine Analog	134
Figure 4.18 Photoredox Cross-Coupling: Single Electron Transmetalation.....	135
Figure 4.19 Summary of Biological Activity of Oxetane Derivatives	137
Figure 4.20 Summary of Biological Activity of Phenyl Allylic Alcohol Family	139

LIST OF SCHEMES

Scheme 1.1 Wolff-Kishner Reduction of Jervine to Cyclopamine.....	6
Scheme 1.2 Acid-Catalyzed Ring Opening and Aromatization of Cyclopamine	7
Scheme 1.3 Generation of Isosteroid Backbone through Wagner-Meerwein Rearrangement of Cholesterol.....	7
Scheme 1.4 Biomimetic Diastereoselective Total Synthesis of Cyclopamine	10
Scheme 1.5 Cyclopropanation/Ring Expansion to <i>D-homo</i> -cyclopamines.....	13
Scheme 1.6 Synthesis of Original Estrone Analog	19
Scheme 1.7 Synthesis of Fused F-Ring Saturated Derivative	23
Scheme 1.8 Synthesis of 4- <i>exo</i> Oxetane F-Ring Saturated Derivative	24
Scheme 2.1 Example Synthesis of Des-B Analogs	47
Scheme 4.1 Synthesis of Beta Sulfonamide	89
Scheme 4.2 Synthesis of Alpha Sulfonamide	90
Scheme 4.3 Synthesis of Aryl-Aryl Coupled Analog of Buchwald Hartwig	93
Scheme 4.4 Unexpected Retro-Aldol from Buchwald Hartwig Cyclization	94
Scheme 4.5 Completion of the Phenyl Aryl-Aryl Coupled Analog	95
Scheme 4.6 Synthesis of Hydroxy Phenyl Aryl Coupled Analog	96
Scheme 4.7 Construction of des-C framework	100
Scheme 4.8 Synthesis of Bent Des-C Analogs.....	101
Scheme 4.8 Synthesis of A-Ring Saturated Oxetane Analog.....	104
Scheme 4.9 Wittig-Based Retrosynthesis for Alkylidene Analogs	106
Scheme 4.10 Retrosynthetic Analysis for Alkylidene Derivative.....	106
Scheme 4.11 Generation of Unsaturated Esters	107
Scheme 4.12 Synthesis of Unsaturated Imine.....	109
Scheme 4.13 Ohira Bestmann Synthesis of Proline Alkynes	112
Scheme 4.14 Synthesis of Flexible Scaffolds	113

Scheme 4.15 Synthesis of Allylic Alcohols	116
Scheme 4.16 Completion of Phenyl and Pyridyl Allylic Alcohols	117
Scheme 4.17 Tsuji-Trost Elimination of Allylic Acetate	118
Scheme 4.18 Completion of <i>cis</i> -pyridyl Analog	119
Scheme 4.19 Synthesis of Saturated Analogs of Phenyl Construct	122
Scheme 4.20 Synthesis of Methyl Ether	122
Scheme 4.21 Synthesis of Cyclobutane Analog	124
Scheme 4.22 Synthesis of Unsaturated Enone	125
Scheme 4.23 Synthesis of Oxetanone Scaffold.....	127
Scheme 4.24 Synthesis of Bare Oxetanone	127
Scheme 4.25 Synthesis of Carbon Framework of Pyrrolidine Allylic Alcohols.....	128
Scheme 4.26 Nucleophilic Addition to Steroid Aldehyde	130
Scheme 4.27 Deprotection of Secondary Carbamate	130
Scheme 4.28 Synthesis of Secondary Tosylate for Elimination.....	131
Scheme 4.29 Elimination Attempts of Secondary Tosylate	131
Scheme 4.30 Completion of Flexible Pyrrolidine Analog	132
Scheme 4.31 Attempted Photoredox Cross-Coupling of Vinyl Bromide	136

LIST OF ABBREVIATIONS

Ac	acetyl
Ac ₂ O	acetic anhydride
AcOH	acetic acid
CAN	acetonitrile
atm	1 atmosphere
BINAP	2,2'-bis(diphenylphosphino)-1,1'-binaphthyl
Bn	benzyl
Boc	<i>tert</i> -butoxycarbonyl
<i>n</i> -BuLi	<i>n</i> -butyllithium
<i>s</i> -BuLi	<i>s</i> -butyllithium
<i>t</i> -BuLi	<i>t</i> -butyllithium
cat.	Catalytic
CeCl ₃	cerium trichloride
CI	chemical ionization
CYC	cyclopamine
d	doublet
δ	chemical shift in parts per million
DCM	dichloromethane

dd	doublet of doublets
DMF	dimethylformamide
DMSO	dimethyl sulfoxide
EI	electron impact ionization
ESI	electrospray ionization
Et	ethyl
Et ₂ O	diethyl ether
EtOAc	ethyl acetate
EtOH	ethanol
H ₂ O	water
HMPA	hexamethylphosphoramide
HRMS	high resolution mass spectrometry
Hz	hertz (s ⁻¹)
IR	infrared spectroscopy
<i>iPr</i>	isopropyl
<i>J</i>	coupling constant in Hertz
LDA	lithium diisopropylamide
m	multiplet
<i>mCPBA</i>	<i>meta</i> -chloroperoxybenzoic acid
Me	methyl

MeOH	methanol
MHz	megahertz
min	minutes
mL	milliliter(s)
mmol	millimole(s)
MsCl	mesylchloride
<i>m/z</i>	mass to charge ratio
NaH	sodium hydride
NaN ₃	sodium azide
NMR	nuclear magnetic resonance
PCC	pyridinium chlorochromate
Pd(OAc) ₂	palladium acetate
Ph	phenyl
PPh ₃	triphenylphosphine
ppm	parts per million
q	quartet
rt	room temperature
s	singlet
sat.	saturated
t	triplet

TBAF	tetra- <i>n</i> -butylammonium fluoride
TBS	<i>tert</i> -butyldimethylsilyl
TBDPS	<i>tert</i> -butyldiphenylsilyl
<i>t</i> -BuOH	<i>tert</i> -butyl alcohol
Tf ₂ O	trifluoromethanesulfonic anhydride
THF	tetrahydrofuran
TLC	thin-layer chromatography
Trit	trityl
TsCl	toluenesulfonyl chloride
XPhos	2-(dicyclohexylphosphino)-2',4',6'- triisopropylbiphenyl
wt	weight

Chapter 1. The Sonic Hedgehog Pathway

Section 1.1 Overview of the Sonic Hedgehog (SHH) Pathway

1.1.1 Discovery of the Hedgehog (*Hh*) Signaling Pathway

For the majority of the 20th century, it was not well understood how a developing embryo could temporally and spatially differentiate at the cellular level. In 1980, Nüsslein-Volhard and Wieschaus discovered over a dozen individual genes that altered the segmentation patterns in the larva of the fruit fly, *Drosophila melanogaster*. The genes they identified were determined to be essential for proper embryonic development, and the associated proteins were classified as the Hedgehog (Hh) signaling pathway.¹ Using genetic sequence alignment, Echelard and coworkers discovered three homologous genes in mice: *Desert Hedgehog (Dhh)*, *Indian Hedgehog (Ihh)* and *Sonic Hedgehog (Shh)*.² *Shh* was reported to be the most widely expressed homolog and is involved in key aspects of embryological development.

1.1.2 Role of Sonic Hedgehog (SHH) Pathway in Embryogenesis

Since their discovery and isolation, the various proteins associated with the Hedgehog (Hh) signaling pathway have been recognized as key components of cellular differentiation and growth. The most widely studied *Hh* homolog, *Shh*, has been linked to patterning of the neuronal tube as well as many other biological processes.³ Levin and coworkers determined that the SHH pathway is responsible for the light-to-right axis of symmetry in developing chick embryos.⁴ It has been shown that disruptions of the SHH

pathway result in severe embryonic malformations. These malformations range from minor disruption of bilateral symmetry to cyclopia, the most severe aberration.⁵

The SHH signaling pathway consists of two key transmembrane proteins, multiple intracellular proteins, and numerous nuclear targets (**Figure 1.1**). To begin the signal transduction, a functional HH protein is released from a parent cell. The HH protein is modified at both the N- and C- termini by the addition of a palmitic acid and cholesterol, respectively. This dually lipidated protein can then bind to the extracellular surface and activate the twelve-pass transmembrane receptor protein Patched (PTC).⁶ Once activated, PTC releases its inhibitory hold on seven-pass transmembrane protein Smoothed (SMO).^{7,8}

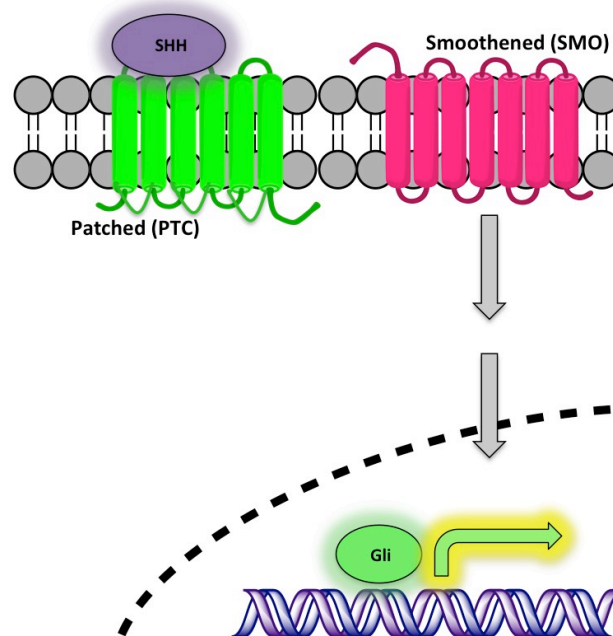


Figure 1.1 Proteins and Cellular Targets of the Sonic Hedgehog Pathway

It is believed that the binding of HH to PTC initiates the translocation of SMO from an intracellular vesicle to the cell surface.³ On the cell surface, the cytosolic tail of

SMO is phosphorylated which allows for the mediation of the downstream cytosolic events. Once activated, SMO will signal cytosolic proteins such as Suppressor of Fused (SUFU) and glioma (GLI). After activation, the GLI proteins are internalized into the nucleus where they can act as transcription factors. Once all necessary nuclear proteins are sequestered, the transcription of the *Gli* genes will begin promoting cellular growth and differentiation.⁹

1.1.3 The Link Between Sonic Hedgehog Pathway and Cancer

Shortly after the discovery of the above-mentioned signaling pathway, it was quickly determined that Hedgehog plays a key role in embryonic pattern formation, including bilateral symmetry. Interestingly, the activation of the Hedgehog pathway is only necessary for embryogenesis and modest tissue homeostasis in adult cells. However, aberrant activation of the pathway was linked to tumor initiation and growth. Up-regulation of the SHH pathway has been associated with both basal cell carcinoma (BCC)^{10,11} and medulloblastoma, as well as numerous other cancers (lung, gastric, pancreatic, and prostate).¹²

In the 1960's, scientists identified a familial variant of basal cell carcinoma, a non-invasive skin cancer that often results in disfigurement and destruction of surrounding tissues.¹³ This familial variant is known as Gorlin's Syndrome, or Nevoid Basal Cell Carcinoma Syndrome. Using a genetic screen, it was later determined that mutations in the *Ptc1* protein were the common link between these two forms of skin cancer.¹⁴ These mutations prevent *Ptc* from inhibiting *Smo*, which results in a constitutively activated SHH pathway. Like the inherited variant of BCC, point mutations along the SHH pathway have been shown to be responsible for a large portion of sporadic BCC's. BCC is the

most common form of cancer in the Western hemisphere, and with a growth rate of over one million new cases annually, there is a high demand for novel chemotherapeutics.

Similar to BCC, medulloblastoma, a pervasive pediatric brain cancer that develops in the cerebellum, has been associated with genetic mutations throughout the SHH pathway. During the development of the cerebellum, the SHH pathway is responsible for neuronal differentiation that leads to the proliferation of cerebellar granular neuronal precursor (GNP) cells. Using a mouse model, Scott and coworkers showed the relationship between *Ptc* and *gli* and the development of medulloblastoma.¹⁵ Furthermore, blockage of the Hedgehog pathway resulted in inhibition of cancer cell growth and reduced tumor size.¹² This study strongly suggests that [inhibitors of the Sonic Hedgehog Pathway](#) could serve as anti-cancer targets.

Section 1.2 The Inhibition of the Sonic Hedgehog Pathway

1.2.1 Discovery of the Alkaloid Cyclopamine

During a drought in the summer of 1957, a herd of sheep was forced to search for food at higher elevation. After the drought was over, the sheep that were pregnant during these periods of dry climate gave birth to offspring that exhibited many congenital cranial abnormalities.¹⁶ After this discovery, scientists spent over ten years searching for the cause. By feeding pregnant sheep with a variety of plants native to higher elevations, it was later determined that *Veratrum californicum*, a California corn lily, contained the tetratogenic alkaloids responsible for this phenotype.¹⁷ In 1968, Keeler successfully isolated the major alkaloids from the plant: veratramine, alkaloid Q,¹⁸ and cyclopamine

(**Figure 1.2**). After feeding studies, it was determined that cyclopamine was responsible for the plant's teratogenic effects.^{19,20}

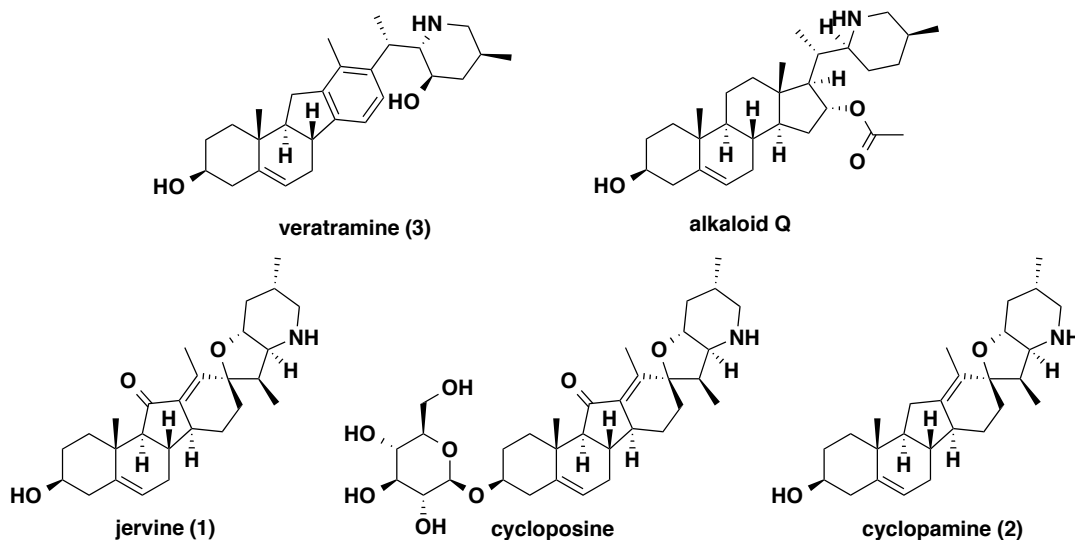
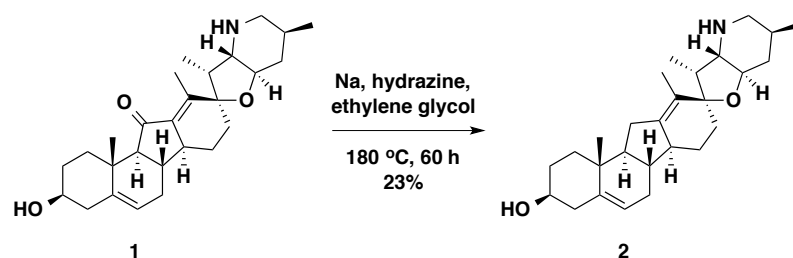


Figure 1.2 Structures of the *Veratrum californicum* Alkaloids

After further experimentation, it was found that there were, in fact, three structurally related alkaloids that induced cyclopia: jervine (1), cycloposine, and cyclopamine (2) (**Figure 1.2**). The latter was structurally related to jervine, and based on crude analysis, it was predicted to be steroidal in nature. To confirm the suspected structure of the novel alkaloid, jervine was submitted to Wolff-Kishner reduction, and the resulting product was identical to that of cyclopamine (**Scheme 1.1**).



Scheme 1.1 Wolff-Kishner Reduction of Jervine to Cyclopamine

This isosteroidal alkaloid exhibits a hexacyclic framework with a *C-nor-D-homo* backbone. Linked to the relatively hydrophobic backbone, cyclopamine contains a functionalized tetrahydrofuran E ring perpendicular to the backbone connected through a spirocyclic allylic ether (**Figure 1.3**). The functionalized piperidine F ring is fused to the tetrahydrofuran ring in a fashion which orients the nitrogen on the alpha face of the molecule while the oxygen lies on the beta face.

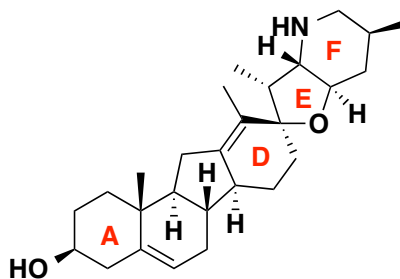
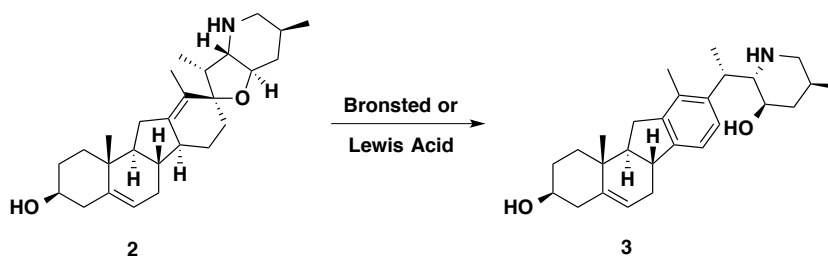


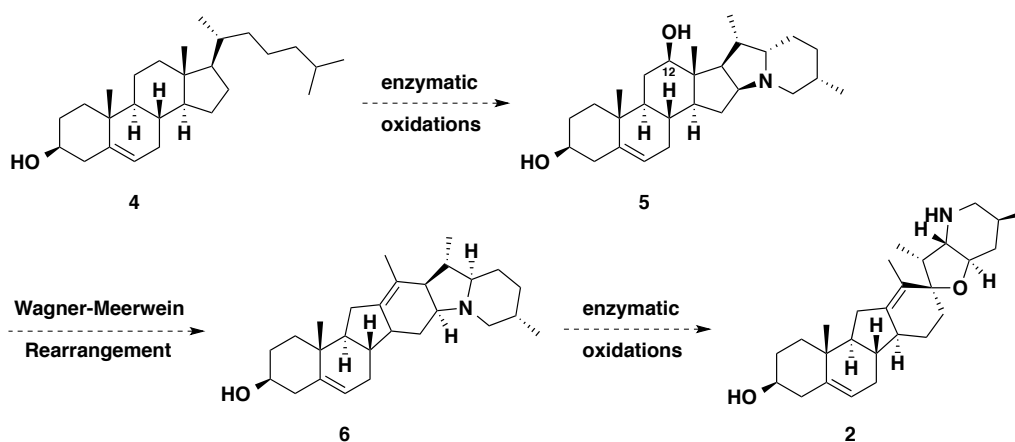
Figure 1.3 Structural Analysis of Alkaloid Cyclopamine

The allylic ether moiety renders this molecule unstable to Brønsted or Lewis acidic conditions, leading to a rapid ring opening and aromatization to yield veratramine (**3**) (**Scheme 1.2**). The loss of the DE spirocycle eliminates all cycloopia-inducing properties of the parent molecule cyclopamine.



Scheme 1.2 Acid-Catalyzed Ring Opening and Aromatization of Cyclopamine

Based on the work of Tscheche and Kaneko, it is believed that cyclopamine is biosynthesized from cholesterol. This was confirmed through feeding studies using ^{14}C -cholesterol (**4**). This study also revealed that cyclopamine is the parent compound that leads to both jervine and veratramine. The isosteroidal backbone is predicted to arise from a Wagner-Meerwein type rearrangement (compound **5** to **6**) via an activated hydroxy-based leaving group (**Scheme 1.3**). Subsequent enzymatic oxidations lead to ^{14}C -cyclopamine.



Scheme 1.3 Generation of Isosteroid Backbone through Wagner-Meerwein Rearrangement of Cholesterol

1.2.2 Linking Cyclopamine to Sonic Hedgehog

Expanding on the work of Keeler, Beachy determined that the *Veratrum californicum* alkaloids were inhibitors of the Sonic Hedgehog pathway.⁵ Using *Shh* knockout mice as a direct comparison, Beachy and coworkers demonstrated that increasing concentrations of jervine and cyclopamine resulted in the same holoprosencephaly phenotype in developing chick embryos. This work further elucidated that the inhibitors do not simply modify the Shh ligand, but instead they were shown to alter the downstream target responses. Similarly, Incardona and coworkers found that cyclopamine disrupts the SHH pathway but not the metabolism of cholesterol, a molecule whose decrease in concentration was shown to result in holoprosencephaly in developing embryos.²¹ Beachy and Incardona both hypothesized that cyclopamine could be acting in the sterol-sensing domain of *Patched* due to its steroid-like structure.

Despite these findings, it remained a mystery how these compounds produced their striking phenotypes. Work by Beachy and coworkers in 2000 suggested a Patched-independent mechanism,²² but in 2002 they showed definitively that cyclopamine acted at the level of Smoothed.²³ By using both a photoaffinity modified cyclopamine as well as BODIPY-cyclopamine (**Figure 1.4**), which can be observed in live cells due to its high levels of fluorescence, Beachy determined that cyclopamine inhibits Sonic Hedgehog by binding to and antagonizing the Smoothed heptahelical bundle. In addition, this work suggested that cyclopamine and Patched (*PTC*) may regulate Smoothed in a similar fashion, although the mechanism of PTC binding to SMO remained unclear.²⁴

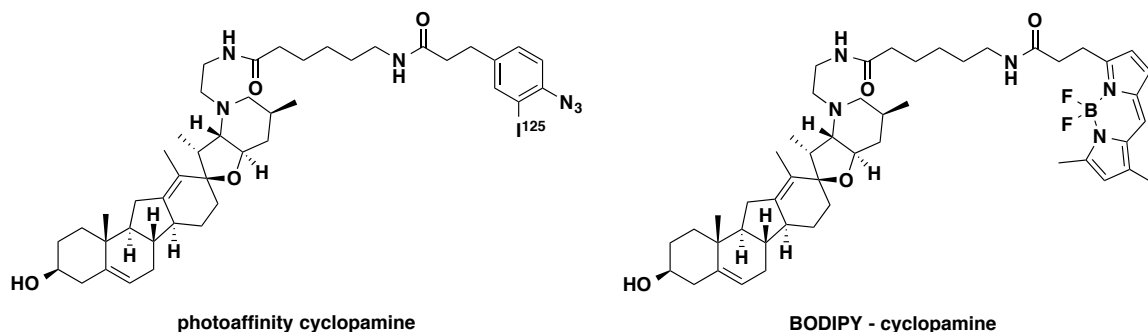


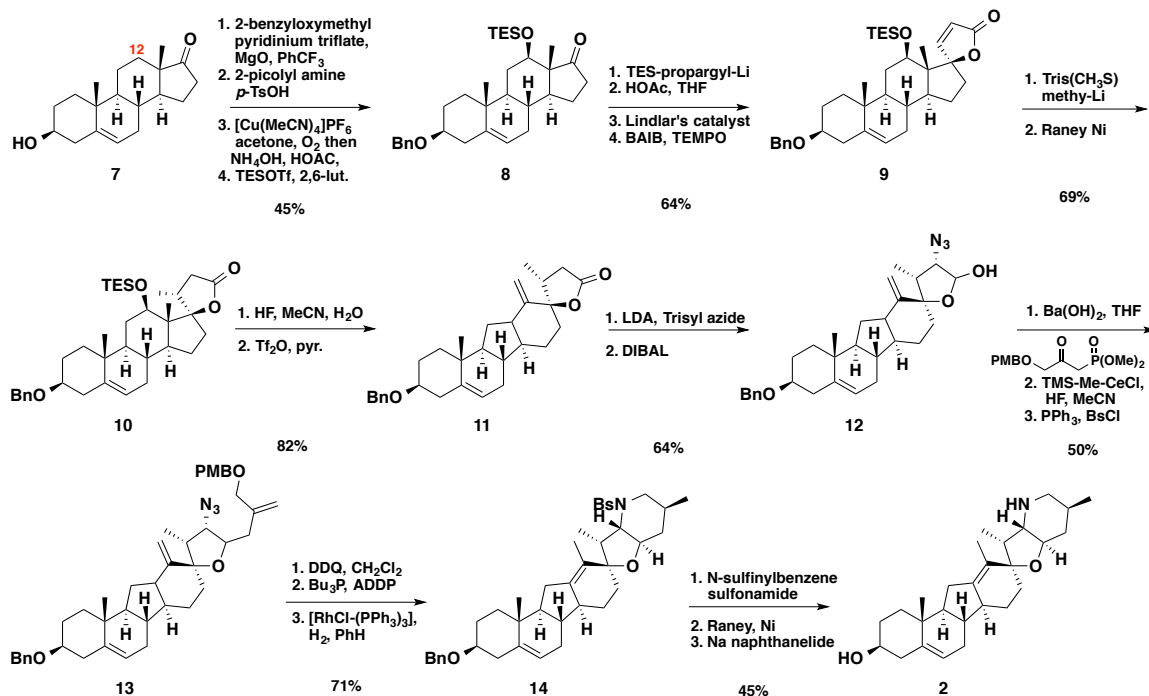
Figure 1.4 Structures of biochemical probe derivatives

1.2.3 Shortcomings of Cyclopamine as a Drug Candidate

Despite its potential as a chemotherapeutic, the shortcomings of cyclopamine are three-fold. In order to pursue the biological possibilities for this molecule, there needs to be a sufficient supply of the parent compound. The first major setback is the low abundance of the alkaloid in plant material. According to the original isolation described by Keeler, isolating cyclopamine requires six extractions, four column chromatography purifications, and three recrystallizations. In addition to the extremely intensive extraction protocol, only 500 milligrams of pure cyclopamine can be extracted from 1 kilogram of dried plant material, providing a 0.05% isolated yield.¹⁹

Since the isolation is not amenable for derivatization and evaluation, synthetic exploration of both cyclopamine and structurally related alkaloids has been of significant interest to the chemistry community. In the late 1960's, both Masamune²⁵ and Johnson²⁶ reported syntheses of jervine and similar constructs, respectively. Since it was shown by Keeler that reduction of the C11 carbonyl of jervine resulted in cyclopamine, these works represent the first formal total synthetic routes to cyclopamine. These routes were both non-stereoselective and low yielding. Nearly fifty years after

their seminal works, Giannis and coworkers published the first diastereoselective and biomimetic total synthesis of the alkaloid cyclopamine.²⁷



Scheme 1.4 Biomimetic Diastereoselective Total Synthesis of Cyclopamine

Summarized in **Scheme 1.4**, the route developed by Giannis allowed for the construction of unnatural analogs of cyclopamine that were previously unexplored and held high potential for biological relevancy. This synthesis utilized copper-mediated C-H activation to install a pivotal C12 hydroxyl, cationic ring expansion/contraction to construct the *C-nor-D-homo* skeleton, and an Alder-ene [reaction](#) to isomerize an exocyclic double bond to the desired internal olefin. In addition, the Giannis research group elaborated commercially available dehydroepiandrosterone and circumvented the intermediacy of jervine.

To begin, Giannis elaborated commercially available dehydroepiandrosterone **7** to TES-protected hydroxy steroid **8** via C-H activation/oxidation sequence. The E-ring carbons were installed using a diastereoselective addition of triethylsilyl propargylate, reduction, and cyclization to afford **9**, which upon addition of a methyl group provided access to **10**, the key intermediate for the Wagner-Meerwein rearrangement. Isosteroid **11** was constructed as desired upon activation of the C12 hydroxyl with triflic anhydride. Functionalization of the alpha carbon of the lactone allowed for installation of the necessary F-ring nitrogen in **12**. A Horner-Wadsworth-Emmons reaction installed the remainder of the carbon skeleton, and azide **13** was reduced and subsequently cyclized using Mitsunobu conditions to provide the EF-ring system of the natural material in **14**. Removal of the protecting groups provided the first diastereoselective synthesis of cyclopamine in just over twenty steps.

Despite the synthetic elegance of this route, the complexity of the natural product and the difficulty to produce material on a biologically useful scale highlight the second major shortcoming of cyclopamine as a chemotherapeutic. The third, and most important, limitation of the molecule is its instability in aqueous acid. Upon entering a mildly acidic environment, the allylic ether of cyclopamine rapidly ring opens and aromatizes (**Scheme 1.2**) and renders the resulting compound inactive. The combination of the aforementioned difficulties have led academic and pharmaceutical laboratories to search for other antagonists of the Hedgehog pathway, through both diversification of the natural alkaloid as well as high-throughput screening to identify new and patentable scaffolds. These efforts are summarized below.

1.2.4 Pharmaceutical Derivatives and Clinical Trials

1.2.4.1 Infinity Pharmaceuticals: IPI-926

Infinity Pharmaceuticals has developed a series of semi-synthetic cyclopamine analogs that shows marked improvement in both cellular activity and metabolic stability. As previously stated, the instability of cyclopamine is attributed to the D-ring allylic ether, which promotes ring opening and aromatization in acidic environments. To circumvent this ring opening, Infinity utilized an oxidation/cyclopropanation/ring-expansion sequence to generate a family of *D-homo-cyclopamine* analogs (**Figure 1.5**).^{28,29}

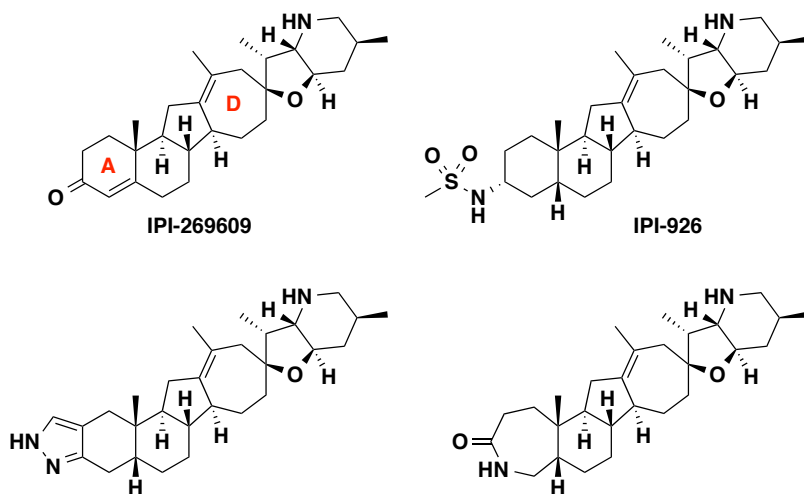
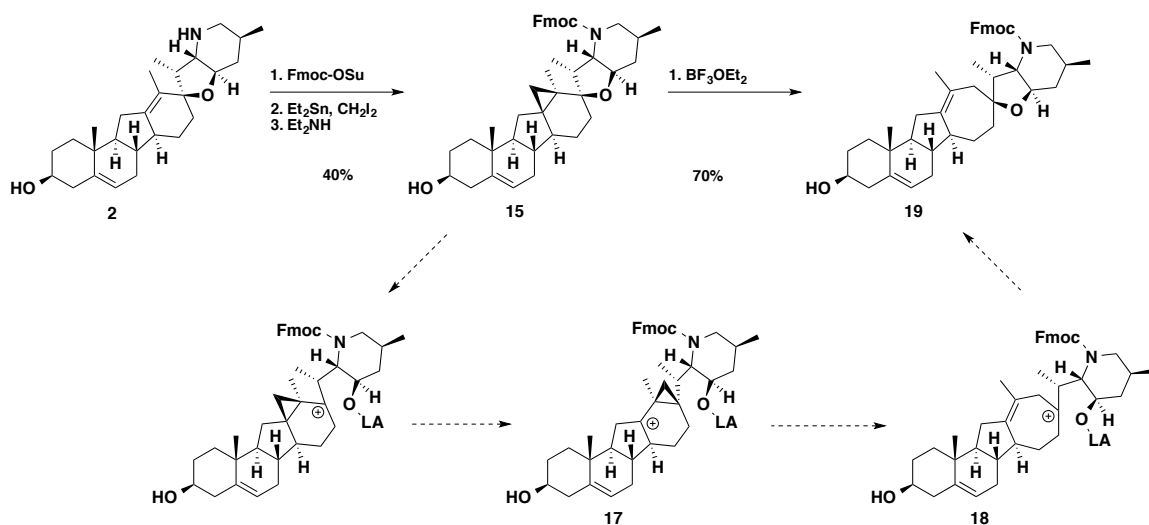


Figure 1.5 Infinity Pharmaceuticals: *D-homo-cyclopamine* Analogs

The major disadvantage to the semisynthetic route is the necessity to grow and harvest acres of corn lilies to isolate cyclopamine in less than one gram per kilogram of dried plant material. This precious starting material must then be carried through five chemical transformations to construct the lead analog, IPI-926. The key cyclopropanation is shown below in **Scheme 1.5**.



Scheme 1.5 Cyclopropanation/Ring Expansion to *D*-homo-cyclopamines

After protection of the secondary amine, the most electron rich double bond of cyclopamine is cyclopropanated to afford **15**. Using Lewis acid-mediated conditions, the six-membered D-ring is expanded through a series of cationic rearrangements (**16-18**) to furnish the homoallylic alcohol **19**. Following this ring expansion, two major modifications remain to produce IPI-926. The stereochemistry of the alcohol on the A-ring of the molecule is inverted and the oxygen exchanged for a methyl sulfonamide to enhance solubility. In addition, the unsaturation at the AB ring fusion is reduced to provide the *cis* decalin, drastically altering the overall three-dimensional shape of the molecule.

After enhancing the pharmacokinetic profile and solubility, IPI-926 has low nanomolar activity and leads to reduced tumor size in a mouse tumor model. IPI-926 performed well in Phase Ia/Ib clinical trials and was given the generic name saridegib. During the clinical trials, saridegib was identified as a Hedgehog inhibitor in the

treatment of chondrosarcoma, an invasive bone cancer that has been linked to constitutive SHH expression. Infinity Pharmaceuticals pulled saridegib from Phase II after it did not perform as anticipated.

1.2.4.2 Curis Pharmaceuticals and Genentech: Cur61414 and GDC-0449

In 2003 a small pharmaceutical company, Curis, released a report that identified a novel, heterocyclic scaffold that inhibited SHH. Cur61414 (**Figure 1.6**) was the first report of a non-cyclopamine like structure that had been identified to inhibit the SHH pathway as well as suppress proliferation in BCC model systems.³⁰ Similar to the aforementioned outcome with IPI-926, Cur61414 was pulled from Phase I clinical trials due to its inability to reduce the proliferation of BCC. This disconnect of *in vivo* and *in vitro* results was speculated to be the result of poor skin penetration. Through a strategic collaboration with Genentech and Evotec, Curis identified a new scaffold that also exhibited potent activity, with the hopes of rescuing their efforts in clinical trials.

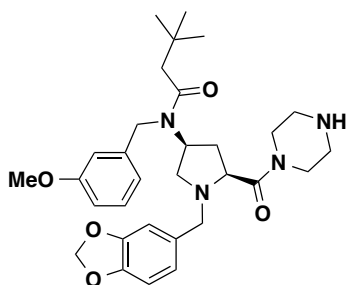


Figure 1.6 Structure of SHH Antagonist Cur61414

Using a murine derived high-throughput screen with a *Gli*-reporter the collaboration quickly identified a potent lead compound. After analyzing the clearance and metabolic stability in human and dog liver microsomes, respectively, it was decided

that this compound was not acceptable to move forward; however, it did provide an excellent starting point. After optimization of the initial benzimidazole lead, Genentech developed GDC-0449 (**Figure 1.7**), a metabolically stable derivative with improved PK properties and increased potency.³¹ GDC-0449 performed well in Phase II clinical trials with patients with advanced BCC, with greater than 50% showing a partial response and decrease in tumor size. In January 2012 GDC-0449 became the first FDA approved Hedgehog Inhibitor to hit the market.

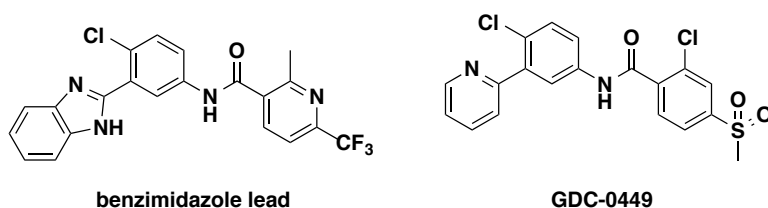


Figure 1.7 Structure of Benzimidazole Lead and SHH Antagonist GDC-0449

Unfortunately, in many cases, patients develop resistance to GDC-0449 by a single point mutation in the gene sequence of SMO, highlighting the necessity for multiple, complimentary forms of [SMO](#)-inhibitory agents for the treatments for BCC.

1.2.4.3 Novartis: NVP-LDE225

Using a library of over ten thousand compounds, Novartis Pharmaceuticals joined the race to find a novel scaffold for SHH inhibition in the early 2000's. By 2009, they had identified 1-amino-4-benzylphthalazines as orally bioavailable antagonists of Smoothed (**Figure 1.8**).³² After an extensive SAR endeavor that increased potency while decreased metabolically labile functionalities, Novartis released the structure of their lead molecule to move into *in vivo* and *in vitro* testing: NVP-LDE225. The 4-amino-

phthalazine core was retained while the benzyl functionality was replaced with a more sterically demanding dimethyl morpholine. Their lead compound displayed excellent pharmacokinetic properties across species, was not a substrate for human CYP450, and showed reduced tumor growth across multiple mouse models.³³

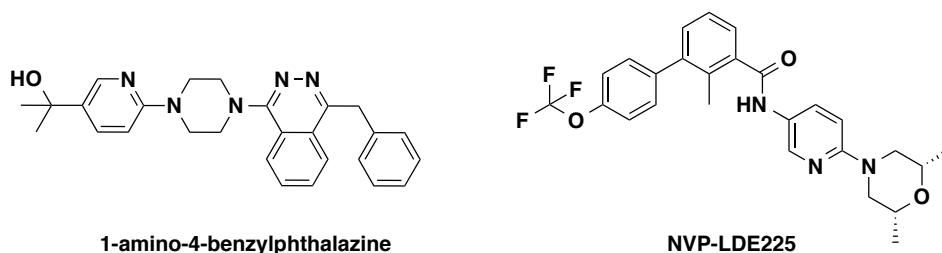


Figure 1.8 Compounds of Interest for Novartis

After successfully completing Phase I clinical trials, NVP-LDE225 entered Phase II targeting patients with advanced basal cell carcinoma. After six months of treatment with the compound, Novartis announced that it had reached a pivotal endpoint of the trial and confirmed that the majority of patients had seen partial or complete responses, indicating a significant tumor response or absence of the disease. The Phase III clinical trial remains ongoing, but in 2014 Novartis filed to market Sonidegib, the trade name given to NVP-LDE225, in the European Union, Switzerland, Australia, and the United States. As of July 2015, the FDA has given Sonidegib approval for the treatment of BCC.

1.2.4.4 Eli Lilly: LY2940680

In 2012, Eli Lilly filed a patent for aryl phthalazines that closely resemble the key structure of the Novartis lead compound (**Figure 1.9**). Their lead aryl phthalazine, LY2940680, has been shown to exhibit low nanomolar activity against the SHH pathway

and has been shown to remain effective in cell lines that develop resistance to GDC-0449. Treatment of $Ptch^{+/-}$ $p53^{-/-}$ transgenic mice, which spontaneously develop medulloblastoma, with oral administration of LY2940680 produced remarkable efficacy and significantly improved their survival. Eli Lilly has recently concluded their Phase II clinical trials in healthy participants.

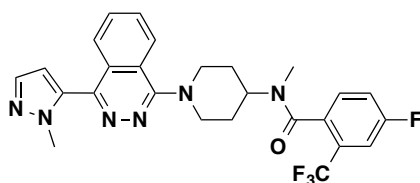


Figure 1.9 Eli Lilly Lead Compound LY2940680

Section 1.3 Development of Steroid-Based Analogs

Since the discovery of cyclopamine and the unveiling of the relevance to cancer biology, there have been a number of approaches taken by pharmaceutical companies to develop novel Sonic Hedgehog inhibitors. Summarized above, these approaches range from isolation and semi-synthesis, utilized by Infinity Pharmaceuticals to develop IPI-926, to more traditional medicinal chemical approaches, such as high-throughput screens and SAR analysis used by Genentech, Novartis, and Eli Lilly. The Winkler Laboratory took interest in this area and decided to use a more targeted design and synthesis technique using the similarities of the cyclopamine carbon skeleton to that of a native steroid.

As mentioned previously, cyclopamine exhibits a *C-nor-D-homo* modification of the traditional ABDC ring system of a steroid (**Figure 1.10**). The Winkler laboratory envisioned using the commercially available estrone backbone as a surrogate for the

pseudo-steroidal backbone of cyclopamine. Preliminary synthetic efforts and biological analysis is summarized below.

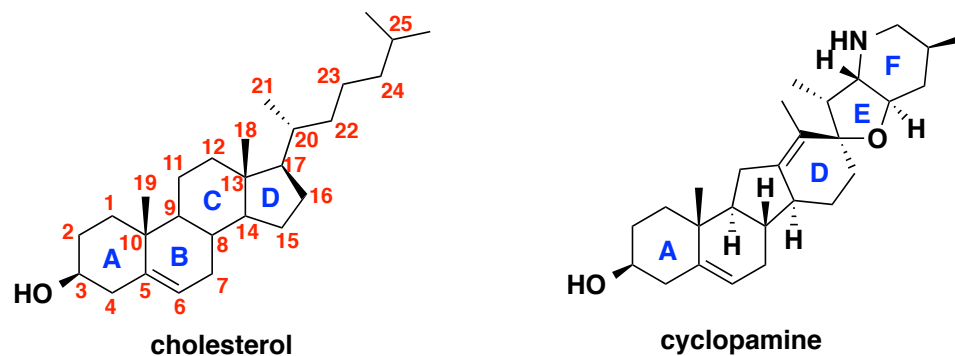


Figure 1.10 Steroid Ring Nomenclature

1.3.1 F-Ring Aromatic Derivatives

The first generation of estrone-derived cyclopamine analogs was designed as a proof-of-principle. Maintaining a linear ABCD backbone and a DE spirocycle, the original estrone analog was constructed to maintain the relationship between the oxygen and nitrogen atoms of the E- and F-rings, respectively. It had been shown that tomatidine, a structurally similar analog with a DE-ring fusion, did not show biological activity (**Figure 1.11**). Therefore, it was essential when designing the first generation analogs to maintain the DE spirocycle. Originally synthesized by Professor Andre Isaacs, the estrone analog was constructed in only four chemical transformations, with a simple protection, lithium mediated addition, Buchwald-Hartwig cyclization, and subsequent deprotection (**Scheme 1.6**).³⁴

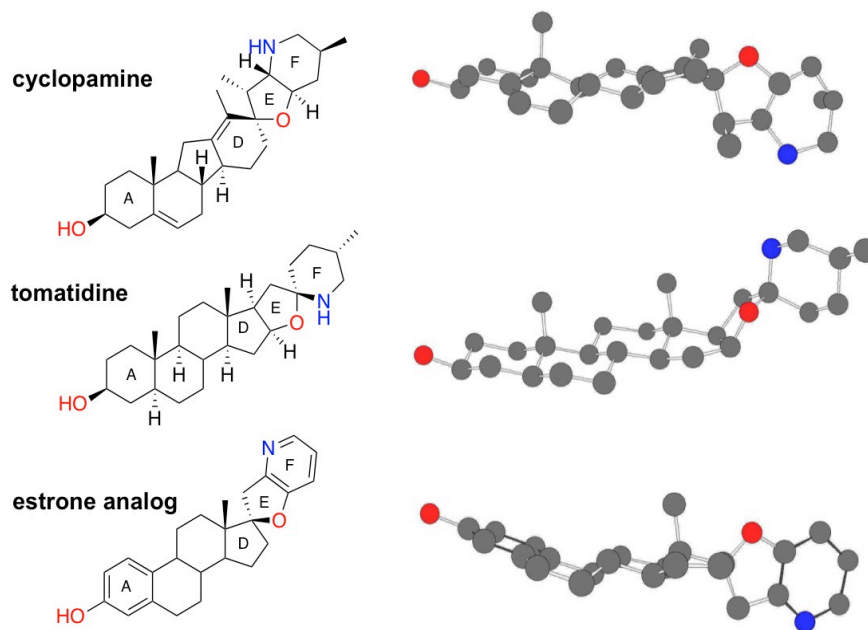
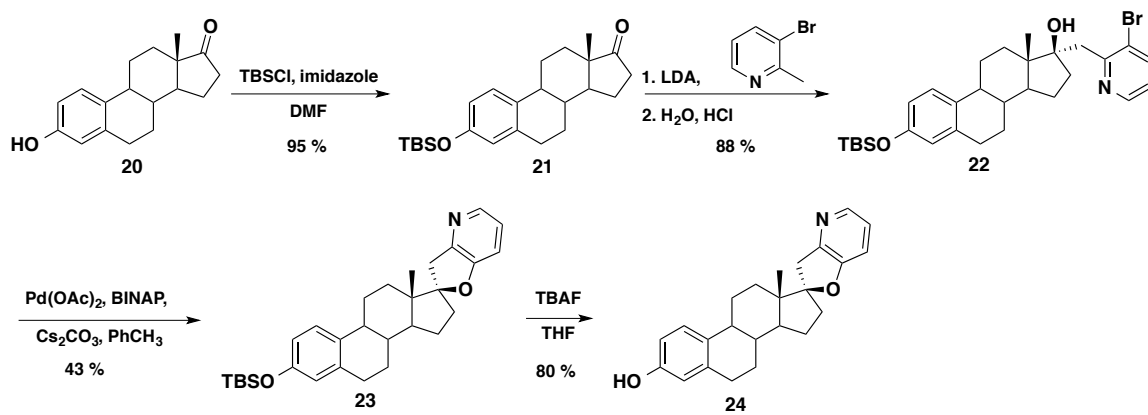


Figure 1.11 Comparison of Cyclopamine, Estrone Analog, and Tomatidine



Scheme 1.6 Synthesis of Original Estrone Analog

In addition, Isaacs prepared a number of analogs to assess various aspects of the proposed two-point binding model (**Figure 1.12**). This binding model proposed that strategic hydrogen bonds could provide the appropriate pharmacophore for both the estrone analog and cyclopamine. The mostly saturated hydrophobic backbone could easily be replaced with another hydrophobic core. To probe this binding model for validity Isaacs designed a C3-deoxygenated analog as well as a C17 epimer (**Figure 1.13**).³⁵

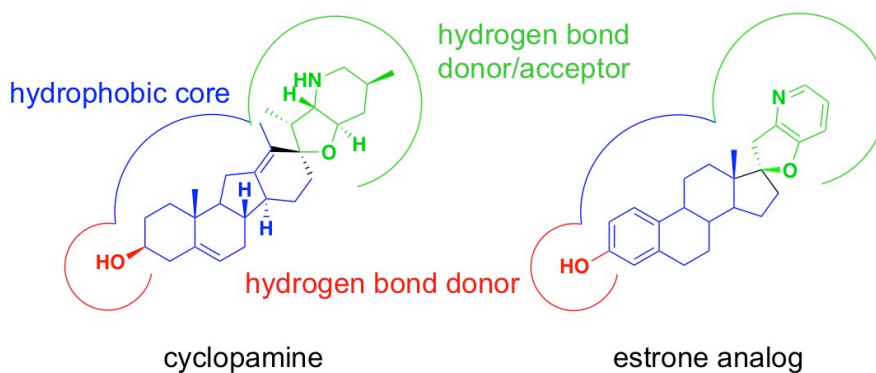


Figure 1.12 Proposed Two-Point Binding Model

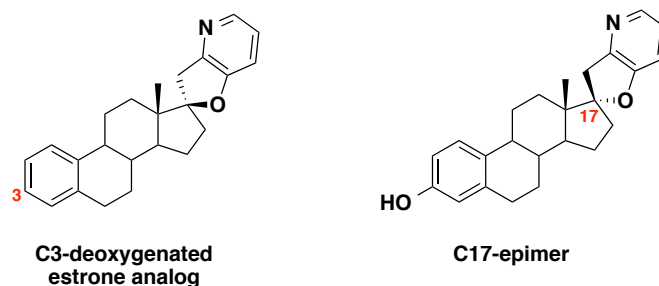


Figure 1.13 Analogs to probe the Two-Point Binding Model

Comparing the structures of the estrone analog relative to cyclopamine, there are two major modifications: the aromatization of both the A- and F-rings, and the hybridization of the F-ring nitrogen. Based on the above-mentioned two-point binding model, the hybridization and basicity of the F ring nitrogen could provide essential hydrogen bonds that enhance potency. The next goal was to synthesize F-ring saturated derivatives that more closely mimicked the EF ring system of cyclopamine.

1.3.2 F-Ring Saturated Derivatives

The F-ring saturated derivatives were envisioned using a two-step cyclization approach. First, the E-ring would be constructed via iodoetherification and then the F-ring would be closed via displacement of the primary tosylate and secondary iodide (**Figure 1.14**). It was anticipated that the stereochemistry of the double bond would be reflected in the 5-*endo* ring closure, where the *cis* olefin would lead to one diastereomeric product, and the *trans* olefin would provide the corresponding diastereomer. Using a common alkyne intermediate, it was envisioned that both diastereomers could be generated, and the importance of stereochemistry could be easily established.

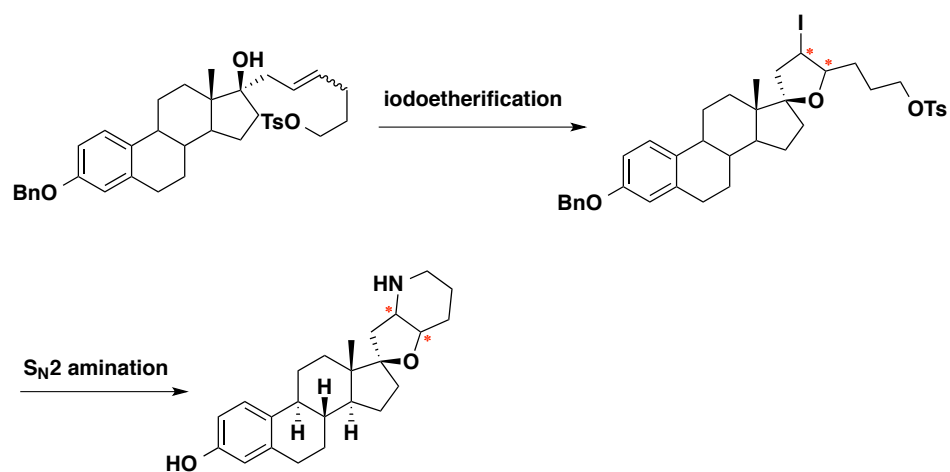
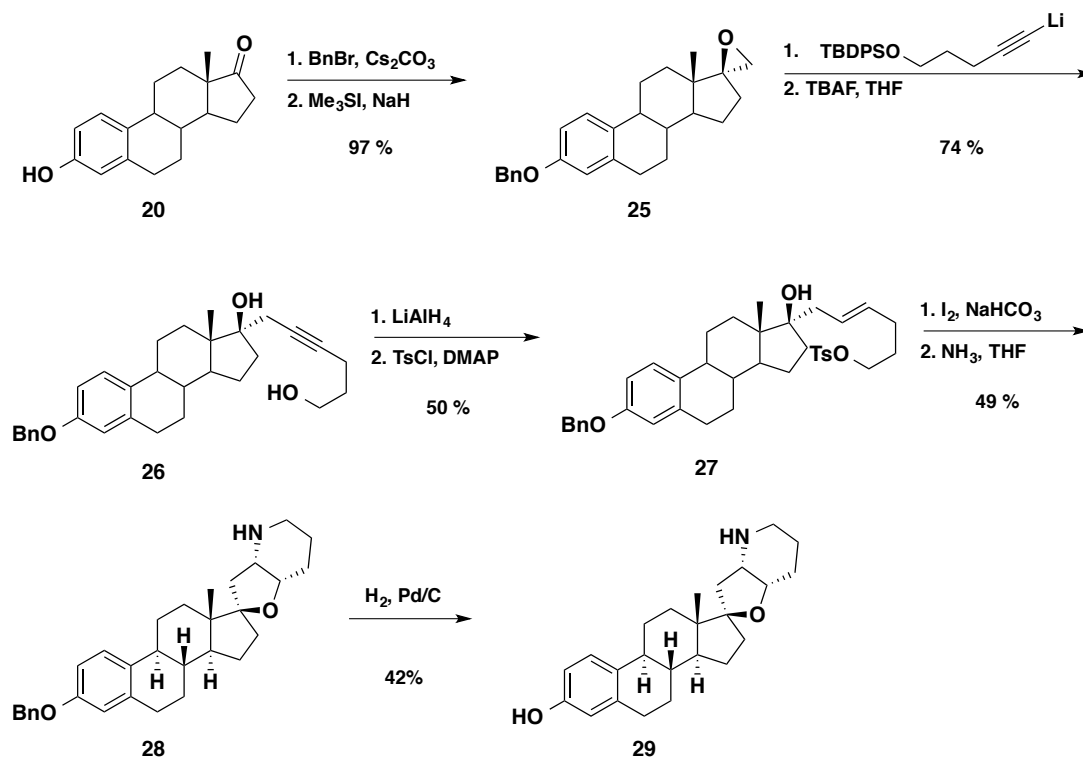


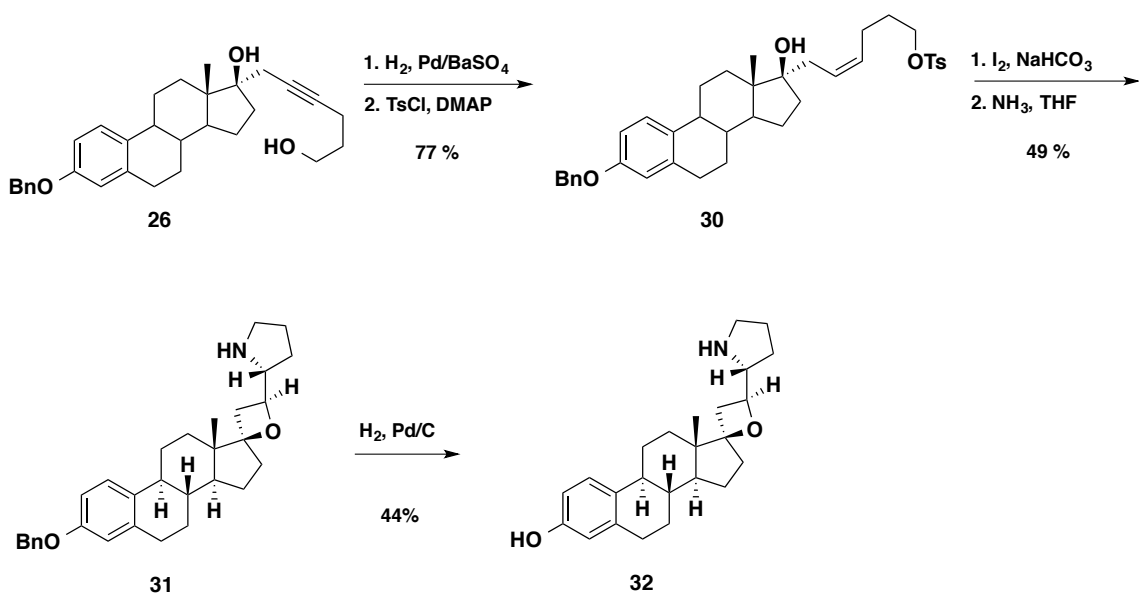
Figure 1.14 Envisioned Approach to F-Ring Saturated Derivatives

To begin, commercially available estrone **20** was protected and treated with trimethylsulfonium iodide to provide epoxide **25**. A silyl protected pentynol was first lithiated and treated with a Lewis acid to afford the epoxide opened product, which could be deprotected with a fluoride source to provide alkyne **26**, a common intermediate for both the *cis*- and *trans*-olefins. Functionalization of the alkyne to the *trans*-alkene via lithium aluminum hydride reduction generated the bis-diol where the most sterically accessible alcohol was activated as the primary tosylate **27**. Upon effecting the key iodine-mediated cyclization, the *trans* olefin precursor afforded the expected *cis* fused EF-ring system of **28** which was deprotected to provide the EF-fused saturated derivative **29** (Scheme 1.7).



Scheme 1.7 Synthesis of Fused F-Ring Saturated Derivative

Similarly, the common alkynyl intermediate **26** was functionalized by reduction to the *cis*-alkene and activation as the primary tosylate **30**. Unexpectedly, the key iodoetherification did not furnish the diastereomeric product of **28**, but instead the exocyclic oxetane **31** was isolated after cyclization with liquid ammonia. Compound **32** was deprotected and evaluated for biological activity (Scheme 1.8).³⁶



Scheme 1.8 Synthesis of 4-exo Oxetane F-Ring Saturated Derivative

1.3.3 Biological Evaluation

The estrone analogs described in **Section 1.3.1** and **1.3.2** were evaluated in two manners: a *Gli*-luciferase reporter assay and inhibition of Granule Neuron Precursors (GNPs). The assays were executed through collaboration with the Dahmane Laboratory in The Wistar Institute. As previously mentioned, the activation of the SHH pathway terminates with the transcription of the *gli* genes. By fusing the *gli* genes to luciferase, a gene with a quantifiable output, an assay was developed that allows for the interpretation of pathway activation. Using the Light2 cells, a mouse 3T3 cell line with a *gli* dependent form of luciferase, the relative potencies of the **24**, **29**, and **32** were established against cyclopamine (**Figure 1.15**).

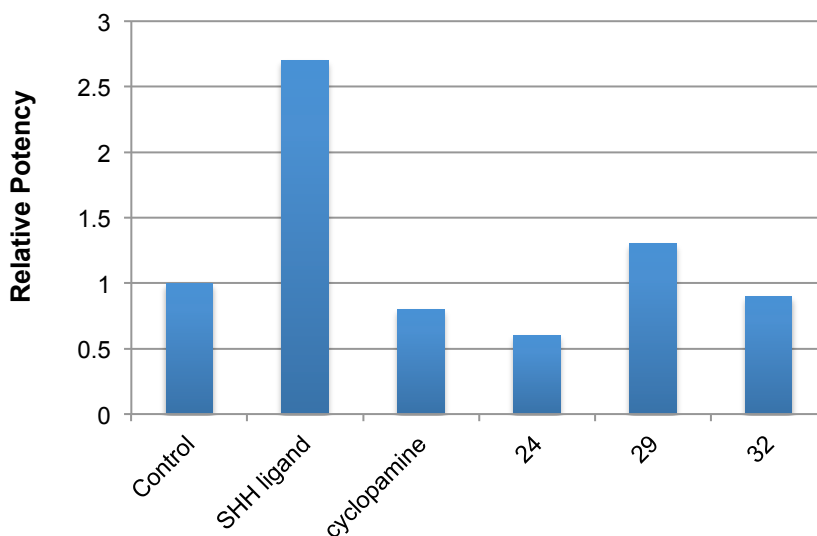


Figure 1.15 Relative Inhibition of *Gli-Luciferase* in SHH Light2 Cells

The Light2 cells were first treated with exogenous SHH ligand and then treated with 10 μ M concentrations of the cyclopamine analogs. As a negative control a portion of cells were left untreated of SHH ligand (control in **Figure 1.15**). Estrone analog **24** showed increased potency relative to the parent cyclopamine whereas the F-ring saturated analogs **29** and **32** both exhibited modest potency.

Using a second set of experiments to generate preliminary biological data, purified mouse P5 GNPs were treated with SHH (600 ng/ mL), alone or in combination with cyclopamine **2** (10 μ M), tomatidine, a negative control (10 μ M), or steroidal analogue **24**, **29**, or **32** (10 μ M). Since the SHH pathway is required for the development of many areas of the brain, SHH alone enhances cell proliferation. Addition of cyclopamine significantly decreases cell proliferation for cells treated with SHH while tomatidine has no effect. At 10 μ M, compounds **24**, **29**, and **32** were equipotent with cyclopamine in inhibiting SHH-induced GNP proliferation (**Figure 1.16**).

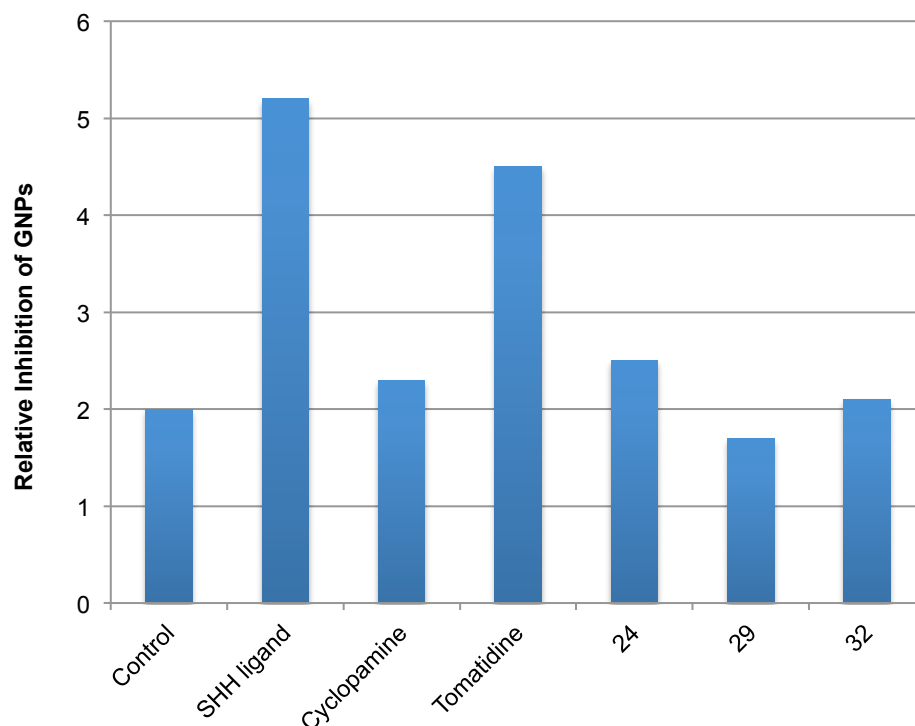


Figure 1.16 Inhibition of SHH-dependent Granule Neuron Precursor Growth

Section 1.4 Conclusions

Due to the metabolic instability of cyclopamine, and the development of GDC-0449 resistant cancers, there is an immediate need for readily available and potent inhibitors of SHH signaling. The Winkler group has initiated a project designed to identify novel compounds that are efficient in blocking the SHH signaling pathway. By using a steroid core to replace the hydrophobic backbone of cyclopamine [previous workers](#) have identified a number of analogs that reduce the activity of SHH in cellular assays.

Section 1.5 References

- (1) Nüsslein-Volhard, C.; Wieschaus, E. Mutations Affecting Segment Number and Polarity in *Drosophila*. *Nature* **1980**, *287*, 795–801.
- (2) Echelard, Y.; Epstein, D. J.; St-Jacques, B.; Shen, L.; Mohler, J.; McMahon, J. a.; McMahon, a. P. Sonic Hedgehog, a Member of a Family of Putative Signaling Molecules, Is Implicated in the Regulation of CNS Polarity. *Cell* **1993**, *75*, 1417–1430.
- (3) Murone, M.; Rosenthal, A.; De Sauvage, F. J. Sonic Hedgehog Signaling by the Patched-Smoothed Receptor Complex. *Curr. Biol.* **1999**, *9*, 76–84.
- (4) Levin, M.; Johnson, R. L.; Stern, C. D.; Kuehn, M.; Tabin, C. A Molecular Pathway Determining Left-Right Asymmetry in Chick Embryogenesis. *Cell* **1995**, *82*, 803–814.
- (5) Cooper, M. K.; Porter, J. A.; Young, K. E.; Beachy, P. A. Teratogen-Mediated Inhibition of Target Tissue Response to Shh Signaling. *Science*. **1998**, *280*, 1603–1607.
- (6) Lum, L.; Beachy, P. a. The Hedgehog Response Network: Sensors, Switches, and Routers. *Science*. **2004**, *304*, 1755–1759.
- (7) Jacob, L.; Lum, L. Deconstructing the Hedgehog Pathway in Development and Disease. *Science*. **2007**, *318*, 66–68.
- (8) Khaliullina, H.; Panáková, D.; Eugster, C.; Riedel, F.; Carvalho, M.; Eaton, S. Patched Regulates Smoothed Trafficking Using Lipoprotein-Derived Lipids. *Development* **2009**, *136*, 4111–4121.

- (9) Peukert, S.; Miller-Moslin, K. Small-Molecule Inhibitors of the Hedgehog Signaling Pathway as Cancer Therapeutics. *ChemMedChem* **2010**, *5*, 500–512.
- (10) Xie, J.; Murone, M.; Luoh, S.-M.; Ryan, A.; Gu, Q. Activating Smoothed Mutations in Sporadic Basal-Cell Carcinoma. *Nature* **1998**, *391*, 90–92.
- (11) Dahmane, N.; Lee, J.; Robins, P.; Heller, P.; Ruiz i Altaba, A. Activation of the Transcription Factor Gli1 and the Sonic Hedgehog Signalling Pathway in Skin Tumours. *Nature* **1997**, *389*, 876–881.
- (12) Berman, D. M.; Karhadkar, S. S.; Hallahan, A. R.; Pritchard, J. I.; Eberhart, C. G.; Watkins, D. N.; Chen, J. K.; Cooper, M. K.; Taipale, J.; Olson, J. M.; et al. Medulloblastoma Growth Inhibition by Hedgehog Pathway Blockade. *Science*. **2002**, *297*, 1559–1561.
- (13) Gorlin, R. J.; Goltz, R. W. Multiple Nevoid Basal-Cell Epithelioma, Jaw Cysts, and Bifid Rib. *N. Engl. J. Med.* **1960**, *262*, 908–912.
- (14) Johnson, R. L.; Rothman, a L.; Xie, J.; Goodrich, L. V; Bare, J. W.; Bonifas, J. M.; Quinn, a G.; Myers, R. M.; Cox, D. R.; Epstein, E. H.; et al. Human Homolog of Patched, a Candidate Gene for the Basal Cell Nevus Syndrome. *Science*. **1996**, *272*, 1668–1671.
- (15) Goodrich, L. V; Milenković, L.; Higgins, K. M.; Scott, M. P. Altered Neural Cell Fates and Medulloblastoma in Mouse Patched Mutants. *Science*. **1997**, *277*, 1109–1113.
- (16) Binns, W.; James, L. F.; Keeler, R. F.; Balls, L. D. Effects of Teratogenic Agents in Range Plants. *Cancer Res.* **1968**, *28*, 2323–2326.

- (17) Keeler, R. F.; Binns, W. Teratogenic Compounds of *Veratrum Californicum* (Durand). II. Production of Ovine Fetal Cyclopia by Fractions and Alkaloid Preparations. *Can. J. Biochem.* **1966**, *44*, 829–838.
- (18) Gaffield, W.; Wong, R. Y.; Lundin, R. E.; Keeler, R. F. Structure of the Steroidal Alkaloid Muldamine and Its Deacetyl Derivative. *Phytochemistry* **1982**, *21*, 2397–2400.
- (19) Keeler, R. F. First Isolation of Veratramine and Alkaloid Q and a Reliable Method for Isolation of Cyclopamine. *Phytochemistry* **1968**, *7*, 303–306.
- (20) Heretsch, P.; Tzagkaroulaki, L.; Giannis, A. Cyclopamine and Hedgehog Signaling: Chemistry, Biology, Medical Perspectives. *Angew. Chem., Int. Ed.* **2010**, *49*, 3418–3427.
- (21) Incardona, J. P.; Gaffield, W.; Kapur, R. P.; Roelink, H. The Teratogenic *Veratrum* Alkaloid Cyclopamine Inhibits Sonic Hedgehog Signal Transduction. *Development* **1998**, *125*, 3553–3562.
- (22) Taipale, J.; Chen, J. K.; Cooper, M. K.; Wang, B.; Mann, R. K.; Milenkovic, L.; Scott, M. P.; Beachy, P. a. Effects of Oncogenic Mutations in Smoothed and Patched Can Be Reversed by Cyclopamine. *Nature* **2000**, *406*, 1005–1009.
- (23) Chen, J. K.; Taipale, J.; Young, K. E.; Maiti, T.; Beachy, P. a. Small Molecule Modulation of Smoothed Activity. *Proc. Natl. Acad. Sci. U. S. A.* **2002**, *99*, 14071–14076.

- (24) Chen, J. K.; Taipale, J.; Cooper, M. K.; Beachy, P. A. Inhibition of Hedgehog Signaling by Direct Binding of Cyclopamine to Smoothed. *Genes Dev.* **2002**, *16*, 2743–2748.
- (25) Masamune, T.; Takasugi, M.; Murai, A.; Kobayashi, K. The Synthesis of Jervine and Related Alkaloids. *J. Am. Chem. Soc.* **1967**, *89*, 4521–4523.
- (26) Johnson, W. S.; Cox, J. M.; Graham, D. W.; Whitlock, H. W. The Total Synthesis of 17-Acetyl-5 α -Etiopjerva-12,14,16-Trien-3 β -Ol. *J. Am. Chem. Soc.* **1967**, *89*, 4524–4526.
- (27) Giannis, A.; Heretsch, P.; Sarli, V.; Stössel, A. Synthesis of Cyclopamine Using a Biomimetic and Diastereoselective Approach. *Angew. Chem., Int. Ed.* **2009**, *48*, 7911–7914.
- (28) Tremblay, M. R.; Lescarbeau, A.; Grogan, M. J.; Tan, E.; Lin, G.; Austad, B. C.; Yu, L. C.; Behnke, M. L.; Nair, S. J.; Hagel, M.; et al. Discovery of a Potent and Orally Active Hedgehog Pathway Antagonist (IPI-926). *J. Med. Chem.* **2009**, *52*, 4400–4418.
- (29) Tremblay, M. R.; Nevalainen, M.; Nair, S. J.; Porter, J. R.; Castro, A. C.; Behnke, M. L.; Yu, L. C.; Hagel, M.; White, K.; Faia, K.; et al. Semisynthetic Cyclopamine Analogues as Potent and Orally Bioavailable Hedgehog Pathway Antagonists. *J. Med. Chem.* **2008**, *51*, 6646–6649.
- (30) Williams, J. a; Guicherit, O. M.; Zaharian, B. I.; Xu, Y.; Chai, L.; Wichterle, H.; Kon, C.; Gatchalian, C.; Porter, J. a; Rubin, L. L.; et al. Identification of a Small Molecule

Inhibitor of the Hedgehog Signaling Pathway: Effects on Basal Cell Carcinoma-like Lesions. *Proc. Natl. Acad. Sci. U. S. A.* **2003**, *100*, 4616–4621.

(31) Robarge, K. D.; Brunton, S. A.; Castanedo, G. M.; Cui, Y.; Dina, M. S.; Goldsmith, R.; Gould, S. E.; Guichert, O.; Gunzner, J. L.; Halladay, J.; et al. GDC-0449 — A Potent Inhibitor of the Hedgehog Pathway. *Bioorg. Med. Chem. Lett.* **2009**, *19*, 5576–5581.

(32) Miller-Moslin, K.; Peukert, S.; Jain, R. K.; McEwan, M. a.; Karki, R.; Llamas, L.; Yusuff, N.; He, F.; Li, Y.; Sun, Y.; et al. 1-Amino-4-Benzylphthalazines as Orally Bioavailable Smoothened Antagonists with Antitumor Activity. *J. Med. Chem.* **2009**, *52*, 3954–3968.

(33) Pan, S.; Wu, X.; Jiang, J.; Gao, W.; Wan, Y.; Cheng, D.; Han, D.; Liu, J.; Englund, N. P.; Wang, Y.; et al. Discovery of NVP-LDE225, a Potent and Selective Smoothened Antagonist. *ACS Med. Chem. Lett.* **2010**, *1*, 130–134.

(34) Winkler, J. D.; Isaacs, A.; Holderbaum, L.; Tatard, V.; Dahmane, N. Design and Synthesis of Inhibitors of Hedgehog Signaling Based on the Alkaloid Cyclopamine. *Org. Lett.* **2009**, *11*, 2824–2827.

(35) Isaacs, A. K.; Xiang, C.; Baubet, V.; Dahmane, N.; Winkler, J. D. Studies Directed toward the Elucidation of the Pharmacophore of Steroid-Based Sonic Hedgehog Signaling Inhibitors. *Org. Lett.* **2011**, *13*, 5140–5143.

(36) Zhang, Z.; Baubet, V.; Ventocilla, C.; Xiang, C.; Dahmane, N.; Winkler, J. D.
Stereoselective Synthesis of F-Ring Saturated Estrone-Derived Inhibitors of Hedgehog
Signaling Based on Cyclopamine. *Org. Lett.* **2011**, *13*, 4786–4789.

Chapter 2. Establishing and Validating a High-Throughput Biological Evaluation

Method

Section 2.1 Summary of Previous Methods of Biological Evaluation¹⁻³

In collaboration with Dr. Nadia Dahmane and her laboratory at the Wistar Institute, the previously described estrone-derived analogs of cyclopamine were tested using two well-established methods of biological evaluation. Both assays were designed to report SHH activity; the first uses a luciferase reporter gene, and the second relies on the inhibition of Granule Neuron Precursor (GNP) cell proliferation, a key step in the development of the cerebellum.

2.1.1 Luciferase Inhibition Assays

One of the most commonly used methods to evaluate SHH activity relies on the downstream cellular target, the *gli* genes. As shown in **Figure 2.1**, the SHH pathway begins with extracellular activation via *Patched* and terminates with the expression of the *gli* genes that promote differentiation and growth. Beachy and coworkers created the Shh-Light2 cell line, derived from an NIH/3T3 cell line, that clonally expresses a stable *gli*-dependent firefly luciferase reporter gene.⁴ The activation of *gli*-dependent firefly luciferase expression is achieved upon treatment of these cells with *Shh*. Treatment of these cells with cyclopamine inhibits SHH-induced activation.

To obtain the relative potencies of the compounds needed for inhibition of SHH signaling, Dahmane and coworkers treated the cells first with SHH ligand to activate the signaling pathway and then treated the cells with ten micromolar concentrations of compound. After a period of incubation, the cells were lysed and the *gli*-dependent

firefly luciferase was activated and the luminescence recorded. The levels of luminescence were analyzed for all compounds at a single concentration and compared directly to the control (SHH induction with no inhibitory compound).

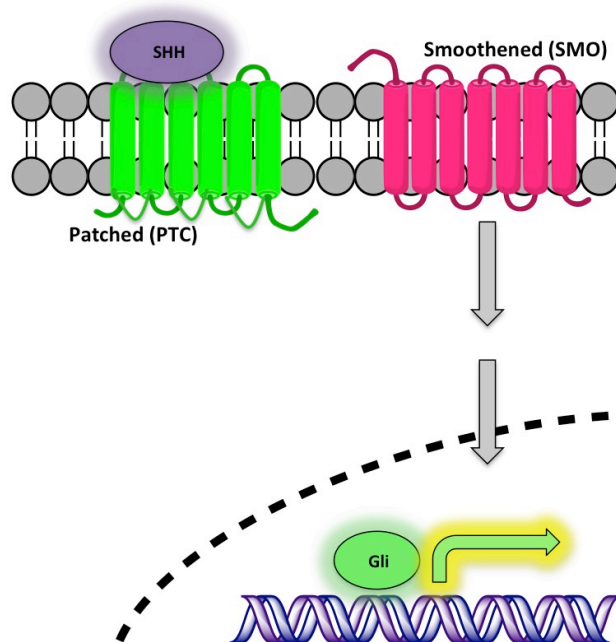


Figure 2.1 Activation of the SHH Signaling Pathway Results in Firefly Luminescence

All previously synthesized estrone-derived cyclopamine analogs were tested using this luciferase reporter assay.

2.1.2 Granule Neuron Precursor (GNP) Cells

During the development of the cerebellum, the SHH pathway is responsible for neuronal differentiation that leads to the proliferation of cerebellar granular neuronal

precursor (GNP) cells. This was first shown by Scott and coworkers who deduced that the division of granule cells in the cerebellum was promoted by Sonic Hedgehog released from Purkinje cells.⁵ Treating these cells with excess SHH resulted in a long-lived proliferative response, whereas blocking the SHH signaling pathway led to a dramatic reduction in proliferation. The Dahmane laboratory used this principal to evaluate the previously synthesized analogs; by treating postnatal day five (P5) mouse GNPs with either SHH or SHH plus compound, the relative potency needed for anti-proliferative activity was established in a luciferase independent assay.

2.1.3 Unanswered Questions from Previous Biological Evaluation Methods

The previously acquired data allows for a comparison of the analogs to cyclopamine at only one concentration. By using only one concentration, it is impossible to quantitatively rank the compounds by potency as only relative activity can be elucidated. In addition, two pieces of information that are essential to consider when analyzing inhibition were absent from the aforementioned assays. The first is to determine the viability of cells at the tested concentrations. Since this *gli*-dependent luciferase assay measures the downstream cellular targets of the SHH pathway, any disruption of the pathway would result in the same output. For example, a dead cell would also have no SHH activation and would present luciferase activity similar to that of an inhibited cell. Additionally, it is essential to assess that the decrease in luminescence is due to the inhibition of the SHH pathway and not simply the inhibition of the luciferase, a key component required for output. The granule neuron precursor assay does address the off-target luciferase inhibition, but this assay is not easily adapted to a high-throughput method.

We desired to pursue these compounds as potential chemotherapeutics for the inhibition of SHH, and it is essential to understand both the viability limitations and potency.

Section 2.2 Development of an In-House Dual Luciferase Reporter (DLR) Assay

Considering the unanswered question outlined above, we embarked on a journey to establish a high-throughput system of analysis. With guidance from Infinity Pharmaceuticals and David Schultz, Director of the Molecular Screening Facility at the Wistar Institute, an assay was established that allowed for statistically robust high-throughput biological evaluation. To enhance efficiency, we opted to use 384-well plates as opposed to the more standard 96-well format, which allows for an 80% decrease in materials. Human error and variability were limited by implementing automated pipetting workstations for the preparation of serially diluted compounds, transfer of compounds to assay plates, and dispensing of all reagents. Two cell lines were used to assess the potencies of the analogs: first, C3H10T1/2, a mouse fibroblast line that required transfection of both the Renilla reporter and the *gli*-dependent firefly genes; and second, the Shh-Light2 cells, which clonally express both Renilla and *gli*-firefly and require no transfection.

2.2.1 Transient Transfection DLR Assay

To begin, C3H10T1/2 cells were transfected with Renilla luciferase, *gli*-firefly luciferase and GFP plasmids. Due to the sensitive nature of a transient transfection, it was important to establish the transfection efficiency using GFP. It was found that there was an ideal cell passage window that allowed for maximum transfection efficiency,

roughly passage 5-8 with the cells never reaching over 80% confluency. With a smaller well-format, low transfection efficiency could lead to a vastly different number of transfected cells per well. We had determined in our pilot assays that the transfection efficiency was correlated inversely to variability and thus needed to be monitored closely. If the cells were not adequately transfected with the Renilla and *gli*-firefly luciferase the induction window, difference between positive and negative control cells was too small to glean any reasonable IC₅₀ data.

In addition to the GFP control, the reporter assay relies on two main plasmids: Renilla luciferase and *gli*-Firefly luciferase. The commercial plasmids were reproduced using a Maxi-Prep and analyzed by restriction enzyme digest to confirm the identities. The Renilla plasmid is constitutively expressed in all cells and acts as a statistical normalizer. The *gli*-Firefly plasmid measures the activity of the SHH signaling pathway by correlating the luminescence generated by firefly luciferase to the transcription of the *gli* genes. An activated pathway culminates with the upregulation of *gli*, which results in an increase in luminescence due to an increase in the production of *gli*-firefly. An inhibited pathway would result in the decrease of transcription of *gli* and therefore a decrease in luminescence.

After a 24 hour incubation post-transfection, the media was changed to a SHH rich media to induce signaling, and various concentrations of our analogs were also added. By using a 384-well format, we could accommodate eight unique concentrations (10 μ M to 2 nM, 3-fold dilutions) of twelve compounds in triplicate. In addition to the analogs, cyclopamine, our control inhibitor, and both positive and negative controls are also included on each assay plate. After incubating for 48 hours, the cells were lysed, and both luciferase signals were read. The Renilla intensity was used to calculate

relative activity ratios. These *gli*-firefly/Renilla ratios were then normalized against the activity of the negative control where no SHH ligand was introduced.

This dual reporter assay relies on the orthogonal activation of the bioluminescent reactions catalyzed by firefly and Renilla luciferases. After lysing the cells, the firefly luciferase is activated first by the addition of a buffer containing beetle luciferin, ATP, and magnesium ions (**Figure 2.2**). This flash of light depletes over time and must be read promptly after mixing. The robotics implemented at the Molecular Screening Facility allowed for the rapid addition of the buffer. It was determined that maximum luciferase activity occurred immediately after mixing.

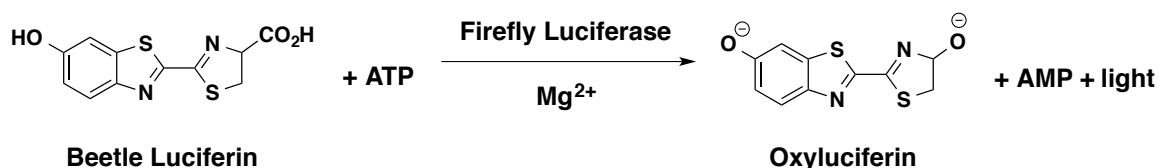


Figure 2.2 Bioluminescent Reaction Catalyzed by Firefly Luciferase

After reading, this firefly luminescence is then quenched with a second buffer that both depletes the remaining ATP and contains coelenterazine luciferin (**Figure 2.3**). This combination serves two purposes: extinguishes the firefly luciferase signal and provides the ligand for the Renilla luciferase. The Renilla signal is not dependent on any reporter gene and should be expressed evenly across all cells. This Renilla expression therefore acts as our normalizer for cell count variability per well.

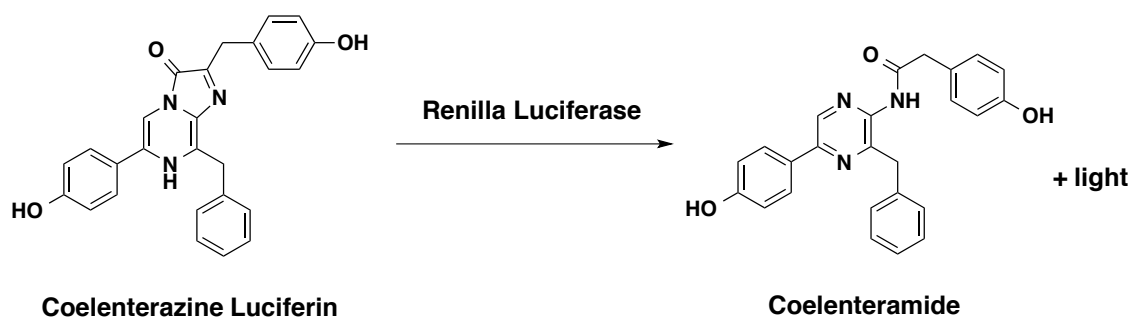


Figure 2.3 Bioluminescent Reaction Catalyzed by Renilla Luciferase

To calculate the potencies, first the firefly luminescence signal in each well is divided by the corresponding Renilla luminescence signal. This value is divided by the negative control, where no SHH ligand or compound has been added. Using GraphPad Prism, the normalized values are plotted against the concentrations, and using a nonlinear regression, the IC_{50} values are determined. After generating these IC_{50} curves, we began to see a wide range of potencies; however, the statistical variability and Hill slopes were too large to reasonably conclude structure activity relationships. It was determined that the smaller cell count per well in combination with the transient transfection was responsible for the statistical error and heightened variability. The data collected from this first generation assay is summarized below (**Figure 2.4 and 2.5**).

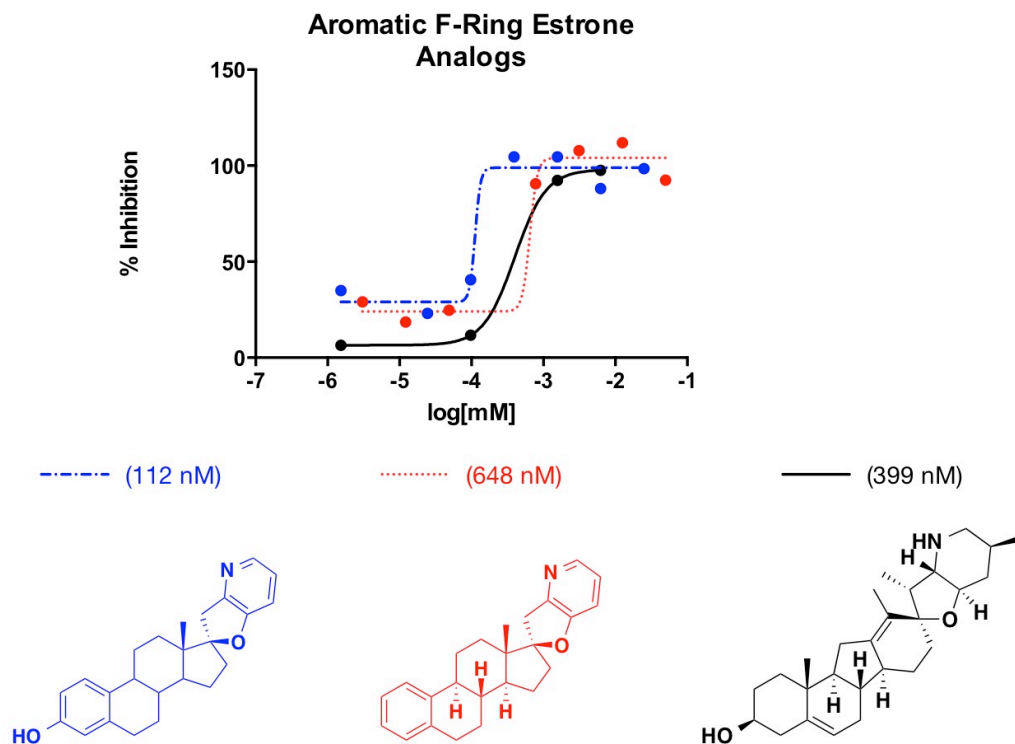


Figure 2.4 IC₅₀ Curves for Aromatic First Generation Analogs

This assay provided insight into the necessity of the C3 hydroxyl for potency (1). Removal of the hydroxyl resulted in a six-fold loss in potency (2). The preliminary data for the F-ring saturated compounds, outlined in **Section 1.3.2**, highlights the 4-exocyclic oxetane as the most potent analog. Although the variability was too large to conclude definitively, we felt reassured that drastic changes to the EF ring system were in fact resulting in changes in the potency of the compounds.

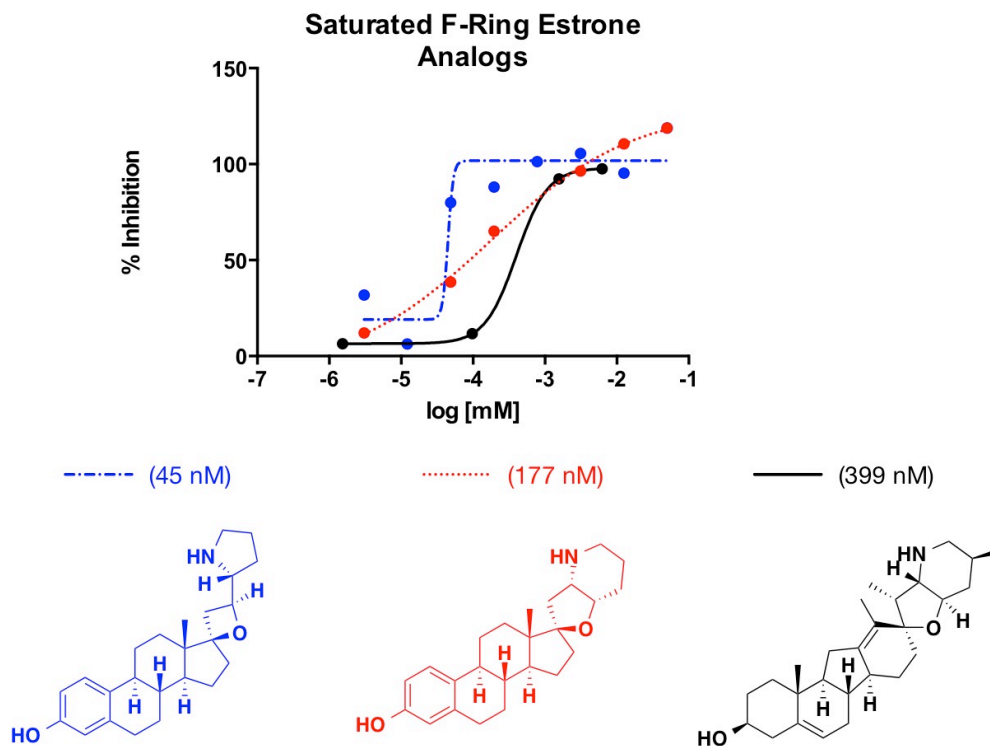


Figure 2.5 IC₅₀ Curves for Saturated First Generation Analogs

This first round of assays had begun to illuminate the approximate IC₅₀ values and the relative rank potencies of the synthesized compounds. However, due to the statistical variability and high Hill slopes, future cell assays were completed with Shh-Light2 cells, a cell line that clonally expresses both the Renilla luciferase and *gli*-firefly luciferase necessary for analysis. Despite the relatively steep IC₅₀ curves, the preliminary analysis did establish the appropriate concentrations needed for analysis. By eliminating the high and low points on the curve, our future assays could make more gradual dilutions, greatly lowering the Hill slope. Additionally, we believed that the Shh-Light2 cells would provide more gradual and smooth IC₅₀ curves, thus providing a more accurate depiction of the relative rank potencies of the analogs.

2.2.2 Constitutively Expressed DLR Assay

As expected, the Shh-Light2 cells provided the statistical robustness that was needed to establish reasonable structure activity relationships between the previously generated estrone analogs. Our preliminary transient transfection assay allowed us to narrow the dosing window and make more gradual dilutions to generate more points along the curves, which decreased the Hill slopes and conserved space on the assay plate. This extra space allowed for each dilution in triplicate on one plate, greatly reducing the variability overall. The data for the F-ring aromatic and saturated estrone analogs are summarized in **Figure 2.6** and **2.7**, respectively.

As suggested by the transient transfection assay, the Shh-Light2 assay confirmed that the C3 hydroxyl is in fact necessary for enhanced potency, as seen in estrone analog **1**. In this cell line, the original estrone analog exhibits modest potency ($111 \text{ nM} \pm 31 \text{ nM}$) relative to cyclopamine **3** ($72 \text{ nM} \pm 27 \text{ nM}$), but activity is diminished when the C3 hydroxyl is removed (**2**, $735 \text{ nM} \pm 256 \text{ nM}$). Most importantly, this analysis corroborates the original findings from the Dahmane Laboratory that the steroidal backbone of estrone is an appropriate and viable surrogate for the nonpolar backbone of cyclopamine. It is also worth noting that other research groups have found that the overall potencies in Shh-Light2 cells to be slightly lower than those found using C3H10T1/2 cells with a transient transfection. For this reason, cyclopamine is always used on every assay plate as a positive control.⁶

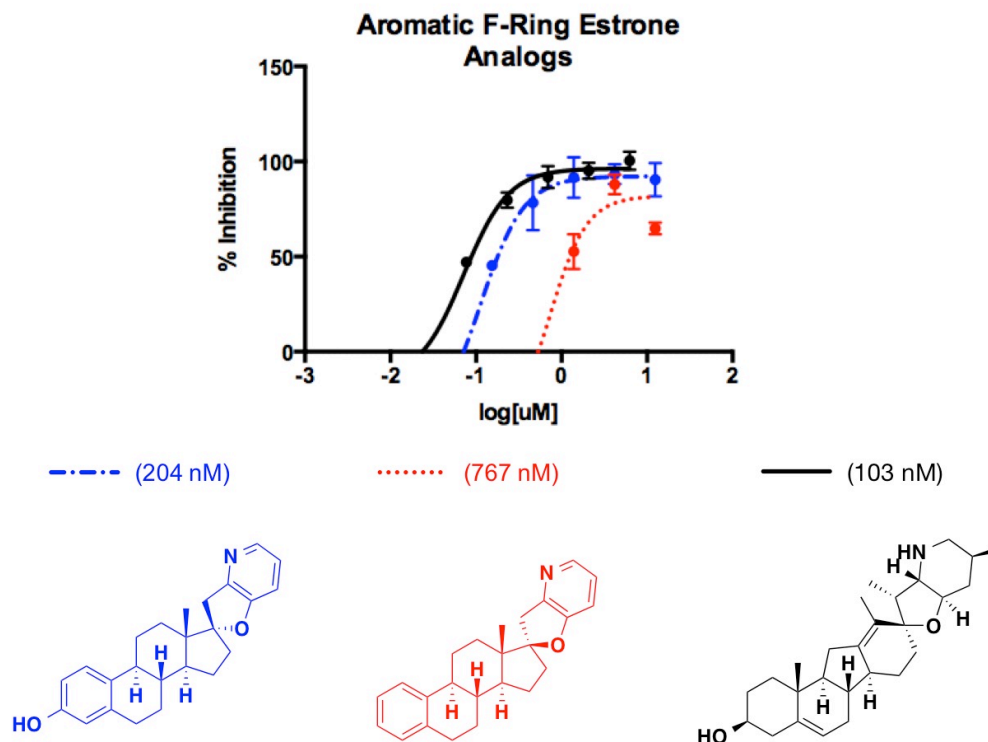


Figure 2.6 IC₅₀ Curves for Aromatic F-Ring Analogs Using Shh-Light2 Cells

As described in **Section 1.3.2**, the F-ring aromatic compounds were originally synthesized quickly in only four steps as a proof of principle, but the F-ring saturated compounds more closely resemble the saturated secondary amine found in cyclopamine in both hybridization and basicity. The 5,6-fused analog **5** has a similar chemical construction to that of cyclopamine, but the *cis* ring fusion in the analog carves out a different chemical space than the *trans* ring fusion found in the natural alkaloid. This stereochemical difference could be responsible for the 20-times loss in potency (1758 nM ± 537 nM).

Interestingly, the oxetane analog **4** exhibited potency twice that of cyclopamine (44 nM ± 8 nM). The exocyclic analog is comprised of an oxetane and pyrrolidine, which have significantly more freedom about the central carbon-carbon bond than the rigid

scaffold present in cyclopamine. Additionally, the five membered ring of the pyrrolidine exposes the nitrogen lone pair more prominently than that of the piperidine in the natural product and offers slightly enhanced basicity. This flexibility and increased availability for hydrogen bonding could explain the increase in potency.

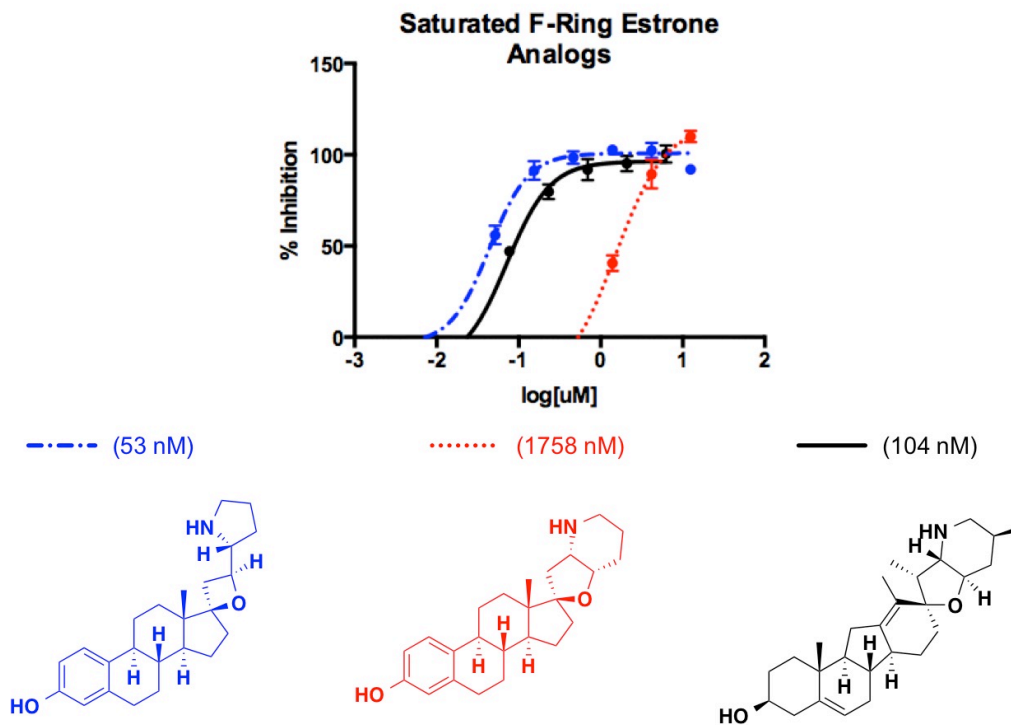


Figure 2.7 IC₅₀ Curves for Saturated F-Ring Analogs Using Shh-Light2 Cells

The statistical analysis for the Shh-Light2 cell line is summarized in **Table 2.1**. The 95 % confidence intervals (CI) were calculated by the predicted standard error of logIC₅₀ generated by Graphpad Prism. The R-squared values for all the IC₅₀ curves signify an excellent fit, and the confidence intervals are relatively small suggesting that this DLR assay can quantitatively rank the estrone analogs according to potency.

Compound	IC50 (nM)	95% CI (nM)	R squared
cyclopamine (3)	72	49 - 106	0.95
oxetane (4)	44	37 - 52	0.98
furan (5)	1528	991 - 2355	0.99
estrone (1)	111	79-156	0.97
deoxy (2)	735	479 - 1128	0.88

Table 2.1 Statistical Analysis of Shh-Light2 DLR Assay

The high and low data points were removed from the analysis, and the concentrations that were later determined to be cytotoxic were also removed due to low Renilla signal. At that stage, it can be concluded that the oxetane **4** is more potent than cyclopamine in inhibiting the SHH signaling pathway, whereas the estrone analog **1** is slightly less potent.

2.2.3 Additional Results of the DLR Assay

In addition to screening the previously described analogs, a series of Des-B analogs (**Figure 2.8**) were screened to assess the necessity of the entire steroid backbone. In collaboration with Dr. Christian Ventocilla, a small library of analogs was developed in hopes to determine the optimal functionalization on the A-ring for maximum potency. By using palladium-catalyzed chemistry with an intermediate coupling partner, a variety of analogs could be constructed through a divergent cross-coupling approach.

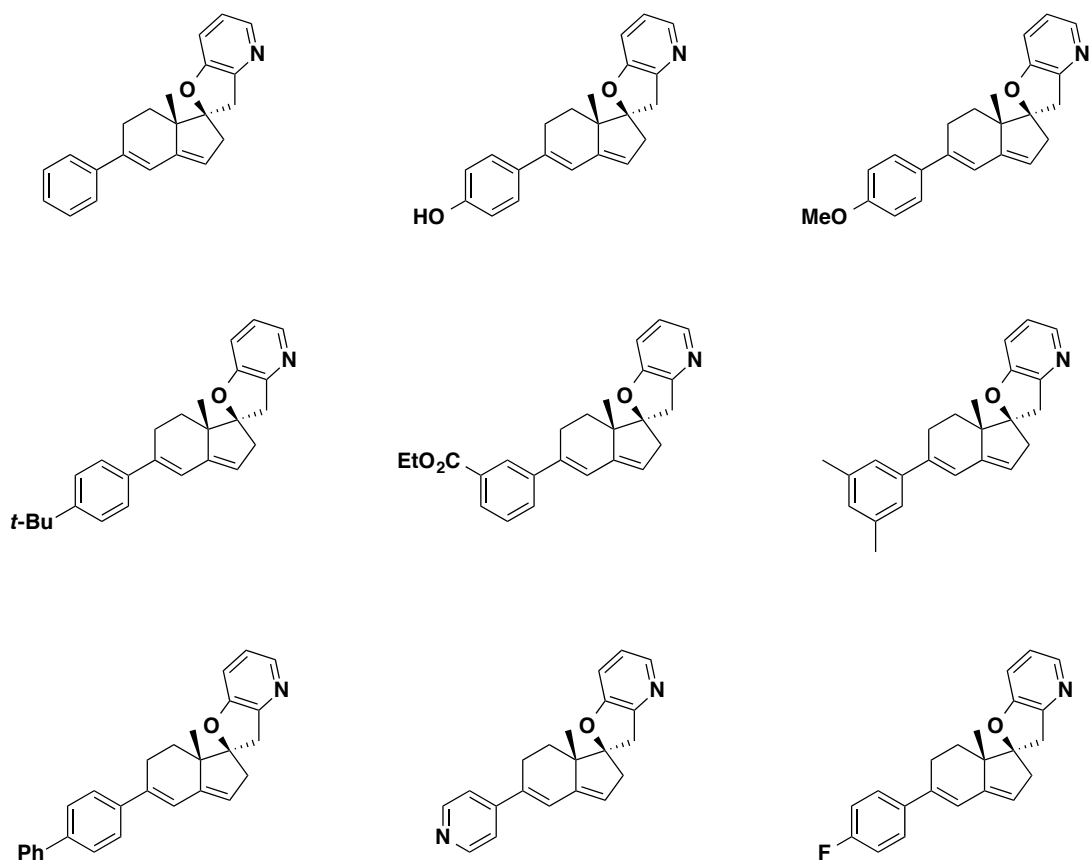
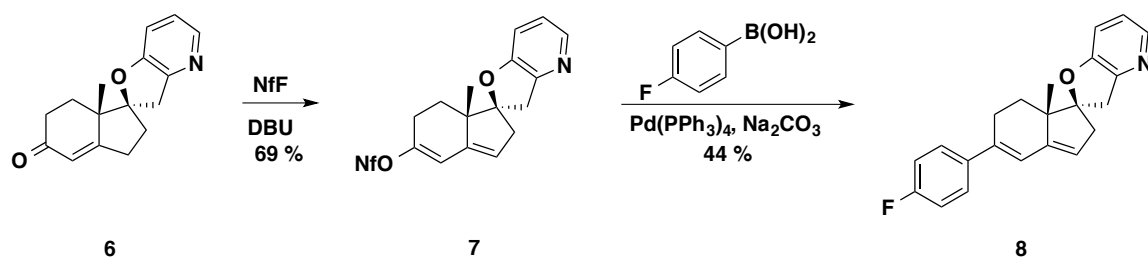


Figure 2.8 Des-B Analogs

The synthesis of these analogs offered a means for late-stage diversification through the palladium mediated cross coupling of vinyl nonaflate **7** with a variety of commercial aryl boronic acids. Spirocycle **6**, synthesized as reported by Dr. Andre Isaacs, was transformed to a stable and isolable nonaflate through reaction with perfluorobutanesulfonyl fluoride in the presence of DBU. This vinyl nonaflate is bench stable and can be purified using silica gel chromatography unlike the corresponding vinyl triflate. The final **des-B** analogs were constructed via a palladium-catalyzed Suzuki reaction. Construction of Fluoro-Des-B analog **8** is outlined below (**Scheme 2.1**).



Scheme 2.1 Example Synthesis of Des-B Analogs

The above analogs were tested in the DLR assay and displayed a wide range of activity. At first glance it appeared that functionalization of the A-ring was responsible for this SAR, but based on the control experiments outlined below, the effects on potency remain unanswered.

Section 2.3 Control Experiments

The assays previously described provide a basic understanding of inhibition but do not confirm the exact mechanism of inhibition. The DLR assay uses a reporter gene as the method of output, and any disruption of the transcription of that gene will result in a decrease in luminescence. It is essential to determine if the SHH signaling pathway is indeed a target of the inhibitors or if the cells are simply dying, as the reporter output would appear the same in an inhibited cell as a dead cell. Our first control experiment was to use a resazurin screen to identify any possible lethal concentrations of our compounds.

Additionally, as described in **Section 2.2.1**, the assay relies on firefly luciferase protein to react with its substrate to produce light. Any disruption of the luciferase protein would also decrease the luminescence signal. To probe this phenomenon, we

implemented a simple biochemical assay with firefly luciferase to probe inhibition of luciferase with our steroidal analogs.

2.3.1 Cell Viability

Moving forward, we wanted to establish any potential issues with cell viability and lethal doses of our compounds. Since the cells were plated in white-walled plates for the luminescence readings, we could not simply visualize cell growth and viability. Using a resazurin screen allowed us to quantitate cell viability, and we established that, at high concentrations (5-10 μM ,) many of the compounds showed little to no cellular activity. Interestingly, all assays that were employed by our previous collaborator used compounds at 10 μM to show relative luciferase activity, providing evidence for the necessity of this screen.

Resazurin is a commonly used dye that acts as an electron receptor in the electron transport chain, and this reduction results in a change in aromatization, and, more importantly, color (**Figure 2.9**). In its oxidized form, resazurin remains non-fluorescent, but in the presence of living cells, the resazurin molecules are reduced, resulting in a change of color and a fluorescent molecule. This change allows for a rapid fluorometric readout that can detect cellular growth. For our purposes, it was important to establish dose concentrations of the compounds at which the cells were unable to survive. These cell lethal doses were eliminated from the analysis.⁷

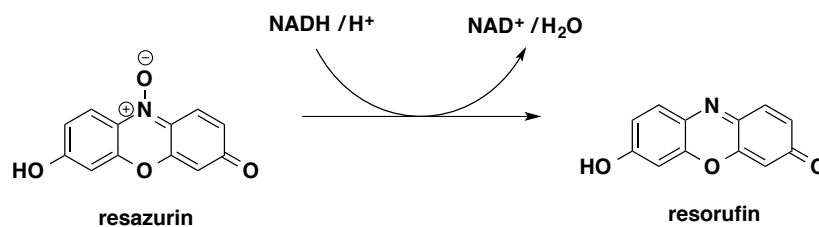


Figure 2.9 Mechanism of Resazurin Oxidation

2.3.2 Luciferase Inhibition

Once IC_{50} curves were generated for previously synthesized analogs, the biological results must be validated. We performed a biochemical assay to probe luciferase inhibition, and interestingly, a majority of our des-B analogs were active in the screen. This suggested that the activity previously demonstrated was not caused by inhibition of the SHH pathway and was instead due to luciferase inhibition. The overall potencies of these compounds therefore cannot be determined by the DLR assay and would require orthogonal methods for screening.

Section 2.4 Summary of Biological Data from First Generation Analogs

As described above, we have confirmed that the hydrophobic steroid backbone is an appropriate surrogate for the more structural complex backbone of cyclopamine. We have identified through our first transient transfection assay the importance of transfection efficiency as well as a concentration window that works best for our steroidal analogs. By adapting this information to the Shh-Light2 cell line, we were able to generate IC_{50} curves for the previously synthesized analogs, including an analog containing an exocyclic oxetane pyrrolidine moiety that has two times the potency of the naturally occurring alkaloid inhibitor cyclopamine.

Section 2.5 Experimental Details

2.5.1 Maxi Prep and Plasmid Purification

Bacterial transformations were executed with DH5 α cells. To a microvial containing 10 μ L DH5 α thawed on ice was added 2 μ L plasmid (8xGli-Luc or pRL-TK) and 2 μ L tris-EDTA. The mixture was then heat shocked at 37 °C for 45 seconds and returned to ice for 2 minutes. Next, 100 μ L of SOC was added to each tube, and the contents spread onto the center of the culture plates. After 24 hours, one colony was selected and incubated for 8 hours at 37 °C in 3 mL LB broth with carbenicillin. This starter culture was then added to 1 L of LB broth and incubated at the same temperature for 24 hours. The cultures were centrifuged at 5,000 rpm for 20 minutes, and the supernatant was removed. Each pellet was suspended in 24 mL of P1 buffer. To this solution was added 48 mL of P2 buffer (0.2 N NaOH/1% SDS), and the resulting slurry mixed gently by inversion. The suspensions were incubated at room temperature for 5 minutes, the tubes inverted, and incubated for another 5 minutes at room temperature. Buffer P3 (48 mL) was added, the suspension mixed and cooled on ice for 30 minutes and then centrifuged for 20 minutes at 25,000 rpm. A Qiagen-2500 column was equilibrated with 35 mL of QBT buffer.

Clarified supernatant was added to the QBT-equilibrated Qiagen-2500 column, allowed to pass through via gravity flow, and the column washed with 250 mL of QC buffer via gravity.

Plasmid DNA was eluted with 35 mL of QF buffer into a fresh and sterile tube. The solution was transferred into a 250 mL conical centrifuge vial and DNA precipitated by adding 30 mL (1 volume) of isopropanol. The precipitate was mixed by inversion and incubated at -20 °C for 30 minutes. The nucleic acids were isolated by centrifugation at

5,000 rpm for 30 minutes. The supernatant decanted, and the pellet suspended in 400 μ L of 1X TE, pH 8.0. To the suspended plasmid DNA was added 1/10th volume 3M sodium acetate, pH 5.5, and 2.5 volumes (1 mL) of ethanol. The plasmid DNA was pelleted by centrifugation for 30 minutes at maximum speed, the supernatant decanted, and rinsed with 1 mL 70 % ethanol. Once the supernatant has been removed, the pellet was suspended in 250-500 μ L of 1X TE, pH 8.0, the DNA quantified by nanodrop, and analyzed by restriction enzyme digest.

2.5.2 Transient Transfection Assay

Day One: C3H10T1/2 cells were seeded in a 6-well plate at approximately 150K cells/well in 3 mL growth media (BME + 10% FBS + 2 mM L-glutamine + Pen/Strep) per well.

Day Two: After 24 hours, to each well was added 1000 ng of total DNA (2:1 ratio 8x Gli-luc:pRL-TK) in 3 μ L GeneJuice and 100 μ L OptiMem. After 8 hours of incubation, the media was removed, and the cells were trypsinized with 0.5 mL trypsin and incubated for 5 minutes before the trypsin was quenched with 1.9 mL growth media. The cells were pooled and plated in a white walled 384-well format (2K cells/well, 40 μ L total volume).

Day Three: Growth media was aspirated from the cells, and 40 μ L either control (BME + 0.5% FBS + 2 mM L-glutamine + Pep/Strep) or induction (BME + 0.5% FBS + 2mM L-glutamine + Pep/Strep + 10% Shh ligand) media was added. Immediately after induction, 50 nL of compound (or DMSO control) was added to each well. The plates were allowed to incubate for 48 hours at 37 °C.

Day Five: The control and induction media was removed and each well washed with 250 μ L PBS. After the PBS was removed, 40 μ L of Passive Lysis Buffer was added and agitated for 15 minutes. Using a cell-plater, 100 μ L of luciferase reagent was added and

the firefly luminescence recorded. After reading, 100 μ L of Stop/Glo buffer was added to quench the firefly and activate the Renilla. The luminescence readings were recorded using a multi-channel plate reader. Percent induction was calculated based on the ratio of firefly:Renilla and corrected with the negative control.

2.5.3 Shh-Light2 Cells DLR Assay

Day One: Shh-Light2 cells were seeded in a white walled 384-well plate at approximately 2K cells/well in 40 μ L growth media (DMEM + 10% FBS + 2 mM L-glutamine + Zeocin) per well.

Day Two: Growth media was aspirated from the cells, and 40 μ L either control (DMEM + 0.5% FBS + 2 mM L-glutamine + Pep/Strep) or induction (DMEM + 0.5% FBS + 2mM L-glutamine + Pep/Strep + 10% Shh ligand) media was added. Immediately after induction, 50 nL of compound (or DMSO control) was added to each well. The plates were allowed to incubate for 48 hours at 37 °C.

Day Four: The control and induction media was removed and each well washed with 250 μ L PBS. After the PBS was removed, 40 μ L of Passive Lysis Buffer was added and agitated for 15 minutes. Using a cell-plater, 20 μ L of luciferase reagent was added and the firefly luminescence recorded. After reading, 20 μ L of Stop/Glo buffer was added to quench the firefly and activate the Renilla. The luminescence readings were recorded using a multi-channel plate reader. In order to determine the percent inhibition, all of the firefly luminescence values were divided by the corresponding Renilla luminescence. These values were then divided by the average of the negative control, where no ligand or compound was added to the cells. The normalized values were then plotted against

the concentrations and, using a two-point non-linear regression, the IC₅₀ curves were generated.

2.5.4 Cell Viability Screen⁷

Day One: Shh-Light2 cells were seeded in a clear 384-well plate at approximately 2K cells/well in 40 µL growth media (DMEM + 10% FBS + 2 mM L-glutamine + Zeocin) per well.

Day Two: 50 nL of compound or DMSO (to replicate the compound plate setup) was added and allowed to incubate at 37 °C for 48 hours.

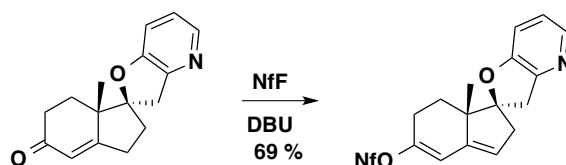
Day Four: Resazurin in ddH₂O (1.2 mM, 40 µL) was added to each well and allowed to incubate at 37 °C for 24 hours.

Day Five: Fluorometric analysis was completed. The wells were excited at 570 nm and the emission was read at 590 nm. The amount of cell growth and reduction of resazurin was estimated.

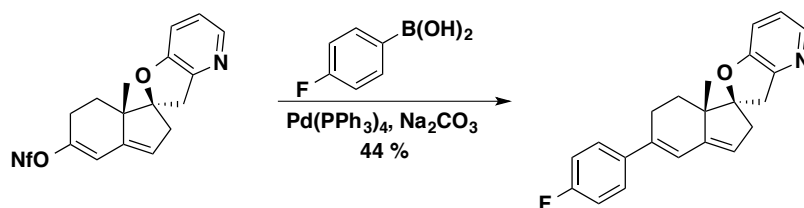
2.5.5 Luciferase Inhibition Assay⁸

To each well of a white opaque 384 well Optiplate was added 20 µL of 2 nM luciferase enzyme solution (1 nM FFluciferase, 50 mM Tris-Acetate pH 7.8, 0.5 mM EDTA, 5 mM MgSO₄, 0.1 % BSA). Compound or DMSO was then added to each well (200 nL). 20 µL of a solution of 2 µM D-Luciferin/ 20 µM ATP was then added to each well to initiate the reaction (1 µM D-luciferin, 10 µM ATP, 50 mM Tris-Acetate pH 7.8, 0.5 mM EDTA, 5 mM MgSO₄, 0.1 % BSA). Luminescence was measured using an EnVision multichannel plate reader and percent inhibition was calculated.

2.5.6 Sample Synthesis of Des-B Analogs



To spirocycle **6** (0.047 g, 0.180 mmol) in THF (1.25 mL) cooled to 0 °C was added DBU (83 μ L, 0.53 mmol) then NfF (98 μ L, 0.53 mmol). The mixture was allowed to warm to 25 °C and stir for 18 h. The mixture was concentrated *in vacuo*, and the resultant residue was purified by flash chromatography (50 % ethyl acetate in hexanes) to afford nonaflate **4** as a viscous yellow oil (0.68 g, 69%): **¹H NMR** (500 MHz, CDCl₃) δ 8.03 (t, J = 3.0 Hz, 1H), 7.01 (d, J = 3.0 Hz, 2H), 6.24 (d, J = 2.0 Hz, 1H), 5.64 (s, 1H), 3.51 (d, J = 16.5 Hz, 1H), 3.07 (d, J = 17.0 Hz, 1H), 2.95 (d, J = 17.0 Hz, 1H), 2.67-2.62 (m, 2H), 2.42 (dd, J = 18.5, 5.5 Hz, 1H), 1.90 (m, 1H), 1.56-1.52 (m, 1H), 1.18 (s, 3H). Nonaflate **7** was carried onto the next reaction within 24 h after its purification to avoid decomposition that was seen with its triflate equivalent.



To nonaflate **7** (0.068 g, 0.126 mmol) in THF:toluene (1:1, 2 mL) was added 4-fluorophenylboronic acid (0.018 g, 0.126 mmol), Pd(PPh₃)₄ (0.008 g, 0.005 mmol), Na₂CO₃ (0.012 g, 0.126 mmol), and water (0.5 mL). The mixture was heated in a sealed flask to 80 °C overnight. The mixture was allowed to cool to room temperature and diluted with CH₂Cl₂ (5 mL) and water (5 mL). The layers were separated, and the aqueous layer

was extracted with CH₂Cl₂ (3 x 5 mL). The organic layers were combined, washed with brine, dried over Na₂SO₄, filtered, and concentrated *in vacuo*. The resultant residue was purified by flash chromatography (50 % ethyl acetate in hexanes) to afford analogue **8** as a pale yellow, waxy solid (0.018 g, 44%). ¹H NMR (500 MHz, CDCl₃) δ 8.02 (dd, *J* = 3.5, 1.0 Hz, 1H), 7.43 (m, 2H), 7.04-7.01 (m, 4H), 6.56 (s, 1H), 5.52 (s, 1H), 3.61 (d, *J* = 16.5 Hz, 1H), 3.09 (d, *J* = 16.5 Hz, 1H), 2.97 (d, *J* = 16.5 Hz, 1H), 2.64-2.59 (m, 3H), 1.87 (dt, *J* = 12.0, 6.0 Hz, 1H), 1.61 (m, 1H), 1.21 (s, 3H); ¹³C NMR (125 MHz, CDCl₃) δ 163.4, 161.4, 153.5, 151.5, 146.0, 141.5, 137.3, 137.0, 126.9, 122.4, 119.9, 119.6, 115.3, 98.3, 47.0, 44.2, 39.3, 28.5, 25.9, 18.0; FTIR (thin film) 2928, 1600, 1508, 1429, 1278, 993, 833 cm⁻¹; HRMS (ESI) *m/z* calcd for C₂₃H₂₄NO₂ (M + H)⁺ 334.1607, found 334.1607.

Section 2.6 References

- (1) Isaacs, A. K.; Xiang, C.; Baubet, V.; Dahmane, N.; Winkler, J. D. Studies Directed toward the Elucidation of the Pharmacophore of Steroid-Based Sonic Hedgehog Signaling Inhibitors. *Org. Lett.* **2011**, *13*, 5140–5143.
- (2) Winkler, J. D.; Isaacs, A.; Holderbaum, L.; Tatard, V.; Dahmane, N. Design and Synthesis of Inhibitors of Hedgehog Signaling Based on the Alkaloid Cyclopamine. *Org. Lett.* **2009**, *11*, 2824–2827.
- (3) Zhang, Z.; Baubet, V.; Ventocilla, C.; Xiang, C.; Dahmane, N.; Winkler, J. D. Stereoselective Synthesis of F-Ring Saturated Estrone-Derived Inhibitors of Hedgehog Signaling Based on Cyclopamine. *Org. Lett.* **2011**, *13*, 4786–4789.

- (4) Taipale, J.; Chen, J. K.; Cooper, M. K.; Wang, B.; Mann, R. K.; Milenkovic, L.; Scott, M. P.; Beachy, P. a. Effects of Oncogenic Mutations in Smoothed and Patched Can Be Reversed by Cyclopamine. *Nature* **2000**, *406*, 1005–1009.
- (5) Wechsler-Reya, R. J.; Scott, M. P. Control of Neuronal Precursor Proliferation in the Cerebellum by Sonic Hedgehog. *Neuron* **1999**, *22*, 103–114.
- (6) Petrova, E.; Rios-Esteves, J.; Ouerfelli, O.; Glickman, J. F.; Resh, M. D. Inhibitors of Hedgehog Acyltransferase Block Sonic Hedgehog Signaling. *Nat. Chem. Bio.* **2013**, *9*, 247–249.
- (7) Perrot, S.; Dutertre-Catella, H.; Martin, C.; Warnet, J.-M.; Rat, P. A New Nondestructive Cytometric Assay Based on Resazurin Metabolism and an Organ Culture Model for the Assessment of Corneal Viability. *Cytom. Part A* **2003**, *55*, 7–14.
- (8) Auld, D. S.; Southall, N. T.; Jadhav, A.; Johnson, R. L.; Diller, D. J.; Simeonov, A.; Austin, C. P.; Inglese, J. Characterization of Chemical Libraries for Luciferase Inhibitory Activity. *J. Med. Chem.* **2008**, *51*, 2372–2386.

Chapter 3. Computational Analysis and Molecular Modeling

Section 3.1 Analysis of Seven Pass Transmembrane Smoothened

As discussed in Chapter 1, Smoothened (SMO) is an integral component of the Sonic Hedgehog (SHH) Signaling Pathway, a cellular signaling mechanism that is essential for embryonic growth and development, and is inappropriately upregulated in numerous cancer cell lines. This pathway becomes activated when a hedgehog ligand binds to Patched (PTC) and thus releases its repressive hold on seven pass transmembrane protein SMO. Since the discovery of cyclopamine, a naturally occurring alkaloid that inhibits the SHH signaling pathway at the level of SMO, there have been numerous attempts to discern the binding site of antagonism through protein crystallography.

Despite their abundance throughout the proteome, crystallography of transmembrane proteins has proven to be a difficult problem in the field of chemical biology. Residing in the lipid bilayer, a majority of these proteins have a highly hydrophobic exterior that makes the purification, solubilization, and stabilization exceedingly challenging to master.¹ Over the past five years the abundance of transmembrane structures has rapidly increased due to the advancing of membrane preps and the development of stabilizing groups.² This chapter will discuss the recent advances in the crystallography of Smoothened.

3.1.1 First Crystal Structure

Using an engineered construct of human SMO receptor, Ray Stevens and coworkers published the first crystal structure of the transmembrane protein crystallized with a known antagonist, LY2940680 with a resolution of 2.3 Å.³ This truncated construct

had a shortened C-terminus that did not interfere with ligand binding and also was expressed with an extracellular thermostabilized apocytochrome *b*₅₆₂RIL (BRIL) at the N-terminus. These modifications eliminated an intracellular unstructured tail and helped to induce crystallinity. A dimeric crystal was obtained using a lipidic method, which allows the protein to congregate inside a lipid membrane for enhanced structural organization.⁴

Due to the lack of structural information prior to the Stevens' publication, the classification of SMO as a canonical GPCR had been controversial. The amino acid sequence of SMO demonstrates high similarity to Frizzled (FZD), a seven pass transmembrane protein integral in the WNT signaling pathway. Both proteins contain seven helices that pass through the membrane, a cysteine-rich extracellular domain, a linker between the two, and an intracellular carboxy domain. Despite the overall spatial similarities described by Stevens, SMO exhibits less than 10 % sequence alignment with a classical GPCR, and for this reason, SMO and FZD have been classified as GPCR proteins, class F. Based on phylogenetic analysis, the class F GPCRs are more conserved than class A, indicating their essential roles in cellular proliferation.

The crystal structure of SMO (**Figure 3.1**) highlights the seven helices that pass through the membrane, with an additional helix VIII lying perpendicular to the protein, along the inside of the cellular membrane. For clarity, only one monomer of the crystal is shown with the BRIL functionality removed. Outside of the lipid bilayer, an extracellular linker domain and extracellular loops partially cover a long hydrophobic cavity. This aqueous exposed pocket is where LY2940680 was found to bind. The ligand burrows deep into the pocket and resides partially within the membrane space.

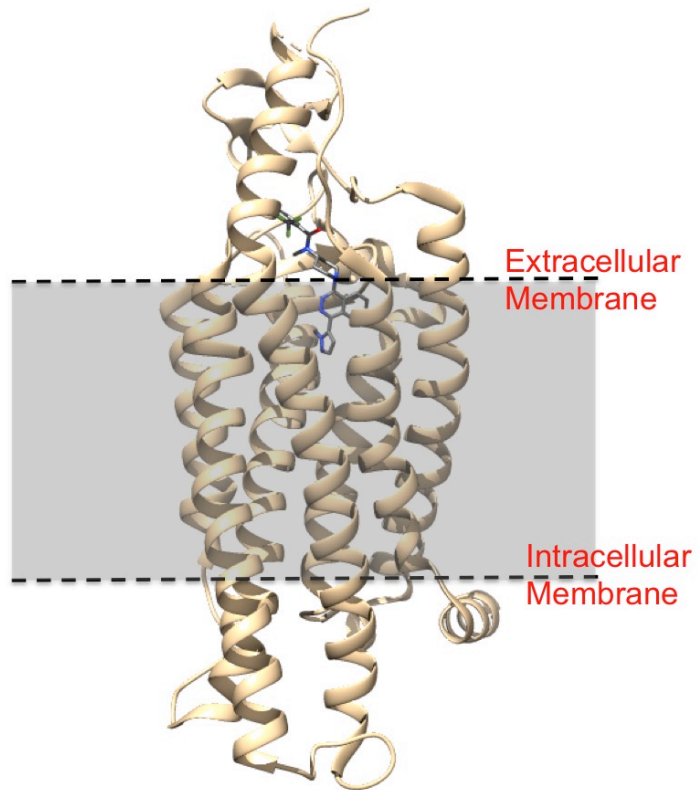


Figure 3.1 Overall Structure of Human SMO with Antagonist LY2940680

The crystal structure gave rise to the first ligand-protein interaction diagram, illuminating specific residues interacting with the ligand. Most notably, [Arg 400](#) and [Asp 219](#) have key hydrogen bonding interactions with the phthalazine and amide backbone, respectively (**Figure 3.2**). Towards the top of the pocket, there is the potential for pi-pi overlap with [Phe 383](#) and the decorated electron poor aromatic ring of the ligand. Similarly, there is the potential of an aromatic overlap between [His 470](#) and the methylated pyrazole at the opposite end of the molecule. Additionally, inside the binding pocket there are numerous water molecules that do not directly interact with LY2940680 but form a larger network of integral hydrogen bonds.

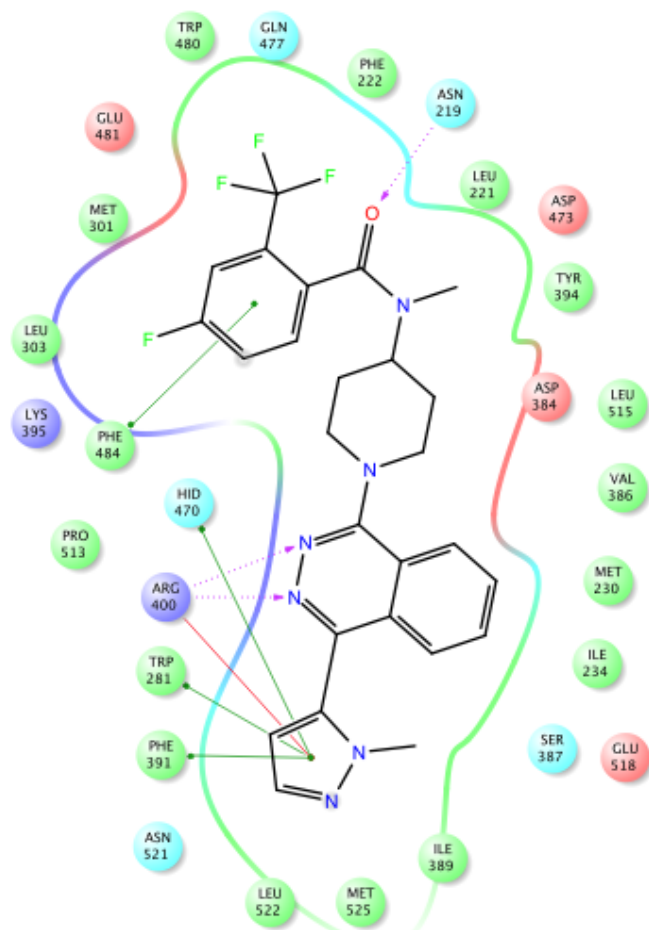


Figure 3.2 Ligand Interactions in Binding Pocket (LY2940680)

Most interestingly, Asp 473, a residue that confers resistance to GDC0449 when mutated, participates in this network of water-mediated hydrogen bonds.⁵

3.1.2 Current State of Crystallography

Shortly after the seminal publication, Stevens co-published with Weierstall and Cherezov a novel method for developing and growing lipidic cubic phase crystals for diffraction.⁶ This work featured the first crystal structure of SMO bound to the natural alkaloid cyclopamine. Unfortunately, by using the method that resulted in the successful

crystallization of SMO with LY2940680, they isolated only low quality crystals. The only crystals isolated of reasonable quality resulted in a low-resolution structure, but they could identify the binding pocket of the alkaloid within the receptor (**Figure 3.3**).

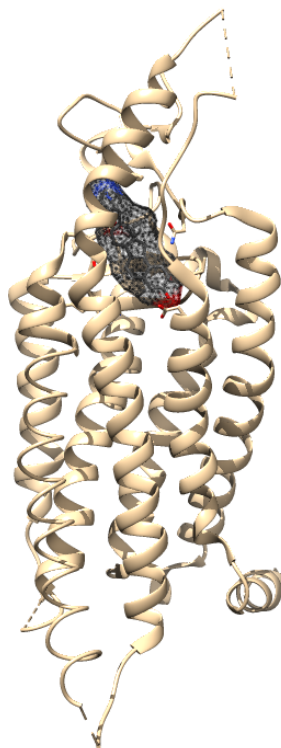


Figure 3.3 Density Map of Cyclopamine Bound to Human SMO

Due to the low-resolution of the crystal (4.5 Å), it was impossible to determine exactly how the ligand was binding within the pocket. Previous studies using KAAD-cyclopamine, an analog of the natural compound with a bulky substituent placed on the secondary amine of the F-ring, demonstrated no loss of inhibitory activity. With this in mind, Stevens and coworkers oriented cyclopamine in the binding pocket with the secondary amine facing the extracellular environment (**Figure 3.4**) in order to accommodate the added bulky group.

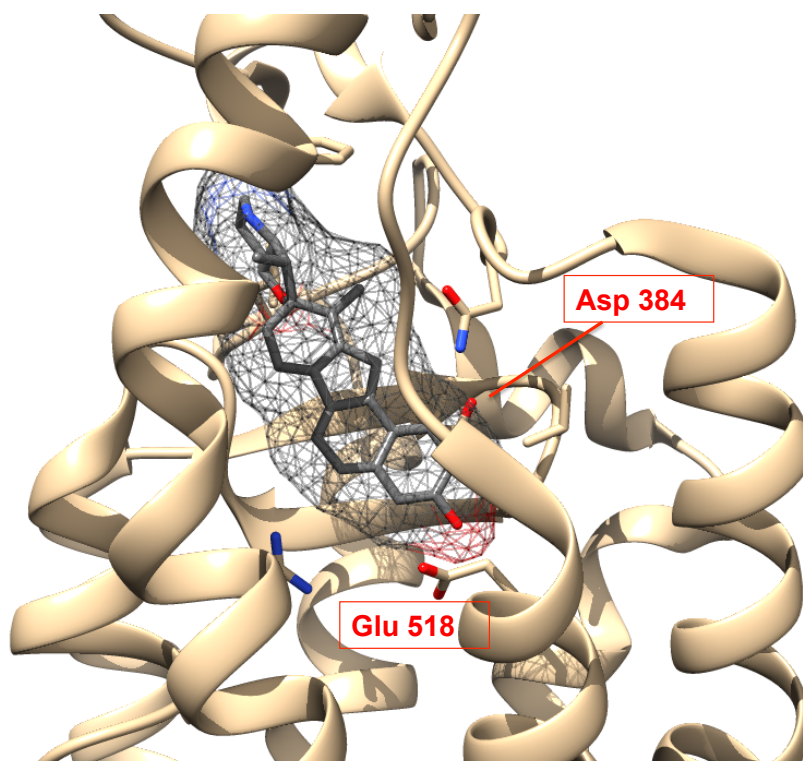


Figure 3.4 Close Up View of Cyclopamine in Binding Pocket

Looking closely at the predicted binding orientation of cyclopamine, the hydroxyl on the A-ring buried deep within the pocket appears to be anchored by potential hydrogen bonds with Glu 518 and Asp 384. The allylic ether and secondary amine do not appear to have any beneficial contacts within the binding pocket, but the secondary amine may serve a purpose to enhance solubility. A map of potential interactions is outlined in **Figure 3.5**.

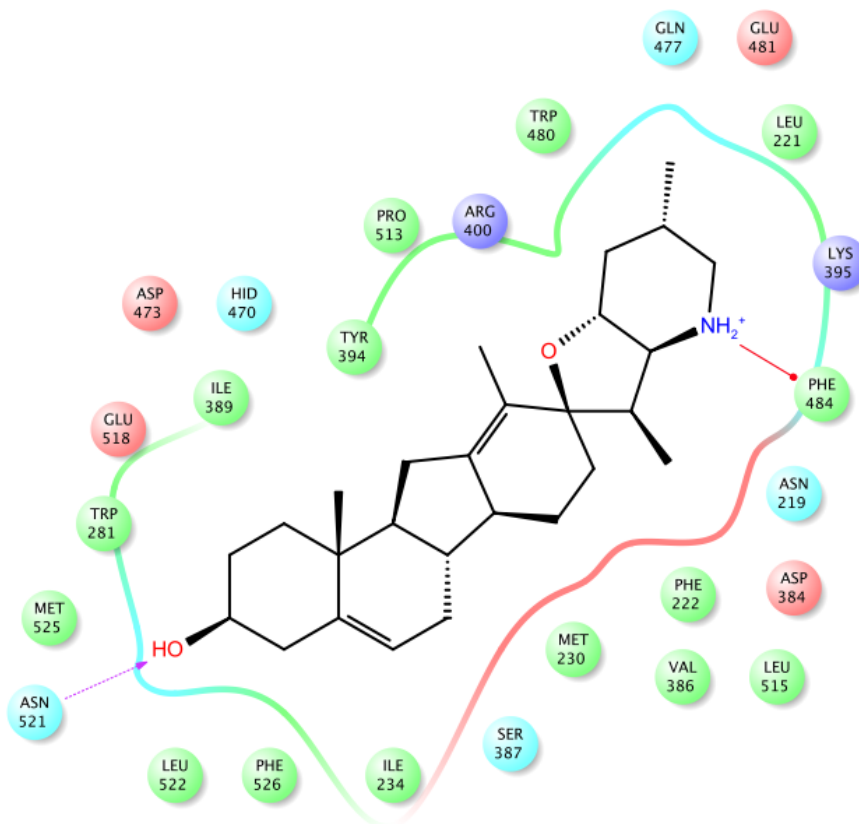


Figure 3.5 Ligand Interactions in Binding Pocket (Cyclopamine)

Shortly after the release of the cyclopamine complex crystal structure, Stevens and coworkers released three more structures of SMO bound to a variety of ligands: antagonists SANT1 and Anta XV and agonist SAG1.5.⁷ The binding sites for these ligands all reside within the same pocket, but interestingly, the binding of SANT1 extended much deeper than the rest of the ligands (**Figure 3.6**). This sub-pocket, unique to the binding of SANT1, lies well within the lipid bilayer and is far removed from the aqueous exposed ligand entrance.

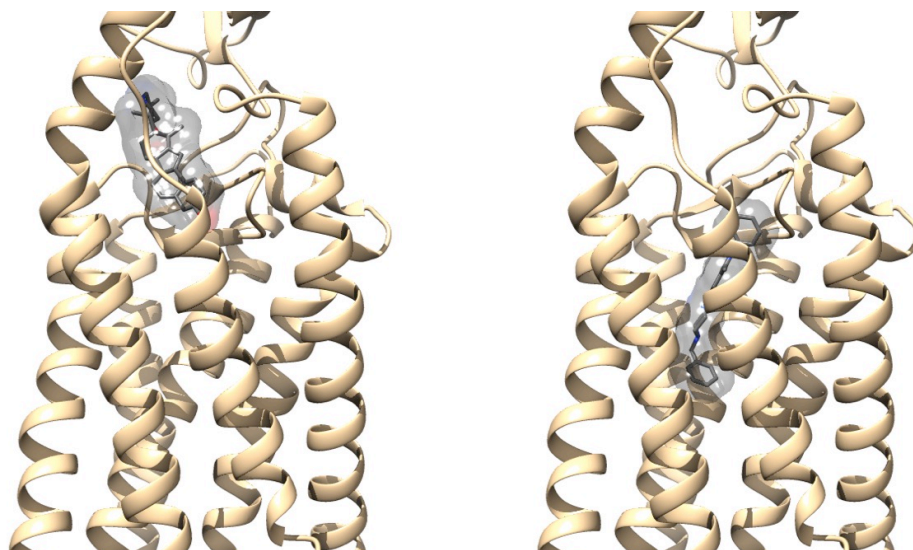


Figure 3.6 Comparison of Cyclopamine and SANT1 Binding Pocket

This unique method of binding SANT1 relative to the other antagonists suggests that, depending on the functionalities within the molecules, there may be more than one possible binding orientation that leads to suppression of the protein. It has been shown that the depth of binding is ligand dependent and can vary greatly. With this information in hand, the next step in the analysis of our analogs was to assess their possible interactions in the binding pocket and to design novel analogs that could enhance those interactions.

Section 3.2 Rigid Protein Molecular Modeling

The publication of the first crystal structure of SMO began to shed light on the pharmacophore of LY2940680. Despite this advance, the various positions occupied by the antagonists in combination with the unresolved cyclopamine structure, there are still questions that remain unanswered. Using molecular modeling we began to hypothesize

what aspects of these molecules could be interacting with the protein to provide the inhibitory effects that were seen in the cellular assays.

3.2.1 Introduction to AutoDock Vina

First introduced by Trott and Olson, AutoDock Vina is a molecular docking program that predicts the most probable non-covalent bonding orientation of an input ligand and receptor protein.⁸ Using a rigid protein, AutoDock Vina allows the energy-minimized ligands to have flexibility, defined by a set number of rotatable bonds, and to sample numerous orientations within a pre-defined docking site. The docking site can span the entire surface of the protein, but for our analyses, we selected the long hydrophobic cavity within SMO that has been shown to bind both agonists and antagonists.⁷

AutoDock Vina allows for the rapid formation of docking poses that are scored by predicted binding energy. The Vina program has been shown to have a high correlation between the predicted free energy of binding and the experimentally calculated energies. In order to begin the analysis, the ligand is first prepared by defining the rigid and rotatable bonds using AutoDock Tools, the protein crystal structure is converted to a PDBQT file to recognize both atom charge and type, and the docking grid box is defined in three-dimensional space. Once all parameters are defined, the docking results and scores are generated in under five minutes and can be processed. By maintaining a rigid protein, AutoDock Vina can very quickly generate the various poses and score them based on steric repulsion, hydrogen bonding, and hydrophobicity.

3.2.2 Analysis of Previously Synthesized Analogs

Using the recently published crystal structure of SMO, we began analyzing our original estrone analogs, both F-ring saturated and aromatic, to hypothesize which potential residues could be responsible for potency. As a proof of principle, we first demonstrated using LY2940680 and the SMO receptor in its apo form that we could recapitulate the docking pose observed in the original crystallization paper (**Figure 3.7**).

Albeit not a perfect match, the residues highlighted in the crystallography paper were still in close proximity to the corresponding heteroatoms of LY2940680. Specifically, Arg400 showed an interaction with the phthalazine ring system, and the fluorinated aromatic ring demonstrated pi-pi overlap with Phe 484. Satisfied with these results, we moved to a small series of our estrone analogs.

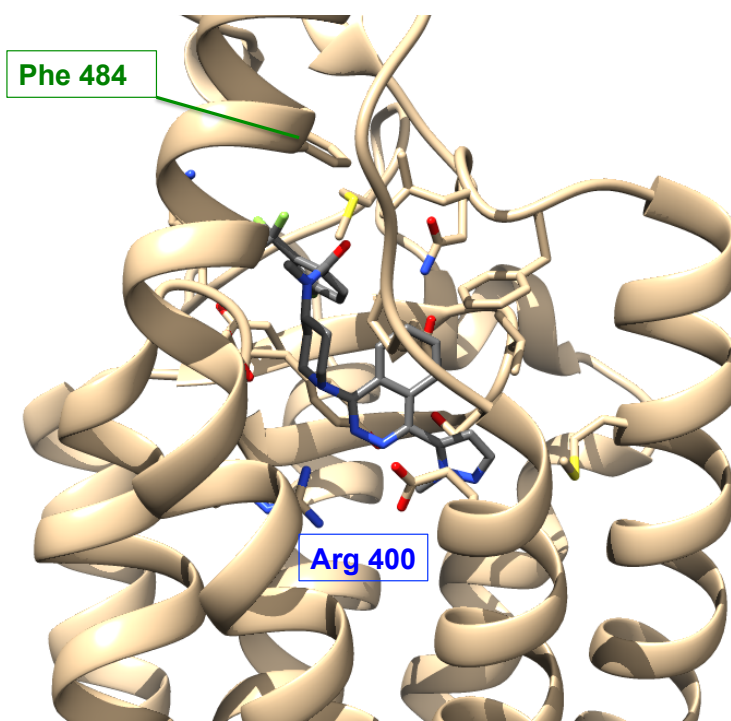


Figure 3.7 Vina Predicted Binding Orientation of LY2940680 with SMO

Looking first at cyclopamine, AutoDock Vina positioned the ligand with the EF-ring system deep in the pocket and the A-ring hydroxyl exposed to the aqueous surroundings (**Figure 3.8**). This binding orientation does not align with the SAR data that has previously been shown. According to Beachy, very large substituents can be placed on the secondary amine without loss in potency, which would require the amine to be configured facing the extracellular environment.⁹ Unfortunately, the proposed binding of cyclopamine does not match the SAR provided by Beachy, or the crystal structure published by Stevens.

Despite these inconsistencies, the binding affinity calculated *in silico* was relatively low compared to both the steroidal analogs and known inhibitors docked with SMO. This low binding affinity may be indicative of a poor compatibility and lack of positive interactions predicted by the software. Additionally, the axial methyl at the AB ring fusion creates a hydrophobic clash with the binding pocket that also would disfavor this binding mode, thus offering an explanation for the low proposed binding affinity.

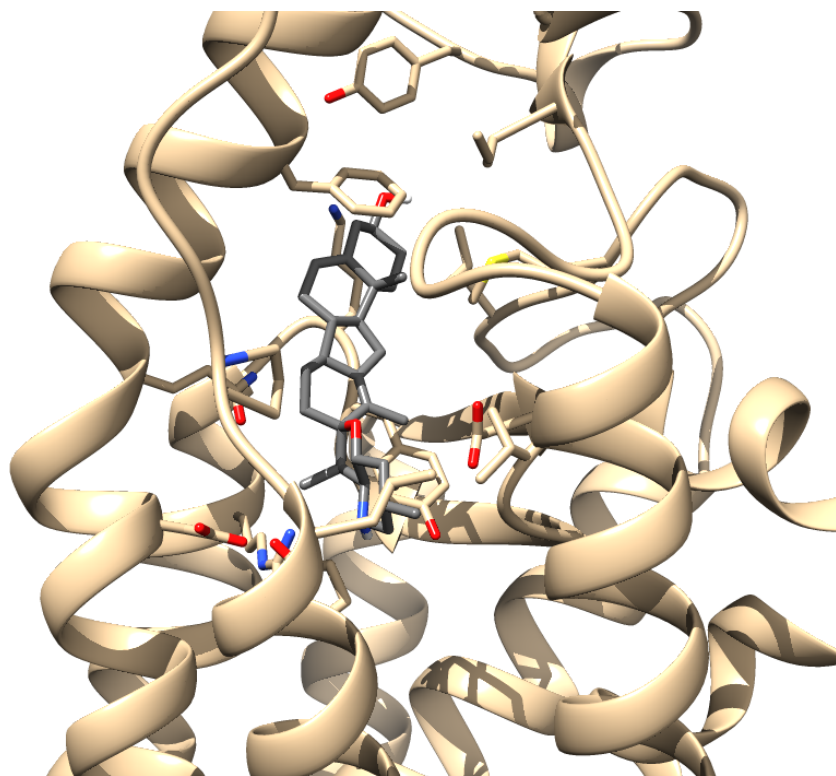


Figure 3.8 Vina Predicted Binding Orientation of Cycloamine with SMO

In comparison, the original estrone analog had a much stronger predicted binding affinity with the rigid receptor SMO. In this predicted binding model, the estrone analog was positioned with the aromatic A-ring anchored by a pi-pi stack with [Phe 484](#) while allowing for the free hydroxyl to interact with [Lys 395](#) (**Figure 3.9**). The unsaturated EF spirocycle was buried deep in the pocket, establishing a potential salt bridge with [Asp 384](#). Due to the aromaticity of the A ring, there is no axial methyl that would conflict with hydrophobic binding pocket. The more compact steroid backbone may, in fact, be a more suitable replacement for the more voluminous cycloamine ABCD core.

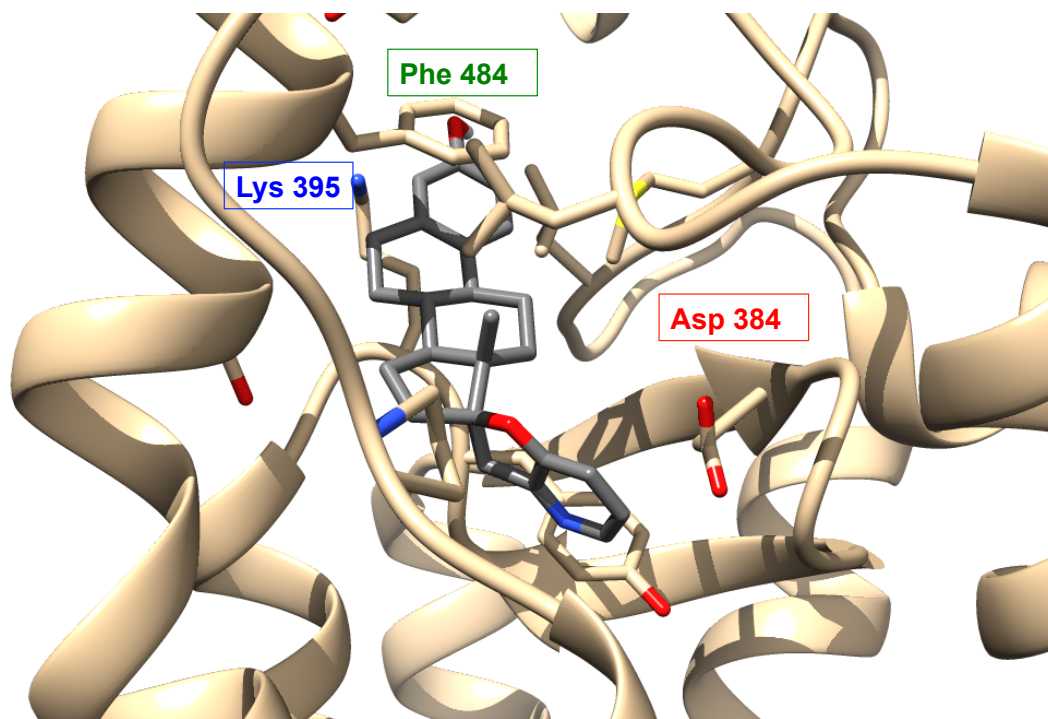


Figure 3.9 Vina Predicted Binding Orientation of Estrone Analog with SMO

Similar to the estrone analog, the most probable predicted binding orientation for the oxetane derivative positioned the aromatic A ring for optimal pi-pi stacking with [Phe 484](#) and in proximity to hydrogen bond with lysine 395 (**Figure 3.10**). Unique to this saturated exocyclic analog, the basic secondary amine of the pyrrolidine F ring has the potential to hydrogen bond with both [Arg 400](#), a residue found to interact with LY2940680, and also [Tyr 394](#). Although, in this predicted binding mode, the oxetane is too far away from any residues to form direct hydrogen bonds, the availability of the lone pairs for water-mediated hydrogen bonding is not precluded.

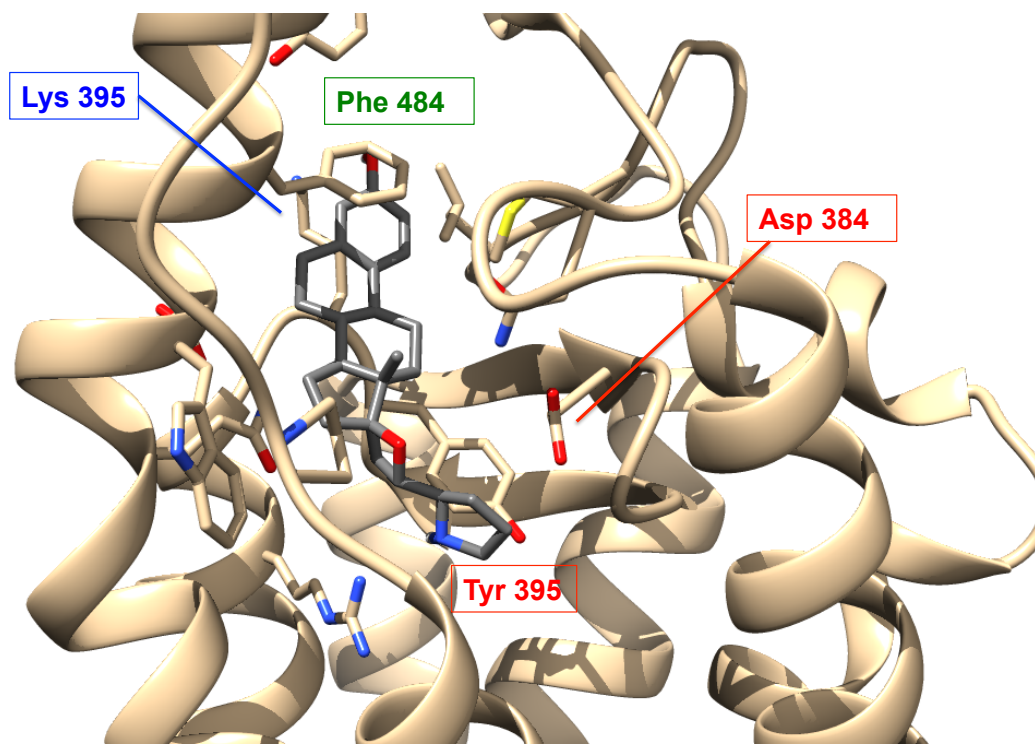


Figure 3.10 Vina Predicted Binding Orientation of Oxetane with SMO

The biological testing summarized in [Chapter 2](#) confirms that the major modifications (saturation, connectivity, ring size, stereochemistry) to the EF ring system of the estrone-derived analogs contribute vastly to their potencies. Through rigid modeling with AutoDock Vina, it is predicted that the aromatic A-ring acts to anchor the analogs in an orientation that places the variable EF scaffold deep inside the binding pocket. Due to the major differences in potencies based on the composition of the EF scaffolds, the biological data would suggest that these aspects of the molecules are oriented in a fashion for high impact with the receptor. Similarly, the *in silico* work suggests the importance of the C3 hydroxyl hydrogen bonding interaction with [Lys 395](#), correlating with the decrease in potency upon loss of the C3 hydroxyl group.

3.2.3 Conclusions from Rigid Molecular Modeling

AutoDock Vina allowed for the rapid creation of possible binding modes for the previously synthesized analogs with the published crystal structure of receptor SMO. Since the receptor was crystallized with a ligand, all of the side chains were oriented in the best possible confirmation for the interaction with LY2940680. It has been shown that this GPCR-like protein is flexible in binding and can accommodate ligands of various sizes. The limitations of AutoDock Vina are such that the receptor must stay rigid, despite the movement and flexing of the ligands.

Looking carefully at the now available crystal structures of SMO, all three have a ligand positioned in the same binding pocket. However, the orientation of multiple side chains (R400, F391, Q518, Y323, and E477) vary greatly dependent on the ligand. For this reason, another molecular modeling system was implemented that allowed for both a flexible receptor and rotatable ligand.

Section 3.3 Flexible Protein Molecular Modeling

Many docking programs rely entirely on a rigid receptor given to the program. In reality, the receptor is flexible and accommodates each ligand uniquely, responding to its shape and chemical composition. Using SMO as the receptor protein, Schrodinger Induced Fit Docking (IFD) allows for the protein to move in response to each ligand conformation. IFD generates a variety of potential structures that would have been impossible to model using a rigid protein receptor and ranks them according to relative binding affinity.

3.3.1 Introduction to Schrodinger Induced Fit Docking Suite

The Schrodinger Induced Fit Docking Suite utilizes two major protocols, Glide and Prime, in order to modify both the input ligand and receptor protein. Glide, or Grid-Based Ligand Docking with Energetics, generates the possible ligand conformations that could be docked into the receptor. Glide allows for all possible tautomers to be generated as well as a variety of protonation states dictated by a target pH. Using a series of criteria, the program breaks a ligand into a relatively stable core (rigid ring systems) and rotatable regions (side chains with more flexibility). A series of conformations is then given for each ligand.

The conformations are then scanned in the receptor gridbox for a best fit. By utilizing an exhaustive approach, Glide places each conformation at various points within the active site and scans for potential clashes or positive interactions. The next phase of refinement locates the potential hydrogen bond donating and accepting atoms within the ligand and calculates the distances to corresponding hydrogen bond participating residues in the receptor. The final stage of refinement assesses the van der Waals interactions and electrostatic maps of both ligand and receptor. A combination of the aforementioned scores constructs a hierarchy of ligand conformations within the receptor and ranks them based on their Induced Fit Docking Score.

3.3.2 Analysis of Previously Synthesized Analogs

Using the Schrodinger IFD program, the previously synthesized saturated and unsaturated estrone analogs were evaluated for binding with the receptor SMO. With the crystal structure provided by Stevens, the protein was first preprocessed for any missing residues, and then the ligand (LY2940680) was removed and a series of the synthesized analogs docked in that binding pocket. Side chains within five angstroms

from the ligands were allowed to maneuver to provide a more optimized docking pose specific to each ligand.

Looking first at cyclopamine (**Figure 3.11**), the nonaromatic A-ring is buried deep in the binding pocket with the EF-ring system facing the extracellular environment. As described above, the secondary amine of the F-ring has been functionalized with large substituents with no loss of potency, thus adding validity to this docking pose. The hydrophobic backbone lies parallel to the transmembrane helices, placing the axial methyl at the AB fusion relatively close to the surface of the pocket. The hydrophobic backbone maintains a close proximity to the relatively hydrophobic binding pocket.

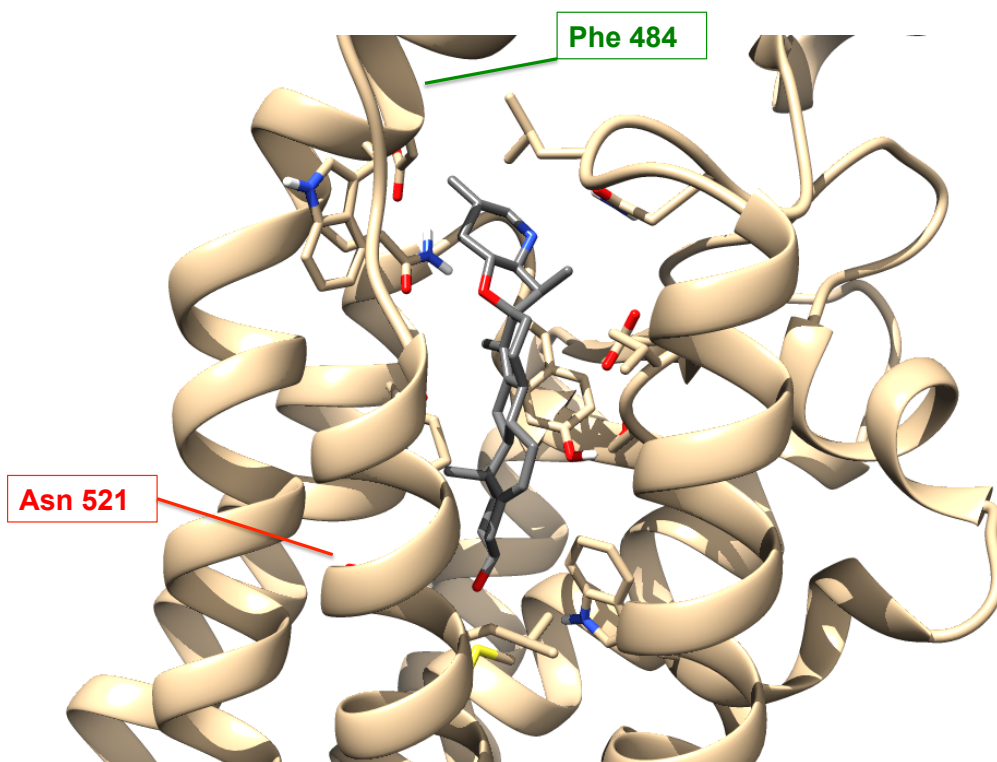


Figure 3.11 IFD Predicted Binding of Cyclopamine with SMO

As depicted in **Figure 3.12**, the protonated piperidine is capable of adopting an orientation at the top of the pocket that results in a cation-pi interaction with Phe 484.¹⁰ The allylic ether, which is responsible for the molecule's acid sensitivity, does not come in contact with any residues that could increase the binding affinity. The C3 hydroxyl, buried deep inside the pocket, picks up a favorable interaction with the amide on the side chain of Asn 521.

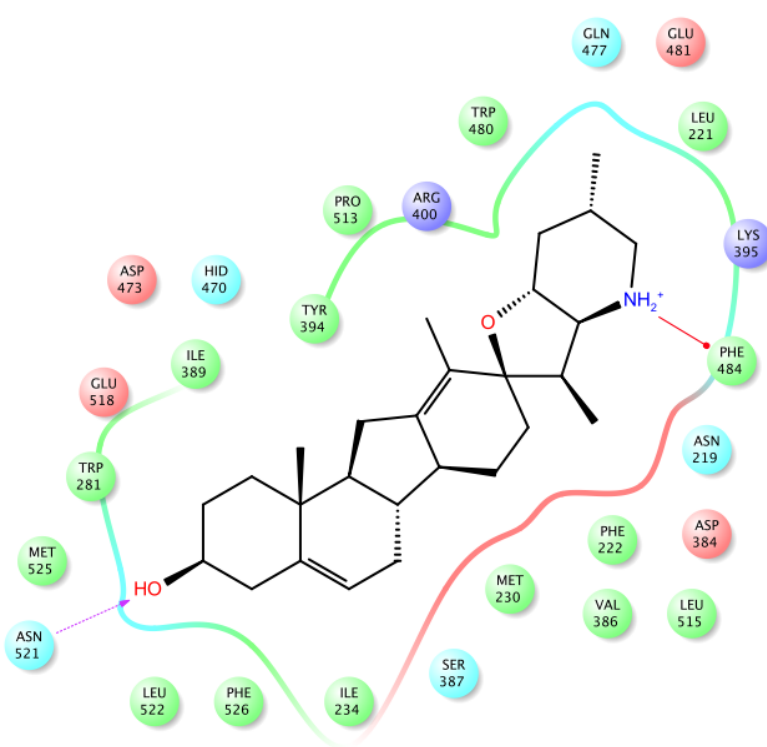


Figure 3.12 IFD Ligand Interaction Diagram: Cyclopamine with SMO

When comparing the predicted docking orientation of cyclopamine with the estrone analog, the most striking difference is the relative orientation of the molecules with respect to the pocket (**Figure 3.13**). All of the previously synthesized estrone-derived analogs orient in a fashion that places the aromatic A-ring closest to the extracellular space and the EF-ring system buried in the pocket. Additionally, with an

aromatized A-ring, there is no axial methyl at the AB-ring fusion, allowing for more space within the pocket.

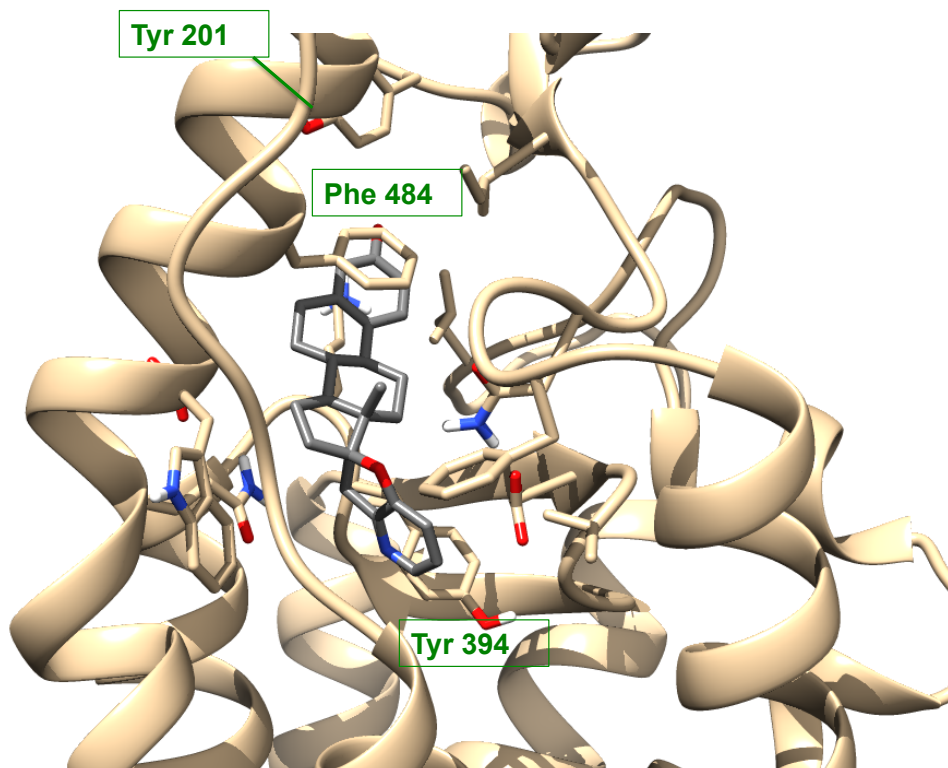


Figure 3.13 IFD Predicted Binding of Estrone Analog with SMO

Looking more closely at the most probably docking pose of the estrone analog and receptor SMO, there are quite a number of positive interactions identified throughout the steroid (**Figure 3.14**). Similar to cyclopamine, the hydrophobic backbone runs parallel with the helices and does not conflict with any hydrophilic or charged residues. Unique to the estrone analog is the ability of the aromatic A-ring to pi-pi stack with Phe 484. The orientation of the C3 hydroxyl is available in some docking poses to interact through a hydrogen bond with Tyr 207 (not shown), but the hydroxyl facing the exterior of the protein could also simply assist in solubility.

Towards the top end of the molecule, the furan oxygen, similar to the allylic ether, does not have any specific interactions of its own. However, the unsaturated pyridine F-ring exhibits a pi-pi stack with Tyr 394 and interacts with a strategic water molecule to contribute to a network of hydrogen bonds.

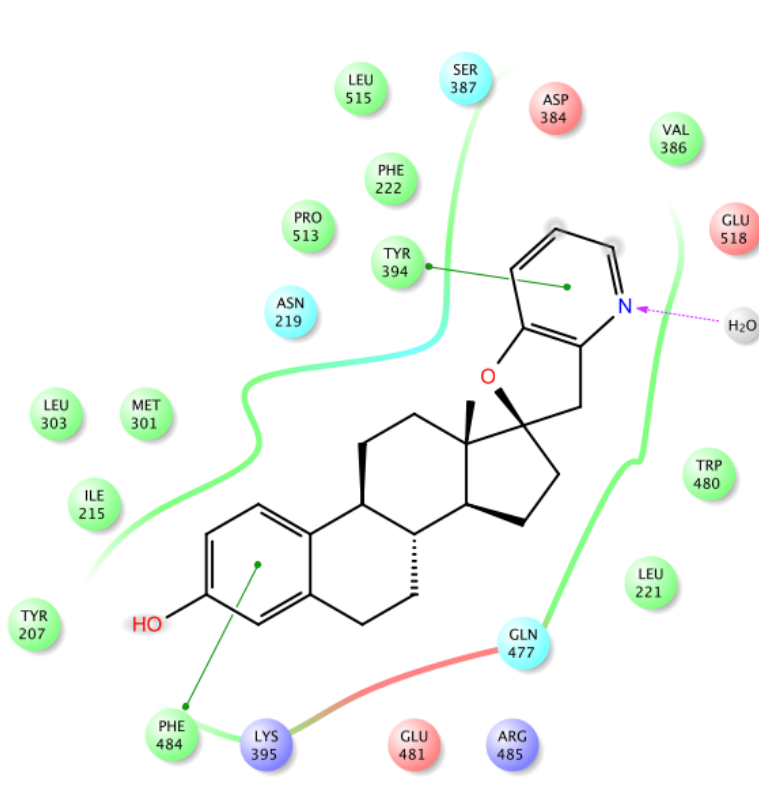


Figure 3.14 IFD Ligand Interaction Diagram of Estrone Analog with SMO

Similar to the estrone analog, the C3 deoxy analog docking study demonstrated all of the same interactions as the previously described analog and also oriented the compound with the A-ring towards the extracellular space and the EF-rings buried into the pocket (**Figure 3.15**). Surprisingly, without the electron-donating group on the aromatic ring, the pi-pi interaction that was present with the previously described estrone analog is no longer predicted by the software (**Figure 3.16**).

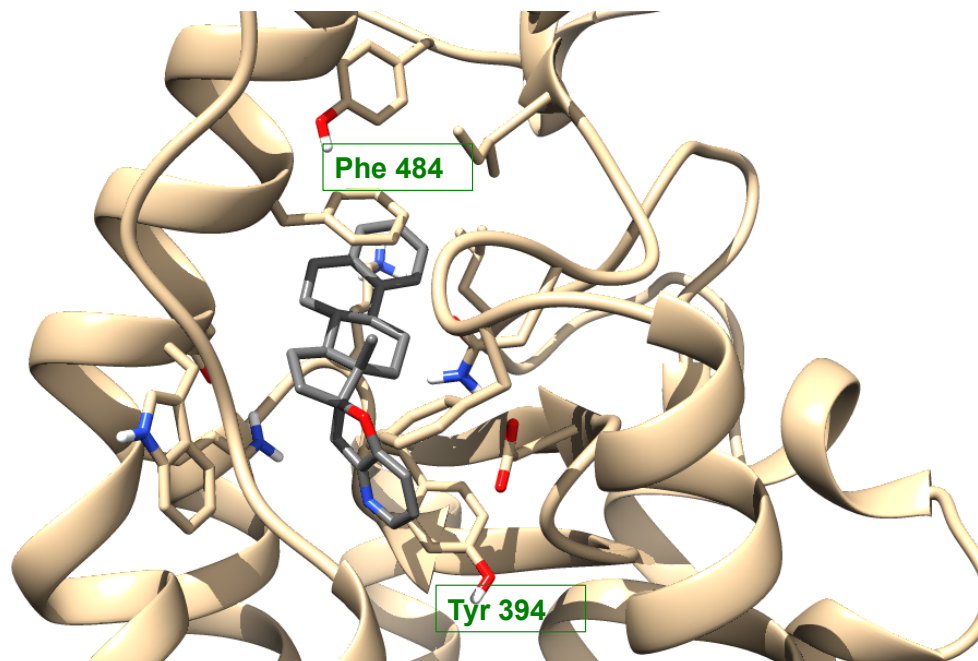


Figure 3.15 IFD Predicted Binding of Deoxy Estrone Analog with SMO

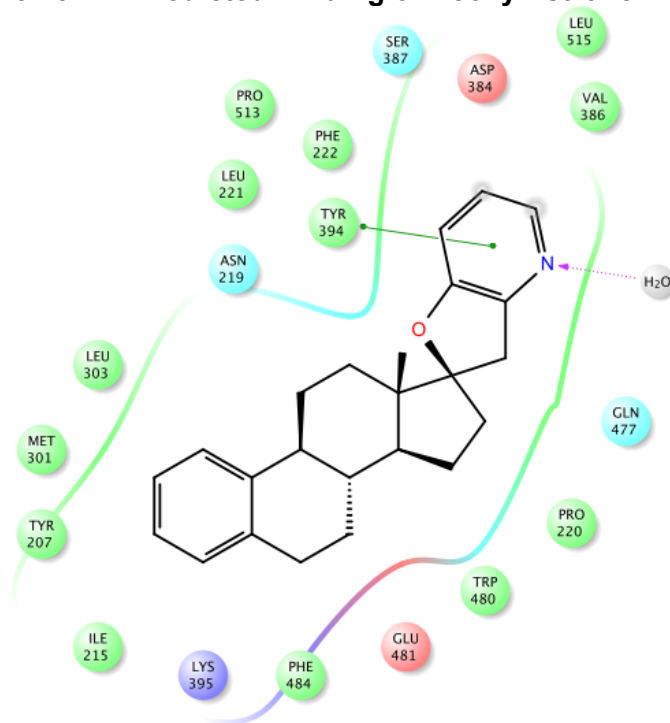


Figure 3.16 IFD Ligand Interaction Diagram of Deoxy Estrone Analog with SMO

Lastly, the oxetane analog has a very different EF-ring system than the aforementioned unsaturated F-ring analogs. As a proof of principle, the estrone analogs were synthesized as efficiently as possible, using pyridine as the aromatic F-ring. Comparing the structure of these analogs to cyclopamine, the sp_3 secondary amine present in cyclopamine varies greatly with respect to basicity and hybridization than the sp_2 pyridine nitrogen described above. The oxetane analog is comprised of a saturated F-ring, albeit one atom smaller, but the pyrrolidine in the oxetane analog provides a more accurate structural approximation to the piperidine seen in cyclopamine.

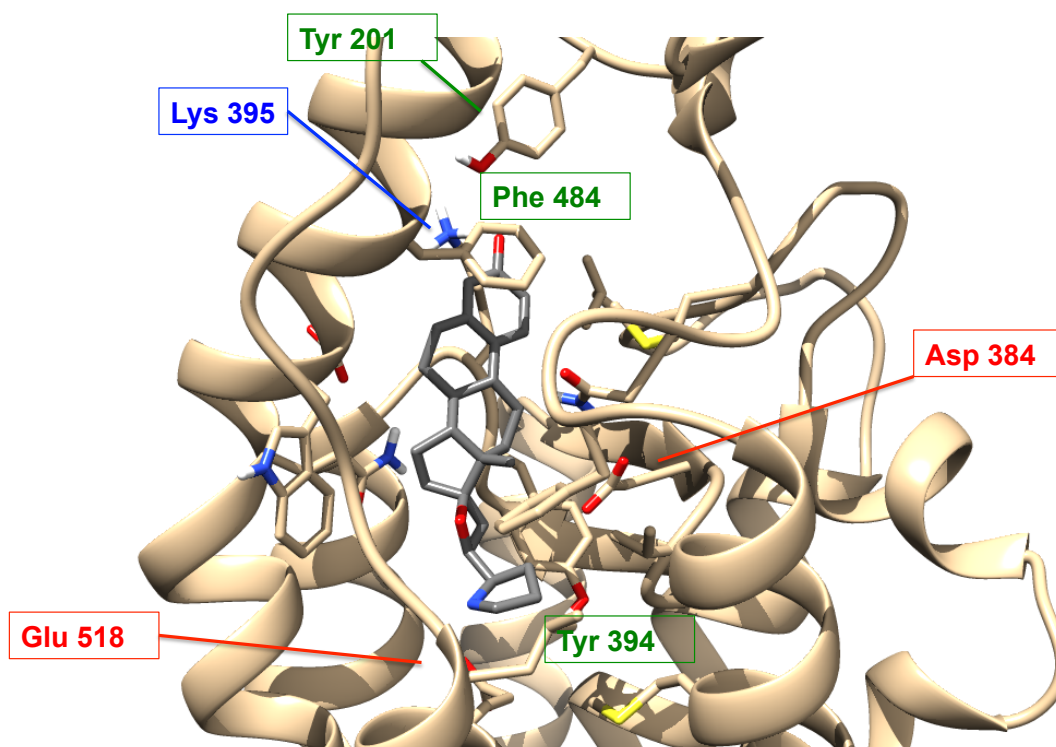


Figure 3.17 IFD Predicted Binding of Oxetane Analog with SMO

The most probable docking pose for the oxetane analog with SMO identifies a large number of interactions. Like the other estrone derived compounds, the aromatic A-

ring overlaps at the top of the pocket with Phe 484 and shows a hydrogen bond with Lys 395 (**Figure 3.17**). The hydrophobic backbone lies in the same hydrophobic cavity, and the EF-rings are at the base of the pocket. Despite the oxetane ether having the propensity for hydrogen bonding, no interactions are predicted by the modeling.¹¹ The protonated pyrrolidine, however, is capable of adapting an orientation that picks up many hydrogen bond donating and accepting interactions (**Figure 3.18**).

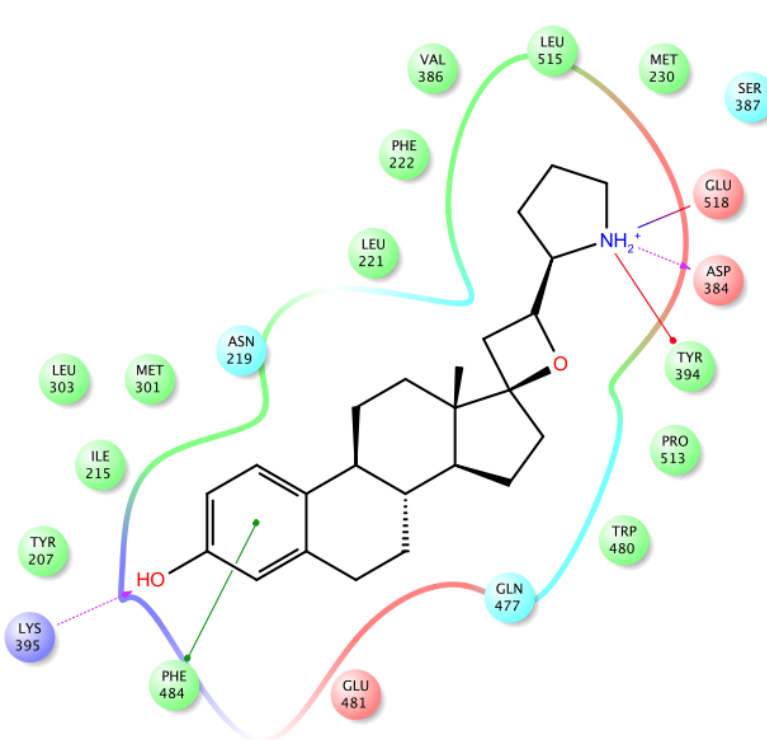


Figure 3.18 IFD Ligand Interaction Diagram of Oxetane Analog with SMO

The exocyclic pyrrolidine may be able to interact with many residues such as Glu 518, Asp 384, or Tyr 394 in the depths of the pocket due to the rotational freedom about the carbon-carbon bond connecting the E and F-rings. Unlike the unsaturated estrone analogs, the exocyclic pyrrolidine is not limited to one conformation. The five membered

ring can pucker in either direction to adopt the conformation with the most favorable hydrogen bonding interactions.

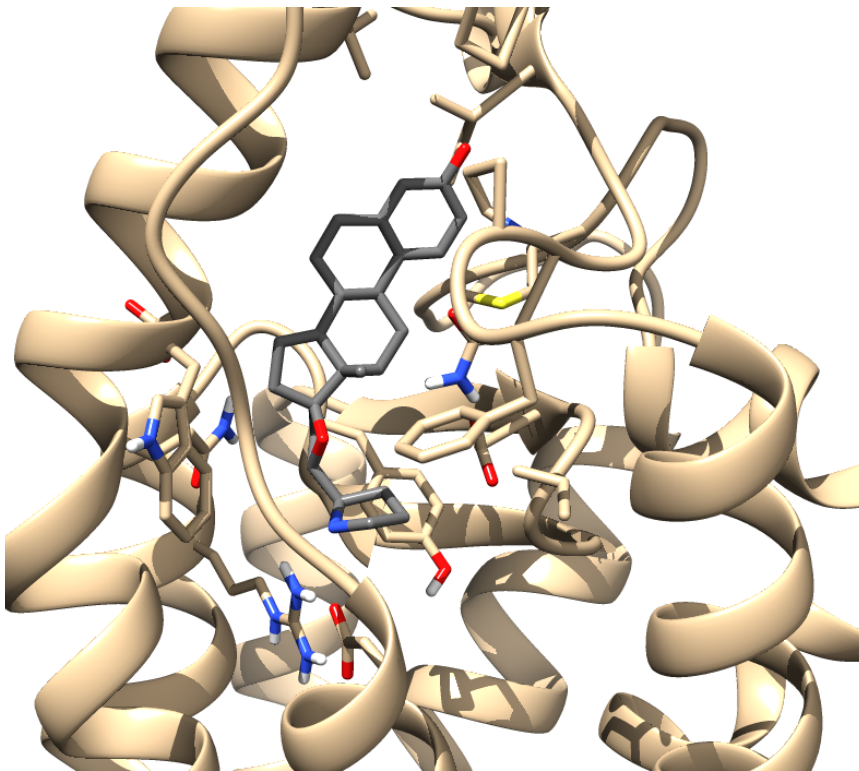


Figure 3.19 IFD Predicted Binding of Oxetane Analog with Mutant SMO

To address *in silico* the importance of the pi-pi overlap with the aromatic A-ring, Phe 484 was mutated to a glycine. After reevaluating the predicted binding affinity with the mutant protein, the steroid-derived analog rotates slightly in the pocket since the anchoring pi-pi stack is no longer present. The importance of the aromatic A-ring is currently being investigated synthetically and will be described in Chapter 4.

3.3.3 Conclusions and Correlation with Biological Data

Once all of the IFD had been completed, it was important to determine the relevancy of the modeling. Since we had recently completed generating IC₅₀ curves for the analogs described above, the IC₅₀ values can be plotted against the IFD score predicted by the software (**Figure 3.20**). Interestingly, the modeling and the biological data correlate with a relatively high statistical validity. Using a nonlinear regression with two degrees, a logarithmic curve fits the data with an R squared of 0.84.

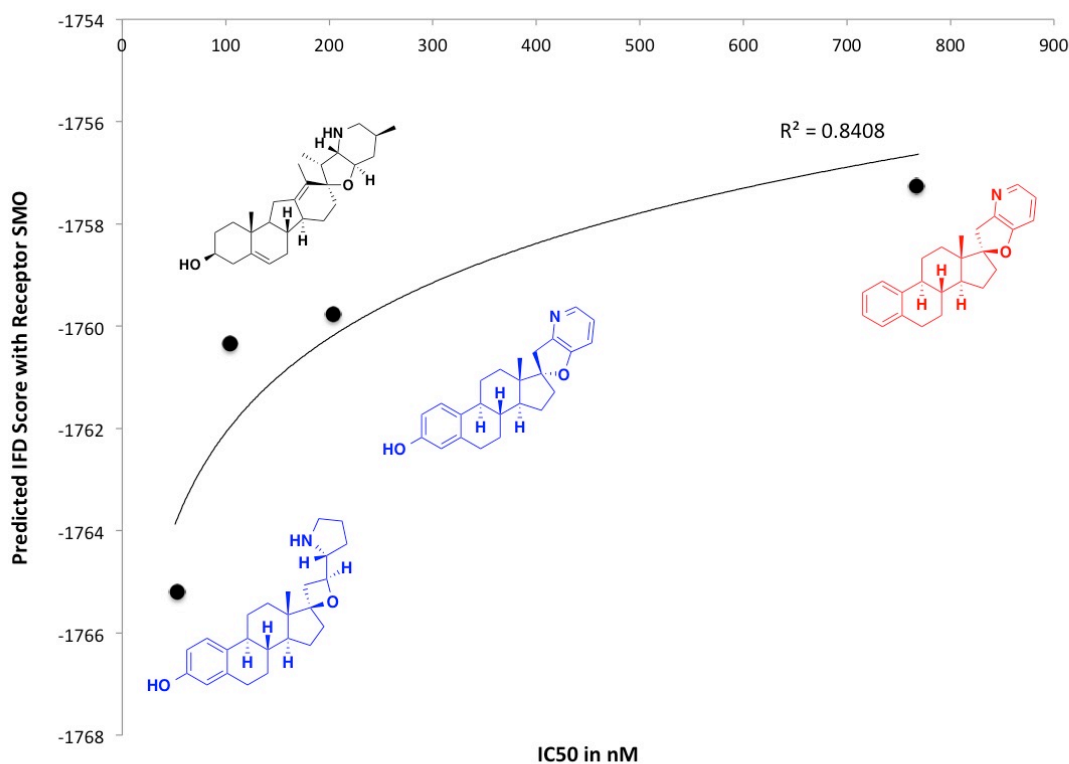


Figure 3.20 Correlation of IC₅₀ from DLR Assay and IFD Docking Score

Additionally, by plotting the logIC₅₀ against the IFD score, a linear trend line with a similar R squared is observed (**Figure 3.21**).

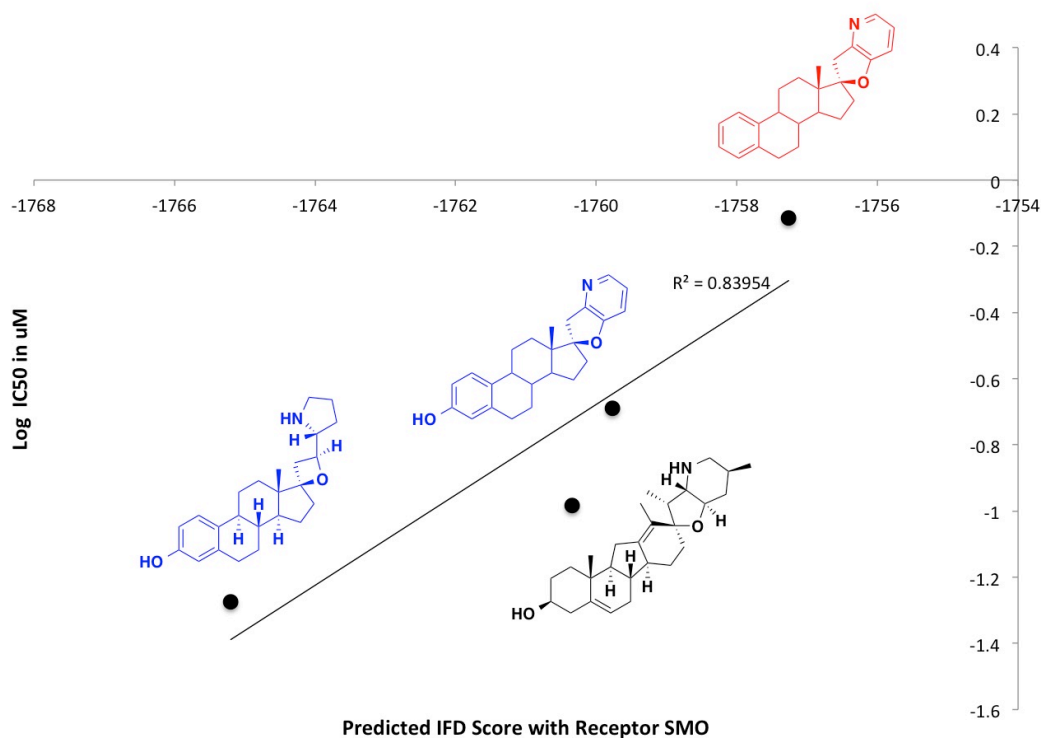


Figure 3.21 Correlation of $\log IC_{50}$ from DLR Assay and IFD Docking Score

Looking back at the molecular modeling in combination with the results from the Dual Luciferase Reporter (DLR) Assay in Chapter 2, there is a definite SAR that can be elucidated. Comparing cyclopamine with the estrone analog, their relatively similar potencies indicate that the steroid backbone is an appropriate surrogate for the steroidal-like *C-nor-D-homo* system of cyclopamine. The modeling suggested that the hydrophobic backbones have little involvement with the binding, but the axial methyl present in cyclopamine due to the nonaromatic A-ring may be detrimental. In addition to the lack of an axial methyl, the aromaticity of the A-ring does not appear to be insignificant. The potential for a pi-pi stack with phenylalanine 484 is prominent in all

docking poses and helps to orient these synthetic analogs with the EF system in the base of the pocket.

The majority of the SAR of the synthetic analogs revolves around the EF ring systems, once again highlighting that these functional groups most likely lie inside the pocket where the interactions are more meaningful than the extracellular space. When comparing the oxetane, the most potent analog, to the estrone analog, the flexibility of the EF system and the hybridization and basicity of the pyrrolidine may be responsible for the increase in potency. The potential connections between the secondary amine and Glu518 or Asp384 may offer a hydrogen bonding network that stabilizes the predicted interaction between ligand and protein.

Section 3.4 Future Directions

With a molecular modeling program validating the biological data, it is now possible to design new analogs from multiple directions. In order to synthesize novel and potent analogs, the biological data in combination with the molecular modeling will provide more guidance than blind design. The goal of the project is to develop molecules synthesized from commercially available, non-plant derived sources that could serve as potential chemotherapeutics. A library of analogs was designed to explore the hypotheses described throughout this chapter. Chapter 4 will outline our efforts in designing, synthesizing, and evaluating analogs that probe the importance of the aromatization of the A-ring, the hybridization of the F-ring, the presence of the E-Ring, and the overall flexibility of the molecules.

Section 3.5 References

- (1) Carpenter, E. P.; Beis, K.; Cameron, A. D.; Iwata, S. Overcoming the Challenges of Membrane Protein Crystallography. *Curr. Opin. Struct. Biol.* **2008**, *18*, 581–586.
- (2) Milić, D.; Veprintsev, D. B. Large-Scale Production and Protein Engineering of G Protein-Coupled Receptors for Structural Studies. *Front. Pharmacol.* **2015**, *6*, 1–24.
- (3) Wang, C.; Wu, H.; Katritch, V.; Han, G. W.; Huang, X.-P.; Liu, W.; Siu, F. Y.; Roth, B. L.; Cherezov, V.; Stevens, R. C. Structure of the Human Smoothed Receptor Bound to an Antitumour Agent. *Nature* **2013**, *497*, 338–343.
- (4) Landau, E. M.; Rosenbusch, J. P. Lipidic Cubic Phases: A Novel Concept for the Crystallization of Membrane Proteins. *Proc. Natl. Acad. Sci. U. S. A.* **1996**, *93*, 14532–14535.
- (5) Yauch, R. L.; Dijkgraaf, G. J. P.; Alicke, B.; Januario, T.; Ahn, C. P.; Bazan, J. F.; Kan, Z.; Seshagiri, S.; Hann, C. L. Smoothed Mutation Confers Resistance to a Hedgehog Pathway Inhibitor in Medulloblastoma. *Science*. **2009**, *326*, 572–575.
- (6) Weierstall, U.; James, D.; Wang, C.; White, T. a; Wang, D.; Liu, W.; Spence, J. C. H.; Bruce Doak, R.; Nelson, G.; Fromme, P.; et al. Lipidic Cubic Phase Injector Facilitates Membrane Protein Serial Femtosecond Crystallography. *Nat. Commun.* **2014**, *5*, 3309–3314.
- (7) Wang, C.; Wu, H.; Evron, T.; Vardy, E.; Han, G. W.; Huang, X.-P.; Hufeisen, S. J.; Mangano, T. J.; Urban, D. J.; Katritch, V.; et al. Structural Basis for Smoothed

- Receptor Modulation and Chemoresistance to Anticancer Drugs. *Nat. Commun.* **2014**, *5*, 4355–4365.
- (8) Trott, O.; Olson, A. J. Software News and Update AutoDock Vina : Improving the Speed and Accuracy of Docking with a New Scoring Function , Efficient Optimization , and Multithreading. *J. Comput. Chem.* **2009**, *31*, 455–461.
- (9) Chen, J. K.; Taipale, J.; Cooper, M. K.; Beachy, P. A. Inhibition of Hedgehog Signaling by Direct Binding of Cyclopamine to Smoothed. *Genes Dev.* **2002**, *16*, 2743–2748.
- (10) Dougherty, D. A. Cation- π Interactions Involving Aromatic Amino Acids. *J. Nutr.* **2007**, *137*, 1504–1508.
- (11) Berthelot, M.; Besseau, F.; Laurence, C. The Hydrogen-Bond Basicity pKHB Scale of Peroxides and Ethers. *Eur. J. Org. Chem.* **1998**, 925–931.

Chapter 4. Design and Synthesis of Second Generation Analogs

After the establishment of a method for high-throughput biological evaluation and a computational model for activity, families of analogs were designed to test hypotheses originating from the biological data or specifically to assess the validity of the docking experiments. When looking at the various antagonists of the Hedgehog pathway developed by pharmaceutical companies (**Chapter 1.2.4**), it is unclear which aspects of these molecules are responsible for the potency, and there is no clear pharmacophore that can be deduced. Although the crystal structure of Smoothed bound to LY2940680 sheds light on important binding interactions, it cannot be assumed that each analog would interact with the same residues in the binding pocket.

After identifying a lead compound, we had hoped to use synthetic chemistry in combination with our biological evaluation to design molecules to tease out the underlying molecular features responsible for the potency of the oxetane-pyrrolidine analog.

Section 4.1 Sulfonamides

IPI-926, the semi-synthetic analog designed by Infinity Pharmaceuticals,¹ is synthesized via three major modifications to cyclopamine. First, the AB-ring fusion is reduced to the *cis*-decalin and then the acid-labile allylic ether undergoes ring expansion through a cyclopropanation sequence to construct the more stable homo-allylic ether. Additionally, a methyl sulfonamide is installed on the A-ring, mostly to increase the overall solubility of the molecule.

Looking at the predicting binding orientation of IPI-926 (**Figure 4.1**), the methyl sulfonamide is placed in the depths of the binding pocket, in close proximity to tyrosine 394 (**Figure 4.2**).

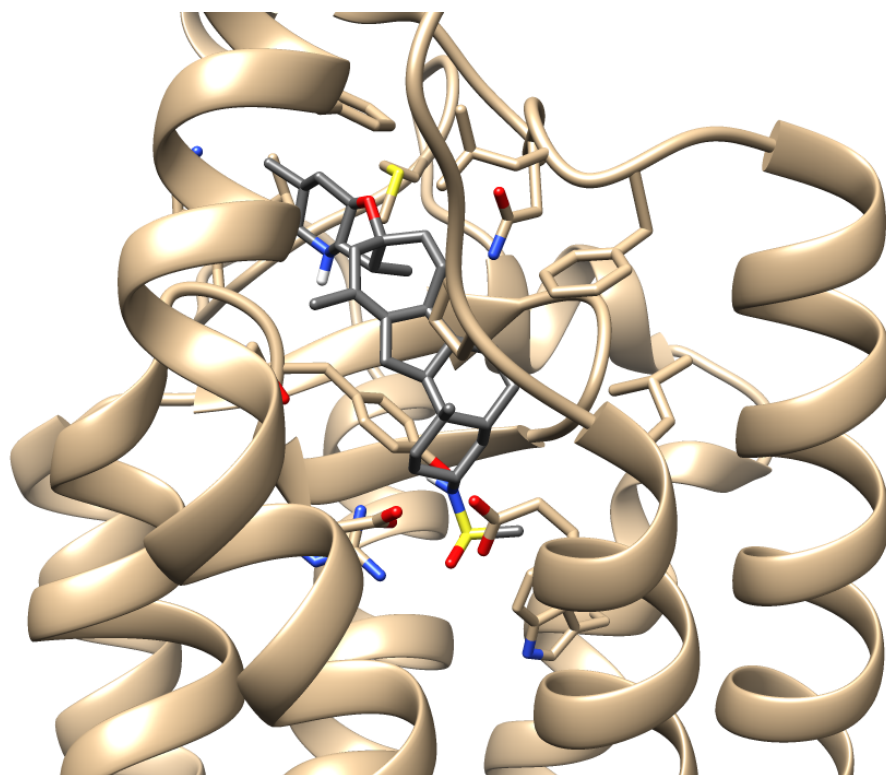


Figure 4.1 Predicted Binding Orientation of IPI-926 with SMO

In order to rule out a minimalistic structure of a sulfonamide fused with a steroid backbone, compounds **1** and **2** were synthesized (**Scheme 4.1** and **4.2**). Beginning with TBS protected estrone **3**, reductive amination with ammonium acetate in the presence sodium cyanoborohydride generated beta-amine **4** in good yield. Exclusive synthesis of the beta epimer is consistent with the addition of hydride from the more accessible face

of the molecule, away from the axial C18 methyl. Conversion of the primary amine to the sulfonamide and deprotection afforded the desired beta epimer.

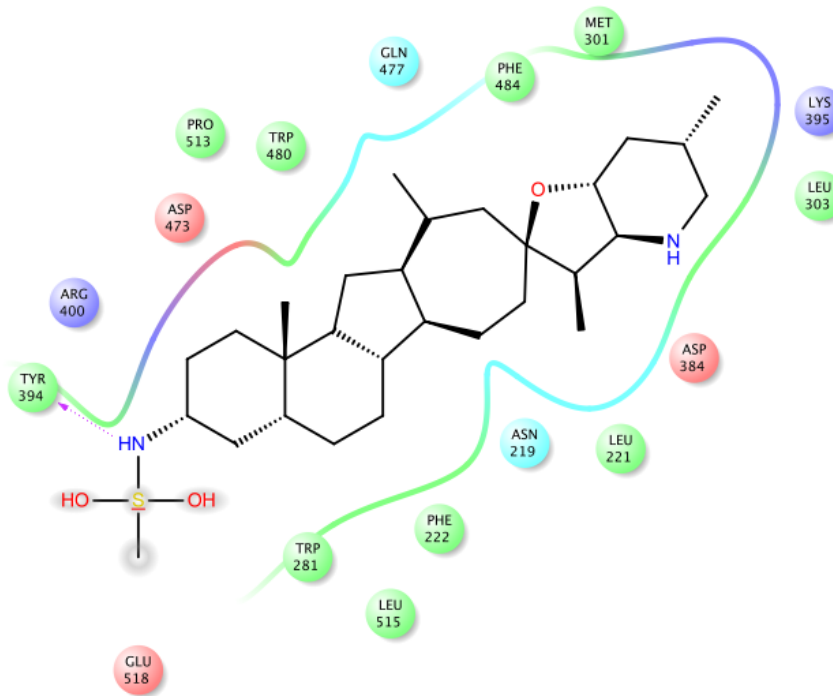
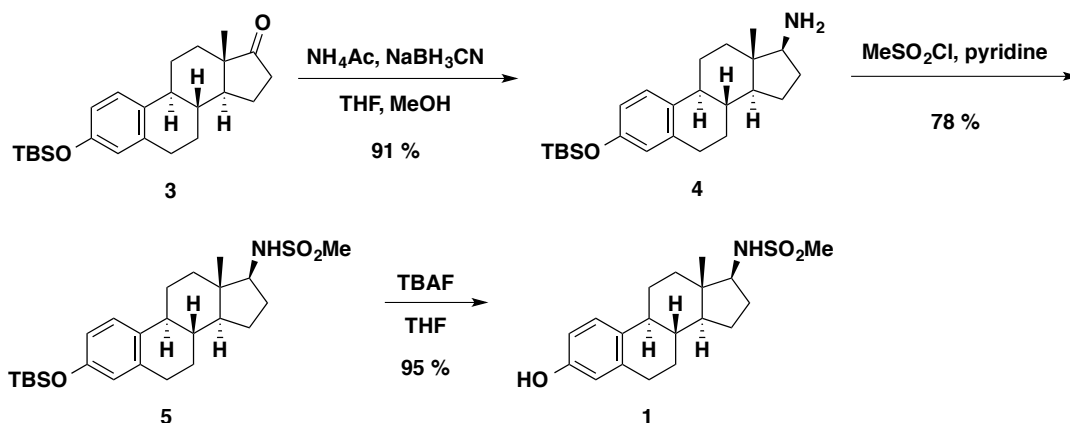
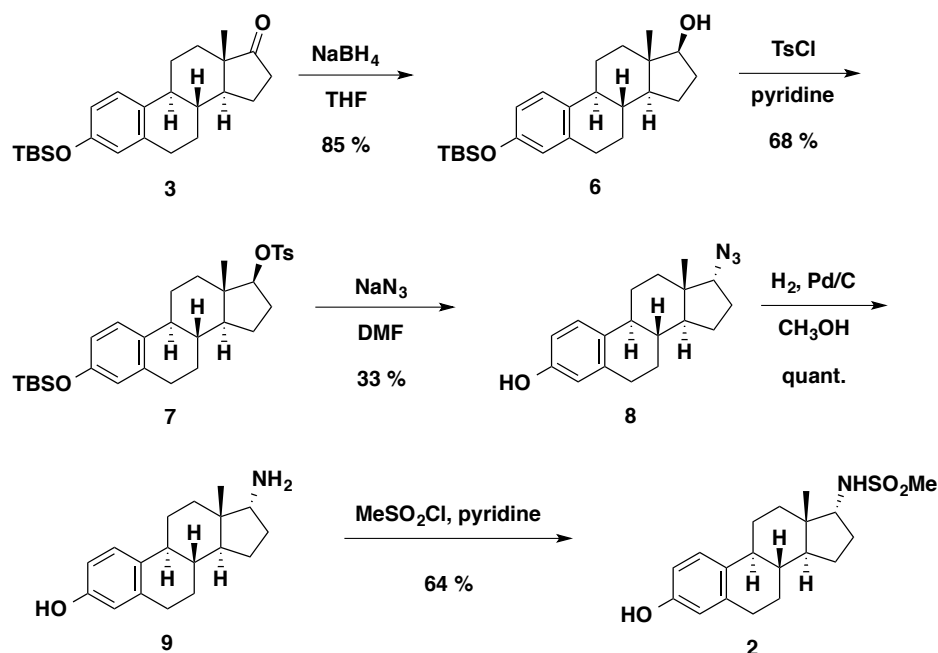


Figure 4.2 Schrodinger Ligand Interaction Diagram for Predicted Binding of IPI-926 with SMO



Scheme 4.1 Synthesis of Beta Sulfonamide

To construct the alpha isomer, protected estrone **3** was reduced from the more accessible face to provide alcohol **6**, which was then activated for displacement as the secondary tosylate **7**. Sodium azide in dimethylformamide, heated to reflux, installed the necessary nitrogen, temporarily masked as azide **8**. The low yield of this displacement reaction is attributed to the hindered nature of the secondary neopentyl tosylate. Hydrogenolysis resulted in reduction of the azide functionality as well as deprotection of the silyl ether to afford phenol **9**. Using a slight excess of methanesulfonyl chloride in pyridine, the desired alpha isomer **2** was isolated (**Scheme 4.2**).



Scheme 4.2 Synthesis of Alpha Sulfonamide

When both the alpha and beta isomers were tested in our Dual Luciferase Reporter (DLR) assay, we were pleased to find that these simple constructs were relatively inactive, suggesting that elaboration of the EF-ring system is necessary for activity. Relative to cyclopamine, the beta isomer exhibited loss in potency by a factor of eight, whereas the alpha isomer featured a reduction in potency by a factor of twenty. This difference in activity contradicts the original model proposed by Winkler, suggesting that the relationship between the oxygen and nitrogen of cyclopamine was essential for activity (**Figure 4.3**).

To summarize briefly, cyclopamine, the active inhibitor, is comprised of a DE-spirocycle, placing the oxygen above its iso-steroidal backbone, on the beta face, and the nitrogen, below the steroid backbone, on the alpha face. Tomatidine, an inactive

pseudo-isomer, lacks this spirocycle, and does not maintain this relative relationship between the oxygen, nitrogen, and steroidal backbone.

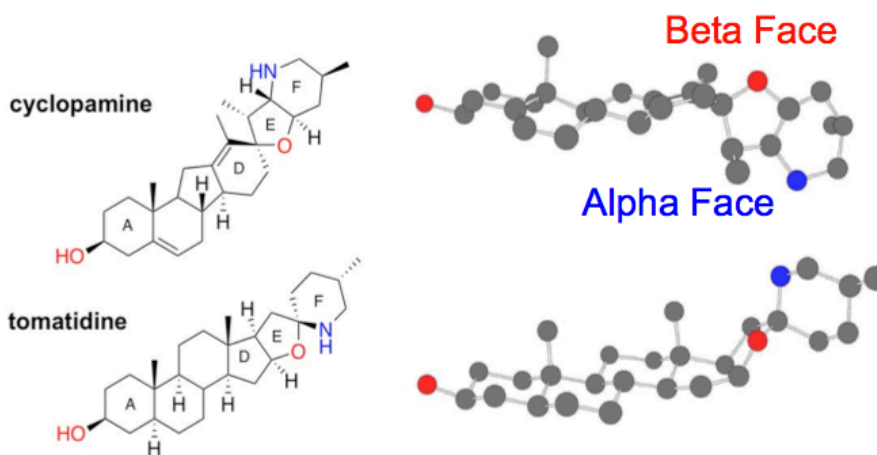


Figure 4.3 Proposed Binding Model: Alpha versus Beta Face

This model highlighted the suspected importance of the placement of the oxygen and nitrogen relative to the backbone. The increased activity of compound **2** relative to **1** demonstrates that having a nitrogen functionality on the alpha face is not preferred to the beta face in these simple constructs.

Section 4.2 Aryl-Aryl Coupled Analogs

Looking at the numerous available crystal structures of SMO bound to a ligand, the depth of the binding pocket varies depending on the analog present in the active site. This long, narrow, hydrophobic cavity spans almost thirty angstroms. The predicted docking positions of the estrone-derived analogs all show a positive interaction between a phenylalanine at the top of the pocket with the aromatic A-ring. This orientation of the

molecules leaves the majority of the pocket unoccupied. To address the importance of the depth of the pocket, I designed two aryl-aryl coupled analogs that could potentially pi-pi stack with an additional aromatic ring, forcing the EF rings deeper into the binding pocket (**Figure 4.4**).

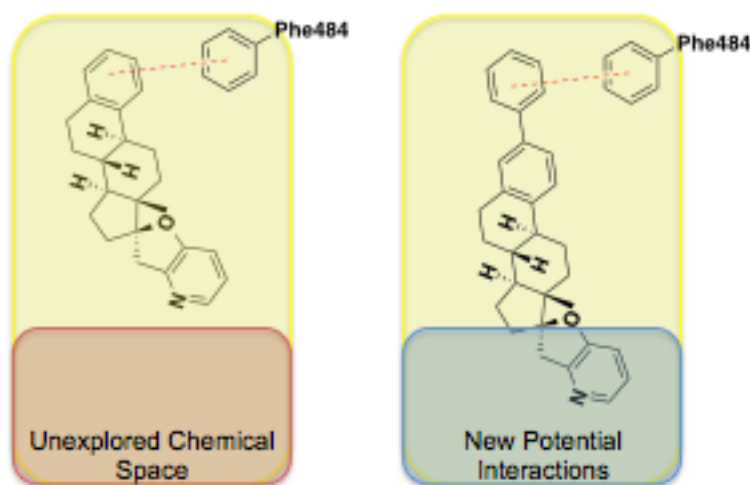
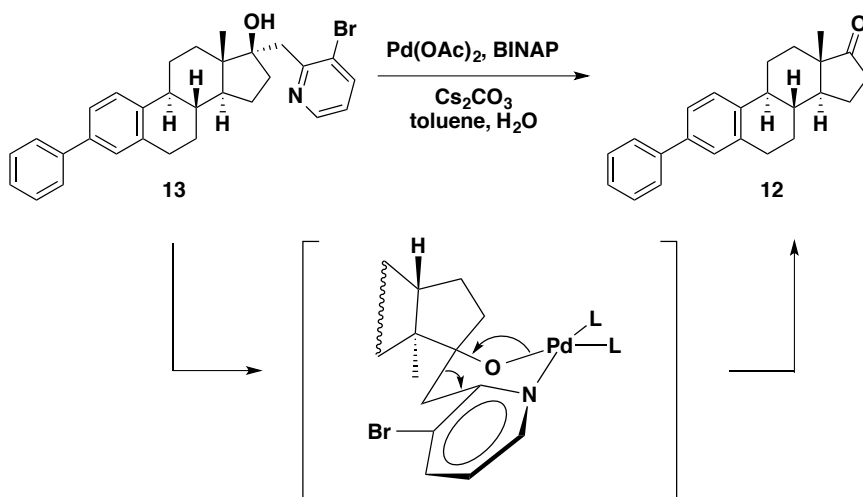


Figure 4.4 Depth of Pocket Hypothesis for Aryl-Aryl Coupled Analogs

To begin, two analogs were designed with a simple EF spirocycle while maintaining the aromatic F-ring of the original analogs. Although the saturated system provided more potency, the aromatic pyridine-derived analogs demonstrated great SAR thus far and were significantly easier to synthesize as a proof of purpose. Starting from commercially available estrone **10**, the C3 phenol was activated as the aryl triflate **11**. Palladium-mediated Suzuki cross-coupling with phenyl boronic acid allowed for the construction of the aryl-aryl system. Using freshly prepared lithium diisopropyl amide and 2-betabromopicoline, the benzylic lithium anion was added to the alpha-face of the

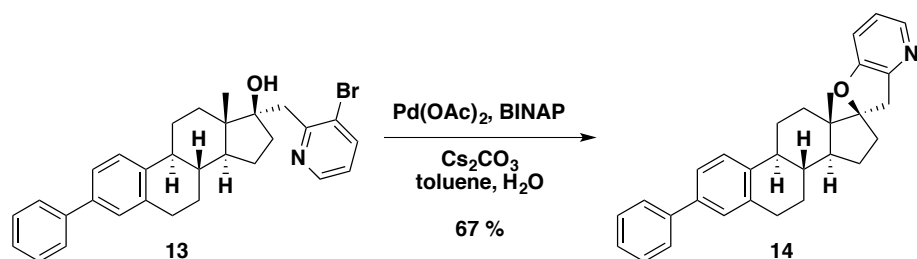
Completion of the phenyl-coupled analog was proposed to culminate with an intramolecular Buchwald Hartwig cyclization of alcohol **13**. Unfortunately, initial attempts of cyclization with palladium acetate and BINAP afforded only the retro-aldol product shown below (**Scheme 4.4**). Niwa and coworkers have shown that 2-pyridylmethyl species can undergo chelation-assisted cleavage of C_{sp3}-C_{sp3} bonds with palladium acting as a Lewis Acid.²



Scheme 4.4 Unexpected Retro-Aldol from Buchwald Hartwig Cyclization

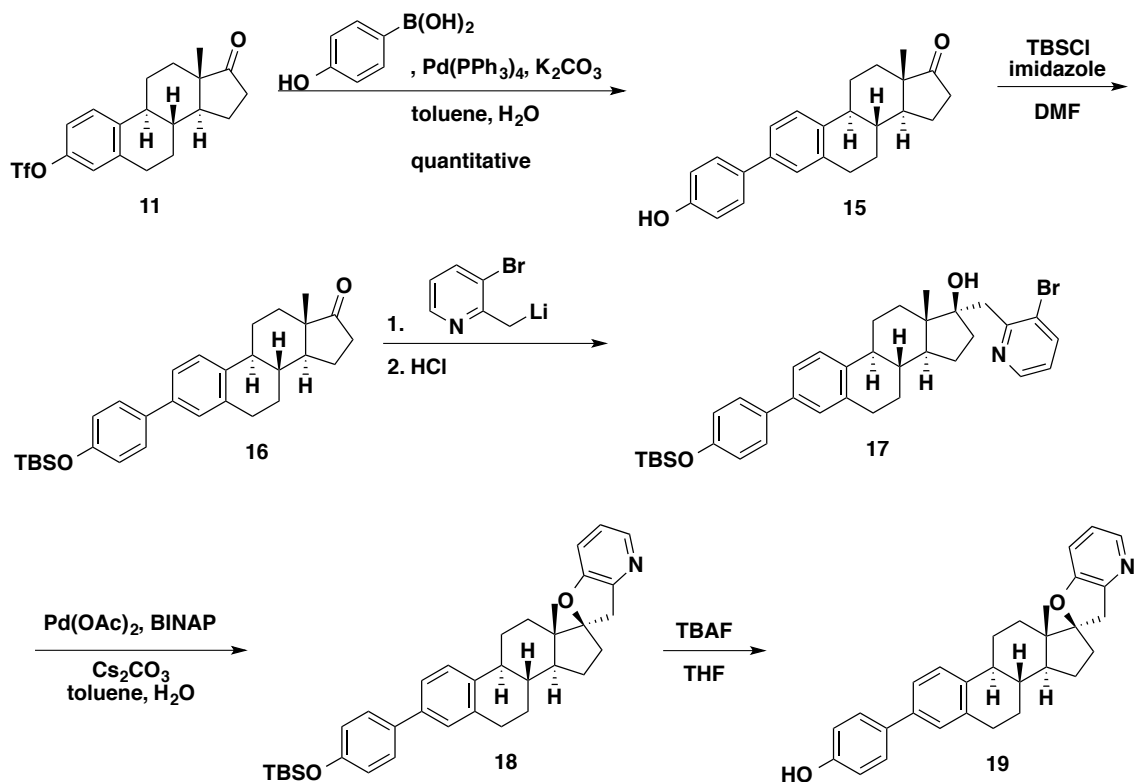
When constructing the original estrone analog, Isaacs reported consistently low yields of the desired spirocycle.³ I have found that in order to improve this yield and eliminate this retro-aldol pathway, the active catalyst must be preformed before the introduction of the Lewis basic nitrogen. By simply flash heating the palladium acetate with BINAP in toluene at 100 °C for 90 seconds followed by the addition of substrate, base, and water provided enough time and energy for the active Pd(0) catalyst to form

without interference from the nitrogen. Following this procedure, the desired analog **14** was isolated for analysis (**Scheme 4.5**).



Scheme 4.5 Completion of the Phenyl Aryl-Aryl Coupled Analog

In a similar fashion, the hydroxy phenyl aryl-coupled analog was constructed beginning with aryl triflate **11** (**Scheme 4.6**). Palladium-mediated Suzuki coupling with 4-hydroxyphenyl boronic acid⁴ provided the aryl-aryl system in compound **15**, which was protected as silyl ether **16**. Following the same series of addition and cyclization, bromo alcohol **17** was generated and subsequently cyclized using palladium acetate to afford spirocycle **18**. Deprotection of the alcohol with TBAF gave the desired analog **19**.



Scheme 4.6 Synthesis of Hydroxy Phenyl Aryl Coupled Analog

Biological evaluation of the compounds suggests that delving deeper into the pocket may not be necessary for the steroid analogs. Comparison of the phenyl aryl extended analog to the parent compound showed that activity was lost upon addition of the aryl group (**Figure 4.6**). When looking back to the crystal structure of cyclopamine bound to SMO, the majority of the molecule was positioned very close to the extracellular surface. The hydrophobic backbone of the alkaloid interacted with very few charged residues, whereas SANT-1, buried deep into the pocket interacted with exclusively polar residues (**Figure 4.7**).⁵

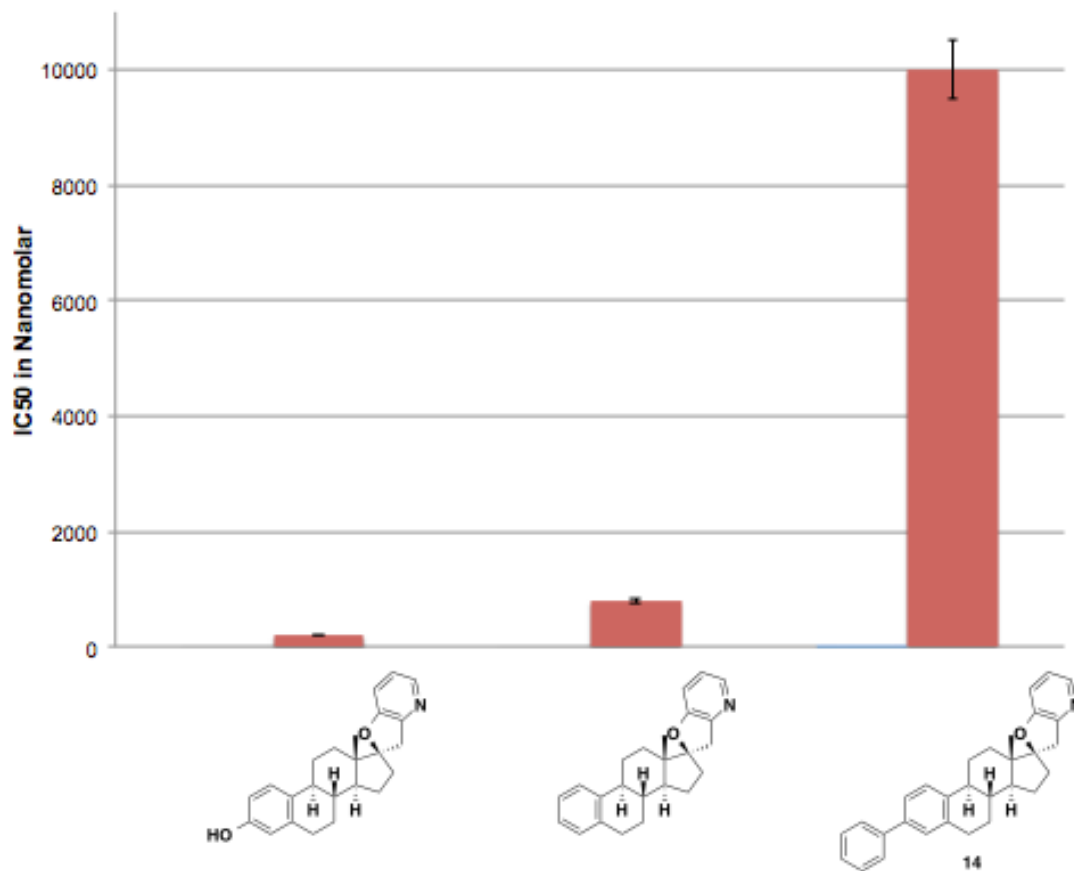


Figure 4.6 Biological Activity for Aryl-Aryl Coupled Analogs

This analysis in combination with the loss of activity in the DLR assay for the aryl-aryl extended analogs suggests that the structure of the steroid backbone should not be altered. Presuming that this hydrophobic backbone occupies that same cavity as cyclopamine, the EF-ring system should be exposed to the top polar portion of the pocket. Accumulation of additional favorable interactions may be accomplished by extending polar functionalities off of the pyridine system as opposed to pushing the hydrophobic backbone deeper into the charged part of the binding pocket.

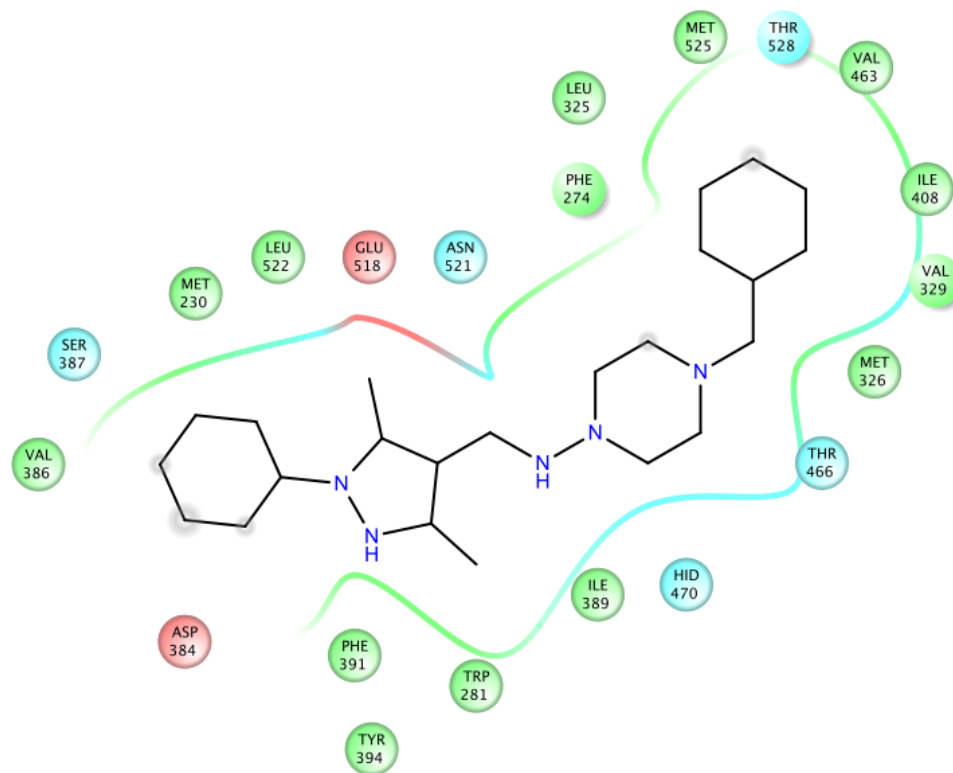
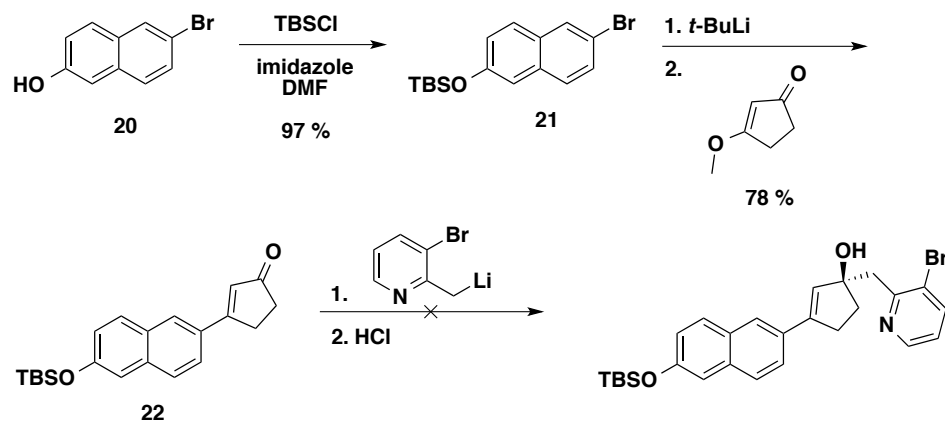


Figure 4.7 Ligand Interaction Diagram for SANT-1 with SMO

Section 4.3 Des-C Analogs and the Importance of Shape

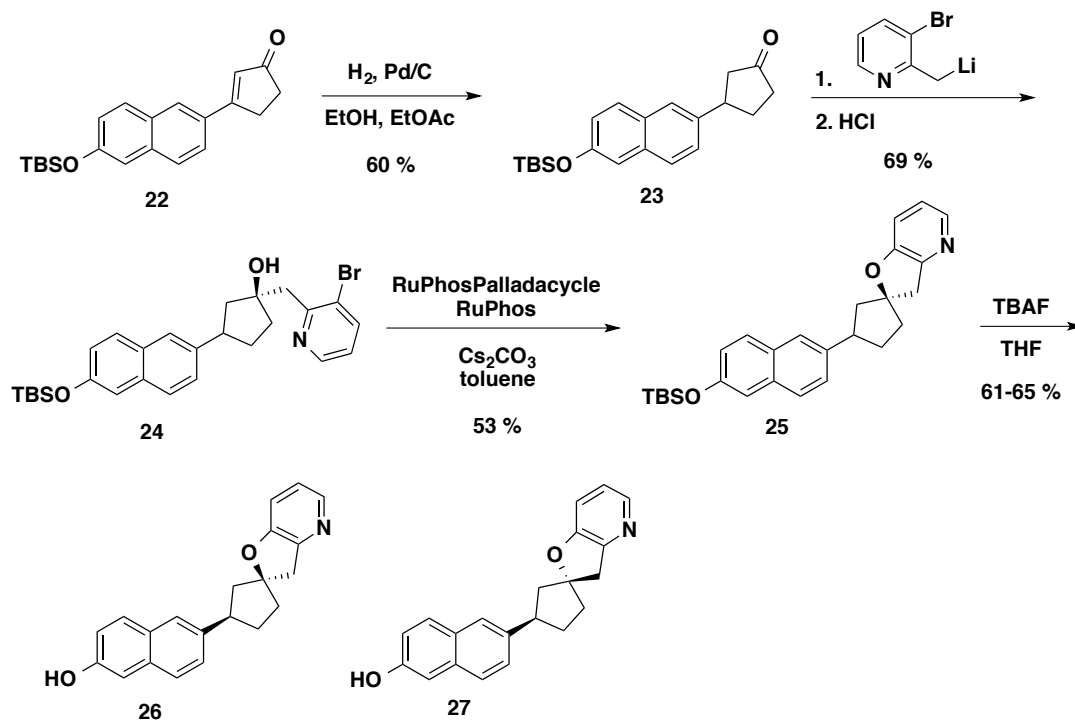
When looking at both the lead compounds synthesized by Infinity Pharmaceuticals and Eli Lilly, despite the vast differences in chemical identities, the overall shapes of the molecules are similar (**Figure 4.8**).⁶ These boomerang, or bent, molecules both adopt very different shapes as compared to the natural alkaloid cyclopamine. As Stefan Peukert, the SMO antagonist program director at Eli Lilly, indicated that all of their most active compounds exhibited the same overall bent shape, I decided to investigate the importance of shape in our system.



Scheme 4.7 Construction of des-C framework

The saturated cyclopentanone **23** generated from the reduction of **22** was a more competent electrophile, and lithiated beta-bromopyridine could be added without the use of cerium to construct alcohol **24** as a mixture of diastereomers. A preformed RuPhosPalladacycle was used to effect the Buchwald Hartwig reaction to construct a separable mixture of diastereomeric spirocycles **25**. Deprotection of the aryl silyl ethers with TBAF provided epimeric des-C analogs that placed the oxygen on the concave face in **26** and on the convex face in **27** (Scheme 4.8).

These truncated Des-C analogs were not potent in our DLR assay, and similar to the Des-B analogs discussed in Chapter 1, compound **26** was shown to inhibit luciferase. As the inhibitory activity towards SMO cannot be determined for substrates that inhibit firefly luciferase, compound **26** was removed from the analysis. Interestingly, compound **27**, where the oxygen faces the convex face and the nitrogen of the pyridine lies on the concave side, did not inhibit luciferase; however, this compound was also inactive in the DLR assay.



Scheme 4.8 Synthesis of Bent Des-C Analogs

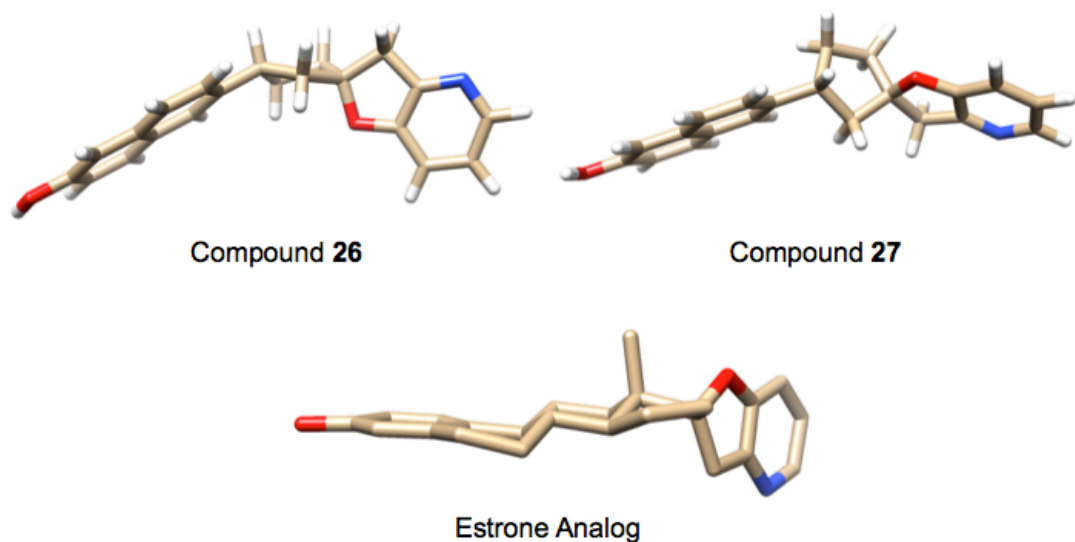


Figure 4.9 Relative Shapes of Des-C Analogs in Comparison to Original Analog

Moving forward, the overall linear nature of our molecules does appear to serve a purpose within the binding pocket, but more importantly, it prevents these steroid analogs from inhibiting luciferase, allowing for the analysis of these molecules with our previously established DLR assay. Additionally, by starting from commercially available estrone with no need to modify the ABCD ring system, we can synthesize more readily available analogs directly.

Section 4.4 Androsterone Derived Oxetane Analog

Described above, the use of estrone as a hydrophobic surrogate for the backbone of cyclopamine, although initially selected for practicality and ease of synthesis, appears to be more important than originally hypothesized. It has been shown that truncation of the backbone, both with Des-B and Des-C systems, result in loss of potency as well as incompatibility with our DLR assay. Additionally, the computational modeling proposed a strong pi-pi interaction between the aromatic A-ring of estrone and a phenylalanine at the top of the binding pocket. To probe the importance of aromaticity of the steroid backbone, an analog containing the exocyclic oxetane pyrrolidine on an androsterone backbone was designed.

Compared to estrone, androsterone, an endogenous steroid that has a fully saturated ABCD ring system, exhibits more structural similarity to the natural alkaloid cyclopamine. Based on the biological evaluation of the previously synthesized analogs, it is clear that the subtle changes in the EF-ring systems are involved in activity of the

molecules. By placing the most potent variation of the EF-ring system on the androsterone backbone the role of the aromatic A-ring can be elucidated (**Figure 4.10**).

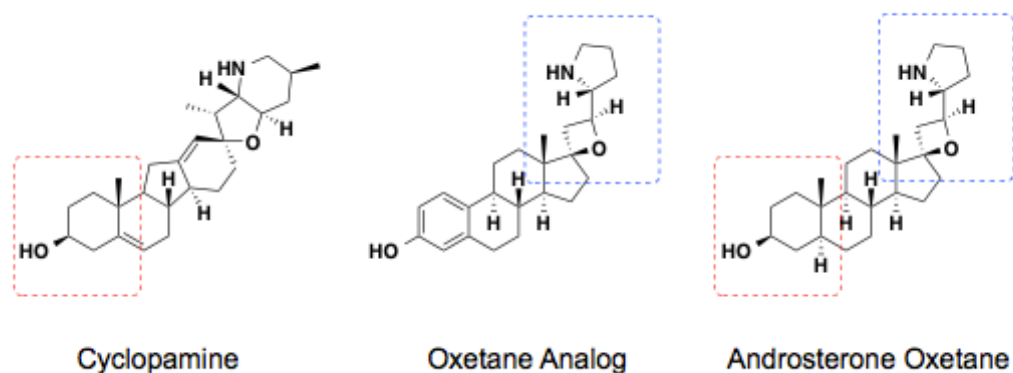
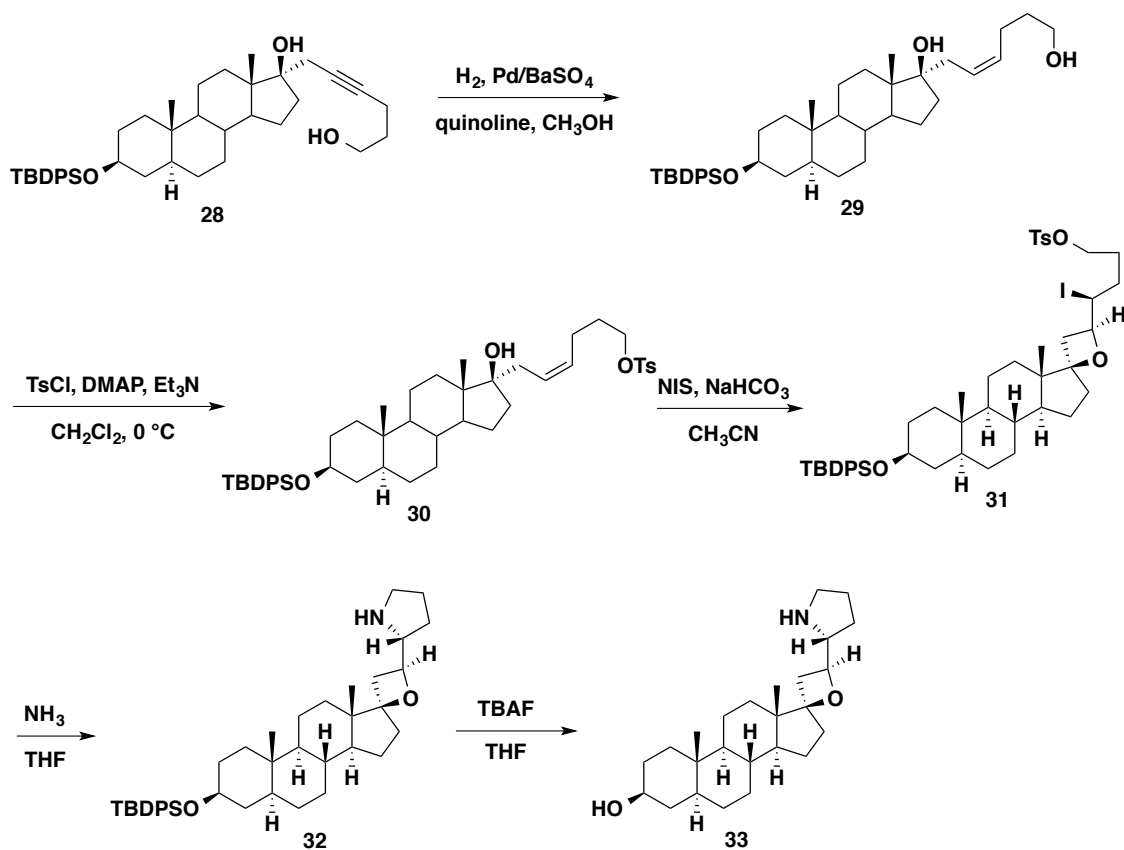


Figure 4.10 Development of Androsterone Oxetane Analog

Following the synthesis first developed by Dr. Zhihui Zhang, Dr. Michelle Estrada constructed the androsterone oxetane analog using an amended procedure that was optimized for reproducibility (**Scheme 4.8**). The key alkynyl diol **28** was constructed from commercially available starting materials via an epoxidation and subsequent ring opening. The alkyne was reduced to the *cis* alkene **29** using Lindlar's catalyst, and the primary alcohol was selectively activated for displacement as tosylate **30**.

The key transformation was originally carried out with iodine, but upon replication of these results, it was found that the oxetane moiety was unstable in acidic environments. By switching the source of electrophilic iodine to *N*-iodosuccinimide, the 4-exocyclic iodoetherification was both reproducible and scalable. Using these newly developed conditions, tosylate **30** was cyclized to oxetane **31**. Using liquid ammonia to

displace both the secondary iodide and primary tosylate constructs pyrrolidine **32**, and deprotection of the silyl ether unveils the alcohol, completing the synthesis of the androsterone oxetane analog **33** (Scheme 4.8).



Scheme 4.8 Synthesis of A-Ring Saturated Oxetane Analog

The biological evaluation of this analog further validated the computational model and confirmed that the aromaticity of the A-ring is essential for activity (**Figure 4.11**). The predicted IFD score for the binding of analog **33** correlates well with the curve generated from predicted values of previously tested compounds. Moving forward, we

believe that estrone is an ideal backbone to use for the development of SMO antagonist analogs for multiple reasons. First, this material is non-plant derived and is commercially available. Additionally, steroids are well-tolerated within the body, and lastly, the estrone backbone has an aromatic A-ring that is important for activity of these analogs as inhibitors of the SHH signaling pathway.

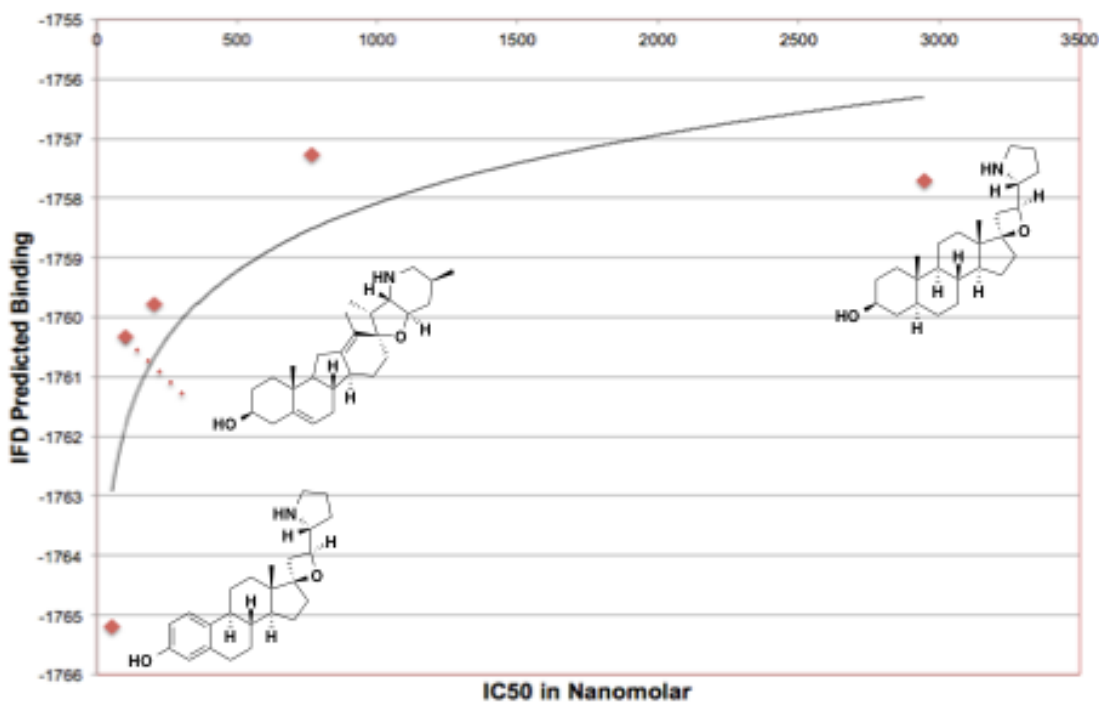


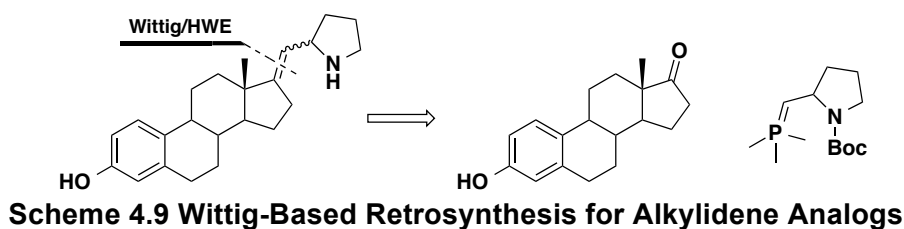
Figure 4.11 IFD Predicted Binding Affinity for Androsterone 33

Section 4.5 Establishing the Role of Oxygen

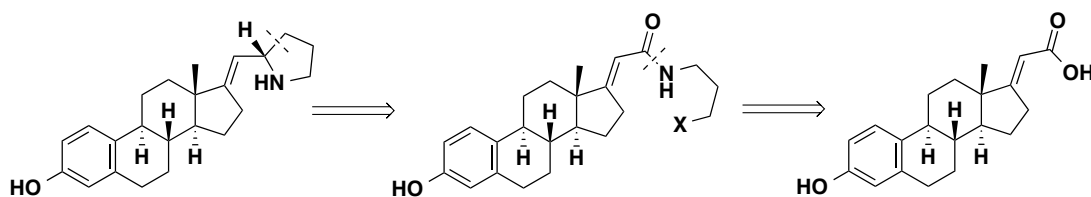
Upon analysis of the most potent analog and its predicted binding orientation, it is unclear what role, if any, the oxygen atom plays. To assess the involvement of the oxygen in binding affinity, a series of analogs were designed that lack the oxetane

functionality. Using a carbon-carbon double bond as a surrogate for the oxetane ring, we began to explore the development of des-E ring analogs.

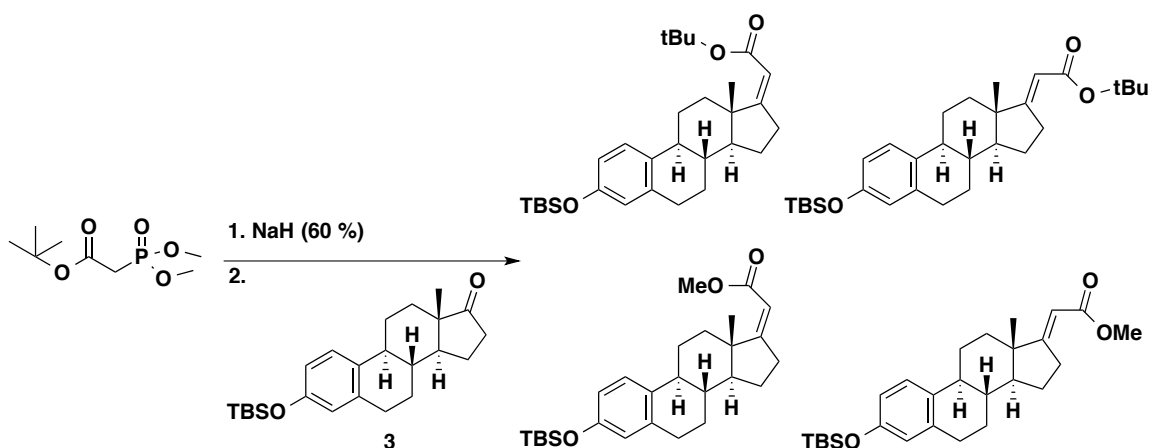
The first route designed to access the deoxygenated analog was using estrone as an electrophile and a proline-derived ylide to construct the carbon-carbon bond using traditional Wittig chemistry (**Scheme 4.9**). After synthesizing the ylide component in four steps from proline, all attempts to produce the final product resulted in only deprotonation of the alpha protons of the steroid and enolization of the carbonyl.



The second retrosynthetic design of these analogs involved construction of the F-ring last with the selective deprotonation of the allylic C-H bond and cyclization on a primary leaving group.⁸ This allylic system would be accessed from the reduction of an amide, the latter of which would be synthesized from a peptide coupling between a steroid derived carboxylic acid and a protected primary amine (**Scheme 4.10**).



To begin, a Horner-Wadsworth-Emmons olefination with *tert*-butyl *P,P*-dimethylphosphonoacetate and protected estrone **3** was carried out to construct a mixture of *E* and *Z* isomers of the unsaturated butyl esters (**Scheme 4.11**).⁹ Due to the bulky substituent on the ester, the alkene isomers can be separated on silica. Upon scale up of this reaction, the product was contaminated with both isomers of the unsaturated methyl ester. This byproduct could not be removed from the desired products resulting in an unproductive mixture. The only method of purification resulting in modest yields of pure materials was preparatory thin layer chromatography.



Scheme 4.11 Generation of Unsaturated Esters

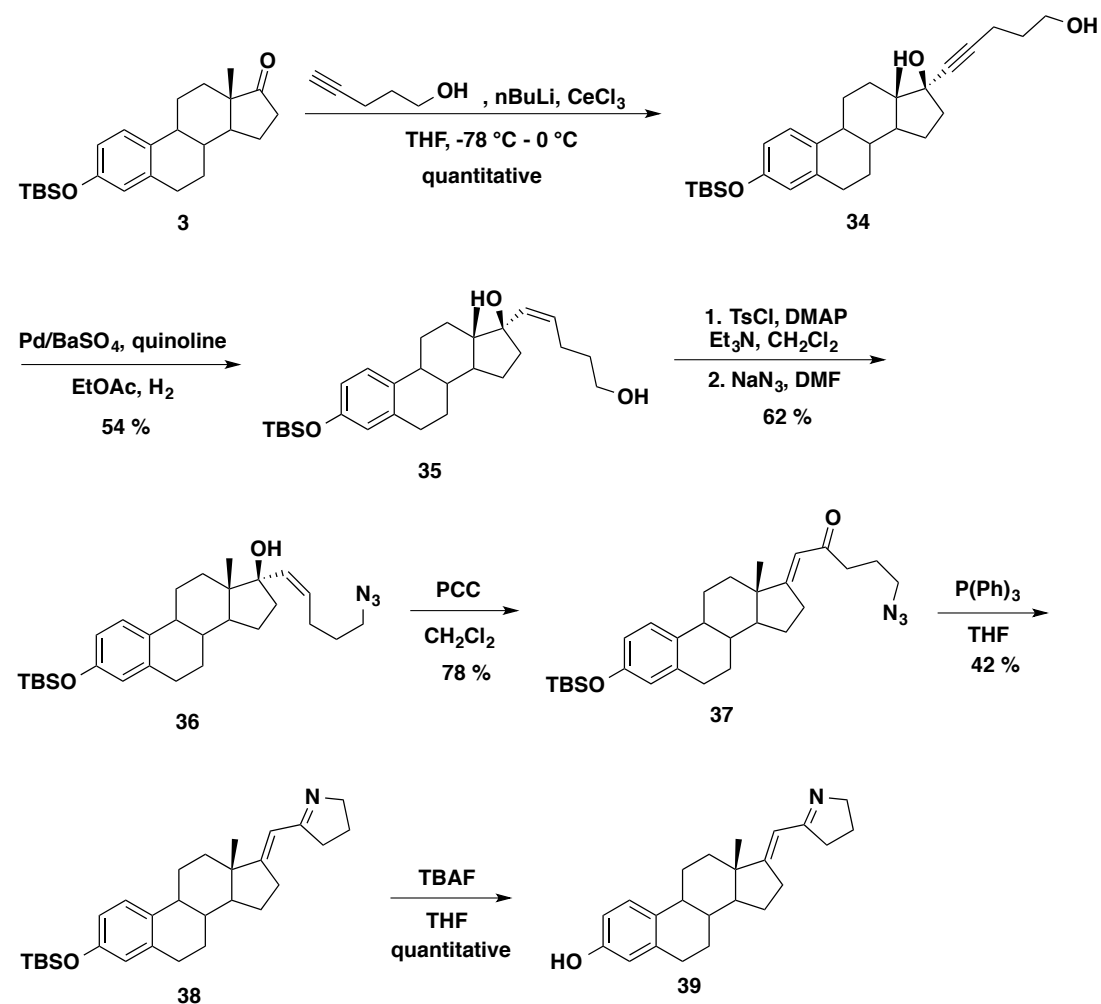
Despite the initial positive results with this pathway, the difficulty in obtaining appreciable amounts of materials for the key steps proved to be problematic. To circumvent this problem of scalability, a third-generation route was devised.

Beginning with protected estrone **3**¹⁰ (**Scheme 4.12**), the addition of the cerium dianion of pentyn-1-ol afforded diol **34** in excellent yields. The use of cerium trichloride was necessary to attenuate the basicity of the lithium anion, which, when added to **3**, resulted in only enolization and isolation of starting material. Reduction of the alkyne to

the *cis* alkene with Lindlar's catalyst gave diol **35**, which could be selectively functionalized at the more available primary alcohol. Activation of the primary alcohol as a tosylate allowed for the displacement with sodium azide to install the necessary amine functionality of **36**.

Azido alcohol **36** underwent a chromium-mediated [allylic](#) oxidation to afford the unsaturated enone **37**; the stereochemistry of the double bond was confirmed by two-dimensional NMR (noe). To cyclize the F-ring, a one pot Staudinger-Aza-Wittig reaction sequence was designed with triphenylphosphine.¹¹ First, the azide was reduced via an intermediate iminophosphorane. Following the activation of the azide, the iminophosphorane attacks the carbonyl intramolecularly and expels triphenylphosphine oxide, generating the unsaturated imine **38**. Removal of the protecting group affords compound **39**, an unsaturated des-E analog. Attempts towards selective reduction of the imine in a 1,2 fashion proved unsuccessful. A variety of conditions were screened but ultimately only the 1,4 reduced product or destruction of the pyrrolidine ring were observed.

Compound **39** allows for the evaluation of several structural features as compared to the lead oxetane. First, the removal of the oxygen atom will provide insight as to whether the lone pairs of the oxygen are useful in binding. Additionally, at biological pH, the imine will most likely be protonated, offering a similar, but distinct, hydrogen-bonding partner. Lastly, the unsaturation in this molecule could serve as a Michael acceptor allowing for non-reversible binding and increased affinity for SMO.



Scheme 4.12 Synthesis of Unsaturated Imine

Based on the molecular modeling, the geometry of the double bond does not appear to make a large difference in binding affinity. The hydrophobic backbone has enough room in the pocket to completely flip over suggesting that the most favorable orientation of the heterocycle would be predominant. Biological evaluation of this unsaturated imine revealed a complete loss in potency, suggesting that the role of the oxygen may be more than simply providing an orientation for the pyrrolidine.

Section 4.6 Rigidity versus Flexibility

Although compound **39** is not an exact deoxygenated mimic of the lead compound, thus far, it has been suggested that the oxygen atom is contributing to the potency of the analogs. Our next objective was to illuminate whether the rigid scaffold would be preferred to a more flexible linker. Despite the high potency of the oxetane analog, the rigid nature of the ligand may not offer the best possible fit within the binding pocket. To explore the role of rigidity as well as distance, we designed alkyne and alkane derivatives that maintained the oxygen and nitrogen heteroatoms in the most potent analog (**Figure 4.12**).

Using energy minimized structures, the distances between the oxygen and nitrogens were calculated. The oxetane analog maintains a distance of approximately three angstroms, whereas these analogs offer more space between the heteroatoms and also allow for more possible binding conformations. When comparing these two scaffolds, the alkyne isomer offers much less conformational freedom than the alkane isomer, and we hoped to utilize this difference to elucidate the importance of flexibility. Additionally, the alkane derivatives could adopt many unique conformers to orient the pyrrolidine in the most productive manner for binding whereas the alkyne isomers can act more as a rigid ruler.

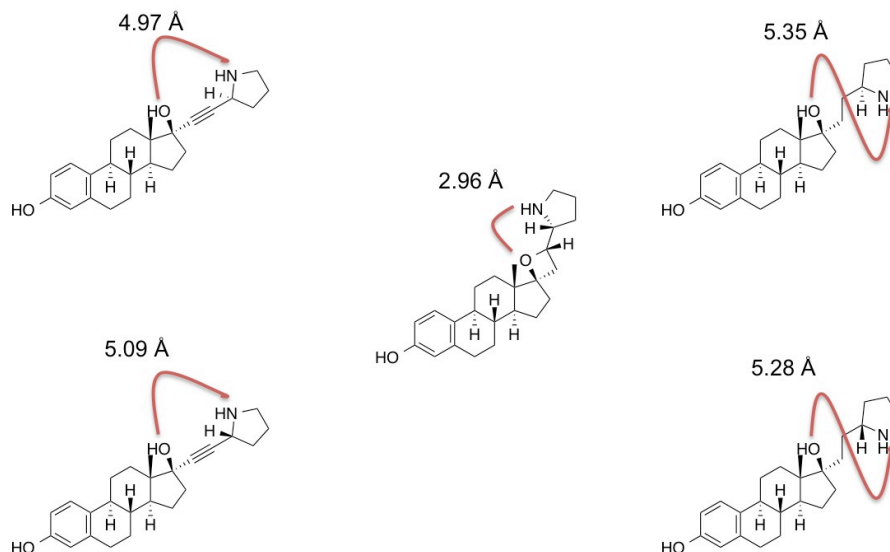


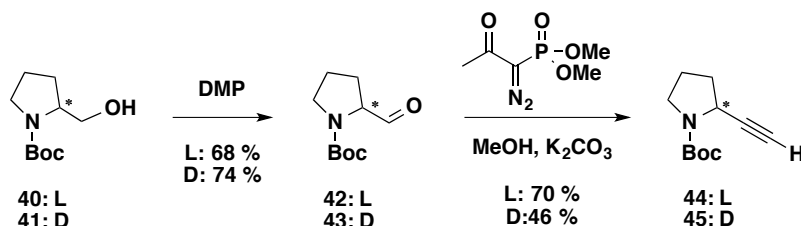
Figure 4.12 Heteroatom Distances for Rigid and Flexible Analogs

To begin, our first set of analogs maintained the carbon framework of the oxetane analog but opens the strained four membered ring allowing for the pyrrolidine to sample more conformations inside the binding pocket. Both L- and D- proline analogs were developed. Based on the computational modeling and energy minimized structures, we felt that the L- and D-derived analogs would have similar potencies. Although not derived from an amino acid, the oxetane analog exhibits the same chirality as D-proline. We hoped to show that both epimers would perform similarly, thus eliminating the need to carry forward the unnatural amino acid.

The carbon framework was assembled through the addition of protected alkynes derived from proline. Alkynes **44** and **45**¹² were achieved through an Ohira-Bestmann homologation of the chirally pure prolinals **42** and **43**.^{13,14} The aldehydes were

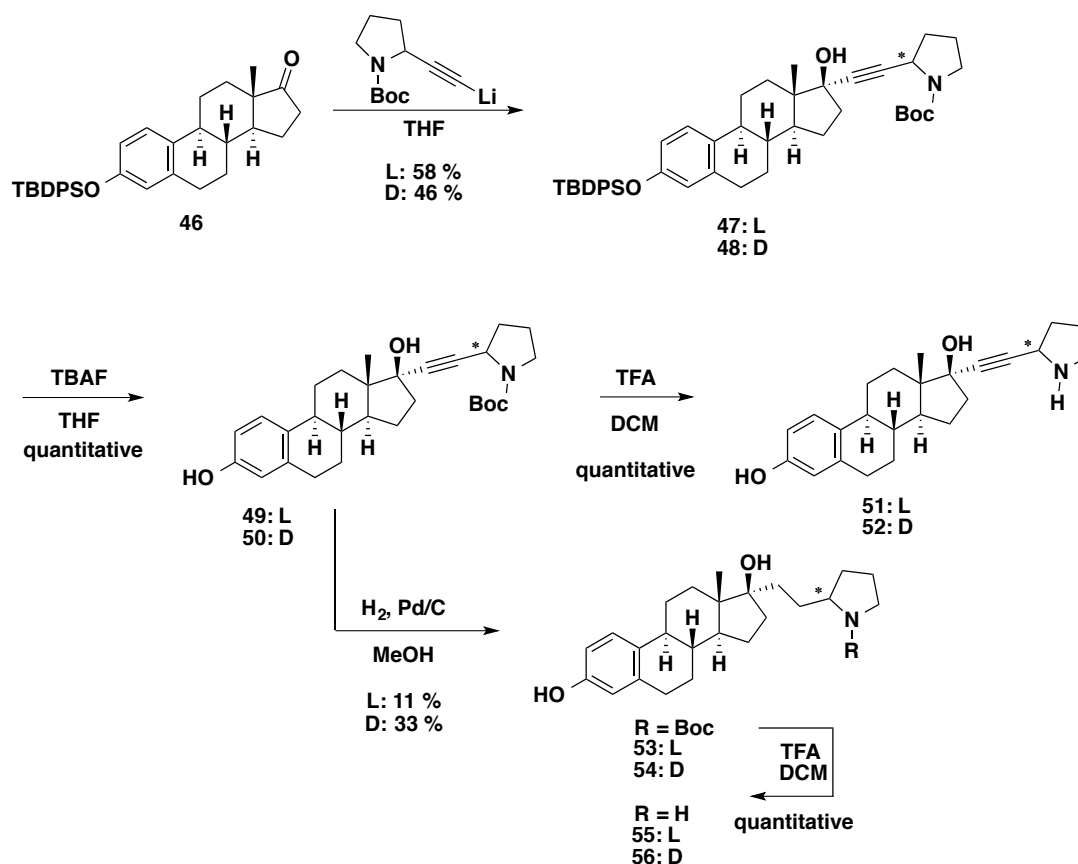
synthesized from the corresponding Boc-prolinols via oxidation with Dess Martin

periodinane (Scheme 4.13).



Scheme 4.13 Ohira Bestmann Synthesis of Proline Alkynes

Using TBDPS protected estrone **46**, the alkyne nucleophile **44** was added to afford alcohol **47** (Scheme 4.14). Use of excess nucleophile and slow addition of the electrophile resulted in the desired product with minimal recovery of starting material. The A-ring of the alkynyl alcohol **47** was deprotected with TBAF and carried forward through two distinct pathways. After exposure to trifluoroacetic acid, the carbamate was removed to unveil a secondary amine, and the resulting alcohol **51** was tested for activity. Additionally, protected alkyne **49** was reduced to give the saturated ring opened analog **53** which was deprotected to furnish **55**. Both **51** and **55** were pursued for biological activity. All transformations were also carried out with the D-proline variant (even numbered analogs).



Scheme 4.14 Synthesis of Flexible Scaffolds

Removal of the oxetane ring allows the pyrrolidine more freedom to rotate around multiple bonds. The alkyne analog possesses a much smaller window of space for pyrrolidine to occupy, whereas the fully saturated linker can rotate around multiple carbon-carbon single bonds, offering the widest range. Biological evaluation of these analogs offered valuable information (**Figure 4.13**). First, the removal of the oxetane resulted in a global loss of potency. Interestingly, the D-proline derived analogs consistently showed greater potency than the L-derived counterparts. Also, the alkyne analogs resulted in a completely inactive compound whereas the alkane analogs, although not as potent as the lead, were significantly more active.

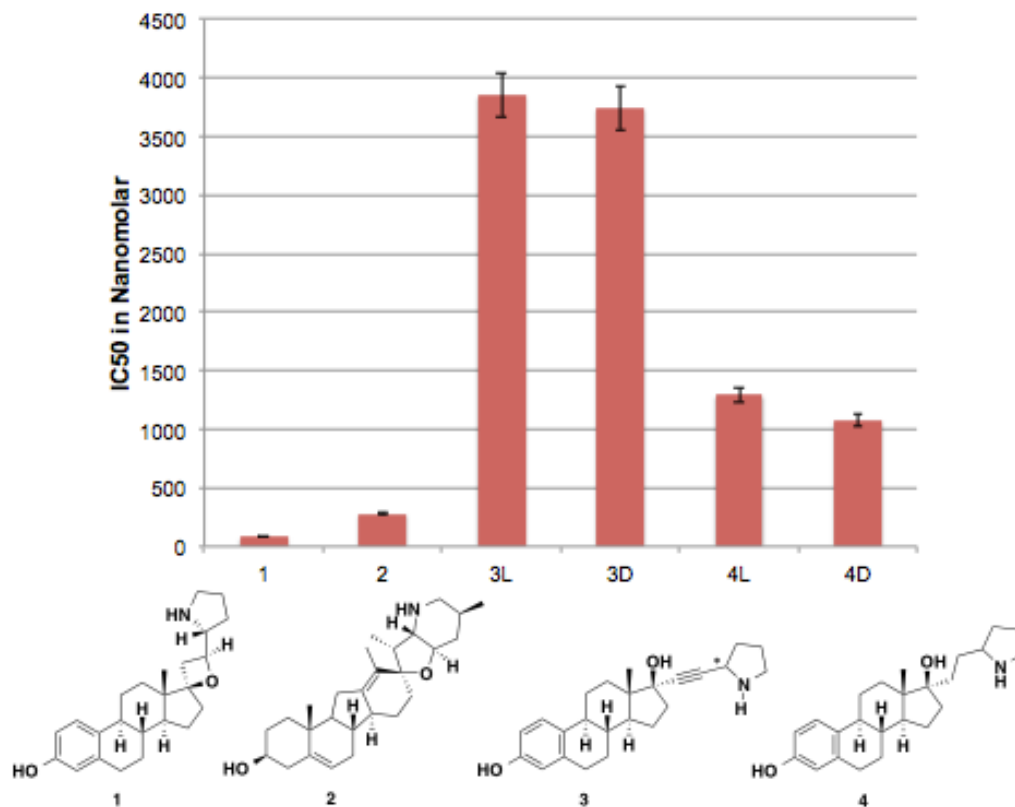


Figure 4.13 IC₅₀ Data for Flexible Linked Analogs

Section 4.7 Regenerating Rigidity without Oxygenation

To further pursue the role of rigidity and oxidation, a route was designed to construct des-E alkylidene analogs via the addition of hydride to a Tsuji-Trost pi-allyl system (**Figure 4.14**). The pivotal allylic acetates would be functionalized from the allylic alcohols, which in turn would be generated by addition of the steroidal vinyl anion to a variety of aldehydes.

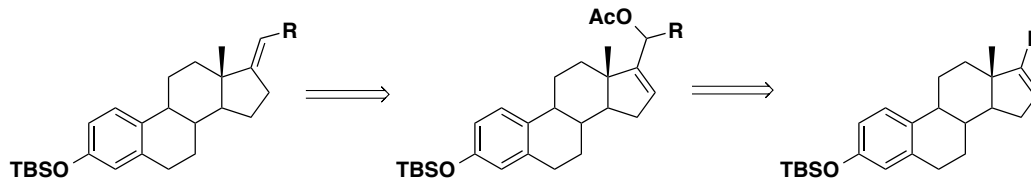
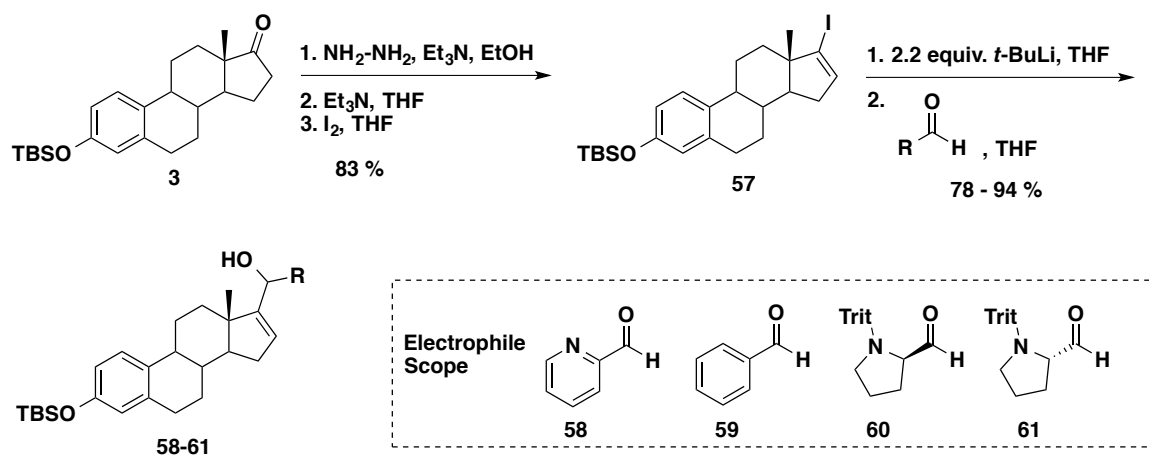


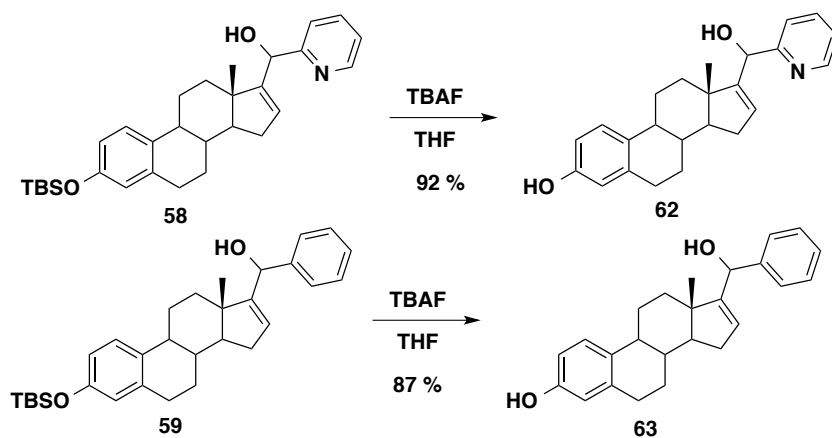
Figure 4.14 Retrosynthetic Design of Alkylidene Analogs

Beginning with protected estrone **3** (**Scheme 4.15**), the carbonyl was first converted to the hydrazone with hydrazine and base. After removal of the solvent, sequential addition of triethylamine followed by iodine resulted in the elimination of nitrogen gas and the construction of vinyl iodide **57**. Lithium halogen exchange proceeded smoothly with a variety of electrophiles featuring both saturated and unsaturated rings to generate a small library of allylic alcohols **58-61**. It is noteworthy that the nature of the protecting group on the prolinal was essential for reactivity. Benzylic and carbamate protecting groups were too small, and only recovered dehalogenated vinyl product was observed. Switching to the large trityl protecting group prevented this reactivity.¹⁵



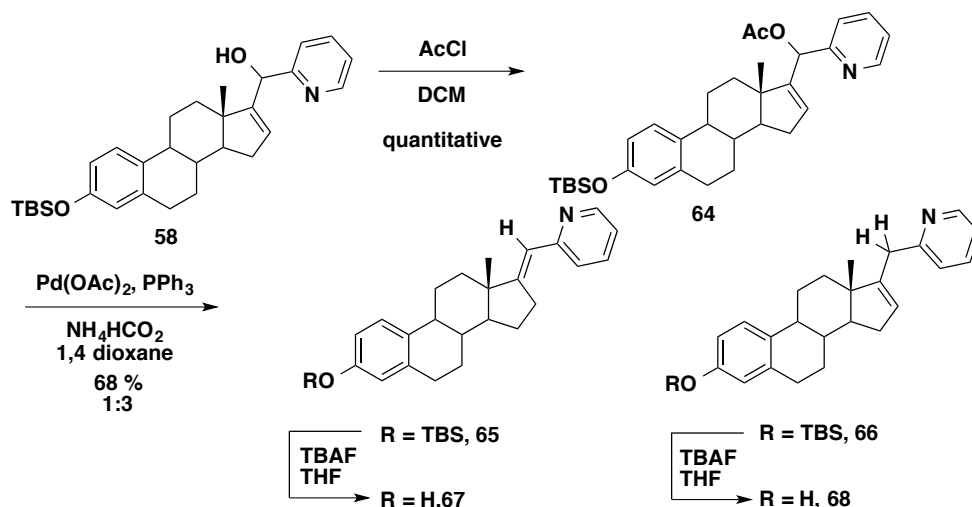
Scheme 4.15 Synthesis of Allylic Alcohols

At this stage we had hoped to isolate this intermediate and evaluate the allylic alcohols for biological activity. Deprotection of the pyridyl and phenyl derived analogs proceeded without issue to afford **62** and **63**, respectively (**Scheme 4.16**). Unfortunately, every condition employed to remove the trityl group from the sterically encumbered environment resulted in decomposition of either the aromatic system or the allylic alcohol. Completion of the saturated pyrrolidine analogs will be discussed in later sections.



Scheme 4.16 Completion of Phenyl and Pyridyl Allylic Alcohols

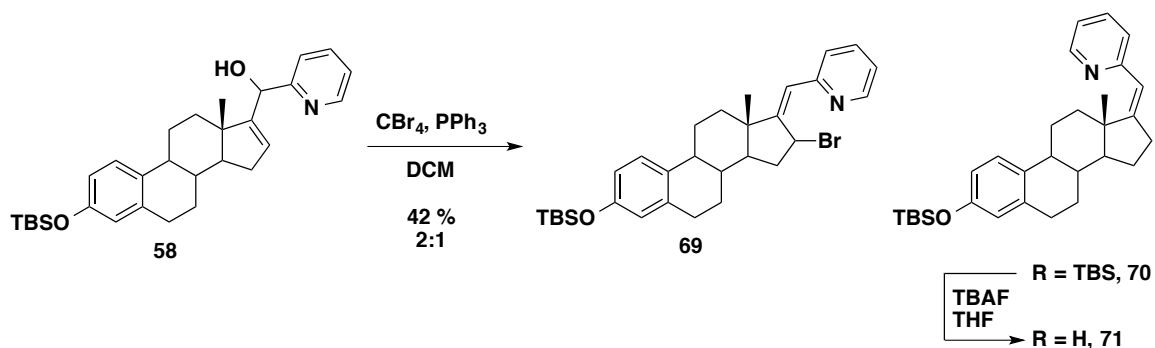
At this point, we were ready to pursue the key transformation. Allylic alcohol **58** was converted to acetate **64** in excellent yield with acetyl chloride (**Scheme 4.17**). Tsuji-Trost pi-allyl chemistry was implemented with palladium acetate and ammonium formate as the source of hydride.¹⁶ Although the transformation occurred in a relatively high overall yield, the ratio of unconjugated (**66**) to conjugated (**65**) product was 3:1 for the undesired isomer.



Scheme 4.17 Tsuji-Trost Elimination of Allylic Acetate

Both analogs were carried forward through deprotection to generate the conjugated *trans*-alkene **67** and unconjugated isomer **68**. Our main goal using this route was to construct both aromatic and saturated analogs through this elimination process. The pilot analysis with the pyridyl ring suggested that there was a preference for the unconjugated product, even in the presence of an aromatic group. This preference could be due to allylic strain in the conjugated product. For this reason, we believed that with saturated analogs the barrier to generate exocyclic isomers would be too high.

By switching the method of activation and elimination via Appel conditions with triphenylphosphine and carbon tetrabromide, we saw both isomers of the conjugated vinyl bromide (**Scheme 4.18**). Upon purification on silica gel, the *cis*-alkene isomer was identified as the unexpected dehalogenated species **70**. Deprotection of compound **70** with TBAF in THF completed the set of *E*-, *Z*-, and unconjugated pyridine isomers for biological analysis.



Scheme 4.18 Completion of *cis*-pyridyl Analog

Biological evaluation of this family of analogs revealed a wide range of potencies (Figure 4.15). First, despite the original hypothesis that both the oxygen and nitrogen were essential for activity, the second most potent analog, phenyl allylic alcohol **63**, does not contain a second heteroatom. Interestingly, the pyridine derivative of the allylic alcohol **62** does not exhibit this same activity. One possible explanation for this difference is that the allylic ether **63** is simply acting as an electrophile inside the binding pocket. Activation of the alcohol would activate the alkene for nucleophilic attack and displacement of the activated hydroxyl. In the presence of a Lewis acidic amino acid, the oxygen of the phenyl allylic alcohol could be activated. Conversely, in the pyridyl analog **62**, the nitrogen may preferentially become activated, resulting in a weaker electrophile.

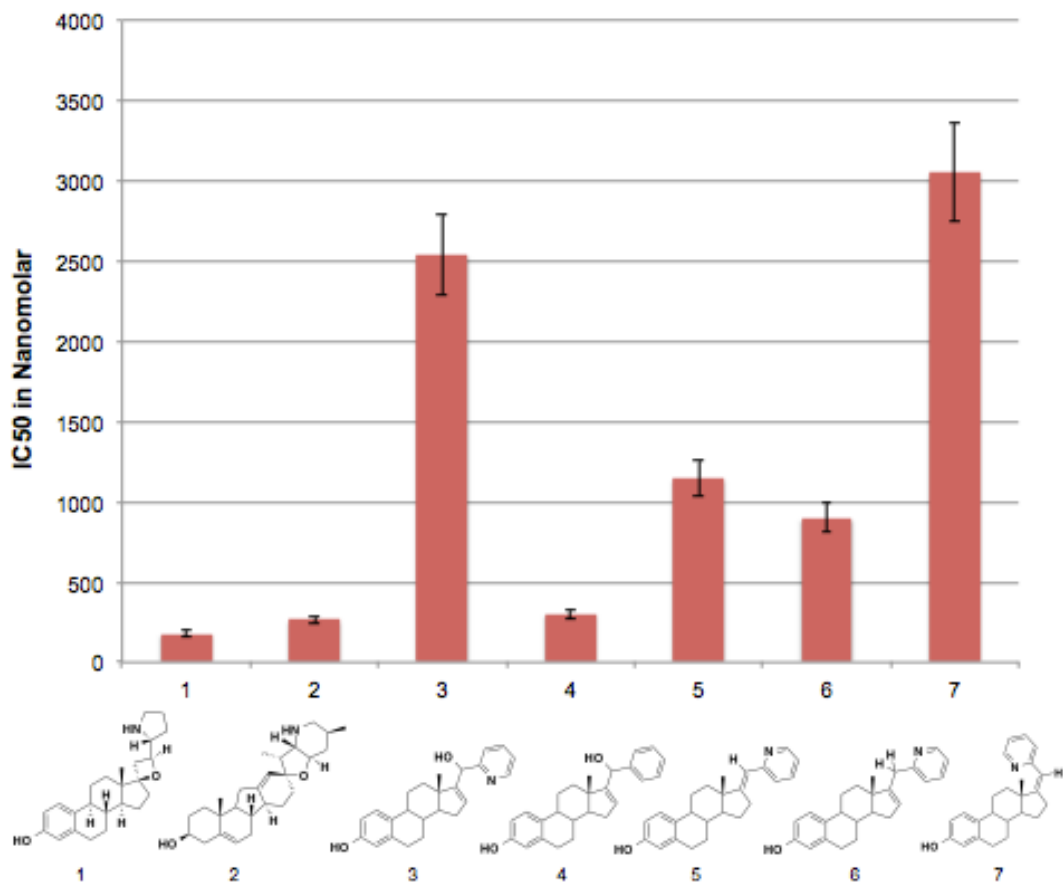


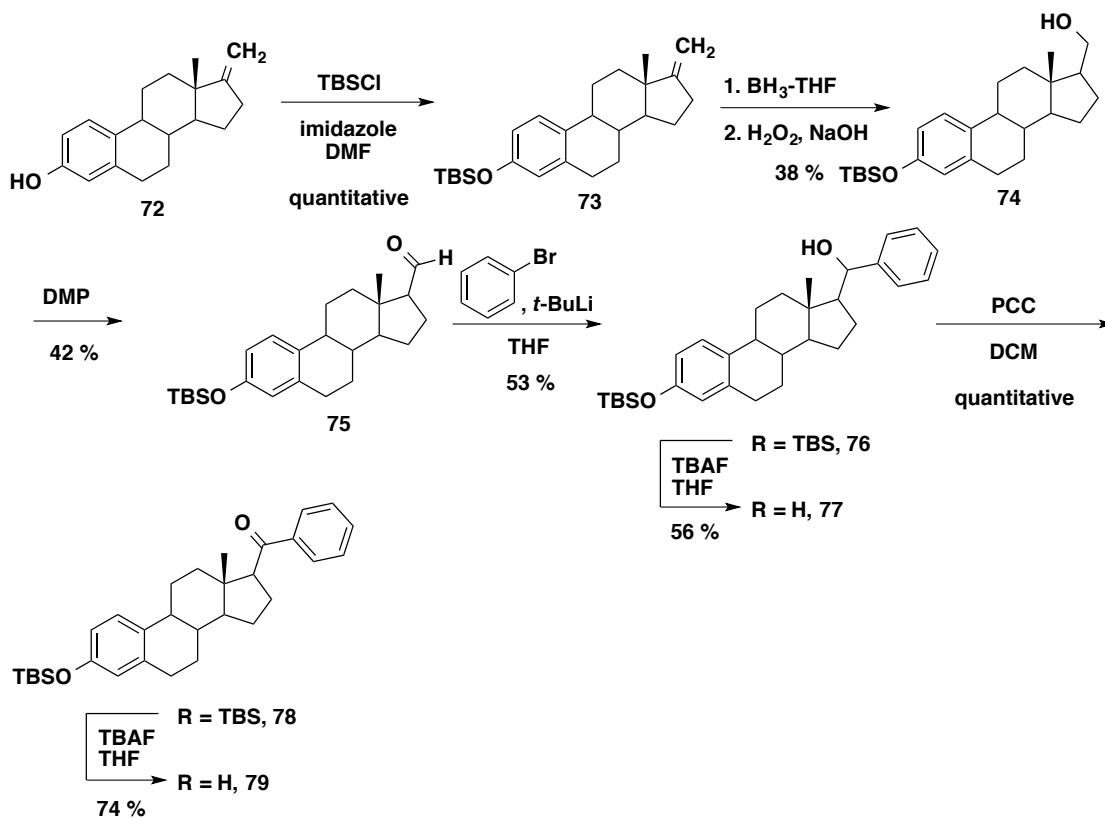
Figure 4.15 Biological Activities of Allylic Alcohols and Derivatives

Furthermore, the relationship between *E*-, *Z*-, and unconjugated pyridyl alkenes is especially interesting. The *trans*-alkene **67** and the unconjugated isomer **68** possess approximately the same potency. On the other hand, *cis*-alkene **71** exhibited a complete loss in potency. Moving forward, construction of exclusively *cis*-alkenes did not seem necessary.

Section 4.8 Second Generation Derivatives of Phenyl Allylic Alcohol

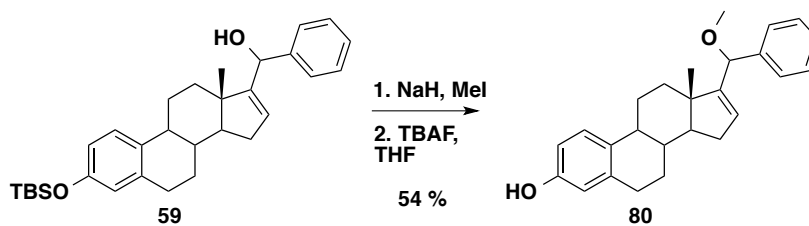
With an identification of another potent analog, it is important to tease out the necessary functionality required for this activity. As previously mentioned, the allylic alcohol may become activated inside the binding pocket and serve as an electrophile. To test this hypothesis, a series of modified compounds were constructed that either removed the ability of the molecule to act as an electrophile through unsaturation or enhanced the ability to act as an electrophile by oxidation. Disruption of the hydrogen-bonding network was also investigated while maintaining the unsaturation.

First, two saturated analogs were synthesized to assess the importance of the potential electrophilicity of the allylic alcohol system (**Scheme 4.19**). Beginning with methylene estrone **72**, protection of the free phenol as the silyl ether provided methylene **73**. Hydroboration and oxidation of the methylene provided primary alcohol **74**, which was selectively oxidized to aldehyde **75** with Dess Martin Periodinane, furnishing our electrophilic partner. Lithium halogen exchange with *tert*-butyllithium and bromobenzene followed by addition of **75** assembled the saturated alcohol **76**. Oxidation of the benzylic alcohol with PCC afforded ketone **78**. Both alcohol **76** and ketone **78** analogs were deprotected with TBAF and isolated for biological testing as **77** and **79**, respectively.



Scheme 4.19 Synthesis of Saturated Analogs of Phenyl Construct

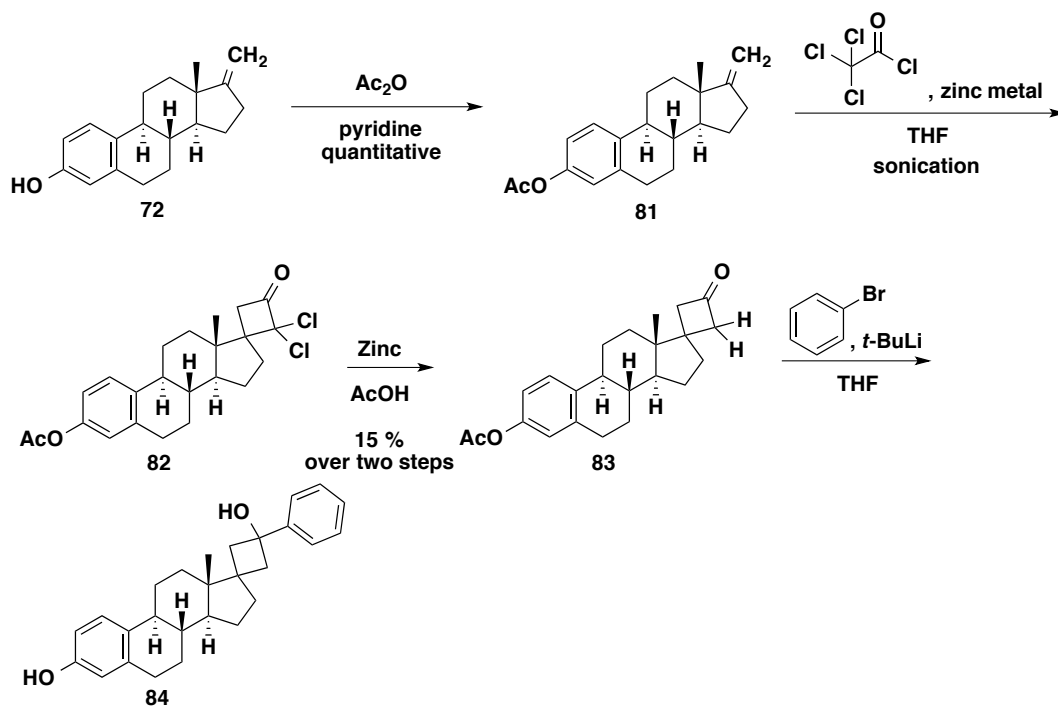
To explore the role of hydrogen bonding, the methylated allylic ether was generated [from 59](#) with methyl iodide and deprotected with TBAF to isolate **80** for analysis (**Scheme 4.20**).



Scheme 4.20 Synthesis of Methyl Ether

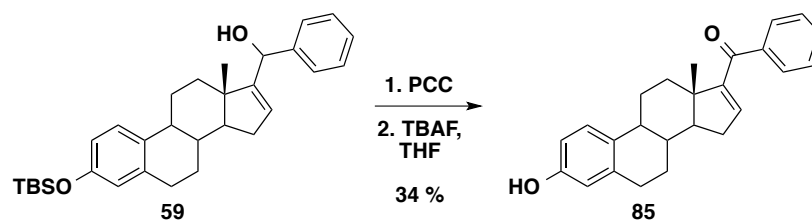
The allylic alcohol **63** (**Scheme 4.16**) shows interesting inhibitory effects on the SHH pathway. Conversely, biological evaluation of the saturated derivatives **77** and **79** showed a complete loss in inhibitory activity, suggesting that the allylic alcohol is responsible for the biological activity of this analog. Additionally, the capping of the allylic alcohol as methyl ether **80** resulted in a complete loss in activity furthering the hypothesis that the allylic alcohol is the essential functionality for inhibition. This activity could be due to the electrophilic nature of an activated allylic alcohol. Or alternatively, the allylic alcohol could be oxidized by extracellular proteins to the enone, and this functionality could be serving as a Michael acceptor. Both the saturated analogs **77** and **79**, as well as the methyl ether **80** would not be capable of oxidation to an enone, and would not serve as potential pro-drug Michael acceptors.

To further explore the hypothesis that electrophilicity is involved in potency, a more rigid version of the phenyl alcohol was also designed to eliminate the possibility for nucleophilic attack. Using cyclobutane as a rigid scaffold, a saturated variant of the phenyl allylic alcohol was synthesized beginning with methylene estrone **72**. Acylation of the phenol was necessary for future transformations. Acylated steroid **81** underwent a [2+2] cyclization with dichloroketene, generated *in situ* from trichloroacetylchloride and freshly activated zinc.^{17,18} Dechlorination of the resulting dichloride **82** with zinc and acetic acid afford cyclobutanone **83**. Lithiated benzene was added in excess to both deprotect the phenol as well as to add to the cyclobutanone, providing analog **84** (**Scheme 4.21**).



Scheme 4.21 Synthesis of Cyclobutane Analog

Upon biological evaluation, this rigid scaffold was also inactive, further suggesting the importance of the allylic alcohol for potency. The final analog designed to test this hypothesis was the oxidation of the allylic alcohol to the conjugated enone (**Scheme 4.22**). If the enone demonstrates similar potency to the allylic alcohol it would suggest the *in vivo* oxidation of the allylic alcohol system to the enone.



Scheme 4.22 Synthesis of Unsaturated Enone

To access the desired enone, compound **59**, the benzylic alcohol, was oxidized using pyridinium chlorochromate to furnish the protected enone, which was deprotected for analysis with TBAF to give **85**. Although this compound showed some loss in potency relative to the parent allylic alcohol **63**, the potential for an activated electrophile appears to be essential for the potency of this family of analogs.

At this point, the biological data has revealed two distinct ligands that inhibit SMO with excellent potency (**Figure 4.16**).

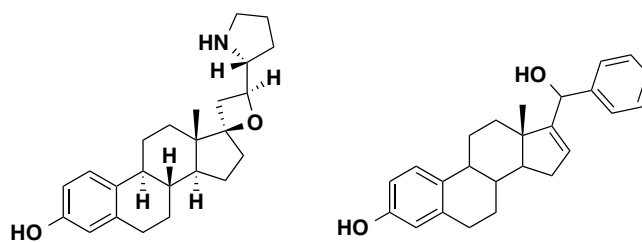


Figure 4.16 Side by Side Comparison of Lead Analogs

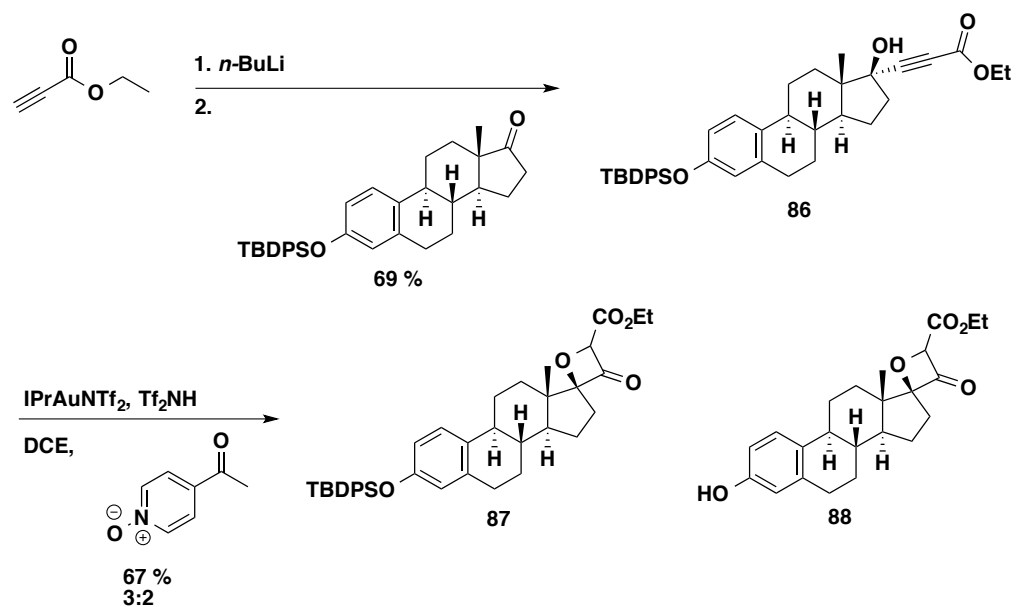
The first, the oxetane analog, consists of an exocyclic oxetane pyrrolidine EF-ring scaffold, and it has been shown that removal of the rigid framework or elimination of the oxygen atom results in the loss of potency. The second, the phenyl allylic alcohol, is

comprised of only one heteroatom and has the potential to act as an electrophile. There is the possibility that upon activation the oxetane ring system could also serve as a potential electrophile. It has been shown that a variety of nucleophiles can add to oxetane ring systems, especially in the presence of mild acid.^{19–21}

Section 4.9 Analyzing the Importance of the Nitrogen

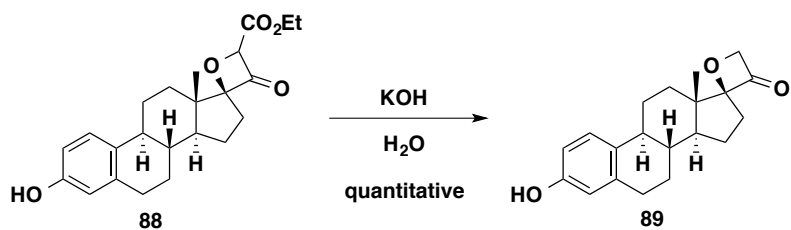
The biological data summarized above demonstrates that there are two unique scaffolds that exhibit inhibitory activity on the SHH pathway. Despite their structural differences, one similarity is the presence of a potential Lewis basic oxygen atom. Looking back at the lead analog, we postulated whether the oxetane alone was sufficient to drive potency or if the exocyclic pyrrolidine also played a role. To address this question, analogs were designed that lacked the pyrrolidine F-ring. Using a gold catalyzed cyclization approach, a small sample of oxetanones was generated that maintained the oxetane E-ring but lacked the pyrrolidine.

To achieve these compounds, ethyl propionate was deprotonated with *n*-butyllithium and added to TBDPS-protected estrone to afford compound **86**. Using a novel method described by Zhang, oxetanones **87** and **88** were obtained in modest yield.²² Due to the hindered nature of the neopentyl alcohol, it was essential for the ester to be directly conjugated with the alkyne for activation of the triple bond for cyclization. Comparison of this reaction to an adamantyl control substrate, which undergoes facile cyclization at lower temperatures, highlights the hindered nature of this steroidal tertiary alcohol.



Scheme 4.23 Synthesis of Oxetanone Scaffold

Compound **88** was analyzed for potency and also carried forward through a base-induced decarboxylation to generate analog **89** (Scheme 4.23).

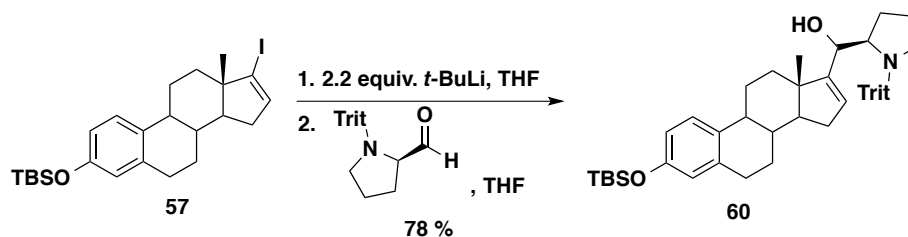


Scheme 4.24 Synthesis of Bare Oxetanone

Although these oxetanones are not an exact des-F mimic, they do afford the quick access to structurally related analogs. Pleasingly, compounds **88** and **89** showed no biological activity, highlighting the importance for the oxetane analogs to be comprised of more than simply a four-membered ring. Although it seems unlikely that the ketone prevents inhibitory function, further studies to examine the role of the additional carbonyl would need to be conducted to confirm the importance of the pyrrolidine F-ring.

Section 4.10 Access to Pyrrolidine Containing Derivatives

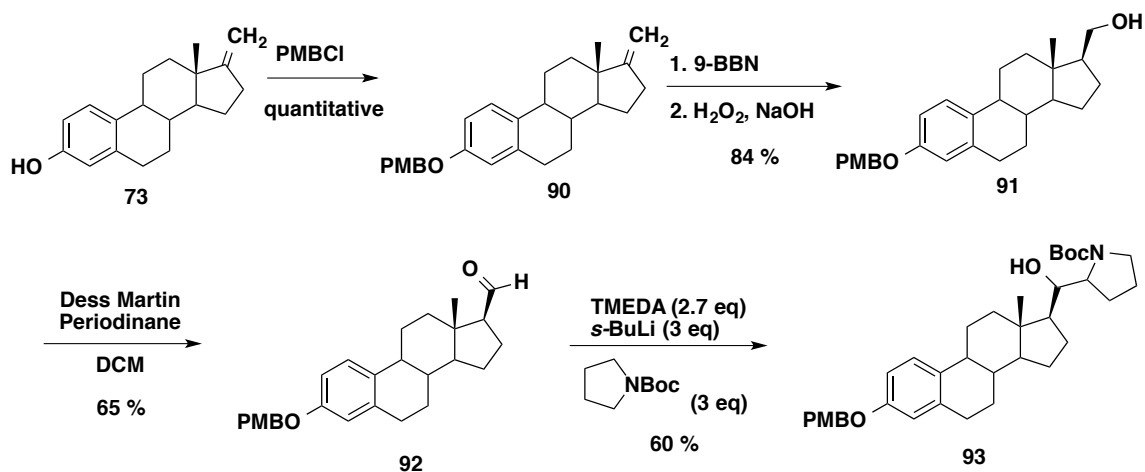
As described in **Section 4.9**, the biological evaluation of preliminary oxetanone derivatives suggest that the pyrrolidine ring is contributing to the activity of the lead oxetane analog. The next family of compounds synthesized maintains a similar spatial relationship between the oxygen and the secondary amine but would allow for more flexibility in the pocket. Additionally, the alcohol intermediate could be used to generate a variety of analogs with varying oxidation states. **Section 4.7** highlighted efforts towards the saturated F-ring analogs through the use of lithium halogen exchange with vinyl iodide **57** and subsequent addition to trityl protected prolinals (**Scheme 4.25**).



Scheme 4.25 Synthesis of Carbon Framework of Pyrrolidine Allylic Alcohols

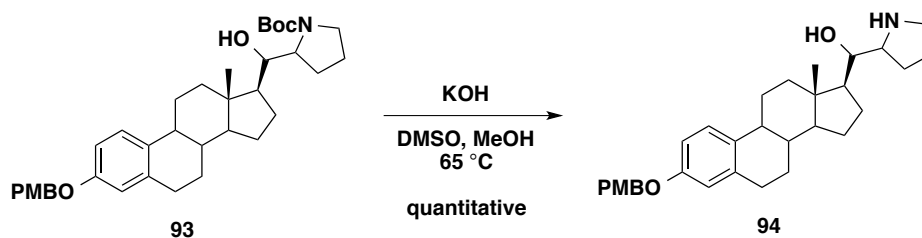
Functionalization of the resulting allylic alcohol **60** proved more difficult than anticipated. Activation of the allylic alcohol as either the corresponding mesylate or acetate resulted in either no product formation or decomposition. Removal of the trityl protecting group with dilute acid resulted in complex mixtures, and hydrogenation attempts at elevated pressures were unsuccessful. Addition of the vinyl anion to aldehydes with alternative nitrogen protecting groups were fruitless and resulted in only isolated of the protonated vinyl species. With these discouraging results, a second-generation route was designed.

By switching the nucleophilic and electrophilic partner, the second generation route to these analogs featured the addition of a lithiated pyrrolidine to the corresponding steroidal aldehyde (**Scheme 4.26**). Beginning with the methylenated estrone **73**²³, the free phenol was protected as the *para*-methoxybenzyl ether **90**. Hydroboration with 9-BBN followed by oxidation afforded **91** as a single beta-epimer in excellent yield. Dess Martin periodinane selectively oxidized the resulting primary alcohol to aldehyde **92** for coupling. After optimization for temperature and time, the lithiation of Boc-pyrrolidine with *sec*-butyllithium in the presence of TMEDA successfully constructed the full carbon framework of alcohol **93** as a mixture of three inseparable diastereomers.



Scheme 4.26 Nucleophilic Addition to Steroid Aldehyde

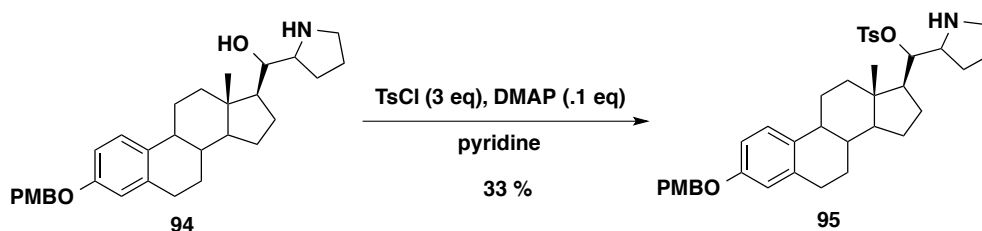
This newly formed secondary alcohol was exceedingly hindered and unreactive to numerous elimination and oxidation conditions. In order to functionalize the alcohol for elimination the carbamate must first be removed (**Scheme 4.27**). Using traditional acidic deprotection conditions resulted in the destruction of the PMB protection group; however, strong basic conditions resulted in a quantitative yield of the desired product.²⁴



Scheme 4.27 Deprotection of Secondary Carbamate

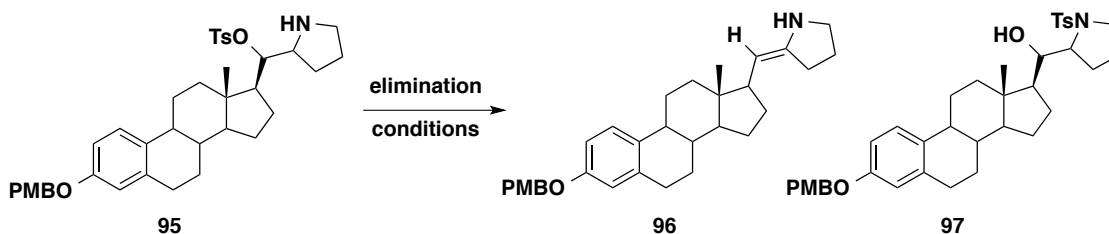
At this stage, there were two families of analogs that were proposed. The first would retain the oxygenation and would highlight the importance of flexibility, whereas

the second would be formed from the elimination of a molecule of water and could be used to assess the importance of both heteroatoms. With compound **94** in hand, a series of elimination conditions were attempted that resulted in no reactivity or destruction of the aromatic ring. However, activation of the secondary alcohol as tosylate **95** was obtained in a modest yield (**Scheme 4.28**).



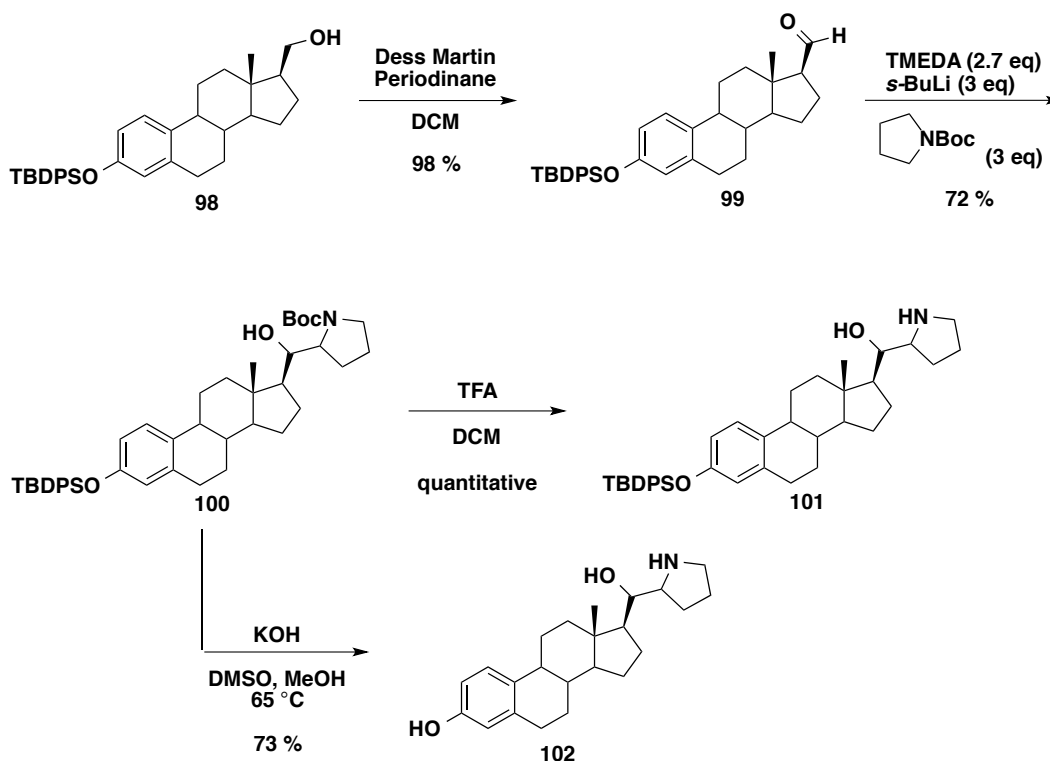
Scheme 4.28 Synthesis of Secondary Tosylate for Elimination

With **95** in hand, a variety of bases and conditions were employed to generate the desired allylic amine. Unfortunately, the only products isolated were enamine **96** and a suspected tosyl-transferred product **97** (**Scheme 4.29**).



Scheme 4.29 Elimination Attempts of Secondary Tosylate

Additionally, when using a model system for removal of the PMB protecting group, it was discovered that oxidative methods further oxidized the resulting free phenol and acidic conditions resulted in destruction of the alkene.²⁵ Moving forward, we transitioned our focus to a more orthogonal protecting group that could be removed with mild conditions in the presence of alkene functionalities (**Scheme 4.30**).



Scheme 4.30 Completion of Flexible Pyrrolidine Analog

Using the chemistry described above, the addition of lithiated Boc-pyrrolidine to aldehyde **99** generated alcohol **100** as a mixture of three diastereomers. At this stage, it was possible to selectively remove the carbamate in the presence of the silyl ether to generate **101**; however, it was also possible to achieve global deprotection with the

basic deprotection conditions described previously to furnish **102** as the first flexible variant of the lead oxetane analog with a vicinal relationship between the two heteroatoms.

To complete the synthesis of this family of derivatives, dehydration of compound **101** was attempted to construct the rigid alkene analog. Based on our previous analysis of the elimination of tosylate **95**, it was believed that elimination from an activated alcohol would also provide the undesired enamine. Conversion of alcohol **101** to a ketone, trapping the enolate as the enol triflate and reducing to furnish the desired alkene, was envisioned to avoid the undesired product. To our disappointment, all efforts to oxidize the alcohol, protected (**100**) or deprotected (**101**), were unsuccessful. Additional experiments using the acid chloride as the electrophile are currently being pursued.

Interestingly, the biological evaluation of the flexible analog **101** did not show inhibitory activity against the SHH pathway, suggesting once again, the importance of the oxetane ring. The oxetane also may be serving an essential role as a hydrogen bond receptor whereas analog **101** is more of a hydrogen bond donor.

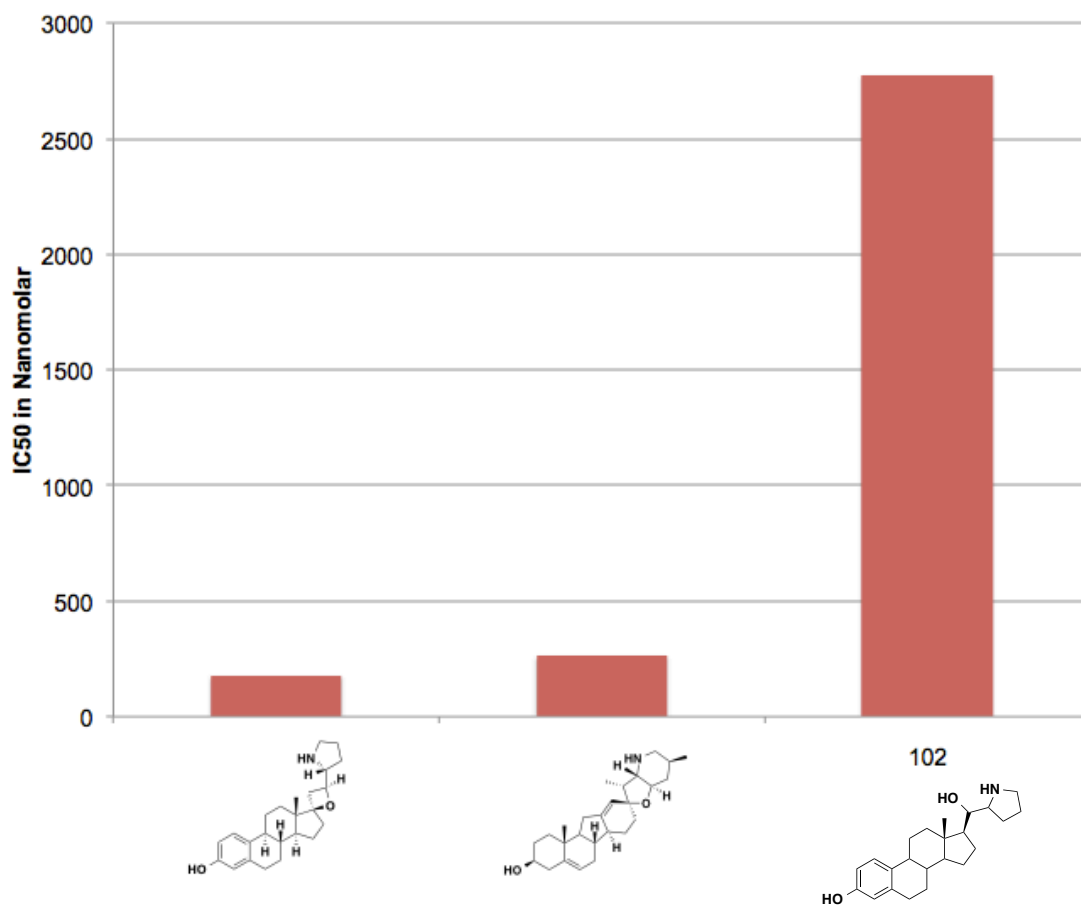


Figure 4.17 Biological Activity of Flexible Pyrrolidine Analog

Section 4.11 Cross-Coupling Approach to Alkylidene Analog

As outlined in the above section, efforts towards functionalizing, eliminating, or oxidizing the sterically hindered secondary alcohol proved difficult. In order to circumvent the issue of late stage installation of the alkene, a third-generation approach was taken using novel photoredox cross-coupling chemistry designed by the Molander group (**Figure 4.18**).²⁶ Using pyrrolidine trifluoroborate and a steroidal vinyl halide, the photoactivated dual catalysis of iridium and nickel would couple the C_{sp3} and C_{sp2} atoms

of interest. First, the photoactivated iridium would cleave the C-B bond generating a carbon centered radical alpha to the nitrogen. Nickel would insert into the vinyl halide bond, and then the carbon-centered radical could coordinate to the nickel to create a pentacoordinate species. Reductive elimination of the allyl amine would allow for recycling of the catalyst.

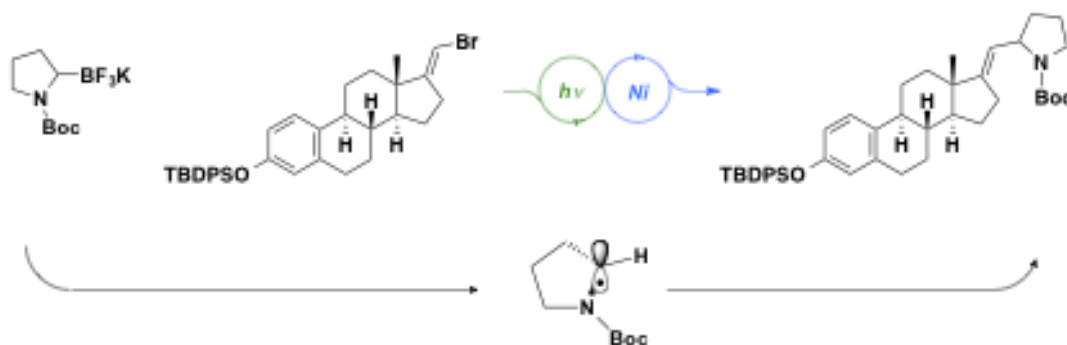
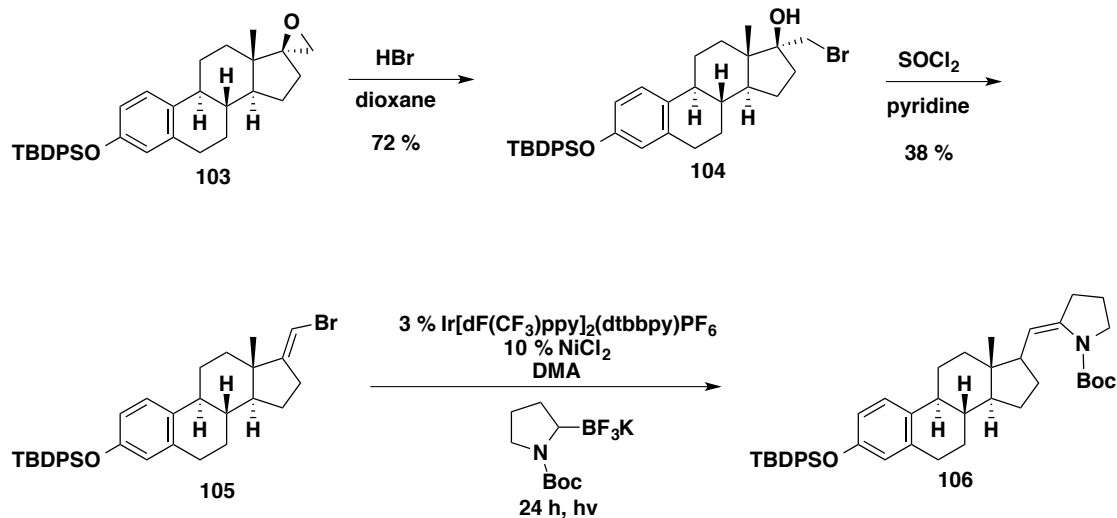


Figure 4.18 Photoredox Cross-Coupling: Single Electron Transmetalation

To construct the necessary vinyl bromide, a one-step procedure using the halogenated Wittig reagent was unsuccessful. An alternative route was designed to access the desired vinyl bromide which required only two chemical transformations from the known epoxide (**Scheme 4.31**). Acid-catalyzed epoxide opening of **103** with aqueous hydrobromic acid afforded halohydrin **104** in good yield. Elimination of the tertiary alcohol with thionyl chloride in pyridine produced a mixture of vinyl halide **105** and an allylic halide byproduct that were separable by column chromatography.²⁷



Scheme 4.31 Attempted Photoredox Cross-Coupling of Vinyl Bromide

With the assistance of John Tellis, the graduate student that designed the seminal photoredox cross-coupling work, and Simon Berritt, the Director of the Merck High-Throughput Experimentation Laboratory at Penn, a small screen was designed to test solvent, additives, and ligands in the photoredox reaction. Analysis of the crude reaction mixtures identified the product by mass, and the best set of conditions was scaled to a full plate. Despite the overall low yield, this unoptimized reaction represents the first use of a steroidal vinyl bromide in conjunction with photoredox catalysis for the assembly of novel analogs. After purification and deprotection, it was determined that the only product formed was the undesired enamine. With this information, the stability of the allyl amine in acidic and aqueous environments remained a concern. The nature of this chemical pathway suggested that the construction of the allyl amine occurs first followed by isomerization to the more thermodynamically favorable enamine.²⁸

Section 4.12 Conclusions

Through the development of in-house high-throughput biological evaluation and a computational model for potency, the Winkler [Laboratory](#) continues to design and synthesize steroid-derived inhibitors of the SHH signaling pathway. To date, we have identified two unique scaffolds that offer potency at, or near, the level of the alkaloid cyclopamine. Small perturbations to the EF-rings of the synthesized ligands result in drastic changes in potency. To date, we have identified both an oxetane-pyrrolidine analog with potency five times that of cyclopamine (**Figure 4.19**). Additionally, we have recently found a family of allylic alcohols and their derivatives with variable potencies, with the most potent phenyl allylic alcohol potentially acting as an irreversible electrophile (**Figure 4.20**).

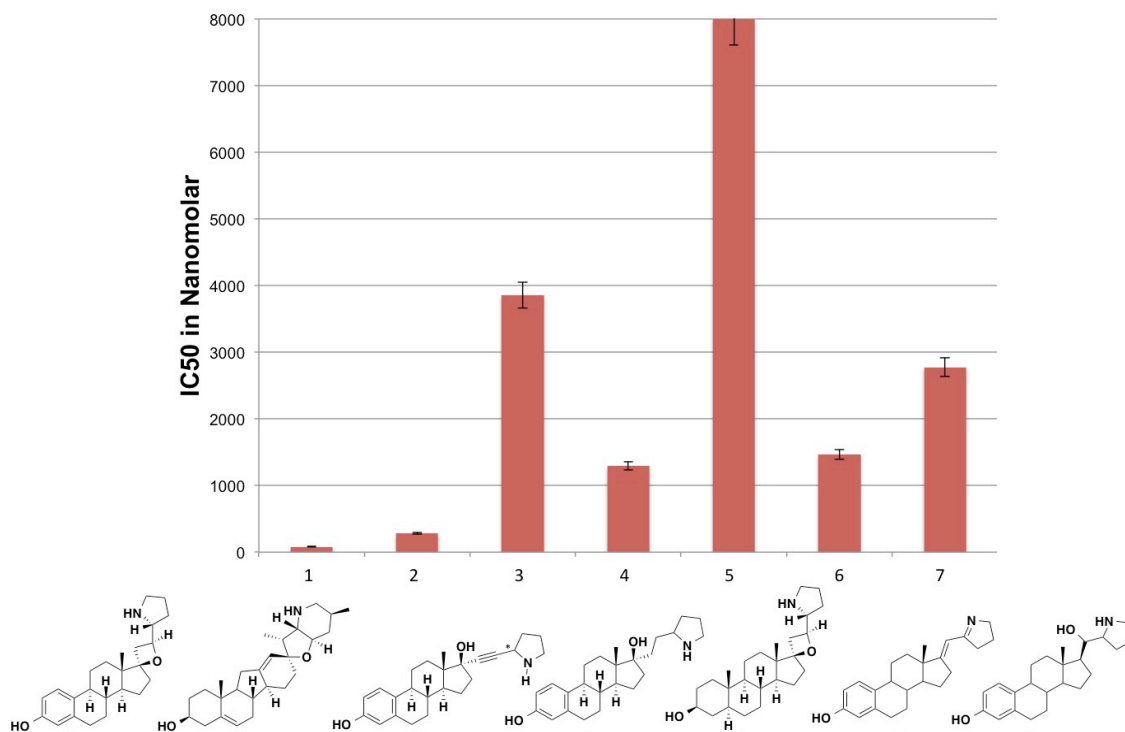
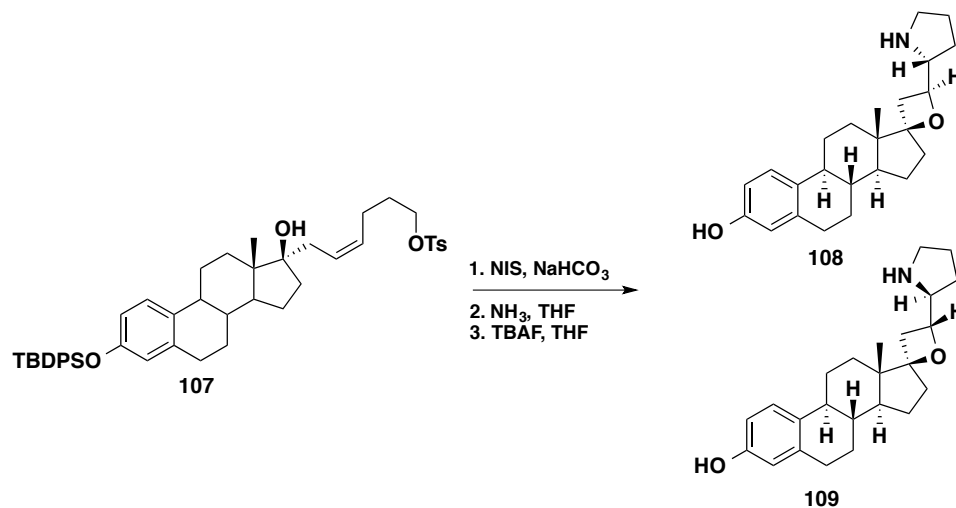


Figure 4.19 Summary of Biological Activity of Oxetane Derivatives

To summarize the oxetane family, any disruption of the four-membered ring results in a loss of biological activity. The role of this four-membered ring remains unclear.

Recently, Dr. Estrada has shown that the use of excess NIS as the electrophilic iodine source results in increased yields of the key iodoetherification step. With this increased yield, the isolation of a second minor diastereomer is now possible (**Scheme 4.32**). Side-by-side biological testing of a 2:1 mixture of diastereomers (**108:109**) and the known oxetane show similar potencies, suggesting the role of stereochemistry is non-essential. Interestingly, ring opened variants such as **56** (**Figure 4.19, column 4**) and **102** (**Figure 4.19, column 9**) show only modest activity suggesting that the constraint of this cyclic system is essential.



Scheme 4.32 Isolation of Two Oxetane Epimers

Turning to the family of phenyl allylic alcohols, any modification that prevents the molecule from acting as an electrophile results in the loss of activity. Conversion of the allylic alcohol to the enone results in a mild loss of potency, suggesting that the enone is

not the active for of the ligand. With this data, it could be concluded that the oxetane moiety and the allylic alcohol are acting as a electrophilic trap in the binding pocket of SMO. Activation of either the lone pairs of the oxetane or the alcohol would render these molecules susceptible to attack from neighboring amino acids. Lastly, it has been shown that the selection of estrone as the hydrophobic surrogate is essential for activity.

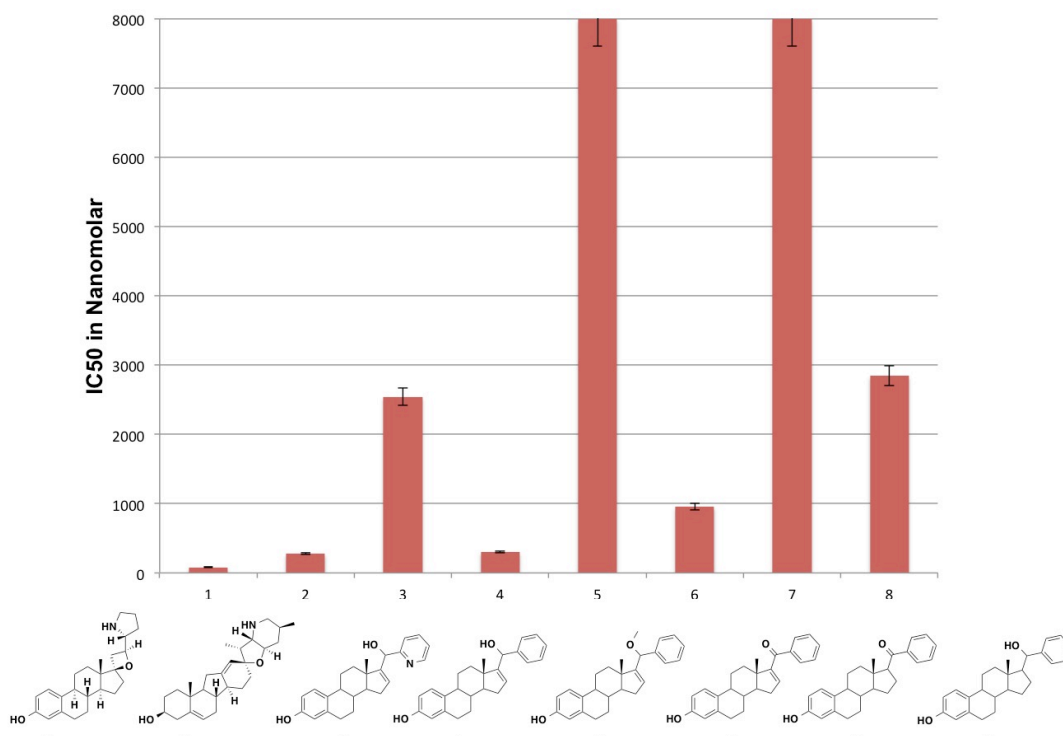


Figure 4.20 Summary of Biological Activity of Phenyl Allylic Alcohol Family

Section 4.13 References

- (1) Tremblay, M. R.; Lescarbeau, A.; Grogan, M. J.; Tan, E.; Lin, G.; Austad, B. C.; Yu, L. C.; Behnke, M. L.; Nair, S. J.; Hagel, M.; et al. Discovery of a Potent and

- Orally Active Hedgehog Pathway Antagonist (IPI-926). *J. Med. Chem.* **2009**, *52*, 4400–4418.
- (2) Niwa, T.; Yorimitsu, H.; Oshima, K. Palladium-Catalyzed 2-Pyridylmethyl Transfer from 2-(2-Pyridyl)ethanol Derivatives to Organic Halides by Chelation-Assisted Cleavage of Unstrained Csp³-Csp³ Bonds. *Angew. Chem., Int. Ed.* **2007**, *46*, 2643–2645.
- (3) Winkler, J. D.; Isaacs, A.; Holderbaum, L.; Tatard, V.; Dahmane, N. Design and Synthesis of Inhibitors of Hedgehog Signaling Based on the Alkaloid Cyclopamine. *Org. Lett.* **2009**, *11*, 2824–2827.
- (4) Kusuma, B. R.; Zhang, L.; Sundstrom, T.; Peterson, L. B.; Dobrowsky, R. T.; Blagg, B. S. J. Synthesis and Evaluation of Novologues as C-Terminal Hsp90 Inhibitors with Cytoprotective Activity against Sensory Neuron Glucotoxicity. *J. Med. Chem.* **2012**, *55*, 5797–5812.
- (5) Weierstall, U.; James, D.; Wang, C.; White, T. a; Wang, D.; Liu, W.; Spence, J. C. H.; Bruce Doak, R.; Nelson, G.; Fromme, P.; et al. Lipidic Cubic Phase Injector Facilitates Membrane Protein Serial Femtosecond Crystallography. *Nat. Commun.* **2014**, *5*, 3309–3314.
- (6) Wang, C.; Wu, H.; Katritch, V.; Han, G. W.; Huang, X.-P.; Liu, W.; Siu, F. Y.; Roth, B. L.; Cherezov, V.; Stevens, R. C. Structure of the Human Smoothed Receptor Bound to an Antitumour Agent. *Nature* **2013**, *497*, 338–343.

- (7) Johnson, D. C.; Widlanski, T. S. Cerium (III) Chloride-Mediated Reactions of Sulfonamide Dianions The Sulfonamide Functional Group Has Received Con-. *J. Org. Chem.* **2003**, *68*, 5300–5309.
- (8) Serino, C.; Stehle, N.; Park, Y. S.; Florio, S.; Beak, P. ChemInform Abstract: Asymmetric Syntheses of N-Boc 2-Substituted Pyrrolidines and Piperidines by Intramolecular Cyclization. *J. Org. Chem.* **1999**, *64*, 1160–1165.
- (9) Kouznetsov, V.; Cruz, U. M.; Zubkov, F. I.; Nikitina, E. V. An Efficient Synthesis of 17-Epi-Ethynylestradiol. *Tetrahedron* **2006**, *54*, 4277–4282.
- (10) Winkler, J. D.; Isaacs, A.; Holderbaum, L.; Tatard, V.; Dahmane, N. Design and Synthesis of Inhibitors of Hedgehog Signaling Based on the Alkaloid Cyclopamine. *Org. Lett.* **2009**, *11*, 2824–2827.
- (11) Langer, P.; Shojaei, H.; Greifswald, D.-; E-mail, G. Fragmentation ' Reactions of 1-Azido-2-Hydroxy-4 , 6-Dioxohexanes. *Chem. Comm.* **2003**, 3044–3045.
- (12) Jepsen, T. H.; Kristensen, J. L. In Situ Generation of the Ohira-Bestmann Reagent from Stable Sulfonyl Azide: Scalable Synthesis of Alkynes from Aldehydes. *J. Org. Chem.* **2014**, *79*, 9423–9426.
- (13) Cuthbertson, J. D.; Unsworth, W. P.; Moody, C. L.; Taylor, R. J. K. The Total Synthesis of (+)-Elaeokanidine A: Natural Product or Isolation Artefact? *Tetrahedron Lett.* **2015**, *56*, 3123–3126.
- (14) Pietruszka, J.; Witt, A. Synthesis of the Bestmann-Ohira Reagent. *Synthesis.* **2006**, 4266–4268.

- (15) Liu, P.; Hong, S.; Weinreb, S. M. Total Synthesis of the Securinega Alkaloid (-) - Secu'amamine A. *J. Am. Chem. Soc.* **2008**, *130*, 7562–7563.
- (16) Muchow, G.; Brunel, J. M. Pd⁰ -Catalyzed Hydrogenolysis of a Bicyclic Allylic Diacetate. *Eur. J. Org. Chem.* **2013**, *2013*, 6449–6454.
- (17) Paryzek, Z.; Blaszczyk, K. Synthesis and Stereochemistry of Steroidal Spirocyclobutanones. *Liebigs. Ann. Chem.* **1990**, 665–670.
- (18) Błaszczyk, K.; Koenig, H.; Paryzek, Z. Cyclobutanone Approach to the Synthesis of Cardenolides. *Eur. J. Org. Chem.* **2005**, 749–754.
- (19) Lajunen, M.; Koskinen, J.-M. Acid-Catalyzed Hydrolysis of Oxetane. *Acta Chem. Scand.* **1994**, *48*, 788–791.
- (20) Pritchard, J. G.; Long, F. a. The Kinetics of the Hydrolysis of Trimethylene Oxide in Water, Deuterium Oxide and 40% Aqueous Dioxane. *J. Am. Chem. Soc.* **1958**, *80*, 4162–4165.
- (21) Searles, S.; Butler, C. F. Reactions of Alcohols and Phenols with Trimethylene Oxide. *J. Am. Chem. Soc.* **1954**, *76*, 56–58.
- (22) Ye, L.; He, W.; Zhang, L. Gold-Catalyzed One-Step Practical Synthesis of Oxetan-3-Ones from Readily Available Propargylic Alcohols. *J. Am. Chem. Soc.* **2010**, *132*, 8550–8551.
- (23) Panchapakesan, G.; Dhayalan, V.; Dhatchana Moorthy, N.; Saranya, N.; Mohanakrishnan, A. K. Synthesis of 2-Substituted 17 β -hydroxy/17-Methylene

Estratrienes and Their in Vitro Cytotoxicity in Human Cancer Cell Cultures.

Steroids **2011**, *76*, 1491–1504.

- (24) Zheng, Z.; Perkins, B. L.; Ni, B. Diarylprolinol Silyl Ether Salt as New Eff Water-Soluble & Recyclable Organocat Asymm Michael Addition on Water. *J. Am. Chem. Soc.* **2010**, *132*, 50–51.
- (25) Chen, D.; Xu, C.; Deng, J.; Jiang, C.; Wen, X.; Kong, L.; Zhang, J.; Sun, H. Proton-Exchanged Montmorillonite-Mediated Reactions of Methoxybenzyl Esters and Ethers. *Tetrahedron* **2014**, *70*, 1975–1983.
- (26) Tellis, J. C.; Primer, D. N.; Molander, G. a. Single-Electron Transmetalation in Organoboron Cross-Coupling by Photoredox/Nickel Dual Catalysis. *Science*. **2014**, *345*, 433–436.
- (27) Hillisch, A.; Von Langen, J.; Menzenbach, B.; Droescher, P.; Kaufmann, G.; Schneider, B.; Elger, W. The Significance of the 20-Carbonyl Group of Progesterone in Steroid Receptor Binding: A Molecular Dynamics and Structure-Based Ligand Design Study. *Steroids* **2003**, *68*, 869–878.
- (28) Birladeanu, L.; Andrews, D. W.; Pagnotta, M. Conjugative Interaction in the Orthogonal Enamine, 1 -Azabicyclo[3.2.2]non-2-Ene. *J. Am. Chem. Soc.* **1985**, *6*, 3813–3817.

Section 4.14 Experimental Details

Experimental Results

General Methods

Solvents used for extraction and purification were HPLC grade from Fisher. Unless otherwise indicated, all reactions were run under an inert atmosphere of argon.

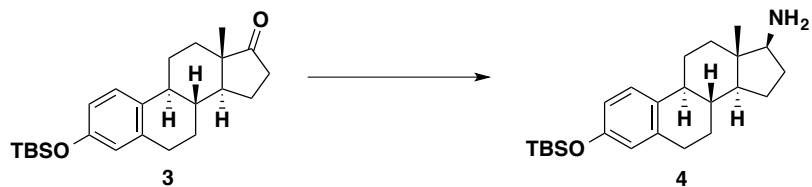
Anhydrous tetrahydrofuran, ethyl ether and toluene were obtained via passage through an activated alumina column. VWR pre-coated silica gel plates (250 μm , 60 F254) were used for analytical TLC. Spots were visualized using 254 nm ultraviolet light, with either ceric ammonium molybdate or potassium permanganate stains as visualizing agents.

Chromatographic purifications were performed on Sorbent Technologies silica gel (particle size 32-63 microns). ^1H and ^{13}C NMR spectra were recorded at 500 MHz and 125 MHz, respectively, in CDCl_3 on a Bruker AM-500 or DRX-500 spectrometer.

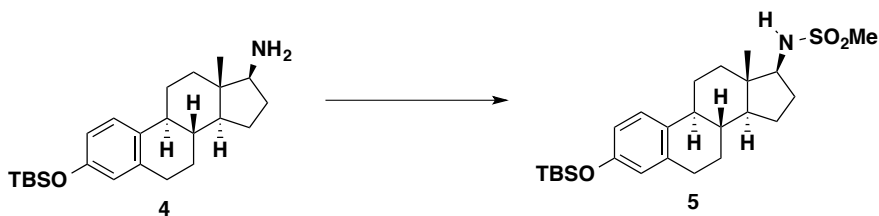
Chemical shifts are reported relative to internal chloroform (δ 7.26 for ^1H , δ 77.17 for ^{13}C). Infrared spectra were recorded on a NaCl plate using a Perkin-Elmer 1600 series Fourier transform spectrometer. High-resolution mass spectra were obtained by Dr. Rakesh Kohli at the University of Pennsylvania Mass Spectrometry Service Center on an Autospec high resolution double-focusing electrospray ionization/chemical ionization spectrometer with either DEC 11/73 or OPUS software data system. Melting points were obtained on a Thomas Hoover capillary melting point apparatus and are uncorrected.

Experimental Details

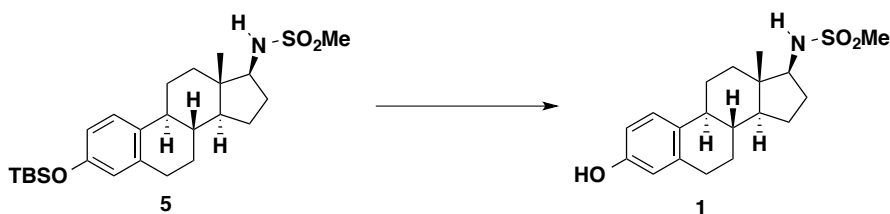
Section 4.1 Sulfonamides



To a solution of protected estrone **3** (274 mg, 0.71 mmol) in THF (14 mL, 0.05 M) and methanol (4.7 mL, 0.15 M) at 25 °C was added ammonium acetate (546 mg, 7.10 mmol) and sodium cyanoborohydride (135 mg, 2.14 mmol). The slurry was allowed to stir overnight at 25 °C before being quenched with water (10 mL). The aqueous was extracted with ethyl acetate (3x 15 mL), washed with brine (10 mL), and dried over sodium sulfate. The organics were removed *in vacuo* and the crude residue was purified by silica gel chromatography with 10% methanol in DCM as the eluent to yield the product **4** as a white film (247 mg, 91 %). Spectral data matches the reported. ¹H NMR (500 MHz, CDCl₃): δ 7.14-7.09 (m, 1H), 6.63-6.56 (m, 2H), 3.76 (s, 1H), 2.82 (t, *J* = 8.9 Hz, 2H), 2.33-1.80 (m, 8H), 1.52-1.26 (m, 5H), 0.98 (s, 8H), 0.91 (d, *J* = 5.6 Hz, 1H), 0.79 (s, 1H), 0.20 (t, *J* = 3.4 Hz, 5H).

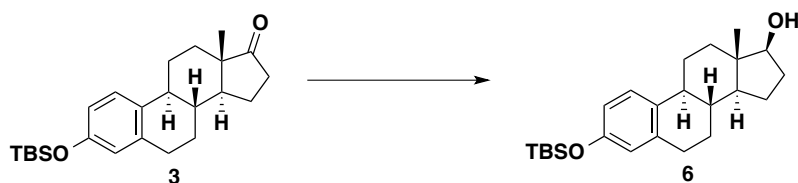


To a solution of amine **4** (247 mg, 0.64 mmol) in dry pyridine (2.1 mL, 0.3 M) at 0 °C was added methanesulfonyl chloride (60 μ L, 0.77 mmol). The reaction was stirred at 0 °C for 2 hours before quenching with deionized water (10 mL). The aqueous was extracted with ethyl acetate (3x 15 mL) and dried over sodium sulfate. The organics were removed *in vacuo* to afford the crude sulfonamide that was purified by silica gel chromatography with DCM as the eluent to afford sulfonamide **5** as a white film (260 mg, 88 %). ¹H NMR (500 MHz; CDCl₃): δ 7.11 (d, *J* = 8.4 Hz, 1H), 6.62 (dd, *J* = 8.4, 2.6 Hz, 1H), 6.55 (d, *J* = 2.6 Hz, 1H), 4.57 (dd, *J* = 9.0, 8.0 Hz, 1H), 3.02 (d, *J* = 0.3 Hz, 3H), 2.88-2.78 (m, 2H), 2.34-2.17 (m, 3H), 2.04 (dt, *J* = 12.2, 3.1 Hz, 1H), 1.89-1.74 (m, 3H), 1.58-1.22 (m, 7H), 0.98 (s, 9H), 0.88 (s, 3H), 0.19 (s, 6H). ¹³C NMR (126 MHz; CDCl₃): δ 153.6, 137.8, 132.7, 126.3, 120.1, 117.4, 89.7, 49.2, 43.9, 43.5, 38.6, 38.4, 36.6, 29.6, 28.1, 27.2, 26.1, 25.9, 23.2, 18.3, 11.9, -4.2. FTIR (thin film) 3023, 2929, 2857, 1607 cm⁻¹. HRMS (ES) Calcd. for C₂₅H₄₁NO₃Si: 463.2576 (M+D)⁺, found 465.2457.



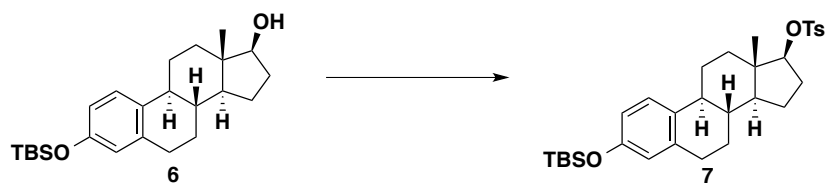
To a solution of sulfonamide **5** (26 mg, 0.05 mmol) in THF (560 μ L, 0.1 M) at 25 C was added tetrabutylammonium fluoride (112 μ L, 0.11 mmol) dropwise and stirred for two hours. The reaction was quenched with saturated ammonium chloride (1 mL) and extracted with ethyl acetate (3x 5 mL), dried with sodium sulfate and concentrated *in vacuo*. The crude product was purified with silica gel chromatography with a gradient of 0-10 % methanol in DCM as the eluent to afford compound **1** as a white film (18 mg, 95

%). **¹H NMR** (500 MHz; CDCl₃): δ 6.87 (d, *J* = 8.4 Hz, 1H), 6.37 (dd, *J* = 8.4, 2.7 Hz, 1H), 6.31 (d, *J* = 2.7 Hz, 1H), 4.32 (dd, *J* = 9.1, 7.8 Hz, 1H), 4.28 (s, 2H), 2.81 (s, 3H), 2.57 (dt, *J* = 10.4, 4.9 Hz, 2H), 2.09-1.94 (m, 3H), 1.78 (dt, *J* = 11.9, 2.8 Hz, 1H), 1.65-1.54 (m, 4H), 1.26-1.01 (m, 7H), 0.63 (s, 3H). **¹³C NMR** (126 MHz; CDCl₃): δ 154.2, 137.5, 130.8, 126.0, 114.9, 112.5, 89.6, 43.4, 43.0, 38.4, 37.5, 36.1, 29.2, 27.6, 26.8, 25.7, 22.7, 11.3. **FTIR** (thin film) 3443, 2922, 1617, 1498 cm⁻¹. **HRMS** (ES) Calcd. for C₁₉H₂₇NO₃S: 349.1712 (M+Cl)⁻, found 385.1463.



To a solution of protected estrone **3** (469 mg, 1.22 mmol) in THF (12 mL, 0.1 M) at 0 °C was added sodium borohydride (46 mg, 1.22 mmol) in one portion. The slurry was stirred at this temperature for three hours before quenching with saturated ammonium chloride (10 mL). The aqueous was extracted with ethyl acetate (3x, 10 mL), dried over sodium sulfate, and the solvent removed *in vacuo*. The crude product **6** was clean and no further purification was required (400 mg, 85%). **¹H NMR** (500 MHz; CDCl₃): δ 7.12 (d, *J* = 8.5 Hz, 1H), 6.62-6.55 (m, 2H), 3.75-3.72 (m, 1H), 2.81 (dt, *J* = 11.2, 5.2 Hz, 2H), 2.30 (dt, *J* = 9.9, 3.6 Hz, 1H), 2.20-2.10 (m, 2H), 1.94 (dt, *J* = 12.6, 3.2 Hz, 1H), 1.88-1.84 (m, 2H), 1.74-1.69 (m, 2H), 1.59 (s, 2H), 1.52-1.25 (m, 22H), 0.98 (s, 9H), 0.78 (s, 3H), 0.19 (s, 6H). **¹³C NMR** (126 MHz; CDCl₃): δ 164.5, 153.5, 143.6, 137.99, 137.94, 133.2, 126.27, 126.08, 125.5, 125.0, 120.1, 117.3, 113.7, 100.21, 100.13, 82.1, 50.2, 44.2, 43.4, 39.0, 36.9, 34.8, 31.8, 30.8,

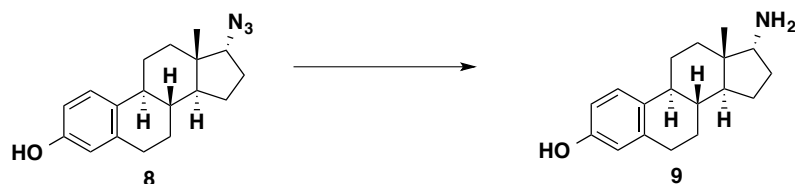
29.8, 29.2, 27.4, 26.4, 25.9, 25.4, 23.3, 22.8, 18.3, 14.3, 11.6, 11.2, -4.2. **FTIR** (thin film): 3330, 2926, 1606, 1496 cm^{-1} .



Tosyl chloride (226 mg, 1.2 mmol) was added in one portion to a solution of alcohol **6** (229 mg, 0.6 mmol) in dry pyridine (2 mL, 0.3 M) and stirred at 25 °C overnight. The reaction was neutralized with concentrate hydrochloric acid and diluted with water to precipitate product. The crude product was collected via filtration and purified by silica gel chromatography with 10 % ethyl acetate in hexanes as the eluent to afford product **7** (219 mg, 67 %). **¹H NMR** (500 MHz; CDCl_3): δ 7.82 (d, J = 8.3 Hz, 2H), 7.35 (dd, J = 8.6, 0.6 Hz, 2H), 7.09 (d, J = 8.2 Hz, 1H), 6.61 (dd, J = 8.4, 2.7 Hz, 1H), 6.55 (d, J = 2.6 Hz, 1H), 4.36 (dd, J = 9.0, 7.8 Hz, 1H), 2.80 (dd, J = 10.9, 5.6 Hz, 2H), 2.47 (s, 3H), 2.22 (dq, J = 13.7, 3.6 Hz, 1H), 2.12 (td, J = 11.1, 3.9 Hz, 1H), 2.01-1.96 (m, 1H), 1.85-1.64 (m, 4H), 1.46-1.26 (m, 4H), 1.17-1.10 (m, 2H), 0.99 (s, 9H), 0.84 (s, 3H), 0.19 (s, 6H). **¹³C NMR** (126 MHz; CDCl_3): δ 153.4, 149.6, 144.5, 137.6, 134.3, 132.6, 129.8, 127.9, 126.2, 120.0, 117.3, 89.9, 49.1, 43.8, 43.35, 43.32, 38.5, 36.2, 29.5, 27.8, 27.1, 25.95, 25.77, 23.1, 21.7, 18.2, 11.8, -4.3. **FTIR** (thin film): 2928, 2837, 1606, 1569 cm^{-1} .

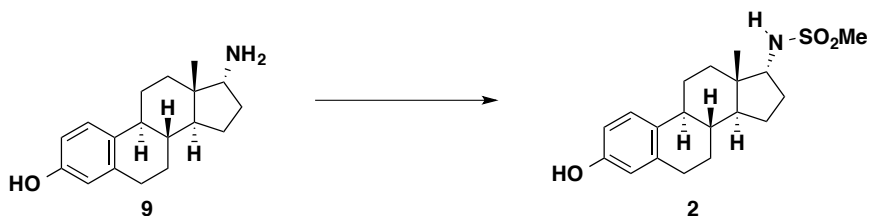


Sodium azide (208 mg, 3.2 mmol) was added in one portion to a solution of tosylate (219 mg, 0.4 mmol) in dry DMF (3 mL, 0.13 M) at 25 °C, and the solution heated to reflux and stirred overnight. The reaction was cooled to 25 °C and quenched with water (10 mL) and extracted with DCM (3x, 15 mL) and the organic solvent removed *in vacuo*. The crude material was purified by silica gel chromatography with 10 % ethyl acetate in hexanes as the eluent to afford the azide **8** as a white film (39 mg, 33 %). Spectra matches that reported. ¹H NMR (500 MHz; CDCl₃): δ 7.16 (d, *J* = 8.5 Hz, 1H), 6.63 (dd, *J* = 8.4, 2.8 Hz, 1H), 6.56 (d, *J* = 2.7 Hz, 1H), 3.59 (d, *J* = 6.6 Hz, 1H), 2.82 (dd, *J* = 10.4, 5.3 Hz, 2H), 2.35 (dd, *J* = 13.4, 3.0 Hz, 1H), 2.23-2.18 (m, 2H), 1.90-1.67 (m, 5H), 1.54-1.26 (m, 6H), 0.79 (s, 3H).



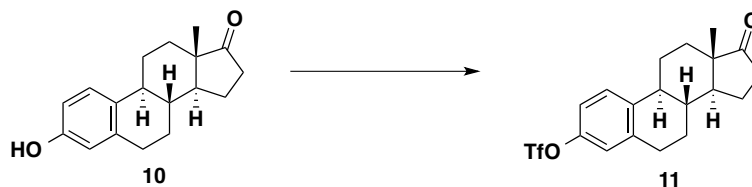
A slurry of azide **8** (39 mg, 0.13 mmol) and Pd/C (10 mg, 10 % by wt) in methanol (1 mL, 0.15 M) was sparged with hydrogen and placed under 1 atm of hydrogen at 25 °C. The slurry was stirred overnight and then diluted with ethyl acetate and filtered through a pad of Celite and the solvent removed *in vacuo*. The crude product **9** was pure and no further chromatography was required (29 mg, quant.), and ¹H NMR data matches reported

spectra. $^1\text{H NMR}$ (500 MHz, CDCl_3): δ 6.98 (d, $J = 8.4$ Hz, 1H), 6.47 (dd, $J = 8.4, 2.7$ Hz, 1H), 6.41 (d, $J = 2.6$ Hz, 1H), 3.98-3.95 (m, 4H), 2.78 (d, $J = 6.5$ Hz, 1H), 2.69-2.65 (m, 2H), 2.22-2.18 (m, 1H), 2.14-2.08 (m, 1H), 2.02-2.00 (m, 1H), 1.78-1.66 (m, 2H), 1.48-1.36 (m, 3H), 1.28-1.22 (m, 3H).

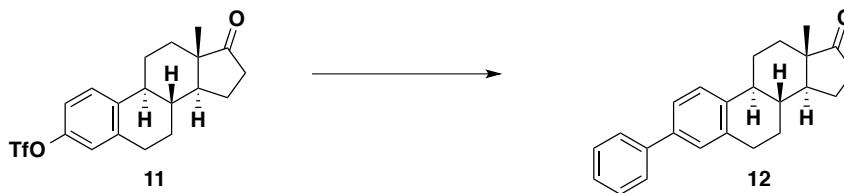


To a solution of amine **9** (27 mg, 0.10 mmol) in dry pyridine (333 μL , 0.3 M) at 0 $^\circ\text{C}$ was added methanesulfonyl chloride (9 μL , 0.12 mmol). The reaction was stirred at 0 $^\circ\text{C}$ for 2 hours before quenching with deionized water (5 mL). The aqueous was extracted with ethyl acetate (2x, 10 mL) and DCM (2x, 1 mL), washed with brine (10 mL) and dried over sodium sulfate. The organics were removed *in vacuo* to afford the crude sulfonamide that was purified by silica gel chromatography with a gradient of 0-10 % methanol in DCM as the eluent to afford sulfonamide **2** as a white film (13 mg, 37 %). $^1\text{H NMR}$ (500 MHz, CDCl_3): δ 7.01 (d, $J = 8.4$ Hz, 1H), 6.51 (dd, $J = 8.4, 2.7$ Hz, 1H), 6.44 (d, $J = 2.6$ Hz, 1H), 3.69 (s, 4H), 3.32 (dd, $J = 8.5, 7.0$ Hz, 1H), 3.25 (dt, $J = 3.2, 1.6$ Hz, 1H), 2.82 (s, 3H), 2.78-2.65 (m, 3H), 2.32-2.21 (m, 3H), 2.09-2.03 (m, 1H), 1.81-1.73 (m, 3H), 1.65-1.55 (m, 3H), 1.46-1.14 (m, 10H), 0.70 (s, 3H). $^{13}\text{C NMR}$ (126 MHz; CDCl_3): δ 154.6, 138.1, 131.4, 126.4, 115.2, 112.7, 62.6, 44.9, 43.5, 41.1, 40.3, 39.2, 33.0, 31.6, 29.7, 28.0, 26.3, 24.2, 18.3. **FTIR** (thin film) 3302, 2932, 1602, 1500 cm^{-1}

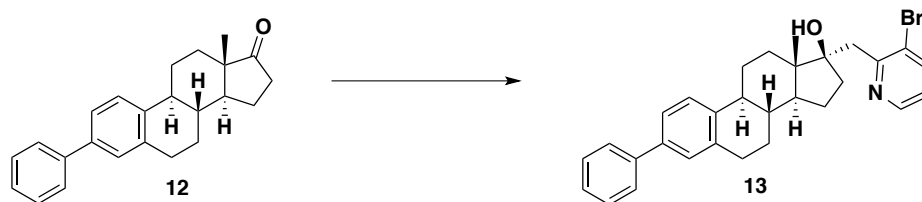
Section 4.2 Aryl-Aryl Coupled Analogs



Triethylamine (1.03 mL, 7.4 mmol) was added to a solution of estrone **10** (1.0 g, 3.7 mmol) in dichloromethane (20 mL, 0.2 M) at 0 °C followed by the dropwise addition of trifluoromethanesulfonic anhydride (684 μ L, 4.1 mmol). The reaction was stirred at 0 °C for two hours, diluted with dichloromethane (20 mL) and quenched with aqueous saturated sodium bicarbonate (25 mL). The aqueous was extracted with dichloromethane (3x 25 mL), and the organics collected, dried over sodium sulfate, and the solvent removed *in vacuo*. The crude product was purified by silica gel chromatography (10 % ethyl acetate in hexanes) to afford **11** as a white film (568 mg, 38 %). Observed spectra correlates with previously reported characterization. $^1\text{H NMR}$ (500 MHz; CDCl_3): δ 7.34 (d, $J = 8.7$ Hz, 1H), 7.03 (dd, $J = 8.6, 2.3$ Hz, 1H), 6.99 (s, 1H), 2.94 (dd, $J = 8.5, 3.8$ Hz, 2H), 2.51 (dd, $J = 18.9, 8.8$ Hz, 1H), 2.42-2.38 (m, 1H), 2.32-2.27 (m, 1H), 2.15 (dt, $J = 18.8, 9.2$ Hz, 1H), 2.09-2.02 (m, 2H), 1.97 (dt, $J = 9.7, 2.7$ Hz, 1H), 1.71-1.44 (m, 6H), 0.91 (s, 3H). $^{13}\text{C NMR}$ (126 MHz; CDCl_3): δ 147.7, 140.4, 139.4, 127.3, 121.3, 118.4, 50.5, 48.0, 44.2, 37.8, 35.9, 31.6, 29.5, 26.2, 25.8, 21.7, 13.9

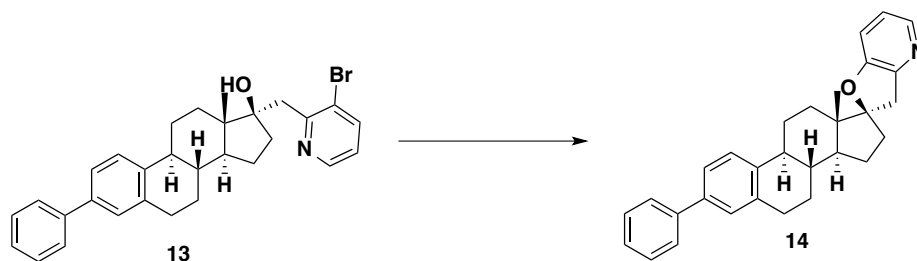


A microwave vial was charged with triflate **11** (214 mg, 0.53 mmol), Pd(PPh₃)₄ (61 mg, 0.05 mmol), phenylboronic acid (71 mg, 0.59 mmol) and K₂CO₃ (242 mg, 1.76 mmol), purged and backfilled with argon. Dry toluene (2.6 mL) and degassed water (0.88 mL) were added and the resulting mixture was allowed to stir at 75 °C for 12 h. The mixture was allowed to cool to 25 °C, quenched with water (10 mL) and extracted with dichloromethane (3x 15 mL). The organics were dried over sodium sulfate, concentrated and purified by silica gel chromatography (20 % ethyl acetate in hexanes) to yield **12** as a white solid (73 mg, 68 %) ¹H NMR (500 MHz; C₆H₆): δ 7.59-7.57 (m, 2H), 7.44-7.31 (m, 6H), 3.00 (dd, *J* = 8.9, 4.0 Hz, 2H), 2.55-2.46 (m, 2H), 2.39-2.34 (m, 1H), 2.20-1.98 (m, 3H), 1.70-1.48 (m, 7H), 0.94 (s, 3H). ¹³C NMR (126 MHz; C₆D₆): δ 141.2, 139.07, 138.97, 137.0, 128.8, 127.9, 127.20, 127.16, 126.0, 124.7, 50.7, 48.2, 44.5, 38.4, 36.0, 31.8, 31.1, 29.7, 26.7, 25.9, 21.8, 14.0. FTIR (thin film) 2930, 1737, 1484 cm⁻¹. HRMS (ES) Calcd. for C₂₄H₂₆O: 330.1984 (M⁺), found 330.1988.



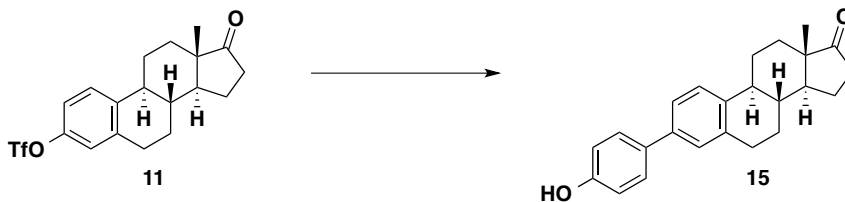
To a solution of diisopropylamine (102 μL, 0.72 mmol) in dry Et₂O (2.9 mL) stirred at -78 °C under argon was added dropwise a solution of 2.3 M *n*-BuLi in hexanes (313 μL, 0.72

mmol). The mixture was stirred at $-78\text{ }^{\circ}\text{C}$ for 1 hour. 2-Methyl-3-bromopyridine (124 mg, 0.72 mmol) was added dropwise. The resulting red mixture was stirred at $-78\text{ }^{\circ}\text{C}$ for 2 h under argon. Steroid **12** (120 mg, 0.36 mmol) in tetrahydrofuran (720 μL) was added dropwise and stirred at $-78\text{ }^{\circ}\text{C}$ for 4 h. The reaction flask was allowed to warm to $25\text{ }^{\circ}\text{C}$ and was quenched slowly with aqueous saturated ammonium chloride (10 mL). The mixture was extracted with ethyl acetate (3x 20 mL), and dried with sodium sulfate. The solvent was removed *in vacuo*, and the crude product was purified by silica gel chromatography (20% ethyl acetate in hexanes) to yield **13** as a white solid (89 mg, 49 %). **$^1\text{H NMR}$** (500 MHz; CDCl_3): δ 8.45 (t, $J = 2.3\text{ Hz}$, 1H), 7.92-7.90 (m, 1H), 7.61-7.59 (m, 2H), 7.45-7.32 (m, 6H), 7.08 (dd, $J = 8.0, 4.7\text{ Hz}$, 1H), 6.36 (s, 1H), 3.36 (d, $J = 15.2\text{ Hz}$, 1H), 3.17 (d, $J = 15.2\text{ Hz}$, 1H), 2.98 (t, $J = 4.3\text{ Hz}$, 2H), 2.39-2.32 (m, 2H), 2.01-1.98 (m, 1H), 1.84-1.60 (m, 8H), 1.48-1.44 (m, 3H), 1.29-1.27 (m, 1H), 1.03 (s, 3H). **$^{13}\text{C NMR}$** (126 MHz; CDCl_3): δ 159.6, 146.7, 141.3, 140.9, 139.8, 138.6, 137.3, 128.8, 127.8, 127.13, 127.06, 125.9, 124.5, 122.87, 122.74, 83.8, 50.0, 47.2, 44.4, 41.8, 39.5, 36.7, 32.7, 29.9, 27.7, 26.4, 23.8, 14.3. **FTIR** (thin film) 3359, 2932, 1575, 1484 cm^{-1} . **HRMS** (ES) Calcd. for $\text{C}_{30}\text{H}_{32}\text{BrNO}$: 501.1667 (M^+), found 502.1746 ($\text{M}+\text{H}^+$).



A microwave vial was charged with $\text{Pd}(\text{OAc})_2$ (3 mg, 0.01 mmol) and BINAP (8 mg, 0.01 mmol) and purged and backfilled with argon. Dry toluene (1.2 mL) and degassed water

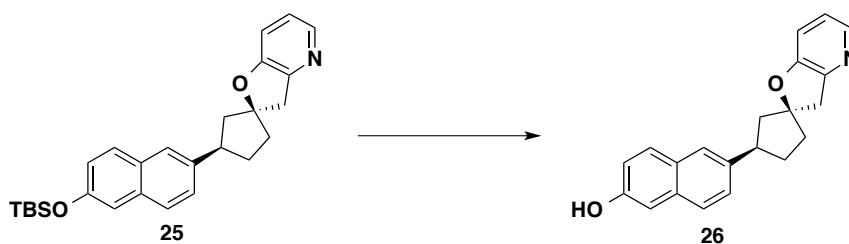
(10 μ L) were added and the resulting mixture was allowed to stir at 110 $^{\circ}$ C for 2 minutes. This solution of precatalyst was transferred to a second microwave vial containing Cs_2CO_3 (29 mg, 0.09 mmol) and alcohol **13** (30 mg, 0.06 mmol). The reaction was stirred at 80 $^{\circ}$ C for 12 hours. The mixture was allowed to cool to 25 $^{\circ}$ C, diluted with ethyl acetate (10 mL), filtered through Celite, concentrated and purified by silica gel chromatography (20% ethyl acetate in hexanes) to yield the spirocycle **14** as a white film (16 mg, 63%). **$^1\text{H NMR}$** (500 MHz; CDCl_3): δ 8.02 (dd, $J = 4.4, 1.2$ Hz, 1H), 7.58 (d, $J = 7.4$ Hz, 2H), 7.44-7.31 (m, 6H), 7.02-6.97 (m, 2H), 3.57 (d, $J = 16.6$ Hz, 1H), 3.03 (d, $J = 16.7$ Hz, 1H), 2.98-2.96 (m, 2H), 2.39-2.29 (m, 3H), 2.05-1.96 (m, 2H), 1.88-1.84 (m, 1H), 1.78 (s, 1H), 1.60-1.42 (m, 7H), 1.06 (s, 3H). **$^{13}\text{C NMR}$** (126 MHz; CDCl_3): δ 153.6, 151.3, 141.21, 141.19, 139.3, 138.8, 137.1, 128.8, 127.9, 127.1, 126.0, 124.61, 124.59, 122.4, 114.9, 98.3, 49.0, 46.4, 44.1, 40.4, 39.2, 37.0, 31.7, 29.8, 27.4, 26.1, 22.6, 14.5. **FTIR** (thin film) 2931, 1601, 1575, 1484 cm^{-1} . **HRMS** (ES) Calcd. for $\text{C}_{30}\text{H}_{31}\text{NO}$: 421.2406 (M^+), found 422.2491 ($\text{M}+\text{H}^+$).



A microwave vial was charged with triflate **11** (144 mg, 0.36 mmol), palladium acetate (2 mg, 0.01 mmol), X-Phos (4 mg, 0.01 mmol), 4-hydroxy-phenylboronic acid (64 mg, 0.47 mmol) and K_2CO_3 (164 mg, 1.19 mmol), purged and backfilled with argon. THF (1.6 mL, 0.2 M) and degassed water (0.4 mL, 0.8 M) were added and the resulting mixture was allowed to stir at 60 $^{\circ}$ C for 12 h. The mixture was allowed to cool to 25 $^{\circ}$ C, quenched

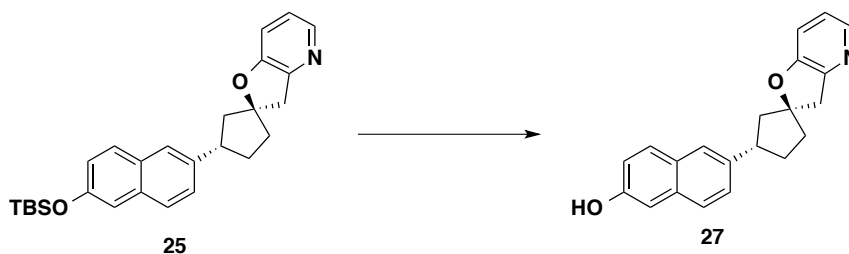
with water (10 mL) and extracted with dichloromethane (3x 15 mL). The organics were dried over sodium sulfate, concentrated and purified by silica gel chromatography with 20 % ethyl acetate in hexanes as the eluent to yield the coupled product **15** as a white film (125 mg, quantitative) $^1\text{H NMR}$ (500 MHz; CDCl_3): δ 7.35-7.32 (m, 2H), 7.26-7.23 (m, 1H), 7.04-7.03 (m, 1H), 7.00 (d, $J = 0.3$ Hz, 1H), 6.94-6.91 (m, 1H), 6.84-6.83 (m, 1H), 4.97-4.96 (m,), 2.96-2.93 (m, 2H), 2.55-2.50 (m, 1H), 2.42-2.38 (m, 1H), 2.32-2.27 (m, 1H), 2.20-2.12 (m, 1H), 2.10-2.02 (m, 2H), 2.00-1.97 (m, 1H), 1.67-1.44 (m, 9H), 0.93-0.90 (m, 3H). $^{13}\text{C NMR}$ (126 MHz; CDCl_3): δ 155.7, 147.7, 140.4, 139.4, 129.8, 127.34, 127.16, 121.4, 120.9, 118.5, 115.4, 100.1, 77.87, 77.74, 77.63, 77.58, 77.32, 77.31, 77.12, 77.06, 50.5, 48.0, 44.2, 37.9, 36.0, 31.6, 29.5, 26.2, 25.8, 21.7, 14.0. **FTIR** (thin film) 3366, 2934, 2865, 1737, 1605 cm^{-1} . **HRMS** (ES) Calcd. for $\text{C}_{24}\text{H}_{26}\text{O}_2$:346.1933, found $[\text{M}+\text{Na}]^+$: 369.2248.

Section 4.3 Des-C Analogs and the Importance of Shape



To a solution of **25** (27 mg, 0.06 mmol) in THF (0.6 mL, 0.1 M) was added TBAF (120 μL , 0.12 mmol) and the reaction for two hours at 25 $^\circ\text{C}$ before being quenched with saturated ammonium chloride (1 mL). The aqueous was extracted with ethyl acetate (2x,

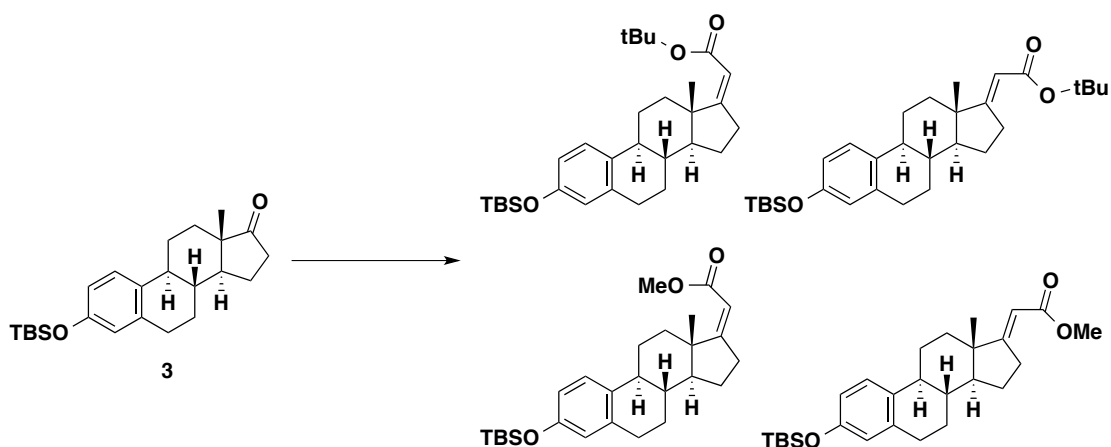
2 mL) and concentrated *in vacuo*. The crude residue was purified by silica gel chromatography with 50 % ethyl acetate in hexanes as the eluent to afford **26** as a white film (12 mg, 61%). **¹H NMR** (500 MHz, CDCl₃): δ 7.88 (dd, *J* = 4.0, 2.3 Hz, 1H), 7.59-7.53 (m, 3H), 7.34 (dd, *J* = 8.5, 1.8 Hz, 1H), 7.04-6.98 (m, 4H), 3.59 (s, 2H), 3.29 (d, *J* = 11.0 Hz, 3H), 2.39 (dd, *J* = 14.4, 9.4 Hz, 1H), 2.31-2.24 (m, 2H), 2.19-2.16 (m, 1H), 2.05-1.95 (m, 1H), 1.87-1.82 (m, 1H). **¹³C NMR** (126 MHz; CDCl₃): δ 154.2, 150.4, 140.2, 139.5, 133.5, 129.0, 128.3, 126.5, 126.1, 125.0, 122.8, 118.2, 116.1, 108.8, 96.4, 47.6, 44.0, 41.9, 40.7, 33.7. **FTIR** (thin film): 2924, 2852, 1604, 1578 cm⁻¹. **HRMS** (ES) Calcd. for C₂₁H₁₉NO₂: 317.1416 (M⁺), found 318.1496 (M+H⁺).



To a solution of **25** (23 mg, 0.05 mmol) in THF (0.5 mL, 0.1 M) was added TBAF (100 μL, 0.10 mmol) and the reaction for two hours at 25 °C before being quenched with saturated ammonium chloride (1 mL). The aqueous was extracted with ethyl acetate (2x, 2 mL) and concentrated *in vacuo*. The crude residue was purified by silica gel chromatography with 50 % ethyl acetate in hexanes as the eluent to afford **27** as a white film (11 mg, 65%). **¹H NMR** (500 MHz, CDCl₃): δ 7.88-7.86 (m, 1H), 7.53 (dt, *J* = 20.0, 10.7 Hz, 3H), 7.23 (dd, *J* = 8.5, 1.6 Hz, 1H), 7.03-6.94 (m, 4H), 3.72 (s, 2H), 3.59-3.55 (m, 1H), 3.31-3.27 (m, 2H), 2.47-2.43 (m, 1H), 2.34 (dt, *J* = 8.8, 4.6 Hz, 1H), 2.28-2.22 (m, 1H), 2.09 (ddd, *J* = 14.6, 9.9, 5.1 Hz, 1H), 1.95-1.84 (m, 2H). **¹³C NMR** (126 MHz;

CDCI₃): δ 153.1, 150.4, 140.4, 139.1, 133.5, 129.0, 128.4, 126.5, 126.0, 124.7, 122.9, 118.3, 116.2, 108.9, 97.0, 48.1, 43.7, 40.8, 39.6, 32.4. **FTIR** (thin film): 2924, 2853, 1604 cm^{-1} . **HRMS** (ES) Calcd. for $\text{C}_{21}\text{H}_{19}\text{NO}_2$: 317.1416 (M^+), found 318.1494 ($\text{M}+\text{H}^+$).

Section 4.5 Establishing the Role of Oxygen



To a solution of *tert*-Butyl P,P-dimethylphosphonoacetate (673 mg, 3.0 mmol) in THF (4.5 mL, 0.22 M) was added NaH (60 % by wt., 130 mg, 3.3 mmol) in small portions to control excessive release of hydrogen gas. Protected estrone **3** (384 mg, 1.0 mmol) was added to the above slurry after 15 minutes, and the reaction mixture was warmed to reflux for 4 hours. The reaction was cooled to 25 °C, diluted with water (10 mL), extracted with ethyl acetate (3x, 15 mL), dried over sodium sulfate, and concentrated *in vacuo*. The crude product was purified by silica gel chromatography with 10 % ethyl acetate in hexanes to isolate a mixture of the four shown products (100 mg). The resulting complex mixture was further purified by preparative thin layer chromatography (1000 μm , 5 % ethyl acetate in hexanes) to isolate three unique fractions; Z-*t*-butyl ester

(24 mg, 5 %), *E*-*t*-butyl and *E*-methyl esters (30 mg, 6 %), and *Z*-methyl ester (14 mg, 3 %).

Z-*t*-butyl ester: $^1\text{H NMR}$ (500 MHz, CDCl_3): δ 7.12 (d, $J = 8.5$ Hz, 1H), 6.55 (d, $J = 2.3$ Hz, 1H), 5.62 (d, $J = 1.8$ Hz, 1H), 1.49 (s, 10H), 1.42-1.39 (m, 6H), 1.04 (s, 3H), 0.98 (s, 9H), 0.19 (d, $J = 2.9$ Hz, 6H).

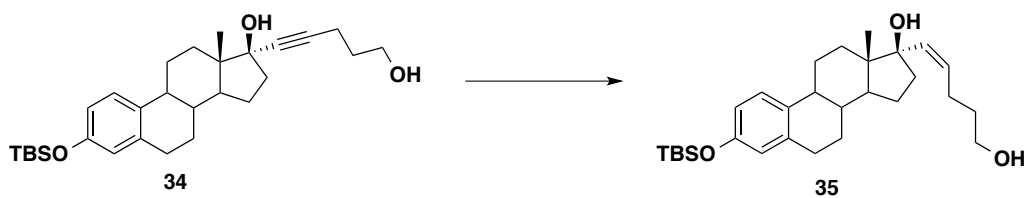
E-*t*-butyl (66 %) and *E*-methyl esters (33 %): $^1\text{H NMR}$ (500 MHz, CDCl_3): δ 7.13 (d, $J = 8.6$ Hz, 1H), 6.62 (dd, $J = 8.4, 2.6$ Hz, 1H), 6.56 (t, $J = 2.9$ Hz, 1H), 5.69 (t, $J = 2.0$ Hz,), 5.50 (t, $J = 2.5$ Hz, 1H), 3.69 (s, 1H), 2.89-2.78 (m, 4H), 2.63-2.19 (m, 3H), 1.98-1.81 (m, 3H), 1.49-1.41 (m, 13H), 1.04 (s, 1H), 0.98 (s, 9H), 0.86 (s, 3H), 0.19 (s, 6H).

Z-methyl ester: $^1\text{H NMR}$ (500 MHz, CDCl_3): δ 7.12 (d, $J = 8.2$ Hz, 1H), 6.62 (dd, $J = 8.4, 2.6$ Hz, 1H), 6.56 (d, $J = 2.6$ Hz, 1H), 5.60 (t, $J = 2.5$ Hz, 1H), 3.70 (s, 3H), 2.90-2.82 (m, 4H), 1.96 (s, 3H), 1.57-1.43 (m, 7H), 0.98-0.97 (m, 9H), 0.86 (s, 3H), 0.19-0.18 (m, 6H).



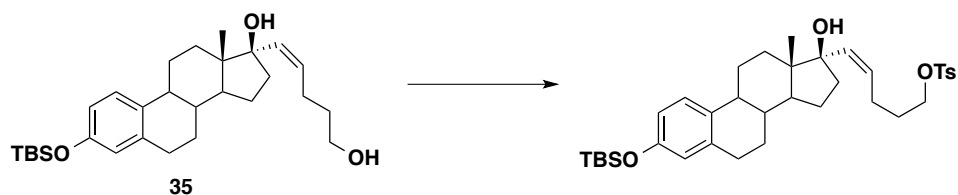
Cerium trichloride heptahydrate (611 mg, 1.64 mmol) was dried in vacuo overnight at 140 °C to remove all water. Once dried, CeCl_3 was stirred in THF (6.6 mL) over night until homogeneous. $n\text{BuLi}$ (1.28 mL, 3.2 mmol) was added to a stirred solution of 4-pentyn-1-ol (135 mg, 1.6 mmol) in THF (3.3 mL) cooled to -78 °C. The resulting yellow solution of dianion was allowed to stir at -78 °C for 30 min. The dianion solution was then warmed to 0 °C and transferred via cannula to a stirring solution of CeCl_3 in THF

(0.25 M) cooled to $-78\text{ }^{\circ}\text{C}$. After an hour of stirring at $-78\text{ }^{\circ}\text{C}$, TBS-estrone **3** (77 mg, 0.2 mmol) in THF (1.5 mL) was added dropwise to the solution held at $-78\text{ }^{\circ}\text{C}$. The reaction was monitored by TLC until complete (1 h). Saturated aqueous NH_4Cl (4 mL) was added in one portion to quench the remaining dianion. The aqueous was extracted with ethyl acetate (3x, 20 mL), the organics combined, washed with brine (20 mL), dried over sodium sulfate, and concentrated *in vacuo* to yield **34** as a white film (84 mg, 90 %). The resulting solid was clean by ^1H NMR and no further purification was necessary. ^1H NMR (500 MHz, CDCl_3): δ 7.12 (d, $J = 8.5$ Hz, 1H), 6.61 (dd, $J = 2.5, 8.5$ Hz, 1H), 6.55 (d, $J = 2.5$ Hz, 1H), 3.76 (t, $J = 6.3$ Hz, 2H), 2.82-2.79 (m, 2H), 2.38 (d, $J = 6.8$ Hz, 2H), 2.35-2.31 (m, 1H), 2.27-2.23 (m, 1H), 2.22-2.16 (m, 2H), 2.02-1.96 (m, 2H), 1.87-1.84 (m, 2H), 1.78 (t, $J = 6.5$ Hz, 2H), 1.74-1.63 (m, 2H), 1.50-1.32 (m, 5H), 0.98 (s, 9H). 0.87 (s, 3H), 0.19 (s, 6H). ^{13}C NMR (126 MHz, CDCl_3): δ 153.39, 137.95, 133.10, 126.27, 120.06, 117.28, 85.53, 84.53, 80.11, 61.81, 49.69, 47.29, 43.85, 39.50, 39.25, 33.10, 31.51, 29.78, 27.44, 26.49, 25.83, 22.93, 18.29, 15.56, 12.98, -4.26 FTIR (thin film): 3359, 2244, 1607, 1496, 1256 cm^{-1} . HRMS (m/z): calcd for $\text{C}_{29}\text{H}_{44}\text{O}_3\text{Si}$: 469.3138, found $[\text{M}+\text{H}]^+$: 469.3131.



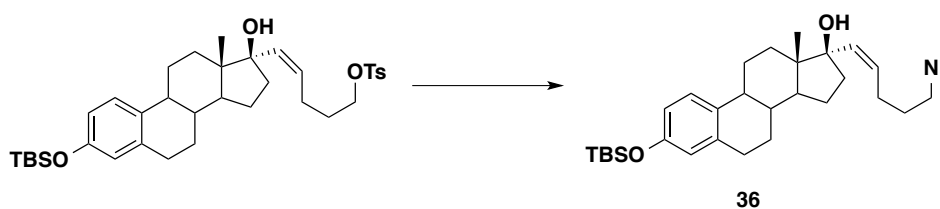
Quinoline (119 mg, 0.26 mmol) was added to a stirred suspension of 5 % Pd/BaSO_4 (119 mg, 0.53 mmol) in ethyl acetate (2.5 mL). After 20 min at $25\text{ }^{\circ}\text{C}$ the alkyne **34** (124 mg, 0.26 mmol) was added. The solvent was sparged with hydrogen, and the resulting

suspension stirred under an atmosphere of H₂ (1 atm) for 2 h. The solution was diluted with 10 mL ethyl acetate then filtered through a pad of celite and concentrated *in vacuo*. The resulting material was purified via silica chromatography with 50 % ethyl acetate in hexanes as the eluent to yield the alkene **35** (97 mg, 54 %) as a white foam. ¹H NMR (500 MHz; CDCl₃): δ 7.11 (d, *J* = 8.5 Hz, 1H), 6.61 (dd, *J* = 2.5, 8.5 Hz, 1H), 6.54 (d, *J* = 2.5 Hz, 1H), 5.61 (d, *J* = 12 Hz, 1H), 5.41 (m, 1H), 3.66 (m, 2H), 2.86-2.75 (m, 2H), 2.65-2.58 (m, 1H), 2.38-2.27 (m, 2H), 2.16-2.11 (m, 2H), 1.90-1.85 (m, 2H), 2.02-1.96 (m, 2H), 1.87-1.84 (m, 2H), 1.78 (t, *J* = 6.5 Hz, 2H), 1.74-1.63 (m, 2H), 1.50-1.77-1.57 (m, 6H), 1.51-1.37 (m, 4H) 1.34-1.26 (m, 2H), 0.98 (s, 9H), 0.87 (s, 3H), 0.19 (s, 6H). ¹³C NMR (126 MHz, CDCl₃): δ 153.42, 137.95, 134.53, 133.18, 131.18, 126.27, 120.05, 117.27, 85.32, 61.05, 49.69, 47.88, 43.88, 40.18, 39.77, 32.17, 31.47, 27.54, 26.49, 25.85, 23.29, 18.31, 13.92, -4.25 FTIR (thin film): 3347, 2929, 2858, 1496, 1255 cm⁻¹. HRMS (*m/z*): calcd for C₂₉H₄₆O₃Si: 470.32, found [M+Na]⁺: 493.3104.



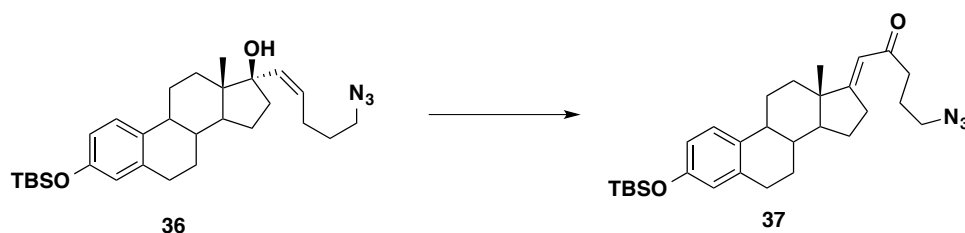
To a solution of alcohol **35** (138 mg, 0.29 mmol) and DMAP (4.0 mg, 0.01 mmol) in dichloromethane (2.9 mL) was added a solution of TsCl (139 mg, 0.73 mmol) in dichloromethane (0.73 mL). The solution was cooled to 0 °C and Et₃N (148 mg, 1.47 mmol) was then added dropwise. After stirring for 12 h at 25 °C, deionized water (10 mL) was added and the mixture was extracted with ethyl acetate (3 × 10 mL). The combined organic solution was dried over MgSO₄ and concentrated *in vacuo*. The residue was

purified by silica gel chromatography (25 % ethyl acetate in hexanes) to afford the tosylate (97 mg, 54 %) as a white foam. **¹H NMR** (500 MHz; CDCl₃): δ 7.80 (d, *J* = 8.5, 2H), 7.33 (d, *J* = 8, 2H), 7.10 (d, *J* = 8.5 Hz, 1H), 6.61 (dd, *J* = 2.5, 8.5 Hz, 1H), 6.54 (d, *J* = 2.5 Hz, 1H), 5.57 (d, *J* = 12 Hz, 1H), 5.34 (m, 1H) 4.11 (m, 2H), 2.82-2.75 (m, 2H), 2.48-2.41 (m, 4H), 2.37-2.32 (m, 1H), 2.28-2.25 (m, 1H), 2.14-2.08 (m, 1H), 2.01-1.97 (m, 1H), 1.89-1.84 (m, 2H), 1.78-1.71 (m, 3H), 1.62-1.36 (m, 8H), 0.98 (s, 9H). 0.91 (s, 3H), 0.19 (s, 6H). **¹³C NMR** (126 MHz, CDCl₃): δ 153.45, 144.75, 137.93, 135.30, 133.46, 133.16, 130.45, 129.93, 128.02, 126.23, 120.04, 117.27, 84.84, 70.34, 60.49, 49.61, 47.75, 43.89, 39.72, 39.66, 32.15, 29.77, 29.32, 27.57, 26.49, 25.84, 25.12 23.34, 21.74, 21.14, 18.29, 14.32, 13.92, -4.25 **FTIR** (thin film): 3551, 2930, 1495, 1176 cm⁻¹. **HRMS**: calcd for C₃₆H₅₂O₅SSi: 624.33, found [M+Na]⁺: 647.3212.



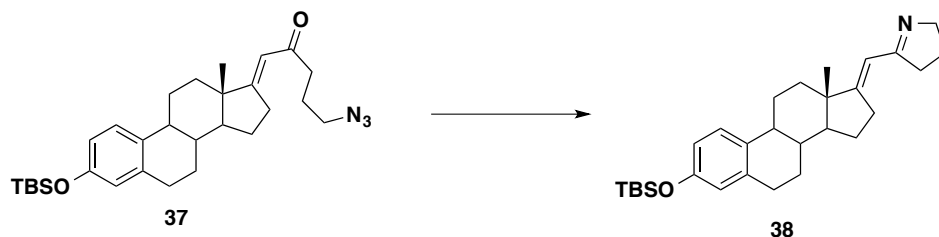
To a solution of tosylate (518 mg, 0.83 mmol) in dimethylformamide (3.3 mL, 0.25 M) was added sodium azide (162 mg, 2.5 mmol) and stirred for 12 h at 25 °C. The reaction was diluted with dichloromethane (15 mL) and quenched with deionized water (10 mL). The layers were separated and the aqueous extracted with dichloromethane (3x 15 mL), the organics washed with brine (10 mL), dried over sodium sulfate, and concentrated *in vacuo*. The crude material was purified with silica gel chromatography (20 % ethyl acetate in hexanes) to afford **36** as a white film (382 mg, 93 %). **¹H NMR** (500 MHz; CDCl₃): δ 7.11 (d, *J* = 8.3 Hz, 1H), 6.61 (s, 1H), 6.55 (d, *J* = 2.6 Hz, 1H), 5.60 (s, 1H),

5.41 (d, $J = 11.8$ Hz, 1H), 3.32 (t, $J = 6.9$ Hz, 2H), 1.72-1.59 (m, 7H), 1.42 (d, $J = 10.3$ Hz, 5H), 0.98 (d, $J = 6.0$ Hz, 9H), 0.93 (s, 3H), 0.19 (q, $J = 2.1$ Hz, 6H). ^{13}C NMR (126 MHz; CDCl_3): δ 153.4, 138.0, 135.2, 133.2, 130.8, 126.3, 120.1, 117.3, 84.9, 51.2, 49.6, 47.8, 43.9, 39.72, 39.71, 32.2, 29.8, 29.1, 27.6, 26.5, 26.3, 25.9, 23.4, 18.3, 14.0, -4.2. FTIR (thin film): 3482, 2929, 2857, 2095, 1606 cm^{-1} . HRMS (m/z): calcd for $\text{C}_{29}\text{H}_{45}\text{N}_3\text{O}_2\text{Si}$: 495.3281, found $[\text{M}-\text{N}_2+\text{H}]^+$: 468.3308.

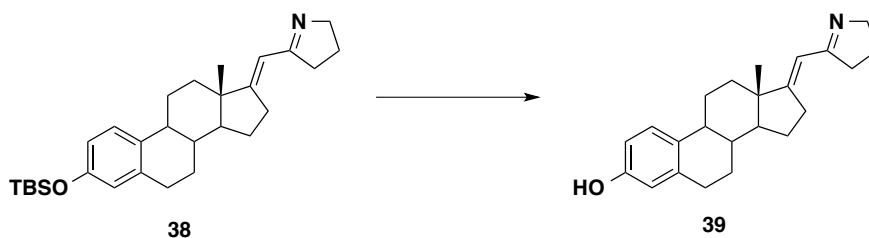


To a solution of allylic alcohol **36** (32 mg, 0.07 mmol) in dichloromethane (0.90 mL, 0.07 M) was added pyridinium chlorochromate (35 mg, 0.16 mmol) in one portion and was stirred for 12 hours at 25 °C. The reaction was diluted with ethyl acetate (5 mL) and filtered through a pad of Celite and concentrated *in vacuo*. The crude material was purified using silica gel chromatography (20 % ethyl acetate in hexanes) to afford **37** as a white foam (18 mg, 56 %). ^1H NMR (500 MHz; CDCl_3): δ 7.12 (dd, $J = 8.6, 4.2$ Hz, 1H), 6.62 (dd, $J = 8.4, 2.6$ Hz, 1H), 6.57-6.56 (m, 1H), 5.99 (t, $J = 2.3$ Hz, 1H), 3.34 (t, $J = 6.7$ Hz, 2H), 2.91-2.79 (m, 3H), 2.62-2.55 (m, 1H), 2.42-2.37 (m, 1H), 2.26-2.21 (m, 1H), 2.00-1.87 (m, 4H), 1.58-1.41 (m, 6H), 1.31-1.26 (m, 4H), 0.98 (s, 9H), 0.87 (s, 3H), 0.19 (s, 6H). ^{13}C NMR (126 MHz; CDCl_3): δ 199.6, 176.1, 153.6, 138.0, 132.9, 126.2, 120.2, 117.4, 115.7, 52.7, 51.1, 46.8, 44.2, 40.5, 38.7, 35.6, 31.6, 29.8, 27.8, 26.7, 25.9,

24.4, 23.5, 18.8, 18.3, -4.2. **FTIR** (thin film): 2928, 2856, 2096, 1741, 1687 cm^{-1} . **HRMS** (m/z): calcd for $\text{C}_{29}\text{H}_{43}\text{N}_3\text{O}_2\text{Si}$: 493.3140, found $[\text{M}+\text{Na}]^+$: 494.3208.

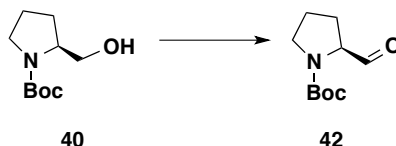


To a solution of azide **37** (60 mg, 0.12 mmol) in tetrahydrofuran (10 mL, 0.07 M) was added triphenylphosphine (132 mg, 0.31 mmol) in one portion and stirred at 25 °C over night and then concentrated *in vacuo*. The crude material was purified with silica gel chromatography (10 % ethyl acetate in hexanes) to afford imine **38** as a white film (25 mg, 42 %). **¹H NMR** (500 MHz; CDCl_3): δ 7.13 (d, $J = 8.5$ Hz, 1H), 6.62 (dd, $J = 8.4, 2.6$ Hz, 1H), 6.56-6.55 (m, 1H), 6.06 (s, 1H), 3.87 (t, $J = 7.4$ Hz, 2H), 2.82-2.69 (m, 5H), 2.01 (d, $J = 11.9$ Hz, 1H), 1.93-1.88 (m, 4H), 1.73 (s, 1H), 1.51-1.41 (m, 5H), 1.26 (d, $J = 6.8$ Hz, 3H), 0.98 (d, $J = 4.0$ Hz, 9H), 0.87 (d, $J = 14.0$ Hz, 3H), 0.19-0.19 (m, 6H). **¹³C NMR** (126 MHz; CDCl_3): δ 174.18, 174.16, 164.5, 153.5, 137.93, 137.92, 133.17, 133.14, 128.2, 126.25, 126.21, 120.17, 120.12, 120.10, 117.36, 117.34, 114.71, 114.69, 114.67, 60.41, 60.39, 60.37, 53.0, 46.4, 44.2, 38.8, 37.7, 36.0, 29.86, 29.82, 29.77, 27.8, 26.8, 25.88, 25.85, 25.78, 24.65, 24.64, 23.1, 19.0, 18.3, -4.2. **FTIR** (thin film): 2928, 2856, 1651, 1607 cm^{-1} . **HRMS** (m/z): calcd for $\text{C}_{29}\text{H}_{43}\text{NOSi}$: 449.3140, found $[\text{M}+\text{H}]^+$: 450.3196.

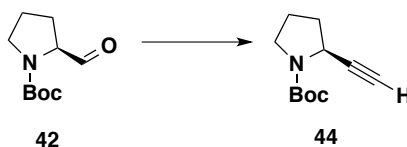


Tetrabutylammonium fluoride (1.0M in THF, 590 μ L, 0.59 mmol) was added dropwise to a solution of imine **38** (106 mg, 0.24 mmol) in tetrahydrofuran (2.4 mL, 0.1 M) at 25 $^{\circ}$ C and stirred for 2 hours. The reaction quenched with saturated NH_4Cl (1 mL) and extracted with ethyl acetate (3x 15 mL) and concentrated *in vacuo*. The crude material purified by silica gel chromatography (10 % methanol in dichloromethane with 1 % ammonium hydroxide) to obtain deprotected imine **39** as a white film (18 mg, 23 %). **^1H NMR** (500 MHz; CDCl_3): δ 6.87 (d, J = 8.5 Hz, 1H), 6.38-6.36 (m, 1H), 6.31 (s, 1H), 5.94 (s, 1H), 3.64-3.61 (m, 2H), 3.09 (dd, J = 1.9, 1.1 Hz, 2H), 2.96-2.93 (m, 2H), 2.72-2.69 (m, 2H), 2.63-2.55 (m, 3H), 2.50-2.44 (m, 1H), 2.18-2.14 (m, 1H), 2.00-1.94 (m, 1H), 1.88-1.82 (m, 2H), 1.82-1.69 (m, 4H), 1.42-0.99 (m, 11H), 0.79 (dd, J = 9.4, 5.2 Hz, 3H), 0.65-0.62 (m, 3H). **^{13}C NMR** (126 MHz; CDCl_3): δ 154.50, 137.82, 132.02, 131.94, 131.19, 128.77, 128.68, 126.29, 115.23, 112.80, 58.74, 52.46, 43.87, 40.21, 38.62, 36.88, 35.43, 30.76, 30.27, 29.66, 29.57, 27.61, 26.53, 24.40, 23.81, 19.65, 18.56, 13.43. **FTIR** (thin film): 3148, 2927, 1638, 1580 cm^{-1} . **HRMS (m/z)**: calcd for $\text{C}_{23}\text{H}_{29}\text{NO}$: 335.2249, found $[\text{M}+\text{H}]^+$: 336.2317.

Section 4.6 Rigidity versus Flexibility

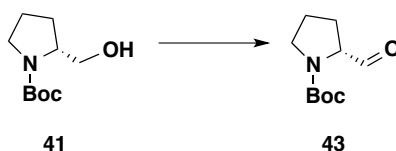


N-Boc-L-Prolinol **40** (1.82 g, 9.0 mmol) was added as a solution in DCM (18 mL, 0.5 M) dropwise to a slurry of Dess Martin periodinane (4.77 g, 11.25 mmol) in DCM (45 mL, 0.25 M) and *t*-BuOH (945 μ L, 9.9 mmol) at 0 °C and stirred for 1.5 hours. The reaction was quenched with saturated sodium thiosulfate (20 mL) and saturated sodium bicarbonate (20 mL) and stirred for 10 minutes at 25 °C. The aqueous was extracted with DCM (3x, 40 mL), dried over sodium sulfate, and concentrated *in vacuo*. The crude residue was purified via silica gel chromatography with 33 % ethyl acetate in hexanes as the eluent to afford *N*-Boc-L-Prolinal **42** as a white film (1.20 g, 68 %). $^1\text{H NMR}$ (500 MHz, CDCl_3): δ 9.55-9.46 (m, 1H), 4.05-4.03 (m, 1H), 3.57-3.43 (m, 2H), 2.13-1.86 (m, 5H), 1.44 (d, $J = 24.8$ Hz, 9H).

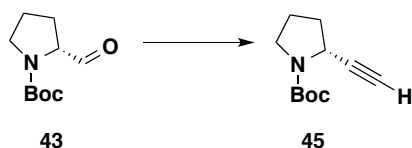


To a slurry of *N*-Boc-L-Prolinal **42** (1.20 g, 6.0 mmol) and potassium carbonate (2.50 g, 18.0 mmol) in methanol (60 mL, 0.1 M) at 25 °C was added freshly prepared Ohira-Bestmann reagent (2.90 g, 15.0 mmol). The solution was allowed to stir overnight at 25 C, before quenching with water (25 mL). The aqueous was extracted with ethyl acetate

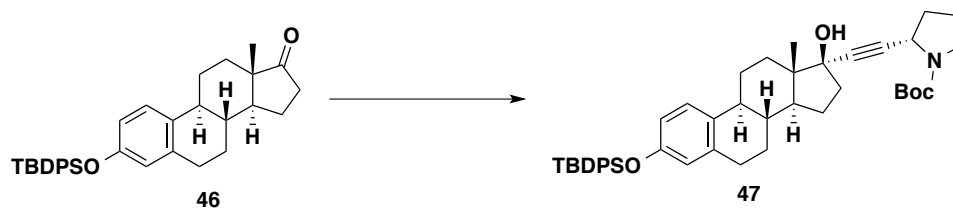
(3x, 40 mL), dried over sodium sulfate, and concentrated *in vacuo*. The crude material was purified with silica gel chromatography with a gradient of 10-25 % ethyl acetate in hexanes as the eluent to afford alkyne **44** as a clear oil (820 mg, 70 %). $^1\text{H NMR}$ matches reported spectra. $^1\text{H NMR}$ (500 MHz, CDCl_3): δ 4.54-4.39 (m, 1H), 3.48-3.30 (m, 2H), 2.21-1.89 (m, 6H), 1.48 (s, 9H).



N-Boc-D-Prolinol **41** (1.20 g, 6.0 mmol) was added as a solution in DCM (12 mL, 0.5 M) dropwise to a slurry of Dess Martin periodinane (3.18 g, 7.5 mmol) in DCM (30 mL, 0.25 M) and *t*-BuOH (630 μL , 6.6 mmol) at 0 °C and stirred for 1.5 hours. The reaction was quenched with saturated sodium thiosulfate (20 mL) and saturated sodium bicarbonate (20 mL) and stirred for 10 minutes at 25 °C. The aqueous was extracted with DCM (3x, 30 mL), dried over sodium sulfate, and concentrated *in vacuo*. The crude residue was purified via silica gel chromatography with 33 % ethyl acetate in hexanes as the eluent to afford *N*-Boc-D-Prolinal **43** as a white film (888 mg, 74 %). $^1\text{H NMR}$ (500 MHz, CDCl_3): δ 9.56-9.46 (m, 1H), 4.04 (dd, $J = 2.2, 0.7$ Hz, 1H), 3.56-3.44 (m, 2H), 2.12-1.84 (m, 5H), 1.48-1.43 (m, 9H).

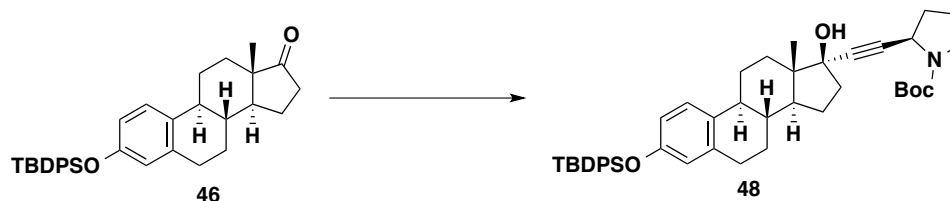


To a slurry of *N*-Boc-D-Prolinal **43** (888 mg, 4.5 mmol) and potassium carbonate (1.90 g, 13.5 mmol) in methanol (45 mL, 0.1 M) at 25 °C was added freshly prepared Ohira-Bestmann reagent (2.14 g, 11.2 mmol). The solution was allowed to stir overnight at 25 C, before quenching with water (25 mL). The aqueous was extracted with ethyl acetate (3x, 30 mL), dried over sodium sulfate, and concentrated *in vacuo*. The crude material was purified with silica gel chromatography with a gradient of 10-30 % ethyl acetate in hexanes as the eluent to afford alkyne **45** as a clear oil (400 mg, 46 %). $^1\text{H NMR}$ matches reported spectra. $^1\text{H NMR}$ (500 MHz, CDCl_3): δ 4.53-4.39 (m, 1H), 3.48-3.30 (m, 2H), 2.20-2.01 (m, 4H), 1.90-1.88 (m, 1H), 1.48 (s, 9H).



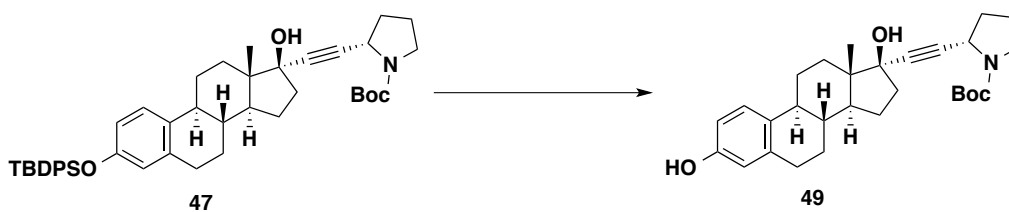
To a solution of alkyne **44** (400 mg, 2.0 mmol) in THF at -78 °C (4 mL, 0.5 M) was added *n*-BuLi (2.6 M, 770 μL , 2.0 mmol) dropwise, followed by protected steroid **46** (508 mg, 1.0 mmol) in THF (10 mL, 0.1M). The reaction was allowed to slowly warm to 25 C over night, and was quenched with saturated ammonium chloride (25 mL). The aqueous was extracted with ethyl acetate (3x, 30 mL), dried over sodium sulfate and concentrated *in vacuo*. The crude residue was purified with silica gel chromatography with 20-33 % ethyl acetate as the eluent to afford alkyne alcohol **47** as a clear oil (411 mg, 58 %) $^1\text{H NMR}$

(500 MHz; CDCl₃): δ 7.73-7.72 (m, 4H), 7.37 (d, *J* = 7.3 Hz, 6H), 6.96 (d, *J* = 8.5 Hz, 1H), 6.53-6.48 (m, 2H), 4.50-4.50 (m, 1H), 3.44 (dt, *J* = 1.0, 0.5 Hz, 1H), 3.31 (dd, *J* = 2.1, 1.1 Hz, 1H), 2.68 (sextett, *J* = 9.5, 7.2 Hz, 2H), 2.24 (dt, *J* = 9.0, 4.0 Hz, 2H), 2.12 (d, *J* = 9.4 Hz, 2H), 1.99 (d, *J* = 13.8 Hz, 3H), 1.89-1.63 (m, 8H), 1.46 (s, 9H), 1.38 (d, *J* = 11.1 Hz, 3H), 1.09 (s, 9H), 0.85 (s, 3H). ¹³C NMR (126 MHz; CDCl₃): δ 160.9, 141.5, 137.8, 135.7, 133.46, 133.42, 129.89, 129.86, 127.8, 126.0, 119.7, 119.1, 116.9, 101.8, 60.5, 49.96, 49.78, 49.74, 43.8, 39.5, 33.06, 33.05, 32.8, 29.7, 28.67, 28.63, 27.4, 26.7, 26.5, 23.0, 21.2, 19.6, 14.4, 13.0. FTIR (thin film): 3418, 2931, 1682, 1606 cm⁻¹. HRMS (m/z): calcd for C₄₅H₅₇NO₄Si: 703.4057, found [M+Na]⁺: 726.3956.

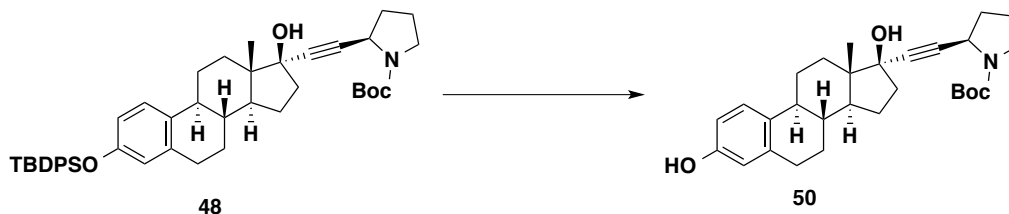


To a solution of alkyne **45** (400 mg, 2.0 mmol) in THF at -78 °C (4 mL, 0.5 M) was added *n*-BuLi (2.6 M, 770 μL, 2.0 mmol) dropwise, followed by protected steroid **46** (508 mg, 1.0 mmol) in THF (10 mL, 0.1M). The reaction was allowed to slowly warm to 25 °C over night, and was quenched with saturated ammonium chloride (25 mL). The aqueous was extracted with ethyl acetate (3x, 30 mL), dried over sodium sulfate and concentrated *in vacuo*. The crude residue was purified with silica gel chromatography with 20-33 % ethyl acetate as the eluent to afford alkynyl alcohol **48** as a clear oil (321 mg, 46 %). ¹H NMR (500 MHz; CDCl₃): δ 7.73 (dd, *J* = 4.0, 2.6 Hz, 4H), 7.43-7.35 (m, 6H), 6.97 (d, *J* = 8.5 Hz, 1H), 6.53-6.49 (m, 2H), 4.49-4.49 (m, 1H), 3.46-3.31 (m, 2H), 2.74-2.62 (m, 2H), 2.24 (ddd, *J* = 10.4, 8.2, 8.1 Hz, 2H), 2.14-2.09 (m, 2H), 2.03-1.98 (m, 3H), 1.90 (d, *J* =

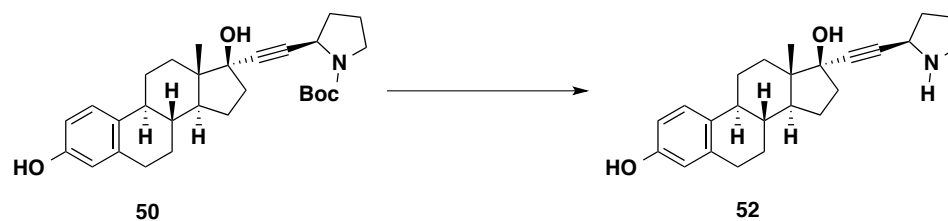
12.7 Hz, 2H), 1.82-1.59 (m, 6H), 1.47 (s, 9H), 1.38 (d, $J = 11.4$ Hz, 4H), 1.09 (s, 9H), 0.85 (s, 3H). $^{13}\text{C NMR}$ (126 MHz; CDCl_3): δ 156.1, 153.4, 137.8, 135.7, 133.44, 133.41, 131.7, 129.9, 127.8, 127.3, 126.0, 119.7, 116.9, 79.7, 60.5, 49.8, 39.5, 33.07, 32.90, 29.7, 28.74, 28.68, 27.4, 26.7, 23.0, 21.2, 19.6, 14.4, 13.4, 13.0. **FTIR** (thin film): 3420, 2930, 1680, 1496 cm^{-1} . **HRMS** (m/z): calcd for $\text{C}_{45}\text{H}_{57}\text{NO}_4\text{Si}$: 703.4057, found $[\text{M}+\text{Na}]^+$: 726.3970.



TBAF (440 μL , 0.44 mmol) was added dropwise to a solution of alkyne **47** (153 mg, 0.22 mmol) in THF (2.2 mL, 0.1 M) at 25 $^\circ\text{C}$. The reaction was quenched after stirring for 12 hours with saturated ammonium chloride (5 mL), extracted with ethyl acetate (3x, 10 mL), dried over sodium sulfate, and concentrated *in vacuo*. The crude residue was purified with silica gel chromatography with 50 % ethyl acetate in hexanes as the eluent to afford free phenol **49** (101 mg, 98 %). $^1\text{H NMR}$ (500 MHz, CDCl_3): δ 7.11-7.02 (m, 1H), 6.69 (d, $J = 8.2$ Hz, 1H), 6.60-6.59 (m, 1H), 4.58-4.51 (m, 1H), 3.48-3.47 (m, 1H), 3.32-3.29 (m, 1H), 2.77-2.71 (m, 2H), 2.25-2.16 (m, 3H), 2.07-1.97 (m, 5H), 1.89-1.60 (m, 6H), 1.41-1.29 (m, 3H), 0.86-0.84 (m, 3H). $^{13}\text{C NMR}$ (126 MHz; CDCl_3): δ 154.47, 154.23, 138.0, 126.4, 115.44, 112.92, 80.12, 60.6, 49.70, 48.33, 47.4, 46.2, 45.65, 43.70, 43.27, 39.5, 39.07, 38.90, 34.01, 33.99, 33.22, 33.03, 28.73, 28.63, 27.33, 26.5, 24.5, 23.79, 23.0, 14.3, 13.0. **FTIR** (thin film): 3351, 2931, 1671, 1499 cm^{-1} . **HRMS** (m/z): calcd for $\text{C}_{29}\text{H}_{39}\text{NO}_4$: 465.2879, found $[\text{M}+\text{Na}]^+$: 488.2781.



TBAF (900 μ L, 0.90 mmol) was added dropwise to a solution of alkyne **48** (320 mg, 0.45 mmol) in THF (4.5 mL, 0.1 M) at 25 °C. The reaction was quenched after stirring for 12 hours with saturated ammonium chloride (10 mL), extracted with ethyl acetate (3x, 15 mL), dried over sodium sulfate, and concentrated *in vacuo*. The crude residue was purified with silica gel chromatography with 50 % ethyl acetate in hexanes as the eluent to afford free phenol **49** (207 mg, 99 %). **¹H NMR** (500 MHz, CDCl₃): δ 7.31 (d, J = 0.5 Hz, 1H), 7.11 (dd, J = 5.6, 0.6 Hz, 1H), 6.70 (d, J = 8.4 Hz, 1H), 6.64 (s, 1H), 3.32-3.31 (m, 2H), 2.81-2.77 (m, 2H), 2.31-1.62 (m, 14H), 0.87 (s, 3H). **¹³C NMR** (126 MHz; CDCl₃): δ 154.5, 154.2, 138.0, 131.76, 126.4, 115.5, 112.94, 86.29, 80.29, 80.07, 79.5, 49.74, 48.34, 47.57, 46.10, 45.66, 43.84, 39.54, 39.09, 33.00, 29.73, 28.60, 27.36, 26.55, 24.60, 23.83, 22.84, 14.3, 12.94. **FTIR** (thin film): 3351, 2931, 1673, 1611 cm^{-1} . **HRMS (m/z)**: calcd for C₂₉H₃₉NO₄: 465.2879, found [M+Na]⁺: 488.2784.

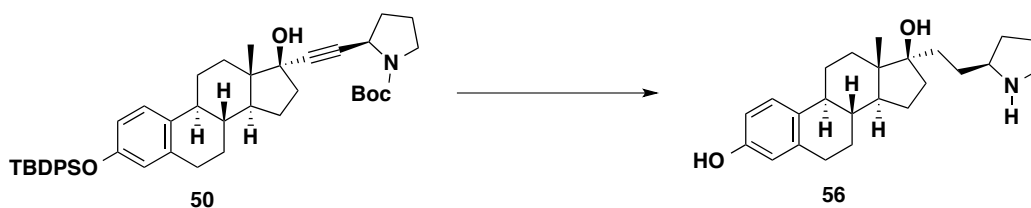


To a solution of carbamate **50** (29 mg, 0.06 mmol) in DCM (600 μ L, 0.1 M) was added TFA (60 μ L, 1.0 M) dropwise. The reaction stirred at 25 $^{\circ}$ C for 3 hours before being concentrated *in vacuo*. The crude material **52** was pure and no further methods of purification were needed (13 mg, 57 %). **$^1\text{H NMR}$** (500 MHz, CDCl_3): δ 7.07-7.06 (m, 1H), 6.57 (dd, $J = 8.4, 2.5$ Hz, 1H), 6.50 (d, $J = 2.3$ Hz, 1H), 4.35 (t, $J = 6.8$ Hz, 1H), 3.39-3.25 (m, 2H), 2.74 (td, $J = 9.8, 7.1$ Hz, 2H), 2.29-1.91 (m, 8H), 1.82-1.78 (m, 1H), 1.71-1.61 (m, 3H), 1.52-1.20 (m, 7H), 0.81-0.79 (m, 3H). **$^{13}\text{C NMR}$** (126 MHz; CDCl_3): δ 154.3, 138.0, 131.4, 126.4, 115.3, 112.8, 92.4, 79.2, 78.7, 47.3, 44.4, 43.8, 39.4, 38.5, 33.1, 32.4, 29.7, 27.3, 26.4, 23.5, 22.9, 12.7. **FTIR** (thin film): 3371, 2928, 1673, 1446 cm^{-1} . **HRMS (m/z)**: calcd for $\text{C}_{24}\text{H}_{31}\text{NO}_2$: 365.2355, found $[\text{M}+\text{H}]^+$: 366.2441.



To a solution of carbamate **49** (17 mg, 0.04 mmol) in DCM (400 μ L, 0.1 M) was added TFA (40 μ L, 1.0 M) dropwise. The reaction stirred at 25 $^{\circ}$ C for 3 hours before being concentrated *in vacuo*. The crude material **51** was pure and no further methods of purification were needed (9 mg, 62 %). **$^1\text{H NMR}$** (500 MHz, CDCl_3): δ 7.05 (d, $J = 8.5$

Hz, 1H), 6.56 (dd, $J = 8.4, 2.6$ Hz, 1H), 6.49 (d, $J = 2.4$ Hz, 1H), 4.33 (dd, $J = 8.8, 5.0$ Hz, 1H), 3.36-3.23 (m, 2H), 2.76-2.72 (m, 2H), 2.29-2.23 (m, 2H), 2.18-1.90 (m, 6H), 1.80-1.76 (m, 1H), 1.69-1.65 (m, 3H), 1.50-1.19 (m, 7H), 0.79-0.78 (m, 3H). $^{13}\text{C NMR}$ (126 MHz; CDCl_3): δ 154.3, 137.9, 131.5, 126.4, 115.2, 112.8, 92.4, 79.2, 78.5, 47.4, 44.4, 43.6, 39.5, 38.5, 33.0, 32.2, 29.7, 27.4, 26.4, 23.5, 22.8, 12.7 **FTIR** (thin film): 3330, 2926, 1674, 1201 cm^{-1} . **HRMS (m/z)**: calcd for $\text{C}_{24}\text{H}_{31}\text{NO}_2$: 365.2355, found $[\text{M}+\text{H}]^+$: 366.2426.



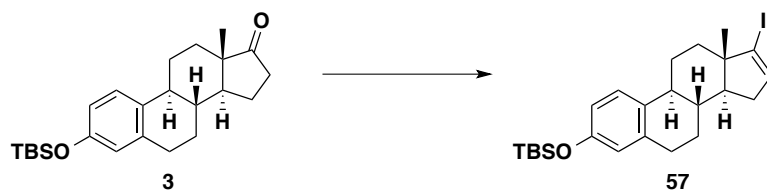
A slurry of alkyne **50** (87 mg, 0.18 mmol) and Pd/C (174 mg, 10 % by wt) in methanol (3.7 mL, 0.05 M) was sparged with hydrogen gas and then placed under 1 atm of hydrogen for 12 hours at 25 °C. The reaction was then diluted with ethyl acetate, filtered through a pad of Celite, and concentrated *in vacuo*. The crude residue was dissolved in DCM (600 μL , 0.1 M) and TFA (60 μL , 1.0 M) was added dropwise at 0 °C and stirred for 1.5 hours. The reaction was concentrate *in vacuo*, and the crude residue purified by silica gel chromatography with 50% ethyl acetate in hexanes as the eluent to afford deprotected product **56** as a clear oil (22 mg, 33 %). $^1\text{H NMR}$ (500 MHz, CDCl_3): δ 7.05-7.02 (m, 1H), 6.54-6.52 (m, 1H), 6.47-6.46 (m, 1H), 3.36-3.32 (m, 1H), 3.28 (dd, $J = 3.0, 1.5$ Hz, 1H), 3.19-3.15 (m, 2H), 2.79-2.67 (m, 2H), 2.19-2.05 (m, 4H), 2.02-1.88 (m, 3H), 1.81-1.73 (m, 3H), 1.66-1.34 (m, 8H), 1.31-1.22 (m, 4H), 1.17-1.11 (m, 5H), 0.53-0.51 (m, 3H). $^{13}\text{C NMR}$ (126 MHz; CDCl_3): δ 154.2, 138.1, 131.9, 126.2, 115.2, 112.6,

100.1, 60.8, 54.8, 50.8, 44.6, 44.1, 42.5, 38.8, 37.9, 31.6, 30.3, 29.7, 28.3, 27.8, 27.4, 26.4, 24.2, 23.5, 12.4. **FTIR** (thin film): 3343, 2926, 1606, 1501 cm^{-1} .



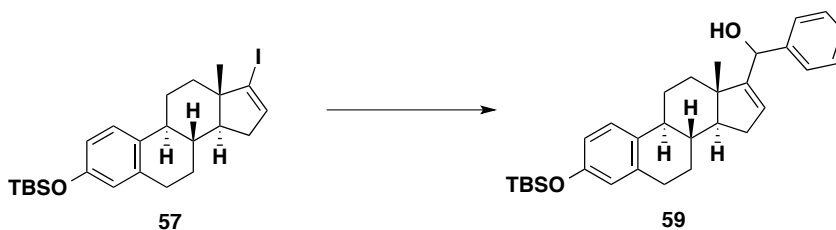
A slurry of alkyne **49** (87 mg, 0.18 mmol) and Pd/C (174 mg, 10 % by wt) in methanol (3.7 mL, 0.05 M) was sparged with hydrogen gas and then placed under 1 atm of hydrogen for 12 hours at 25 °C. The reaction was then diluted with ethyl acetate, filtered through a pad of Celite, and concentrated *in vacuo*. The crude residue was dissolved in DCM (600 μL , 0.1 M) and TFA (60 μL , 1.0 M) was added dropwise at 0 °C and stirred for 1.5 hours. The reaction was concentrate *in vacuo*, and the crude residue purified by silica gel chromatography with 50% ethyl acetate in hexanes as the eluent to afford **55** as a clear oil (9 mg, 11 %). **$^1\text{H NMR}$** (500 MHz, CDCl_3): δ 7.03 (dd, $J = 8.4, 4.1$ Hz, 1H), 6.54-6.46 (m, 2H), 3.38-3.17 (m, 3H), 2.74-2.68 (m, 2H), 2.18-2.05 (m, 3H), 2.02-1.88 (m, 2H), 1.83-1.73 (m, 3H), 1.69-1.52 (m, 5H), 1.45-1.35 (m, 2H), 1.33-1.21 (m, 4H), 1.17-1.07 (m, 6H), 0.53-0.49 (m, 3H). **$^{13}\text{C NMR}$** (126 MHz; CDCl_3): δ 154.2, 138.0, 131.9, 126.2, 115.2, 112.6, 60.7, 54.7, 50.5, 44.7, 44.1, 42.4, 38.8, 37.7, 31.4, 30.2, 29.7, 28.2, 27.8, 27.3, 26.4, 24.2, 23.5, 12.4. **FTIR** (thin film): 3377, 2925, 1682, 1499 cm^{-1} .

Section 4.7 Regenerating Rigidity without Oxygenation



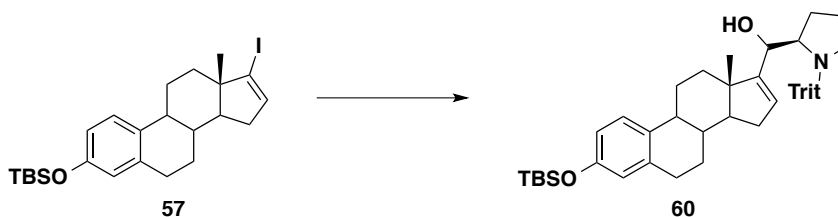
To a slurry of protected estrone **3** (115 mg, 0.3 mmol) in EtOH (30 mL, 0.01 M) at 25 °C was added hydrazone monohydrate (300 mg, 6.0 mmol) and triethylamine (606 mg, 6.0 mmol). The resulting solution was warmed to 70 °C and stirred overnight. The reaction was cooled to 25 °C and concentrated *in vacuo*. The thick white oil was re-dissolved in THF (30 mL, 0.01 M) and triethylamine (840 μ L, 6.0 mmol) was added at 25 °C. To this solution was added iodine (153 mg, 0.6 mmol) in THF (6 mL, 0.1 M) and an evolution of nitrogen gas was observed. The reaction was stirred at 25 °C for 45 minutes before being quenched with saturated sodium thiosulfate (10 mL) and sodium bicarbonate (10 mL). The aqueous was extracted with ethyl acetate (3x, 15 mL), dried over sodium sulfate, and concentrated *in vacuo*. The crude material was purified by silica gel chromatography with 10 % ethyl acetate in hexanes as the eluent to afford the vinyl iodide **57** (72 mg, 49 %). $^1\text{H NMR}$ (500 MHz, CDCl_3): δ 7.11 (d, $J = 8.4$ Hz, 1H), 6.63-6.57 (m, 2H), 6.17 (dd, $J = 3.2, 1.6$ Hz, 1H), 2.84 (dd, $J = 6.6, 2.8$ Hz, 2H), 2.25 (ddd, $J = 14.8, 6.3, 3.2$ Hz, 2H), 2.06 (dd, $J = 11.3, 1.6$ Hz, 1H), 1.74-1.41 (m, 6H), 0.98 (s, 9H), 0.78 (s, 2H), 0.20-0.19 (m, 6H). $^{13}\text{C NMR}$ (126 MHz; CDCl_3): δ 153.6, 137.8, 137.5, 133.0, 126.0, 120.1, 117.3, 112.9, 54.3, 50.5, 44.4, 37.9, 36.5, 33.6, 29.6, 27.6, 26.5, 25.9, 18.3, 15.5, -4.2. **FTIR** (thin film): 3425, 2930, 2858, 1607 cm^{-1} . **HRMS (m/z)**: calcd for $\text{C}_{24}\text{H}_{35}\text{IOSi}$: 494.1502, found $[\text{M}]^+$: 494.1525.

6.60-6.54 (m, 2H), 5.60 (t, $J = 1.5$ Hz, 1H), 5.40 (s, 1H), 2.81 (d, $J = 4.9$ Hz, 2H), 2.22 (dd, $J = 11.1, 7.8$ Hz, 3H), 1.98-1.94 (m, 2H), 1.66 (d, $J = 6.4$ Hz, 1H), 1.57-1.54 (m, 3H), 0.98 (t, $J = 4.3$ Hz, 9H), 0.72 (s, 3H), 0.19-0.17 (m, 6H). ^{13}C NMR (126 MHz; CDCl_3): δ 160.7, 156.9, 153.4, 148.1, 137.9, 136.6, 133.5, 127.7, 125.9, 122.6, 122.1, 120.1, 117.2, 72.4, 57.1, 47.1, 44.4, 37.2, 35.3, 31.1, 29.6, 27.9, 26.4, 25.9, 18.3, 17.1, -4.2
FTIR (thin film): 3392, 2929, 2856, 1606, 1496 cm^{-1} . **HRMS** (m/z): calcd for $\text{C}_{30}\text{H}_{41}\text{O}_2\text{Si}$: 475.2907, found $[\text{M}+\text{H}]^+$: 476.2967.



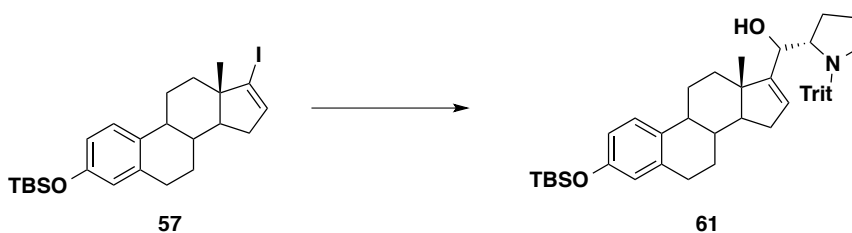
To a solution of iodide **57** (155 mg, 0.31 mmol) in THF (3.1 mL, 0.1 M) at -78 °C was added *t*-butyllithium (625 μL , 0.69 mmol) dropwise. The solution of anion was stirred for 5 minutes prior to the addition of aldehyde (36 mg, 0.34 mmol) in THF (3.4 mL, 0.10 M). The solution was stirred for 1 hour at this temperature before warming to 25 °C and being quenched with saturated ammonium chloride (10 mL). The aqueous was extracted with ethyl acetate (3x, 15 mL), dried with sodium sulfate and concentrated *in vacuo*. The crude reaction mixture was purified by silica gel chromatography with 15 % ethyl acetate in hexanes as the eluent to afford the desired alcohol **59** (76 mg, 52 %). ^1H NMR (500 MHz, CDCl_3): δ 7.42-7.30 (m, 5H), 7.07 (dd, $J = 32.2, 8.5$ Hz, 1H), 6.63-6.56 (m, 2H), 5.67 (dt, $J = 116.5, 1.5$ Hz, 1H), 5.32 (d, $J = 26.2$ Hz, 1H), 2.85 (dt, $J = 10.9, 5.3$

Hz, 2H), 2.29-2.16 (m, 3H), 1.99-1.89 (m, 4H), 1.70-1.41 (m, 6H), 1.00 (d, $J = 0.5$ Hz, 9H), 0.92 (s, 1H), 0.67 (s, 2H), 0.20 (d, $J = 6.3$ Hz, 6H). $^{13}\text{C NMR}$ (126 MHz; CDCl_3): δ 157.8, 157.3, 153.41, 153.38, 143.00, 142.97, 137.9, 133.4, 128.51, 128.35, 128.0, 127.68, 127.65, 127.51, 126.9, 126.08, 125.90, 125.88, 124.5, 120.10, 120.07, 117.21, 117.17, 72.9, 72.3, 57.1, 56.7, 46.79, 46.78, 44.41, 44.31, 37.29, 37.25, 35.29, 35.11, 30.9, 29.67, 29.63, 27.9, 26.44, 26.41, 25.9, 18.3, 16.94, 16.79, -4.2. **FTIR** (thin film): 3434, 2929, 1643, 1495 cm^{-1} . **HRMS** (m/z): calcd for $\text{C}_{31}\text{H}_{42}\text{O}_2\text{Si}$: 474.2954, found $[\text{M}-\text{OH}]^+$: 457.2926.



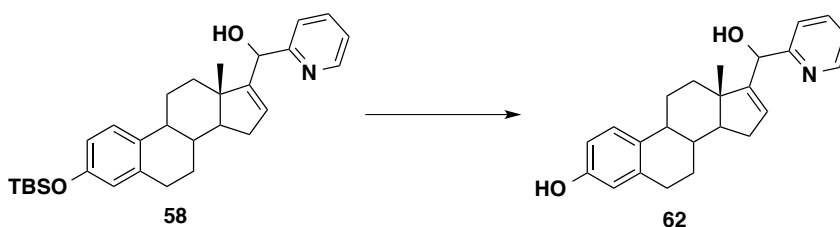
To a solution of iodide **57** (145 mg, 0.30 mmol) in THF (600 μL , 0.5 M) at -78 $^{\circ}\text{C}$ was added *t*-butyllithium (510 μL , 0.66 mmol) dropwise. The solution of anion was stirred for 5 minutes prior to the addition of aldehyde (110 mg, 0.33 mmol) in THF (320 μL , 1.0 M). The solution was stirred for 1 hour at this temperature before warming to 25 $^{\circ}\text{C}$ and being quenched with saturated ammonium chloride (10 mL). The aqueous was extracted with ethyl acetate (3x, 15 mL), dried with sodium sulfate and concentrated *in vacuo*. The crude reaction mixture was purified by silica gel chromatography with 10 % ethyl acetate in hexanes as the eluent to afford the desired alcohol **60** (80 mg, 38 %) and the undesired dehalogenated alkene (60 mg, 54 %). $^1\text{H NMR}$ (500 MHz, CDCl_3): δ 7.63-7.61 (m, 6H), 7.35-7.29 (m, 7H), 7.23 (t, $J = 7.3$ Hz, 3H), 7.10 (d, $J = 8.4$ Hz, 1H), 6.65-6.58 (m, 2H), 5.68 (t, $J = 1.6$ Hz, 1H), 4.77 (s, 1H), 2.86 (d, $J = 24.4$ Hz, 2H), 2.71

(s, 1H), 2.16-2.16 (m, 3H), 1.91 (s, 2H), 1.61-1.56 (m, 3H), 1.40 (dd, $J = 46.1, 33.8$ Hz, 5H), 1.02-1.01 (m, 9H), 0.69 (s, 3H), 0.23-0.22 (m, 6H). ^{13}C NMR (126 MHz; CDCl_3): δ 155.6, 153.4, 144.7, 137.9, 133.5, 130.0, 128.0, 127.73, 127.68, 127.58, 127.4, 126.3, 125.9, 123.9, 120.0, 117.1, 78.2, 73.6, 63.5, 57.6, 53.5, 45.7, 44.3, 37.1, 34.3, 30.9, 29.6, 27.8, 26.2, 25.86, 25.78, 25.1, 18.3, 17.0, -4.2. FTIR (thin film): 3490, 3056, 2928, 1606 cm^{-1} . HRMS (m/z): calcd for $\text{C}_{48}\text{H}_{59}\text{NO}_2\text{Si}$: 709.4315, found $[\text{M}+\text{H}]^+$: 710.4393.

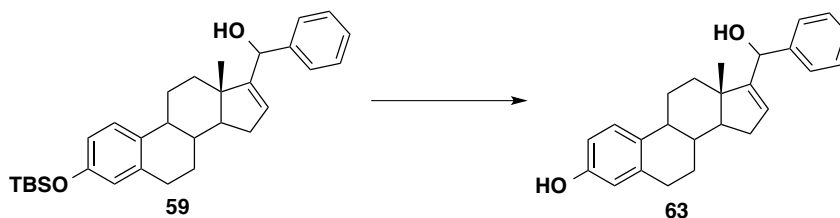


To a solution of iodide **57** (495 mg, 1.0 mmol) in THF (2.0 mL, 0.5 M) at -78 °C was added *t*-butyllithium (1.7 mL, 2.2 mmol) dropwise. The solution of anion was stirred for 5 minutes prior to the addition of aldehyde (403 mg, 1.1 mmol) in THF (1.1 mL, 1.0 M). The solution was stirred for 1 hour at this temperature before warming to 25 °C and being quenched with saturated ammonium chloride (10 mL). The aqueous was extracted with ethyl acetate (3x, 15 mL), dried with sodium sulfate and concentrated *in vacuo*. The crude reaction mixture was purified by silica gel chromatography with 10 % ethyl acetate in hexanes as the eluent to afford the desired alcohol **61** (169 mg, 24 %). ^1H -NMR (500 MHz, CDCl_3): δ 7.60 (d, $J = 8.0$ Hz, 7H), 7.34-7.30 (m, 8H), 7.23 (t, $J = 7.3$ Hz, 3H), 7.11 (d, $J = 8.5$ Hz, 1H), 6.64 (dd, $J = 8.4, 2.6$ Hz, 1H), 6.59 (d, $J = 2.5$ Hz, 1H), 5.69 (d, $J = 1.2$ Hz, 1H), 4.56 (s, 1H), 3.69 (s, 1H), 3.11 (s, 2H), 2.83 (s, 2H), 2.18 (dt, $J = 6.8, 3.6$ Hz, 3H), 1.92-1.89 (m, 2H), 1.54 (s, 2H), 1.47-1.29 (m, 9H), 1.02 (s, 9H),

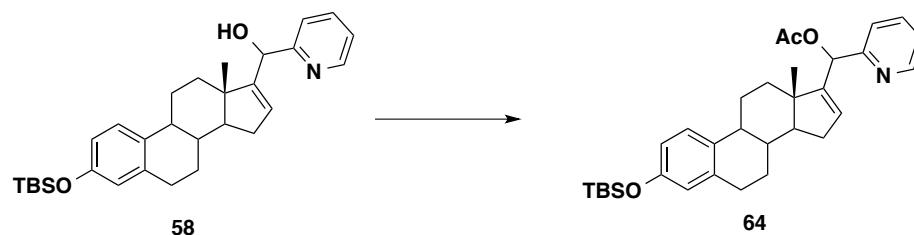
0.68 (s, 3H), 0.24-0.23 (m, 6H). $^{13}\text{C NMR}$ (126 MHz; CDCl_3): δ 155.0, 153.4, 147.0, 144.6, 137.9, 133.4, 130.0, 129.8, 128.05, 128.02, 127.77, 127.66, 127.3, 126.4, 125.9, 123.4, 120.1, 117.2, 78.2, 72.4, 63.4, 55.8, 53.6, 46.5, 44.4, 37.3, 35.0, 34.80, 34.66, 31.7, 31.1, 29.7, 27.9, 27.0, 26.6, 26.3, 25.9, 25.4, 25.1, 22.8, 18.3, 16.5, 14.3, -4.2. **FTIR** (thin film): 3494, 3056, 2929, 1607 cm^{-1} . **HRMS** (m/z): calcd for $\text{C}_{48}\text{H}_{59}\text{NO}_2\text{Si}$: 709.4315, found $[\text{M}+\text{H}]^+$: 710.4394.



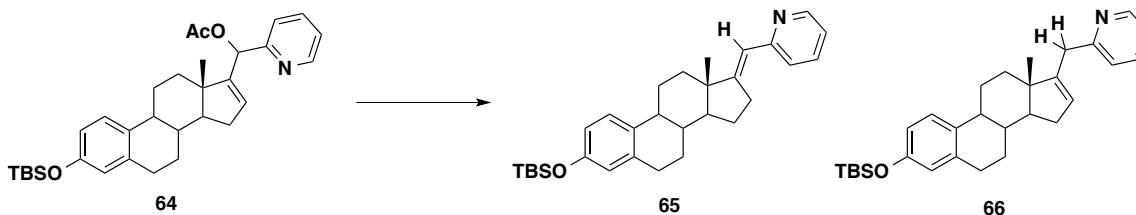
To a solution of alcohol **58** (10 mg, 0.02 mmol) in THF (210 μL , 0.1 M) was added TBAF (40 μL , 0.04 mmol) dropwise at 25 $^\circ\text{C}$ and stirred overnight. The reaction was quenched with saturated ammonium chloride (2 mL) and extracted with ethyl acetate (3x, 10 mL) and the solvent removed *in vacuo*. The crude residue purified via silica gel chromatography with 50 % ethyl acetate in hexanes as the eluent to afford the final product **62** (7 mg, 92 %). $^1\text{H NMR}$ (500 MHz, CDCl_3): δ 8.57 (ddd, $J = 4.9, 1.7, 1.0$ Hz, 1H), 7.67 (td, $J = 7.7, 1.8$ Hz, 1H), 7.32-7.30 (m, 1H), 7.23-7.20 (m, 1H), 7.11-7.10 (m, 1H), 6.62-6.60 (m, 1H), 6.55 (d, $J = 2.7$ Hz, 1H), 5.60 (dt, $J = 3.0, 1.4$ Hz, 1H), 5.39 (d, $J = 0.3$ Hz, 1H), 2.86-2.81 (m, 2H), 2.27-2.17 (m, 3H), 2.00-1.93 (m, 2H), 1.90-1.85 (m, 1H), 1.69-1.32 (m, 10H), 0.70 (d, $J = 4.5$ Hz, 3H). $^{13}\text{C NMR}$ (126 MHz, CDCl_3): δ 170.42, 156.94, 153.55, 148.06, 138.15, 136.25, 127.40, 126.11, 122.36, 121.77, 115.15, 11.48, 75.04, 72.26, 71.71, 56.82, 46.83, 44.08, 36.98, 34.99, 30.81, 29.39, 27.53, 26.24, 16.85. **FTIR** (thin film): 3431, 2928, 2852, 1607, cm^{-1} .



To a solution of alcohol (8 mg, 0.02 mmol) in THF (170 μ L, 0.1 M) was added TBAF (34 μ L, 0.04 mmol) dropwise at 25 $^{\circ}$ C and stirred overnight. The reaction was quenched with saturated ammonium chloride (2 mL) and extracted with ethyl acetate (3x, 10 mL) and the solvent removed *in vacuo*. The crude residue purified via silica gel chromatography with 50 % ethyl acetate in hexanes as the eluent to afford the final product (6 mg, 87 %). **$^1\text{H NMR}$** (500 MHz, CDCl_3): δ 7.41-7.28 (m, 5H), 7.13-7.04 (m, 1H), 6.63-6.54 (m, 2H), 5.79-5.54 (m, 1H), 5.35-5.28 (m, 1H), 4.59-4.57 (m, 1H), 2.87-2.79 (m, 2H), 2.32-2.12 (m, 3H), 2.02-1.85 (m, 3H), 1.69-1.60 (m, 2H), 1.55-1.36 (m, 3H), 1.28-1.22 (m, 2H), 0.91-0.89 (m, 1H), 0.65 (s, 2H). **$^{13}\text{C NMR}$** (126 MHz, CDCl_3): δ 175.29, 175.20, 175.16, 133.03, 128.53, 128.37, 127.68, 127.52, 126.92, 126.09, 115.39, 112.72, 72.91, 72.31, 70.71, 66.91, 57.08, 51.04, 47.70, 46.79, 45.07, 45.05, 44.34, 44.25, 42.82, 38.92, 38.87, 37.34, 37.30, 35.27, 32.00, 30.94, 30.60, 30.50, 30.42, 29.80, 29.65, 29.62, 29.27, 29.06, 29.03, 27.89, 27.85, 27.77, 26.52, 25.67, 25.43, 23.98, 23.85, 23.83. **FTIR** (thin film): 3419, 2926, 1644, 1454 cm^{-1} .



To a solution of alcohol **58** (28 mg, 0.06 mmol) in DCM (60 μ L, 1.0 M) at 0 °C was added dry pyridine (6 μ L, 10.0 M) followed by AcCl (24 mg, 0.3 mmol) and stirred for 1.5 hours at this temperature. The reaction was quenched with HCl (1 N, 3 mL), the aqueous extracted with DCM (3x, 5 mL), dried over sodium sulfate, and concentrated *in vacuo*. The crude acetate **64** was clean and no further purification was necessary. $^1\text{H NMR}$ (500 MHz, CDCl_3): δ 8.61 (ddd, $J = 4.8, 1.8, 0.9$ Hz, 1H), 7.68 (dd, $J = 7.7, 1.8$ Hz, 1H), 7.41-7.40 (m, 1H), 7.23-7.20 (m, 1H), 7.05 (d, $J = 8.5$ Hz, 1H), 6.60-6.58 (m, 1H), 6.54 (d, $J = 2.6$ Hz, 1H), 6.42 (s, 1H), 5.63 (t, $J = 1.6$ Hz, 1H), 2.20-2.16 (m, 3H), 2.14 (s, 3H), 1.26 (s, 2H), 0.97 (d, $J = 5.2$ Hz, 9H), 0.89 (s, 3H), 0.18 (d, $J = 5.9$ Hz, 6H).

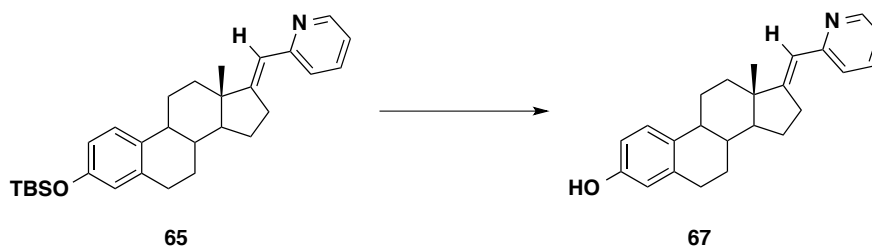


To a solution of acetate **64** (81 mg, 0.16 mmol) in degassed dioxane (1.8 mL, 0.1 M) was added ammonium formate (24 mg, 0.32 mmol), palladium acetate (12 mg, 0.03 mmol) and triphenylphosphine (24 mg, 0.08 mmol). The reaction was stirred at 25 C for 12 hours before being quenched with water (5 mL). The aqueous was extracted with ethyl acetate (3x, 15 mL), dried over sodium sulfate, and concentrated *in vacuo*. The

crude mixture was purified by silica gel chromatography with 20 % ethyl acetate in hexanes as the eluent to afford two products: unconjugated alkene **66** (38 mg, 52 %) and conjugated alkene **65** (12 mg, 16 %).

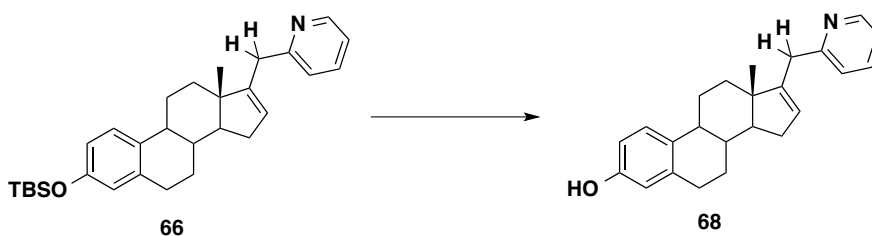
Unconjugated Product 66: $^1\text{H NMR}$ (500 MHz, CDCl_3): δ 8.56-8.55 (m, 1H), 7.63-7.60 (m, 1H), 7.23 (d, $J = 7.9$ Hz, 1H), 7.14-7.08 (m, 2H), 6.61-6.55 (m, 2H), 5.16 (d, $J = 1.1$ Hz, 1H), 3.55 (s, 2H), 2.86-2.80 (m, 2H), 2.30-2.13 (m, 3H), 1.94-1.81 (m, 3H), 1.63-1.54 (m, 3H), 1.43-1.38 (m, 2H), 0.82 (s, 3H), 0.18 (s, 6H).

Conjugated Product 65: $^1\text{H NMR}$ (500 MHz, CDCl_3): δ 8.58-8.57 (m, 1H), 7.63-7.60 (m, 1H), 7.30 (d, $J = 8.0$ Hz, 1H), 7.16 (d, $J = 8.5$ Hz, 1H), 7.05-7.03 (m, 1H), 6.64-6.62 (m, 1H), 6.57 (t, $J = 0.9$ Hz, 1H), 6.28 (s, 1H), 2.95-2.76 (m, 4H), 2.44-2.40 (m, 1H), 2.28-2.23 (m, 1H), 2.12-2.11 (m, 1H), 1.98-1.92 (m, 2H), 1.61-1.26 (m, 8H), 0.98 (d, $J = 1.1$ Hz, 9H), 0.93 (s, 3H), 0.19 (d, $J = 1.2$ Hz, 6H).



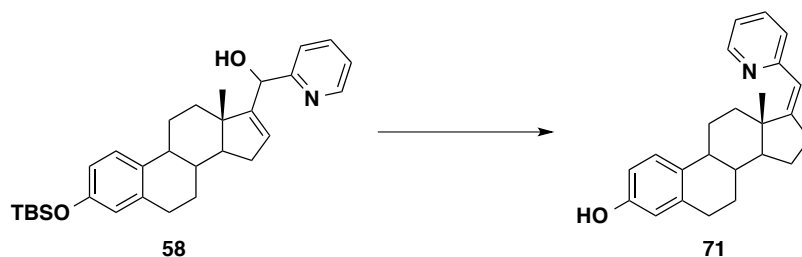
To a solution of alkene **65** (11 mg, 0.02 mmol) in THF (240 μL , 0.1 M) was added TBAF (48 μL , 0.05 mmol) dropwise at 25 $^\circ\text{C}$ and stirred overnight. The reaction was quenched with saturated ammonium chloride (2 mL) and extracted with ethyl acetate (3x, 5 mL) and the solvent removed *in vacuo*. The crude residue purified via silica gel chromatography with 50 % ethyl acetate in hexanes as the eluent to afford the final

product **67** (6 mg, 73 %). $^1\text{H NMR}$ (500 MHz, CDCl_3): δ 8.58-8.57 (m, 1H), 7.69-7.65 (m, 1H), 7.36-7.34 (m, 1H), 7.18-7.16 (m, 1H), 7.10-7.08 (m, 1H), 6.68-6.66 (m, 1H), 6.59 (d, $J = 0.4$ Hz, 1H), 6.33 (t, $J = 0.8$ Hz, 1H), 2.93-2.71 (m, 4H), 2.41-2.38 (m, 1H), 2.25-2.20 (m, 1H), 2.09-2.05 (m, 1H), 1.96-1.91 (m, 2H), 1.59-1.25 (m, 8H), 0.91-0.88 (m, 3H). $^{13}\text{C NMR}$ (126 MHz; CDCl_3): δ 163.8, 159.2, 153.8, 138.3, 132.6, 126.6, 123.1, 120.6, 120.0, 115.5, 113.0, 106.3, 52.8, 46.5, 45.8, 44.2, 38.8, 36.0, 30.00, 29.84, 27.8, 26.9, 24.8, 19.0. **FTIR** (thin film): 3327, 2926, 2845, 1595 cm^{-1} . **HRMS** (m/z): calcd for $\text{C}_{24}\text{H}_{27}\text{NO}$: 345.2093, found $[\text{M}+\text{H}]^+$: 346.2174.



To a solution of alcohol (**67**, 8 mg, 0.02 mmol) in THF (170 μL , 0.1 M) was added TBAF (34 μL , 0.04 mmol) dropwise at 25 C and stirred overnight. The reaction was quenched with saturated ammonium chloride (2 mL) and extracted with ethyl acetate (3x, 10 mL) and the solvent removed *in vacuo*. The crude residue purified via silica gel chromatography with 50 % ethyl acetate in hexanes as the eluent to afford the final product (**68**, 6 mg, 87 %). $^1\text{H NMR}$ (500 MHz, CDCl_3): δ 8.55 (dt, $J = 5.0, 0.9$ Hz, 1H), 7.63 (td, $J = 7.6, 1.8$ Hz, 1H), 7.25 (d, $J = 7.9$ Hz, 1H), 7.16-7.13 (m, 1H), 7.09 (d, $J = 8.4$ Hz, 1H), 6.62 (dd, $J = 8.4, 2.6$ Hz, 1H), 6.57 (d, $J = 2.5$ Hz, 1H), 5.16 (d, $J = 1.4$ Hz, 1H), 3.56 (s, 2H), 2.86-2.76 (m, 2H), 2.29-2.24 (m, 1H), 2.22-2.17 (m, 1H), 2.15-2.11 (m, 1H), 1.95-1.86 (m, 2H), 1.79 (ddd, $J = 12.3, 3.9, 2.4$ Hz, 1H), 1.63-1.50 (m, 3H), 1.43-1.35 (m, 2H). $^{13}\text{C NMR}$

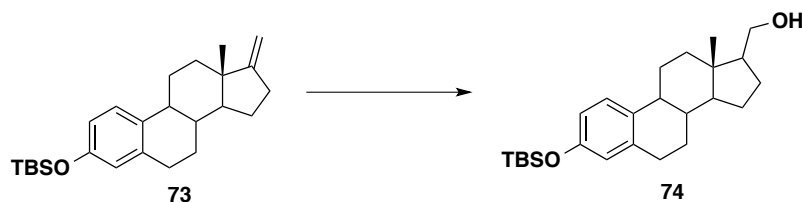
NMR (126 MHz; CDCl₃): δ 160.1, 154.3, 153.5, 148.4, 138.0, 136.8, 132.0, 126.0, 125.0, 124.1, 121.4, 115.2, 112.6, 56.4, 47.1, 45.9, 44.3, 37.5, 36.6, 34.6, 30.9, 29.5, 27.8, 26.4, 15.7 **FTIR** (thin film): 3315, 2926, 2845, 1596 cm⁻¹.



To a solution of alcohol **58** (42 mg, 0.09 mmol) in DCM (600 μL, 0.15 M) was added triphenylphosphine (43 mg, 0.16 mmol) in DCM (1.25 mL, 0.13 M) and carbon tetrabromide (80 mg, 0.24 mmol) in DCM (1.2 mL, 0.2 M). The reaction was stirred at 25 °C for 30 minutes, then concentrated *in vacuo* when no starting material was present by TLC. The crude material was purified by silica gel chromatography with 15 % ethyl acetate in hexanes as the eluent to afford the debrominated alkene (6 mg, 15 %). **¹H NMR** (500 MHz, CDCl₃): δ 7.64 (dd, *J* = 6.9, 1.0 Hz, 1H), 7.32-7.30 (m, 1H), 7.16 (d, *J* = 8.4 Hz, 1H), 6.64 (dd, *J* = 8.4, 2.7 Hz, 1H), 6.59 (d, *J* = 2.6 Hz, 1H), 6.46 (dd, *J* = 6.7, 1.3 Hz, 1H), 6.25 (s, 1H), 2.89 (dd, *J* = 13.4, 6.5 Hz, 3H), 2.60 (s, 1H), 2.41 (s, 2H), 2.30-2.28 (m, 2H), 1.55 (d, *J* = 3.3 Hz, 3H), 1.25 (s, 3H), 1.00 (s, 3H), 0.99-0.98 (m, 9H), 0.20 (dd, *J* = 6.4, 0.7 Hz, 6H). The alkene was solubilized with THF (130 μL, 0.1 M) and TBAF (26 μL, 0.03 mmol) was added dropwise, and the reaction stirred overnight at 25 °C before being quenched with saturated ammonium chloride (2 mL). The aqueous was extracted with ethyl acetate (3x, 5 mL), dried over sodium sulfate and concentrated *in vacuo*. The crude material was purified by silica gel chromatography with 25 % ethyl

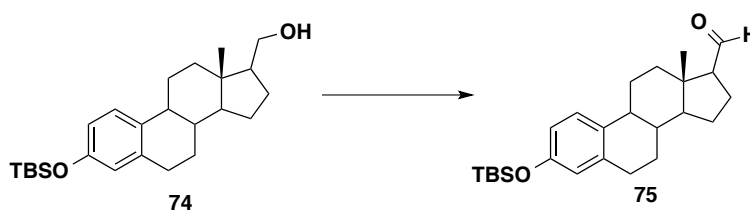
acetate in hexanes as the eluent to afford the deprotected product **71** (4 mg, 89%). ¹H NMR (500 MHz, CDCl₃): δ 7.68-7.66 (m, 1H), 7.35-7.32 (m, 1H), 7.23-7.21 (m, 1H), 6.70-6.67 (m, 1H), 6.63 (dd, *J* = 1.3, 0.7 Hz, 1H), 6.58-6.56 (m, 1H), 6.49 (td, *J* = 1.1, 0.5 Hz, 1H), 6.30-6.25 (m, 1H), 4.54-4.51 (m, 1H), 2.98-2.88 (m, 2H), 2.64-2.63 (m, 1H), 2.47-2.40 (m, 2H), 2.34-2.29 (m, 1H), 2.03 (dtd, *J* = 2.7, 1.4, 0.7 Hz, 1H), 1.93-1.86 (m, 2H), 1.78-1.73 (m, 1H), 1.56-1.56 (m, 3H). FTIR (thin film): 3352, 2920, 2756, 1507 cm⁻¹.

Section 4.8 Second Generation Derivatives of Phenyl Allylic Alcohol



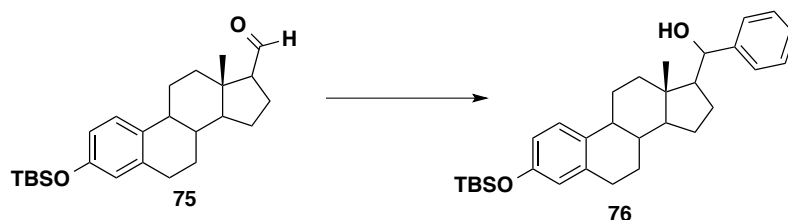
To a solution of TBS-methylene **73** (553 mg, 1.5 mmol) in dry THF (20 mL, 0.08 M) was added a solution of borane in THF (3 mL, 1 M) at 25 °C. The solution was stirred for 2 h or until the consumption of starting material was observed by TLC. The reaction was then cooled to 0 °C and 2N sodium hydroxide in deionized water (3 mL) and 30% aqueous hydrogen peroxide (2 mL) were added. The solution was stirred overnight at 25 °C and then diluted with ethyl acetate (50 mL). The organics were washed with brine (5x, 25 mL) until they tested negative for peroxides and dried over sodium sulfate. The solvent was removed *in vacuo* and the residue purified by silica gel chromatography with 10% ethyl acetate in hexanes to yield the desired alcohol **74** as a white solid (220 mg, 38%) as a 3:1 mixture of β:α epimers. ¹H NMR (500 MHz, CDCl₃): δ 7.12 (d, *J* = 8.4 Hz,

1H), 6.62-6.55 (m, 2H), 3.76 (t, $J = 5.2$ Hz, 1H), 3.59 (t, $J = 5.2$ Hz, 1H), 2.80 (d, $J = 4.0$ Hz, 2H), 2.24 (s, 2H), 2.02 (d, $J = 31.1$ Hz, 1H), 1.89-1.87 (m, 2H), 1.75 (d, $J = 30.2$ Hz, 2H), 1.42-1.25 (m, 9H), 0.98-0.96 (m, 9H), 0.84 (s, 1H), 0.69 (s, 2H), 0.19 (s, 6H). ^{13}C NMR (126 MHz; CDCl_3): δ 153.4, 138.0, 133.4, 126.2, 120.1, 117.2, 64.8, 55.2, 53.6, 53.3, 44.2, 42.3, 39.0, 38.6, 29.8, 28.0, 26.5, 25.87, 25.78, 24.5, 18.3, 12.8, -4.2. FTIR (thin film) 3358, 2923, 2852, 1609 cm^{-1} . HRMS (m/z): calcd for $\text{C}_{25}\text{H}_{40}\text{O}_2\text{Si}$: 400.2798, found $[\text{M}+\text{Cl}]$: 435.2487.



To a solution of alcohol **74** (132 mg, 0.34 mmol) in dichloromethane (680 μL , 0.5 M) at 0 $^{\circ}\text{C}$ was added Dess Martin periodinane (180 mg, 0.43 mmol) in DCM (1.72 mL, 0.25 M). The yellow solution was stirred at 0 $^{\circ}\text{C}$ for 1.5 h until no more SM was observed by TLC. The reaction was quenched with saturated aqueous sodium bisulfate (10 mL) and saturated aqueous sodium bicarbonate (10 mL) and stirred for 15 minutes. The layers were separated and the aqueous extracted with dichloromethane (3x 20 mL). The combined organic layers were washed with brine (15 mL), dried over sodium sulfate and the solvent removed *in vacuo*. The crude residue was purified by silica gel chromatography with 15 % ethyl acetate in hexanes as the eluent to provide the aldehyde **75** as a white film (56 mg, 42 %). ^1H NMR (500 MHz, CDCl_3): δ 9.81 (s, 1H), 7.11 (d, $J = 8.5$ Hz, 1H), 6.62-6.55 (m, 2H), 2.81-2.80 (m, 2H), 2.38-1.35 (m, 16H), 0.97 (s, 9H), 0.96 (s, 1H), 0.80 (s, 2H), 0.19 (t, $J = 0.7$ Hz, 6H). ^{13}C NMR (126 MHz; CDCl_3):

δ 205.1, 153.5, 137.9, 132.9, 126.2, 120.1, 117.3, 63.1, 55.5, 46.6, 45.3, 44.0, 43.6, 39.1, 38.6, 38.4, 29.7, 27.9, 26.2, 25.9, 24.7, 21.3, 18.3, 14.1, -4.2. **FTIR**(thin film): 2924, 2851, 1716, 1608 cm^{-1} . **HRMS (m/z)**: calcd for $\text{C}_{25}\text{H}_{38}\text{O}_2\text{Si}$: 398.2641, found $[\text{M}+\text{H}]^+$: 399.2734.

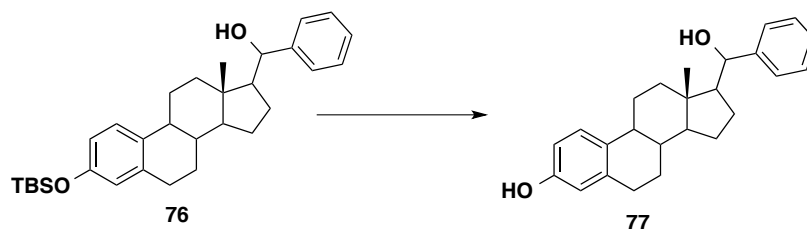


To a solution of bromobenzene (34 μL , 0.32 mmol) in THF (1.3 mL, 0.25 M) at $-78\text{ }^\circ\text{C}$ was added *t*-butyl lithium (630 μL , 0.88 mmol) dropwise and quickly warmed to $25\text{ }^\circ\text{C}$. After 30 minutes, the solution of anion was cooled to $-78\text{ }^\circ\text{C}$ and aldehyde **75** (56 mg, 0.14 mmol) was added in THF (170 μL , 1.0 M) and stirred at this temperature for 1 hour. The reaction was quenched with saturated ammonium chloride (10 mL), the aqueous extracted with ethyl acetate (3x, 10 mL), washed with brine (15 mL). The organics were dried and concentrated *in vacuo*. The crude residue was purified with silica gel chromatography with 15 % ethyl acetate as the eluent to afford the desired alcohol **76** as two separate diastereomers (35 mg, 53 %).

Mixture: $^1\text{H NMR}$ (500 MHz, CDCl_3): δ 7.35-7.27 (m, 5H), 7.14 (dd, $J = 14.1, 8.4$ Hz, 1H), 6.63-6.56 (m, 2H), 4.77 (dd, $J = 187.4, 6.9$ Hz, 1H), 2.82-2.79 (m, 2H), 2.35-2.24 (m, 3H), 1.91-1.83 (m, 4H), 1.67-1.54 (m, 5H), 1.44-1.14 (m, 9H), 0.94-0.93 (m, 2H), 0.84 (s, 1H), 0.19-0.17 (m, 9H). $^{13}\text{C NMR}$ (126 MHz; CDCl_3): δ 153.4, 144.9, 138.0, 133.5, 128.9, 128.56, 128.43, 127.8, 127.1, 126.9, 126.27, 126.20, 120.1, 117.24,

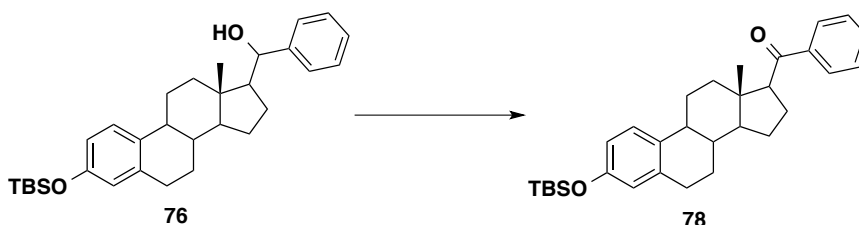
117.17, 73.9, 57.3, 55.2, 54.8, 51.8, 44.1, 43.86, 43.75, 43.3, 40.2, 39.3, 38.8, 29.97, 29.84, 28.0, 26.84, 26.80, 25.88, 25.83, 24.2, 21.72, 21.66, 18.3, 12.6, -4.2. **FTIR** (thin film): 3465, 3028, 2928, 2858, 1607 cm^{-1} . **HRMS (m/z)**: calcd for $\text{C}_{31}\text{H}_{44}\text{O}_2\text{Si}$: 476.3111, found $[\text{M}-\text{OH}]^+$: 459.3087.

Pure Diastereomer: **^1H NMR** (500 MHz, CDCl_3): δ 7.40-7.31 (m, 5H), 6.98 (d, $J = 8.4$ Hz, 1H), 6.56-6.52 (m, 2H), 4.54 (d, $J = 9.4$ Hz, 1H), 2.78 (d, $J = 6.3$ Hz, 2H), 1.96 (t, $J = 9.1$ Hz, 2H), 1.87-1.80 (m, 5H), 1.36-1.20 (m, 7H), 0.74 (s, 3H), 0.19 (s, 6H). **^{13}C NMR** (126 MHz; CDCl_3): δ 153.3, 144.4, 138.0, 133.4, 128.5, 128.1, 127.3, 126.1, 120.0, 117.2, 57.7, 55.4, 43.9, 42.1, 38.5, 38.2, 29.8, 27.9, 26.7, 26.3, 25.9, 24.0, 18.3, 13.1, -4.3. **FTIR** (thin film): 3399, 3029, 2929, 2858, 1607 cm^{-1} . **HRMS (m/z)**: calcd for $\text{C}_{31}\text{H}_{44}\text{O}_2\text{Si}$: 476.3111, found $[\text{M}-\text{OH}]^+$: 459.3079.

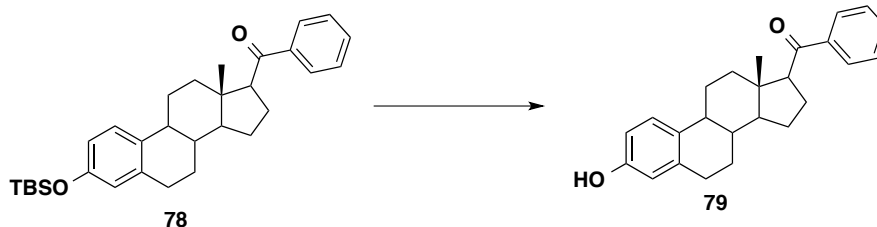


To a solution of alcohol **76** (7 mg, 0.02 mmol) in THF (200 μL , 0.1 M) was added TBAF (40 μL , 0.04 mmol) dropwise at 25 $^\circ\text{C}$ and stirred overnight. The reaction was quenched with saturated ammonium chloride (5 mL) and extracted with ethyl acetate (3x, 10 mL) and the solvent removed *in vacuo*. The crude residue purified via silica gel chromatography with 33 % ethyl acetate in hexanes as the eluent to afford the final product **77** (4 mg, 56 %). **^1H NMR** (500 MHz, CDCl_3): δ 7.40-7.29 (m, 5H), 7.03-7.00 (m, 1H), 6.57-6.53 (m, 2H), 4.57-4.50 (m, 1H), 2.83-2.76 (m, 2H), 2.15-2.09 (m, 1H),

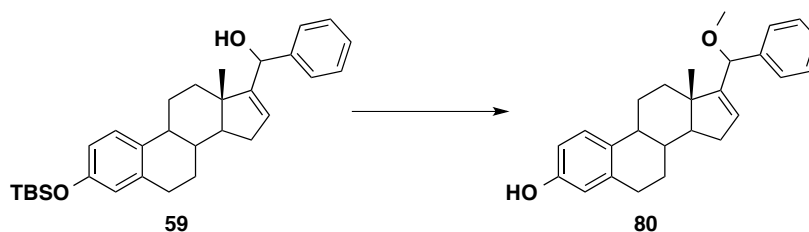
2.08-2.02 (m, 2H), 2.00-1.92 (m, 2H), 1.89-1.75 (m, 3H), 1.67-1.55 (m, 2H), 1.35-1.15 (m, 7H), 0.75-0.72 (m, 3H). $^{13}\text{C NMR}$ (126 MHz; CDCl_3): δ 154.2, 144.3, 138.1, 132.0, 128.4, 127.9, 127.3, 126.2, 115.2, 112.6, 57.5, 55.3, 43.7, 42.0, 38.6, 38.1, 30.9, 29.7, 27.8, 26.7, 26.3, 23.9, 12.9. **FTIR** (thin film): 3347, 2926, 1498 cm^{-1} . **HRMS (m/z)**: calcd for $\text{C}_{25}\text{H}_{30}\text{O}_2$: 362.2246, found $[\text{M}-\text{OH}]^+$: 345.2213.



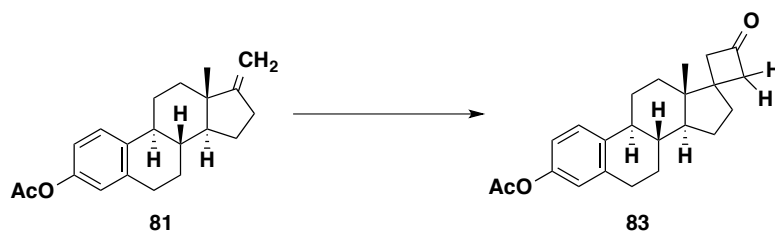
To a solution of alcohol (10 mg, 0.02 mmol) in DCM (210 μL , 0.1 M) was added pyridinium chlorochromate (11 mg, 0.05 mmol) in one portion, and the reaction stirred at 25 $^\circ\text{C}$ for 12 hours. The reaction was diluted with DCM (10 mL) and filtered through a pad of silica and the solvent removed *in vacuo*. The crude product was clean and required no further purification. $^1\text{H NMR}$ (500 MHz, CDCl_3): δ 7.90 (d, $J = 7.3$ Hz, 2H), 7.55 (t, $J = 7.4$ Hz, 1H), 7.46 (t, $J = 7.6$ Hz, 2H), 7.04 (d, $J = 8.5$ Hz, 1H), 6.59-6.55 (m, 2H), 3.58 (t, $J = 8.8$ Hz, 1H), 2.81-2.80 (m, 2H), 2.51-2.48 (m, 1H), 2.23-2.16 (m, 2H), 1.92-1.85 (m, 3H), 1.57-1.50 (m, 5H), 1.45-1.25 (m, 5H), 0.65 (s, 3H), 0.17 (d, $J = 4.7$ Hz, 6H). $^{13}\text{C NMR}$ (126 MHz; CDCl_3): δ 202.3, 153.5, 139.6, 138.0, 133.0, 132.7, 128.52, 128.43, 126.1, 120.1, 117.3, 57.6, 56.4, 45.5, 43.9, 39.6, 39.1, 29.8, 28.0, 26.7, 25.9, 24.7, 24.1, 18.3, 13.9, -4.2. **FTIR** (thin film): 3501, 2928, 1673, 1607 cm^{-1} . **HRMS (m/z)**: calcd for $\text{C}_{31}\text{H}_{42}\text{O}_2\text{Si}$: 474.2954, found $[\text{M}+\text{H}]^+$: 475.3049.



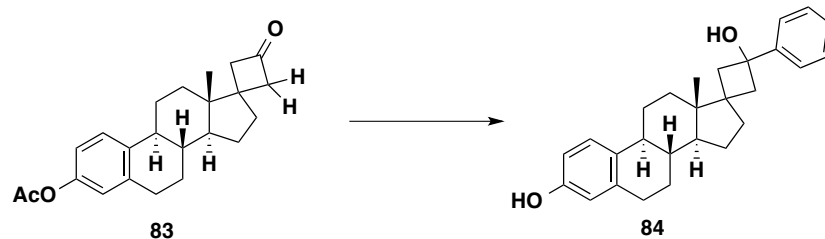
To a solution of alcohol (7 mg, 0.02 mmol) in THF (150 μ L, 0.1 M) was added TBAF (30 μ L, 0.05 mmol) dropwise at 25 $^{\circ}$ C and stirred overnight. The reaction was quenched with saturated ammonium chloride (5 mL) and extracted with ethyl acetate (3x, 10 mL) and the solvent removed *in vacuo*. The crude residue purified via silica gel chromatography with 33 % ethyl acetate in hexanes as the eluent to afford the final product (4 mg, 74 %). **$^1\text{H NMR}$** (500 MHz, CDCl_3): δ 7.91-7.88 (m, 2H), 7.57-7.43 (m, 3H), 7.08-7.05 (m, 1H), 6.60-6.54 (m, 2H), 4.56-4.53 (m, 1H), 3.60-3.55 (m, 1H), 2.85-2.78 (m, 2H), 2.51-2.46 (m, 1H), 2.25-2.15 (m, 2H), 1.96-1.79 (m, 3H), 1.57-1.49 (m, 4H), 1.48-1.32 (m, 4H), 1.32-1.22 (m, 2H), 0.65-0.62 (m, 3H). **$^{13}\text{C NMR}$** (126 MHz; CDCl_3): δ 202.34, 153.53, 139.65, 138.47, 132.75, 130.29, 128.59, 128.49, 126.61, 115.45, 112.85, 57.70, 56.43, 53.64, 45.58, 43.92, 39.61, 39.27, 39.15, 29.92, 29.84, 27.96, 26.83, 24.71, 24.11, 13.90. **FTIR** (thin film): 3397, 2923, 1661, 1499 cm^{-1} . **HRMS** (m/z): calcd for $\text{C}_{25}\text{H}_{28}\text{O}_2$: 360.2089, found $[\text{M}+\text{H}]^+$: 361.2151.



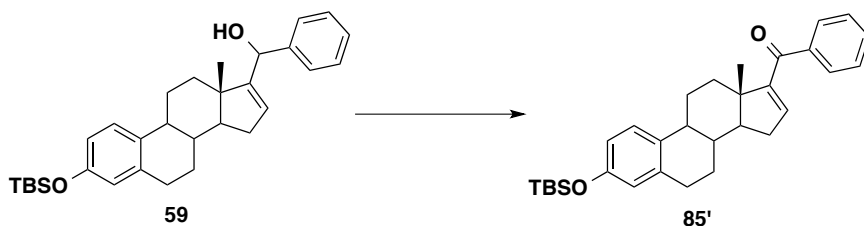
To a solution of alcohol (6 mg, 0.02 mmol) in THF (200 μ L, 0.1 M) was added NaH (60 % by wt, 1 mg, 0.02 mmol) at 25 $^{\circ}$ C. After 30 minutes at 25 C, MeI (3 mg, 0.02 mmol) was added dropwise. The reaction was quenched after stirring for 2 hours at 25 C with saturated ammonium chloride (3 mL), the aqueous extracted with ethyl acetate (3x, 5 mL), dried over sodium sulfate, and concentrated *in vacuo*. The crude residue was dissolved in THF (200 μ L, 0.01 M) and TBAF (20 μ L, 0.02 mmol) was added dropwise. The reaction was stirred at 25 $^{\circ}$ C until reaction complete by TLC, quenched with saturated ammonium chloride (2 mL), extracted with ethyl acetate (3x, 5 mL), and concentrated *in vacuo*. The crude material was purified by silica gel chromatography with 50 % ethyl acetate in hexanes as the eluent to afford the unsaturated methyl ether (4 mg, 54 % over two steps). **$^1\text{H NMR}$** (500 MHz, CDCl_3): δ 7.38-7.29 (m, 5H), 7.19-7.12 (m, 1H), 6.72-6.61 (m, 2H), 5.66-5.44 (m, 1H), 4.73-4.68 (m, 1H), 3.81-3.76 (m, 3H), 3.32-3.29 (m, 3H), 2.92-2.84 (m, 2H), 2.33-2.15 (m, 3H), 2.03-1.87 (m, 3H), 0.94-0.81 (m, 7H), 0.77-0.65 (m, 3H). **$^{13}\text{C NMR}$** (126 MHz; CDCl_3): δ 157.6, 156.0, 155.3, 140.93, 140.91, 138.17, 138.15, 133.16, 133.13, 128.31, 128.30, 128.1, 127.79, 127.61, 127.53, 126.15, 126.13, 125.4, 114.0, 82.0, 81.4, 56.97, 56.87, 56.77, 55.4, 46.87, 46.79, 44.39, 44.33, 37.40, 37.38, 35.12, 34.99, 32.1, 31.04, 31.02, 29.90, 29.87, 29.83, 29.5, 27.9, 26.60, 26.52, 22.9, 16.80, 16.69, 14.3. **FTIR** (thin film): 3583, 2924, 2852, 1609 cm^{-1} .



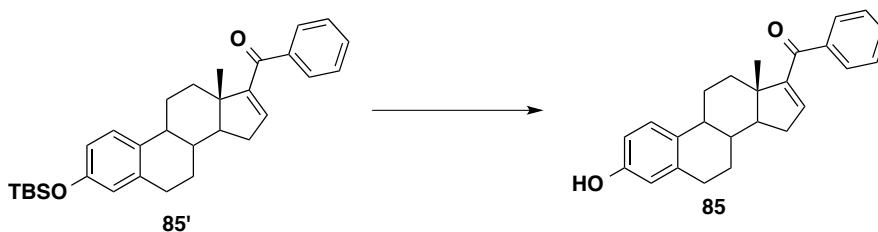
To a microwave vial purged and backfilled with argon preloaded with freshly activated zinc (227 mg, 3.5 mmol) was added methylene (216 mg, 0.7 mmol) in THF (1.4 mL, 0.5 M). The microwave vial was placed in a sonicator bath at 25 °C, and the acid chloride (390 µL, 3.5 mmol) in THF (1.75 mL, 2.0 M) was added dropwise and sonicated for 3 hours. The microwave vial was then heated to 60 °C for 2 hours. The reaction was cooled to 25 °C, quenched with water (10 mL), extracted with ethyl acetate (3x, 10 mL) and concentrate *in vacuo* to furnish dichloroketone **82**. The crude dichlorocyclobutanone was dissolved in acetic acid (7 mL, 0.1 M) and activated zinc (364 mg, 5.6 mmol) was added and the solution refluxed overnight. The solution was cooled to 25 °C and the aqueous extracted with ethyl acetate (3x, 20 mL). The crude reaction was purified with silica gel chromatography with 20-25 % ethyl acetate in hexanes as the eluent to afford the dechlorinated product (37 mg, 11 %). **¹H NMR** (500 MHz, CDCl₃): δ 7.31-7.29 (m, 1H), 6.86-6.80 (m, 2H), 4.08 (q, *J* = 6.6 Hz, 1H), 3.43 (t, *J* = 6.3 Hz, 1H), 3.18-3.15 (m, 1H), 3.06 (ddd, *J* = 17.4, 4.0, 2.4 Hz, 1H), 2.91-2.86 (m, 3H), 2.70 (ddd, *J* = 17.3, 5.8, 2.4 Hz, 1H), 2.51 (ddd, *J* = 17.2, 5.7, 2.4 Hz, 1H), 2.41-2.38 (m, 1H), 2.27 (dt, *J* = 1.6, 0.7 Hz, 4H), 2.24-2.18 (m, 1H), 2.13-2.09 (m, 1H), 1.97-1.85 (m, 3H), 1.47-1.34 (m, 4H), 0.88-0.77 (m, 3H). **¹³C NMR** (126 MHz; CDCl₃): δ 208.3, 171.4, 169.88, 169.87, 148.4, 138.19, 138.15, 137.7, 126.35, 126.26, 126.0, 121.55, 121.49, 121.45, 118.65, 118.61, 118.59, 118.53, 70.2, 64.4, 56.1, 54.2, 53.5, 52.4, 51.24, 51.11, 44.4, 43.77, 43.70, 42.8, 39.44, 39.43, 37.3, 36.96, 36.95, 31.8, 31.0, 29.69, 29.55, 29.47, 29.42, 29.37, 27.55, 27.47, 26.36, 26.34, 26.19, 26.13, 25.95, 25.85, 25.4, 24.1, 21.08, 20.95, 15.65, 15.63, 15.61, 14.6. **FTIR** (thin film): 3503, 2932, 2869, 1766 cm⁻¹. **HRMS (m/z)**: calcd for C₂₃H₂₈O₃: 352.2038, found [M-AcH]⁺: 309.1863.



To a solution of bromobenzene (106 μ L, 1.01 mmol) in THF (4.0 mL, 0.25 M) at $-78\text{ }^{\circ}\text{C}$ was added *t*-butyl lithium (2 mL, 2.9 mmol) dropwise and quickly warmed to $25\text{ }^{\circ}\text{C}$. After 30 minutes, the solution of anion was cooled to $-78\text{ }^{\circ}\text{C}$ and cyclobutanone (80 mg, 0.23 mmol) was added in THF (230 μ L, 1.0 M) and stirred at this temperature for 3 hours. The reaction was warmed to $25\text{ }^{\circ}\text{C}$ before being quenched with saturated ammonium chloride (10 mL), the aqueous extracted with ethyl acetate (3x, 20 mL), washed with brine (25 mL). The organics were dried and concentrated *in vacuo*. The crude residue was purified with silica gel chromatography with 20 % ethyl acetate as the eluent to afford the desired compound (83 mg, 93 %). **$^1\text{H NMR}$** (500 MHz, CDCl_3): δ 7.59-7.32 (m, 5H), 7.23-7.17 (m, 1H), 6.68-6.64 (m, 1H), 6.59 (s, 1H), 2.88-2.81 (m, 2H), 2.63-2.56 (m, 1H), 2.47-2.16 (m, 5H), 1.93-1.82 (m, 4H), 1.68-1.65 (m, 2H), 1.57-1.54 (m, 3H), 1.41-1.34 (m, 3H), 0.82-0.71 (m, 3H). **$^{13}\text{C NMR}$** (126 MHz; CDCl_3): δ 153.49, 146.7, 138.5, 133.0, 128.68, 128.61, 127.51, 126.74, 126.64, 126.0, 125.16, 124.93, 115.38, 112.8, 75.4, 72.8, 71.63, 71.55, 60.6, 55.4, 55.2, 51.17, 50.3, 44.8, 44.39, 44.27, 43.92, 43.88, 42.7, 42.2, 39.9, 39.5, 38.3, 37.8, 33.4, 33.0, 30.3, 29.91, 29.88, 29.86, 28.00, 27.87, 26.57, 26.41, 24.57, 24.46, 21.2, 14.34, , 13.6. **FTIR** (thin film): 3376, 2930, 2867, 1716, 1609 cm^{-1} . **HRMS (m/z)**: calcd for $\text{C}_{27}\text{H}_{32}\text{O}_2$: 388.2402, found $[\text{M}-\text{H}]^+$: 387.2257.



To a solution of alcohol **59** (35 mg, 0.07 mmol) in DCM (700 μ L, 0.1 M) at 25 C was added PCC (40 mg, 0.19 mmol) in one portion. The reaction was stirred at this temperature for 1 hour, diluted with DCM (10 mL) and filtered through a pad of silica. The organics were concentrated *in vacuo* and the crude reaction mixture was purified by silica gel chromatography with 20 % ethyl acetate in hexanes as the eluent to afford the enone **85'** (22 mg, 72 %). $^1\text{H NMR}$ (500 MHz, CDCl_3): δ 7.75-7.74 (m, 1H), 7.52 (d, J = 7.4 Hz, 1H), 7.43 (t, J = 7.6 Hz, 2H), 7.14 (d, J = 8.4 Hz, 1H), 6.63 (dd, J = 8.4, 2.5 Hz, 1H), 6.58 (d, J = 2.5 Hz, 1H), 6.45 (dd, J = 3.1, 1.7 Hz, 1H), 2.87-2.85 (m, 3H), 2.50-2.47 (m, 2H), 2.35 (s, 2H), 2.23-2.20 (m, 1H), 1.80 (d, J = 6.4 Hz, 1H), 1.70-1.61 (m, 4H), 1.50 (dd, J = 12.3, 6.7 Hz, 2H), 1.11 (d, J = 18.2 Hz, 3H), 0.20 (d, J = 2.9 Hz, 6H). $^{13}\text{C NMR}$ (126 MHz; CDCl_3): δ 202.3, 153.5, 139.6, 138.0, 133.0, 132.7, 128.52, 128.43, 126.1, 120.1, 117.3, 57.6, 56.4, 45.5, 43.9, 39.6, 39.1, 29.8, 28.0, 26.7, 25.9, 24.7, 24.1, 18.3, 13.9, -4.2. **FTIR** (thin film): 2929, 2857, 1661, 1609 cm^{-1}



To a stirred solution of protected enone **85'** (22 mg, 0.05 mmol) in THF (500 μ L, 0.1 M) was added TBAF (100 μ L, 0.10 mmol) and the reaction stirred at 25 $^{\circ}$ C over night. The reaction was quenched with saturated ammonium chloride (1 mL), extracted with ethyl acetate (3x, 15 mL), dried over sodium sulfate and concentrated *in vacuo*. The crude product was purified with silica gel chromatography with 50 % ethyl acetate in hexanes as the eluent to afford the desired product **85** (6 mg, 34 %). $^1\text{H NMR}$ (500 MHz, CDCl_3): δ 7.75-7.73 (m, 2H), 7.54-7.51 (m, 1H), 7.44-7.41 (m, 2H), 7.18-7.17 (m, 1H), 6.65-6.63 (m, 1H), 6.46-6.46 (m, 1H), 4.62 (s, 1H), 2.92-2.83 (m, 2H), 2.52-2.46 (m, 2H), 2.38-2.29 (m, 2H), 2.22-2.16 (m, 1H), 1.97-1.93 (m, 1H), 1.83-1.77 (m, 1H), 1.72-1.61 (m, 3H), 1.54-1.46 (m, 2H), 1.11-1.10 (m, 3H), 0.99-0.96 (m, 1H), 0.90-0.85 (m, 1H). $^{13}\text{C NMR}$ (126 MHz; CDCl_3): δ 194.6, 154.0, 153.5, 146.3, 139.5, 138.2, 133.0, 132.0, 129.2, 128.3, 126.5, 115.4, 112.9, 55.8, 47.9, 44.5, 37.2, 34.6, 32.8, 29.6, 28.0, 26.6, 16.3. **FTIR** (thin film) 3419, 2926, 1644, 1454 cm^{-1} .

Section 4.9 Analyzing the Importance of the Nitrogen



To a solution of ethyl propiolate (222 mg, 2.25 mmol) in THF (4.5 mL, 0.5 M) at -78 $^{\circ}$ C was added *n*-BuLi (900 μ L, 2.25 mmol) dropwise. After 15 minutes at -78 $^{\circ}$ C, protected steroid (768 mg, 1.5 mmol) was added in THF (3 mL, 0.5 M). The reaction mixture was allowed to slowly warm to 25 $^{\circ}$ C and was quenched with saturated ammonium chloride

(20 mL) after 5 hours. The aqueous was extracted with ethyl acetate (3x, 20 mL), dried over sodium sulfate, and concentrate *in vacuo*. The crude product was purified via silica gel chromatography with 20-33 % ethyl acetate in hexanes as the eluent. The product **86** was isolated as a yellow oil (626 mg, 69 %). **¹H NMR** (500 MHz, CDCl₃): δ 7.74 (t, *J* = 1.8 Hz, 4H), 7.45-7.37 (m, 6H), 6.98 (d, *J* = 8.5 Hz, 1H), 6.56-6.50 (m, 2H), 4.25 (q, *J* = 7.0 Hz, 2H), 2.72-2.68 (m, 2H), 2.41-2.18 (m, 4H), 2.07-2.02 (m, 1H), 1.83-1.74 (m, 4H), 1.64 (dd, *J* = 9.5, 9.1 Hz, 1H), 1.48-1.39 (m, 4H), 1.39-1.29 (m, 6H), 0.90 (s, 3H). **¹³C NMR** (126 MHz; CDCl₃): δ 153.8, 153.4, 137.7, 135.6, 133.36, 133.32, 132.6, 129.9, 127.8, 126.0, 119.7, 116.9, 90.6, 80.0, 78.2, 62.2, 50.0, 48.0, 43.5, 39.4, 38.7, 34.8, 33.1, 31.7, 29.6, 27.3, 26.7, 26.3, 25.4, 23.1, 22.8, 19.6, 14.27, 14.17, 12.8. **FTIR** (thin film): 3448, 2931, 2857, 1710 cm⁻¹. **HRMS (m/z)**: calcd for C₃₉H₄₆O₄Si: 606.3165, found [M+Na]⁺: 629.3054.

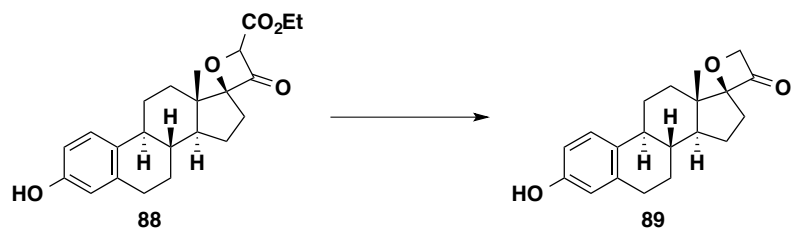


A microwave vial charged with alkyne alcohol **86** (224 mg, 0.37 mmol), IPrAuNTf₂ (16 mg, 0.02 mmol), and 4-acyl-pyridine-*N*-oxide (98 mg, 0.74 mmol) was sealed, purged of air, and backfilled with argon three times. To the microwave vial was added DCE (1.5 mL) and Tf₂NH (122 mg, 0.44 mmol) in DCE (2.1 mL) and the resulting solution was warmed to 80 °C and stirred for 12 hours. The reactions was cooled to 25 °C, quenched with water (10 mL) and extracted with DCM (3x, 15mL). The organics were dried over sodium sulfate and concentrated *in vacuo*. The crude mixture was purified by silica gel

chromatography with 20 % ethyl acetate in hexanes as the eluent to afford two products: silyl protected **87** (92 mg, 41 %) and deprotected **88** (34 mg, 24 %).

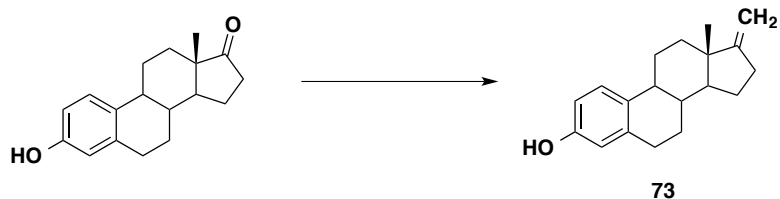
Compound **87**: $^1\text{H NMR}$ (500 MHz, CDCl_3): δ 7.72 (d, $J = 6.2$ Hz, 4H), 7.41-7.38 (m, 6H), 6.94-6.92 (m, 1H), 6.55-6.48 (m, 2H), 5.57 (d, $J = 28.3$ Hz, 1H), 4.32-4.27 (m, 2H), 2.70-2.65 (m, 2H), 2.32-2.10 (m, 5H), 1.95-1.88 (m, 1H), 1.81-1.75 (m, 2H), 1.64-1.59 (m, 2H), 1.53-1.23 (m, 10H), 1.00-0.95 (m, 3H). $^{13}\text{C NMR}$ (126 MHz; CDCl_3): δ 199.35, 199.25, 165.1, 164.5, 153.48, 153.45, 137.64, 137.61, 135.6, 135.3, 134.9, 133.32, 133.29, 133.27, 132.35, 132.25, 129.91, 129.76, 127.8, 126.03, 126.00, 120.63, 120.46, 119.73, 119.69, 117.0, 93.6, 93.2, 62.29, 62.15, 49.8, 49.4, 46.7, 46.5, 43.32, 43.26, 38.87, 38.83, 32.53, 32.37, 31.8, 31.2, 29.5, 27.11, 27.09, 26.7, 25.9, 23.36, 23.30, 19.6, 19.1, 14.39, 14.30, 12.64, 12.57 **FTIR** (thin film): 3502, 3071, 2931, 2857, 1820, 1752 cm^{-1} . **HRMS (m/z)**: calcd for $\text{C}_{39}\text{H}_{46}\text{O}_5\text{Si}$: 622.3115, found $[\text{M}+\text{Na}]^+$: 645.3010.

Compound **88**: $^1\text{H NMR}$ (500 MHz, CDCl_3): δ 7.11 (q, $J = 7.4$ Hz, 1H), 6.63-6.56 (m, 2H), 5.59 (d, $J = 27.2$ Hz, 1H), 4.34-4.25 (m, 2H), 2.85-2.79 (m, 2H), 2.37-2.10 (m, 5H), 1.98-1.91 (m, 1H), 1.91-1.74 (m, 3H), 1.57-1.39 (m, 5H), 1.34 (t, $J = 6.7$ Hz, 3H), 1.00 (dd, $J = 20.5, 13.3$ Hz, 3H). $^{13}\text{C NMR}$ (126 MHz; CDCl_3): δ 199.41, 199.29, 165.2, 164.6, 153.73, 153.69, 145.7, 138.24, 138.18, 138.15, 135.6, 132.09, 131.99, 130.9, 129.9, 127.8, 126.62, 126.61, 124.4, 120.66, 120.50, 115.43, 115.40, 112.9, 93.6, 93.2, 62.36, 62.22, 60.6, 49.7, 49.4, 46.7, 46.5, 43.29, 43.24, 38.97, 38.94, 32.53, 32.37, 31.8, 31.2, 29.6, 29.0, 27.08, 27.06, 26.7, 26.0, 25.7, 24.6, 24.2, 23.36, 23.31, 21.2, 14.40, 14.32, 14.30, 14.18, 12.63, 12.58 **FTIR** (thin film): 3422, 2930, 1819, 1735 cm^{-1} . **HRMS (m/z)**: calcd for $\text{C}_{23}\text{H}_{25}\text{O}_5$: 384.1937, found $[\text{M}+\text{H}]^+$: 385.2016.

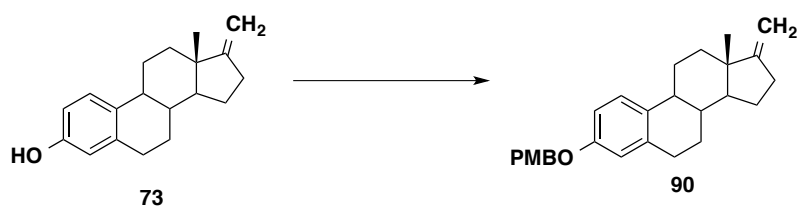


A solution of ketoester (43 mg, 0.11 mmol) in aqueous KOH (8 %, 900 μL , 0.1 M) and THF (100 μL , 1.0 M) was warmed to 45 $^{\circ}\text{C}$ for 12 hours. The reaction was cooled to 25 $^{\circ}\text{C}$, acidified with HCl (1N), and the aqueous extracted with DCM (2x, 20 mL), and 20 % *i*-PrOH in chloroform (1x, 20 mL). The organics were combined, dried over sodium sulfate and concentrate *in vacuo* to afford the product as a slightly yellow oil (34 mg, 384, quantitative). **$^1\text{H NMR}$** (500 MHz, CDCl_3): δ 6.99-6.97 (m, 1H), 6.52-6.45 (m, 2H), 4.01-3.91 (m, 2H), 2.72-2.66 (m, 2H), 2.28-2.16 (m, 2H), 2.07-2.01 (m, 1H), 1.84-1.69 (m, 4H), 1.42-1.31 (m, 3H), 1.31-1.25 (m, 1H), 1.25-1.11 (m, 5H), 0.99-0.90 (m, 3H). **$^{13}\text{C NMR}$** (126 MHz; CDCl_3): δ 176.5, 172.6, 154.2, 137.9, 131.4, 127.5, 126.1, 115.1, 112.6, 94.0, 64.8, 43.3, 39.0, 33.8, 30.3, 29.60, 29.52, 27.3, 26.42, 26.24, 24.0, 14.1. **FTIR** (thin film): 3381, 2927, 1741, 1610 cm^{-1} . **HRMS (m/z)**: calcd for $\text{C}_{20}\text{H}_{24}\text{O}_3$: 312.1725, found $[\text{M}-\text{H}]^-$: 311.1646.

Section 4.10 Access to Pyrrolidine Containing Derivatives



To a slurry of methyltriphenylphosphonium bromide (6.43 g, 18 mmol) in dry toluene (30 mL) was added potassium tert-butoxide (2.02 g, 18 mmol). The slurry was stirred at 80 °C for 2 h then cooled to 25 °C. Estrone (1.62 g, 6 mmol) was added in one portion to the yellow slurry. The reaction mixture was heated overnight at 80 °C. The reaction was cooled to 25 °C and quenched with acetone (25 mL), filtered through a 1 cm pad of silica gel, and concentrated *in vacuo*. The crude material was purified by silica gel chromatography with 33% ethyl acetate in hexanes as the eluent to afford the desired methylene **73** as a white solid (1.36 g, 85%). Spectral data matches reported spectra. ¹H NMR (500 MHz, CDCl₃): δ 7.18 (d, *J* = 8.4 Hz, 1H), 6.64 (dd, *J* = 8.4, 2.7 Hz, 1H), 6.57 (d, *J* = 2.6 Hz, 1H), 4.72 (s, 1H), 4.69 (d, *J* = 2.1 Hz, 2H), 2.87-2.79 (m, 2H), 2.58-2.52 (m, 1H), 2.38-2.18 (m, 3H), 1.99-1.91 (m, 2H), 1.85-1.79 (m, 1H), 1.59-1.35 (m, 5H), 1.25 (ddd, *J* = 12.6, 10.6, 6.4 Hz, 1H).



To a solution of methylene **73** (1.36 g, 5.1 mmol) in dry dimethylformamide (10 mL) was added cesium carbonate (1.80 g, 5.6 mmol) and paramethoxybenzyl chloride (680 μL, 5.1 mmol). The reaction was stirred for 12 h at 25° C before being quenched with deionized water (25 mL). The organics were extracted with ethyl acetate (3x 25 mL), washed with brine (30 mL), and dried with sodium sulfate. The solvent was removed *in vacuo* and the crude material purified by silica gel chromatography with 10% ethyl acetate in hexanes as the eluent to yield the product **90** as a white solid (1.94 g, 98%).

Spectra matches reported data. $^1\text{H NMR}$ (500 MHz, CDCl_3): δ 7.35-7.33 (m, 2H), 7.21 (d, $J = 8.6$ Hz, 1H), 6.91-6.89 (m, 2H), 6.77 (d, $J = 8.5$ Hz, 1H), 6.71 (s, 1H), 4.94 (s, 2H), 4.67 (s, 2H), 3.80 (s, 3H), 2.86-2.84 (m, 1H), 2.53-2.51 (m, 1H), 2.34-2.21 (m, 3H), 1.96-1.94 (m, 2H), 1.84 (s, 1H), 1.58-1.38 (m, 6H), 0.81 (s, 3H).

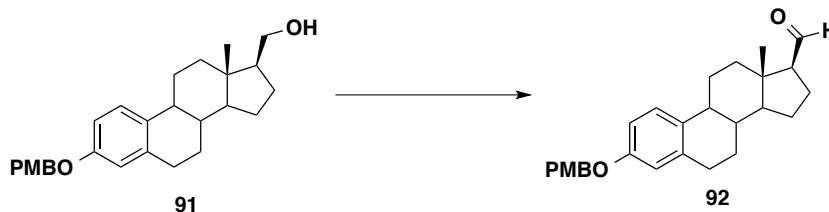


To a solution of PMB-methylene **90** (1.94 g, 5 mmol) in dry THF (20 mL) was added a solution of borane in THF (10 mL, 1 M) at 25 °C. The solution was stirred for 2 h or until the consumption of starting material was observed by TLC. The reaction was then cooled to 0 °C and 2N sodium hydroxide in deionized water (10 mL) and 30% aqueous hydrogen peroxide (6.6 mL) were added. The solution was stirred overnight at 25 °C and then diluted with ethyl acetate (50 mL). The organics were washed with brine (6x 50 mL) until they tested negative for peroxides and dried over sodium sulfate. The solvent was removed *in vacuo* and the residue purified by silica gel chromatography with 30% ethyl acetate in hexanes as the eluent to yield the product **91** as a white solid (1.64 g, 81%) as a 2:1 mixture of β : α epimers. $^1\text{H-NMR}$ (500 MHz; CDCl_3): δ 7.37 (d, $J = 8.6$ Hz, 2H), 7.22 (d, $J = 8.6$ Hz, 1H), 6.94-6.92 (m, 2H), 6.79 (dd, $J = 8.6, 2.6$ Hz, 1H), 6.73 (d, $J = 2.6$ Hz, 1H), 4.97 (s, 2H), 3.83 (s, 3H), 3.77 (dd, $J = 10.5, 6.8$ Hz, 1H), 3.66 (t, $J = 6.6$ Hz,), 3.59 (dd, $J = 10.5, 7.5$ Hz, 1H), 3.38 (dd, $J = 10.5, 7.5$ Hz,), 2.88 (dd, $J = 14.7, 5.4$ Hz, 2H), 2.31-2.22 (m, 2H), 2.04-2.01 (m, 1H), 1.94-1.72 (m, 4H), 1.59-1.27 (m, 9H), 0.87 (s, 1H), 0.71 (s, 2H). $^{13}\text{C NMR}$ (126 MHz; CDCl_3): δ 159.4, 156.8, 138.1, 133.2,

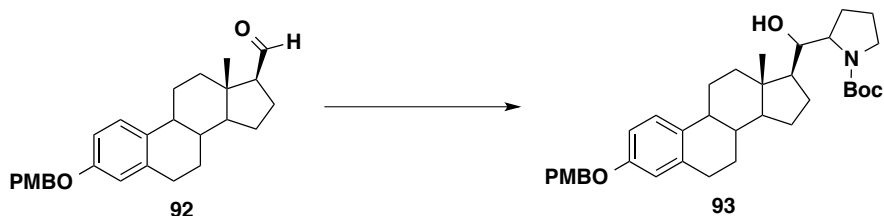
129.5, 129.2, 126.37, 126.34, 114.90, 114.88, 114.0, 112.3, 69.8, 65.1, 64.6, 62.7, 58.7, 55.4, 55.1, 53.2, 53.0, 50.9, 50.6, 44.13, 44.11, 43.9, 43.1, 42.3, 39.2, 38.8, 38.6, 35.3, 34.9, 34.2, 30.01, 29.94, 29.90, 29.88, 28.3, 27.9, 26.57, 26.54, 26.50, 26.49, 25.7, 25.45, 25.43, 24.40, 24.26, 21.0, 19.0, 14.0, 12.6, 8.3. **FTIR** (thin film) 3389, 2931, 2867, 1612, 1515 cm^{-1} .



To a solution of PMB-methylene **90** (2.14 g, 5.5 mmol) in dry THF (11 mL) was added a solution of 9-BBN in THF (22 mL, 0.5 M) at 25 °C. The solution was stirred for 2 h or until the consumption of starting material was observed by TLC. The reaction was then cooled to 0 °C and 2N sodium hydroxide in deionized water (11 mL) and 30% aqueous hydrogen peroxide (6.6 mL) were added. The solution was stirred overnight at 25 °C and then diluted with ethyl acetate (50 mL). The organics were washed with brine (6x 50 mL) until they tested negative for peroxides and dried over sodium sulfate. The solvent was removed *in vacuo* and the residue purified by silica gel chromatography (30% ethyl acetate in hexanes) to yield alcohol **91** as a white solid (1.85 g, 83%) as exclusively the β epimer. **¹H NMR** (500 MHz, CDCl₃): δ 7.34 (d, J = 8.5 Hz, 2H), 7.19 (d, J = 8.6 Hz, 1H), 6.90 (d, J = 8.6 Hz, 2H), 6.77-6.70 (m, 2H), 4.94 (s, 2H), 3.81 (s, 3H), 3.74 (t, J = 5.1 Hz, 1H), 3.59-3.57 (m, 1H), 2.84-2.83 (m, 2H), 2.24 (d, J = 10.6 Hz, 2H), 2.00 (d, J = 12.2 Hz, 1H), 1.91-1.86 (m, 2H), 1.79-1.70 (m, 3H), 1.50-1.31 (m, 7H), 0.68 (s, 3H).

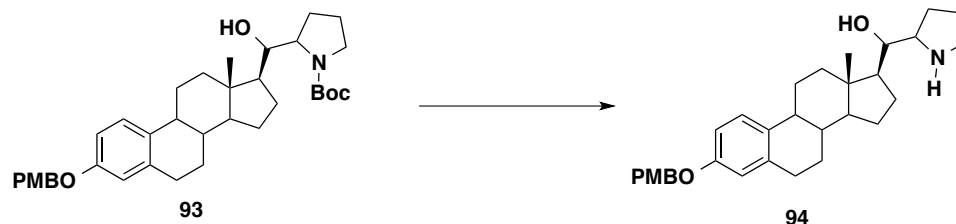


To a solution of alcohol **91** (1.82 g, 4.5 mmol) in dichloromethane (30 mL) at 0 °C was added Dess Martin periodinane (2.84 g, 6.7 mmol). The yellow solution was stirred at 0 °C for 1.5 h until no more SM was observed by TLC. The reaction was quenched with saturated aqueous sodium bisulfate (10 mL) and saturated aqueous sodium bicarbonate (10 mL) and stirred for 15 minutes. The layers were separated and the aqueous extracted with dichloromethane (3x 25 mL). The combined organic layers were washed with brine (15 mL), dried over sodium sulfate and the solvent removed *in vacuo*. The crude residue was purified by silica gel chromatography (dry loaded on 4.5 g Si; 20% ethyl acetate in hexanes) to provide the aldehyde **92** as a white solid (1.19 g, 65 %). ¹H NMR (500 MHz; CDCl₃): δ 9.84 (d, J = 1.9 Hz, 1H), 7.38 (d, J = 8.5 Hz, 2H), 7.23 (d, J = 8.6 Hz, 1H), 6.94 (d, J = 8.6 Hz, 2H), 6.81 (dd, J = 8.5, 2.5 Hz, 1H), 6.75 (d, J = 2.3 Hz, 1H), 4.98 (s, 2H), 3.83 (s, 3H), 2.92-2.88 (m, 2H), 2.42-2.34 (m, 2H), 2.31-2.26 (m, 1H), 2.23-2.15 (m, 2H), 1.94-1.88 (m, 2H), 1.85-1.79 (m, 1H), 1.67 (td, J = 12.9, 3.7 Hz, 1H), 1.58-1.38 (m, 5H), 0.82 (s, 3H). ¹³C NMR (126 MHz; CDCl₃): δ 204.87, 204.83, 159.4, 156.9, 137.9, 132.5, 129.32, 129.21, 126.3, 114.8, 114.0, 112.3, 69.7, 63.0, 55.31, 55.26, 45.1, 43.8, 38.43, 38.29, 29.8, 27.8, 26.2, 24.6, 21.1, 14.0. FTIR (thin film) 2931, 2719, 1715, 1612 cm⁻¹. HRMS (m/z): calcd for C₂₇H₃₂O₃: 404.2351, found [M-H]⁺: 403.2570.

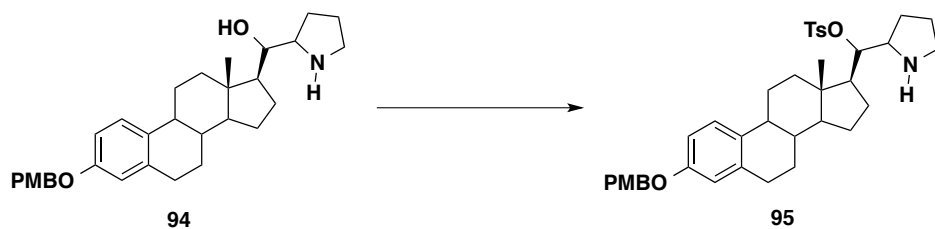


To a solution of *N*-Boc-pyrrolidine (420 mg, 2.45 mmol) and TMEDA (257 mg, 2.21 mmol) in diethyl ether (5.0 mL, 0.5 M) at -78 °C was added *s*-butyllithium (2.0 mL, 2.45 mmol). The reaction was stirred at this temperature for 3 hours before the dropwise addition of aldehyde **92** (333 mg, 0.82 mmol) in THF (1.6 mL, 0.5 M). The reaction was allowed to slowly warm to 25 °C overnight before being quenched with saturated ammonium chloride (20 mL). The aqueous extracted with ethyl acetate (3x, 15 mL), washed with brine (25 mL), and dried over sodium sulfate. The crude material was concentrated *in vacuo* and purified with silica gel chromatography with 33-50 % ethyl acetate in hexanes as the eluent to give a mixture of three major diastereomers of **93** (130 mg, 27 %) ¹H NMR (500 MHz; CDCl₃): δ 7.35 (d, J = 8.4 Hz, 2H), 7.19-7.17 (m, 1H), 6.91 (d, J = 8.1 Hz, 2H), 6.77-6.76 (m, 1H), 6.71 (s, 1H), 4.95 (s, 2H), 4.62-4.60 (m,), 4.41 (s,), 4.32-4.30 (m,), 4.03-3.95 (m,), 3.81 (s, 3H), 3.77-3.51 (m, 2H), 3.27-3.13 (m, 1H), 2.87-2.79 (m, 2H), 2.31-2.18 (m, 2H), 1.98-1.72 (m, 8H), 1.52-1.43 (m, 6H), 0.86-0.75 (m, 3H). ¹³C NMR (126 MHz; CDCl₃): δ 160.9, 159.5, 156.91, 156.84, 138.14, 138.07, 132.7, 129.50, 129.46, 129.40, 129.28, 126.31, 126.27, 114.9, 114.1, 112.46, 112.37, 83.3, 77.4, 69.8, 64.3, 60.5, 55.41, 55.22, 55.0, 54.7, 45.4, 43.9, 43.4, 42.6, 39.2, 38.9, 38.59, 38.42, 31.34, 31.23, 29.99, 29.90, 28.72, 28.68, 28.54, 28.51, 27.88, 27.78, 26.5, 26.34, 26.31, 24.4, 24.0, 21.22, 21.17, 14.3, 13.9. FTIR (thin film) 3443,

2931, 1749, 1688, 1611 cm^{-1} . **HRMS (m/z)**: calcd for $\text{C}_{36}\text{H}_{49}\text{NO}_5$: 575.3611 found $[\text{M}+\text{H}]^+$: 576.3698.

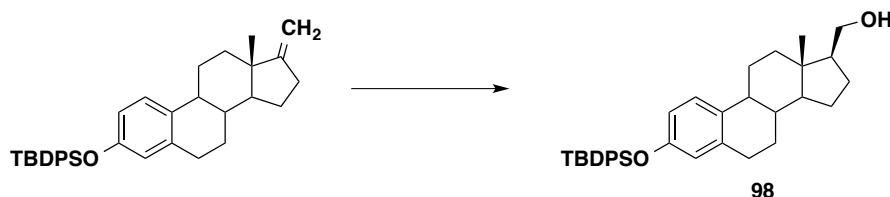


A solution of alcohol **93** (104 mg, 0.18 mmol) and KOH (100 mg, 1.80 mmol) in MeOH (180 μL , 1.0 M) and dry DMSO (1 mL, 0.2 M) was heated to 65 $^{\circ}\text{C}$ for 12 hours. The reaction mixture was cooled to 25 $^{\circ}\text{C}$, quenched with water (10 mL) and extracted with chloroform (2x, 20 mL) and 10 % *i*-PrOH in chloroform (2x, 20 mL). The organics were combined and concentrate *in vacuo*. The crude residue was purified by silica gel chromatography with 4 % methanol in DCM as the eluent to afford the deprotected product **94** (61 mg, 71 %). **^1H NMR** (500 MHz, CDCl_3): δ 7.34 (d, $J = 8.4$ Hz, 2H), 7.20-7.17 (m, 1H), 6.90 (d, $J = 8.4$ Hz, 2H), 6.77-6.70 (m, 2H), 4.95 (s, 2H), 3.81 (s, 3H), 2.98-2.82 (m, 3H), 2.22-2.18 (m, 4H), 1.90-1.86 (m, 10H), 1.39-1.20 (m, 12H), 0.77-0.73 (m, 3H). **^{13}C NMR** (126 MHz; CDCl_3): δ 159.5, 156.9, 133.2, 129.5, 129.3, 126.37, 126.36, 126.34, 114.96, 114.95, 114.92, 114.10, 114.06, 112.38, 112.36, 69.9, 55.4, 55.2, 50.9, 44.10, 44.01, 42.8, 38.7, 29.99, 29.84, 27.9, 26.5. **FTIR** (thin film): 3055, 2929, 1608 cm^{-1} .



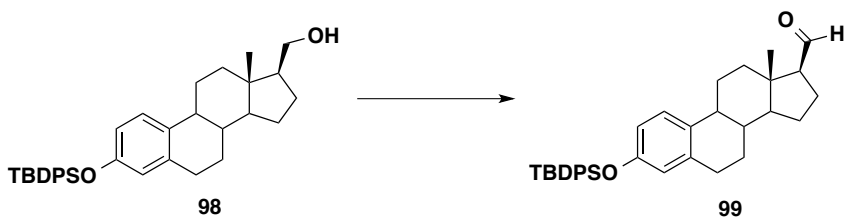
To a solution of alcohol **94** (145 mg, 0.30 mmol) and DMAP (4 mg, 0.03 mmol) in dry pyridine (1 mL, 0.3 M) was added TsCl (172 mg, 0.90 mmol) and the reaction stirred for 12 hours, until the starting material was no longer seen by TLC. The reaction was quenched with water (20 mL) and the aqueous extracted with DCM (3x, 15 mL). The organics concentrated *in vacuo*, and the crude residue purified by silica gel chromatography with 33 % ethyl acetate in hexanes as the eluent to afford the desired tosylate **95** as a mixture of diastereomers (48 mg, 25 %). **¹H NMR** (500 MHz, CDCl₃): δ 7.80-7.70 (m, 2H), 7.35 (quintet, *J* = 8.6 Hz, 4H), 7.20 (dd, *J* = 8.2, 5.1 Hz, 1H), 6.91 (d, *J* = 8.0 Hz, 2H), 6.79-6.76 (m, 1H), 6.71 (s, 1H), 4.96 (s, 2H), 4.56-4.54 (m, 1H), 3.78 (d, *J* = 0.5 Hz, 3H), 3.60 (s, 1H), 3.41-3.35 (m, 2H), 2.89-2.79 (m, 2H), 2.44-2.41 (m, 3H), 2.36-2.10 (m, 3H), 1.95-1.85 (m, 2H), 1.85-1.66 (m, 4H), 1.66-1.50 (m, 3H), 1.50-1.33 (m, 4H), 0.82-0.73 (m, 3H). **¹³C NMR** (126 MHz; CDCl₃): δ 208.7, 171.3, 159.5, 156.9, 143.8, 143.5, 138.16, 138.05, 137.99, 136.1, 134.78, 134.59, 132.7, 129.98, 129.94, 129.92, 129.85, 129.68, 129.44, 129.28, 127.84, 127.76, 127.65, 126.40, 126.35, 126.33, 114.94, 114.91, 114.89, 114.1, 112.45, 112.43, 112.36, 70.9, 69.8, 67.6, 66.1, 64.6, 63.2, 60.55, 60.51, 59.3, 56.2, 55.56, 55.41, 55.0, 52.6, 49.6, 48.9, 48.6, 45.9, 45.4, 44.4, 43.82, 43.71, 43.2, 42.9, 38.85, 38.82, 38.70, 38.63, 38.46, 38.2, 29.99, 29.91, 29.82, 29.27, 29.23, 28.7, 27.93, 27.89, 27.81, 26.82, 26.69, 26.3, 25.9, 24.95, 24.83, 24.63, 24.55, 24.49, 24.45, 24.38, 24.21, 21.7, 21.2, 19.8, 14.3, 14.0, 13.7, 13.4,

12.4. **FTIR** (thin film): 3501, 2927, 1716, 1612. **HRMS (m/z)**: calcd for C₃₈H₄₇NO₅S: 629.3175, found [M+H]⁺: 630.3245.

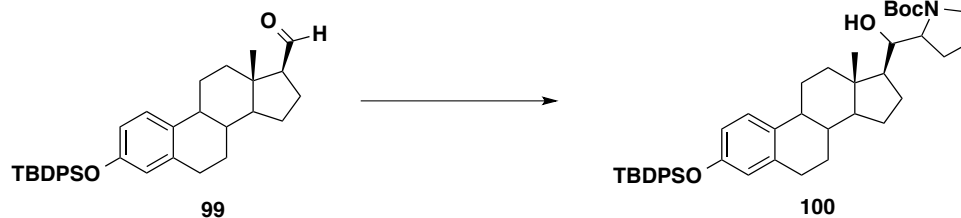


To a solution of TBDPS-methylene (1.93 g, 3.8 mmol) in dry THF (7.6 mL, 0.5 M) was added a solution of 9-BBN in THF (15.2 mL, 7.6 mmol) at 25 °C. The solution was stirred for 2 h or until the consumption of starting material was observed by TLC. The reaction was then cooled to 0 °C and 2N sodium hydroxide in deionized water (7.6 mL) and 30% aqueous hydrogen peroxide (5.2 mL) were added. The solution was stirred overnight at 25 °C and then diluted with ethyl acetate (50 mL). The organics were washed with brine (5x 50 mL) until they tested negative for peroxides and dried over sodium sulfate. The solvent was removed *in vacuo* and the residue purified by silica gel chromatography with 20% ethyl acetate in hexanes as the eluent to yield alcohol **98** as a white solid (746 mg, 37 %) as exclusively the β epimer. ¹H NMR (500 MHz, CDCl₃): δ 7.73-7.73 (m, 4H), 7.44-7.37 (m, 6H), 6.97-6.96 (m, 1H), 6.54 (s, 1H), 6.49 (d, J = 8.5 Hz, 1H), 3.76-3.55 (m, 2H), 2.72-2.64 (m, 2H), 2.18-2.13 (m, 3H), 1.97-1.95 (m, 1H), 1.95-1.80 (m, 3H), 1.76-1.62 (m, 5H), 1.58-1.20 (m, 13H), 0.70-0.67 (m, 3H). ¹³C NMR (126 MHz; CDCl₃): δ 153.3, 137.8, 135.7, 133.41, 133.37, 133.1, 129.9, 127.8, 126.0, 119.7, 116.8, 64.8, 55.1, 53.2, 44.2, 42.3, 38.9, 38.5, 29.7, 27.9, 27.6, 26.7, 26.4, 25.8, 24.4, 22.8, 19.6.

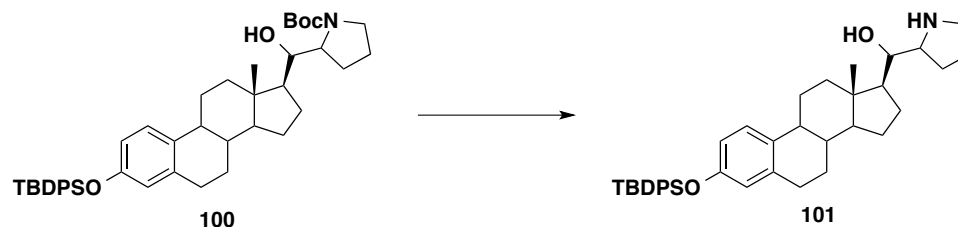
12.7. **FTIR** (thin film) 3389, 2929, 2857, 1606 cm⁻¹. **HRMS (m/z)**: calcd for C₃₅H₄₄O₂Si: 524.3111, found [M+H]⁺: 525.3206.



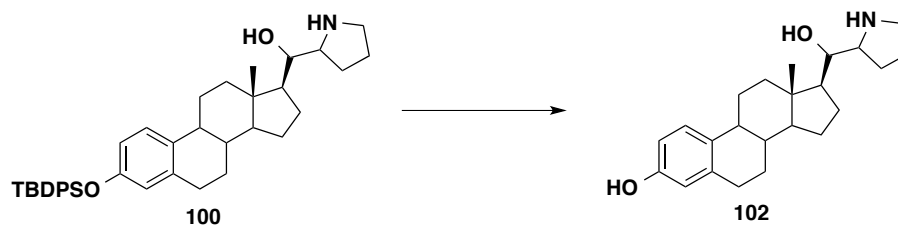
To a slurry of Dess Martin Periodinane (747 mg, 1.76 mmol) in DCM (7 mL, 0.25 M) was added a solution of alcohol **98** (739 mg, 1.4 mmol) in DCM (2.8 mL, 0.5 M) at 0 °C. The yellow solution was stirred at 0 °C for 2 hours until no more SM was observed by TLC. The reaction was quenched with saturated aqueous sodium bisulfate (10 mL) and saturated aqueous sodium bicarbonate (10 mL) and stirred for 15 minutes. The layers were separated and the aqueous extracted with dichloromethane (3x ,20 mL). The combined organic layers were washed with brine (15 mL), dried over sodium sulfate and the solvent removed *in vacuo*. The crude residue was purified by silica gel chromatography with 10% ethyl acetate in hexanes as the eluent to provide the aldehyde **99** as a white solid (627, 86 %). **¹H NMR** (500 MHz, CDCl₃): δ 9.79 (s, 1H), 7.73 (t, *J* = 2.9 Hz, 4H), 7.42-7.37 (m, 6H), 6.96 (d, *J* = 8.5 Hz, 1H), 6.54-6.49 (m, 2H), 2.73-2.67 (m, 2H), 2.48-2.35 (m, 5H), 2.25-2.05 (m, 6H), 1.91-1.68 (m, 9H), 1.62-1.25 (m, 15H), 0.77 (s, 3H). **¹³C NMR** (126 MHz; CDCl₃): δ 205.0, 153.4, 137.7, 135.6, 133.31, 133.27, 132.6, 129.9, 127.8, 125.9, 119.7, 116.9, 63.0, 55.4, 45.2, 43.9, 42.05, 41.99, 38.5, 38.2, 33.4, 29.6, 27.8, 27.3, 26.7, 26.10, 25.94, 25.77, 24.81, 24.64, 21.2, 19.6, 14.0. **FTIR** (thin film) 2929, 2856, 1717, 1606 cm⁻¹. **HRMS (m/z)**: calcd for C₃₅H₄₂O₂Si: 522.2954, found [M+H]⁺: 523.3044.



To a solution of *N*-Boc-pyrrolidine (615 mg, 3.60 mmol) and TMEDA (371 mg, 3.20 mmol) in diethyl ether (7.2 mL, 0.5 M) at -78 °C was added *s*-butyllithium (3.0 mL, 3.60 mmol). The reaction was stirred at this temperature for 2 hours before the dropwise addition of aldehyde **99** (531 mg, 1.20 mmol) in THF (2.4 mL, 0.5 M). The reaction was allowed to slowly warm to 25 °C overnight before being quenched with saturated ammonium chloride (20 mL). The aqueous extracted with ethyl acetate (3x, 20 mL), washed with brine (25 mL), and dried over sodium sulfate. The crude material was concentrated *in vacuo* and purified with silica gel chromatography with 20-50 % ethyl acetate in hexanes as the eluent to give a mixture of three major diastereomers of **100** (510 mg, 72 %). ¹H NMR (500 MHz, CDCl₃): δ 7.73 (d, *J* = 1.3 Hz, 4H), 7.41-7.36 (m, 6H), 6.96-6.93 (m, 1H), 6.54-6.47 (m, 2H), 3.61-3.54 (m, 2H), 3.34-3.14 (m, 3H), 2.72-2.67 (m, 2H), 2.22-2.03 (m, 5H), 1.98-1.66 (m, 12H), 1.47-1.45 (m, 8H), 0.80-0.74 (m, 3H). ¹³C NMR (126 MHz; CDCl₃): δ 160.9, 154.8, 153.37, 153.28, 137.82, 137.77, 135.69, 135.61, 135.56, 135.53, 133.36, 133.34, 133.31, 133.27, 132.6, 129.9, 127.8, 125.86, 125.85, 125.81, 119.72, 119.65, 119.57, 116.81, 116.74, 116.73, 85.0, 83.3, 80.9, 79.0, 64.2, 55.18, 54.99, 46.1, 45.7, 45.4, 45.1, 43.9, 42.5, 38.9, 38.46, 38.28, 35.8, 31.2, 29.68, 29.57, 28.72, 28.67, 28.63, 28.54, 28.50, 28.3, 27.85, 27.77, 27.74, 26.66, 26.47, 26.39, 26.31, 26.22, 26.19, 25.85, 25.75, 24.47, 24.41, 24.0, 21.79, 21.70, 19.6, 13.9. FTIR (thin film) 3458, 2930, 1753, 1691, 1607 cm⁻¹. HRMS (*m/z*): calcd for C₄₄H₅₉NO₄Si: 693.4213, found [M+H]⁺: 694.4298.



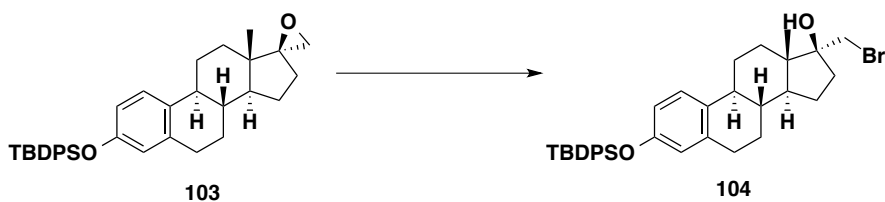
To a solution of alcohol (248 mg, 0.36 mmol) in DCM (3.6 mL, 0.1 M) at 0 °C was added TFA (360 μ L, 1.0 M) dropwise. The reaction mixture was stirred at this temperature for 1 hour and then concentrated *in vacuo* to afford the deprotected material (210 mg, 98 %). **$^1\text{H NMR}$** (500 MHz, CDCl_3): δ 7.73-7.71 (m, 4H), 7.43-7.34 (m, 6H), 6.94-6.92 (m, 1H), 6.54-6.46 (m, 2H), 4.30-4.28 (m, 1H), 3.70-3.51 (m, 3H), 3.17-3.14 (m, 2H), 2.69-2.66 (m, 2H), 1.58-1.25 (m, 12H), 1.08 (s, 9H), 0.73 (s, 3H). **$^{13}\text{C NMR}$** (126 MHz; CDCl_3): δ 161.0, 153.4, 137.8, 135.71, 135.66, 133.36, 133.32, 132.7, 129.9, 127.87, 127.82, 125.8, 119.8, 116.8, 85.0, 83.3, 68.6, 64.3, 55.22, 55.03, 45.4, 45.2, 43.9, 42.6, 39.0, 38.3, 35.8, 31.2, 30.9, 29.6, 28.3, 27.81, 27.77, 26.69, 26.65, 26.51, 26.35, 26.25, 26.23, 25.8, 24.51, 24.46, 24.0, 21.83, 21.74, 19.6, 13.9. **FTIR** (thin film) 2931, 1745, 1607 cm^{-1} . **HRMS (m/z)**: calcd for $\text{C}_{39}\text{H}_{51}\text{NO}_2\text{Si}$: 593.3689, found $[\text{M}+\text{H}]^+$: 594.3765.



To a solution of alcohol **100** (28 mg, 0.05 mmol) in THF (250 μ L, 0.2 M) was added TBAF (100 μ L, 0.10 mmol) dropwise, and the resulting reaction stirred overnight at 25

°C. The reaction was then quenched with saturated ammonium chloride (10 mL), the aqueous extracted with ethyl acetate (3x, 10 mL), dried with sodium sulfate and concentrate *in vacuo*. The crude residue was purified by silica gel chromatography with 50 % ethyl acetate in hexanes as the eluent to afford the product **102** (5 mg, 28 %). **¹H NMR** (500 MHz, CDCl₃): δ 7.08-7.05 (m, 1H), 6.60-6.57 (m, 1H), 6.52-6.51 (m, 1H), 4.29 (t, *J* = 0.4 Hz, 1H), 3.55-3.52 (m, 2H), 3.13-3.12 (m, 1H), 2.78-2.75 (m, 2H), 0.72 (3H). **¹³C NMR** (126 MHz; CDCl₃): δ 161.4, 161.2, 154.3, 138.1, 131.6, 126.48, 126.29, 115.3, 112.8, 83.7, 64.3, 55.13, 54.93, 54.85, 54.5, 45.2, 45.0, 43.90, 43.85, 43.1, 42.6, 38.94, 38.90, 38.62, 38.44, 35.8, 31.15, 31.11, 30.8, 29.7, 28.2, 27.91, 27.74, 27.69, 26.38, 26.34, 26.33, 26.24, 25.7, 24.45, 24.41, 24.38, 23.93, 23.76, 21.72, 21.62, 13.8, 12.5. **FTIR** (thin film) 3289, 2921, 1718 cm⁻¹. **HRMS (m/z)**: calcd for C₂₃H₃₃NO₂: 355.2511, found [M-H]⁺: 354.2431.

Section 4.11 Cross Coupling Approach to Alkylidene Analog



To a solution of epoxide (126 mg, 0.24 mmol) in dioxane (1 mL, 0.25 M) was added HBr (48 % in water, 1 mL, 0.25 M) dropwise at 25 °C. The reaction was stirred at this temperature for three hours before diluting with water (20 mL) and extracting with ethyl

acetate (3x, 15 mL). The organics were washed with sodium bicarbonate (20 mL), then brine (20 mL), dried over sodium sulfate, and the solvent removed *in vacuo*. The crude mixture was purified with silica gel chromatography with 10 % ethyl acetate in hexanes as the eluent to afford the halohydrin product (53 mg, 38 %). **¹H NMR** (500 MHz; CDCl₃): δ 7.74 (dt, *J* = 3.6, 1.7 Hz, 4H), 7.42-7.38 (m, 7H), 6.97 (t, *J* = 8.3 Hz, 1H), 6.57-6.50 (m, 2H), 3.81-3.79 (m, 1H), 3.64 (d, *J* = 10.1 Hz, 1H), 2.73-2.68 (m, 2H), 2.30-1.27 (m, 20H), 1.11 (s, 9H), 0.99 (d, *J* = 9.6 Hz, 3H), 0.90 (dt, *J* = 6.0, 2.7 Hz, 3H). **¹³C NMR** (126 MHz; CDCl₃): δ 153.5, 137.70, 137.57, 135.7, 135.3, 134.9, 133.35, 133.32, 132.5, 132.3, 129.91, 129.77, 127.8, 126.03, 125.95, 119.75, 119.72, 117.07, 116.94, 81.9, 77.42, 77.38, 77.2, 76.9, 50.63, 50.57, 48.1, 47.2, 46.9, 44.1, 43.9, 39.4, 38.4, 36.2, 36.0, 34.8, 32.3, 31.74, 31.71, 29.59, 29.51, 27.6, 27.1, 26.71, 26.66, 26.2, 25.9, 25.4, 23.6, 22.8, 21.7, 20.9, 19.6, 19.2, 15.0, 14.3, 14.0. **FTIR** (thin film) 3453, 2930, 1732, 1606 cm⁻¹. **HRMS (m/z)**: calcd for C₃₅H₄₃BrO₂Si: 602.2216, found [M+H]⁺: 603.2289.



Thionyl chloride (10 μ L, 0.12 mmol) was added dropwise to a solution of halohydrin (53 mg, 0.09 mmol) in dry pyridine (300 μ L, 0.3M) at 25 C. The reaction was quenched after one hour with HCl (2N, 2 mL) and extracted with DCM (3x, 10 mL). The organics were concentrated *in vacuo* and the crude residue purified by silica gel chromatography with 3 % ethyl acetate in hexanes as the eluent to afford the desired vinyl bromide as a yellow

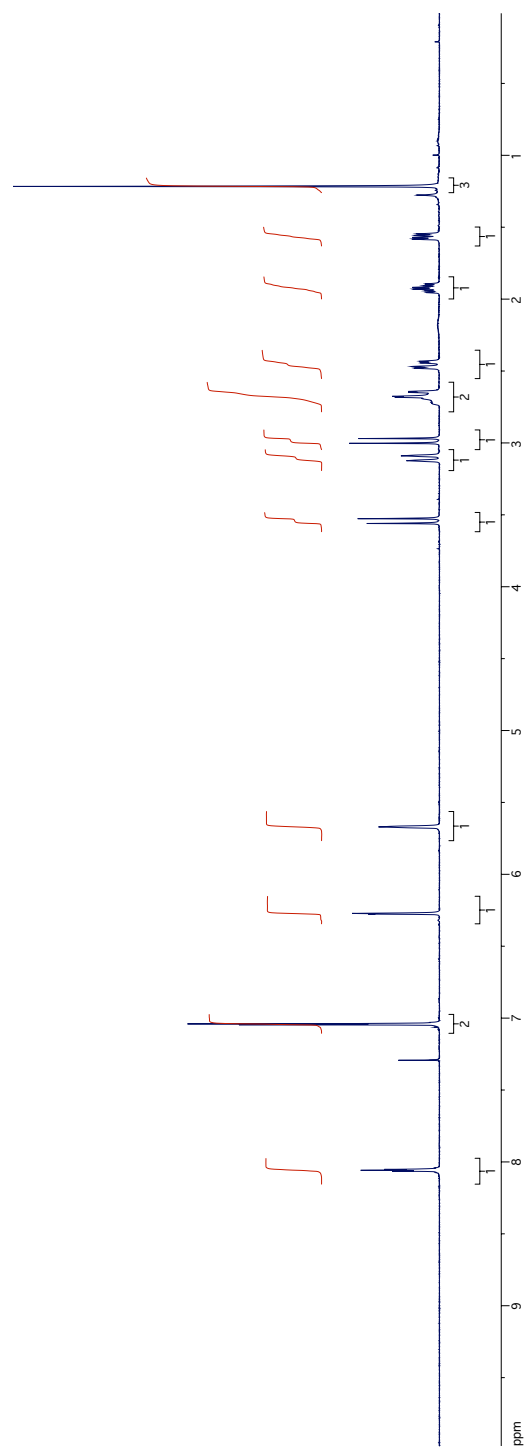
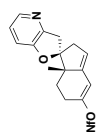
oil (18 mg, 30 %). **¹H NMR** (500 MHz; CDCl₃): δ 7.74-7.72 (m, 4H), 7.44-7.35 (m, 6H), 6.96 (d, *J* = 8.5 Hz, 1H), 6.54-6.48 (m, 2H), 5.80 (s, 1H), 2.73-2.67 (m, 2H), 2.42-2.37 (m, 2H), 2.27-2.26 (m, 1H), 2.18-2.16 (m, 1H), 1.92-1.90 (m, 1H), 1.88-1.83 (m, 2H), 1.48-1.26 (m, 6H), 0.90-0.84 (m, 3H). **¹³C NMR** (126 MHz; CDCl₃): δ 158.1, 153.4, 137.7, 135.7, 133.38, 133.34, 132.7, 129.9, 127.8, 126.0, 119.7, 116.9, 96.3, 77.42, 77.38, 77.2, 76.92, 76.86, 54.4, 46.9, 44.0, 38.7, 35.7, 30.7, 29.6, 27.6, 26.7, 26.4, 23.9, 19.6, 18.8. **FTIR** (thin film) 3071, 2929, 1607, 1496 cm⁻¹. **HRMS (m/z)**: calcd for C₃₅H₄₁BrOSi: 584.2110, found [M+H]⁺: 585.2193.

APPENDIX

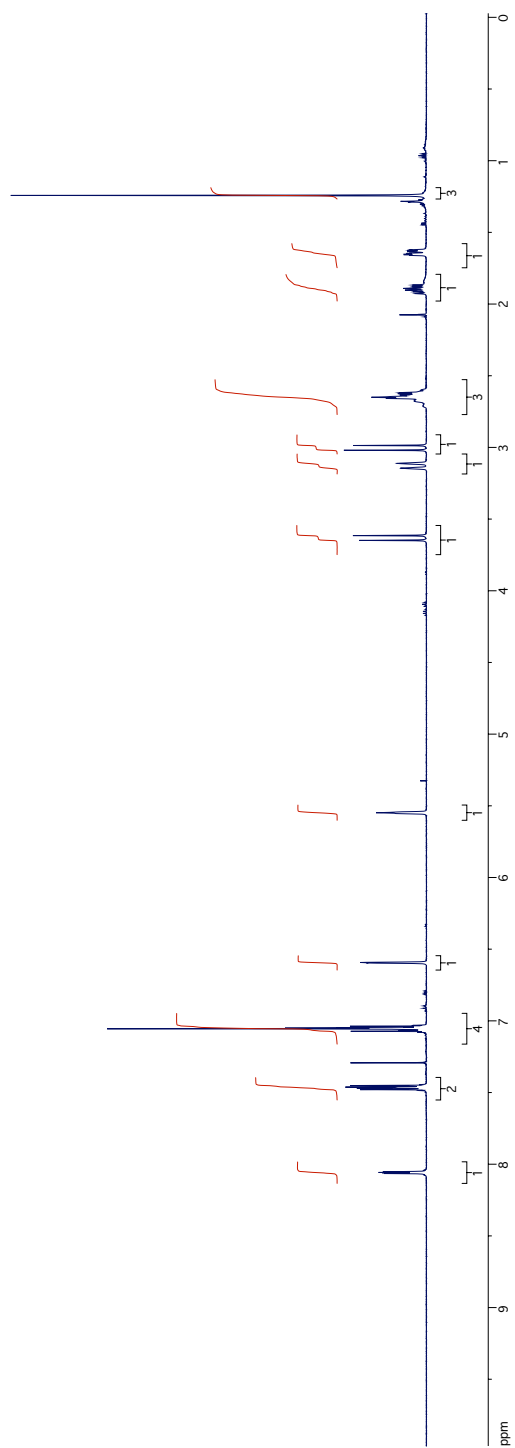
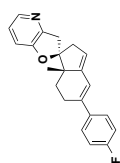
A.1 Spectral Images for Chapter 2

A.2 Spectral Images for Chapter 4

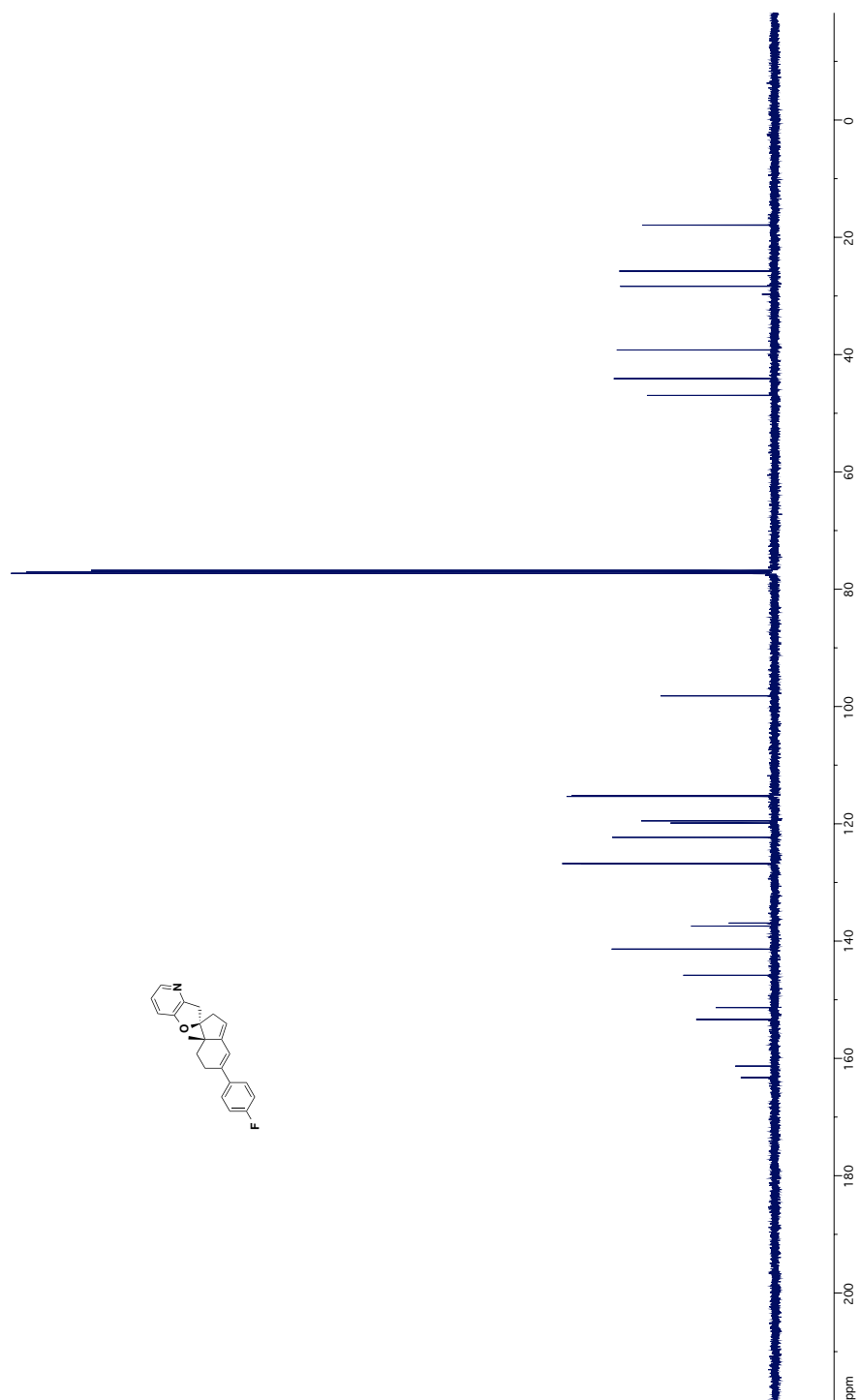
Appendix A.1



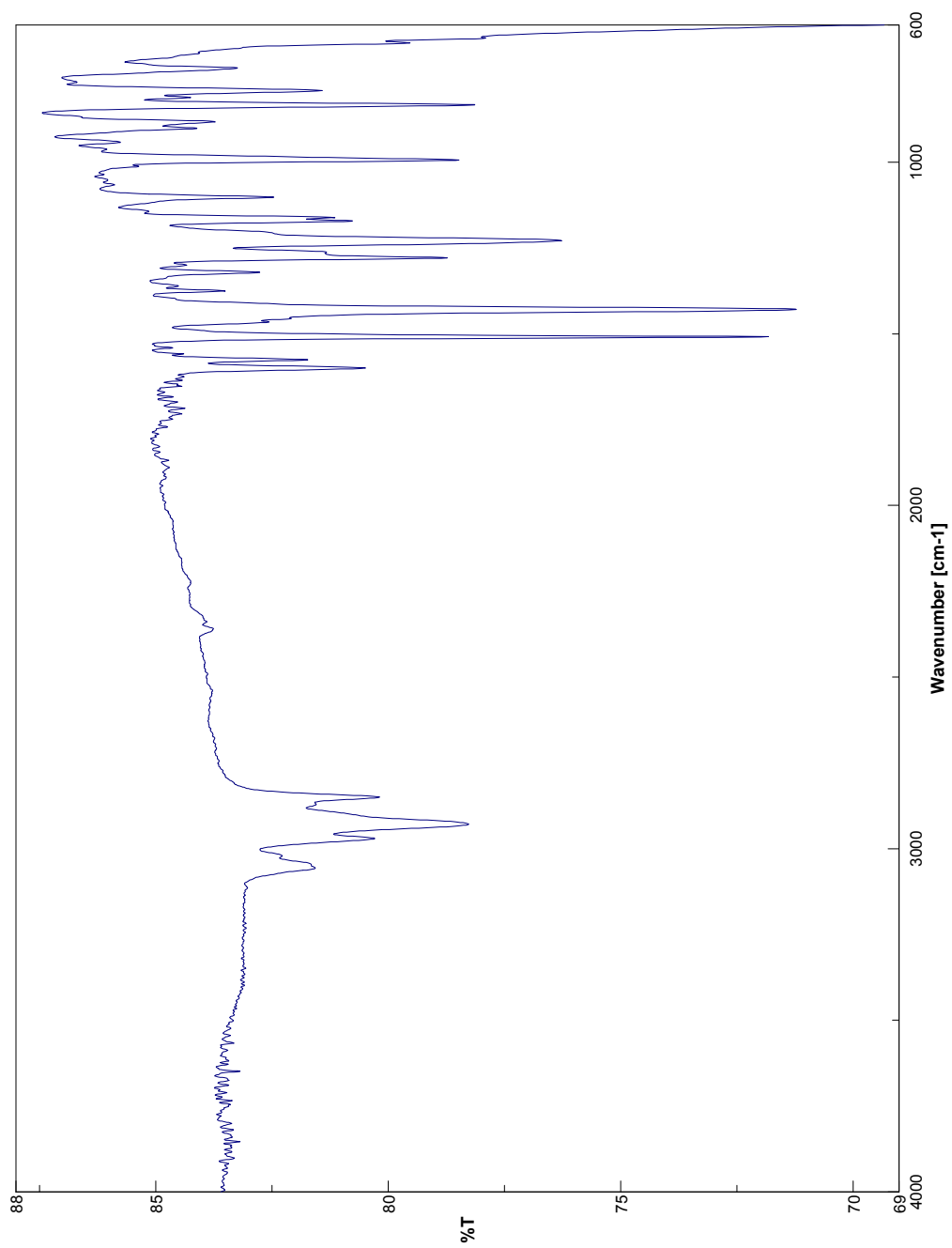
^1H NMR Spectrum of Compound 8



¹H NMR Spectrum of Compound 8

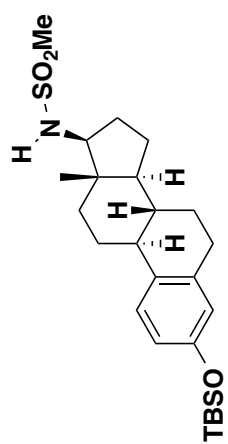


^{13}C NMR Spectrum of Compound 8

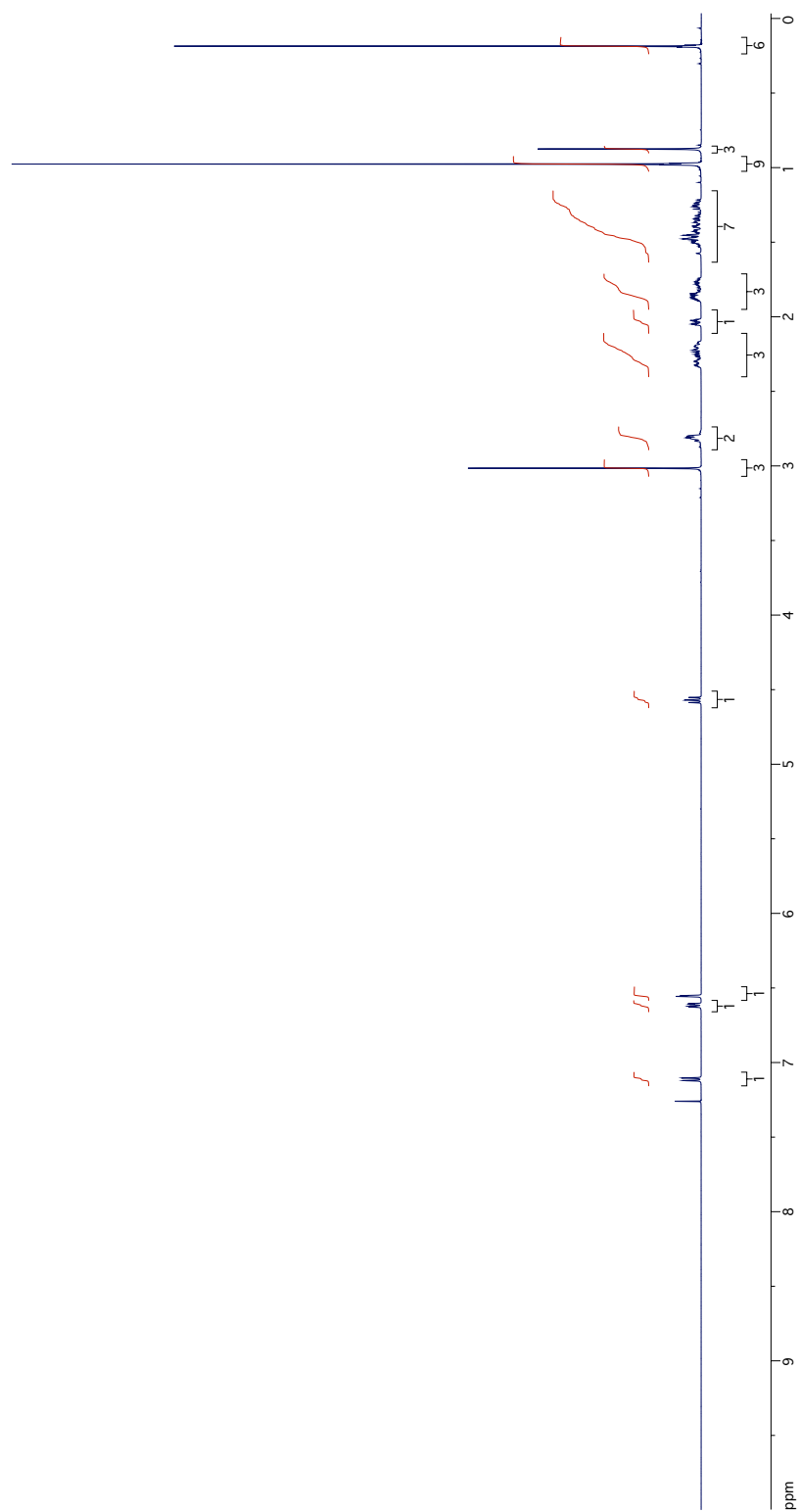


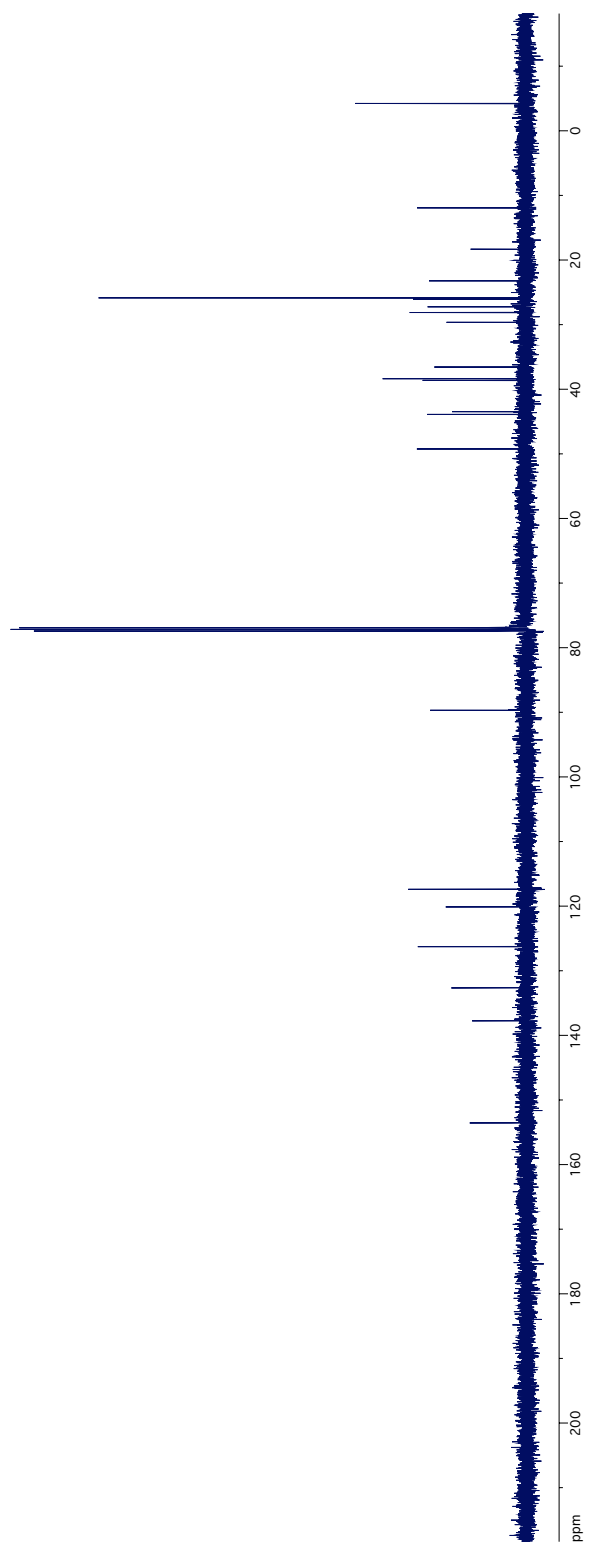
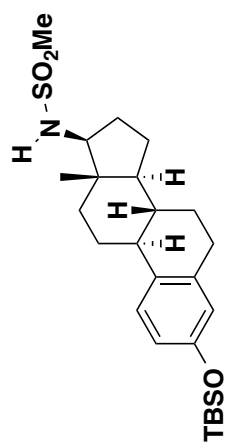
FTIR of Compound 8

Appendix A.2

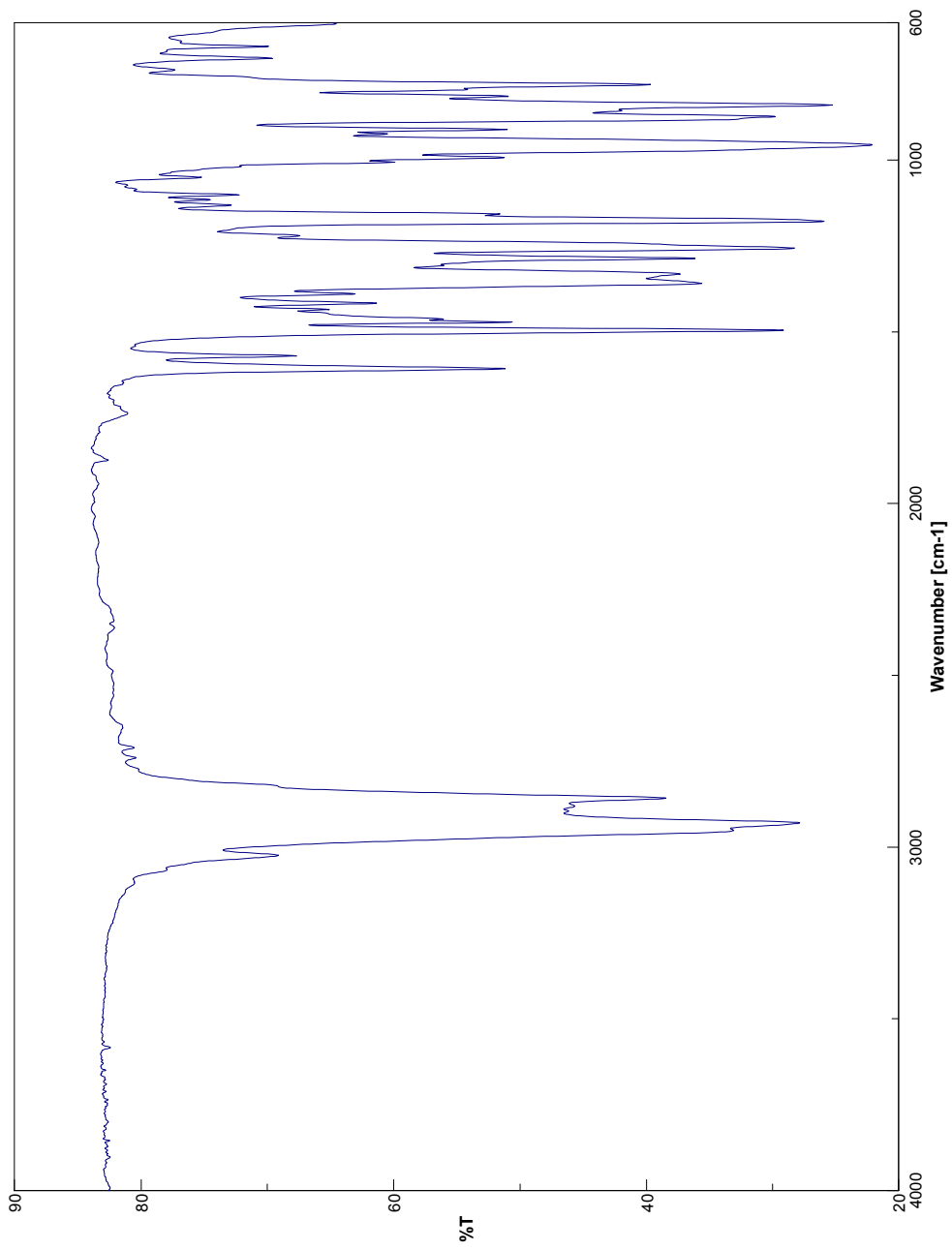


¹H NMR Spectrum of Compound 5

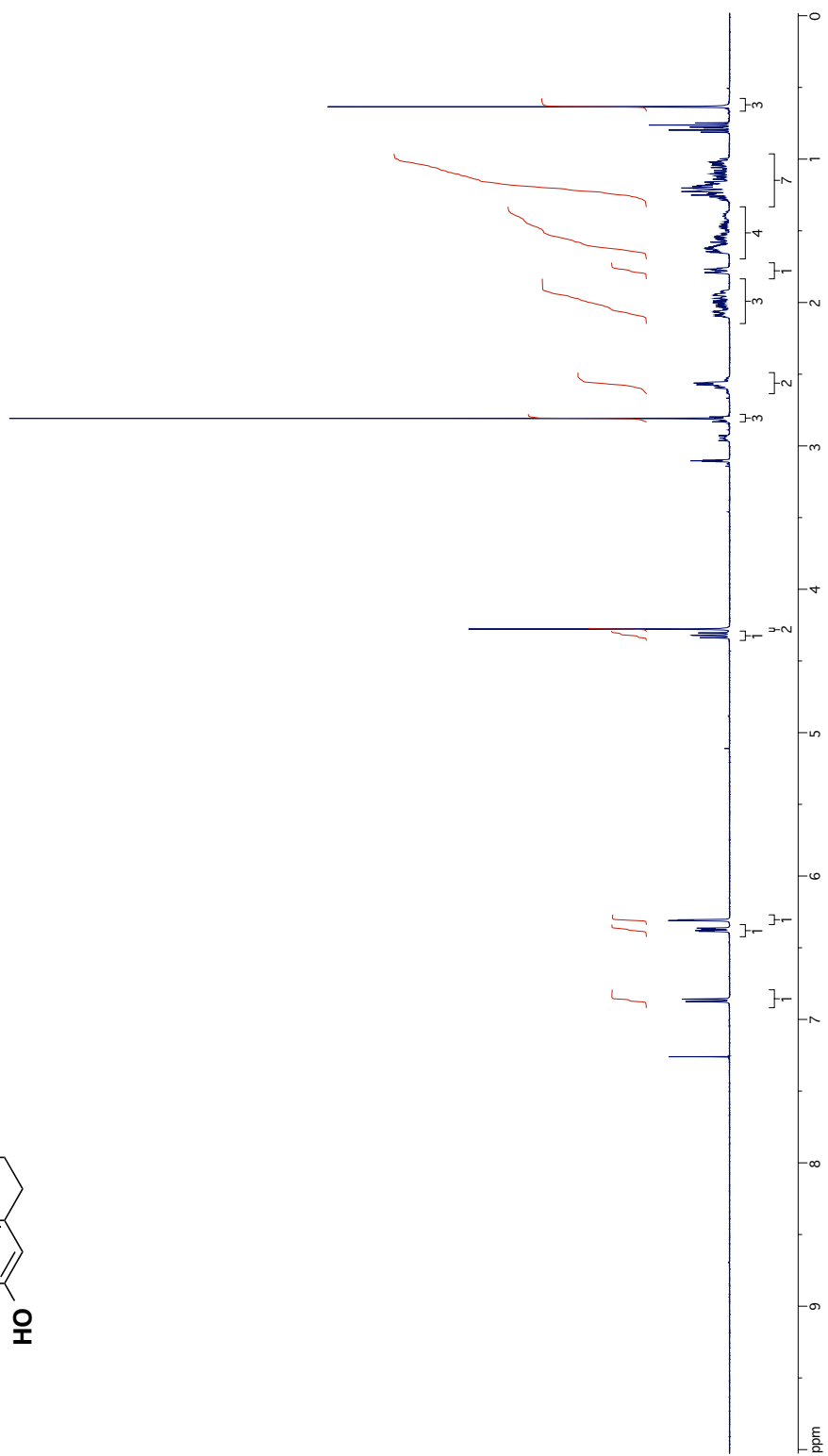
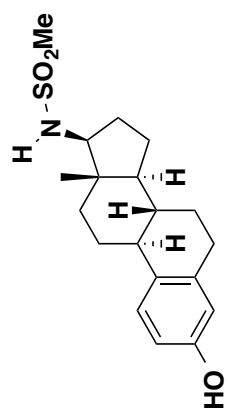




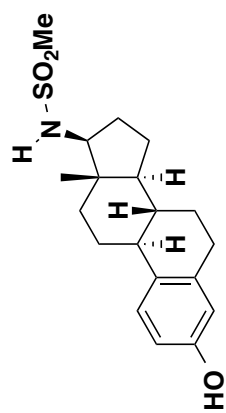
^{13}C NMR Spectrum of Compound 5



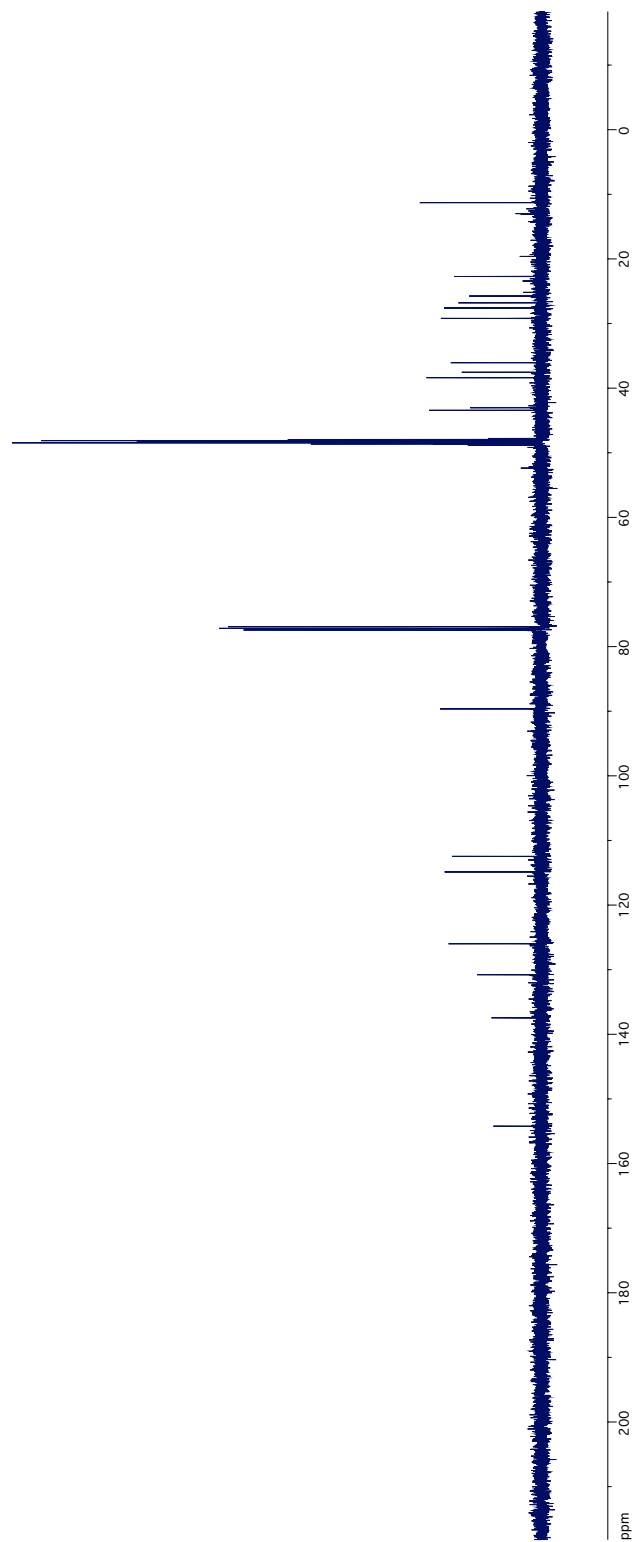
IR Spectrum of Compound **5**

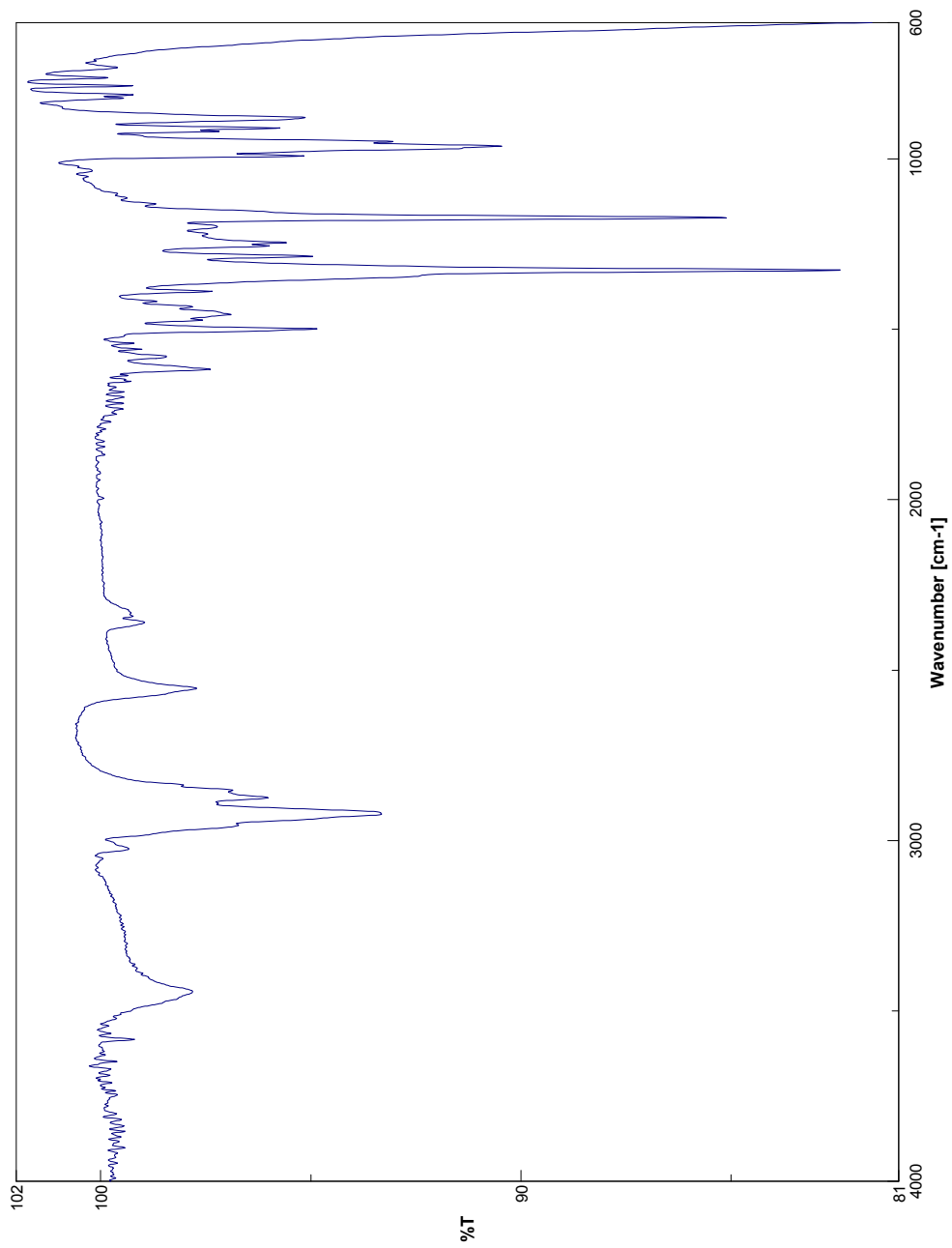


¹H NMR Spectrum of Compound 1

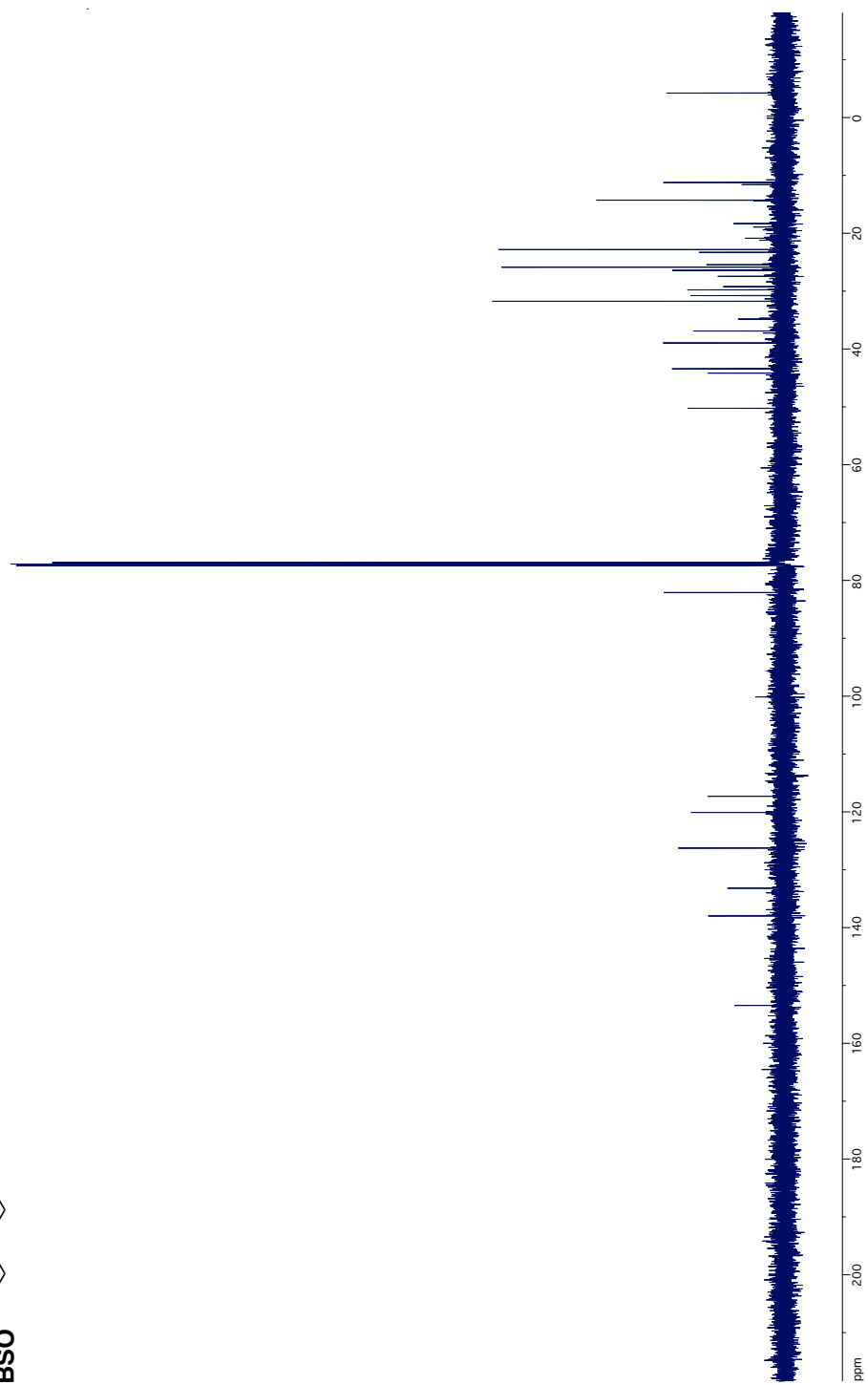
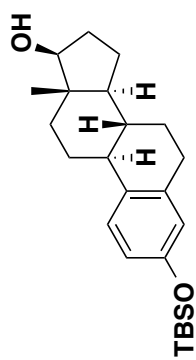


^{13}C NMR Spectrum of Compound 1

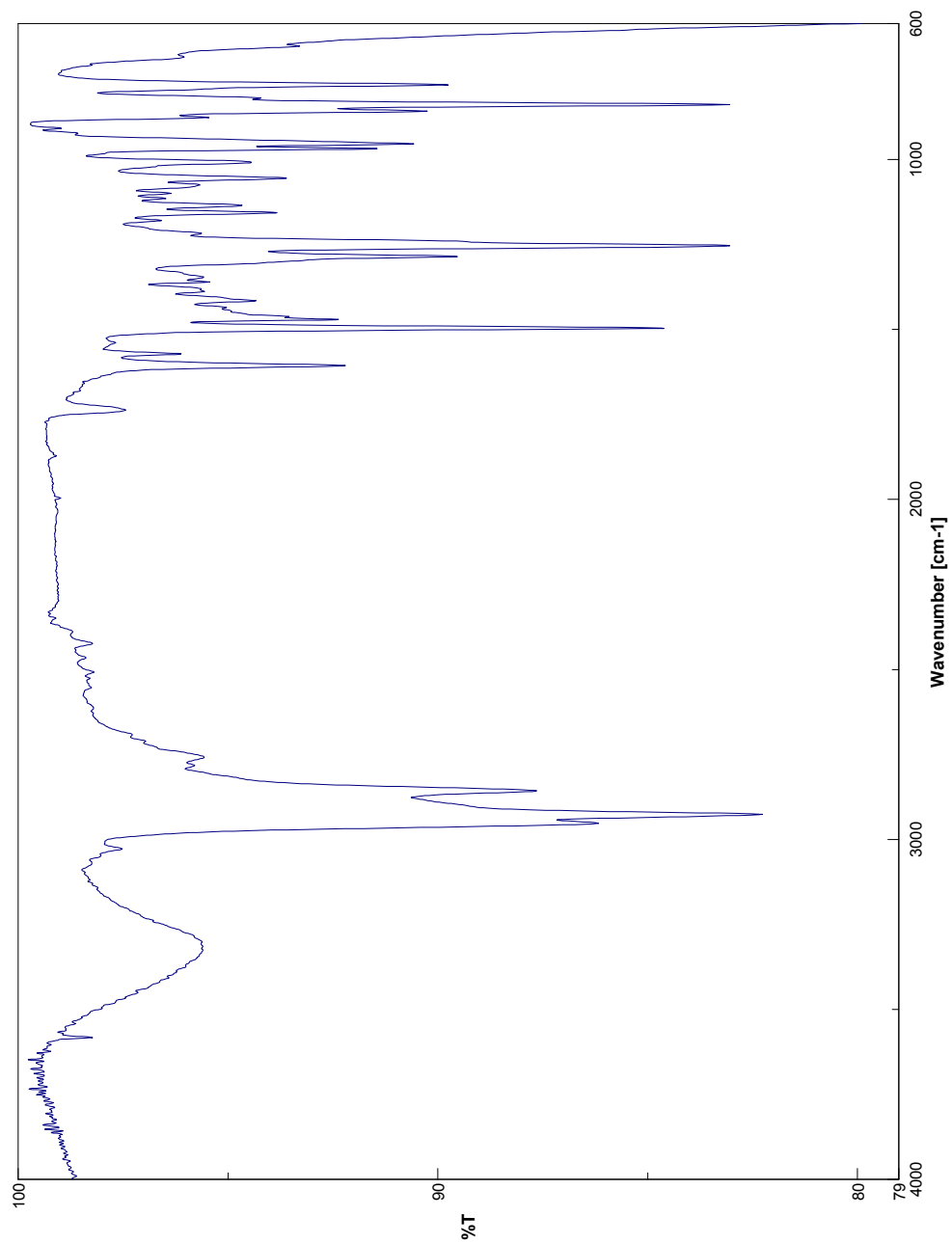




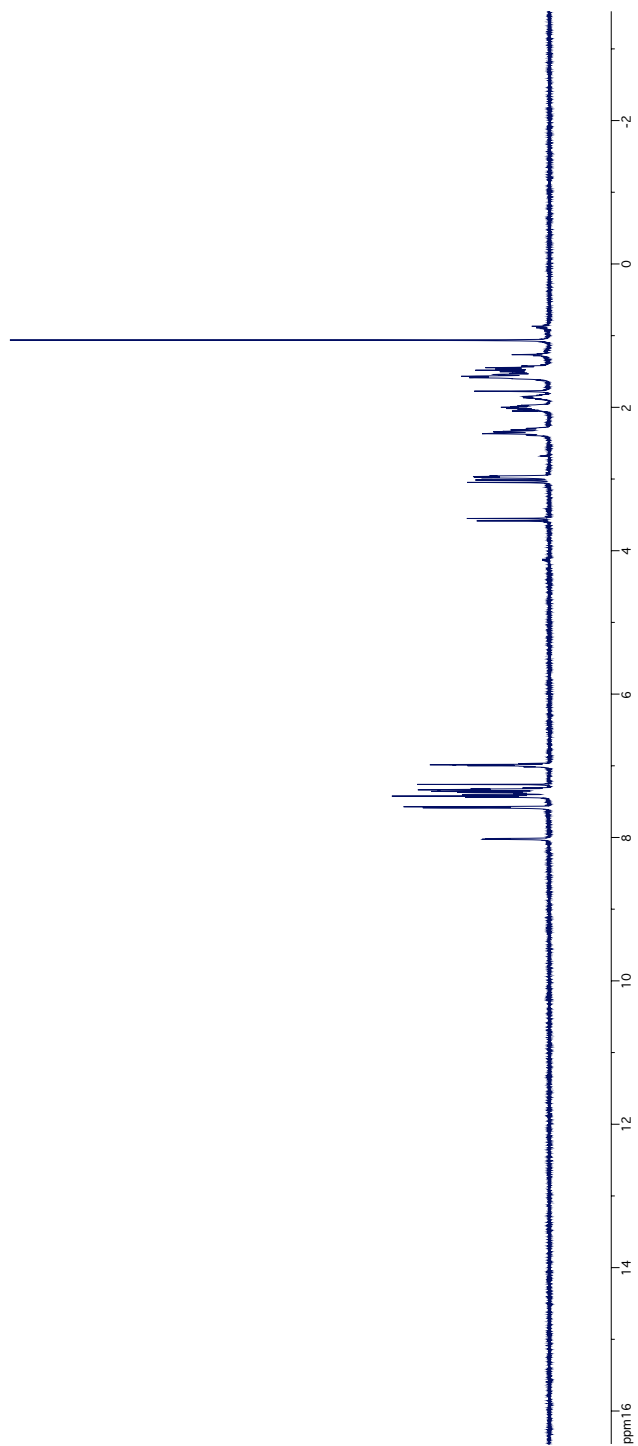
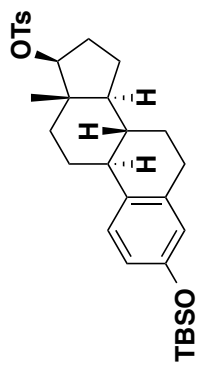
IR Spectrum of Compound 1



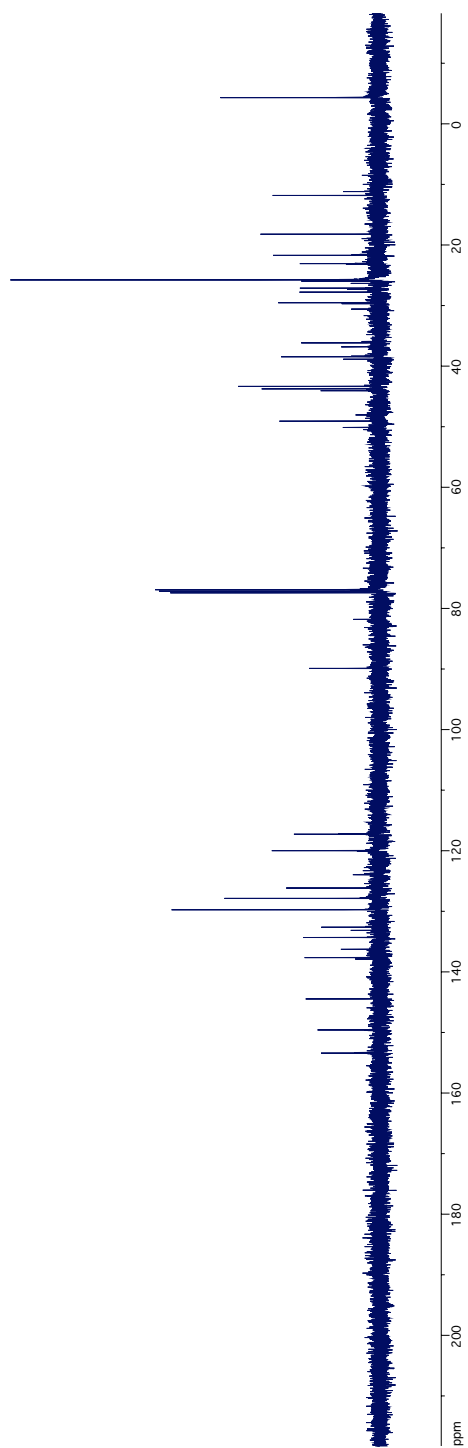
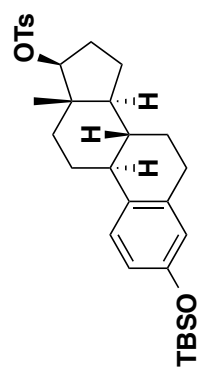
^{13}C NMR Spectrum of Compound 6



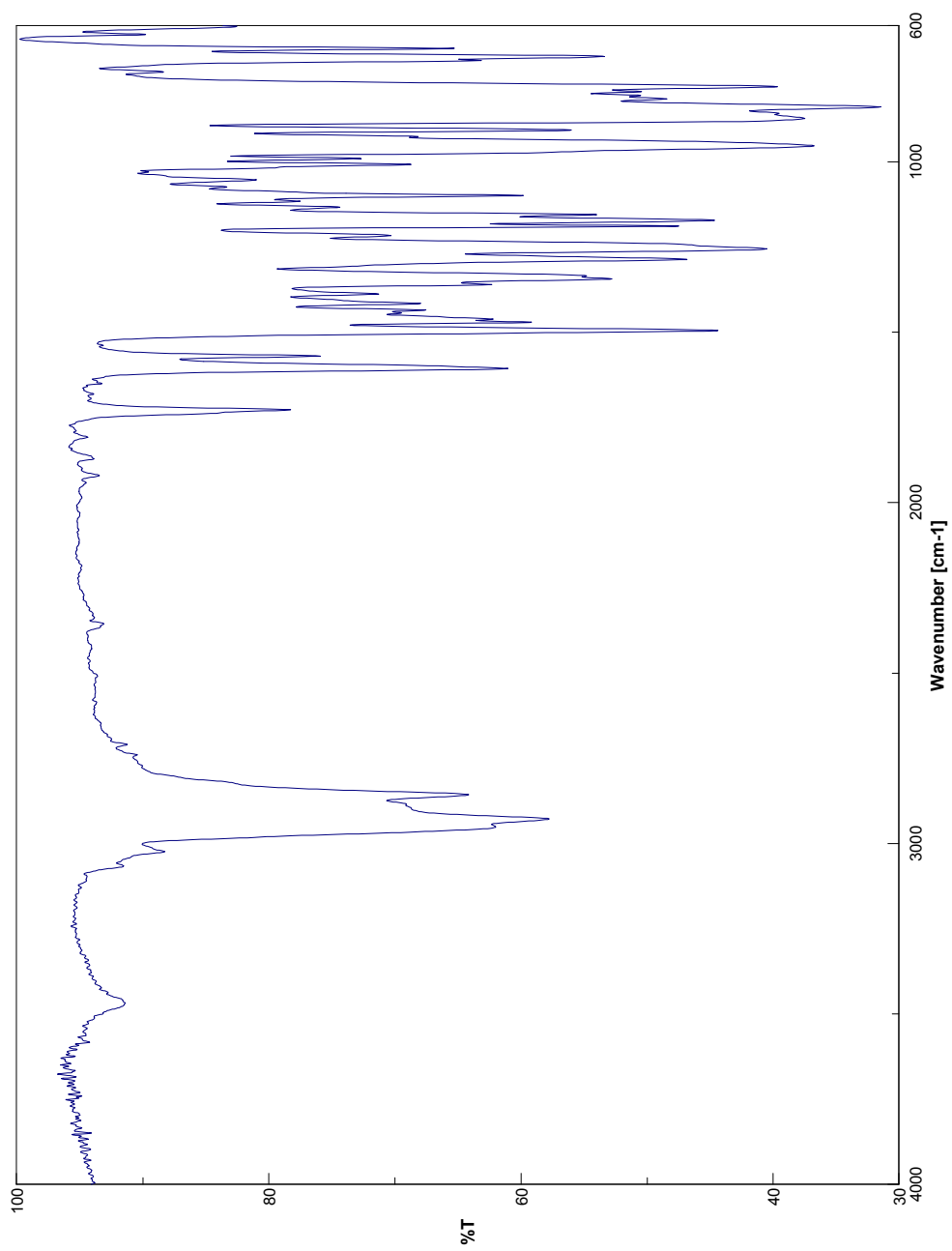
IR Spectrum of Compound **6**



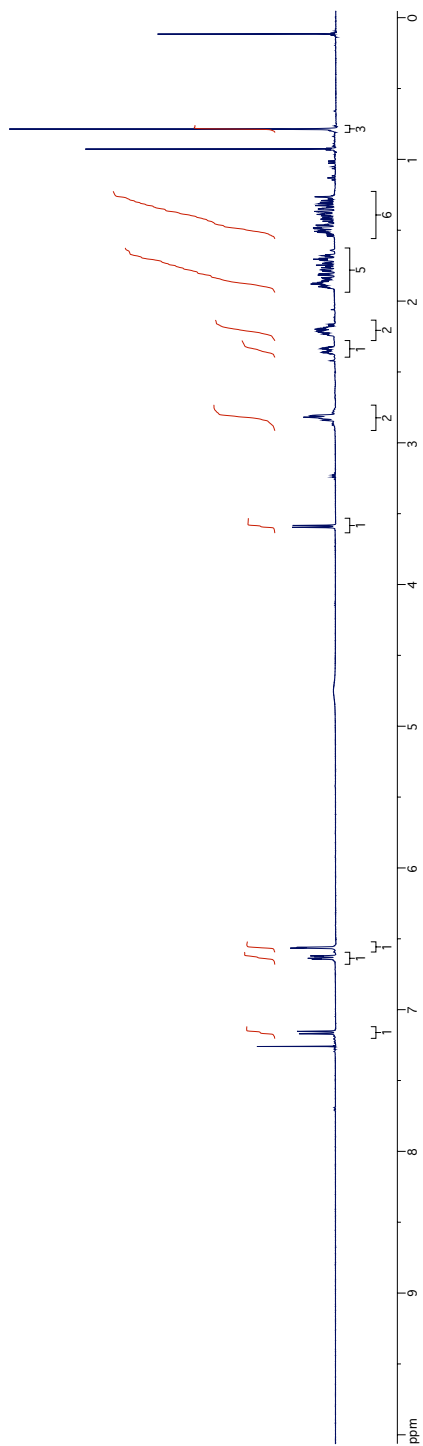
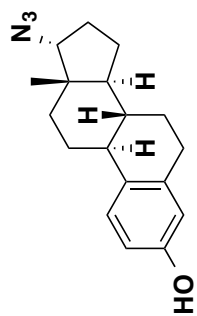
^1H NMR Spectrum of Compound 7



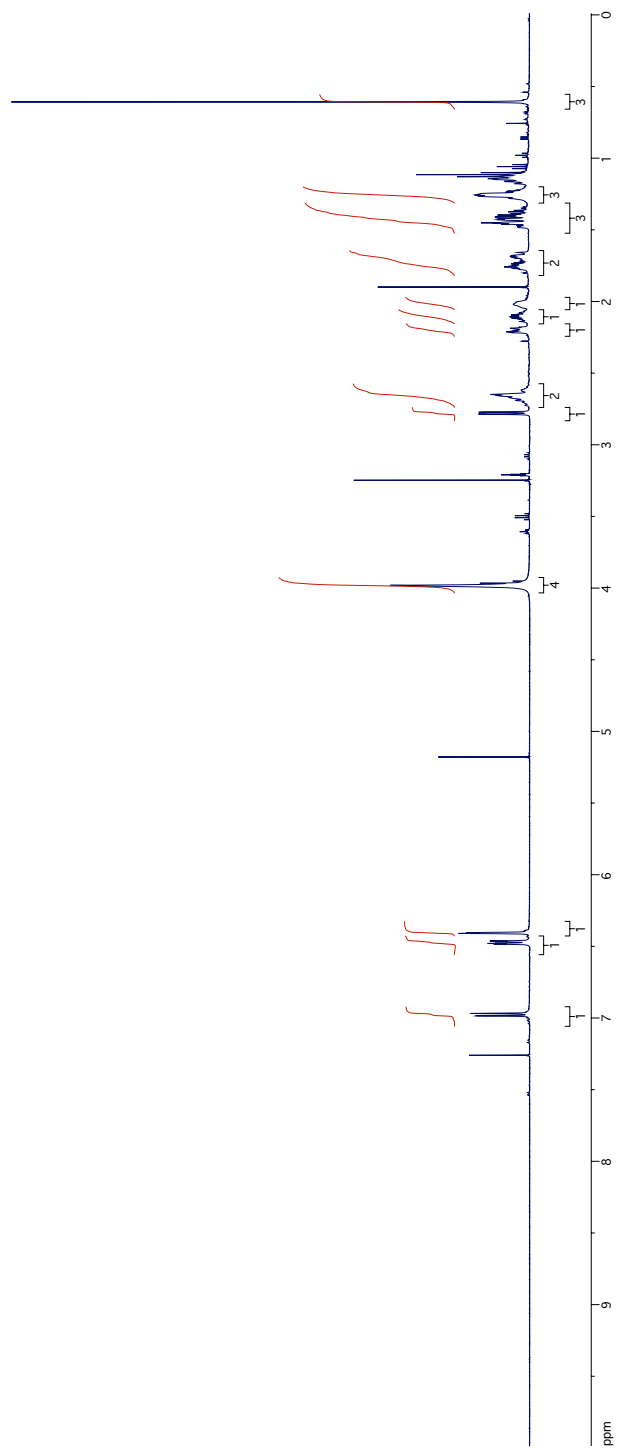
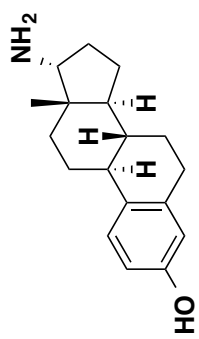
^{13}C NMR Spectrum of Compound 7



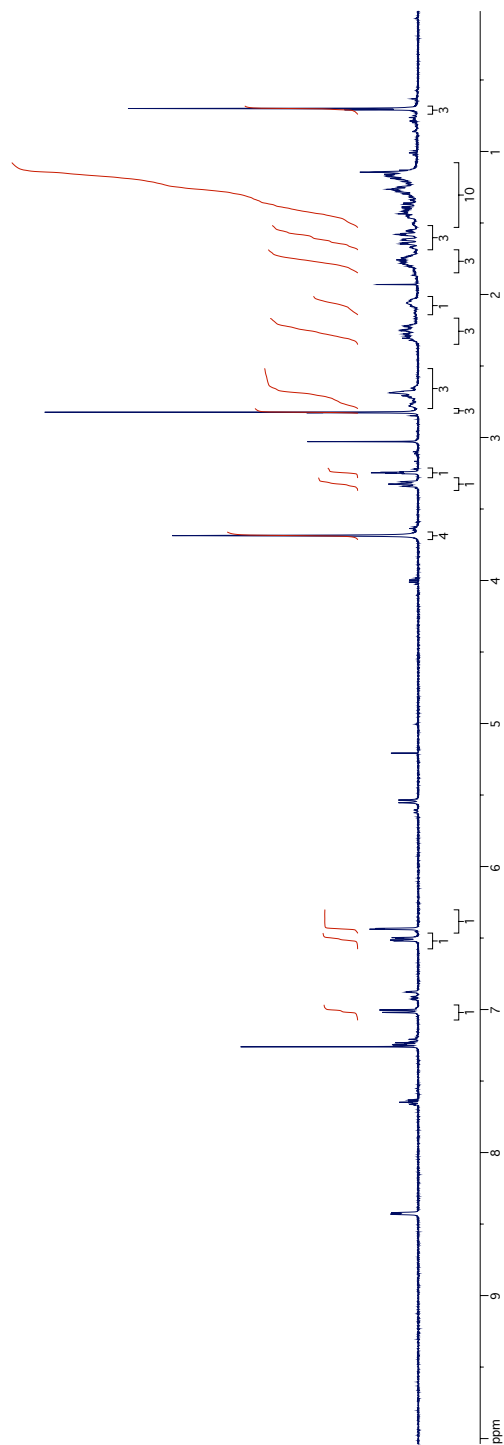
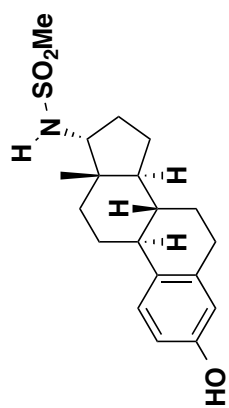
IR Spectrum of Compound 7



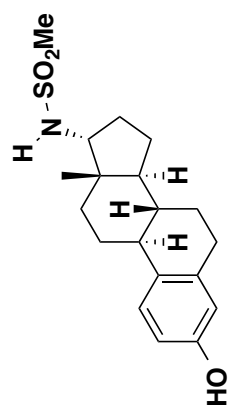
¹H NMR Spectrum of Compound 8



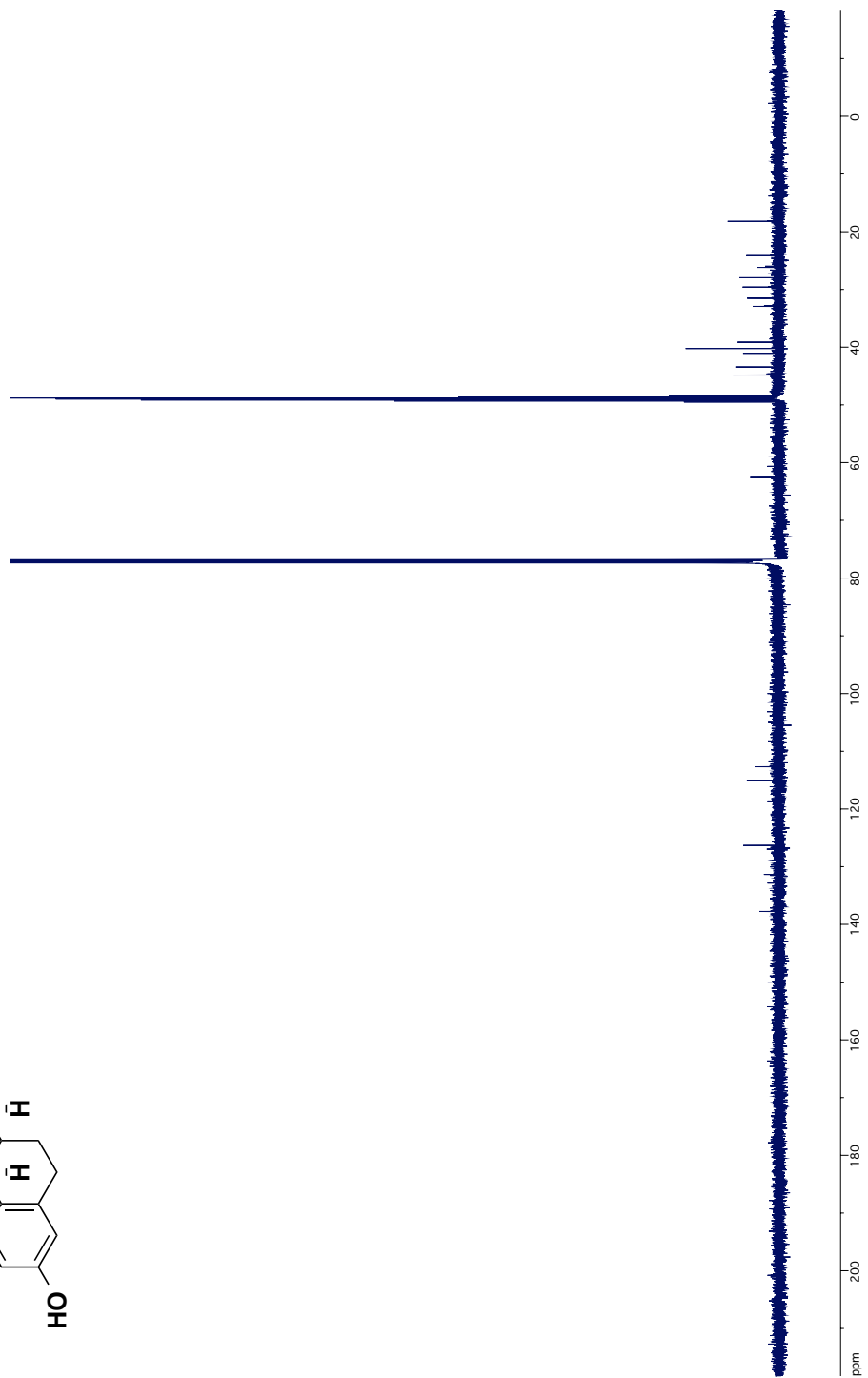
¹H NMR Spectrum of Compound 9

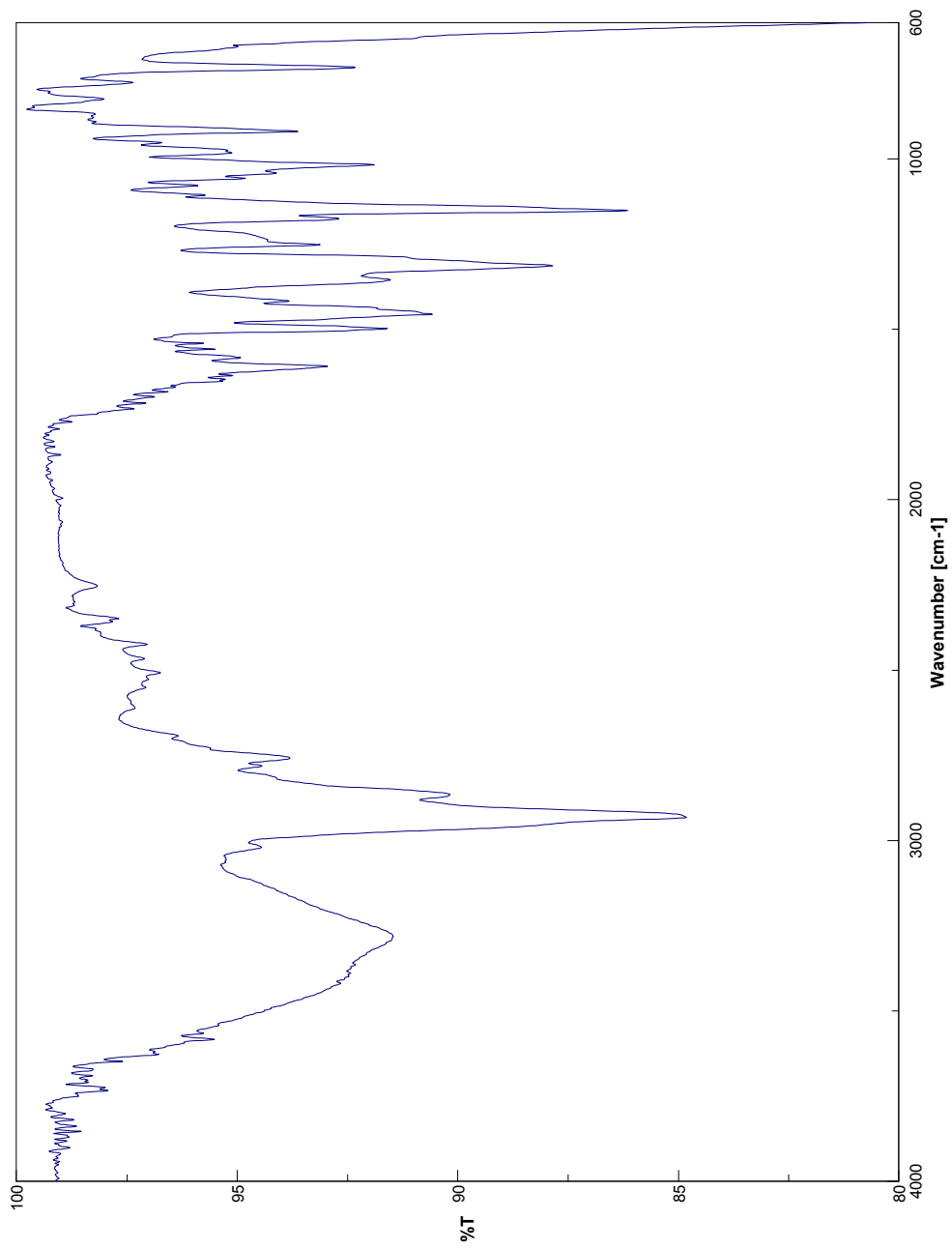


¹H NMR Spectrum of Compound 2

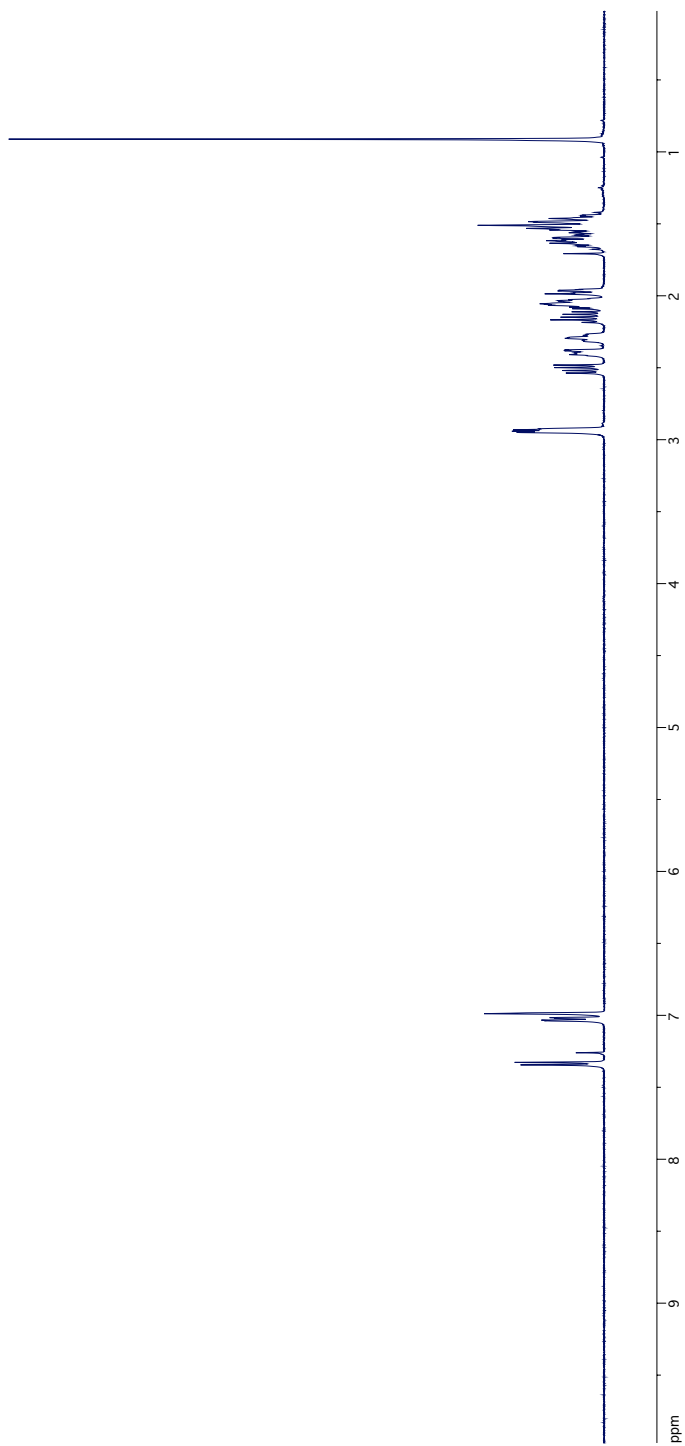
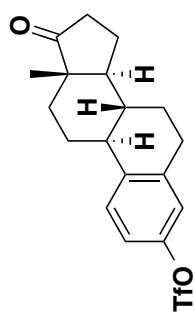


^{13}C NMR Spectrum of Compound 2

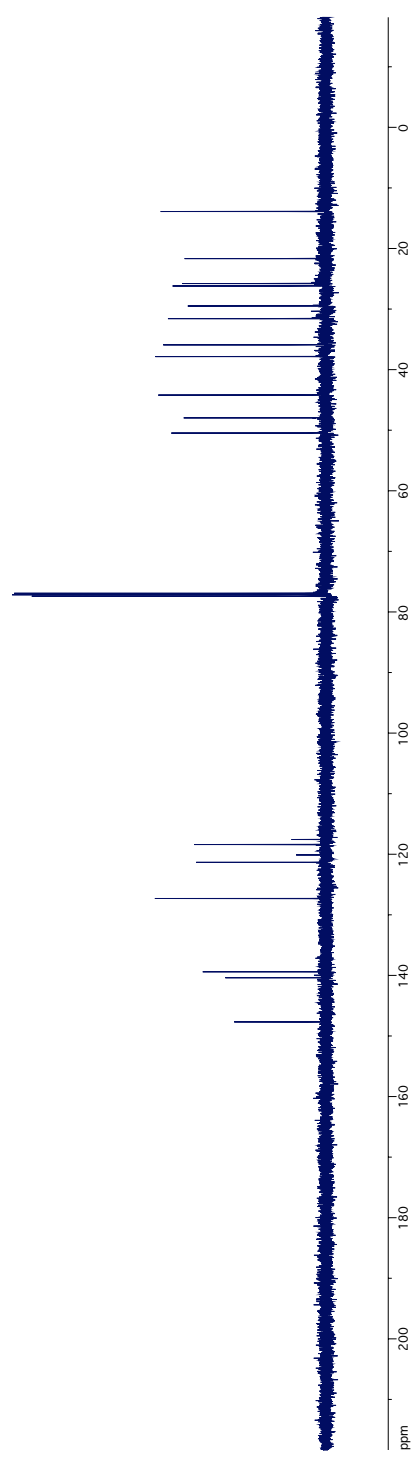
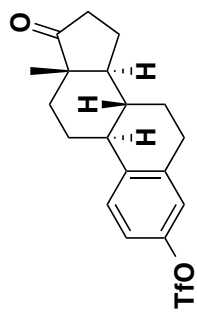




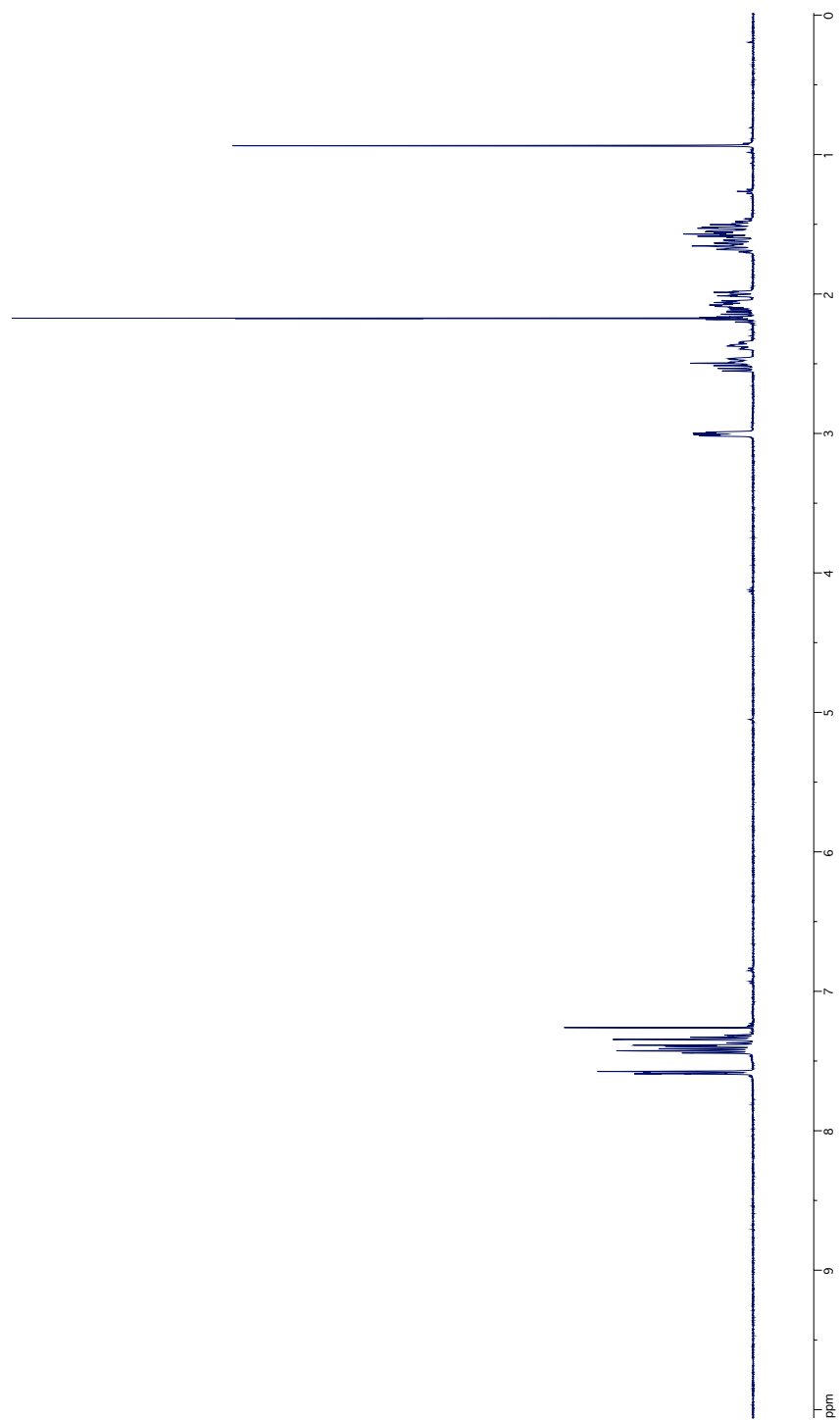
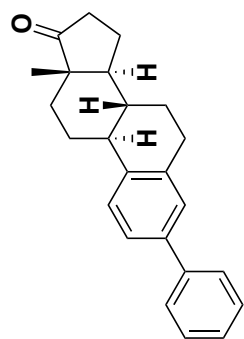
IR Spectrum of Compound 2



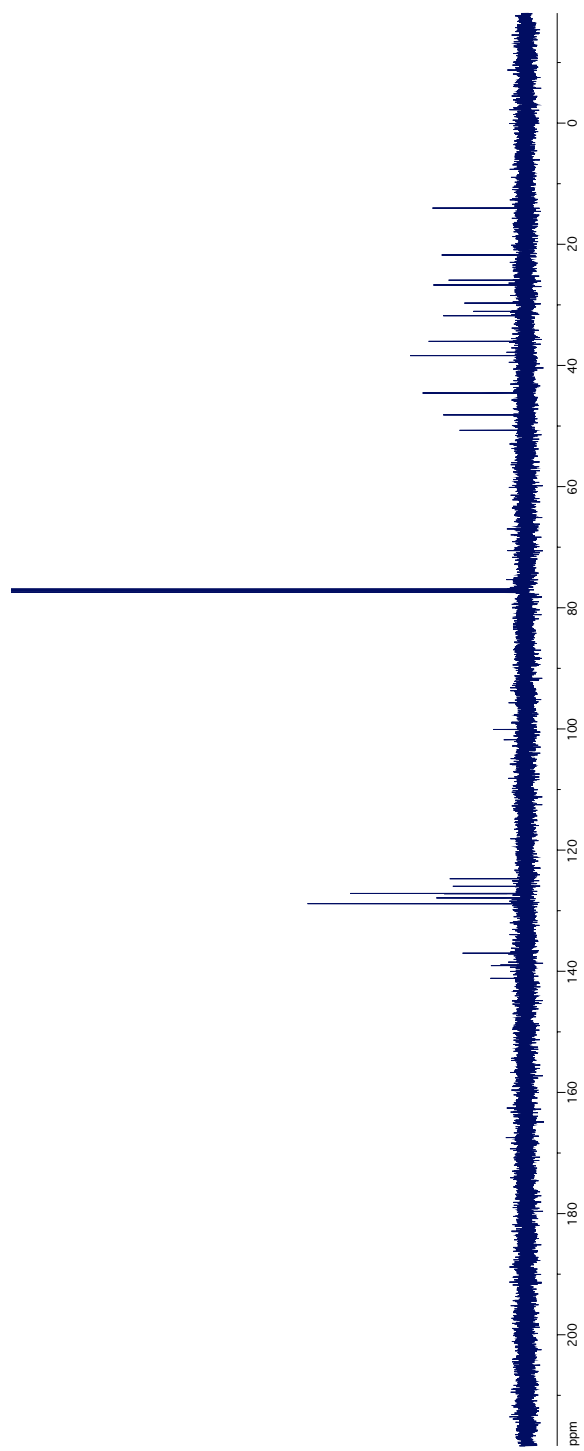
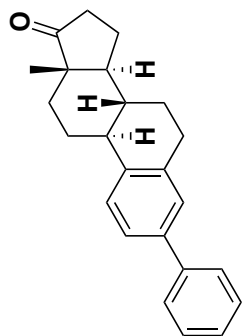
¹H NMR Spectrum of Compound 11



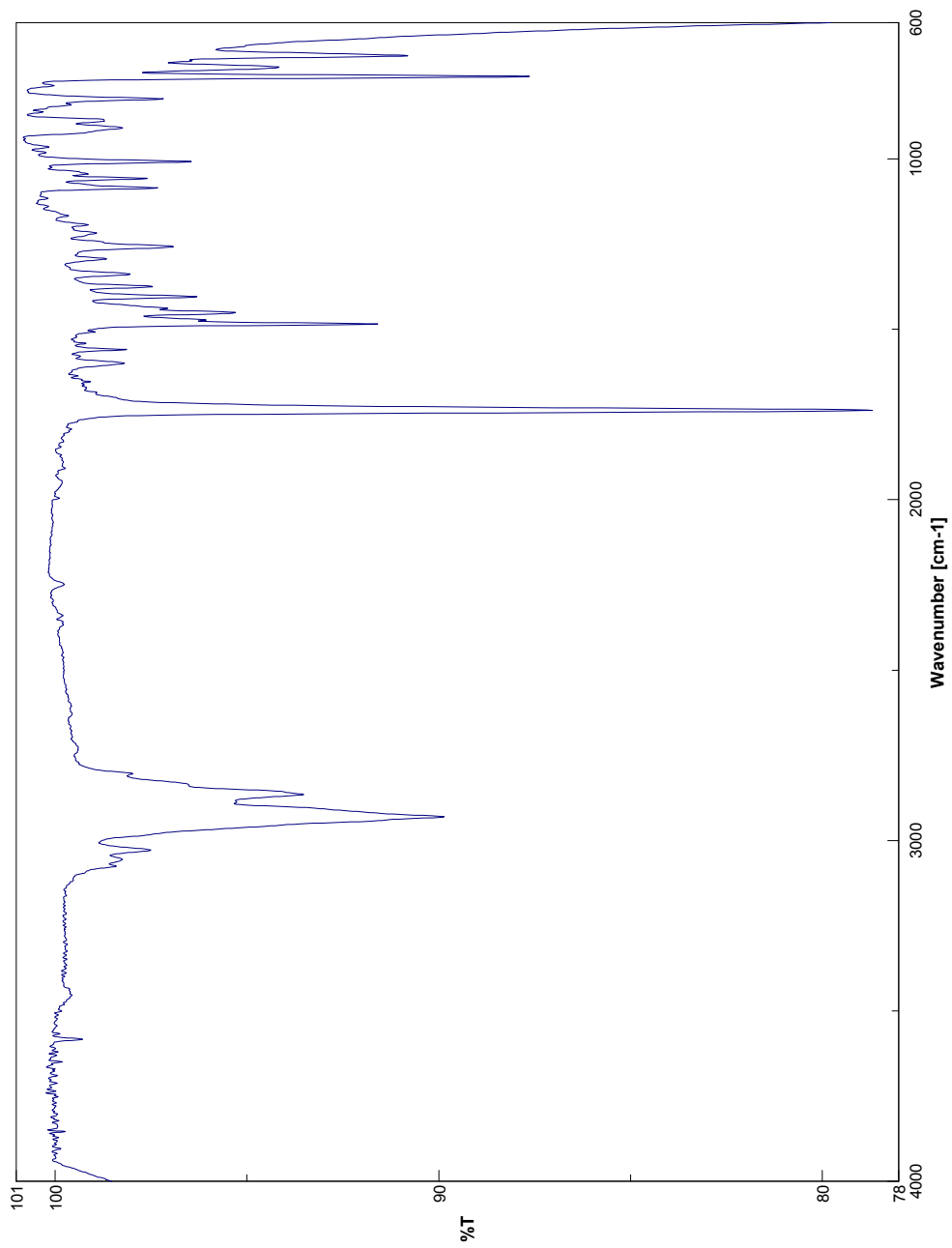
^{13}C NMR Spectrum of Compound 11



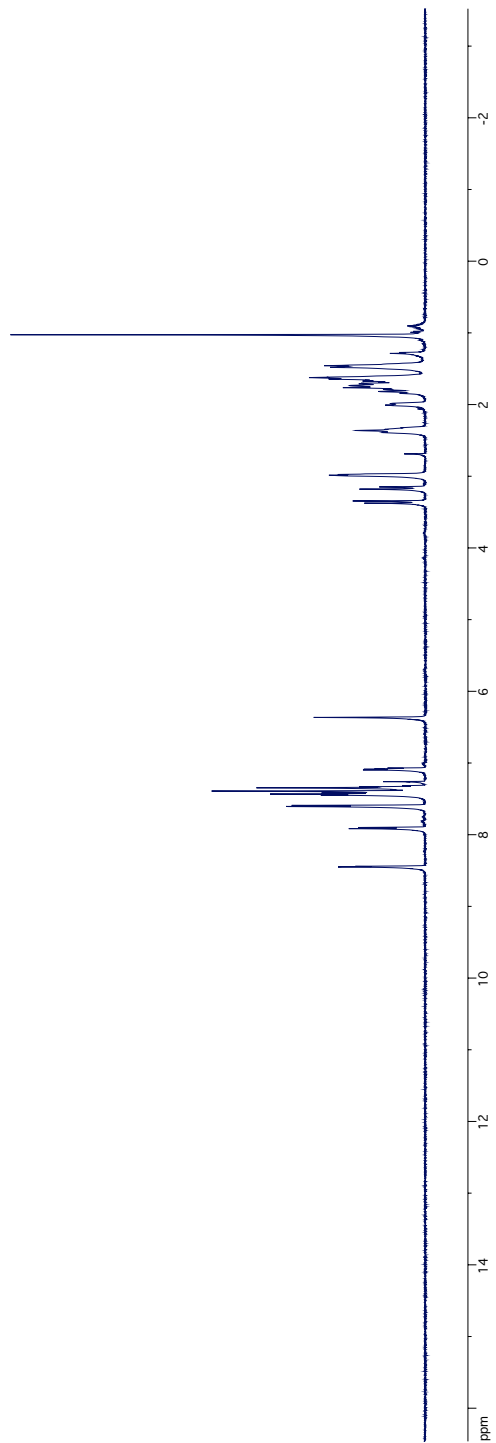
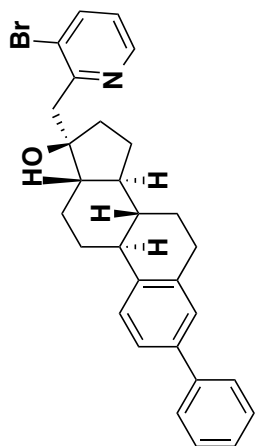
¹H NMR Spectrum of Compound 12



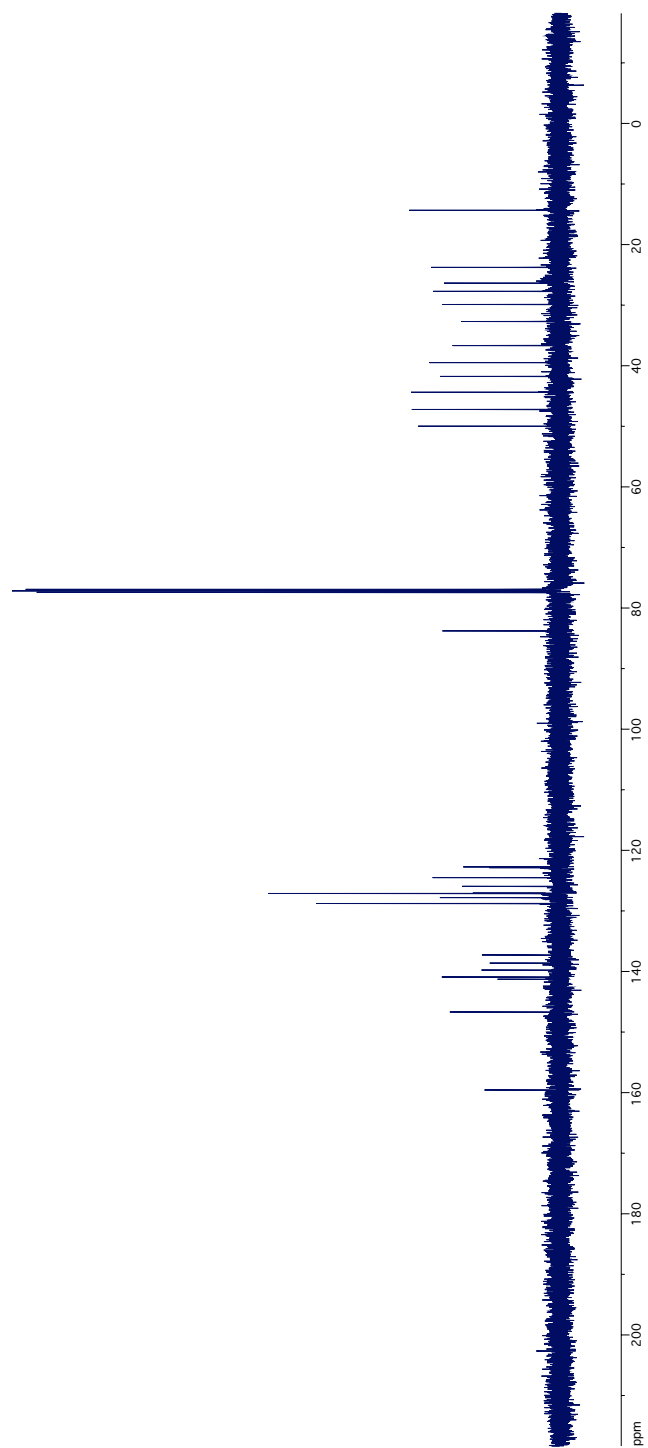
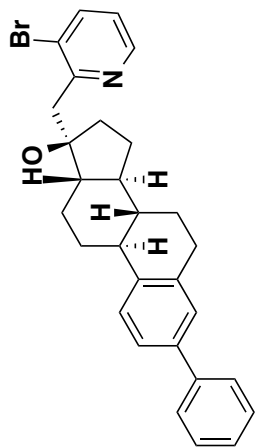
^{13}C NMR Spectrum of Compound 12



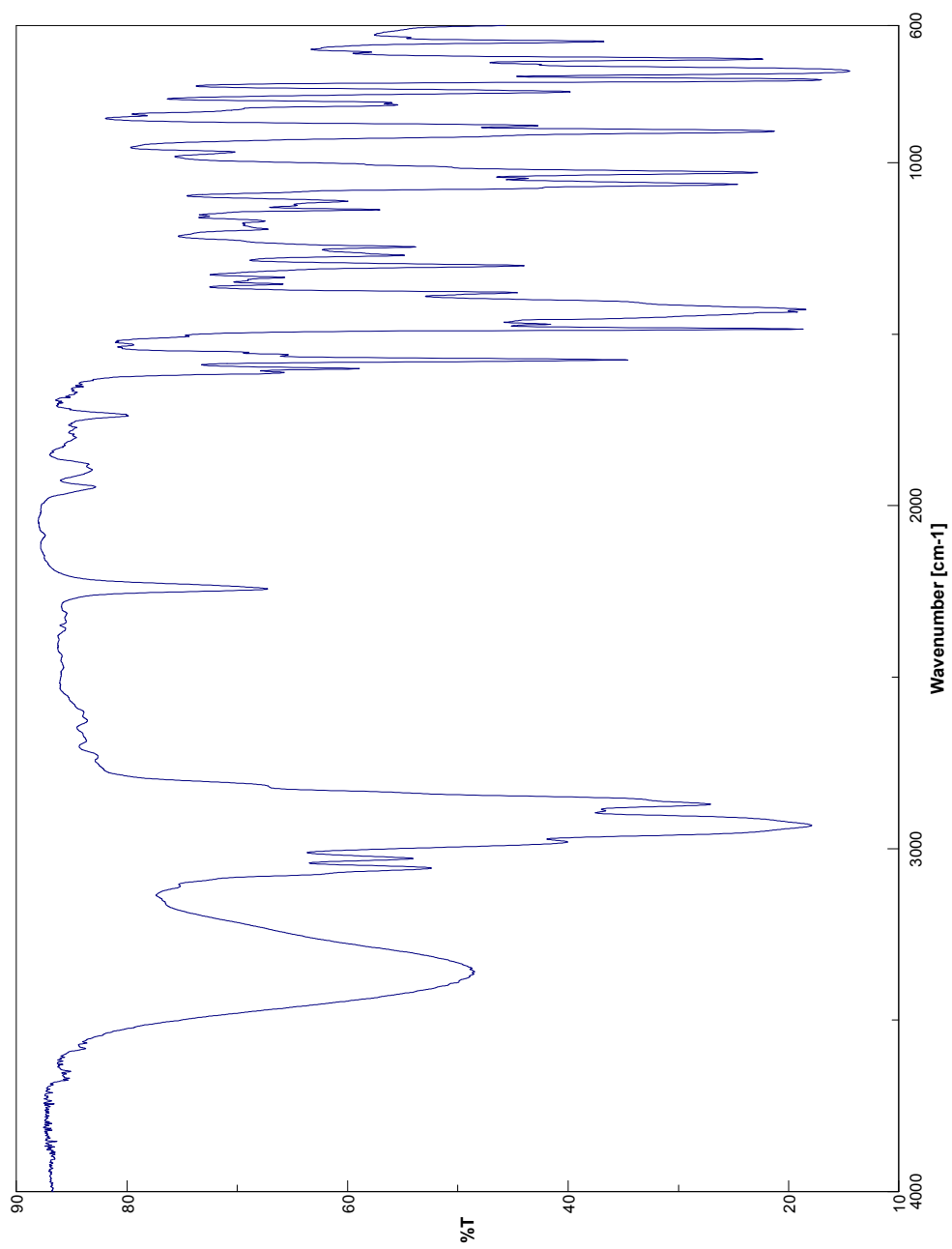
IR Spectrum of Compound **12**



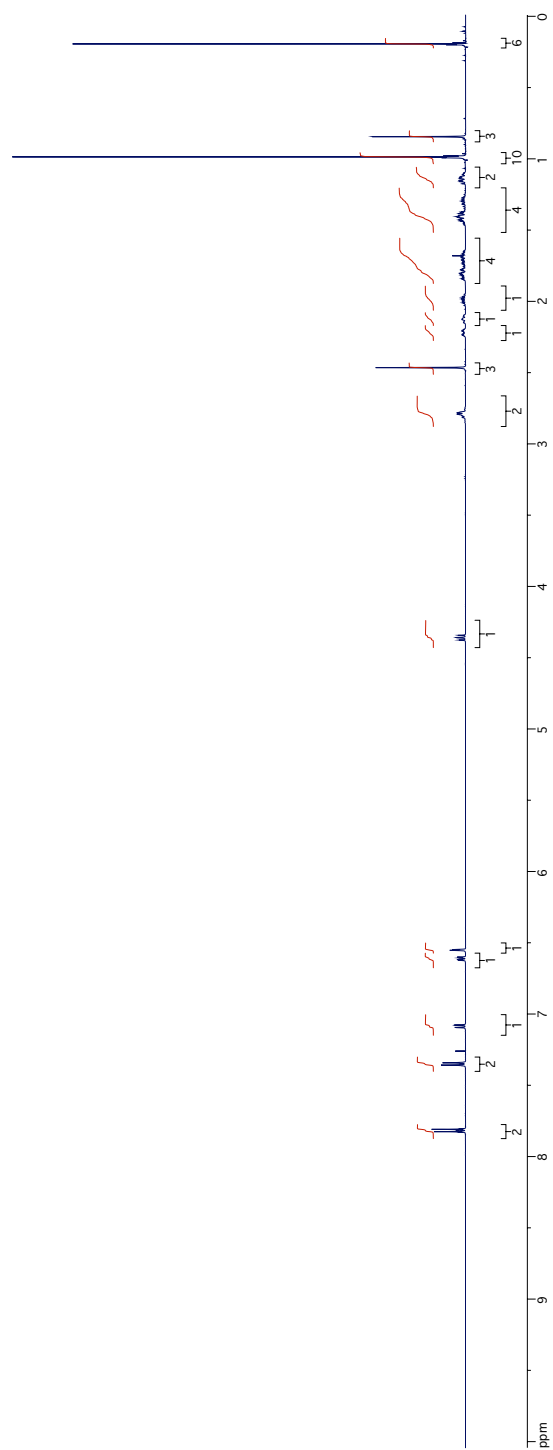
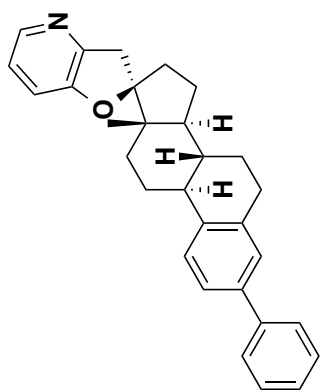
¹H Spectrum of Compound 13



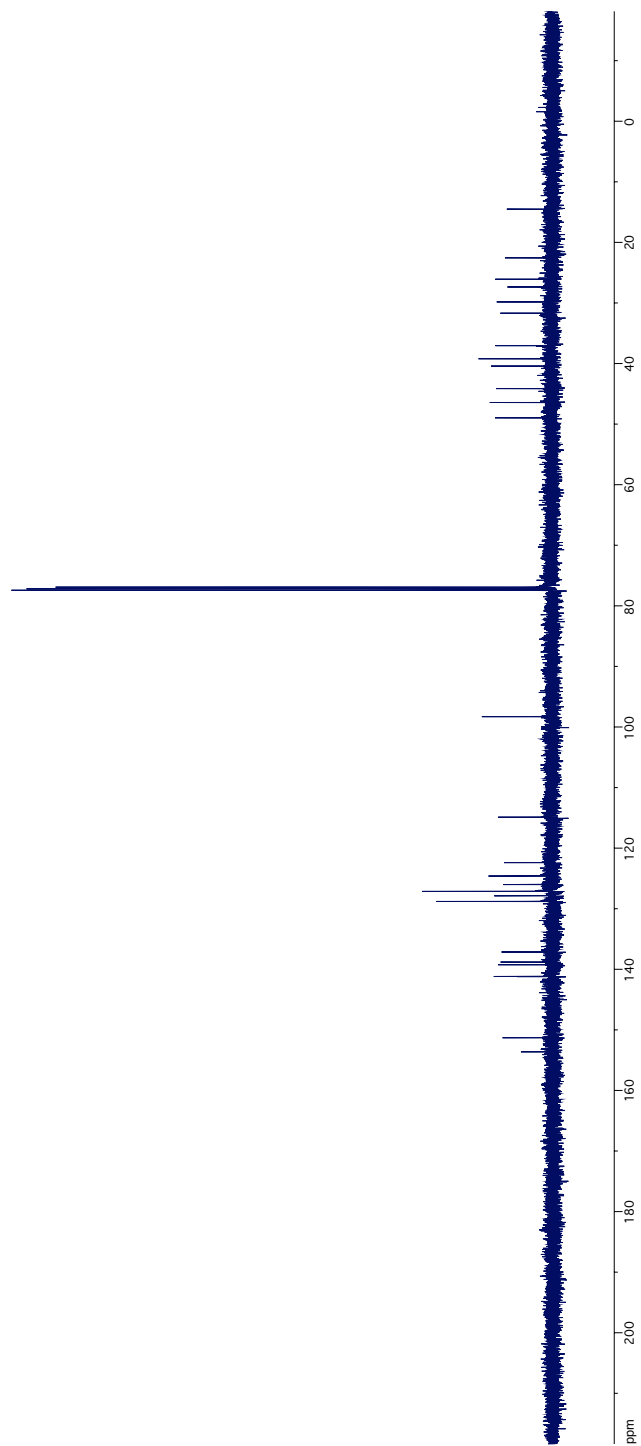
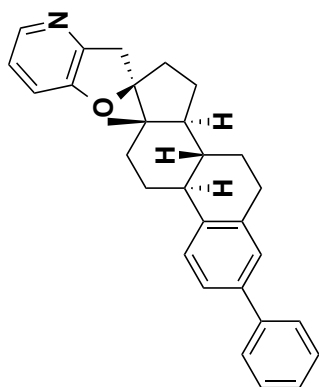
^{13}C NMR Spectrum of Compound 13



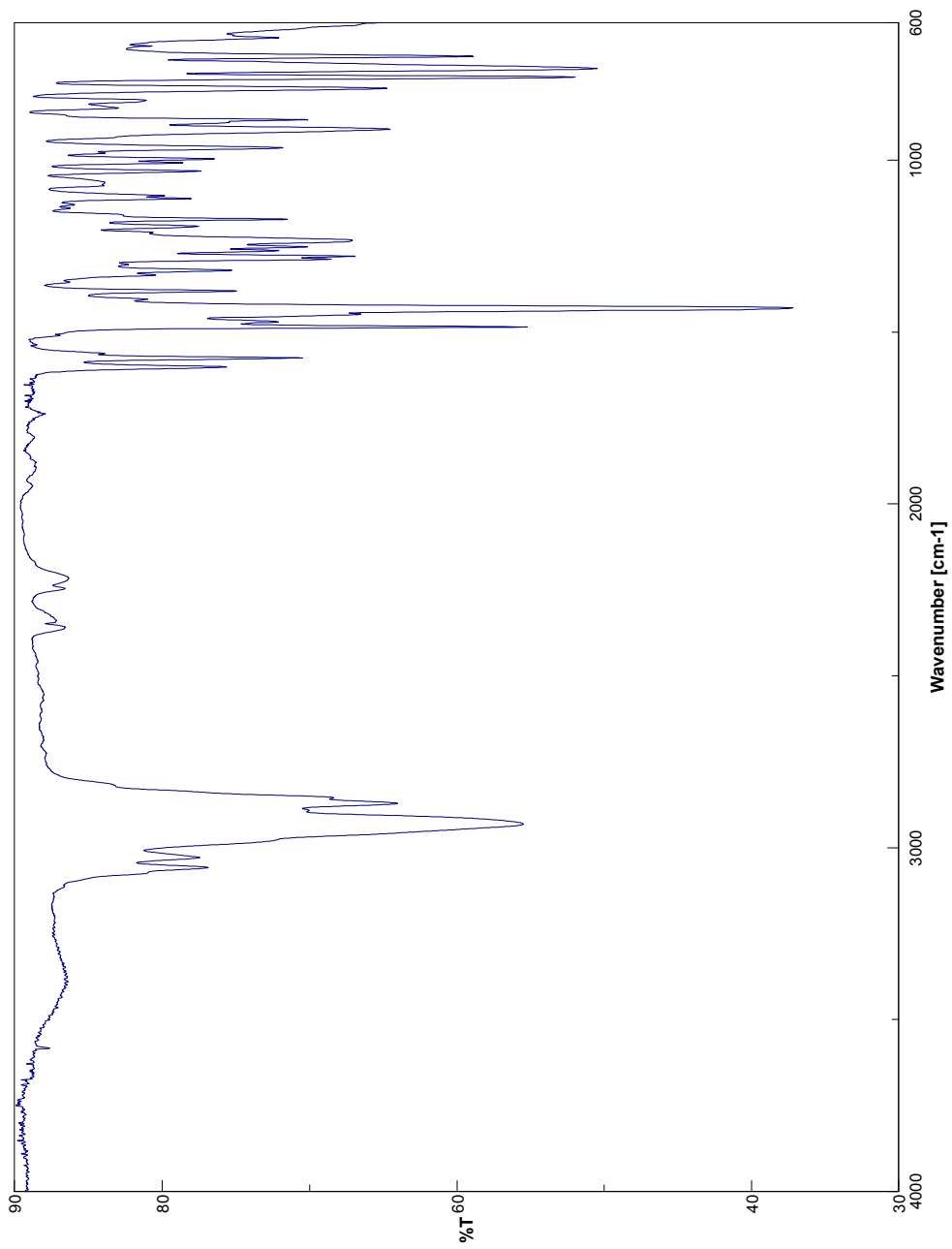
IR Spectrum of Compound **13**



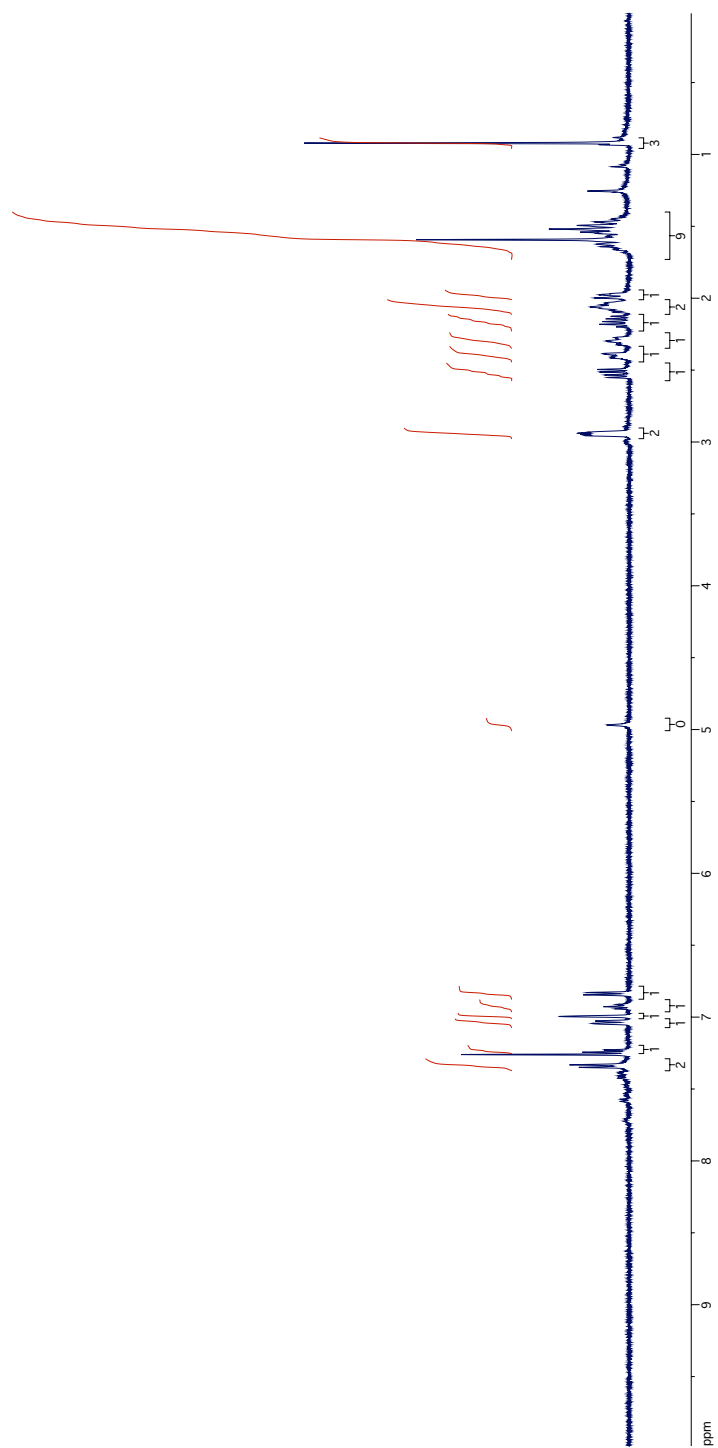
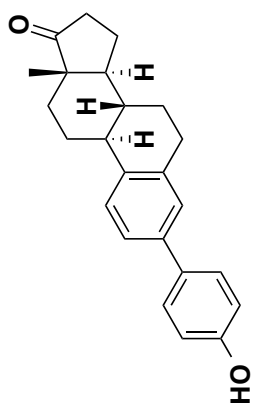
¹H NMR Spectrum of Compound 14



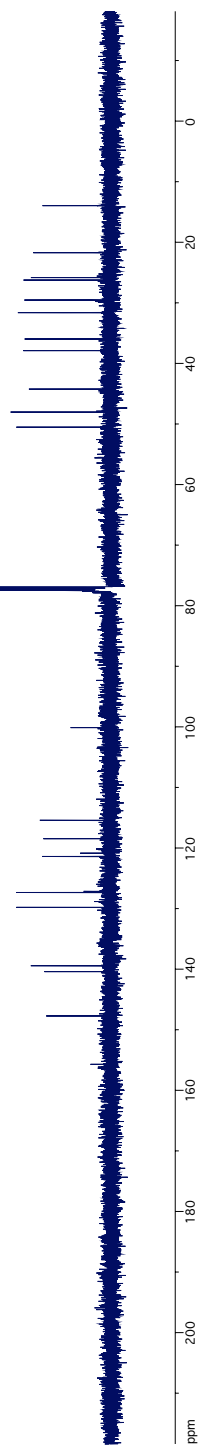
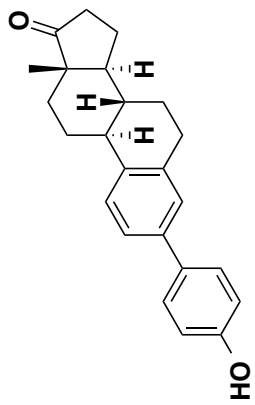
^{13}C NMR Spectrum of Compound 14



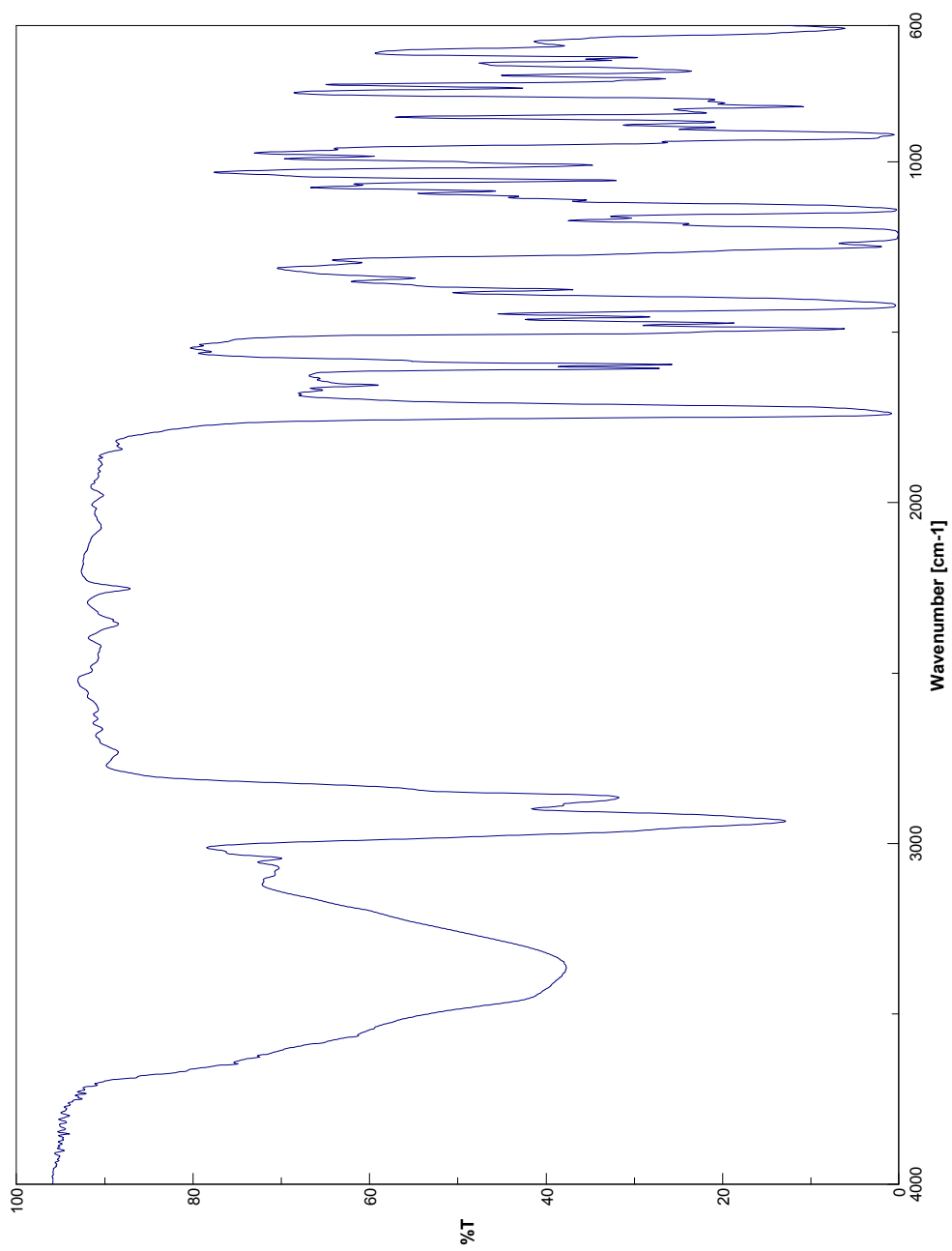
IR Spectrum of Compound **14**



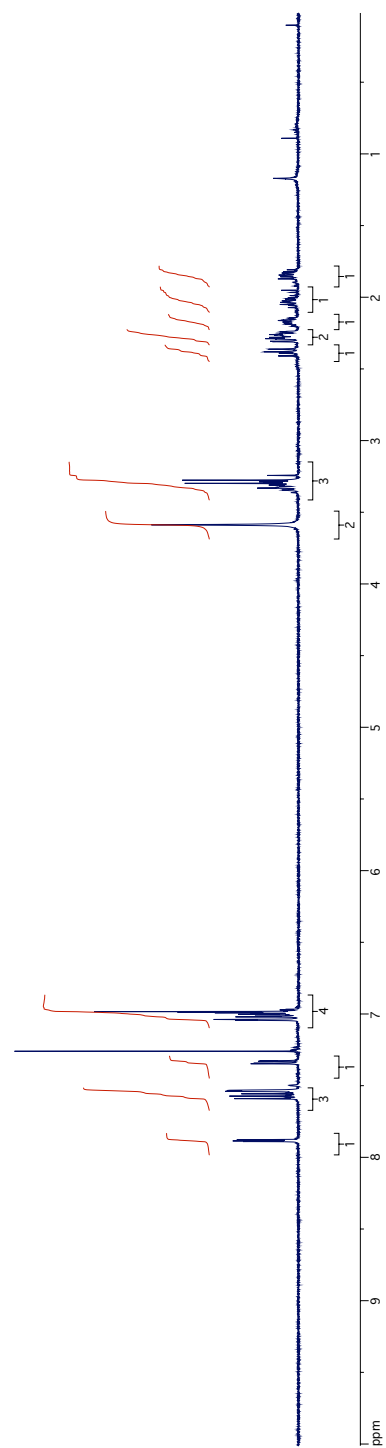
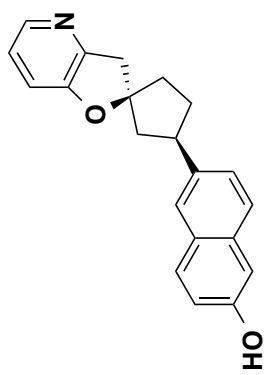
¹H NMR Spectrum of Compound 15



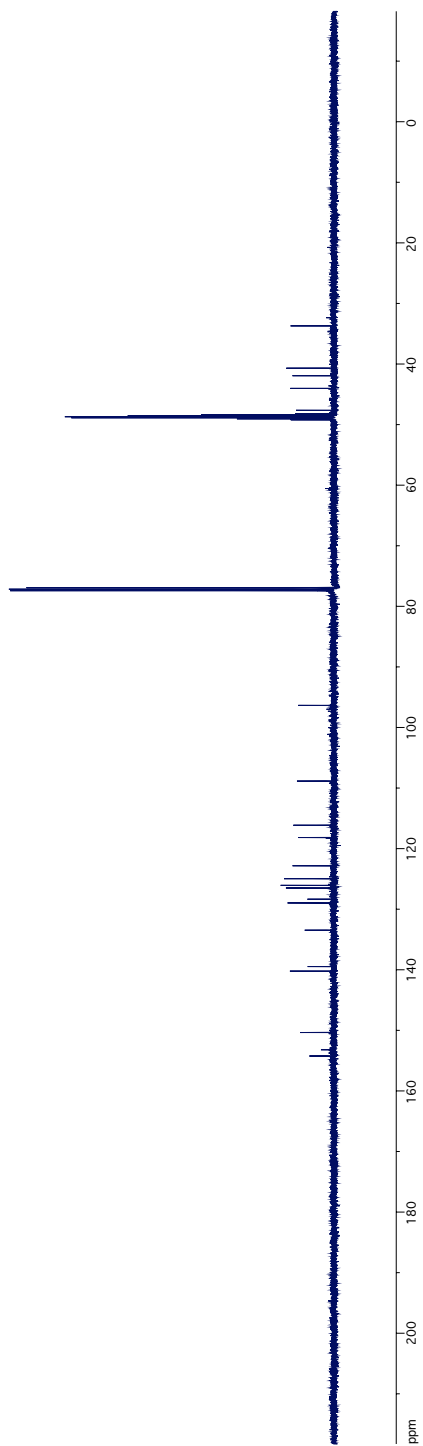
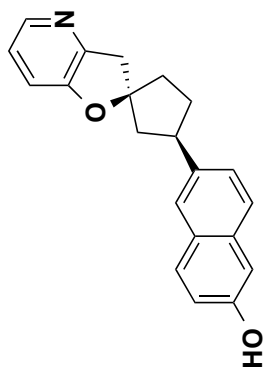
¹³C NMR Spectrum of Compound 15



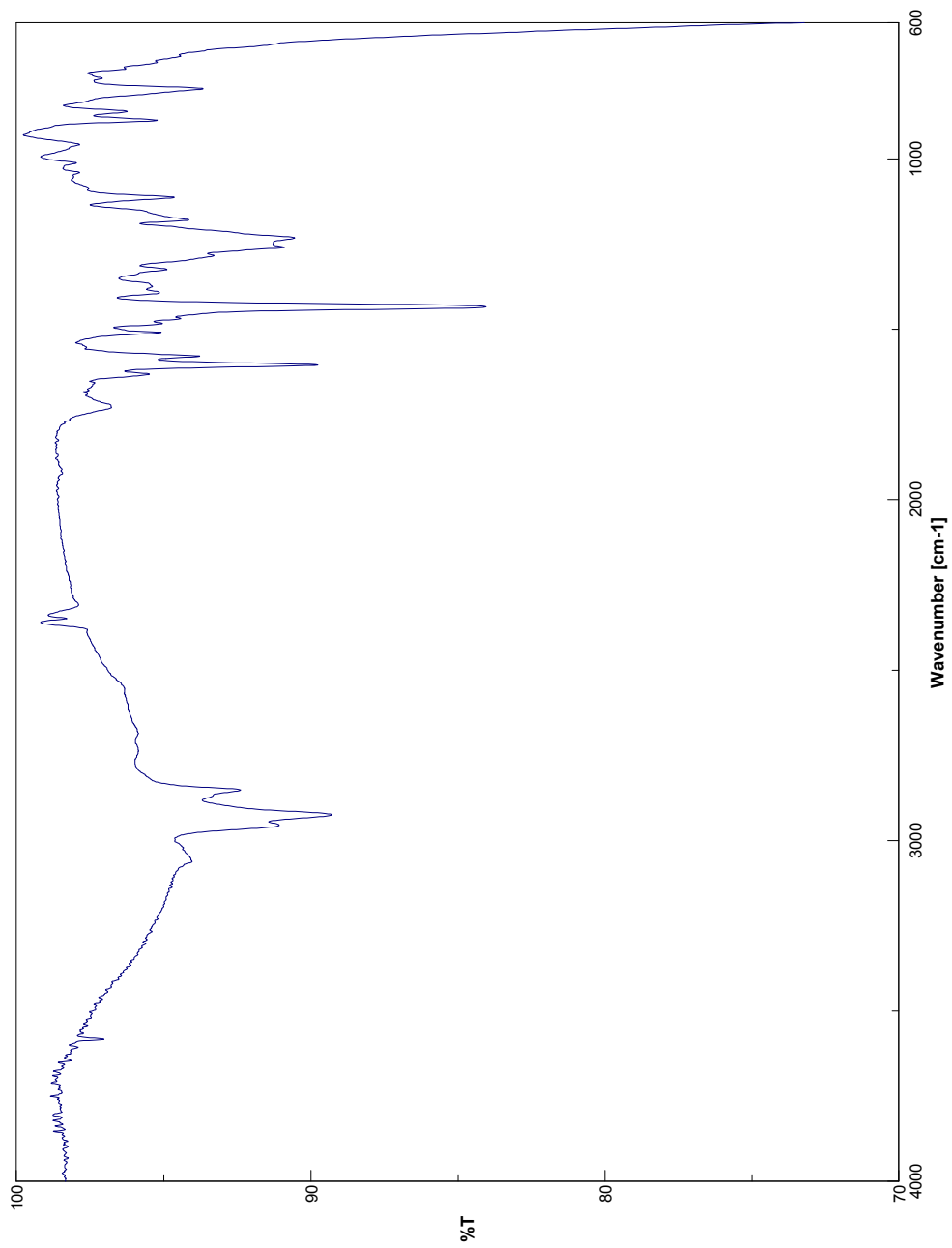
IR Spectrum of Compound **15**



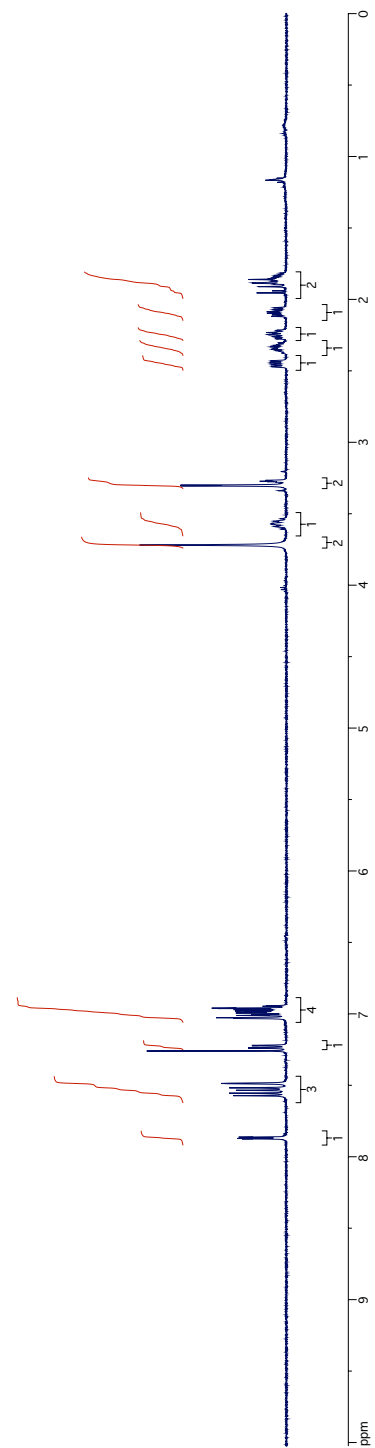
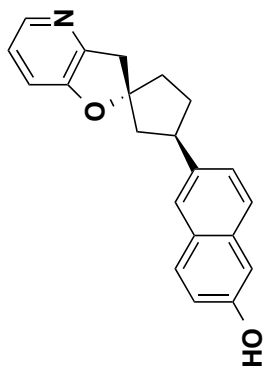
¹H NMR Spectrum of Compound 26



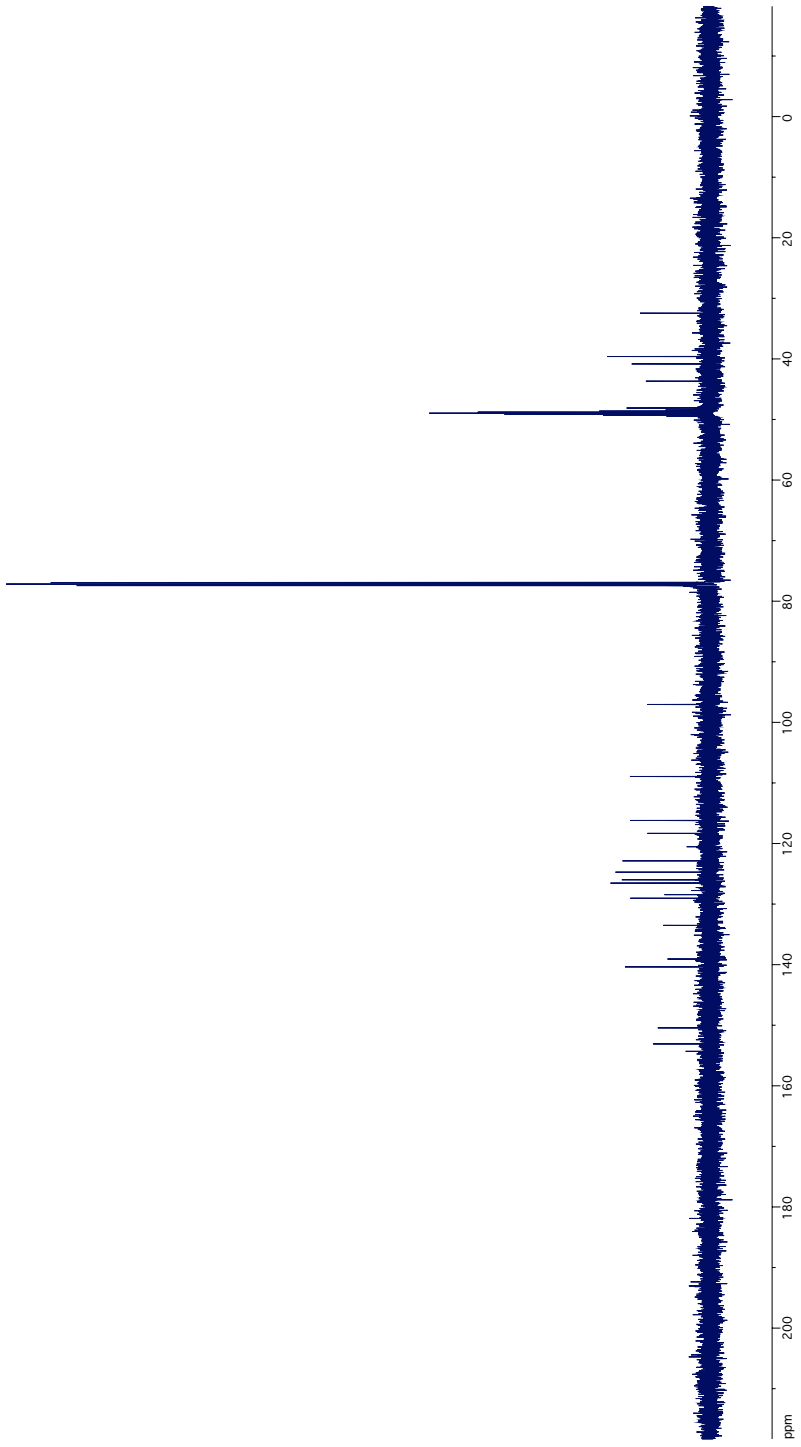
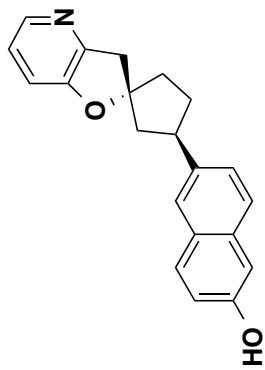
^{13}C NMR Spectrum of Compound 26



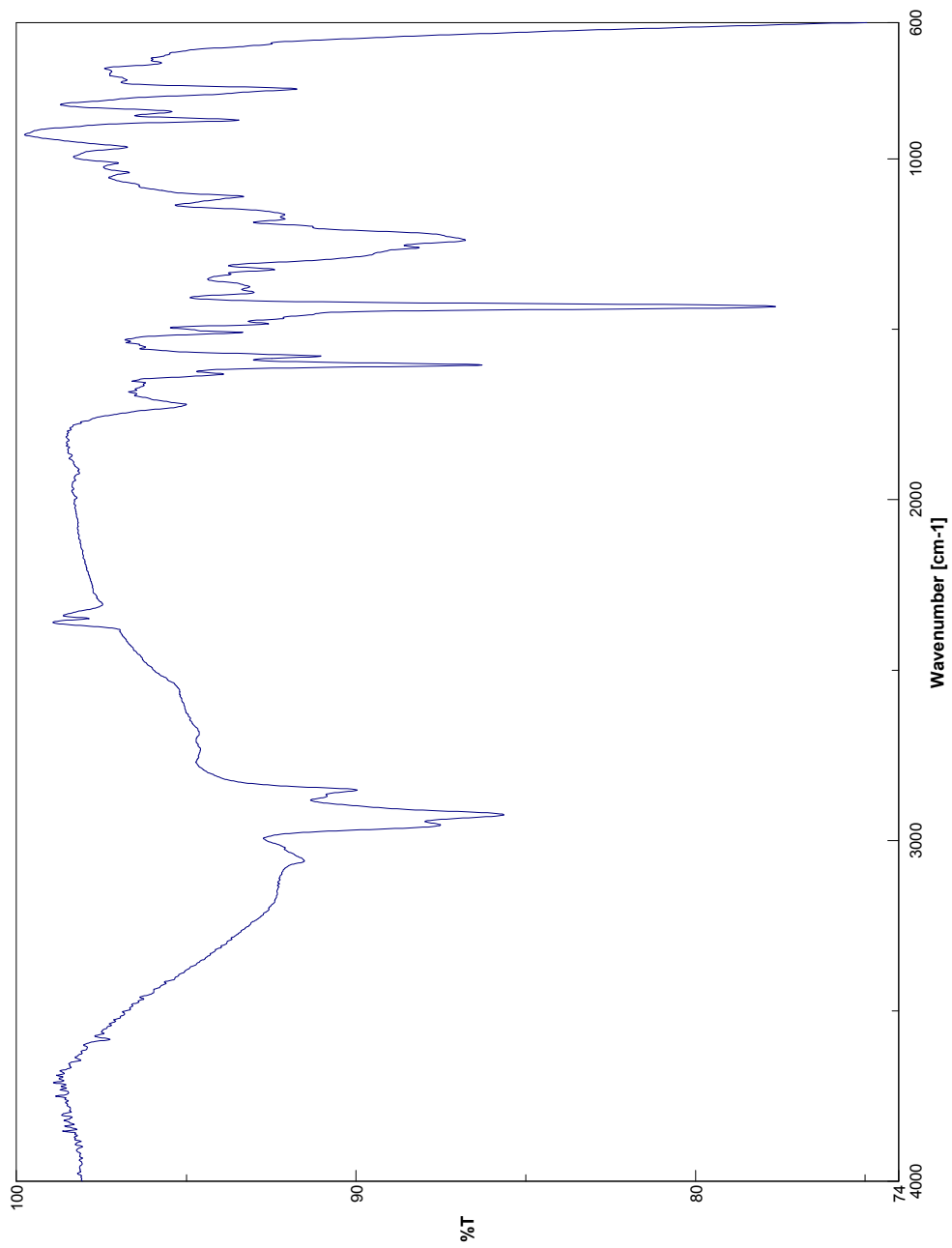
IR Spectrum of Compound **26**



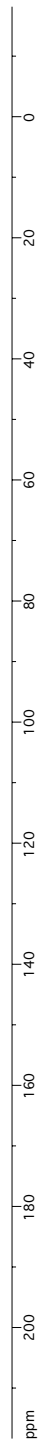
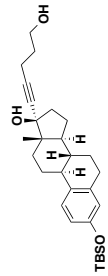
^1H NMR Spectrum of Compound 27



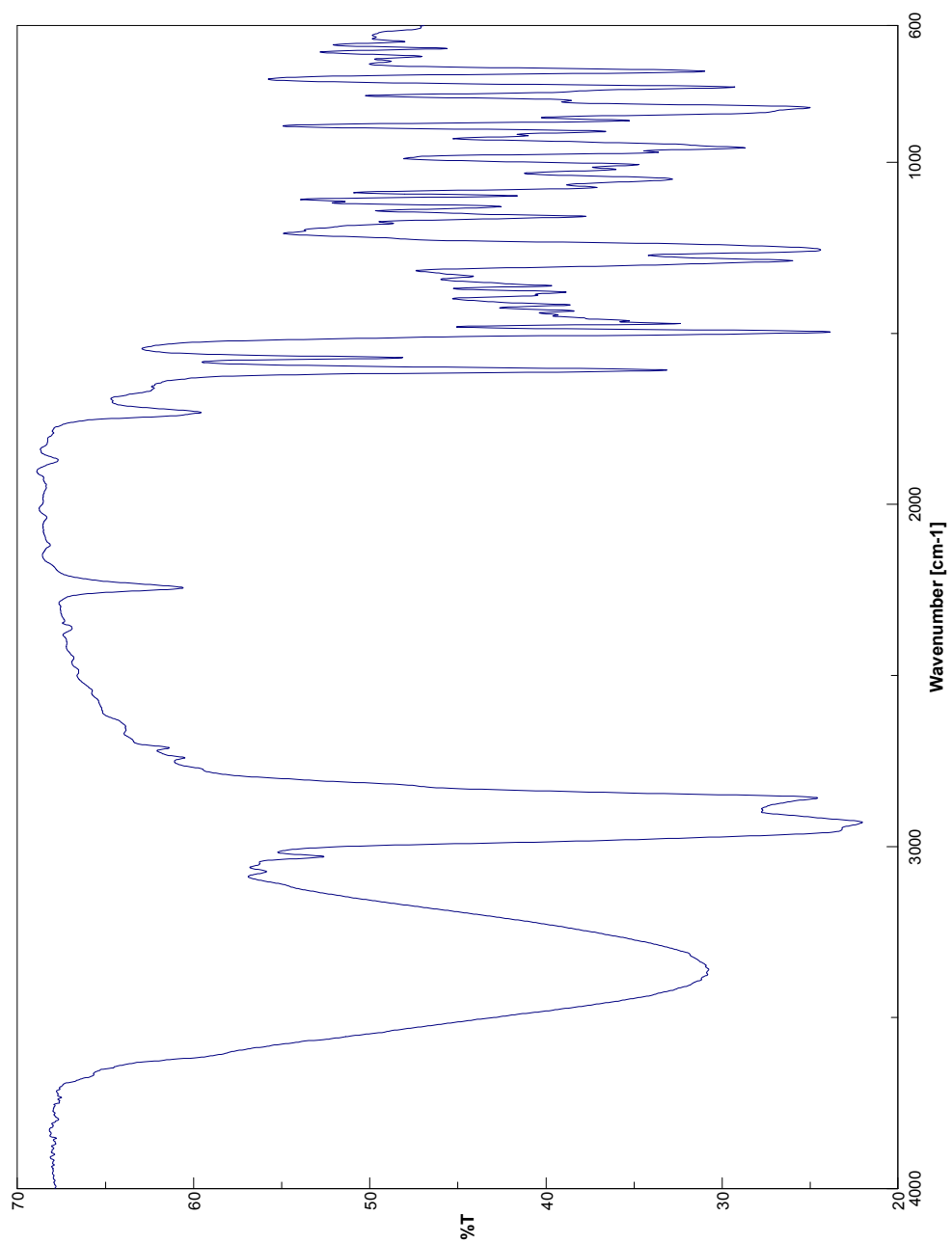
^{13}C NMR Spectrum of Compound 27



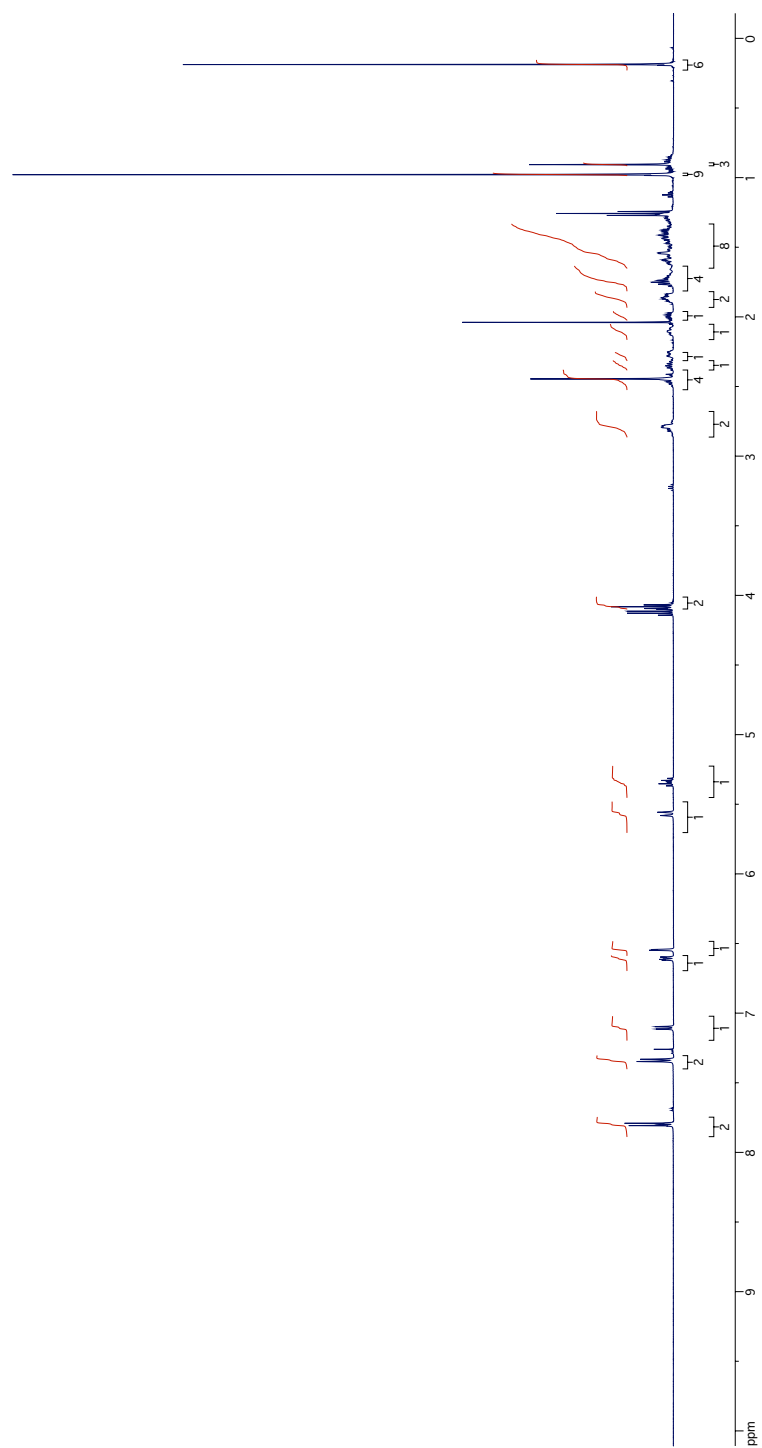
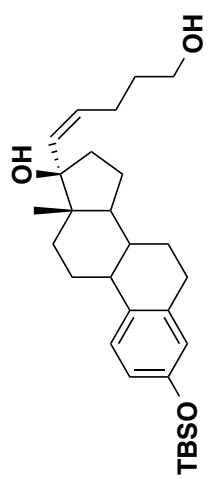
IR Spectrum of Compound **27**
254



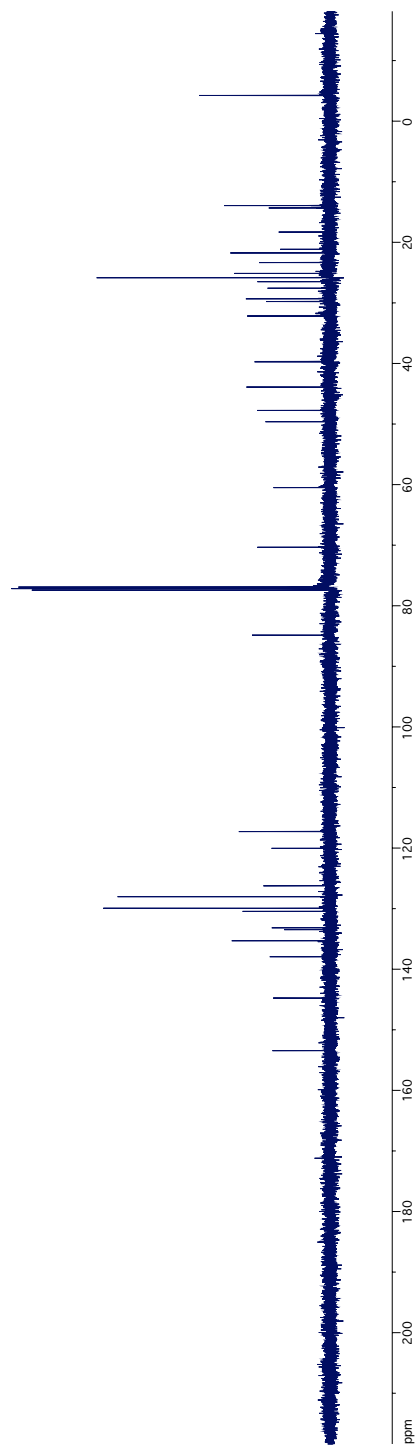
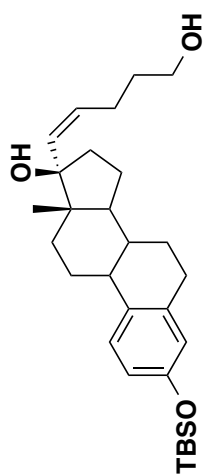
¹³C NMR Spectrum of Compound 34



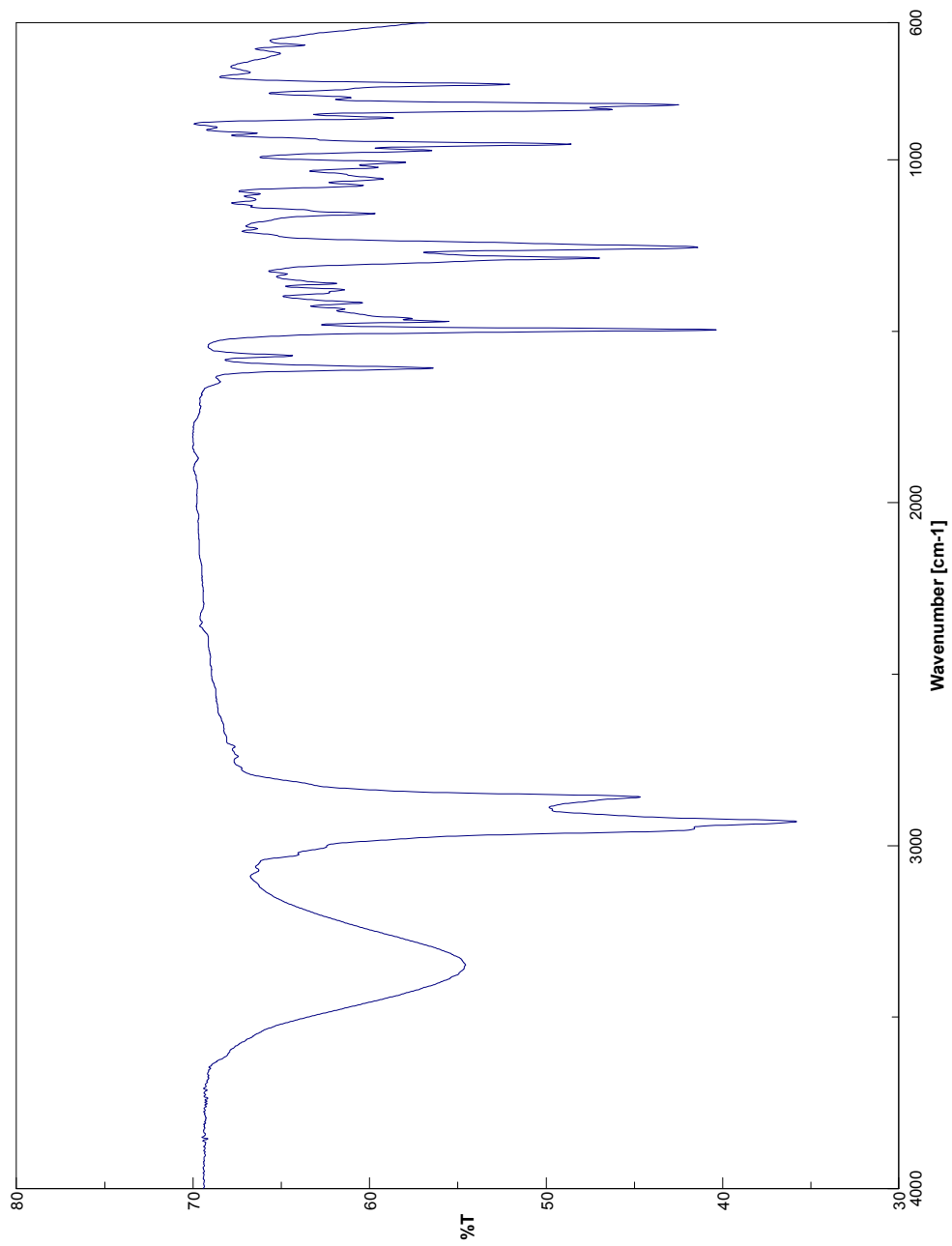
IR Spectrum of Compound **34**



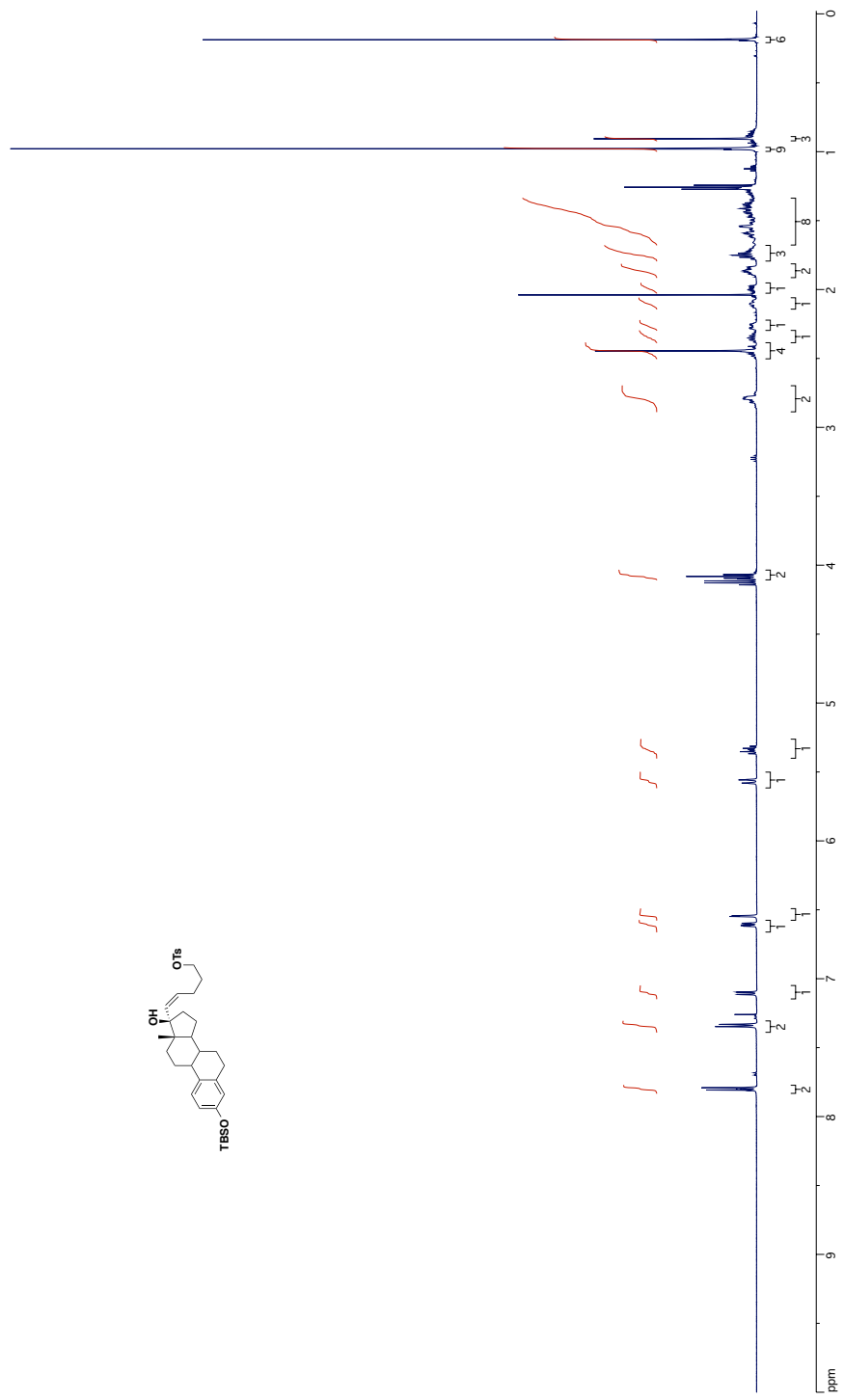
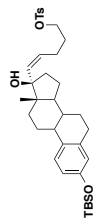
^1H NMR Spectrum of Compound **35**

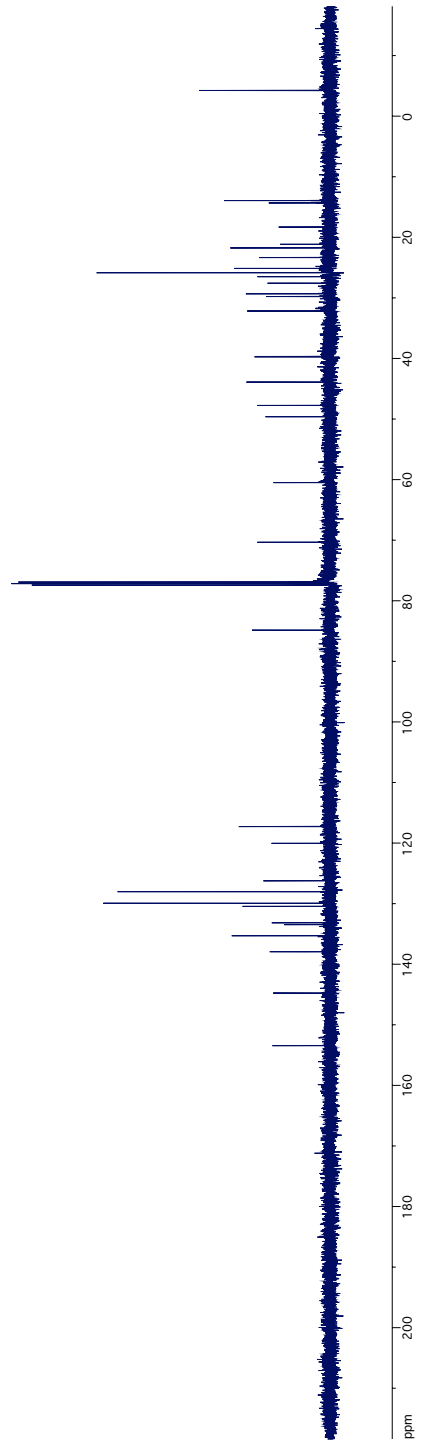
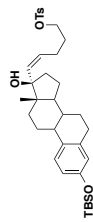


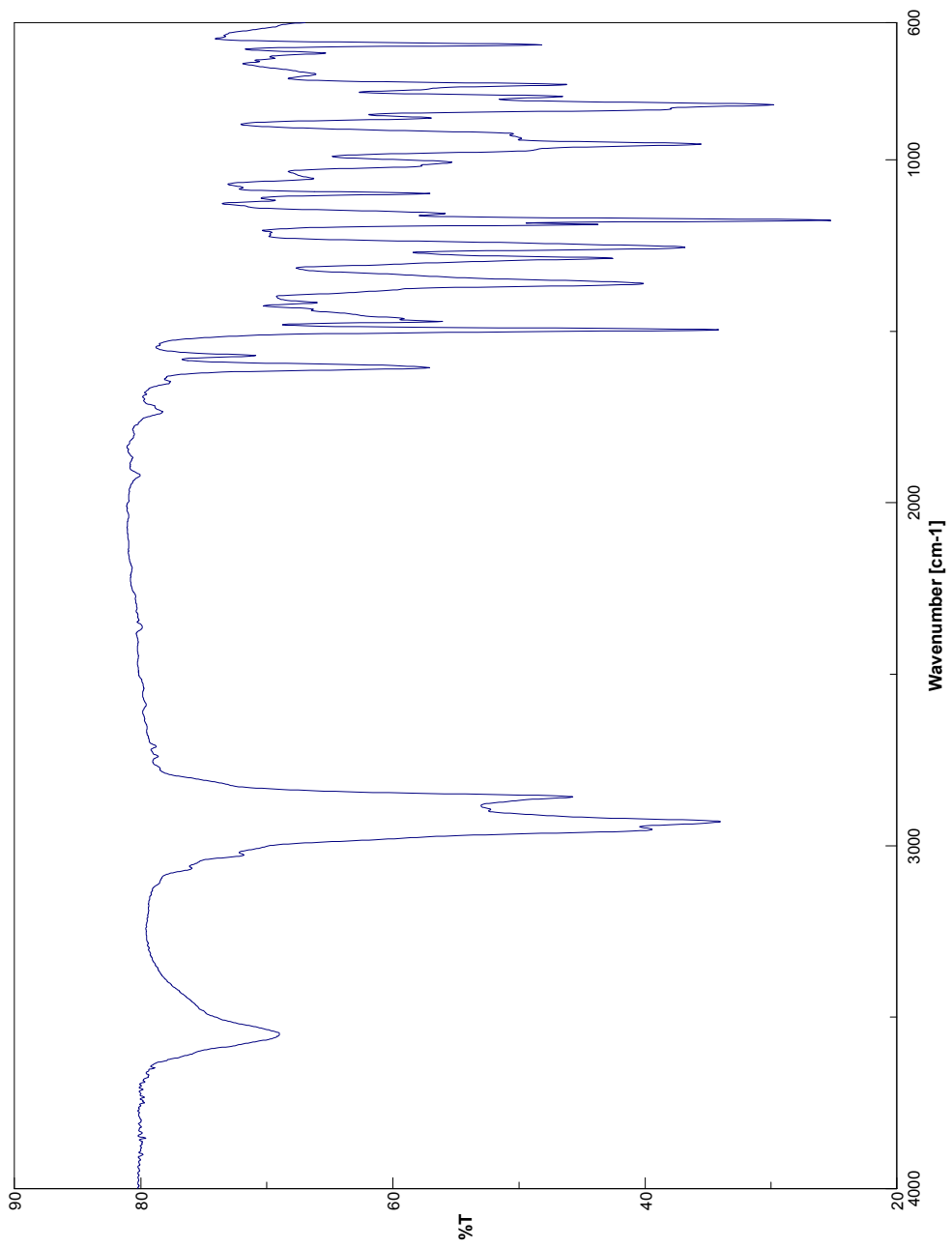
^{13}C NMR Spectrum of Compound 35

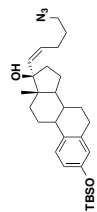
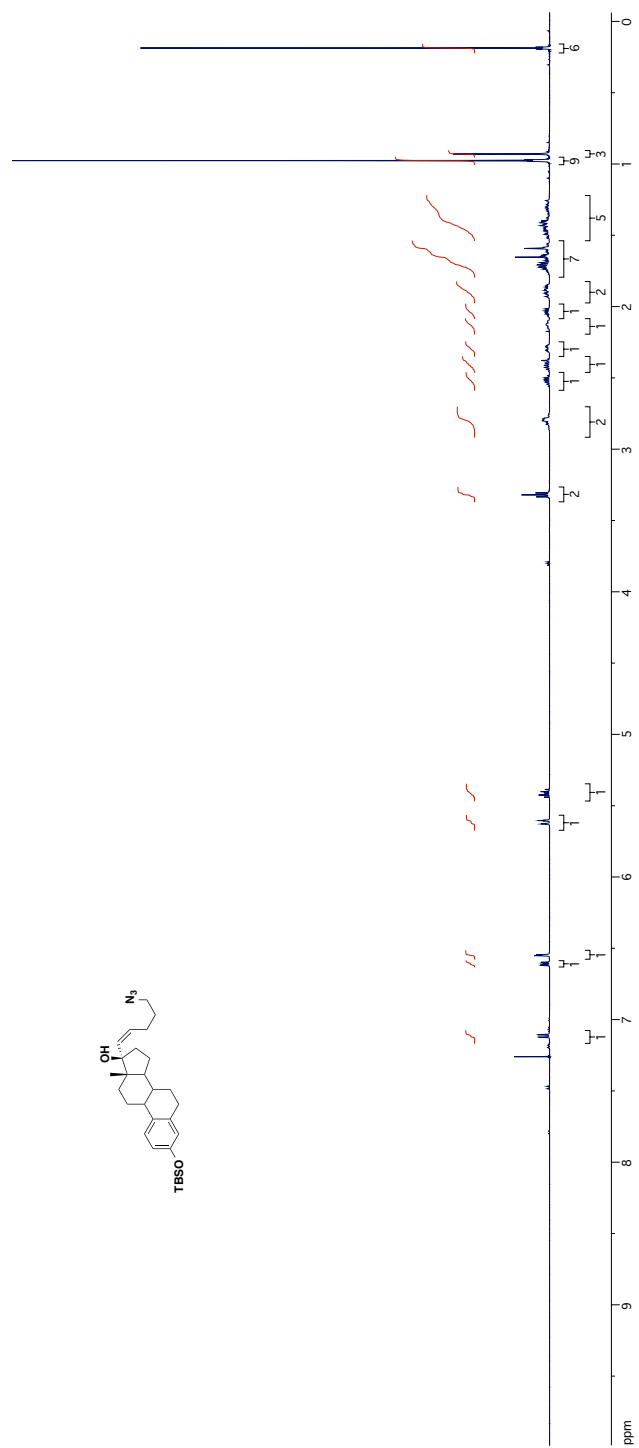


IR Spectrum of Compound **35**
260

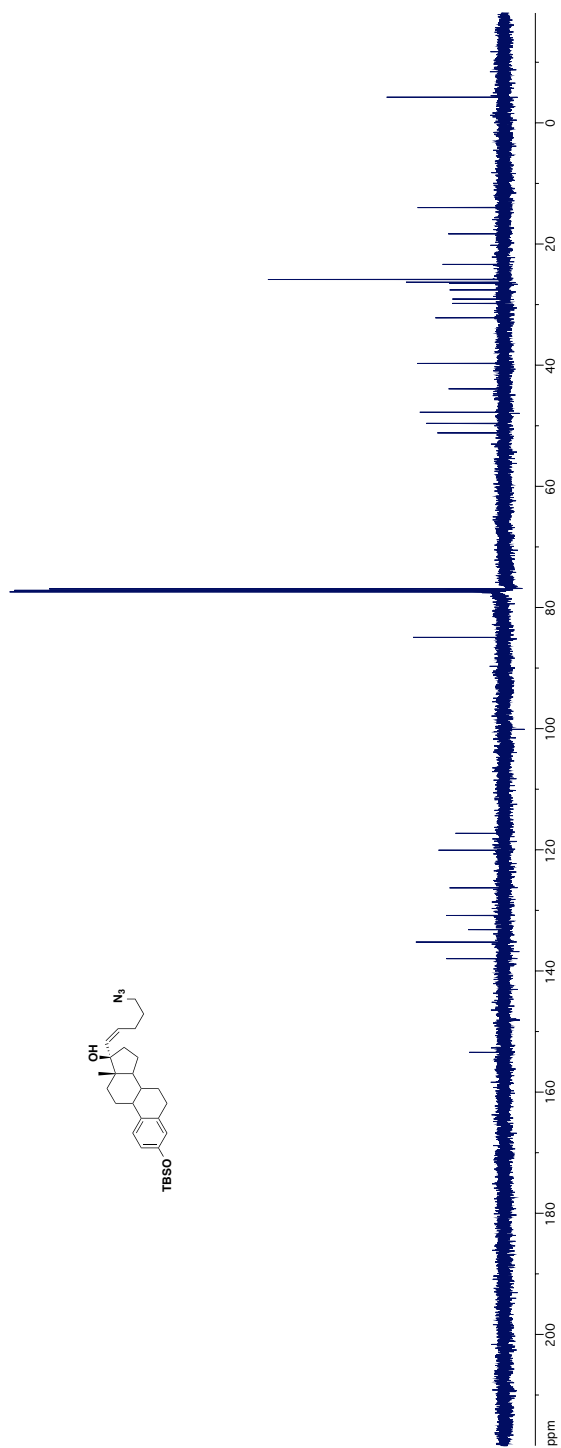
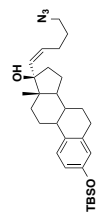




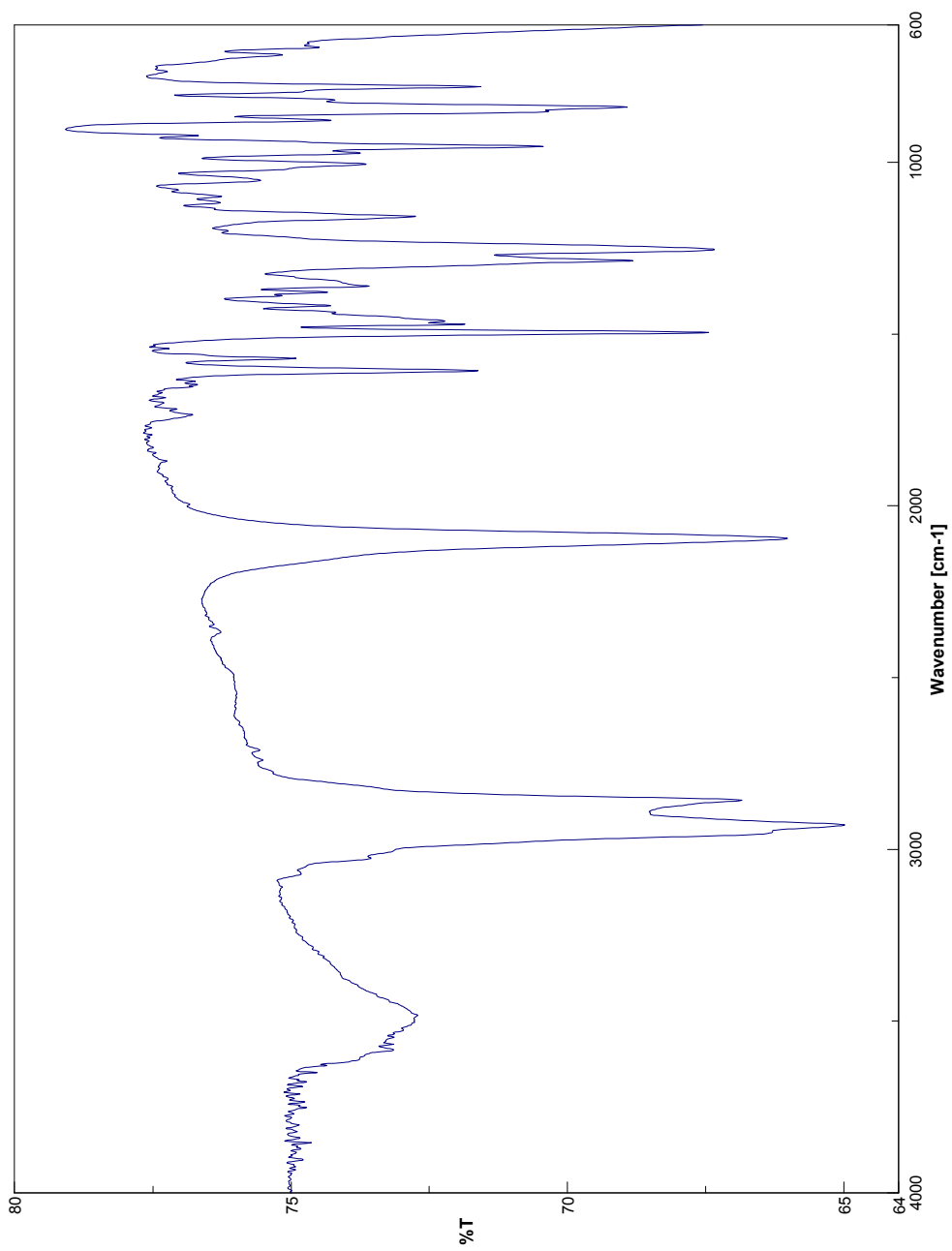




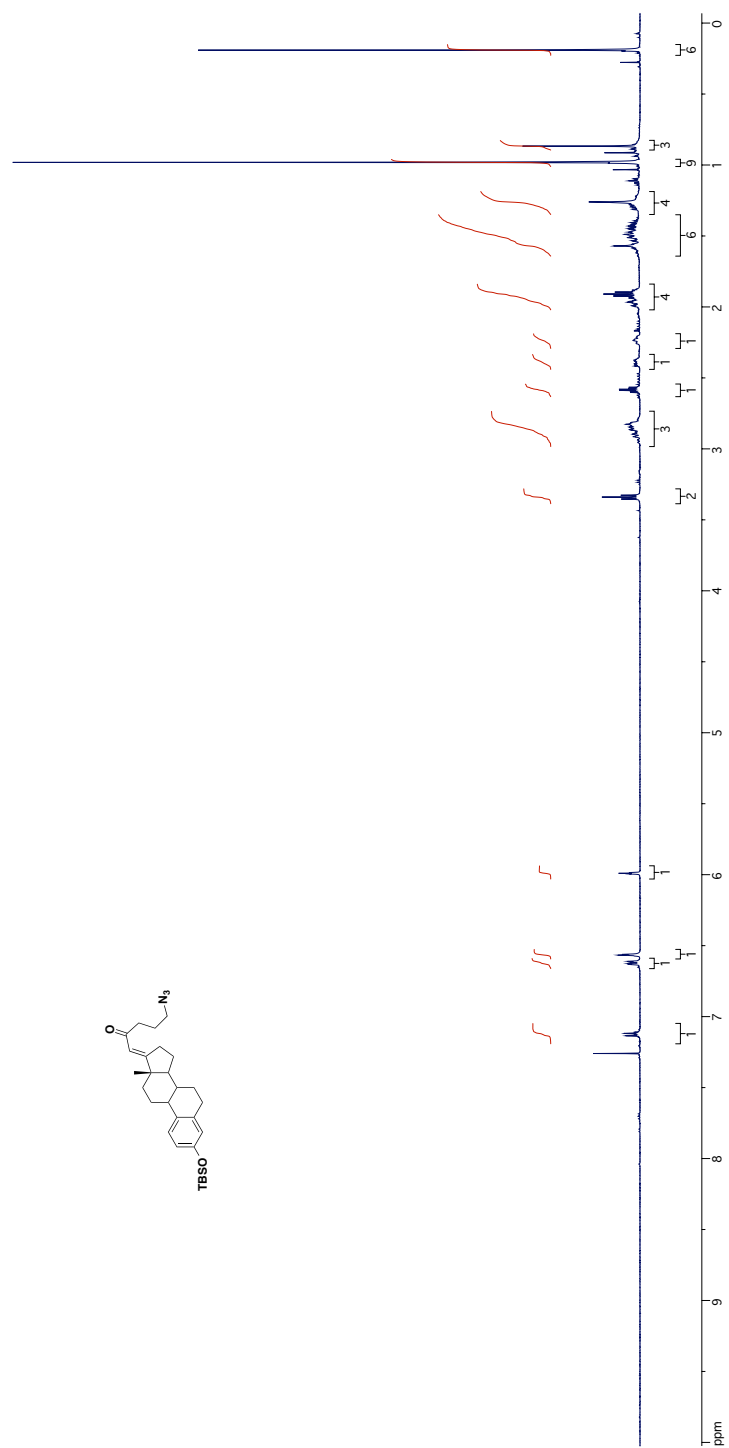
¹H NMR Spectrum of Compound **36**



^{13}C NMR Spectrum of Compound 36



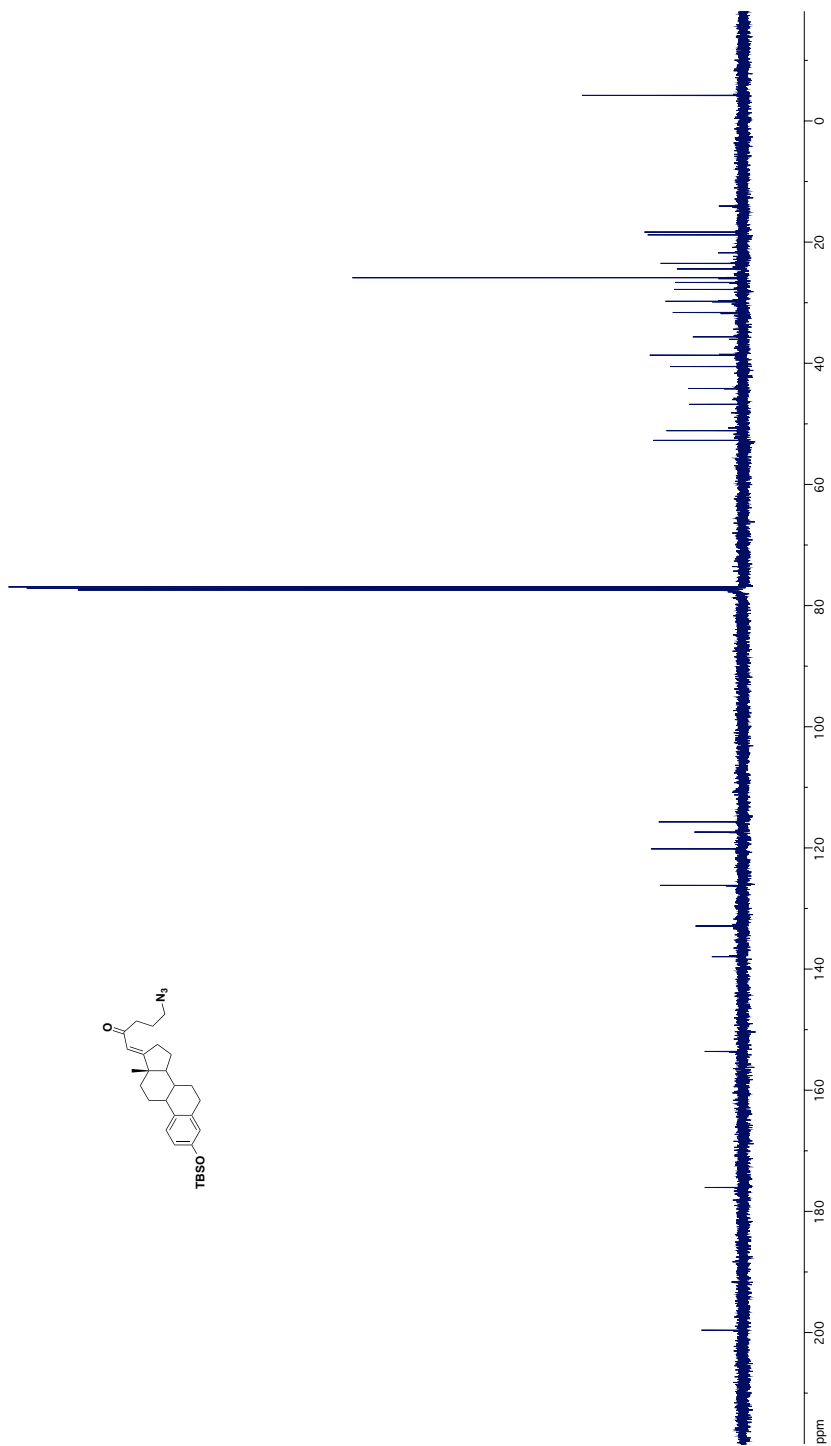
IR Spectrum of Compound **36**

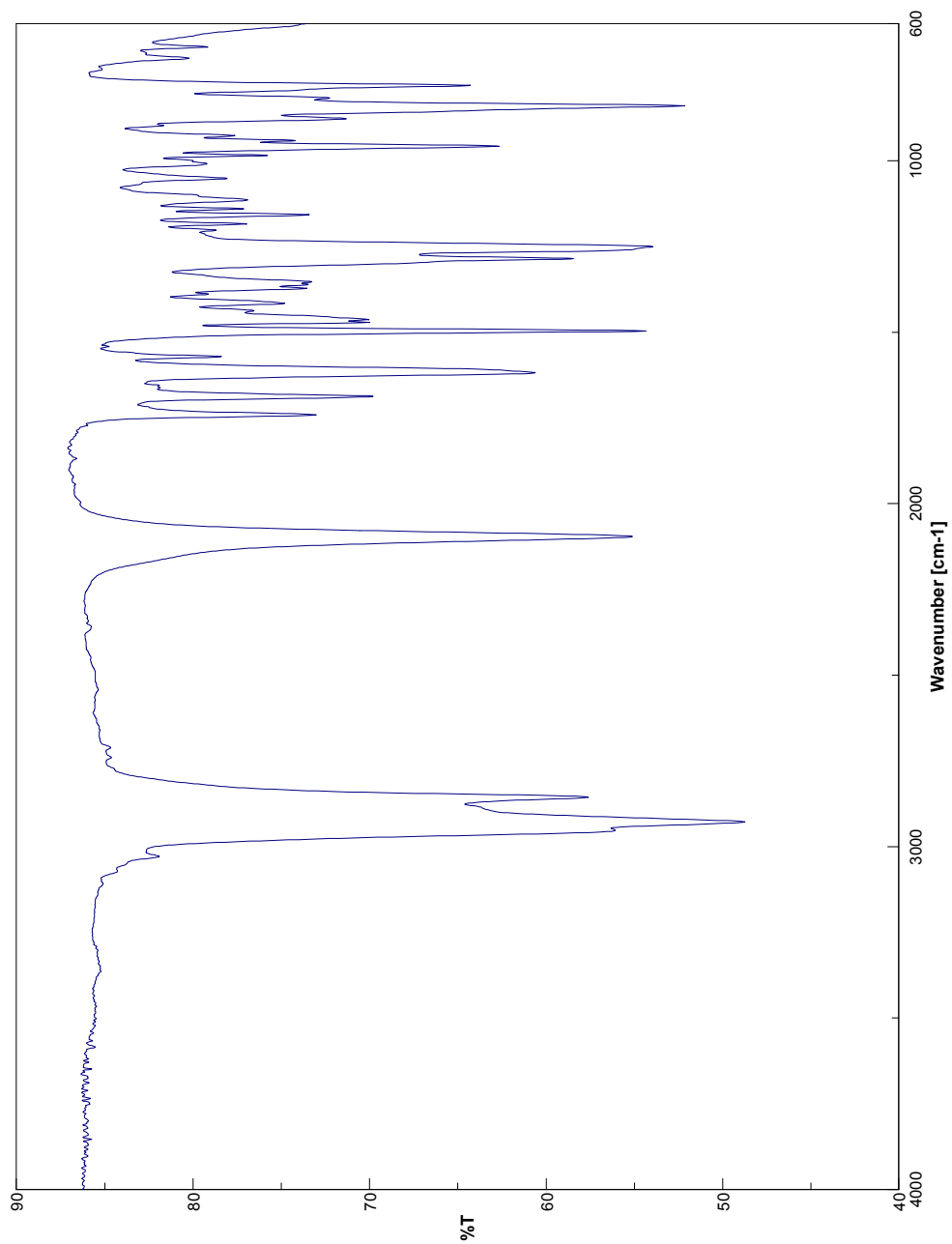


¹H NMR Spectrum of Compound 37

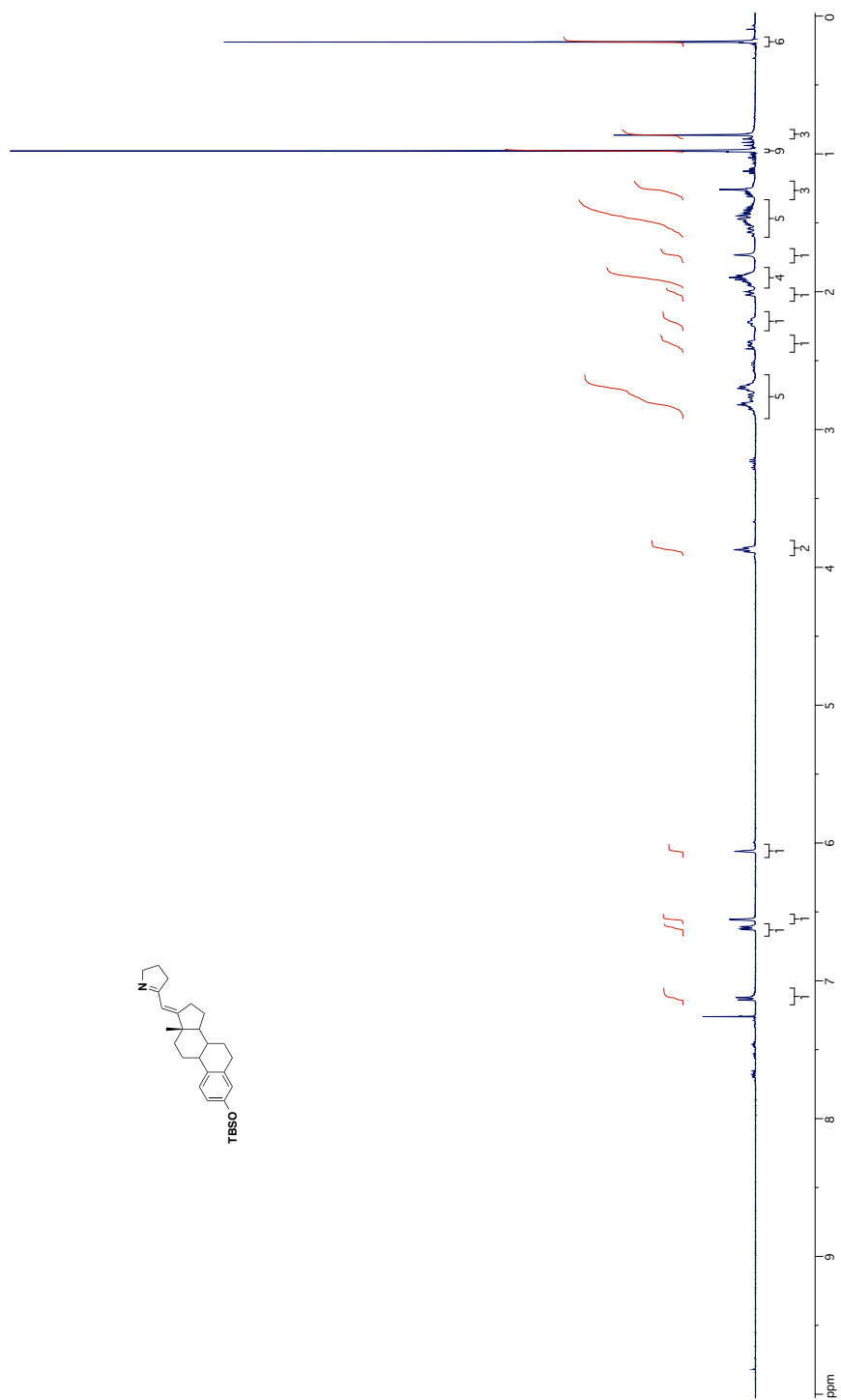
¹³C NMR Spectrum of Compound **37**

268





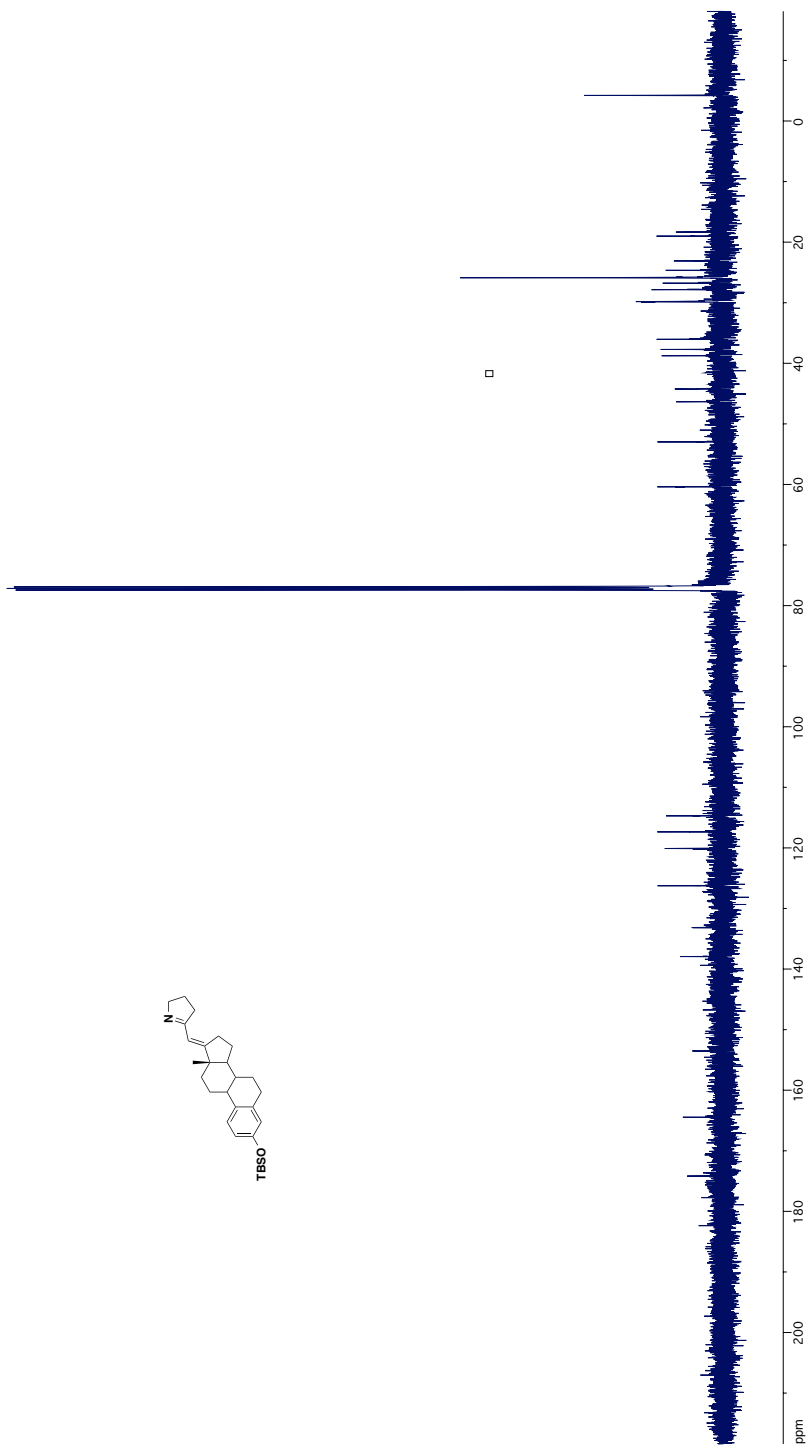
IR Spectrum of Compound **37**

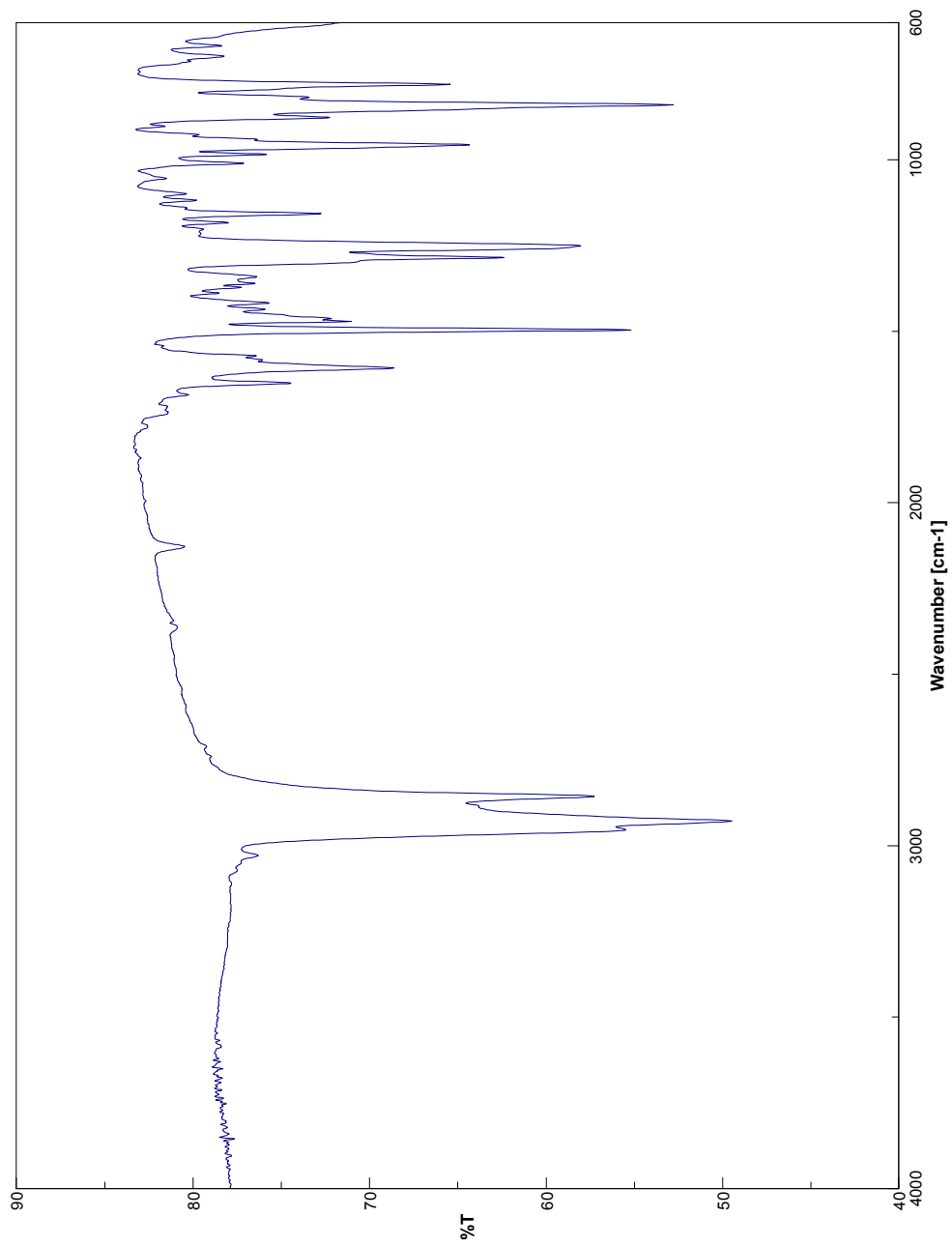


¹H NMR Spectrum of Compound **38**

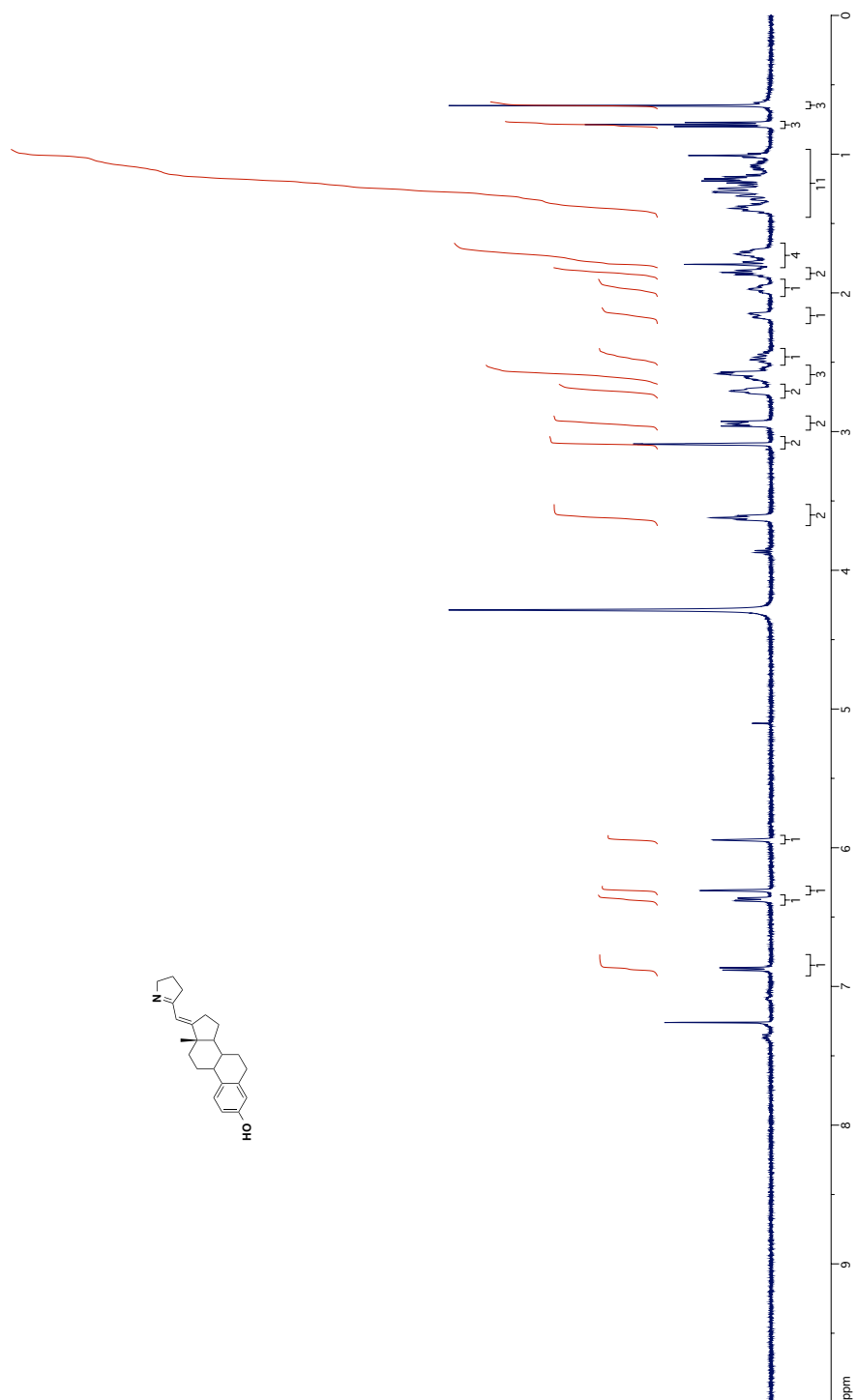
¹³C NMR Spectrum of Compound **38**

271

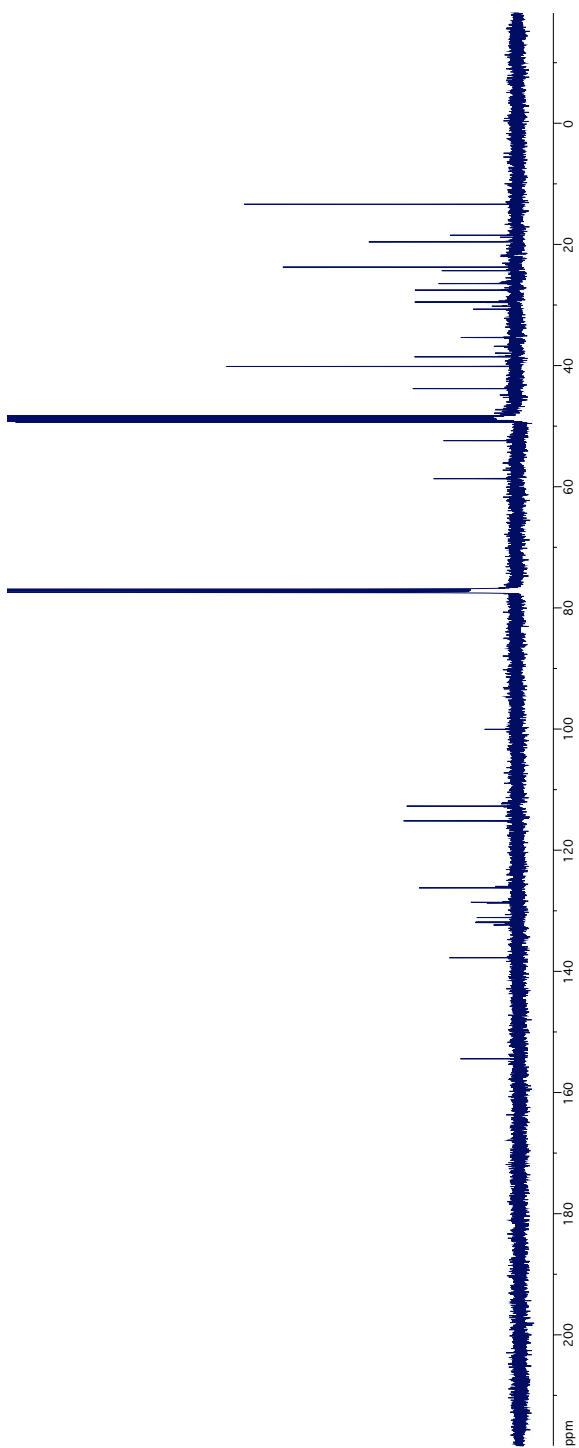
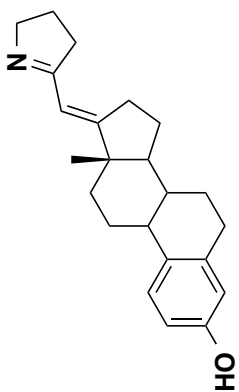




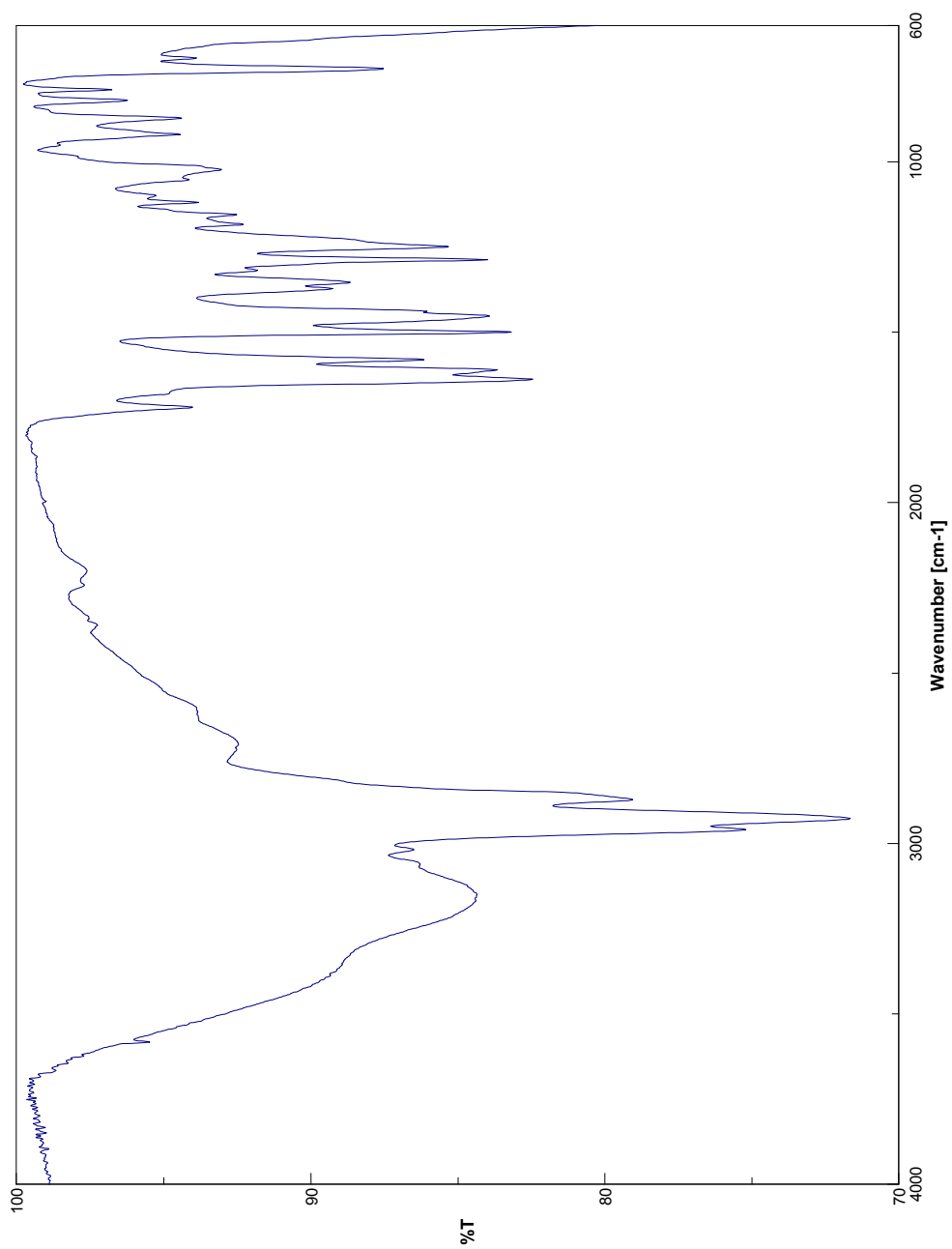
IR Spectrum of Compound **38**



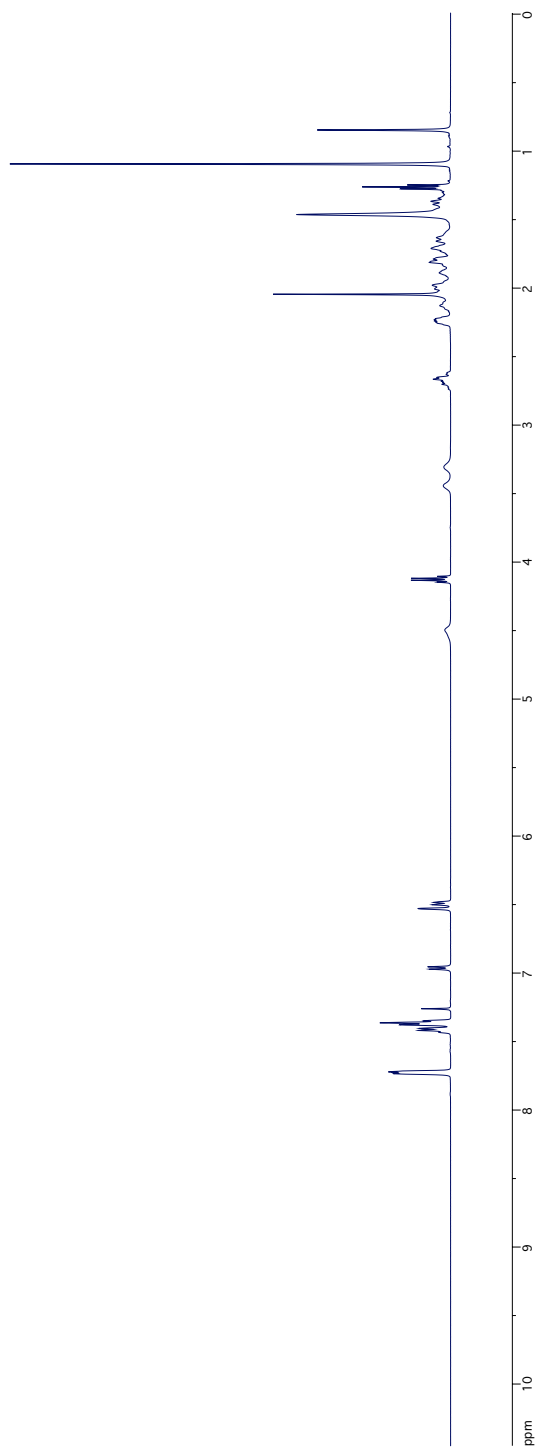
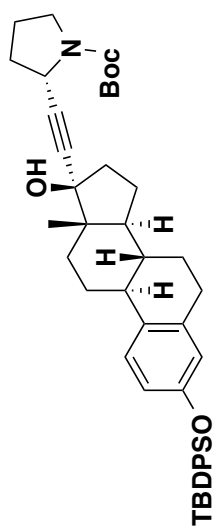
¹H NMR Spectrum of Compound **39**



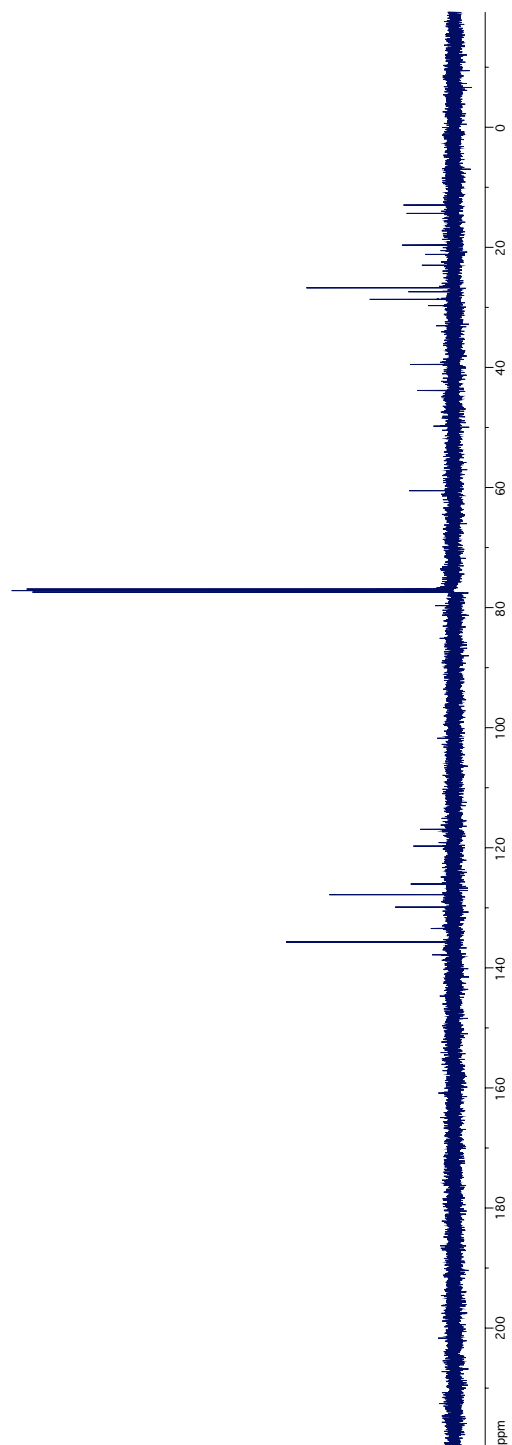
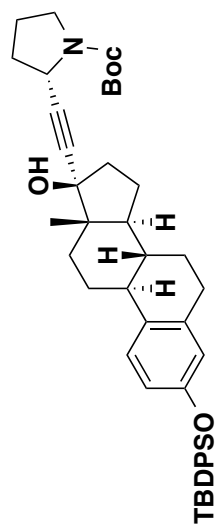
^{13}C NMR Spectrum of Compound 39



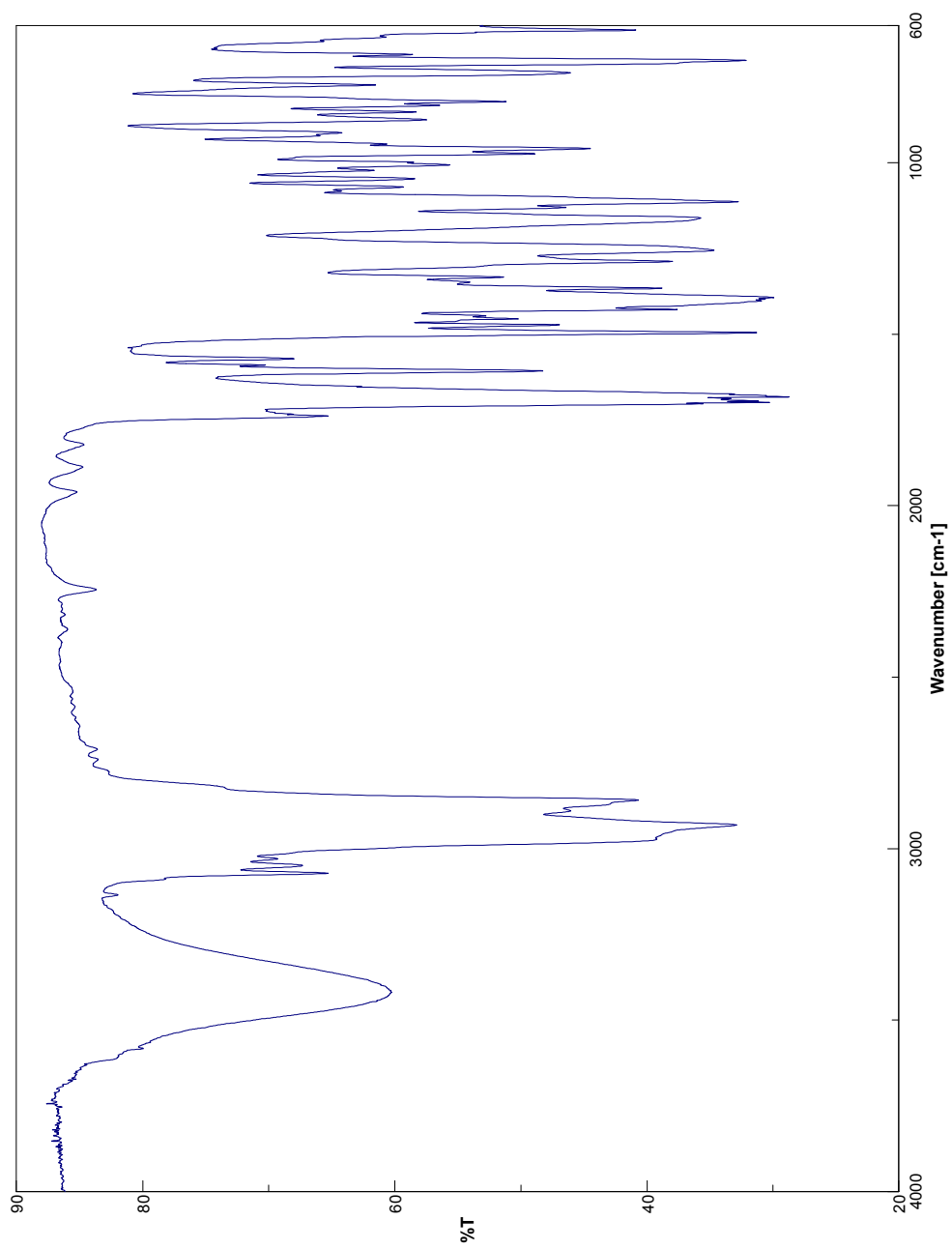
IR Spectrum of Compound **39**



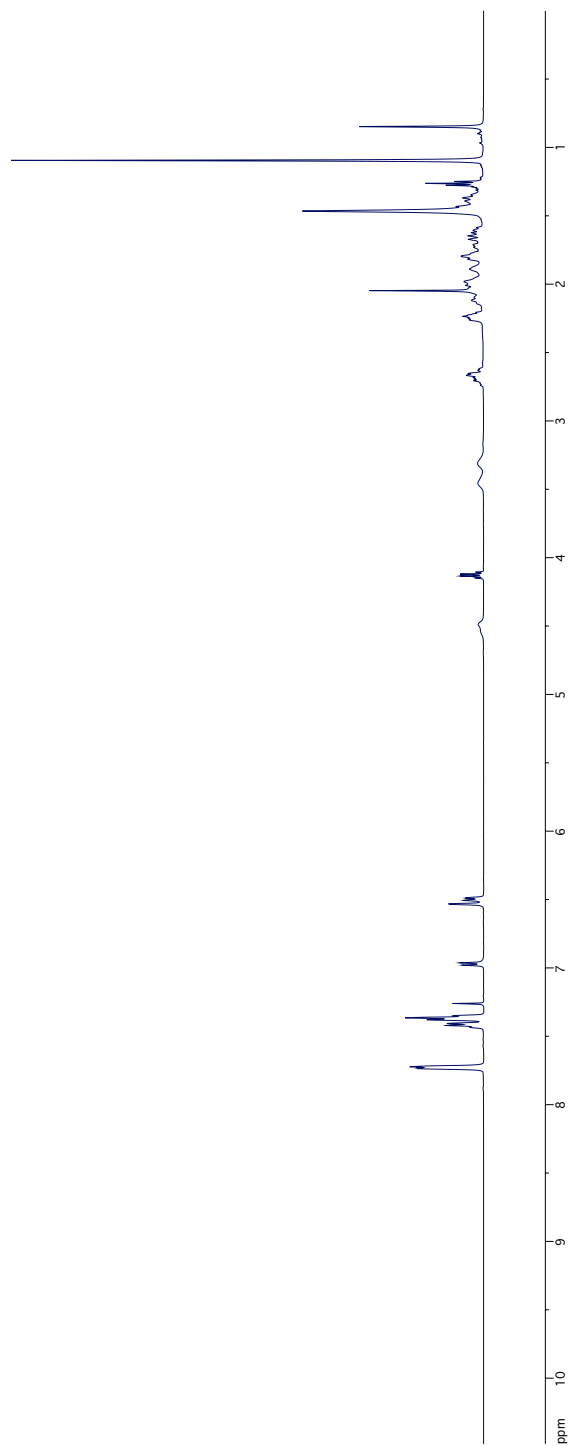
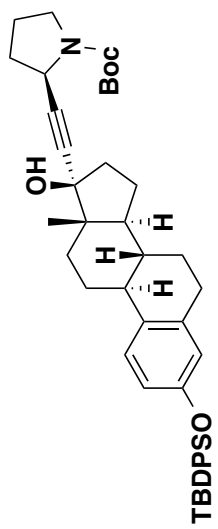
^1H NMR Spectrum of Compound **47**



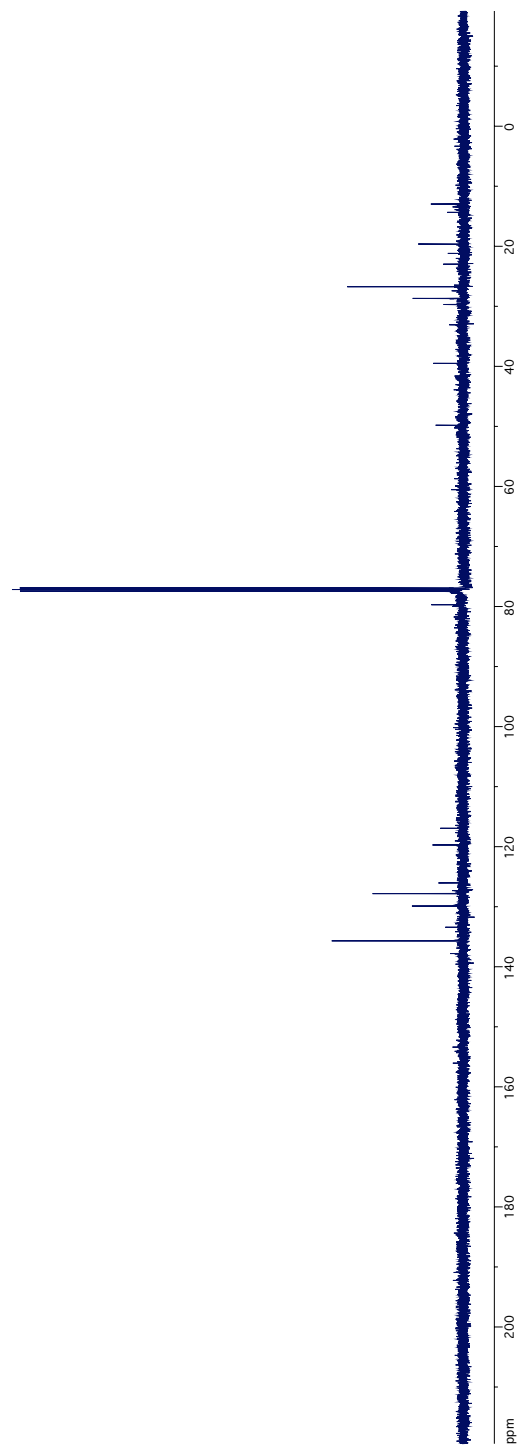
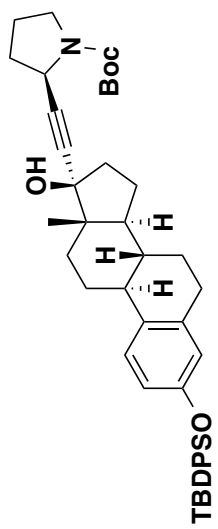
^{13}C NMR Spectrum of Compound 47



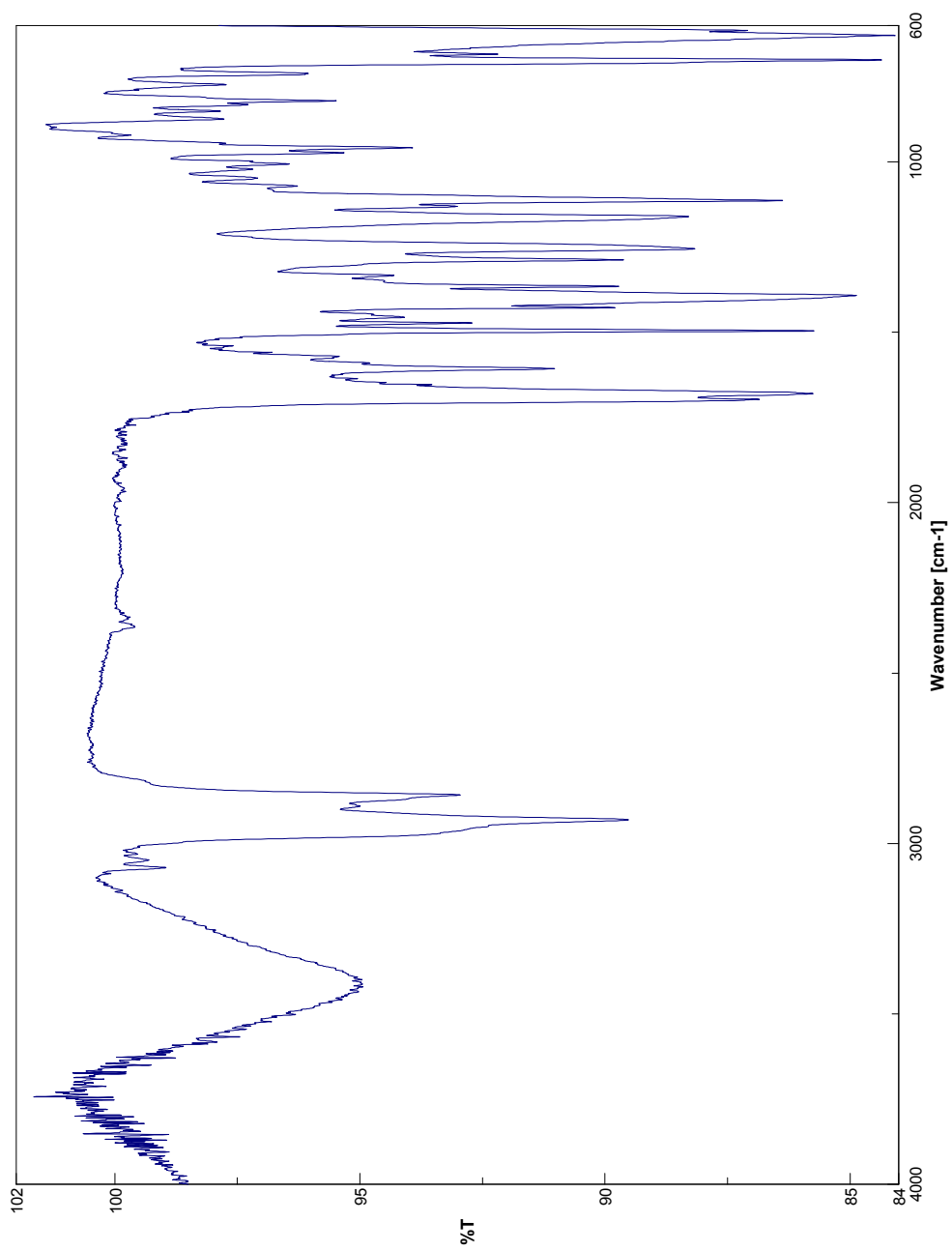
IR Spectrum of Compound **47**



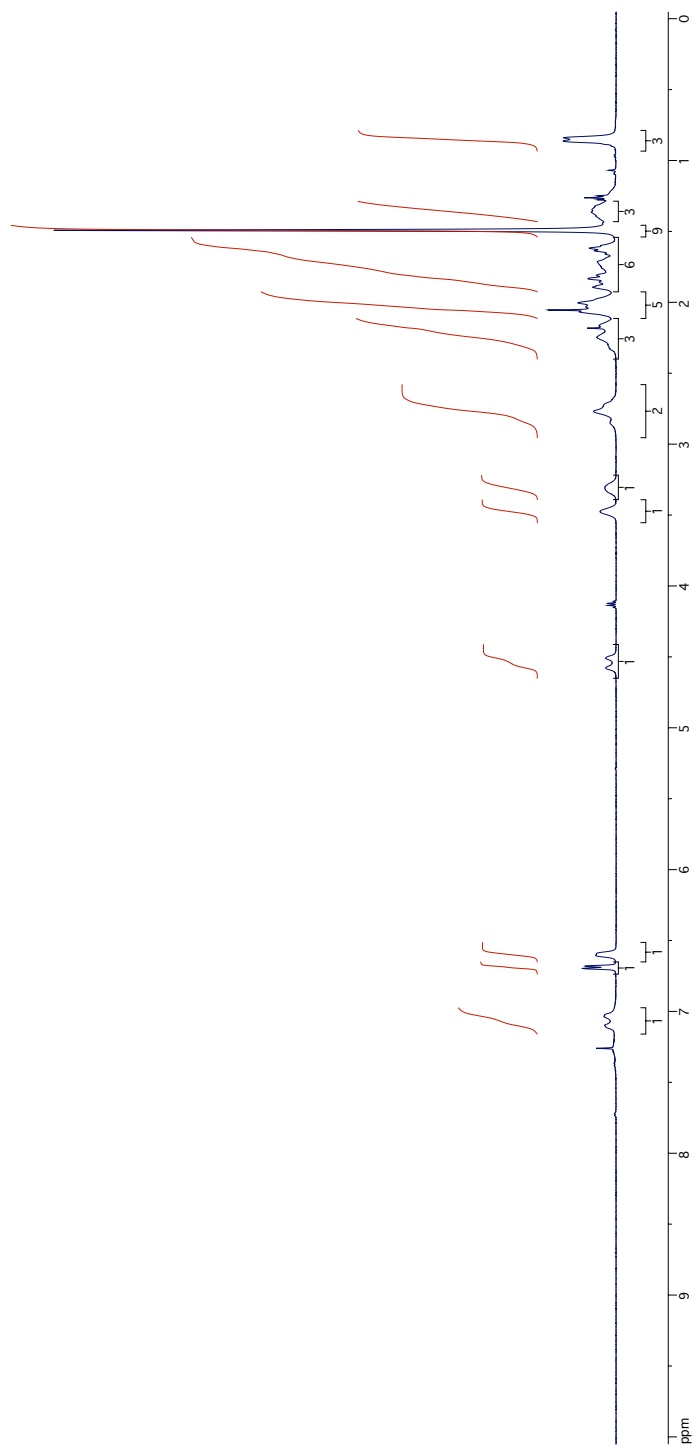
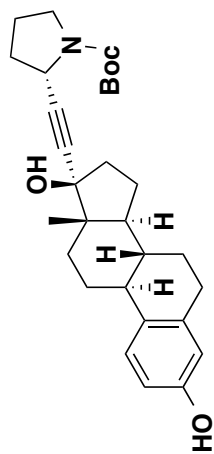
^1H NMR Spectrum of Compound 48



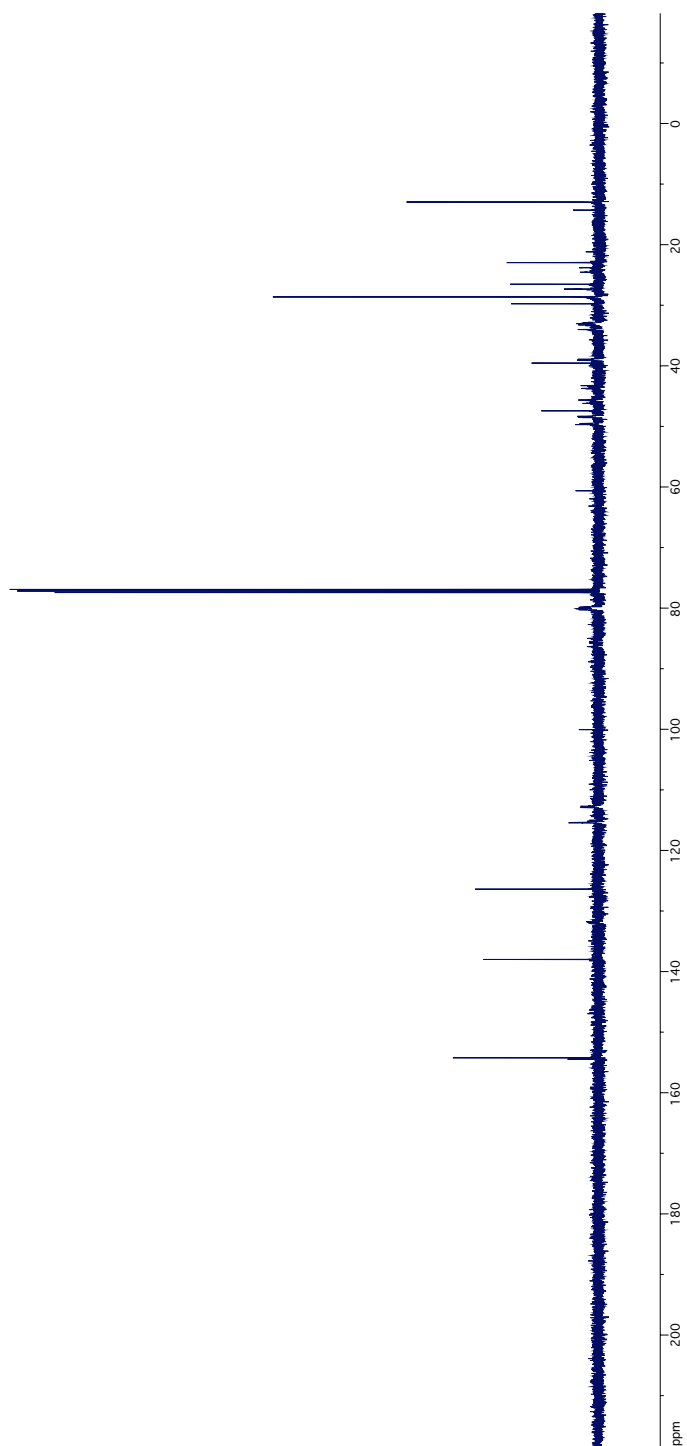
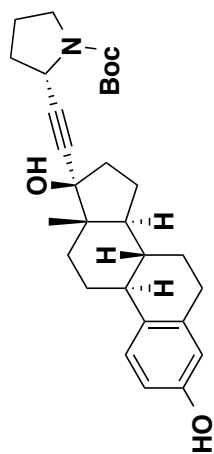
^{13}C NMR Spectrum of Compound **48**



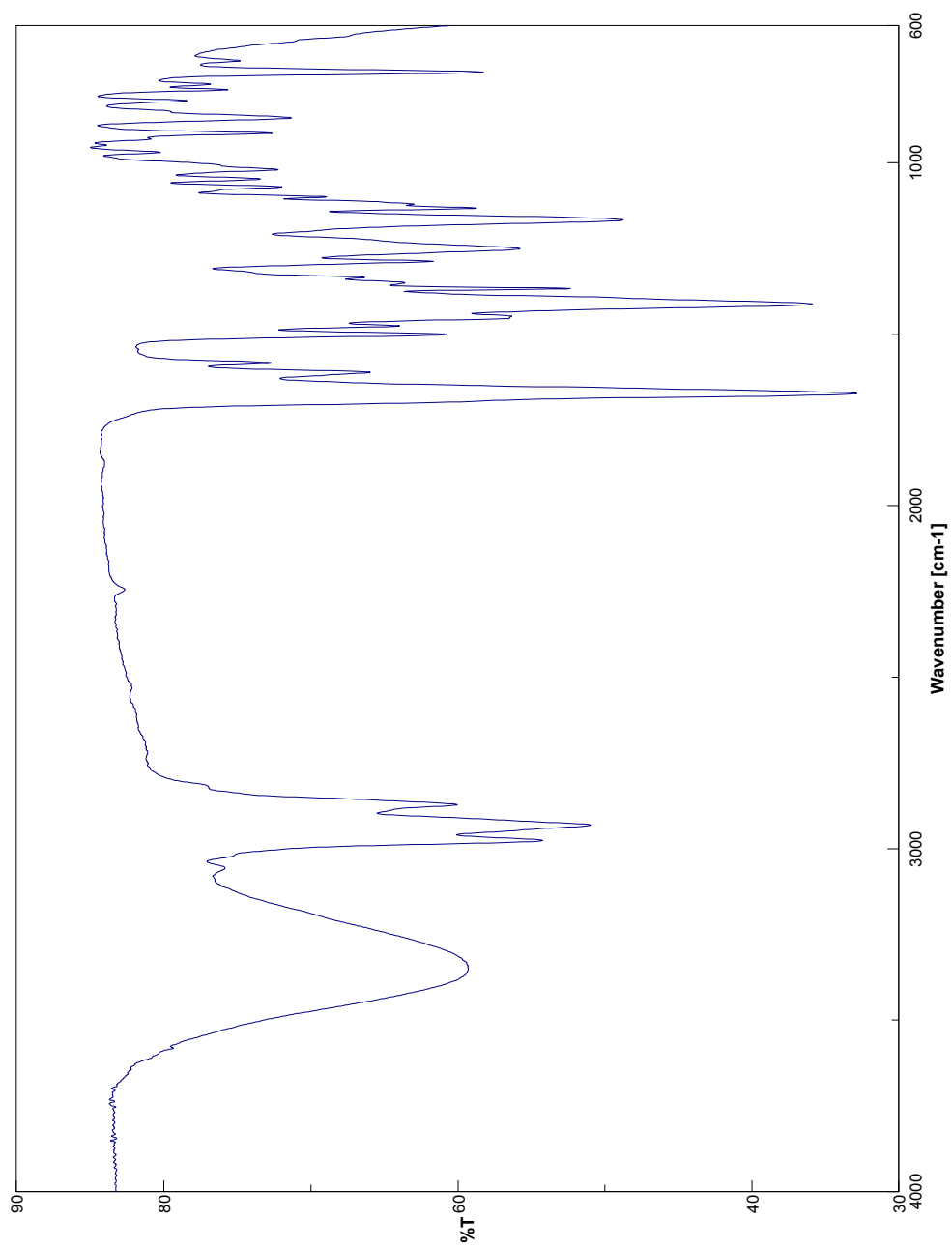
IR Spectrum of Compound **48**



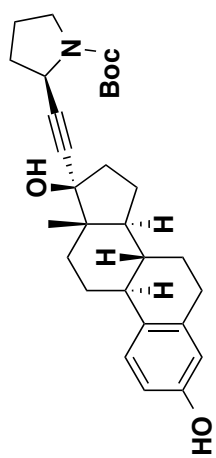
¹H NMR Spectrum of Compound 49



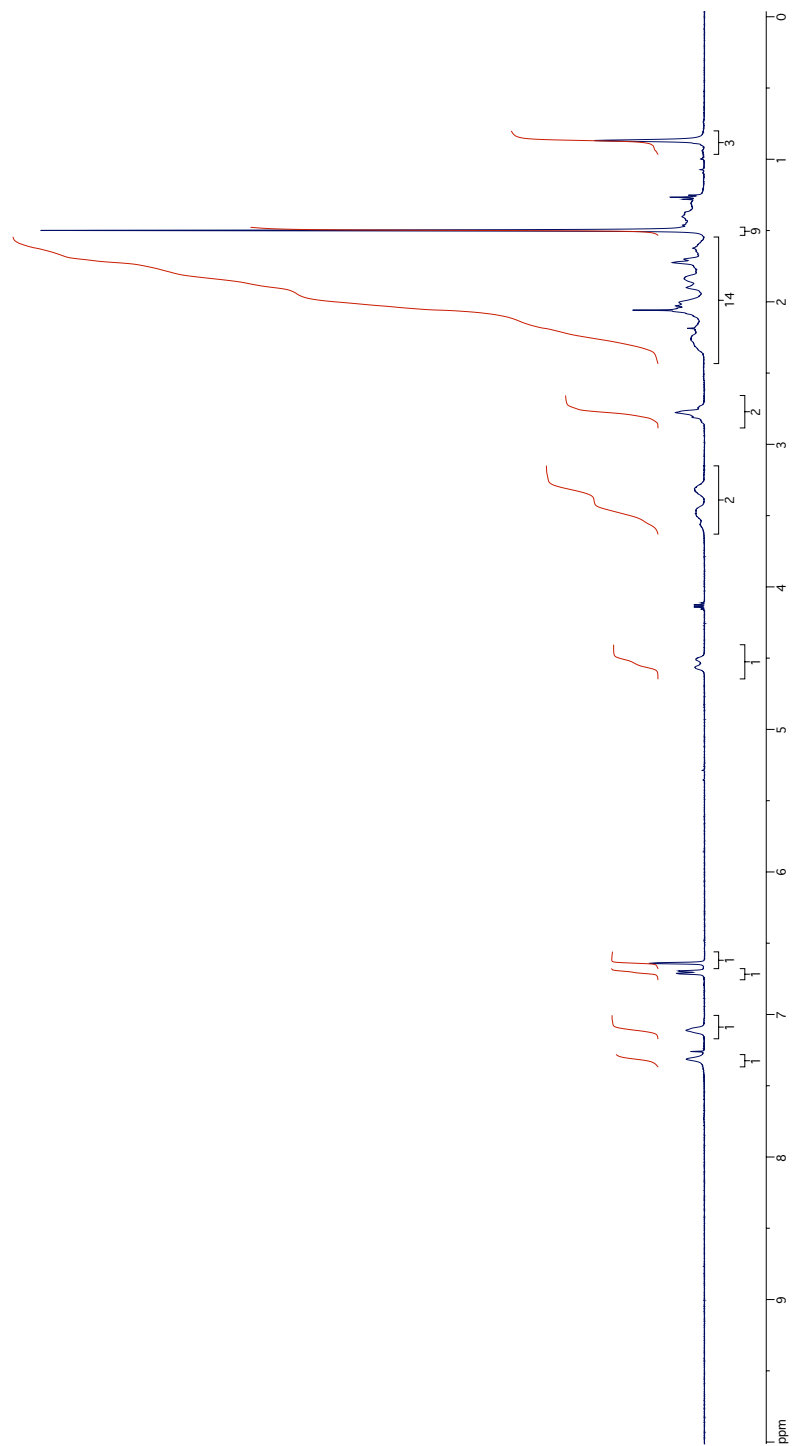
^{13}C NMR Spectrum of Compound 49

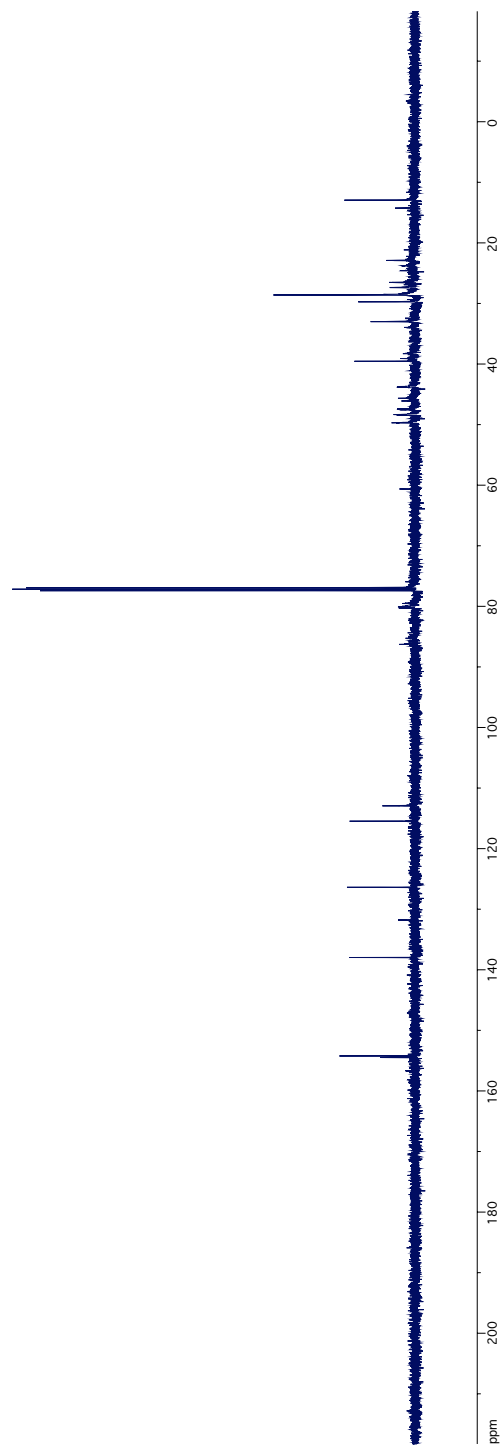
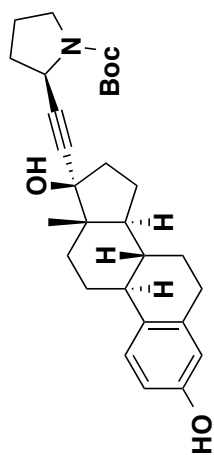


IR Spectrum of Compound **49**

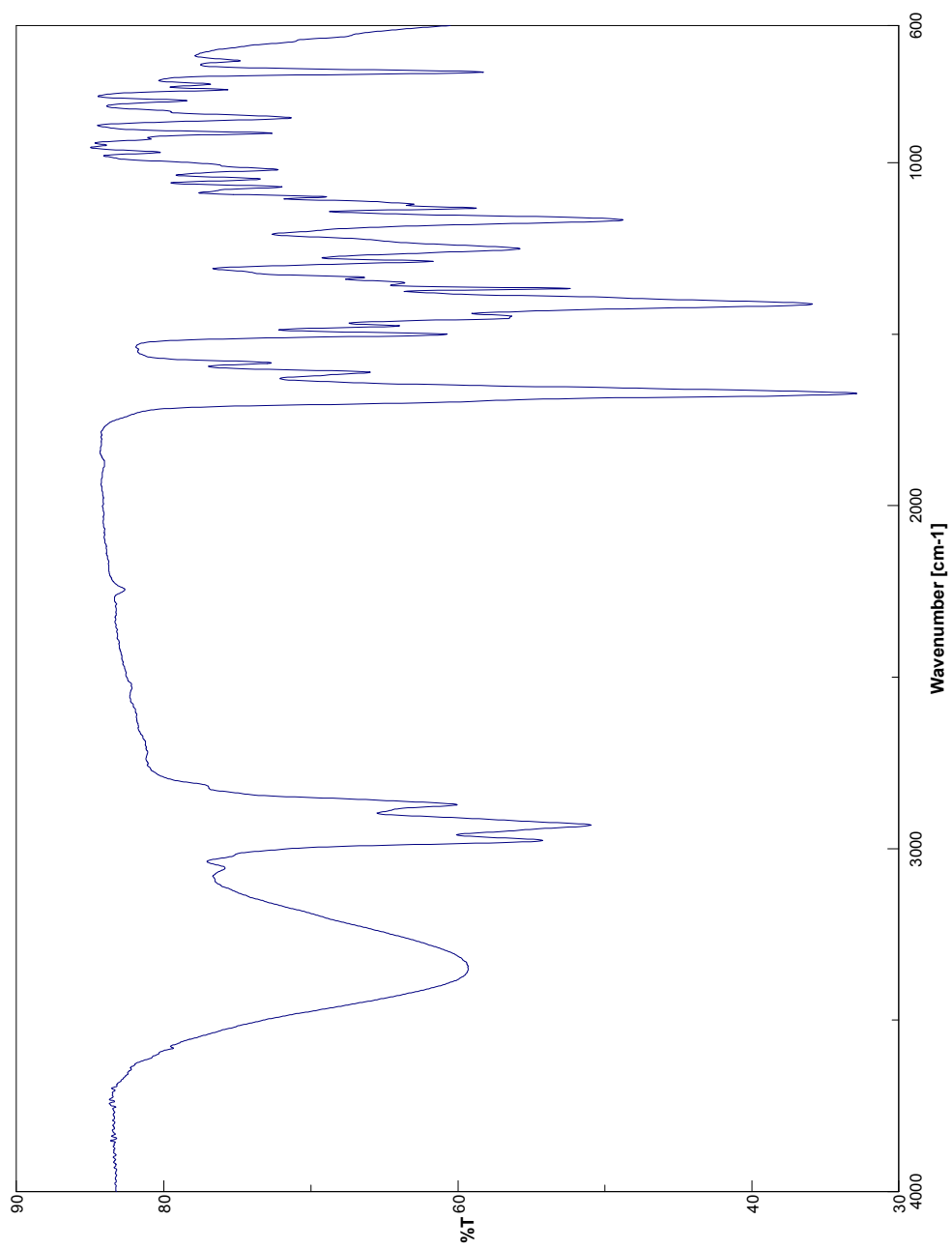


¹H NMR Spectrum of Compound **50**

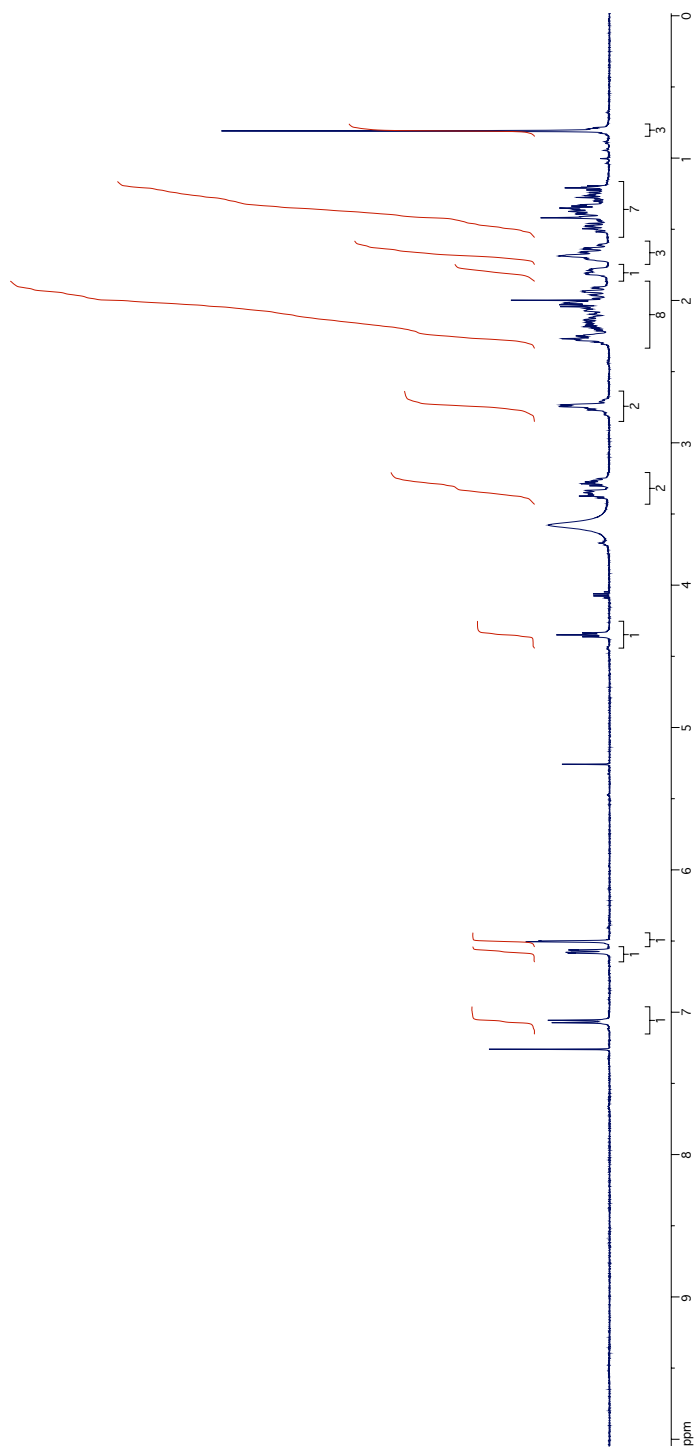
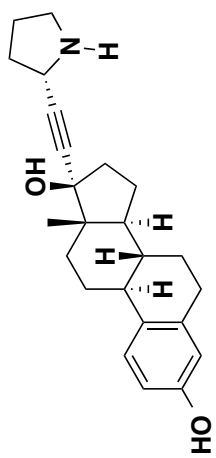




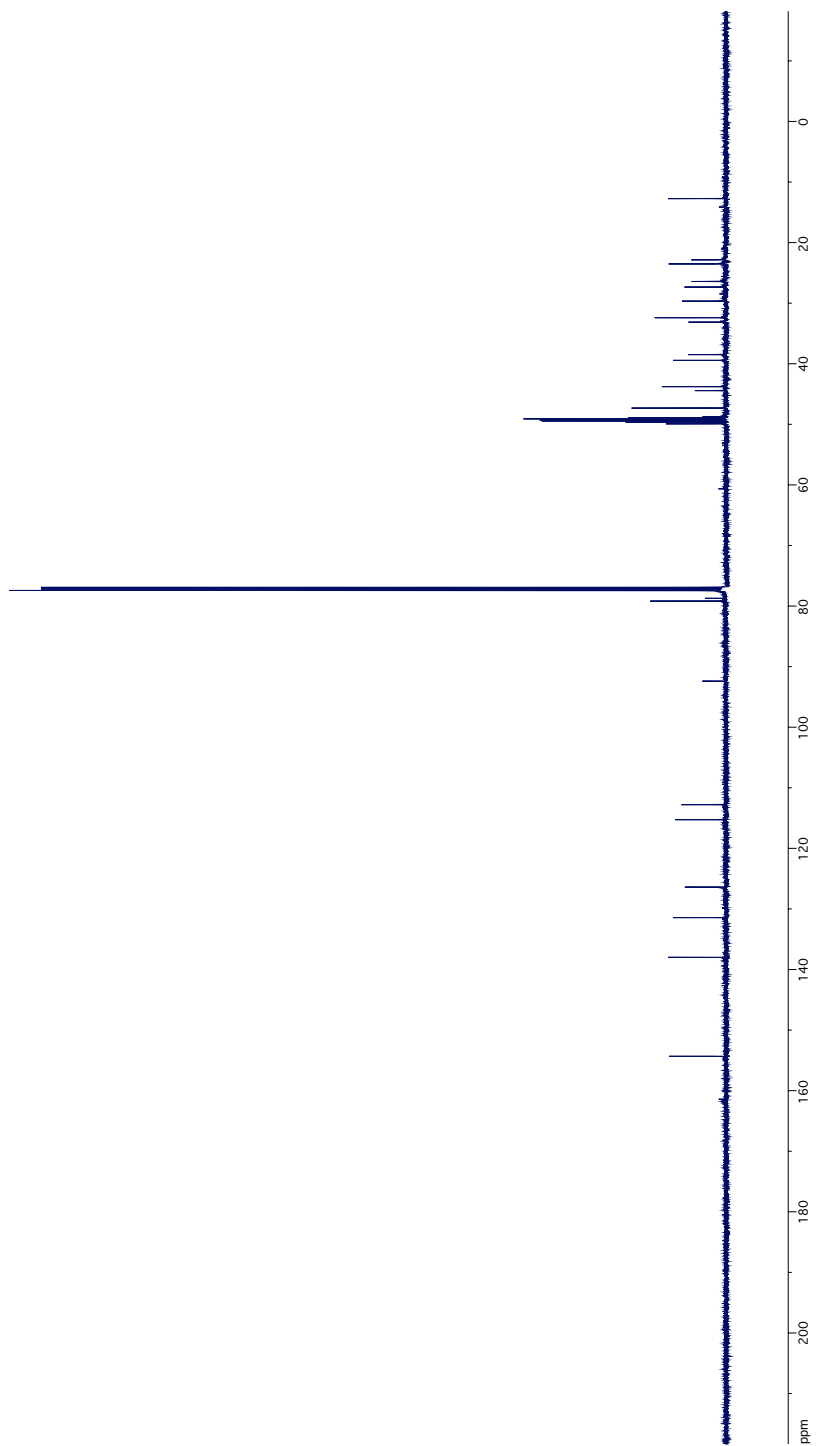
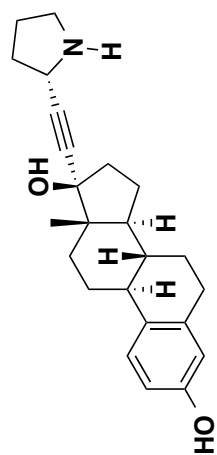
^{13}C NMR Spectrum of Compound 50



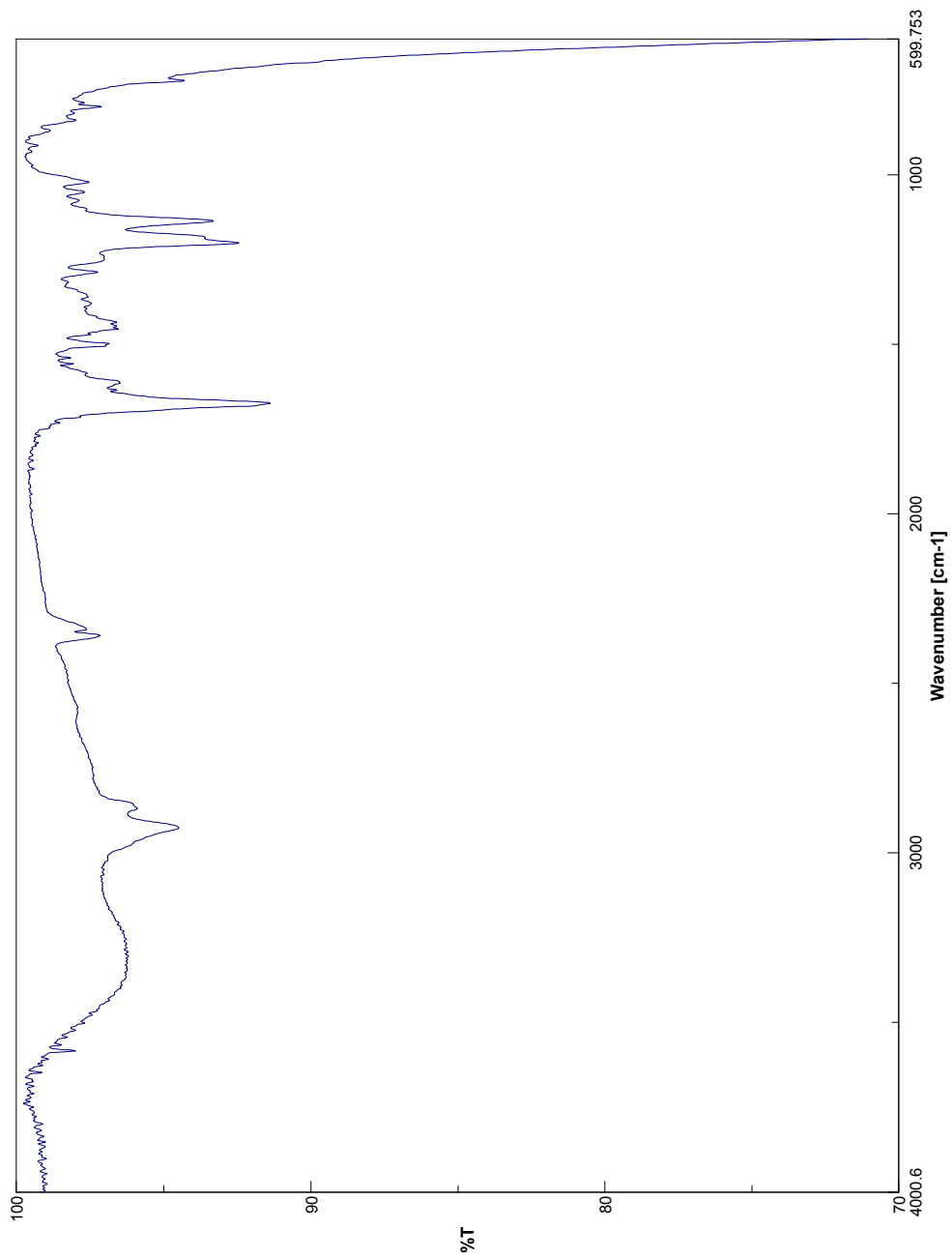
IR Spectrum of Compound **50**



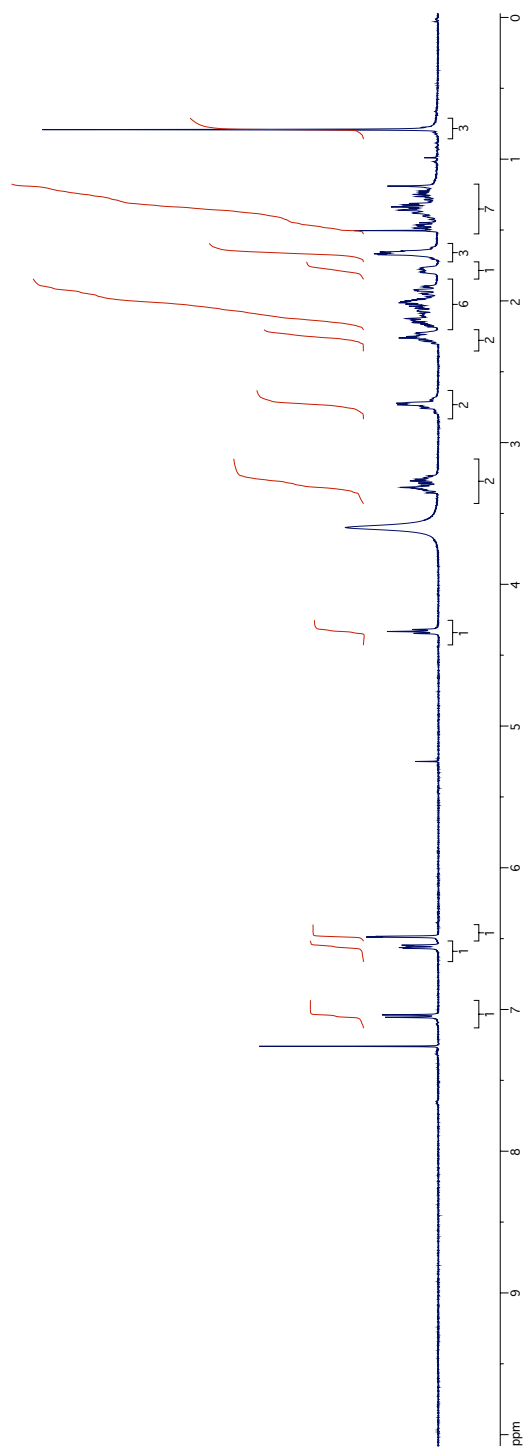
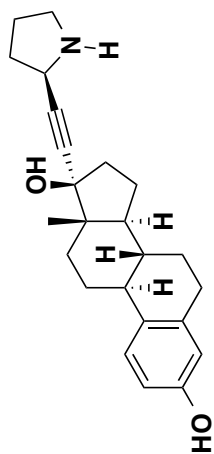
¹H NMR Spectrum of Compound 51



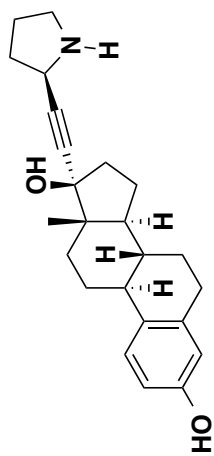
¹³C NMR Spectrum of Compound 51



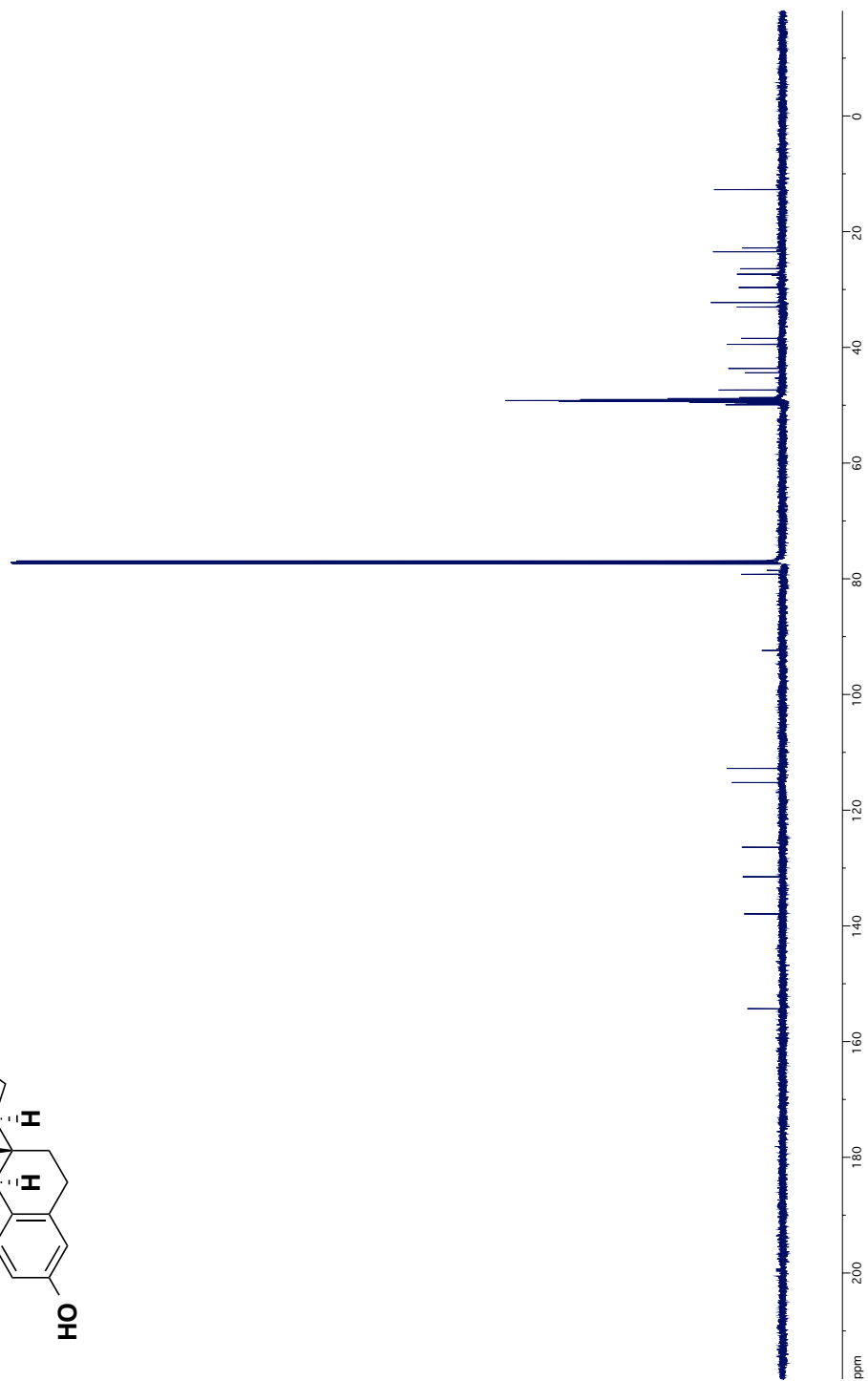
IR Spectrum of Compound **51**

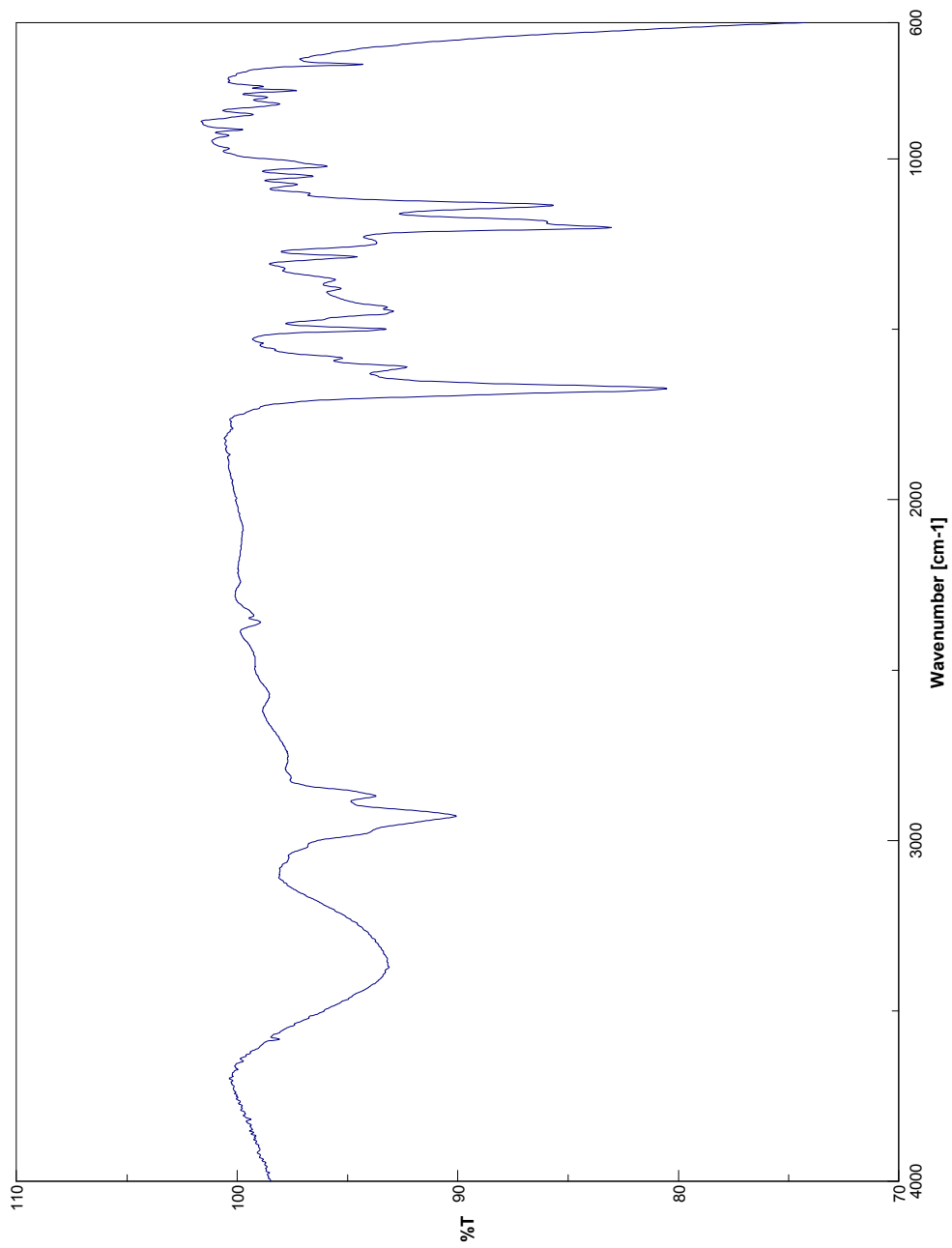


^1H NMR Spectrum of Compound 52

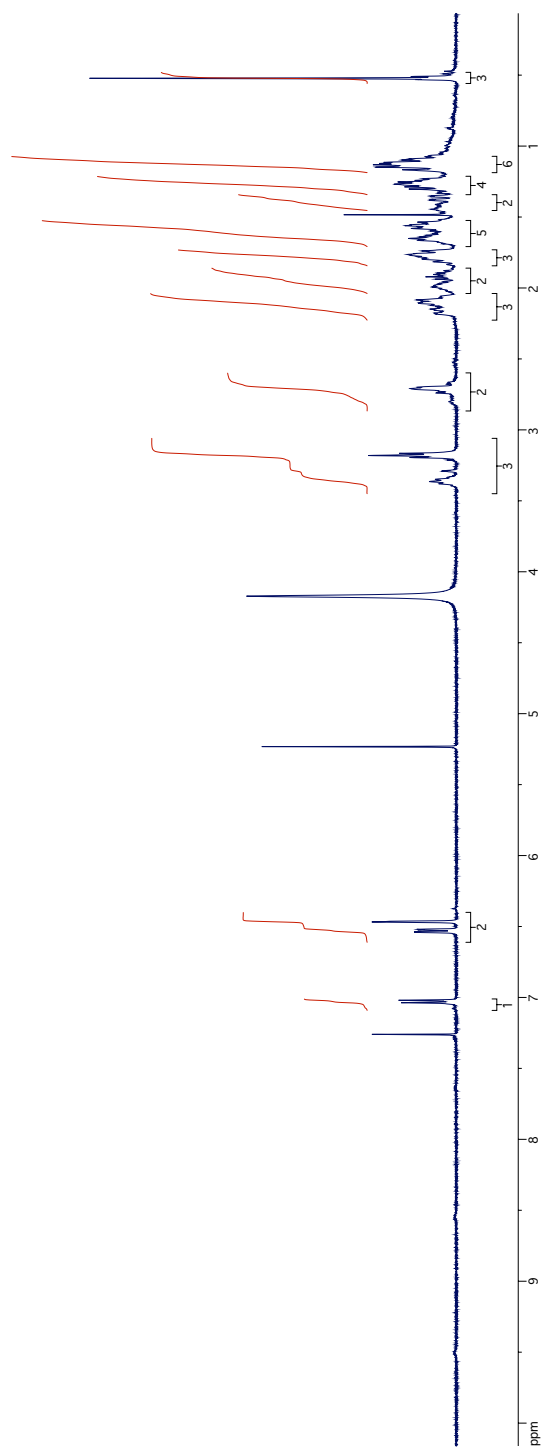
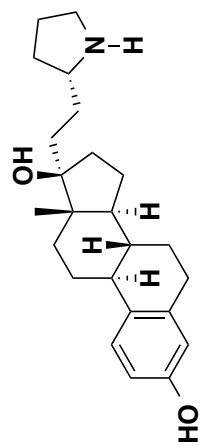


^{13}C NMR Spectrum of Compound **52**

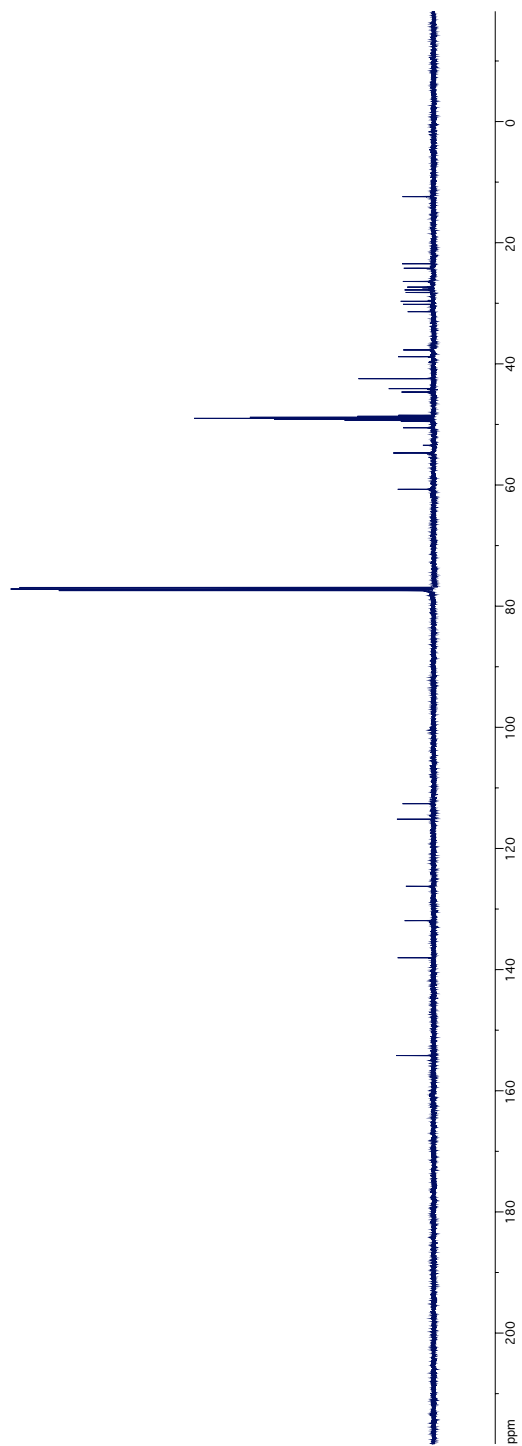
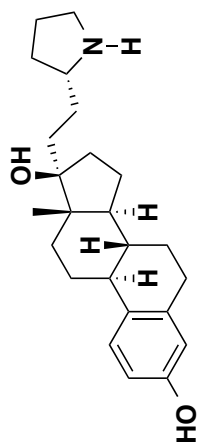




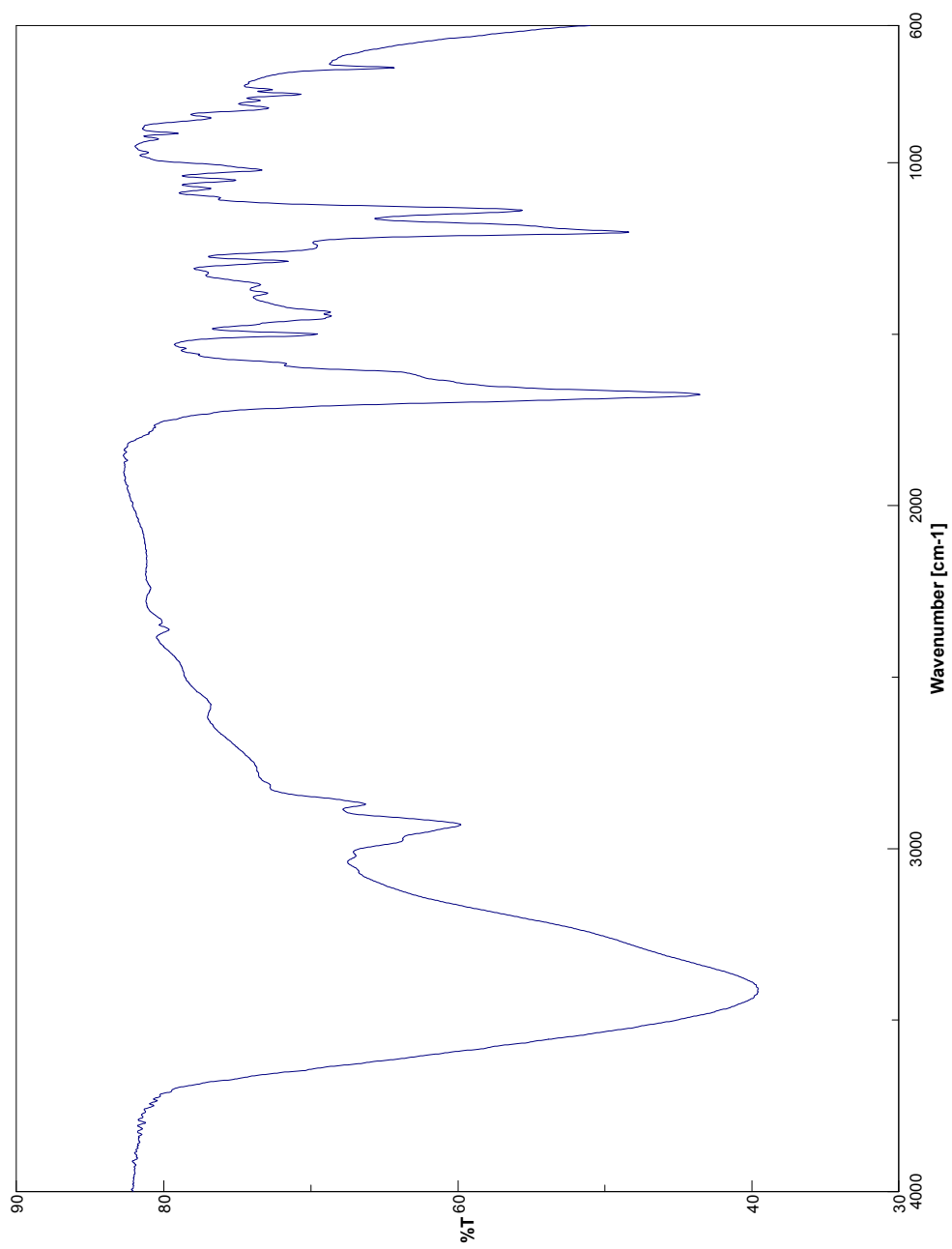
IR Spectrum of Compound **52**



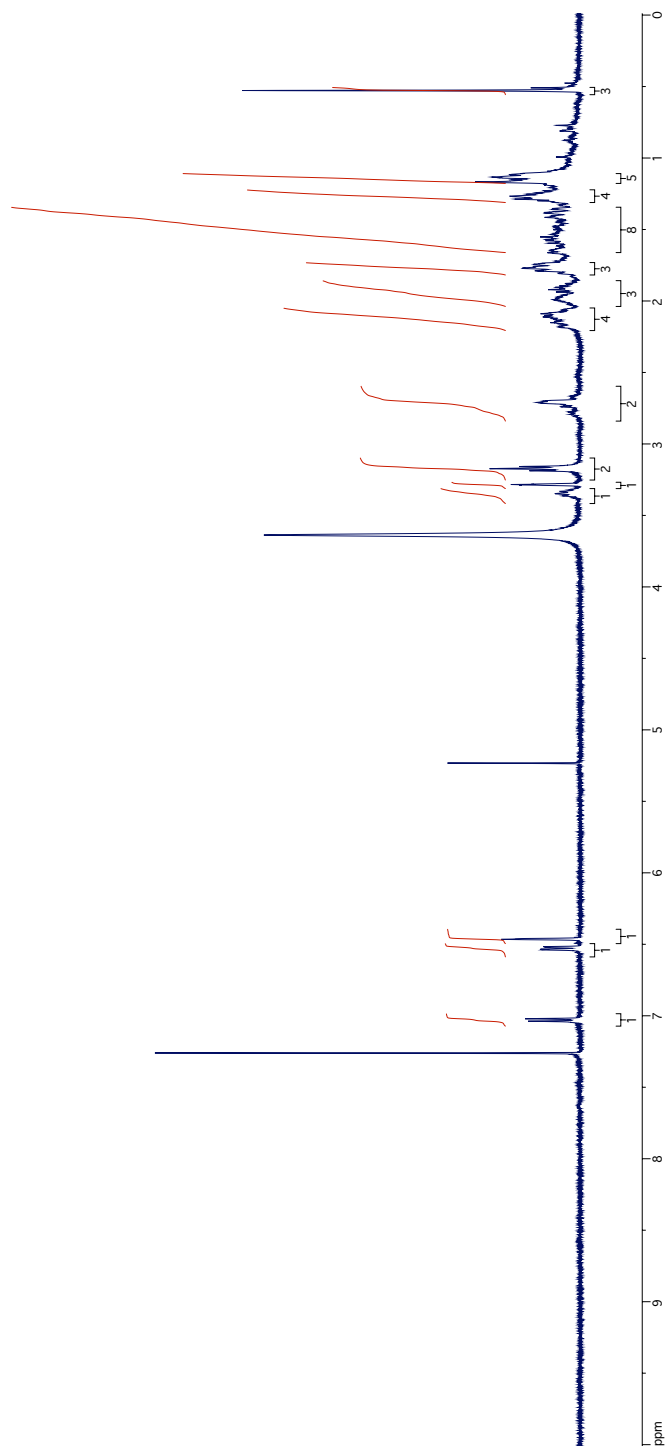
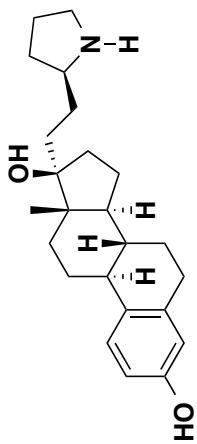
¹H NMR Spectrum of Compound 55



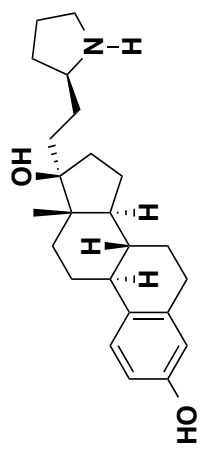
¹³C NMR Spectrum of Compound 55



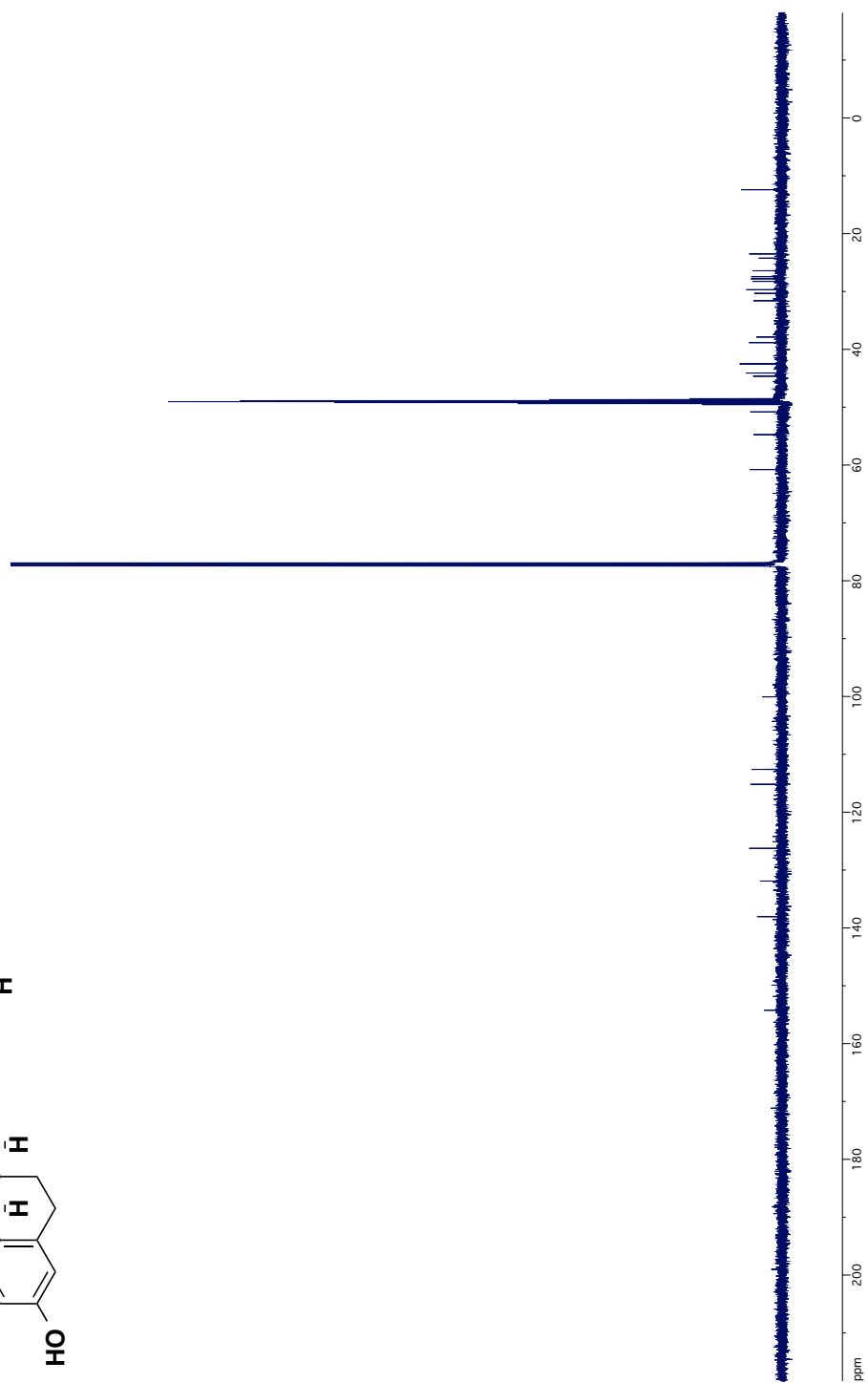
IR Spectrum of Compound **55**

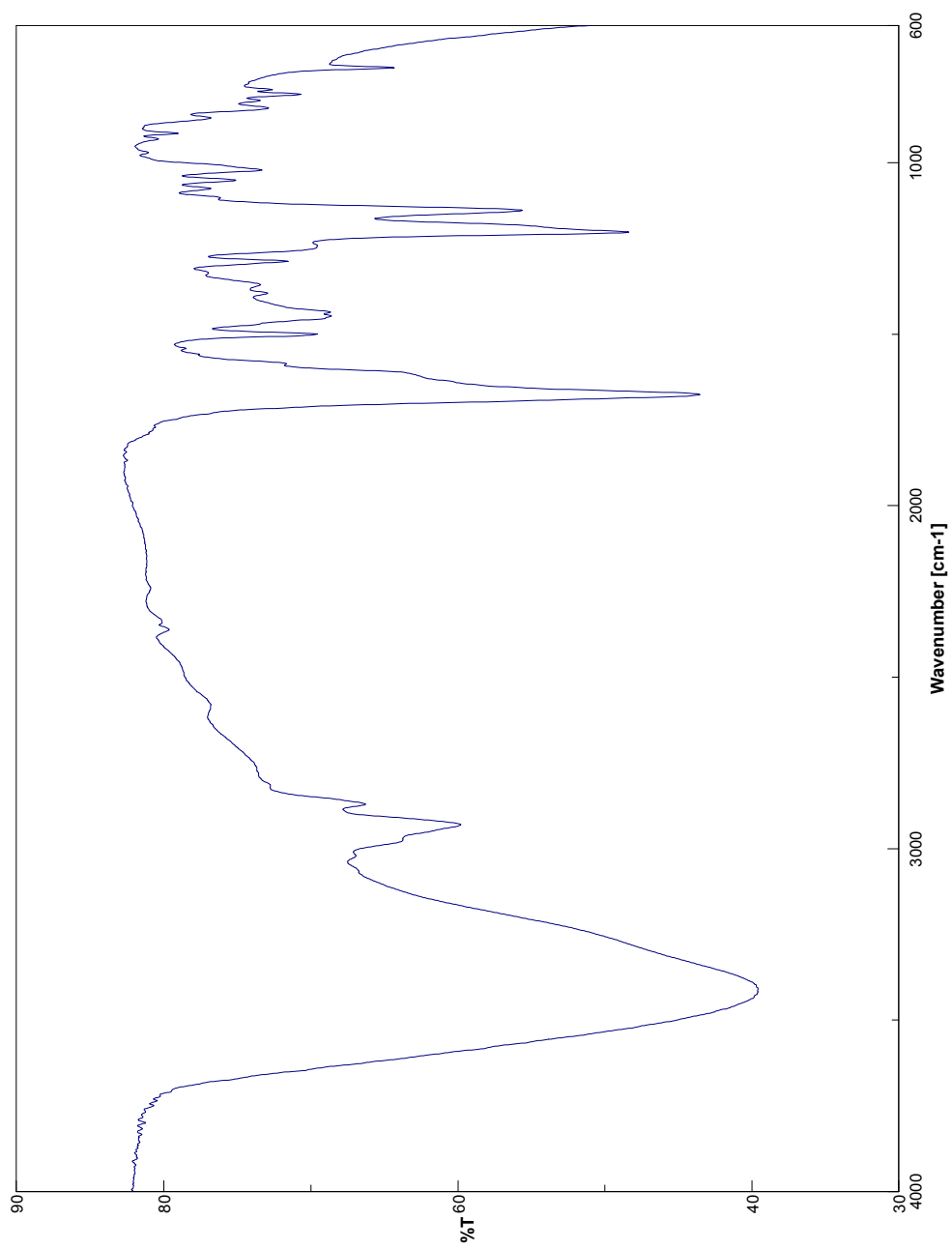


^1H NMR Spectrum of Compound 56

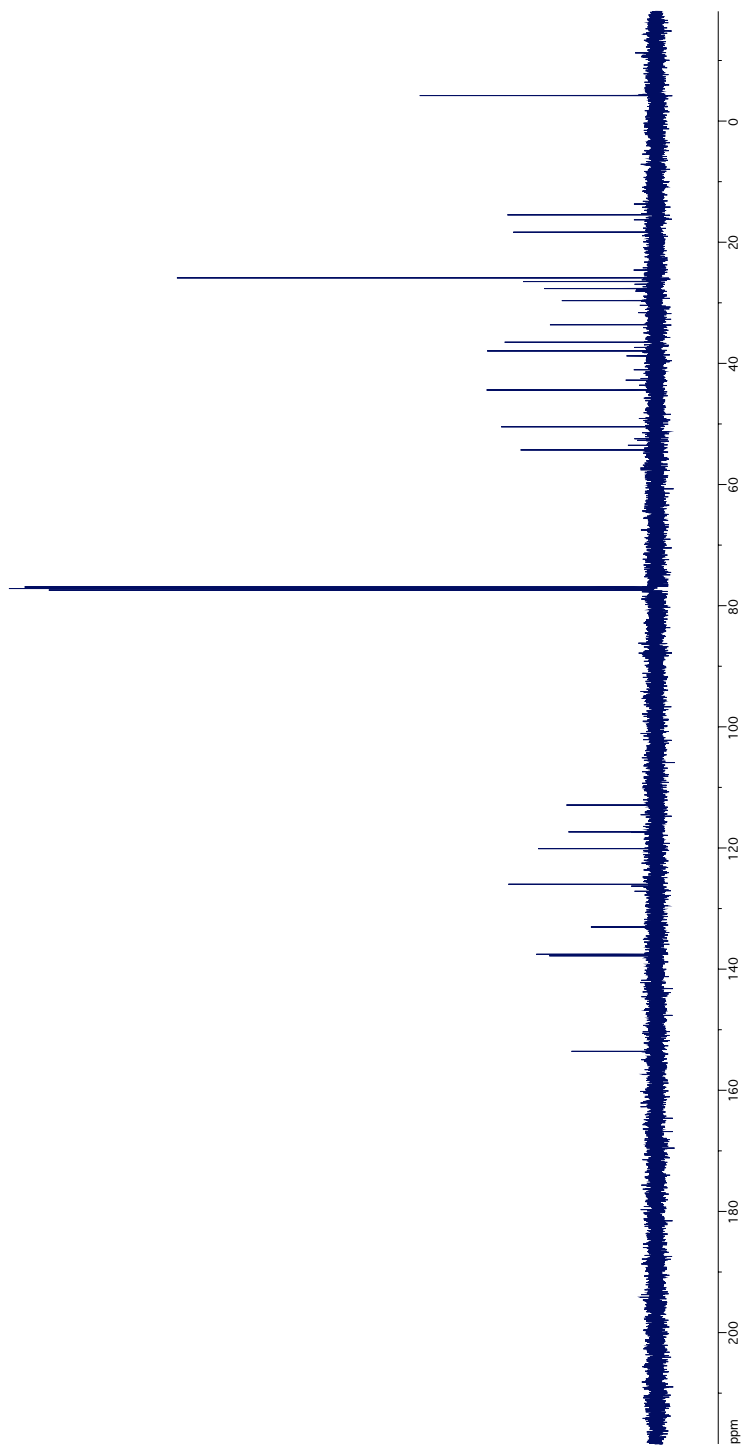
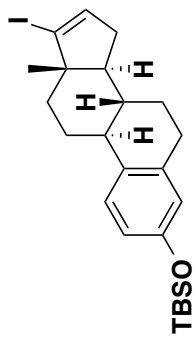


^{13}C NMR Spectrum of Compound **56**

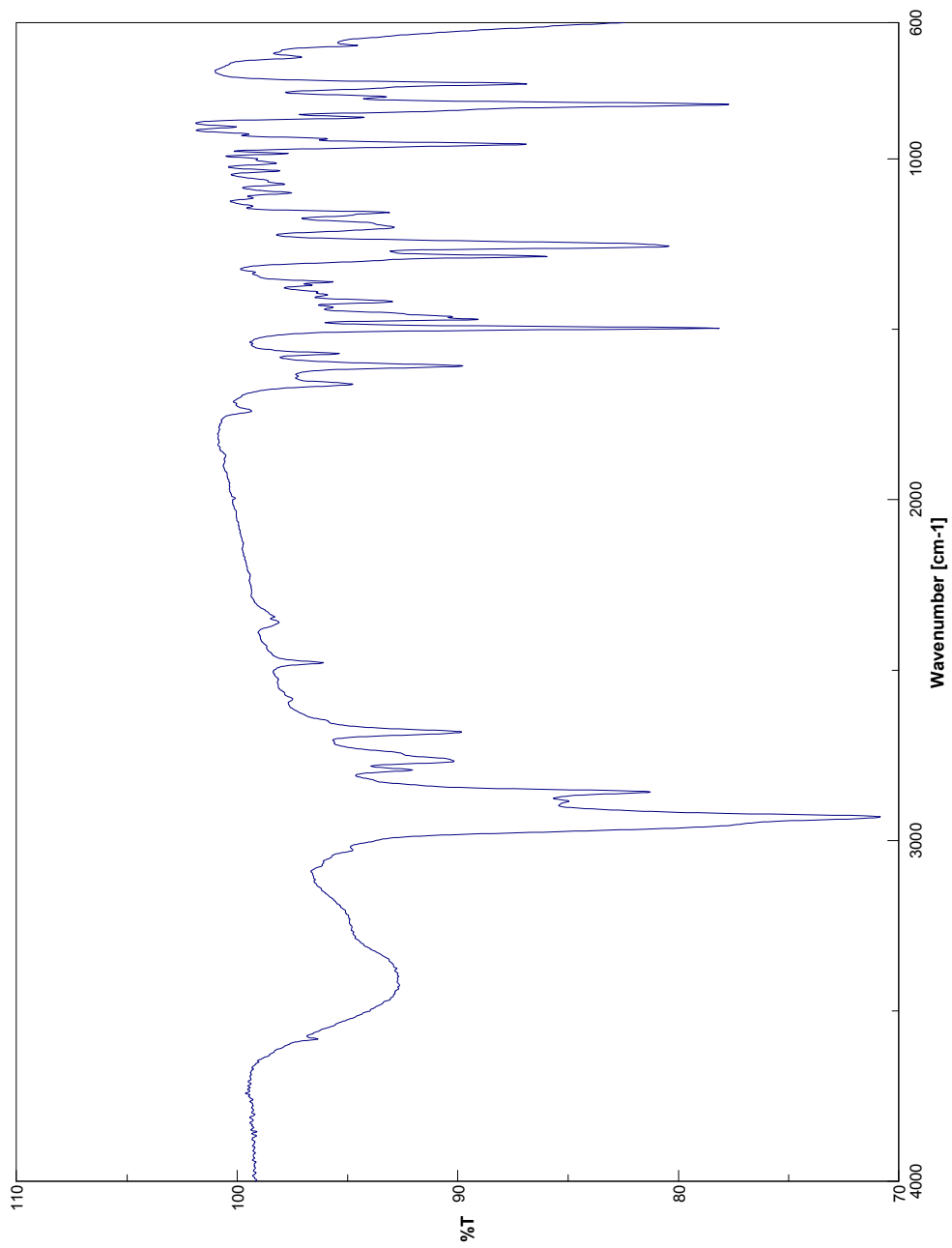




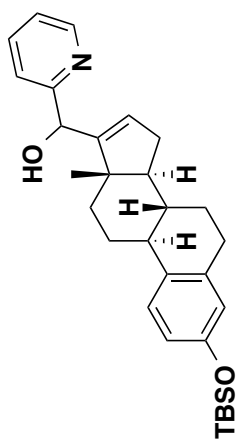
IR Spectrum of Compound **56**



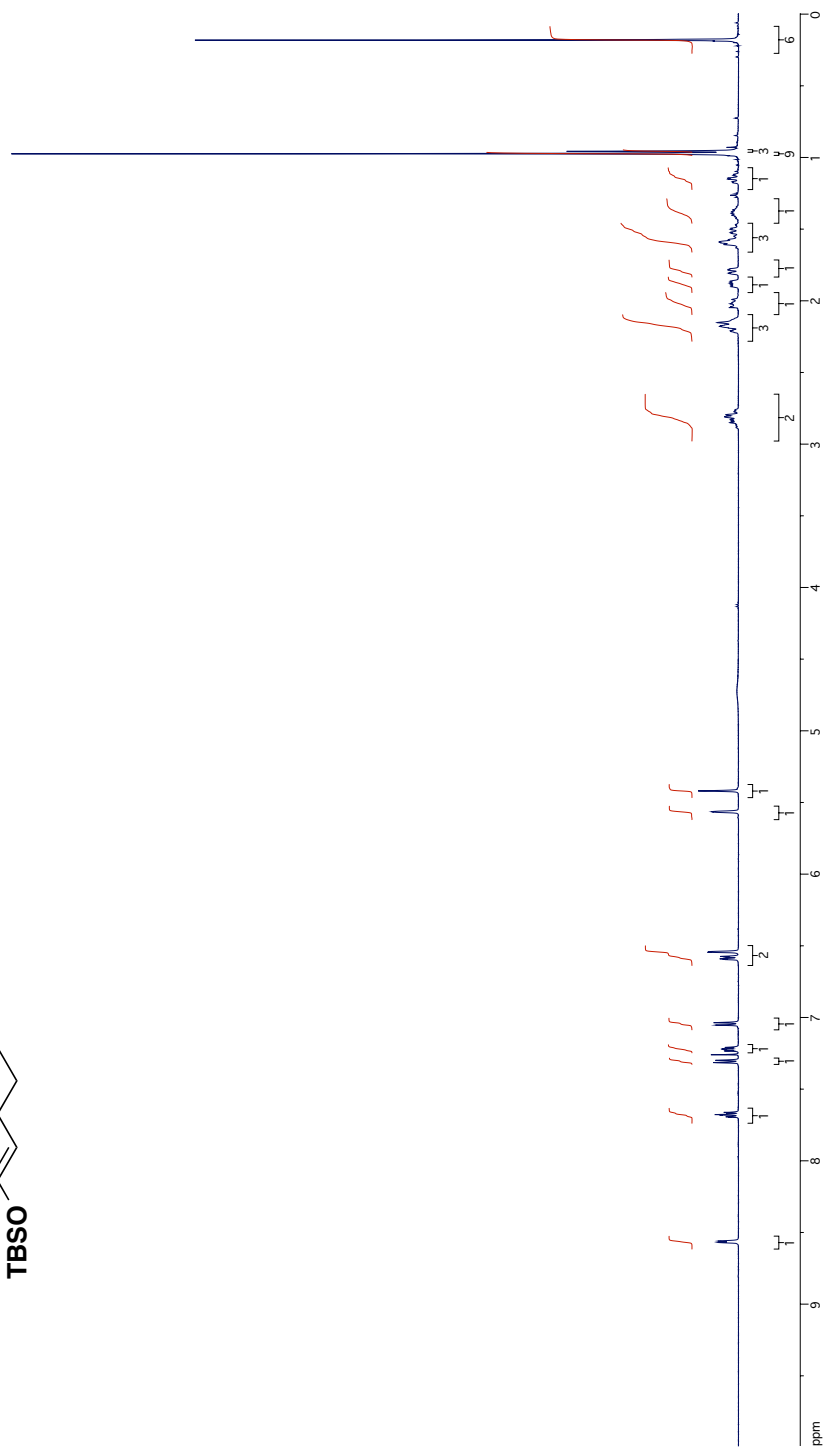
^{13}C NMR Spectrum of Compound **57**

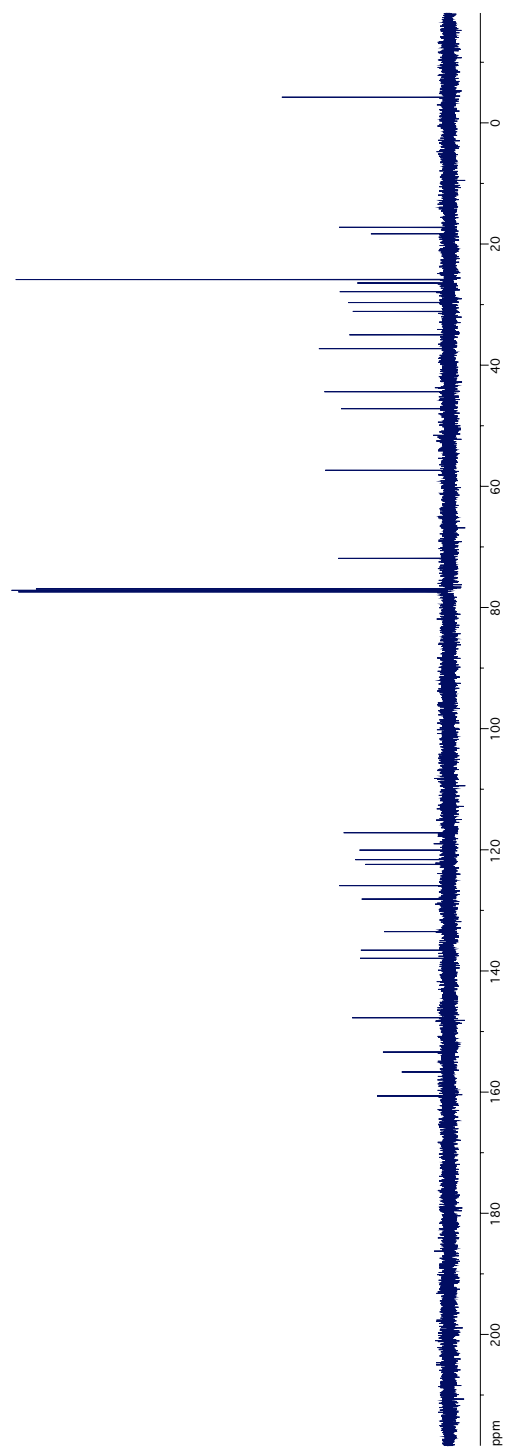
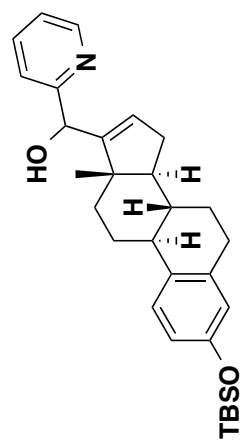


IR Spectrum of Compound **57**

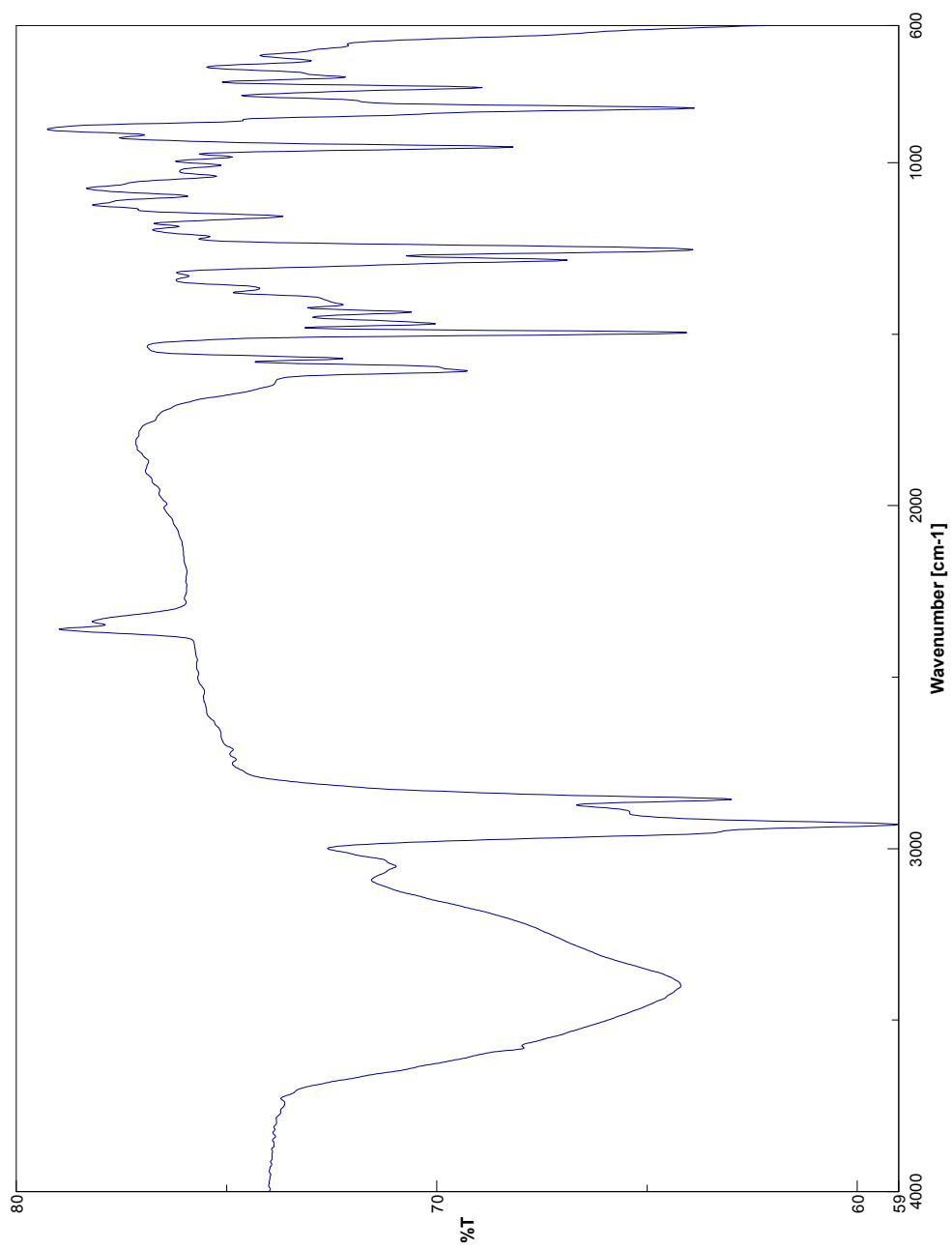


^1H NMR Spectrum of Compound **58a**

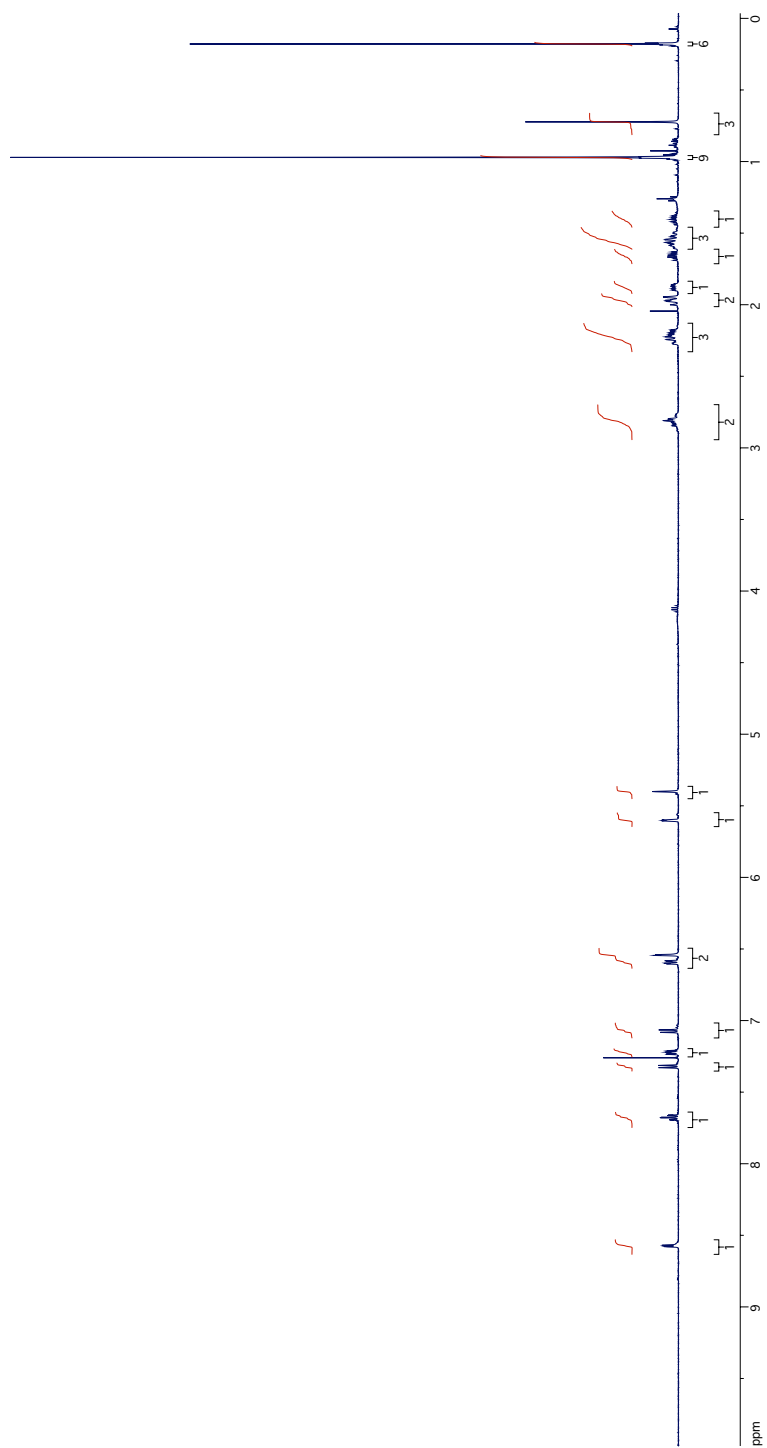
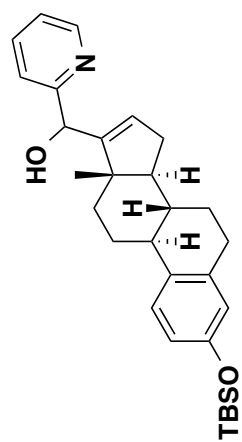




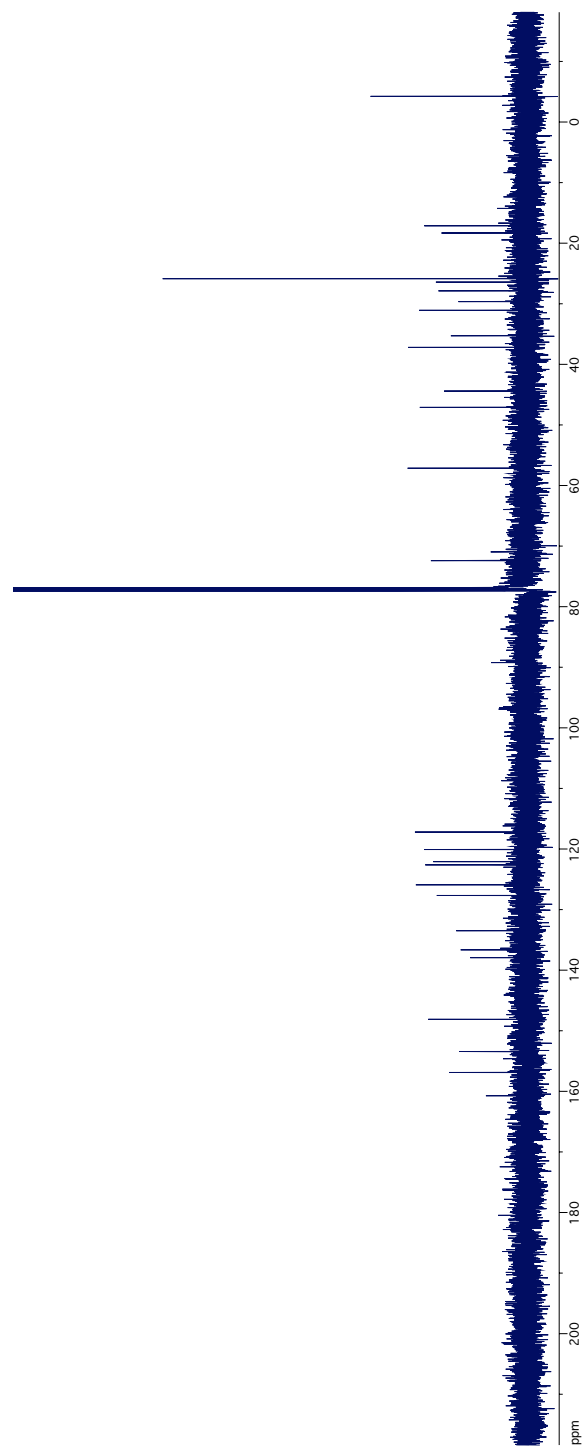
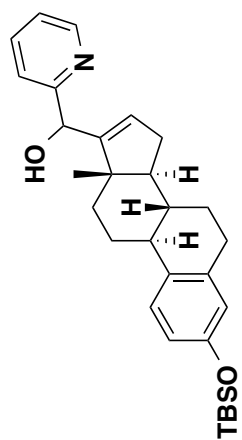
¹³C NMR Spectrum of Compound 58a



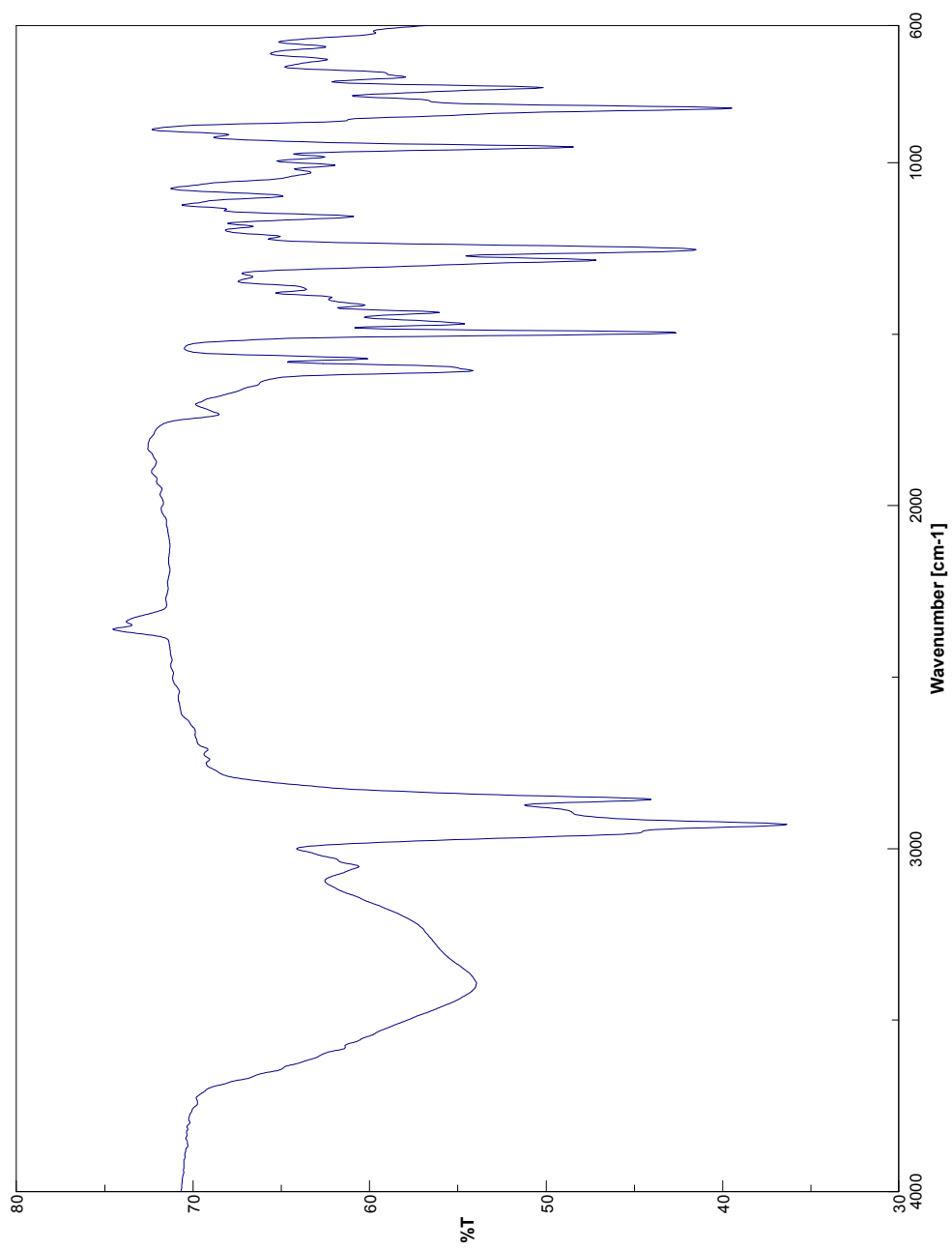
IR Spectrum of Compound **58a**



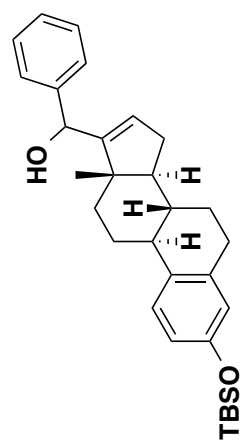
¹H NMR Spectrum of Compound 58b



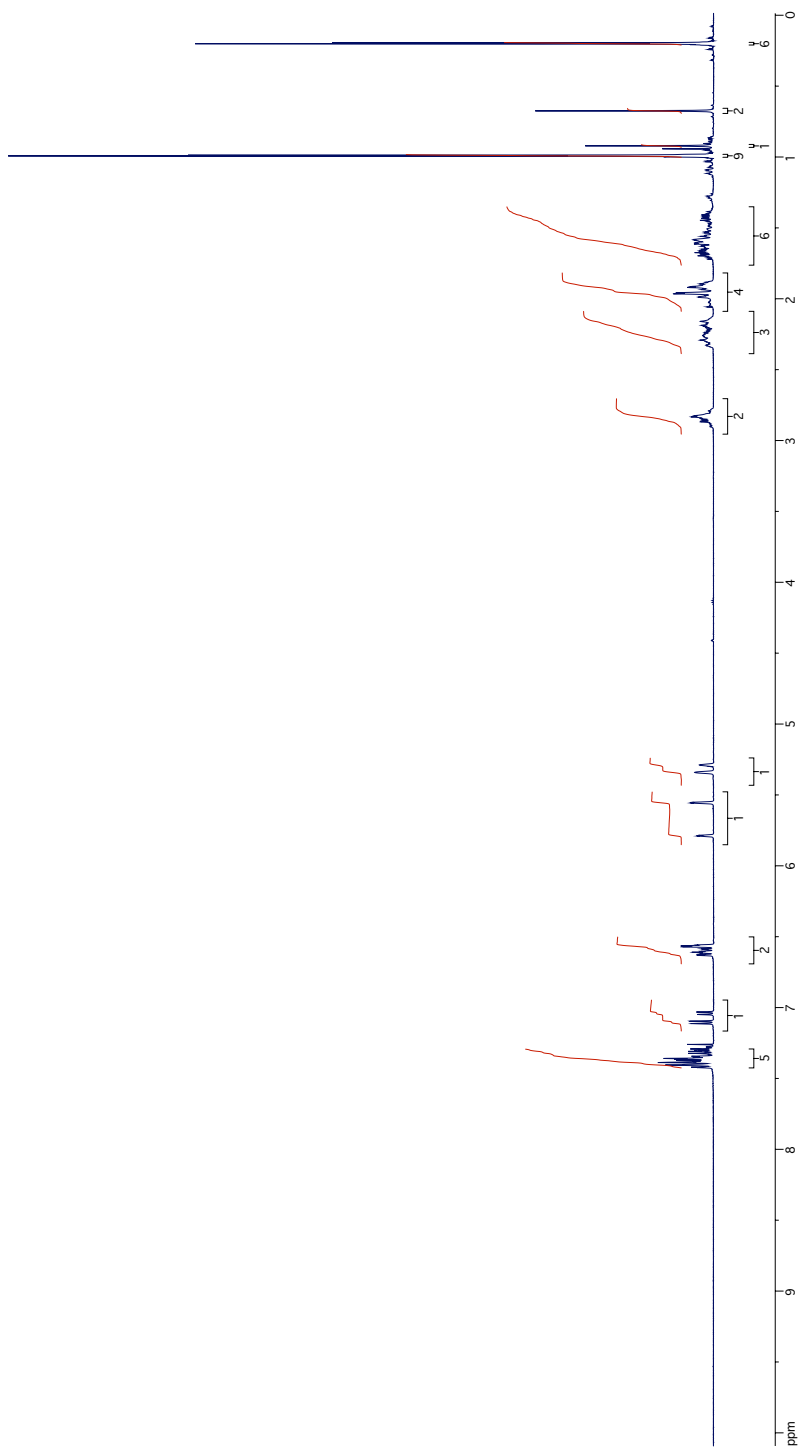
^{13}C NMR Spectrum of Compound 58b

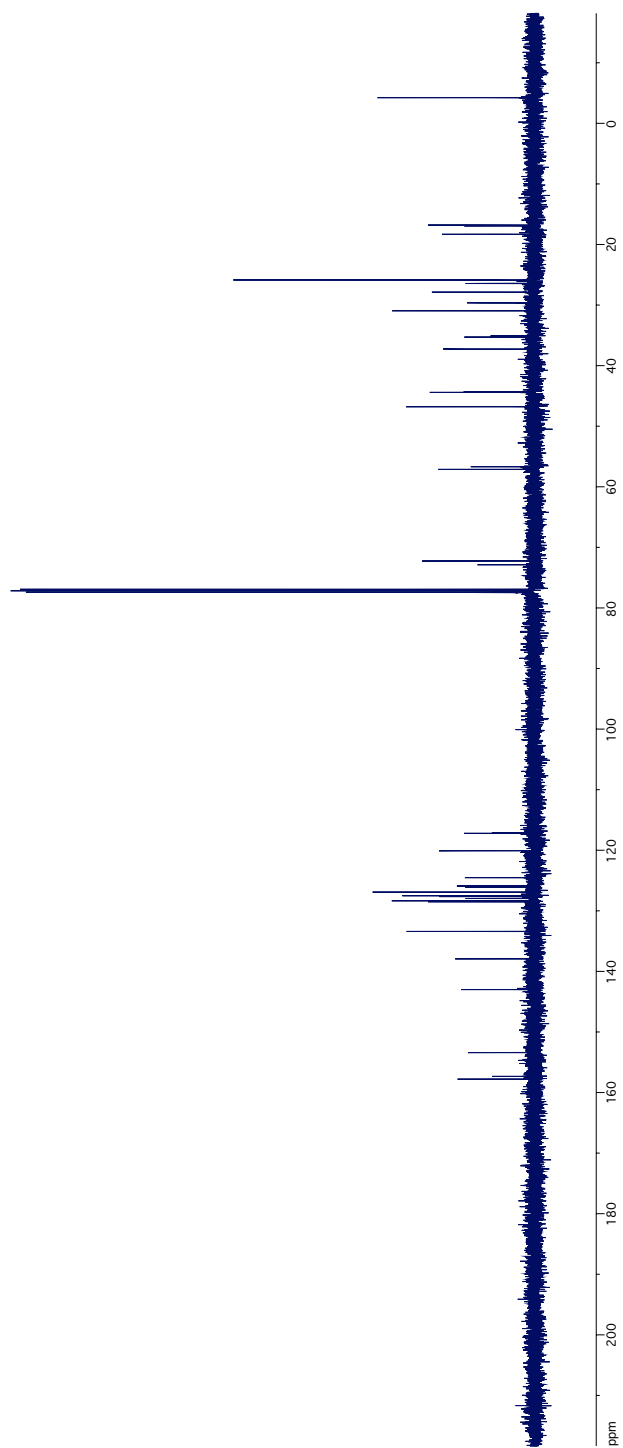
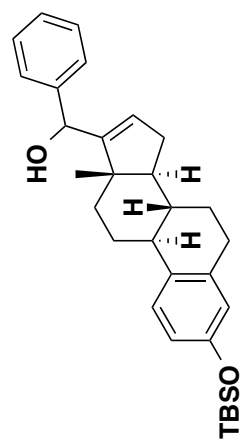


IR Spectrum of Compound **58b**

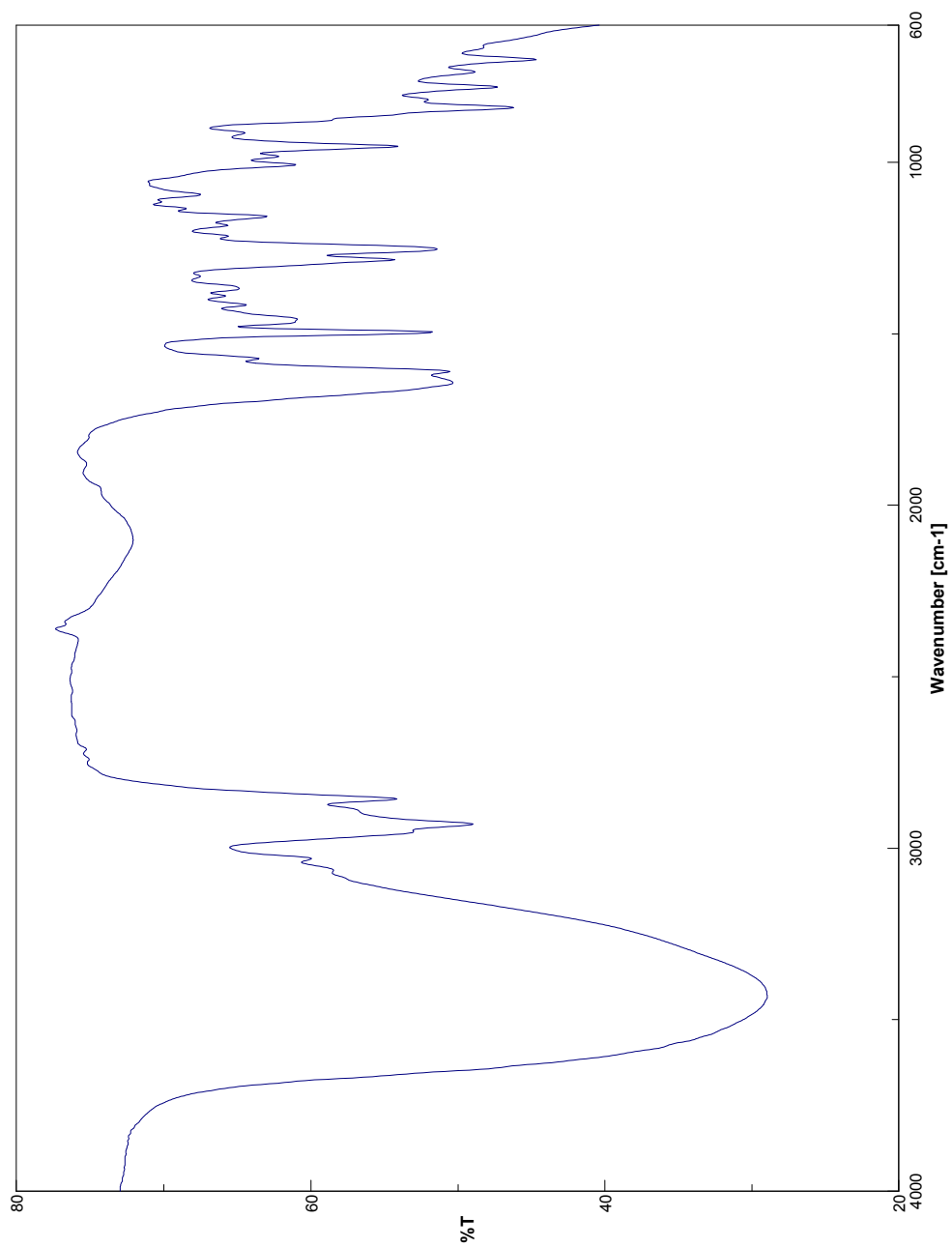


¹H NMR Spectrum of Compound 59

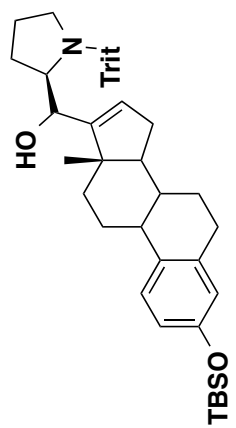




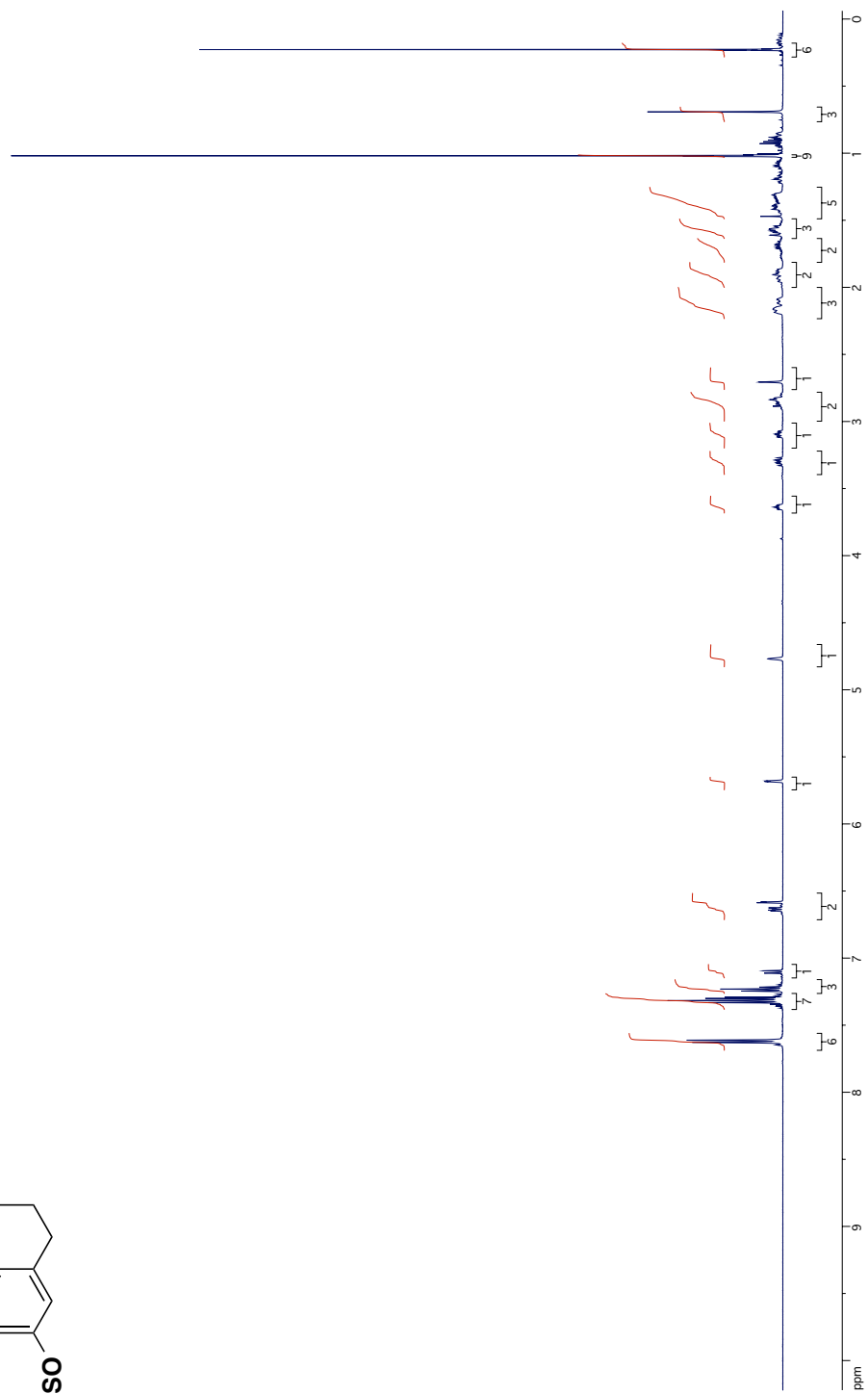
^{13}C NMR Spectrum of Compound 59

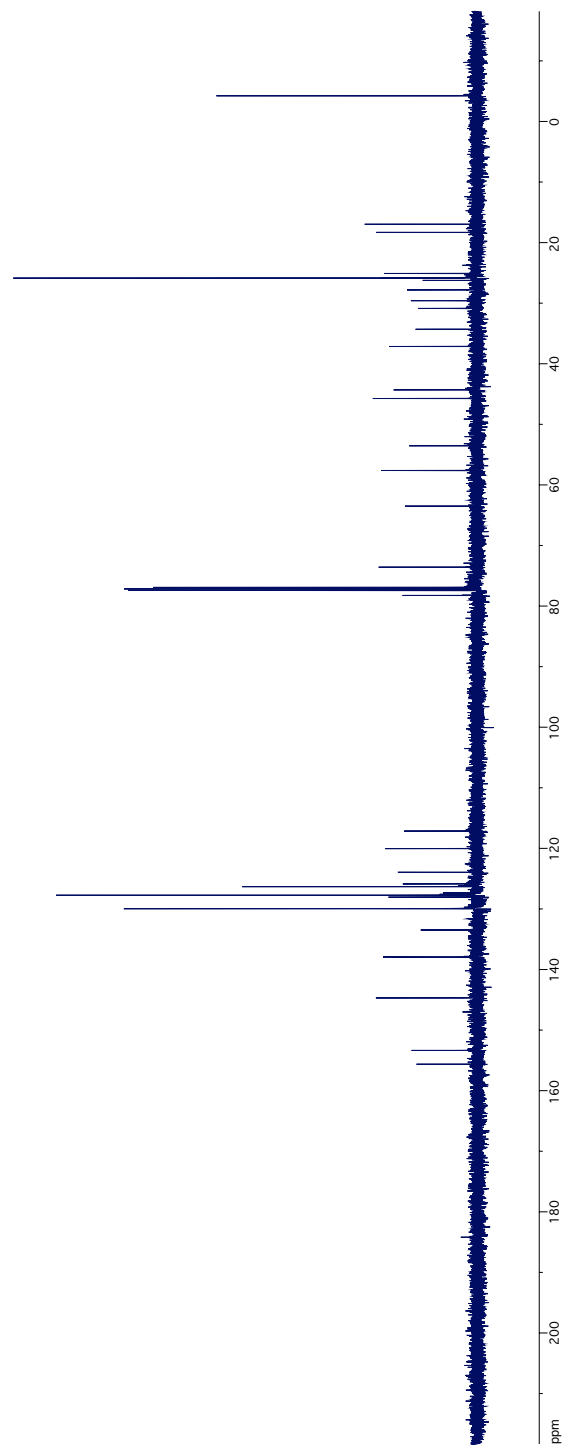
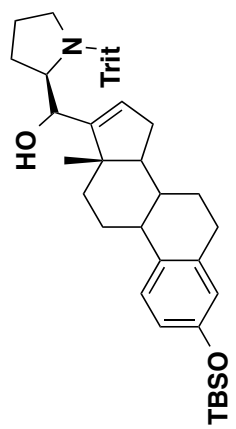


IR Spectrum of Compound **59**

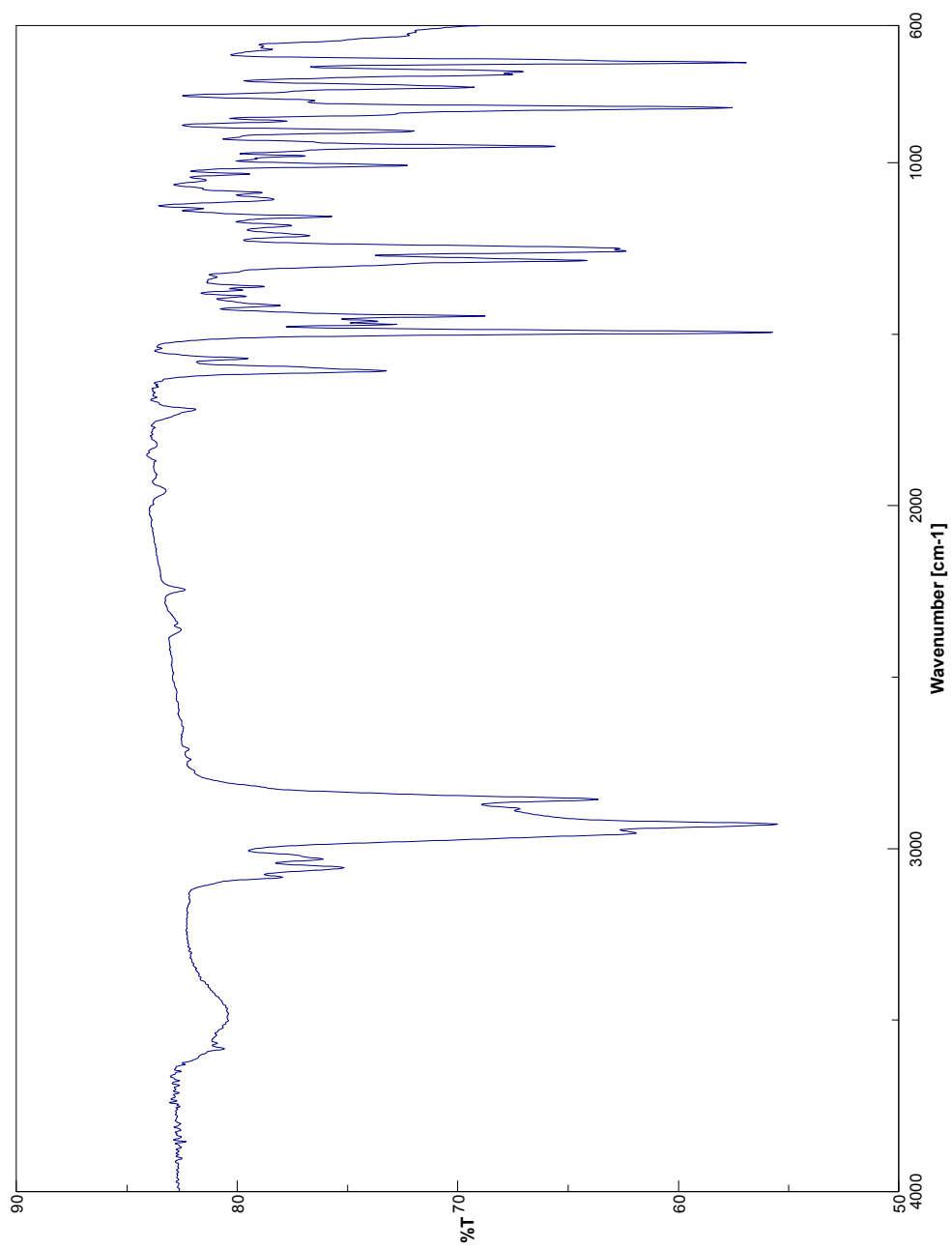


^1H NMR Spectrum of Compound **60**

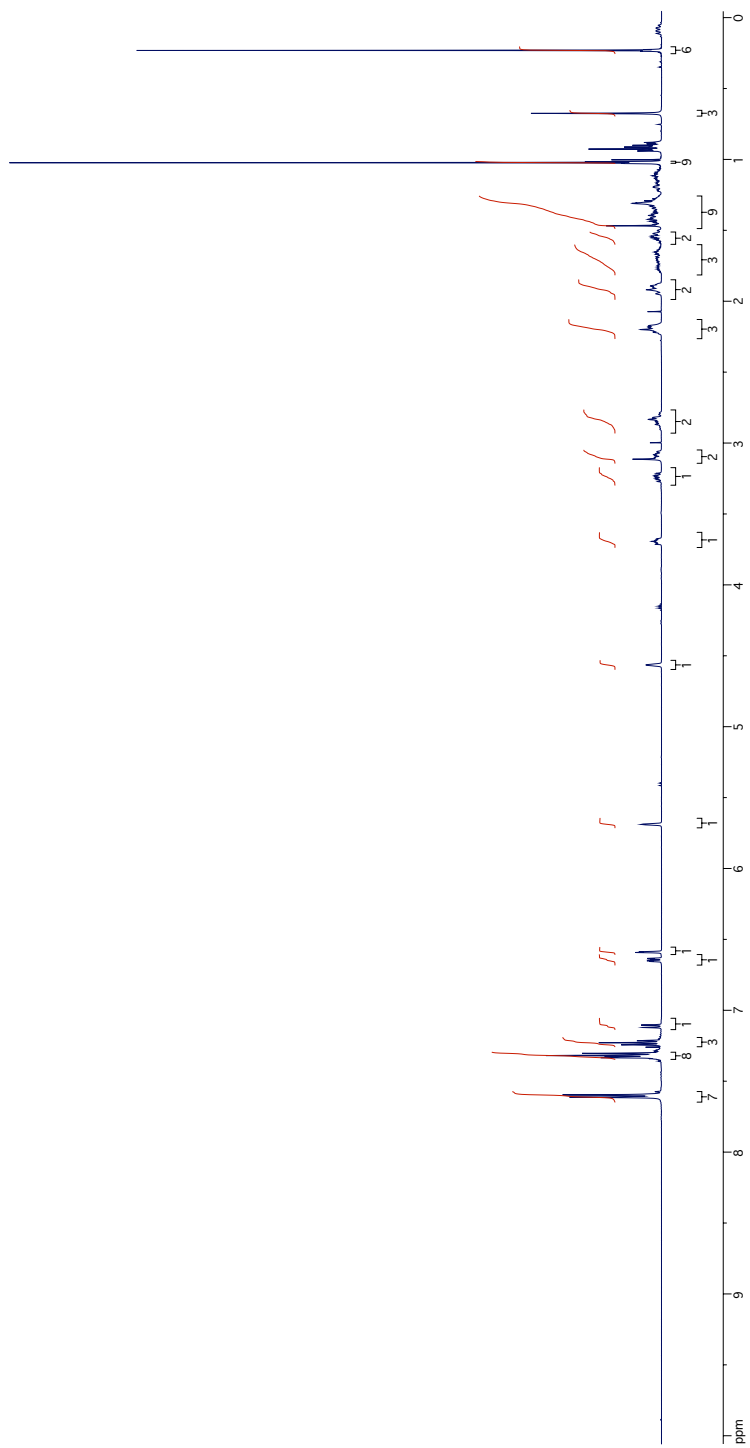
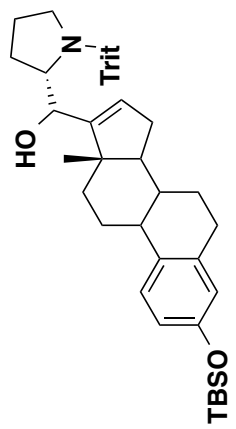




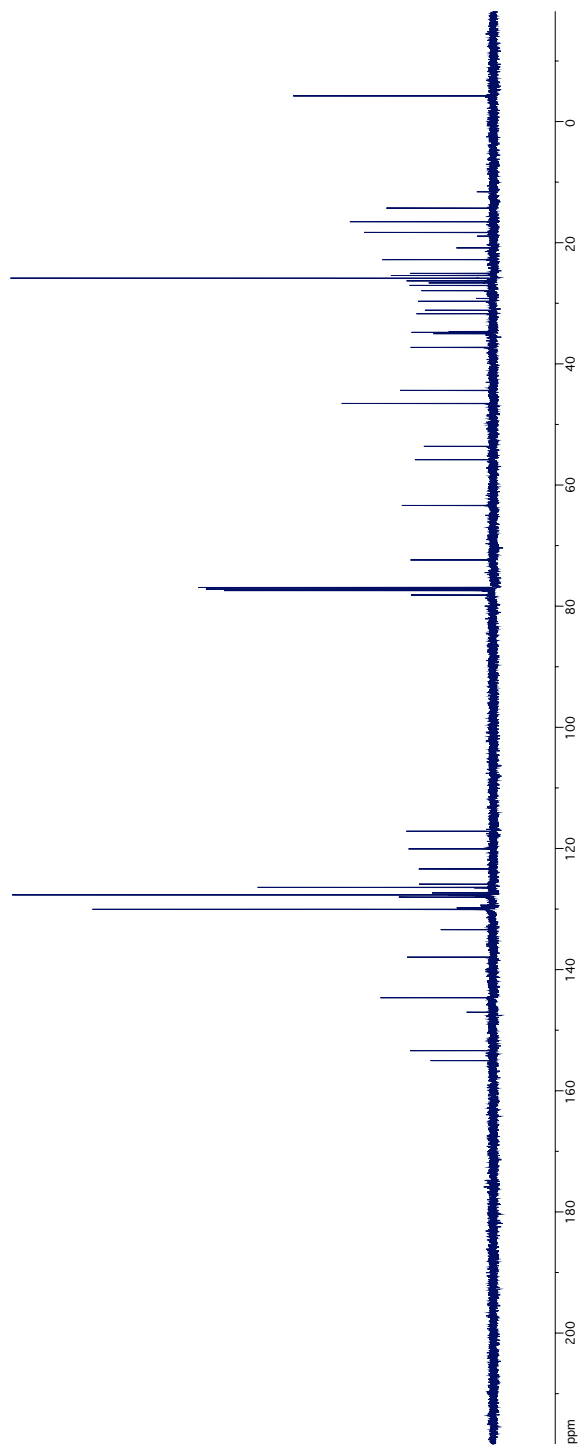
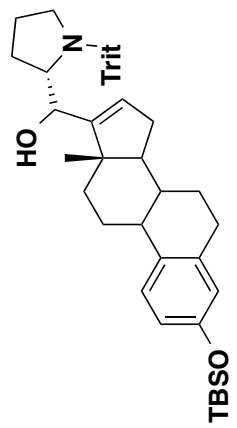
^{13}C NMR Spectrum of Compound 60



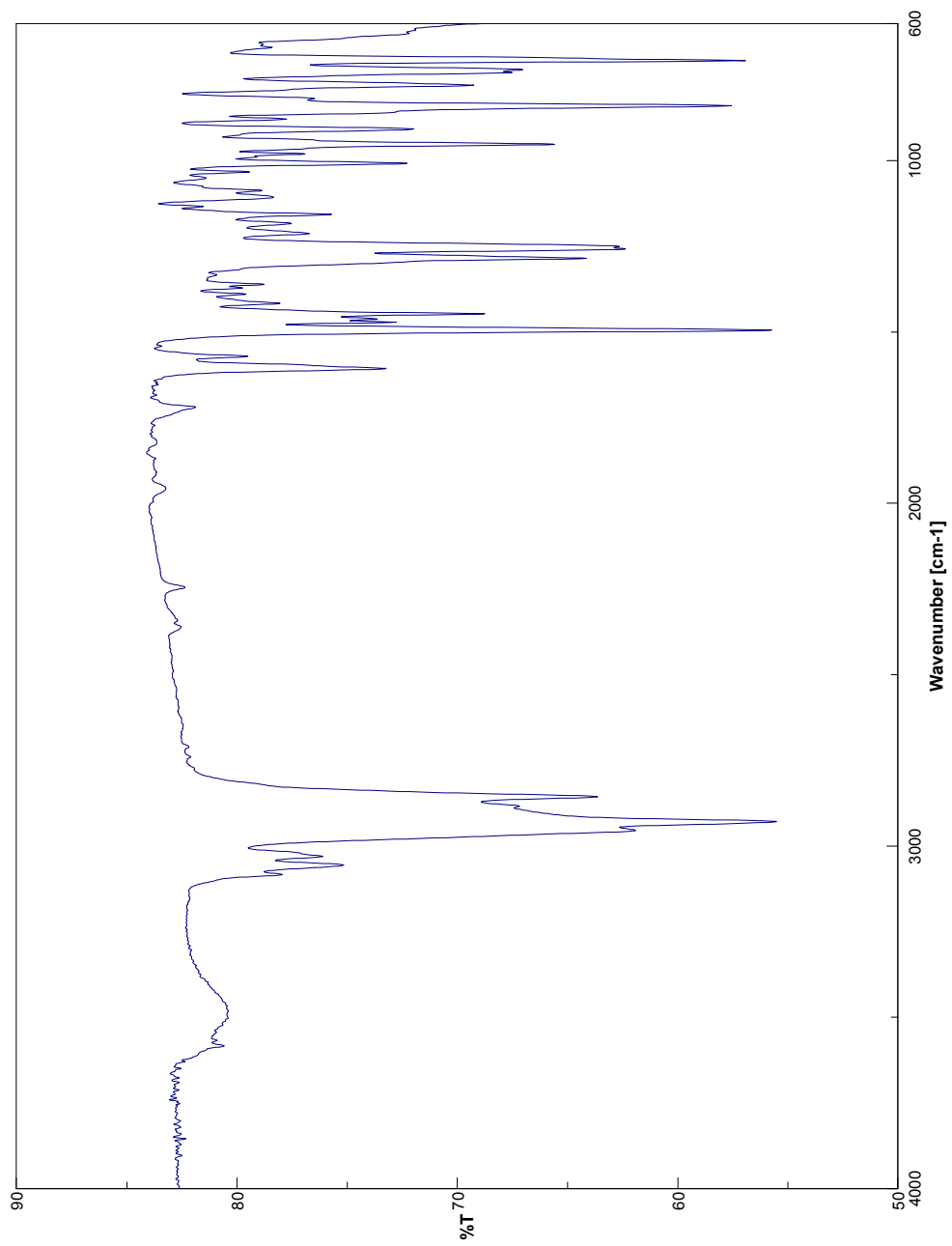
IR Spectrum of Compound **60**



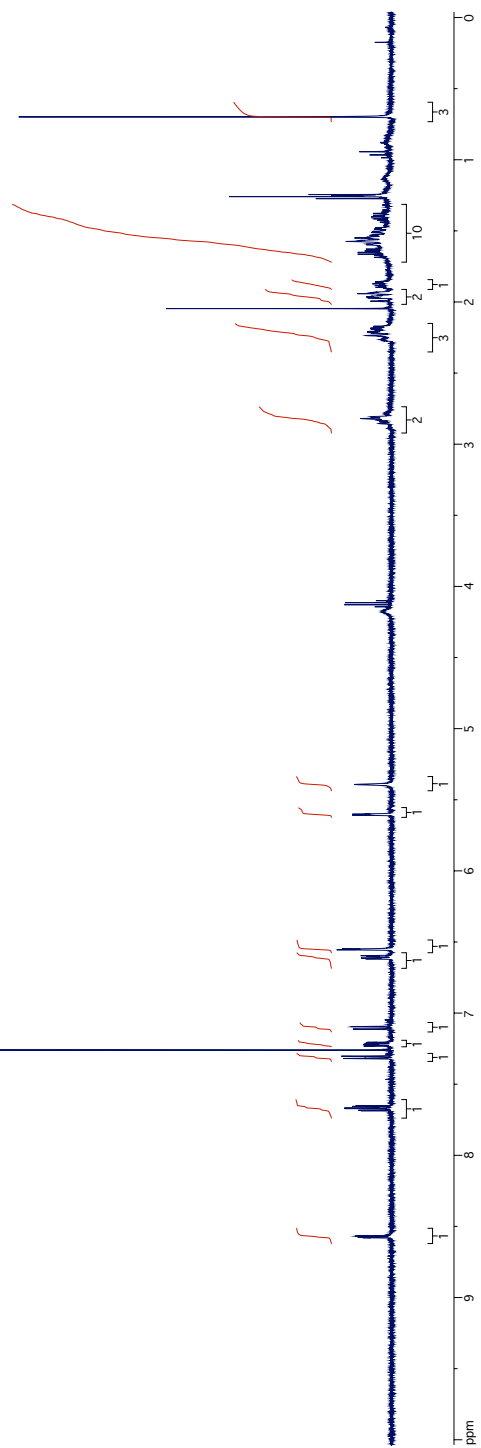
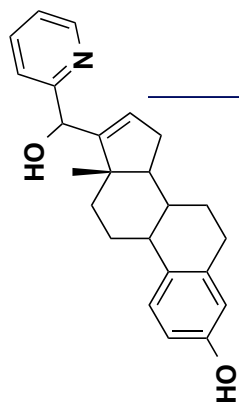
^1H NMR Spectrum of Compound 61



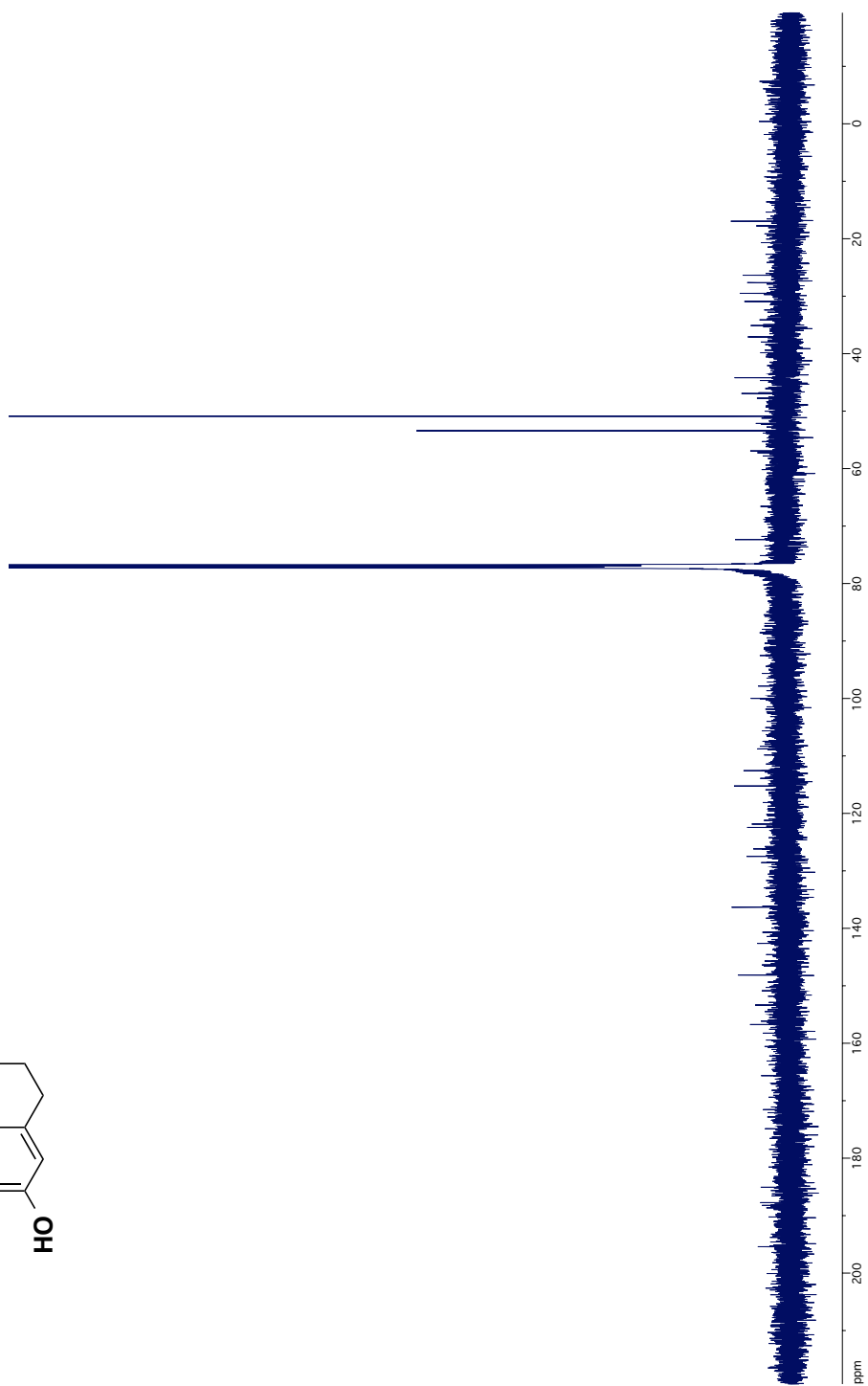
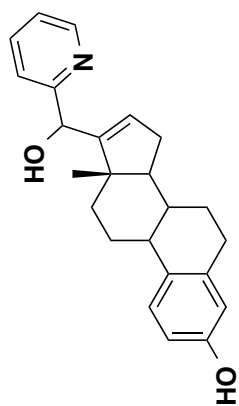
^{13}C NMR Spectrum of Compound **61**



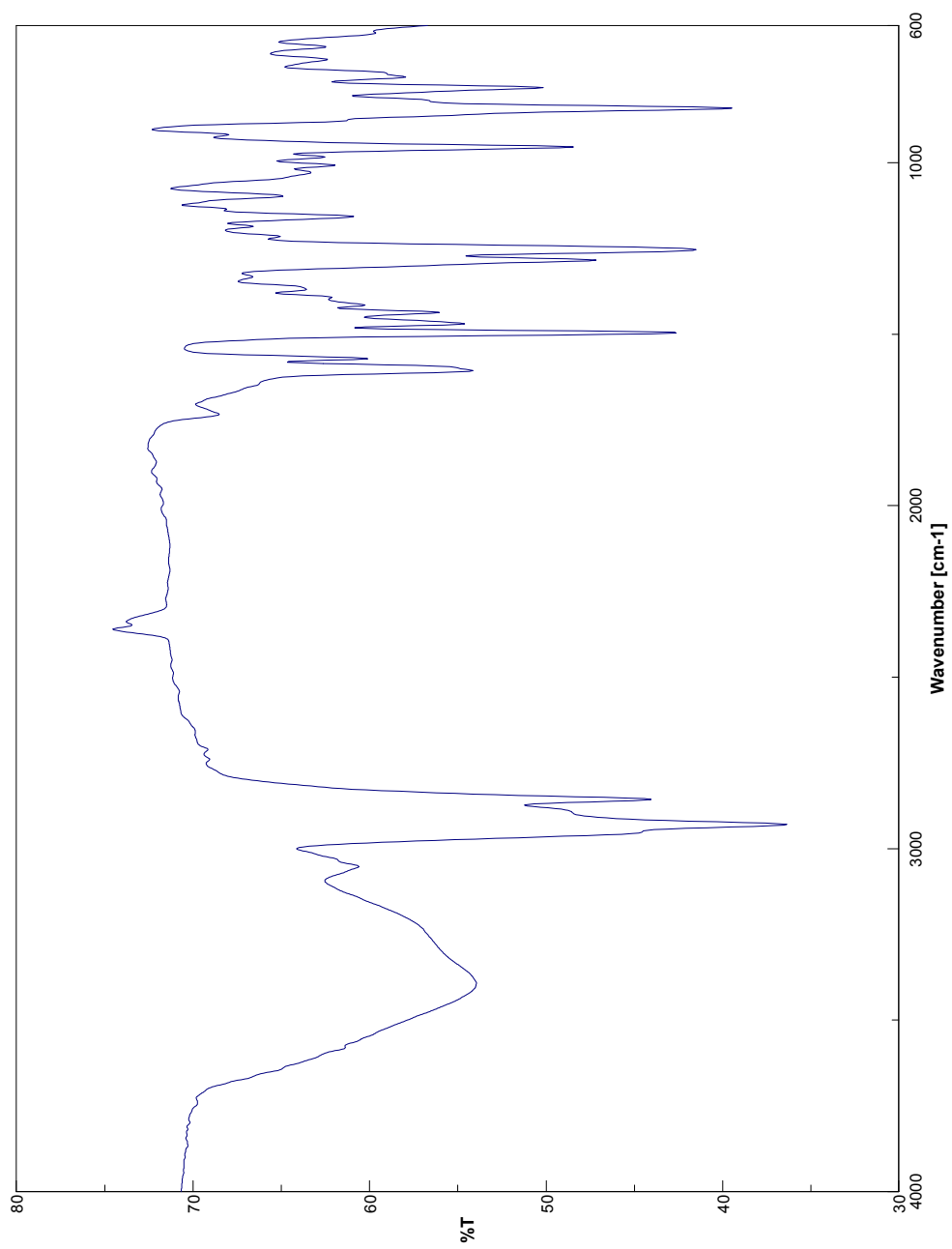
IR Spectrum of Compound **61**



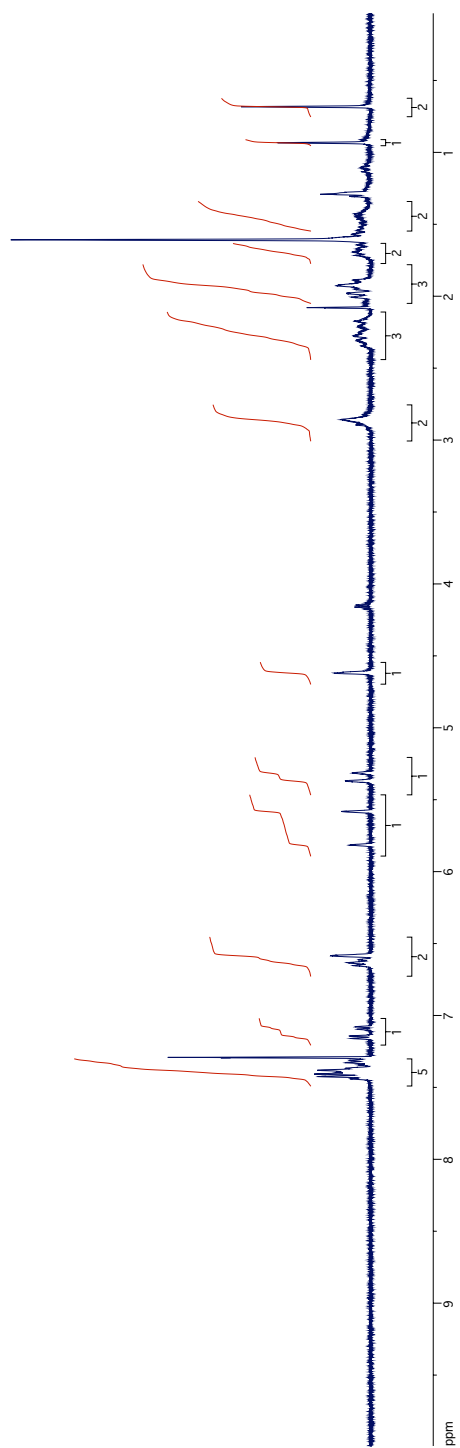
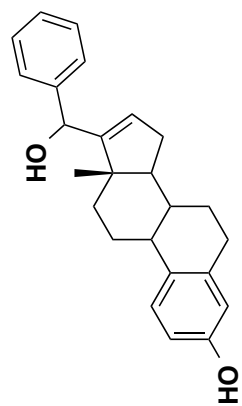
^1H NMR Spectrum of Compound 62



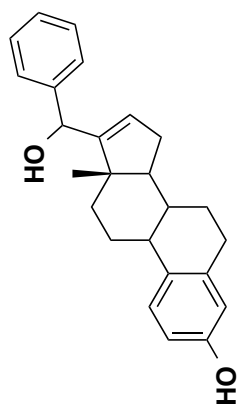
^{13}C NMR Spectrum of Compound 62



IR Spectrum of Compound **62**

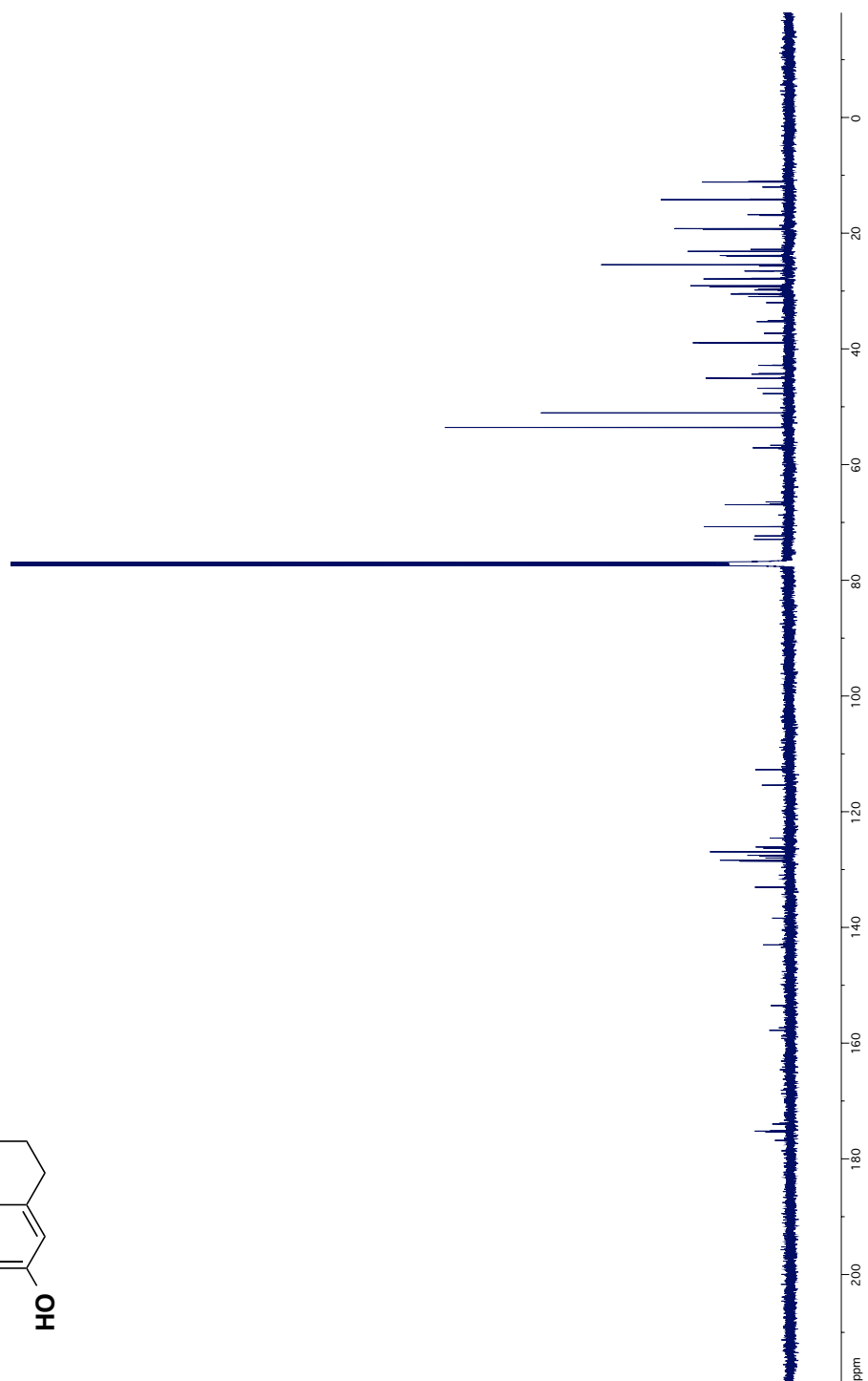


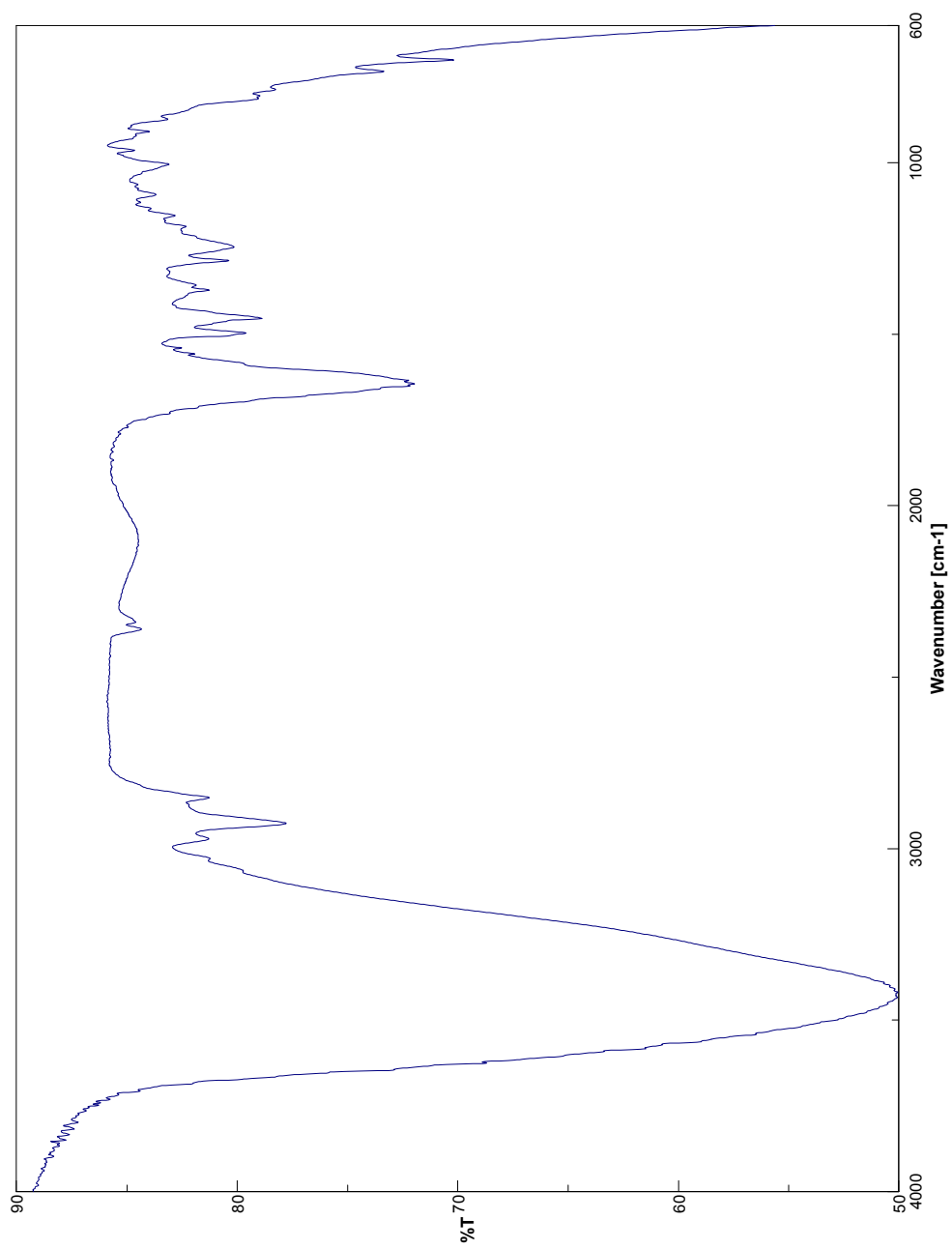
¹H NMR Spectrum of Compound 63



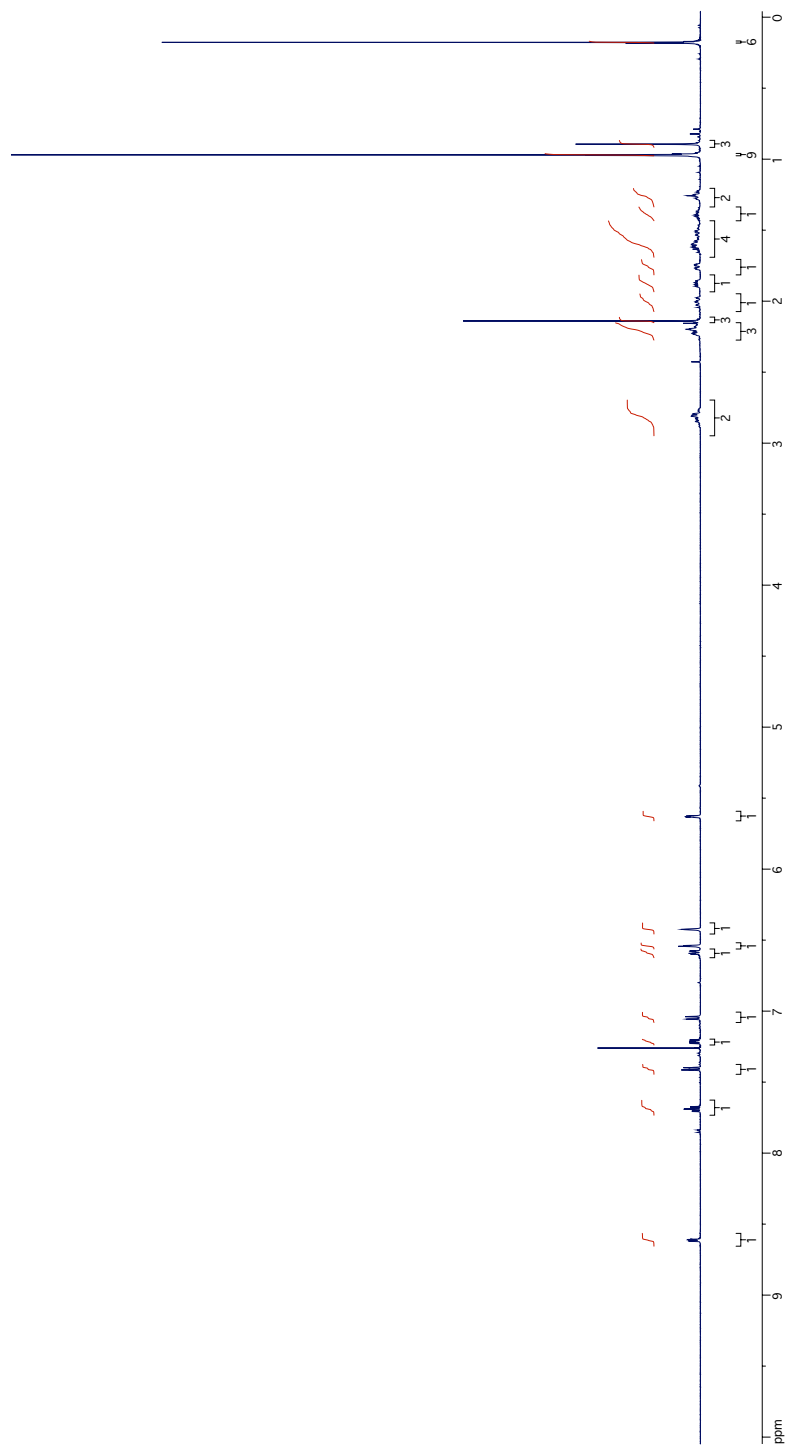
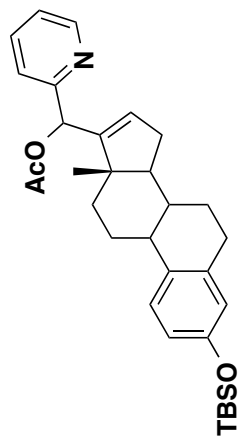
^{13}C NMR Spectrum of Compound **63**

322

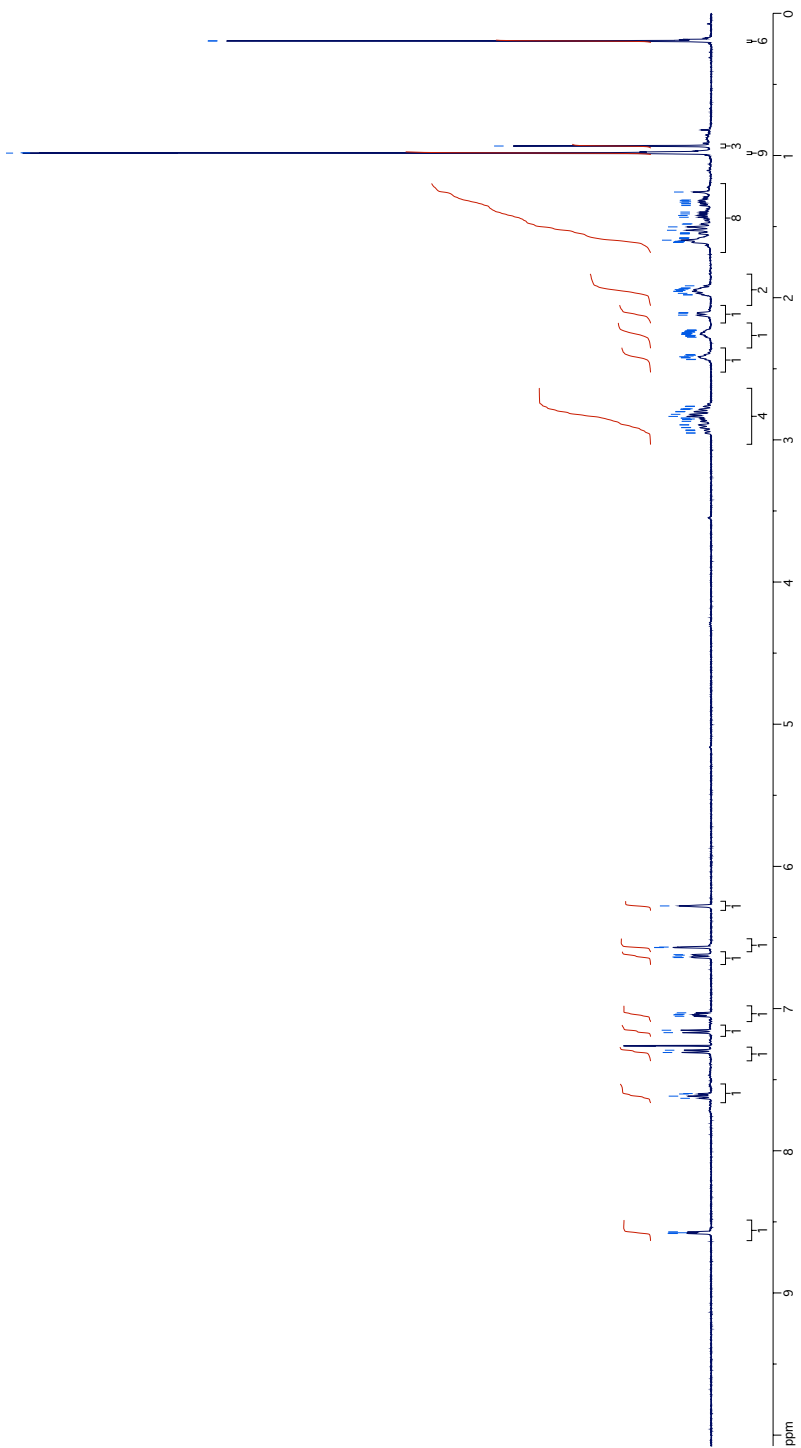
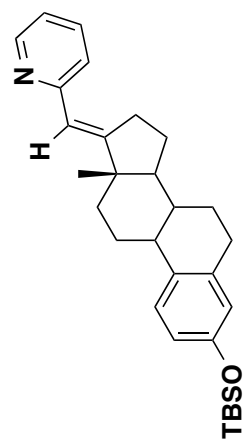




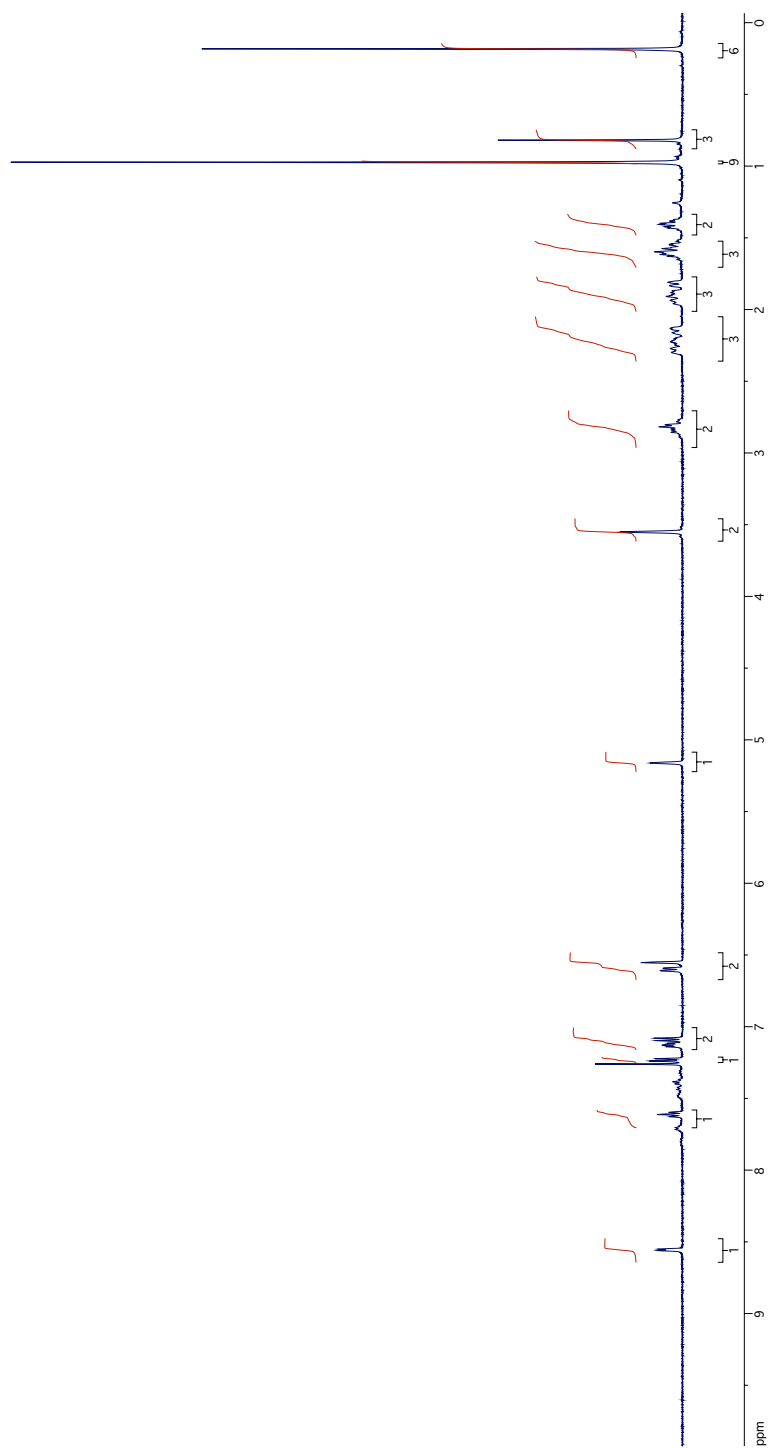
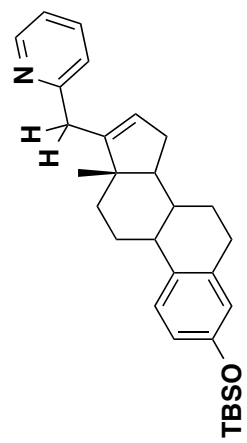
IR Spectrum of Compound **63**



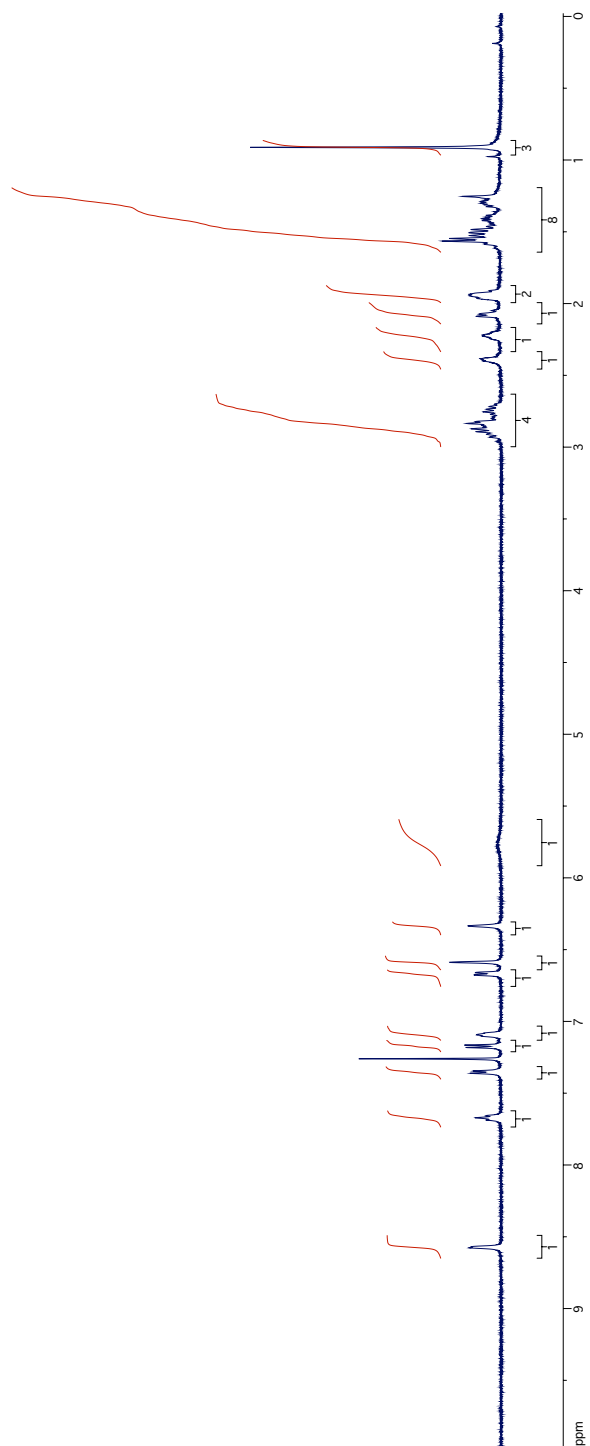
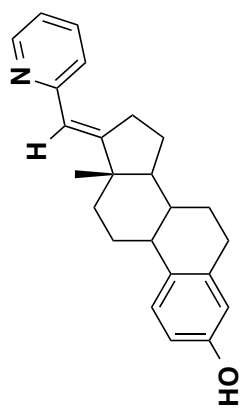
^1H NMR Spectrum of Compound **64**



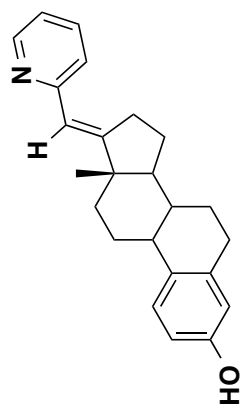
¹H NMR Spectrum of Compound **65**



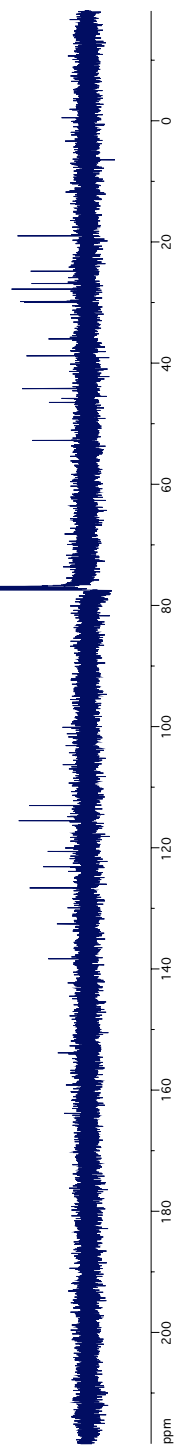
^1H NMR Spectrum of Compound 66

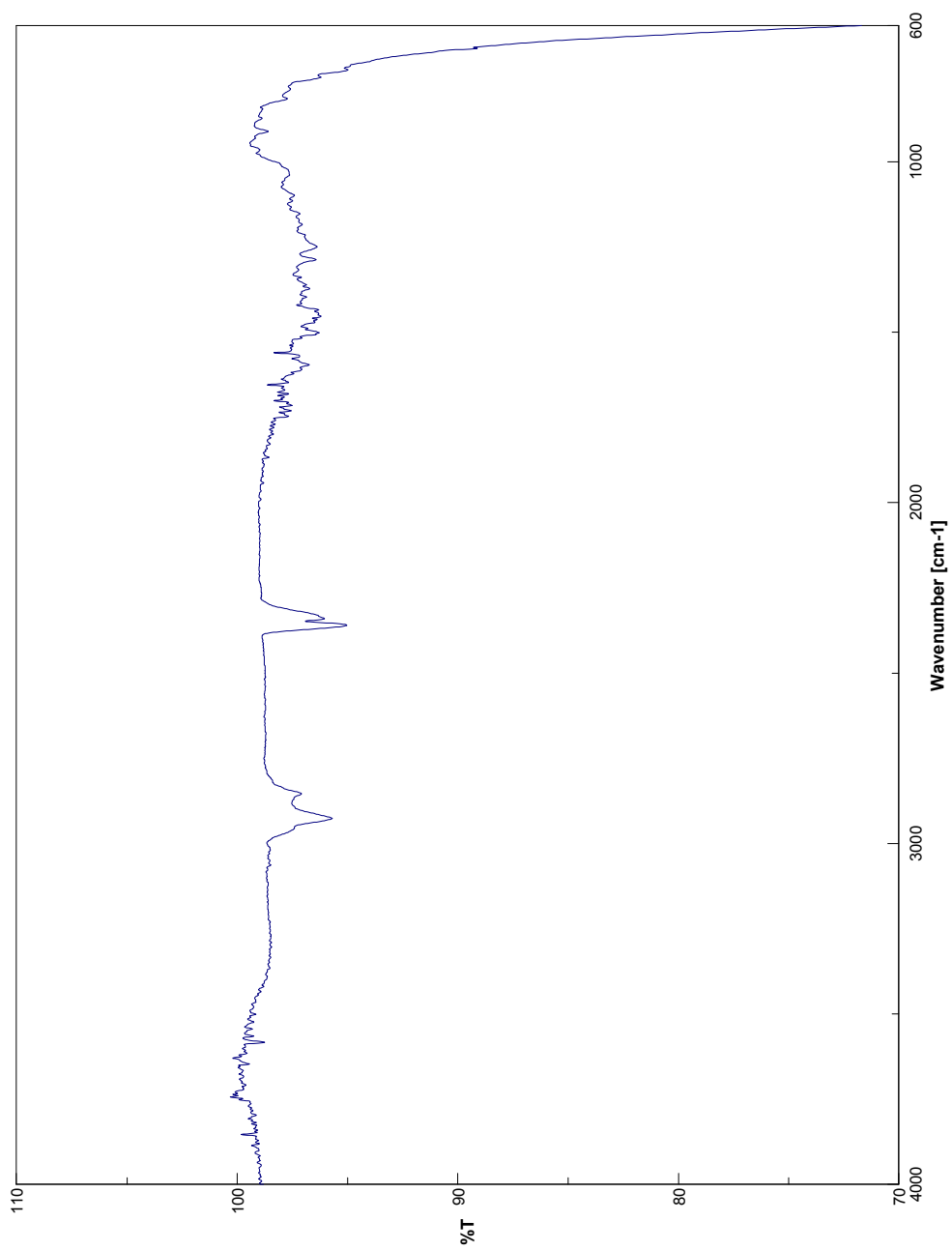


¹H NMR Spectrum of Compound 67

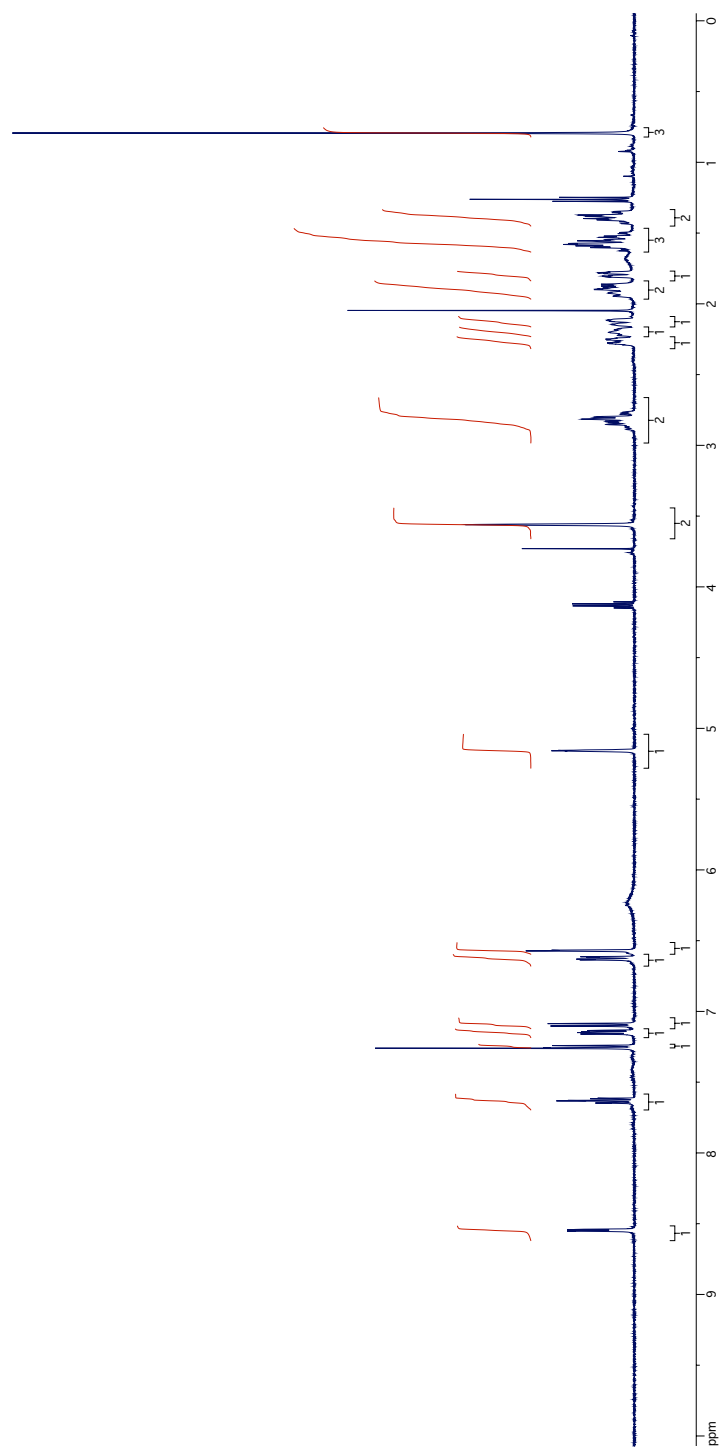
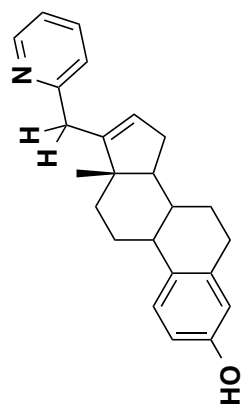


^{13}C NMR Spectrum of Compound 67

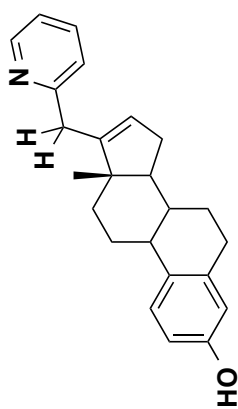




IR Spectrum of Compound **67**

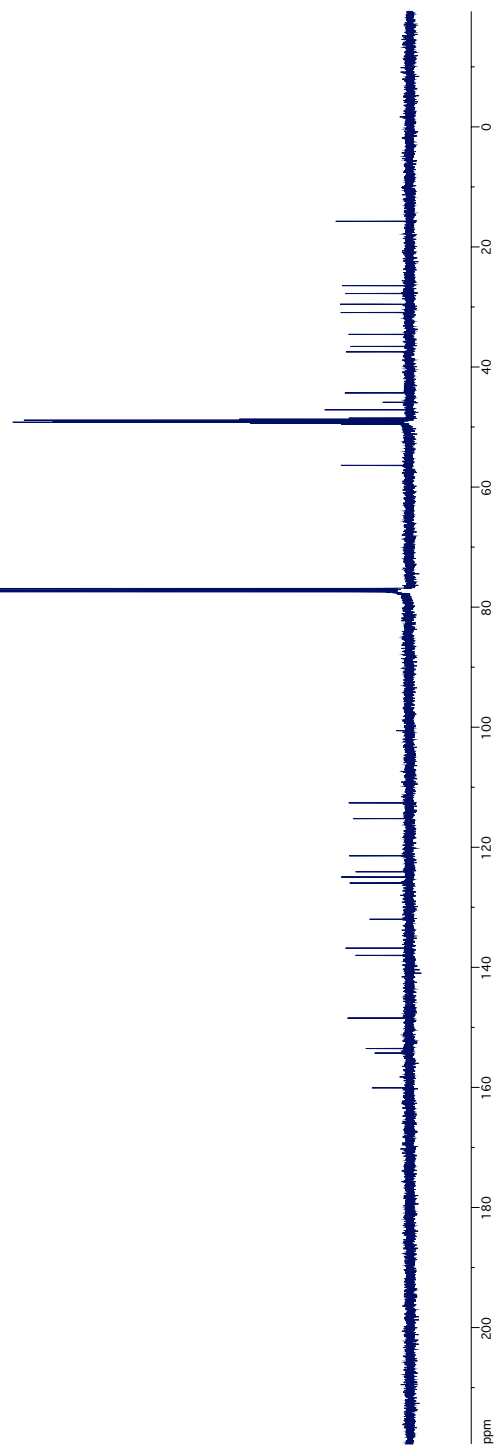


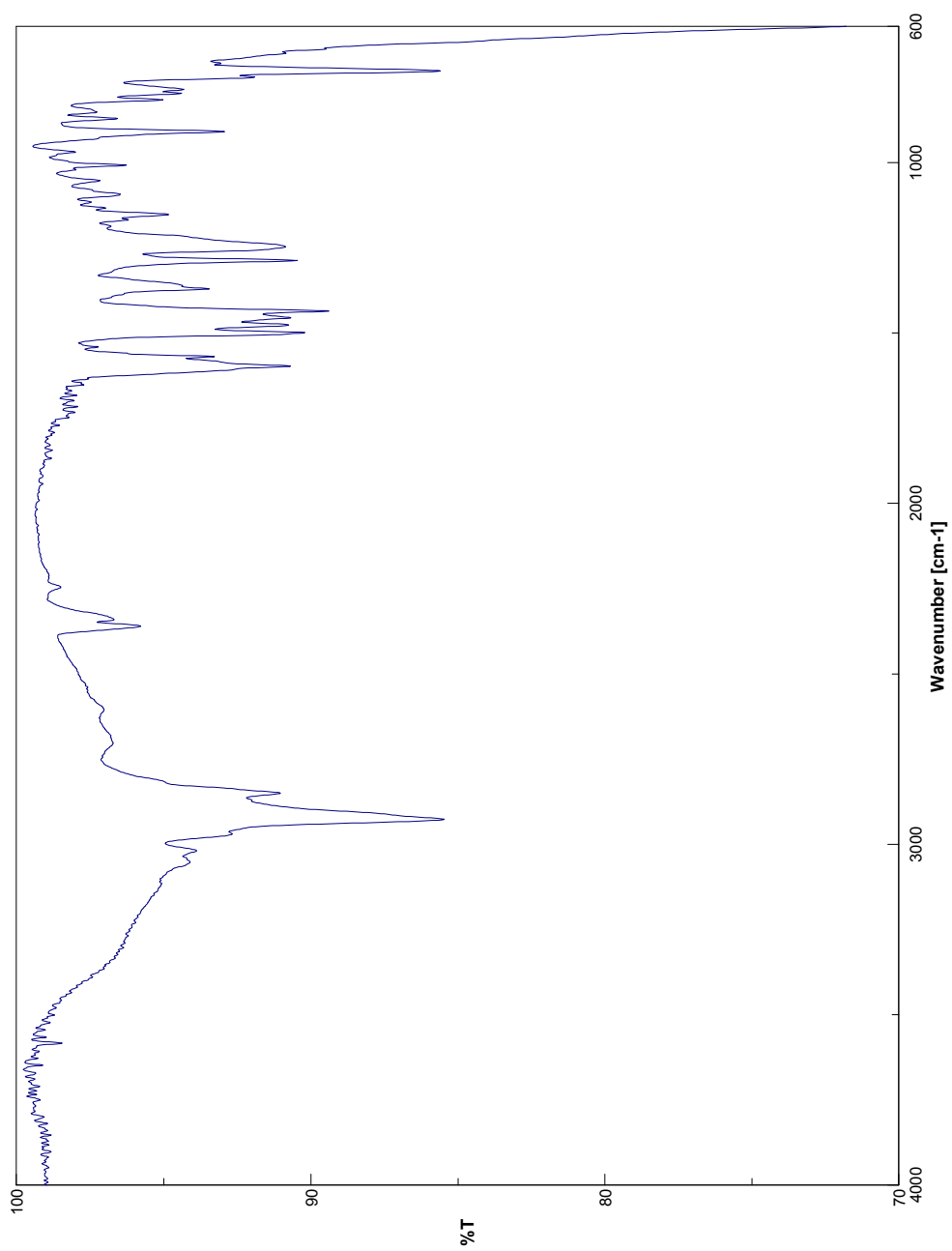
^1H Spectrum of Compound **68**



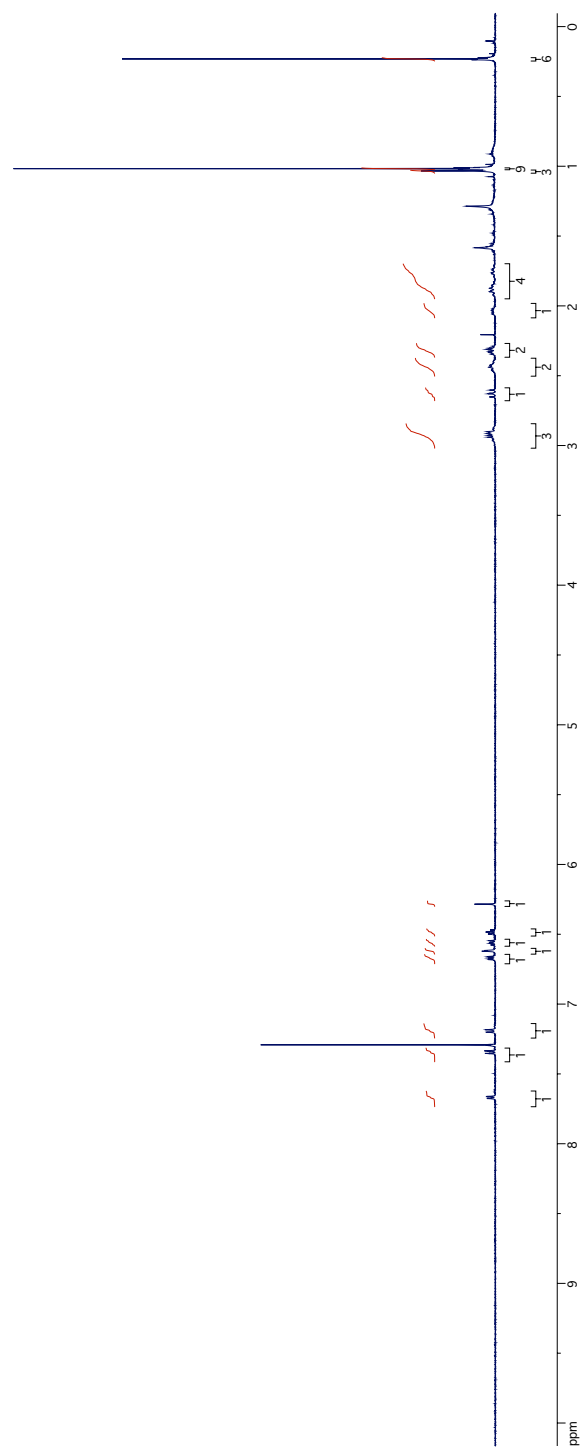
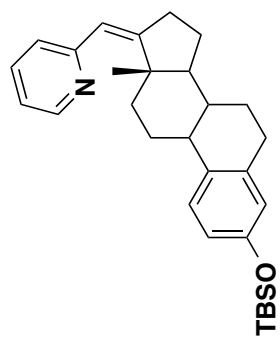
^{13}C NMR Spectrum of Compound 68

331

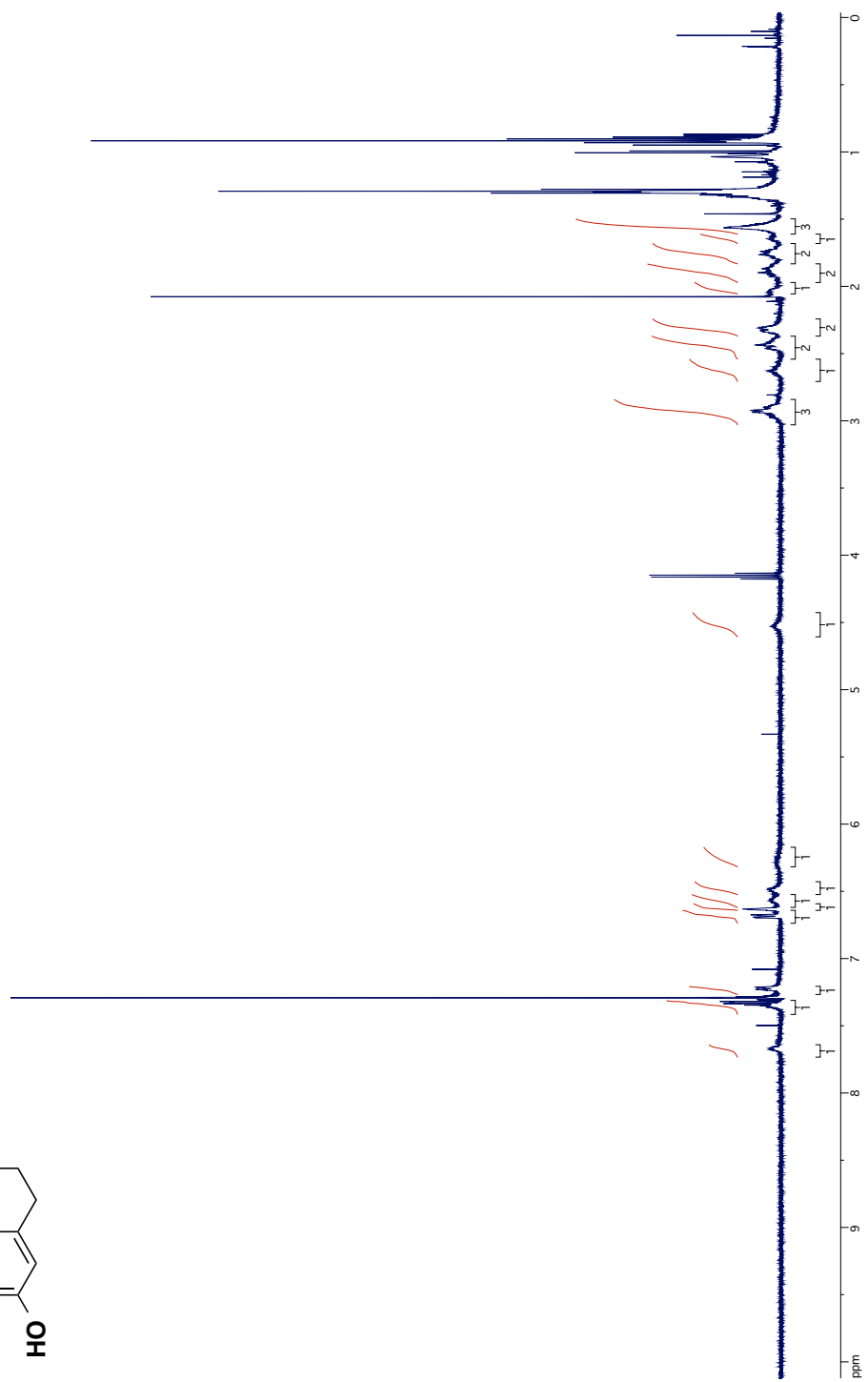
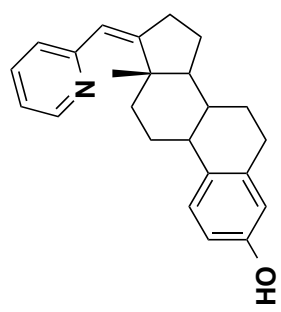




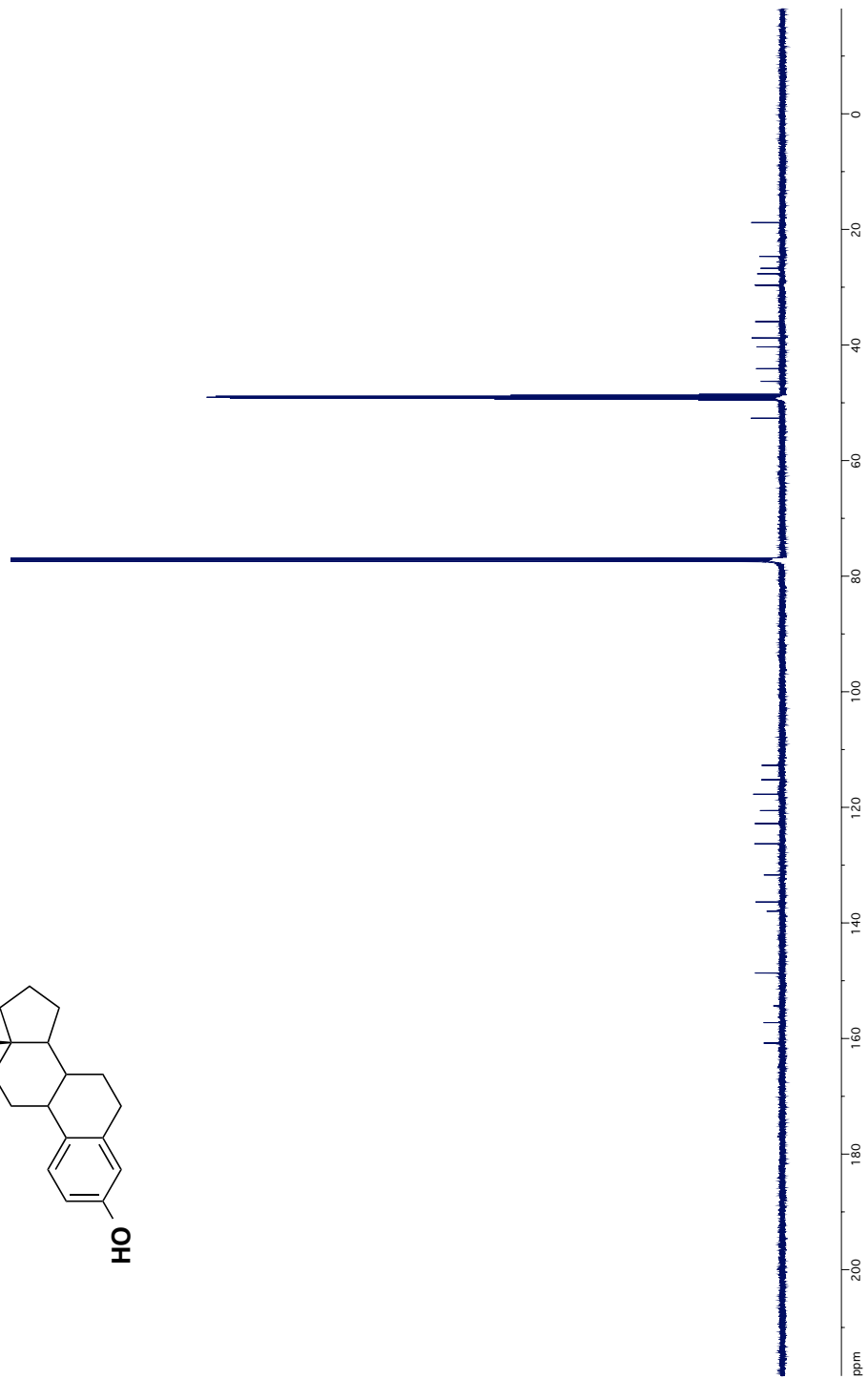
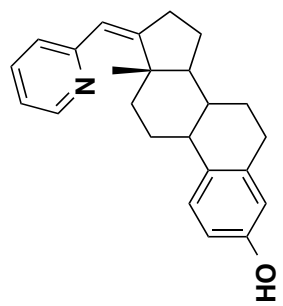
IR Spectrum of Compound **68**



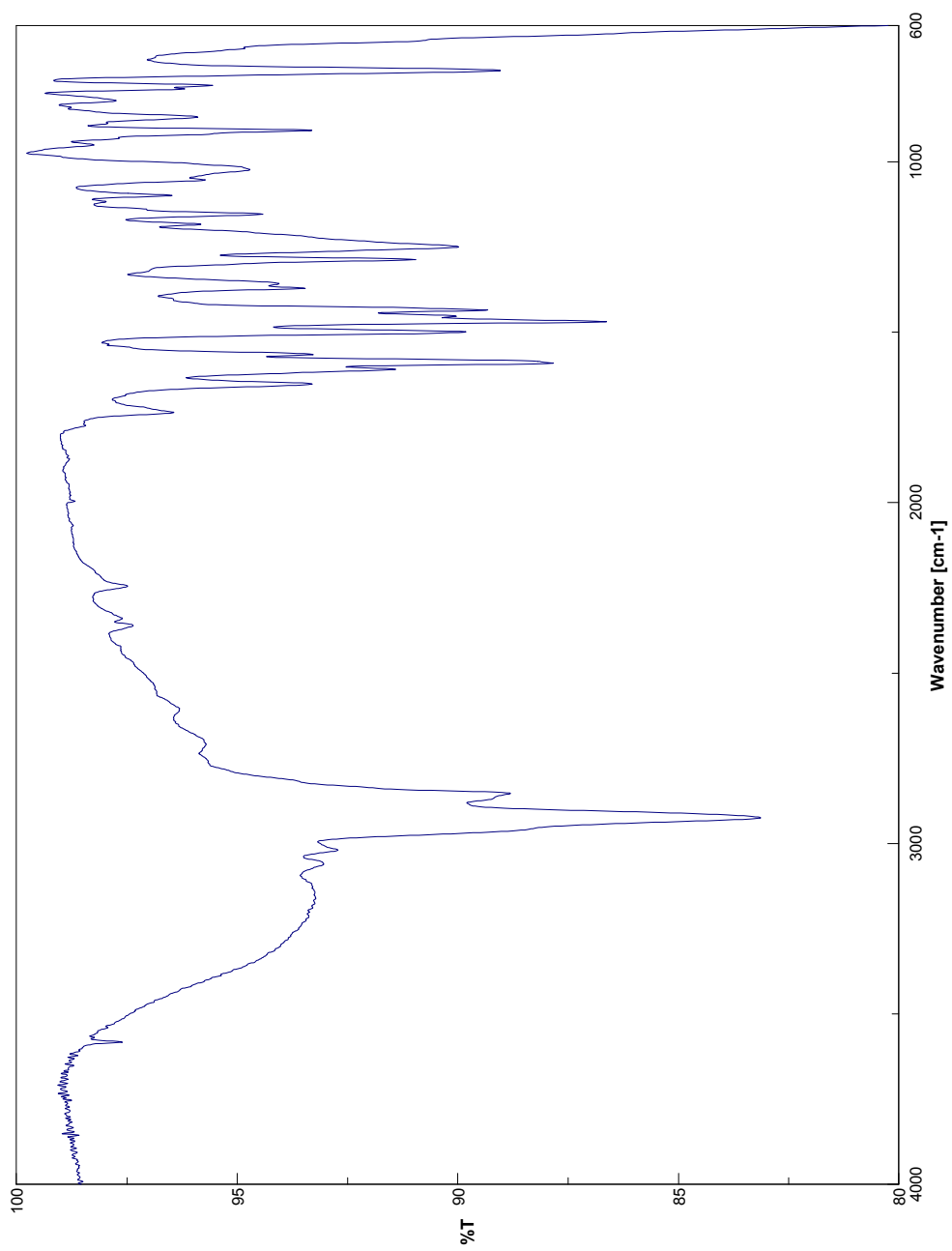
^1H NMR Spectrum of Compound 70



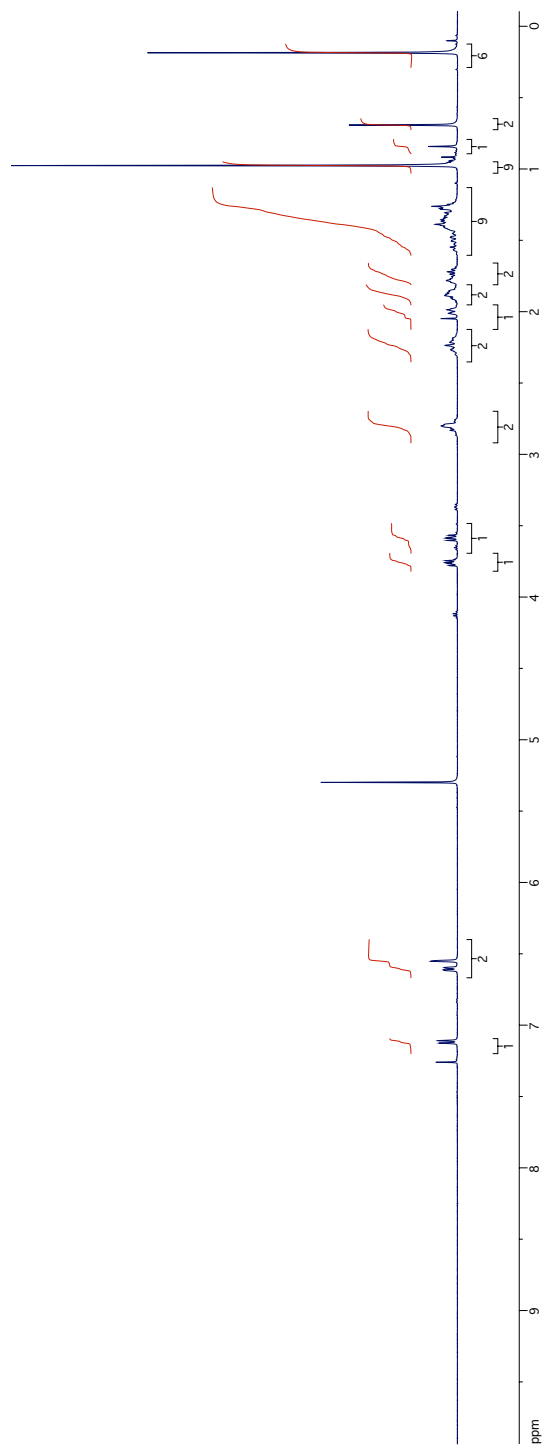
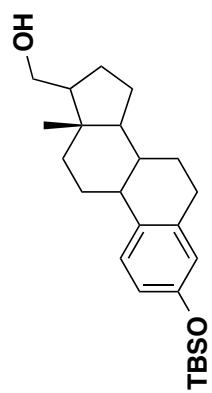
¹H NMR Spectrum of Compound 71



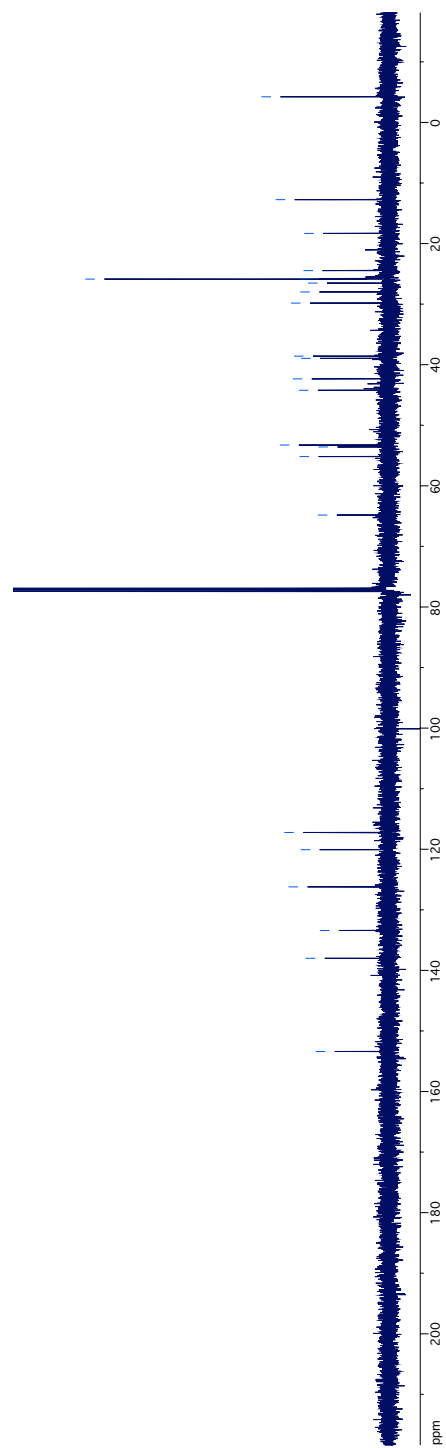
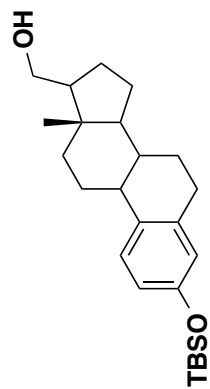
^{13}C NMR Spectrum of Compound 71



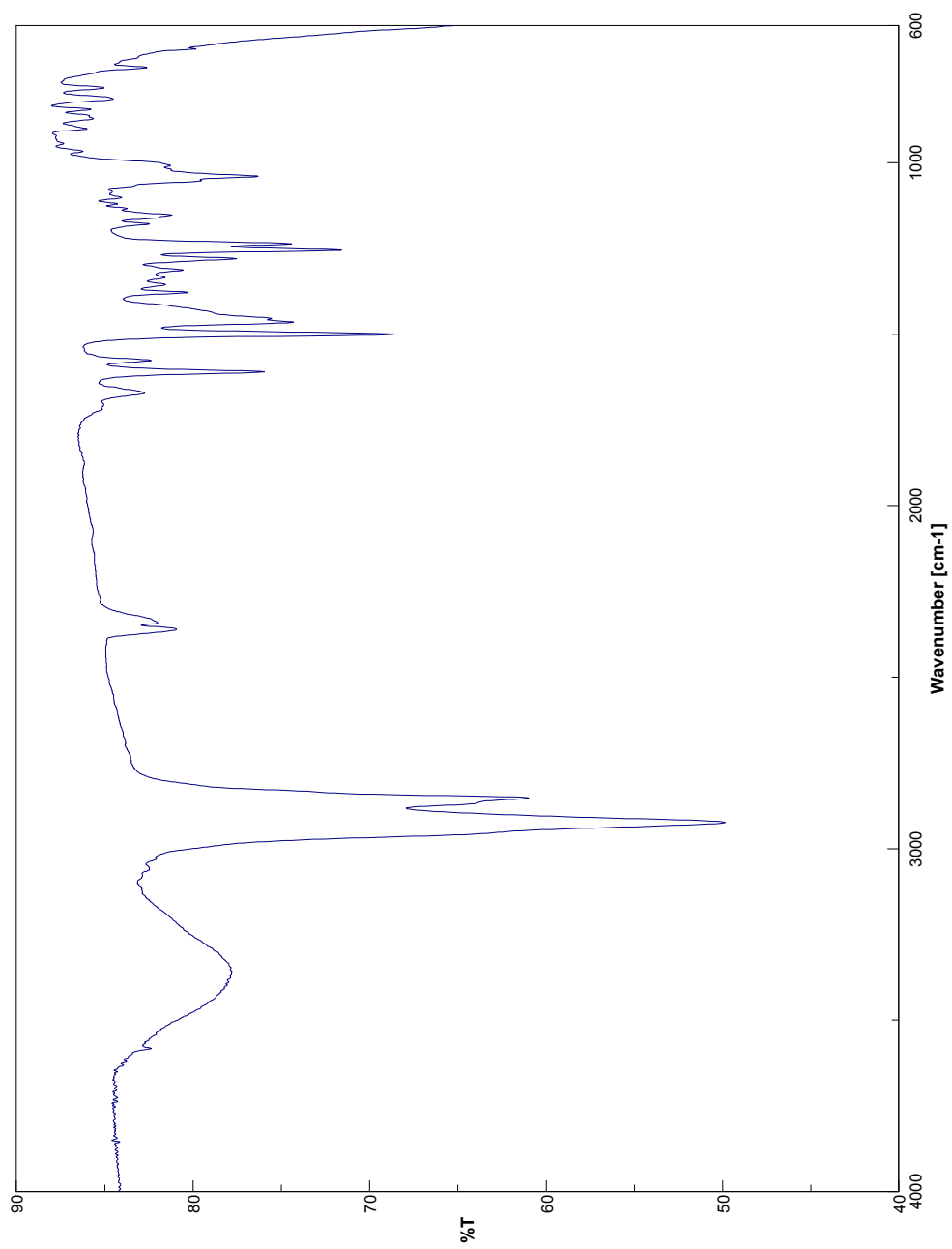
IR Spectrum of Compound 71



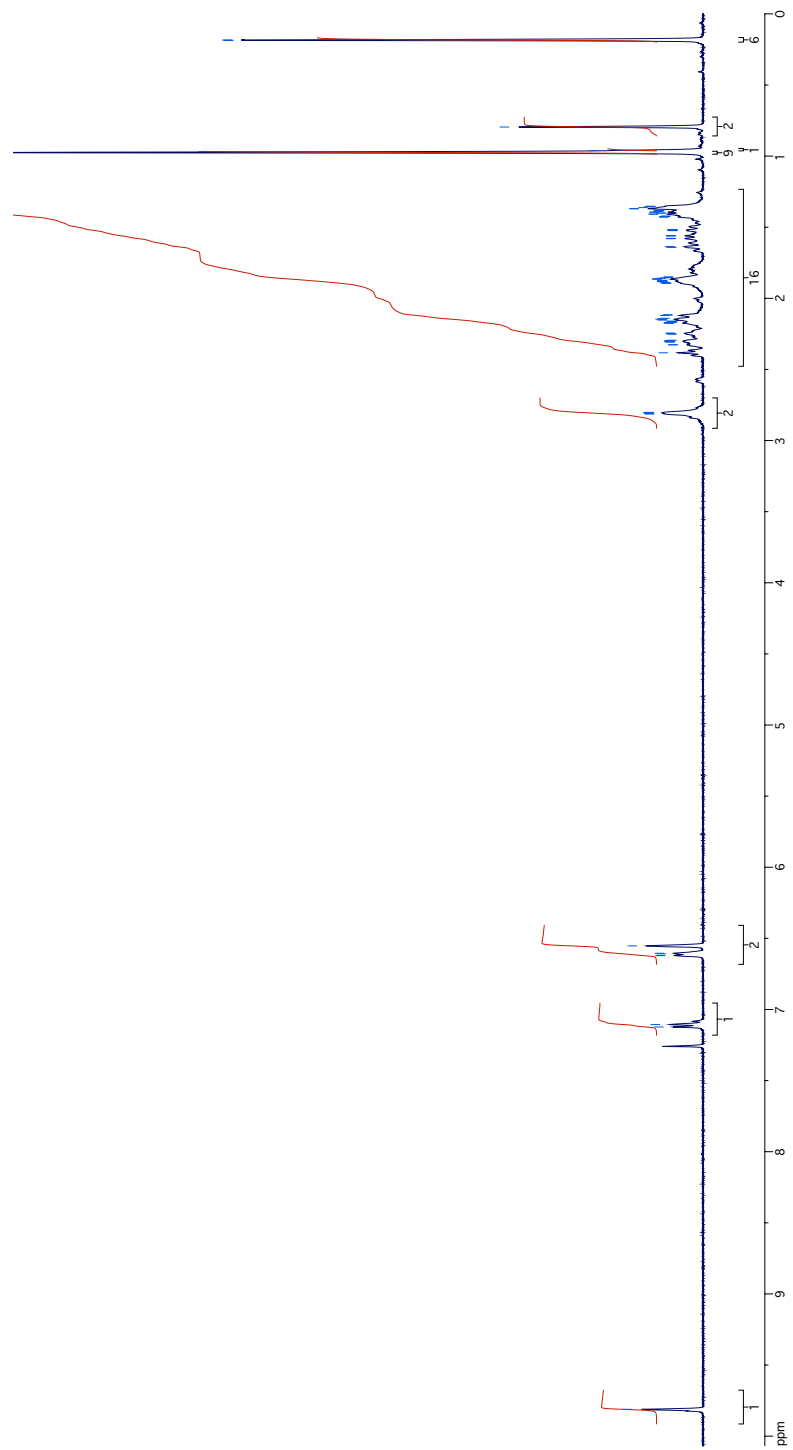
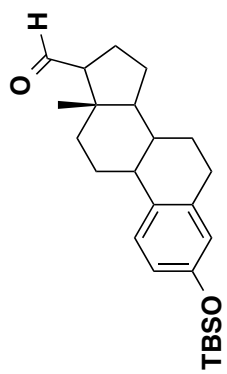
¹H NMR Spectrum of Compound **74**



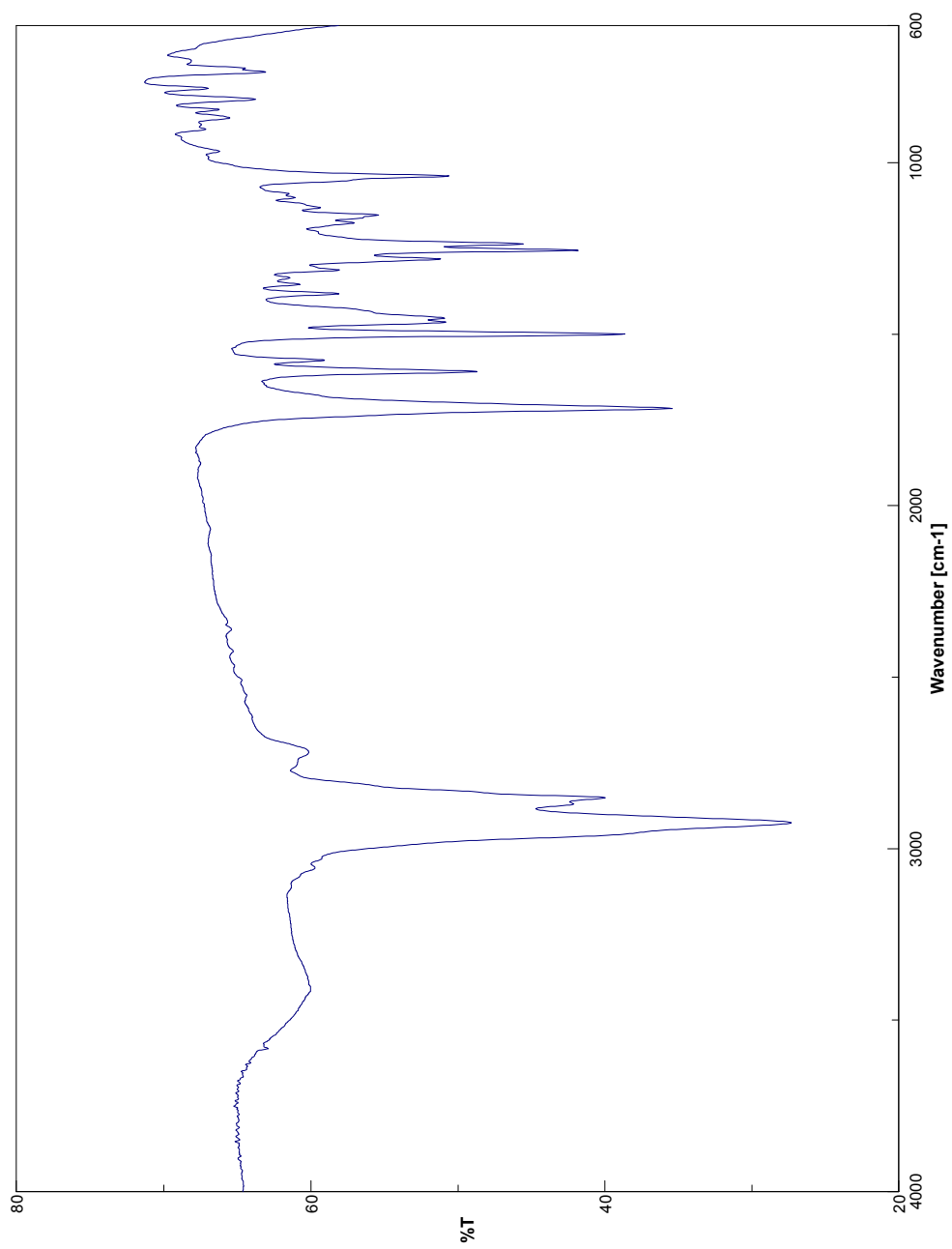
^{13}C NMR Spectrum of Compound 74



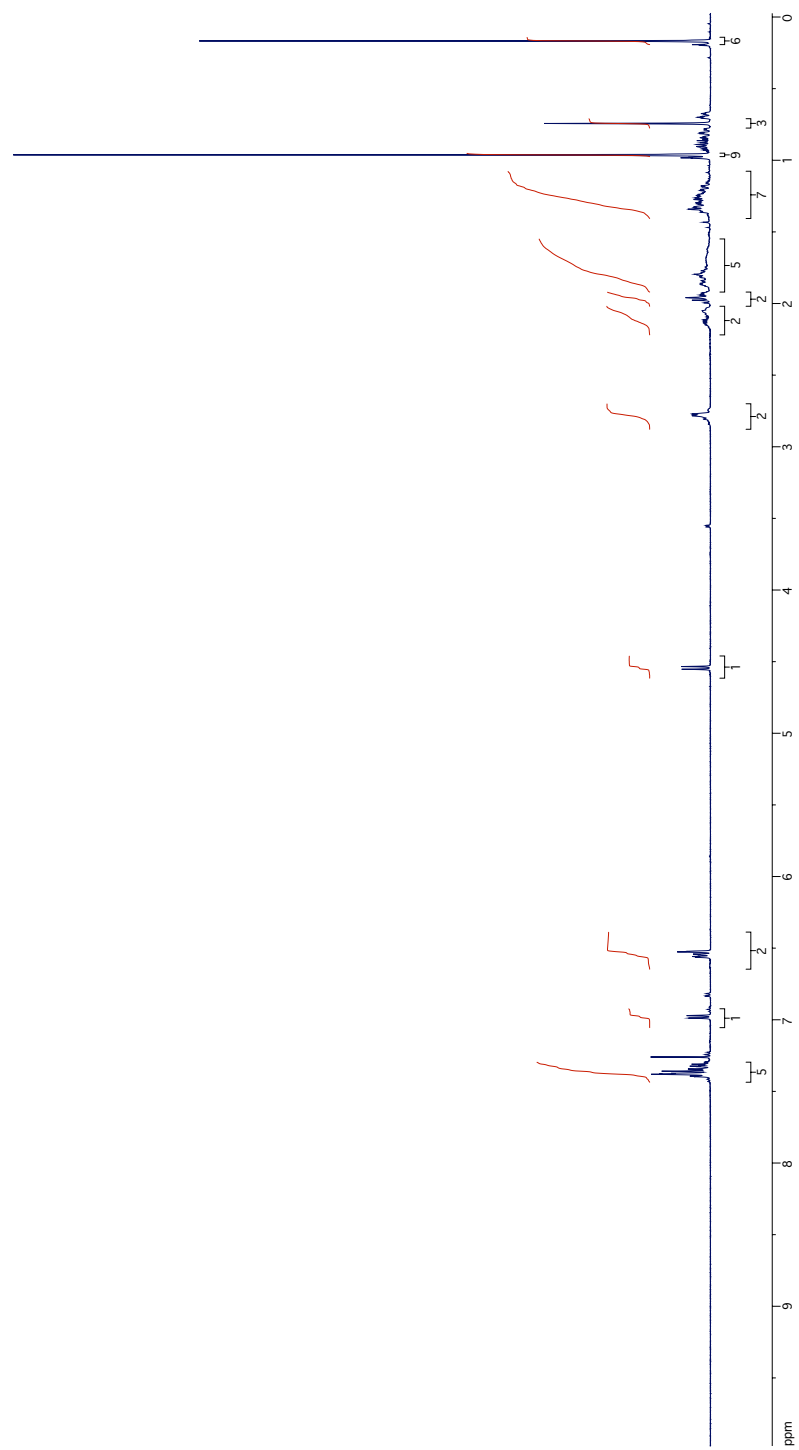
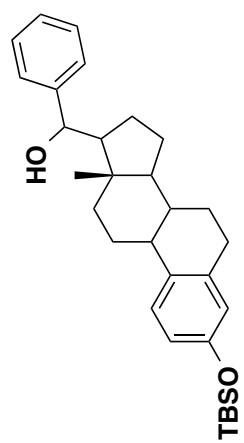
IR Spectrum of Compound 74



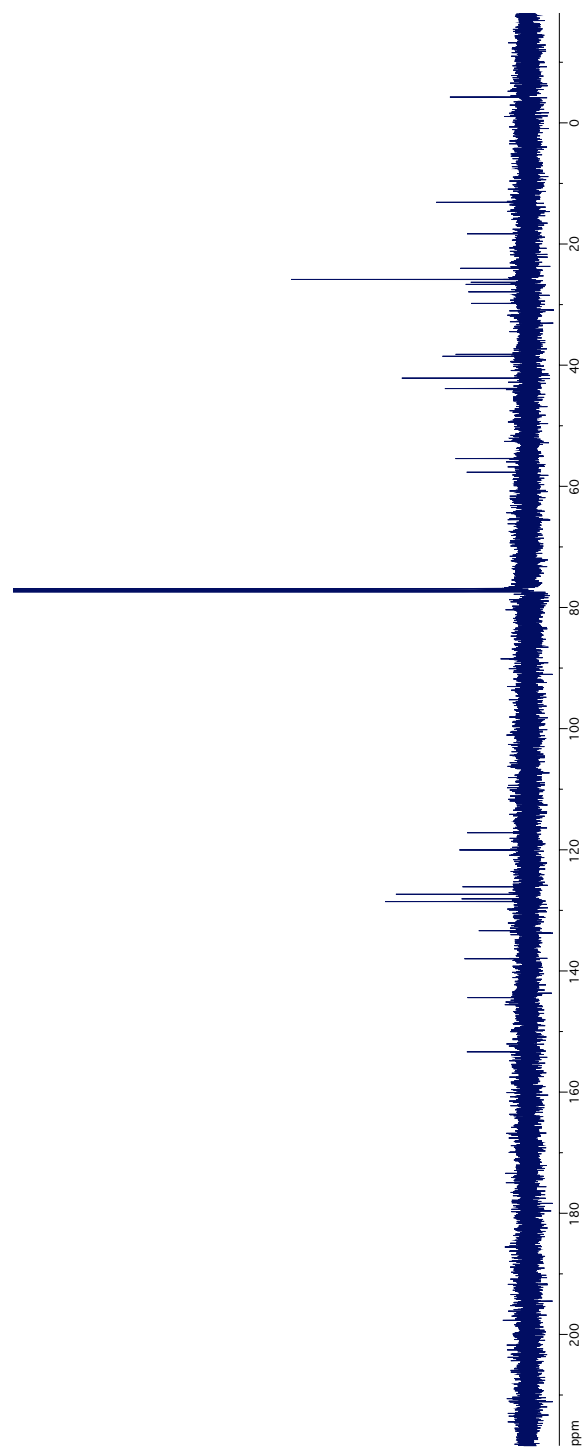
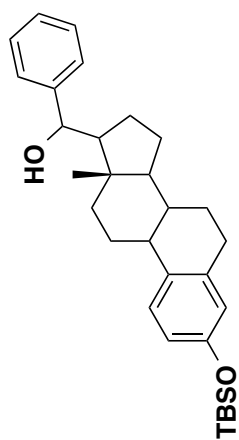
¹H NMR Spectrum of Compound 75



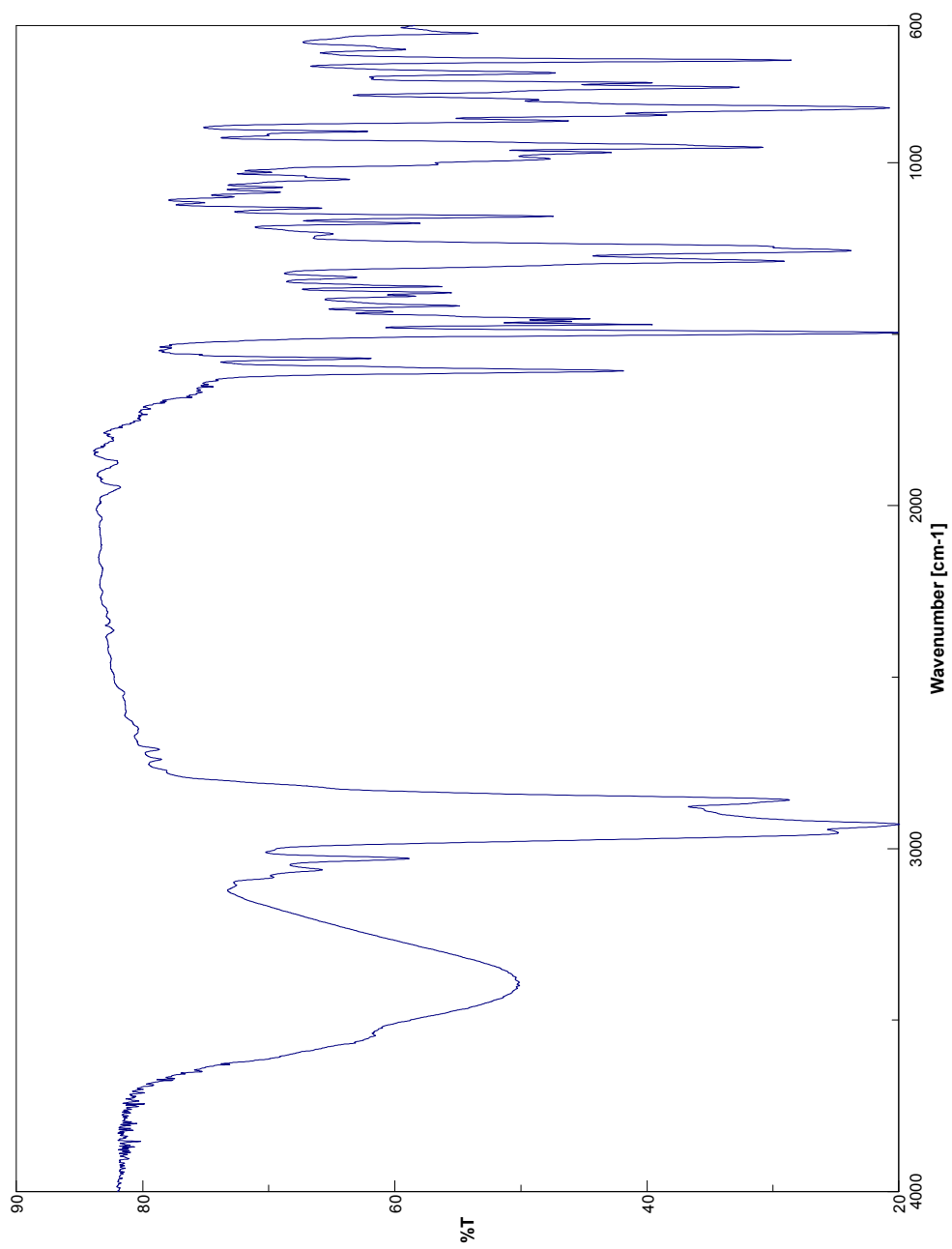
IR Spectrum of Compound **75**



¹H NMR Spectrum of Compound 76

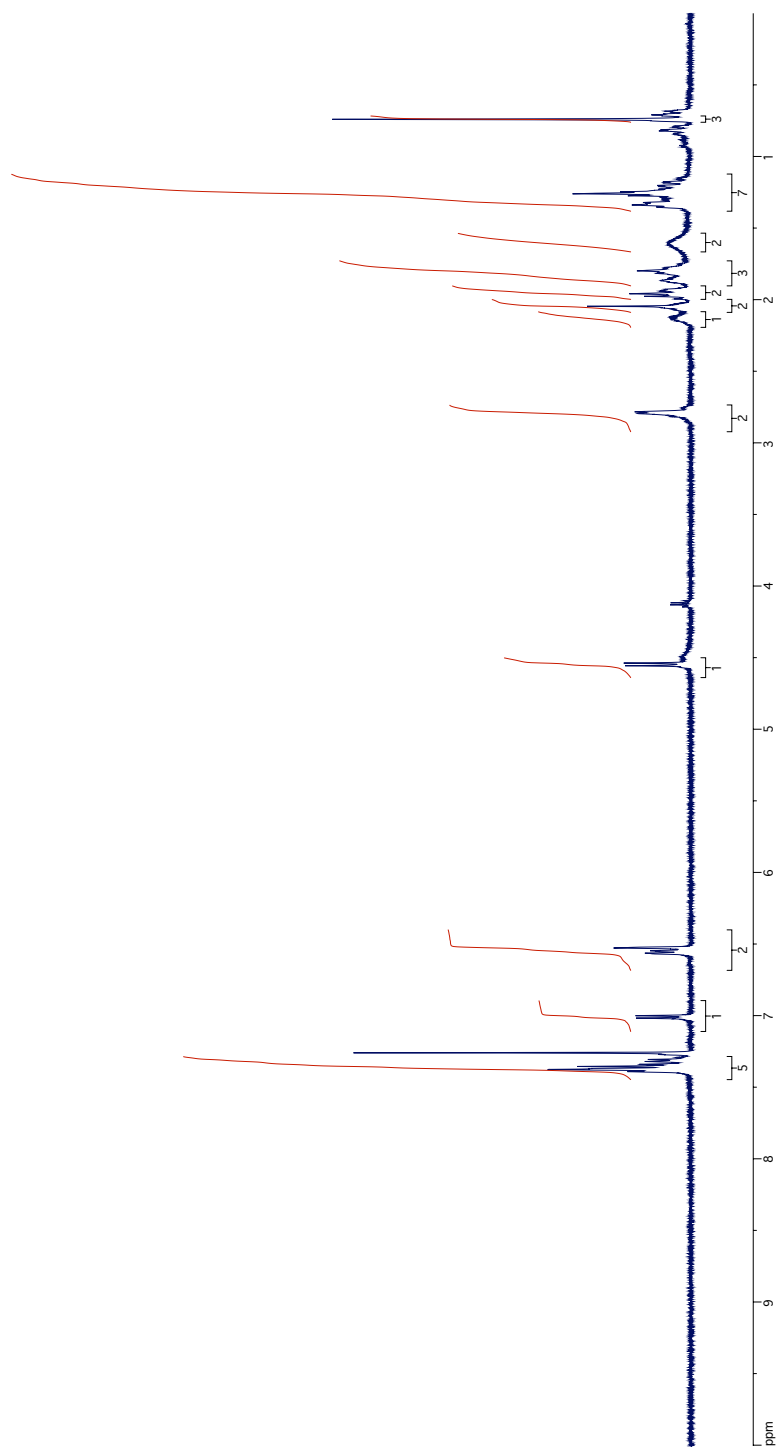
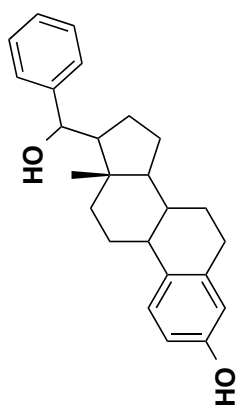


^{13}C NMR Spectrum of Compound 76

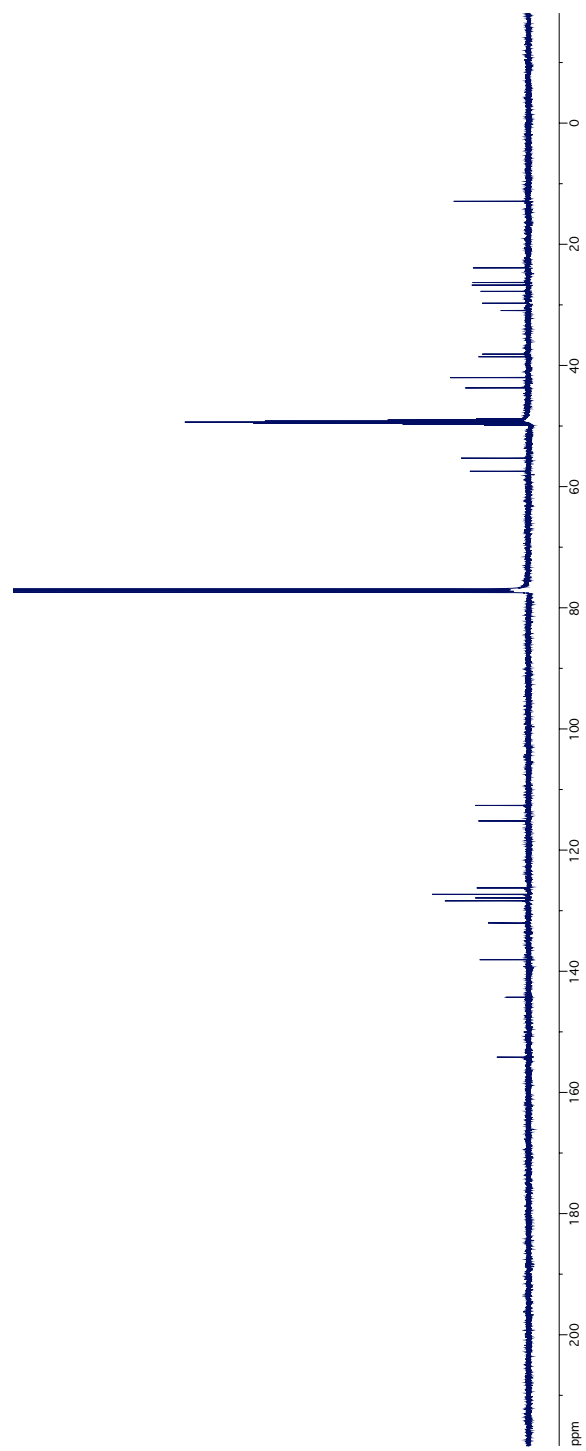
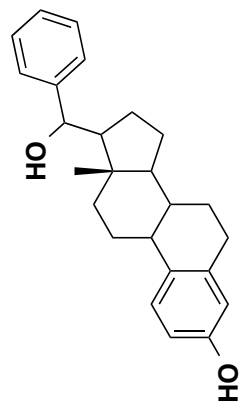


IR Spectrum of Compound **76**

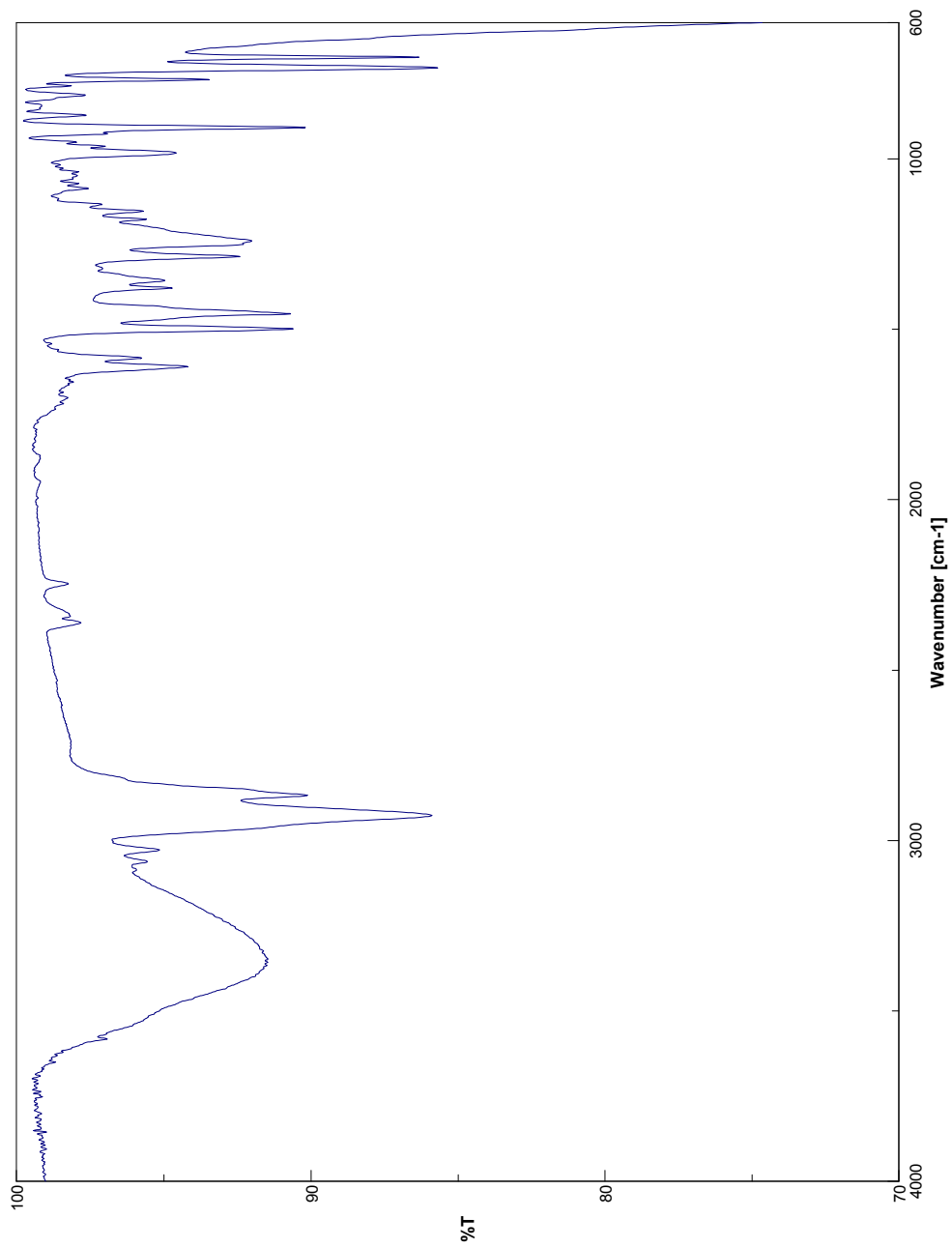
345



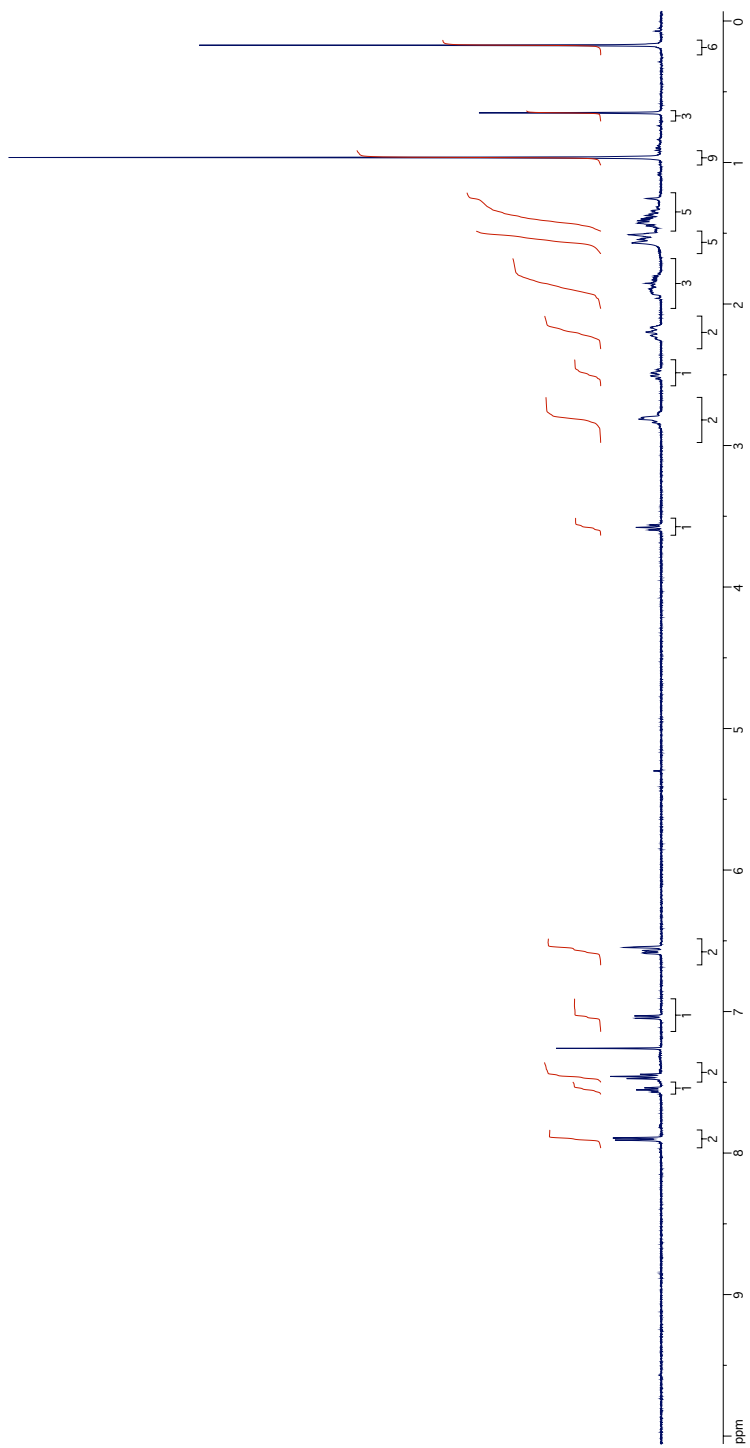
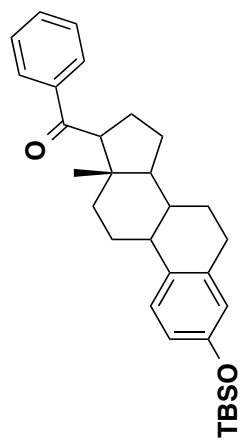
¹H NMR Spectrum of Compound 77



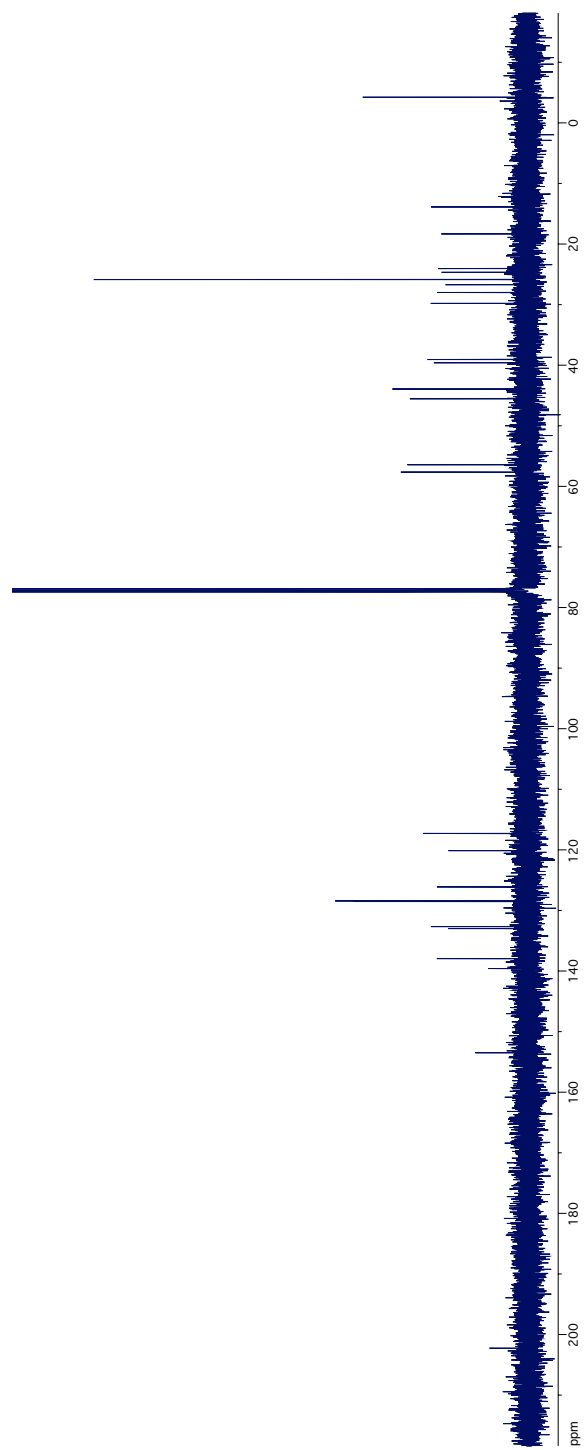
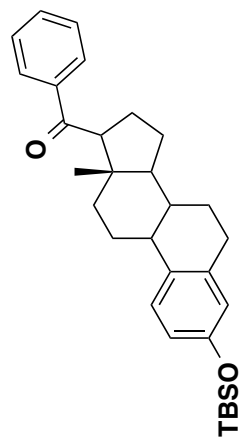
^{13}C NMR Spectrum of Compound 77



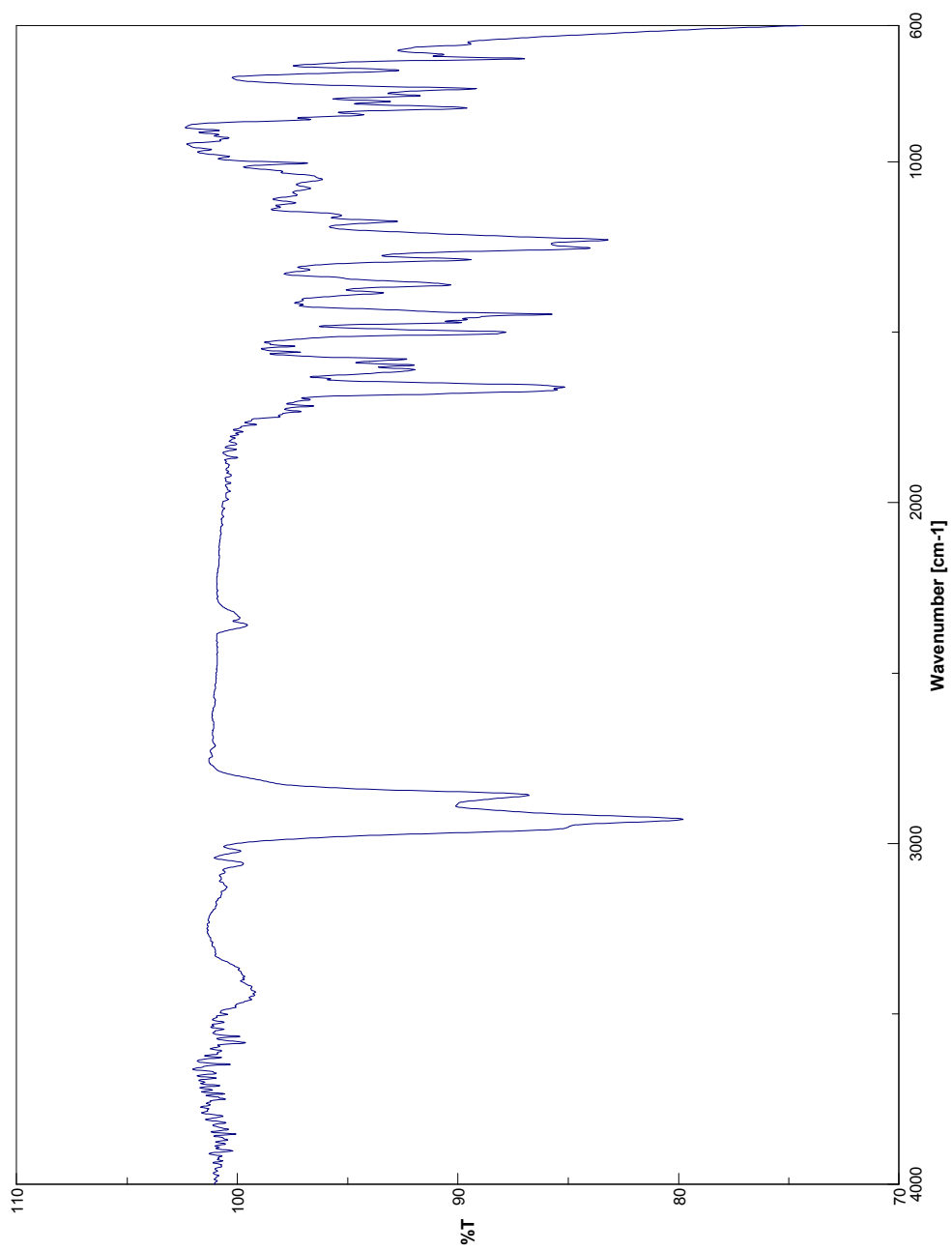
IR Spectrum of Compound 77



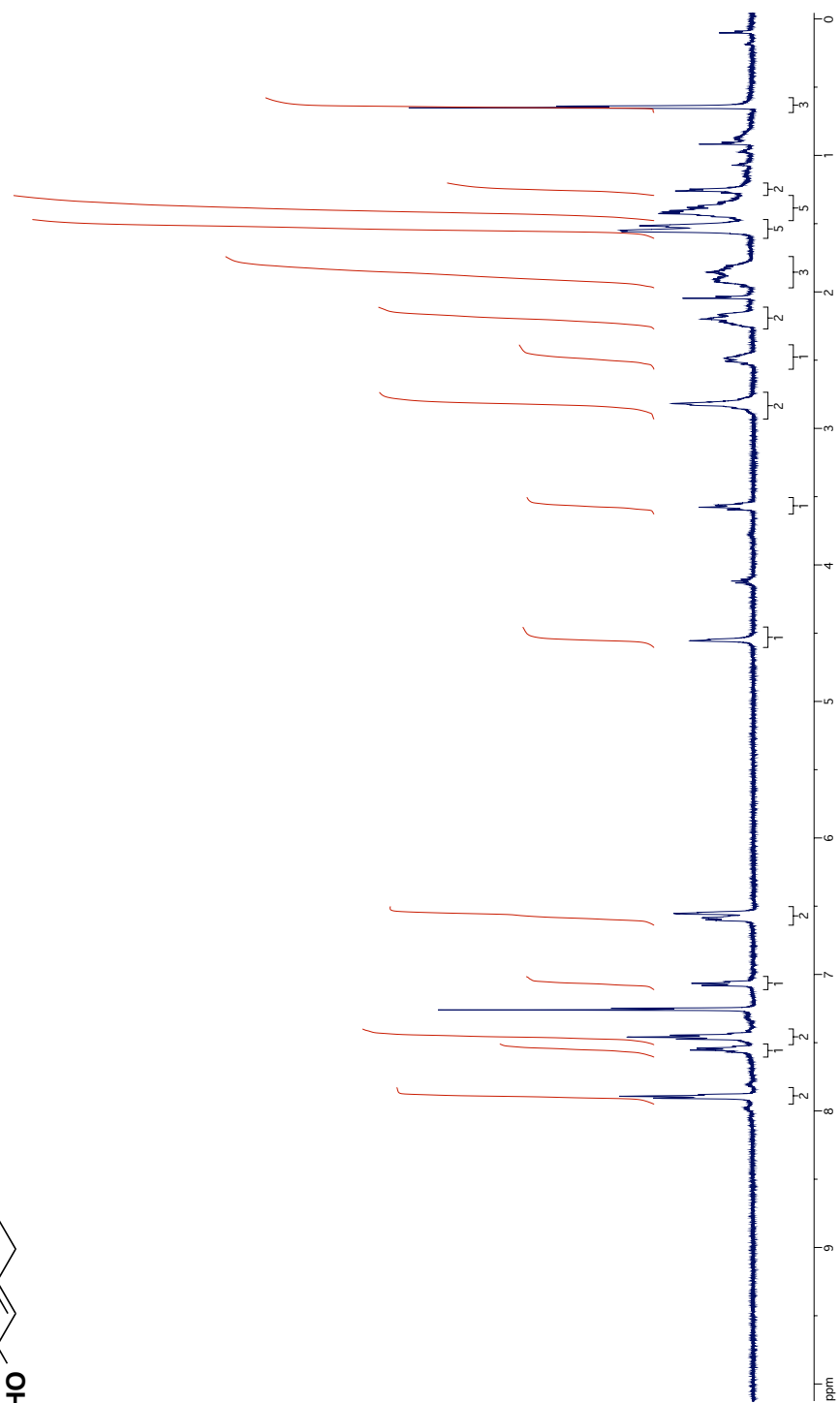
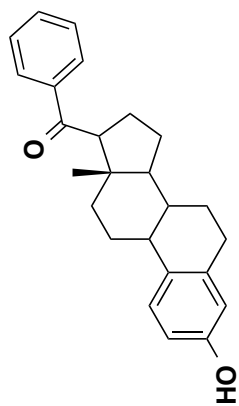
^1H NMR Spectrum of Compound **78**



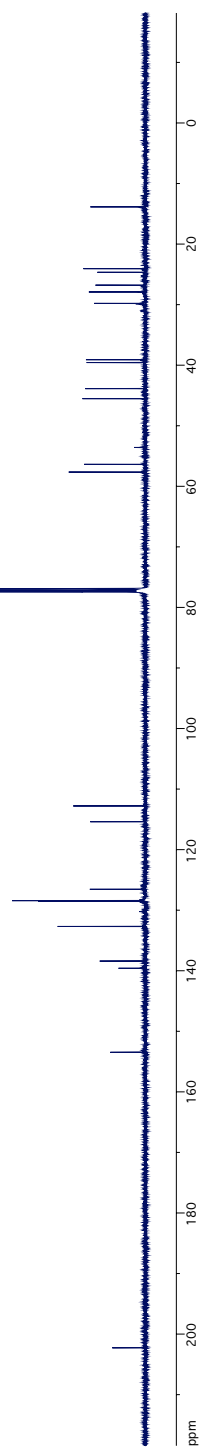
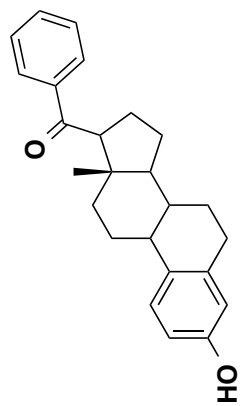
^{13}C NMR Spectrum of Compound 78



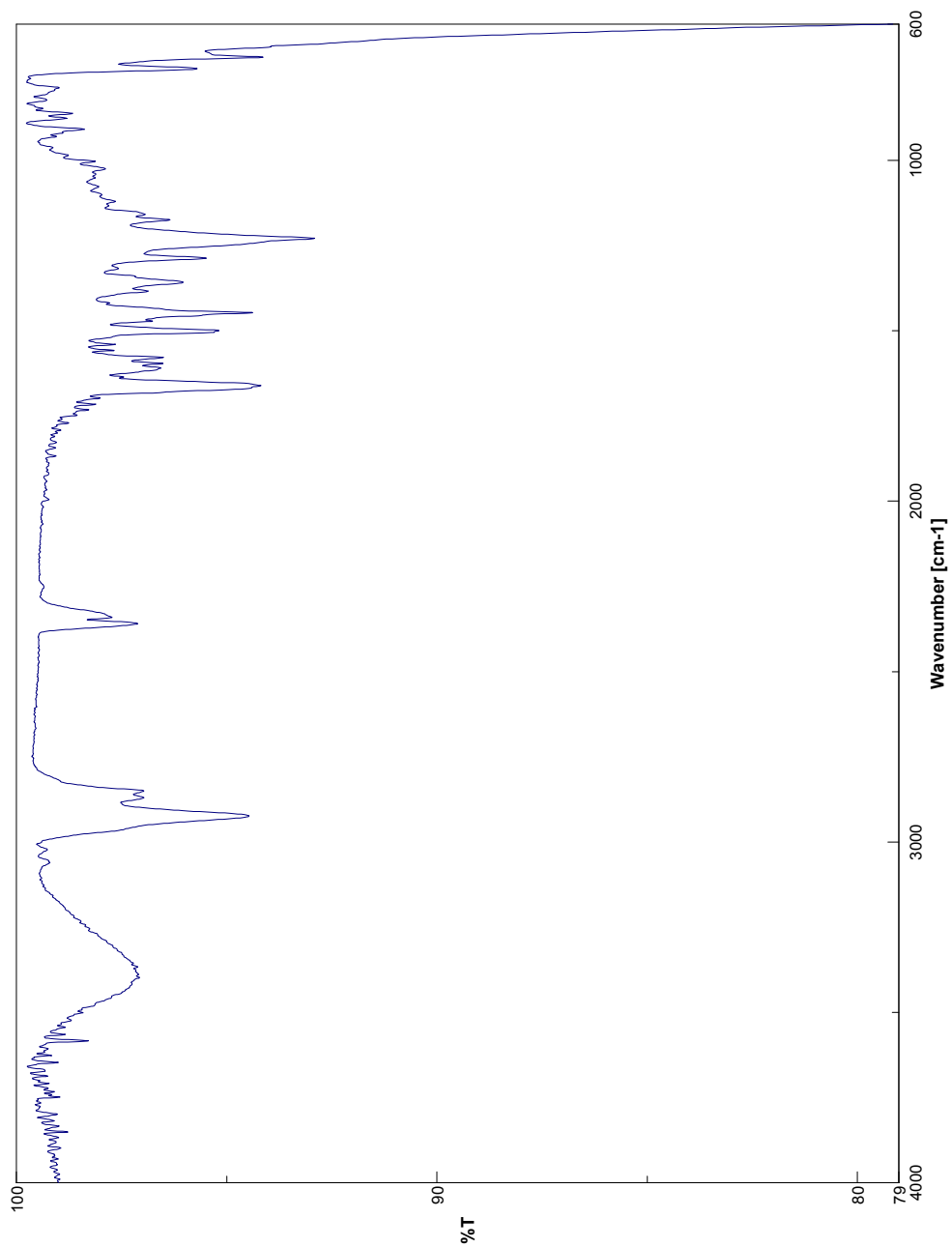
IR Spectrum of Compound 78



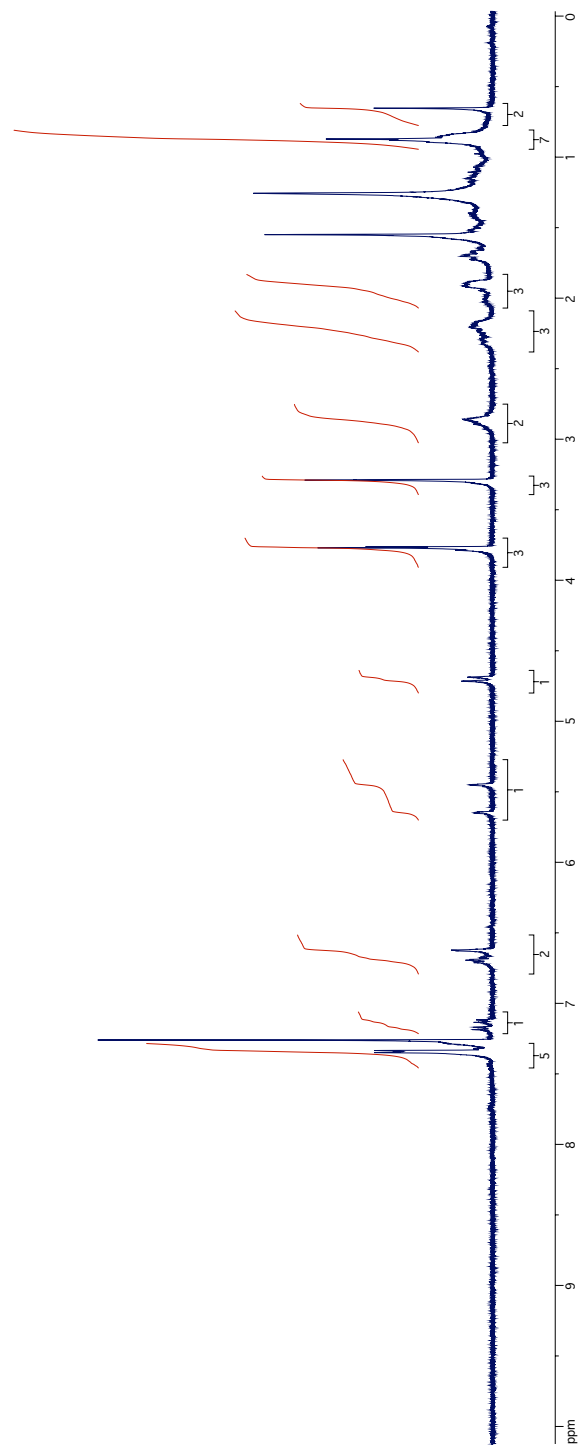
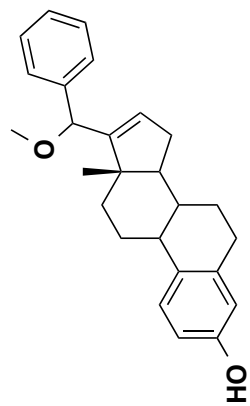
¹H NMR Spectrum of Compound **79**



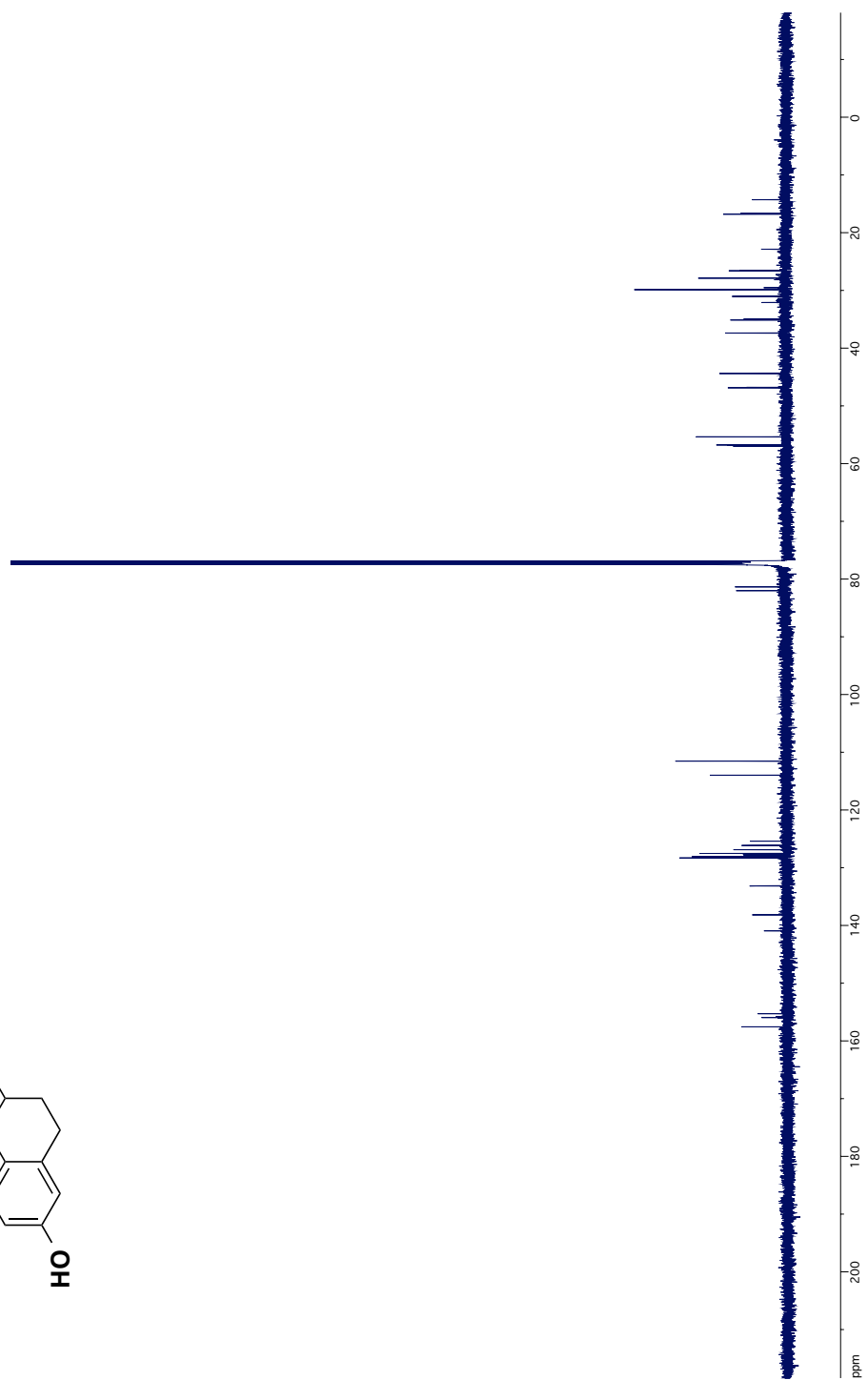
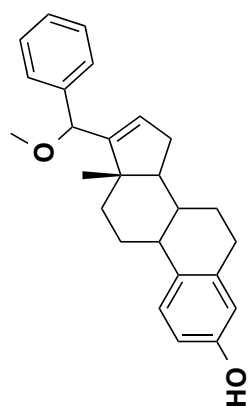
^{13}C NMR Spectrum of Compound 79



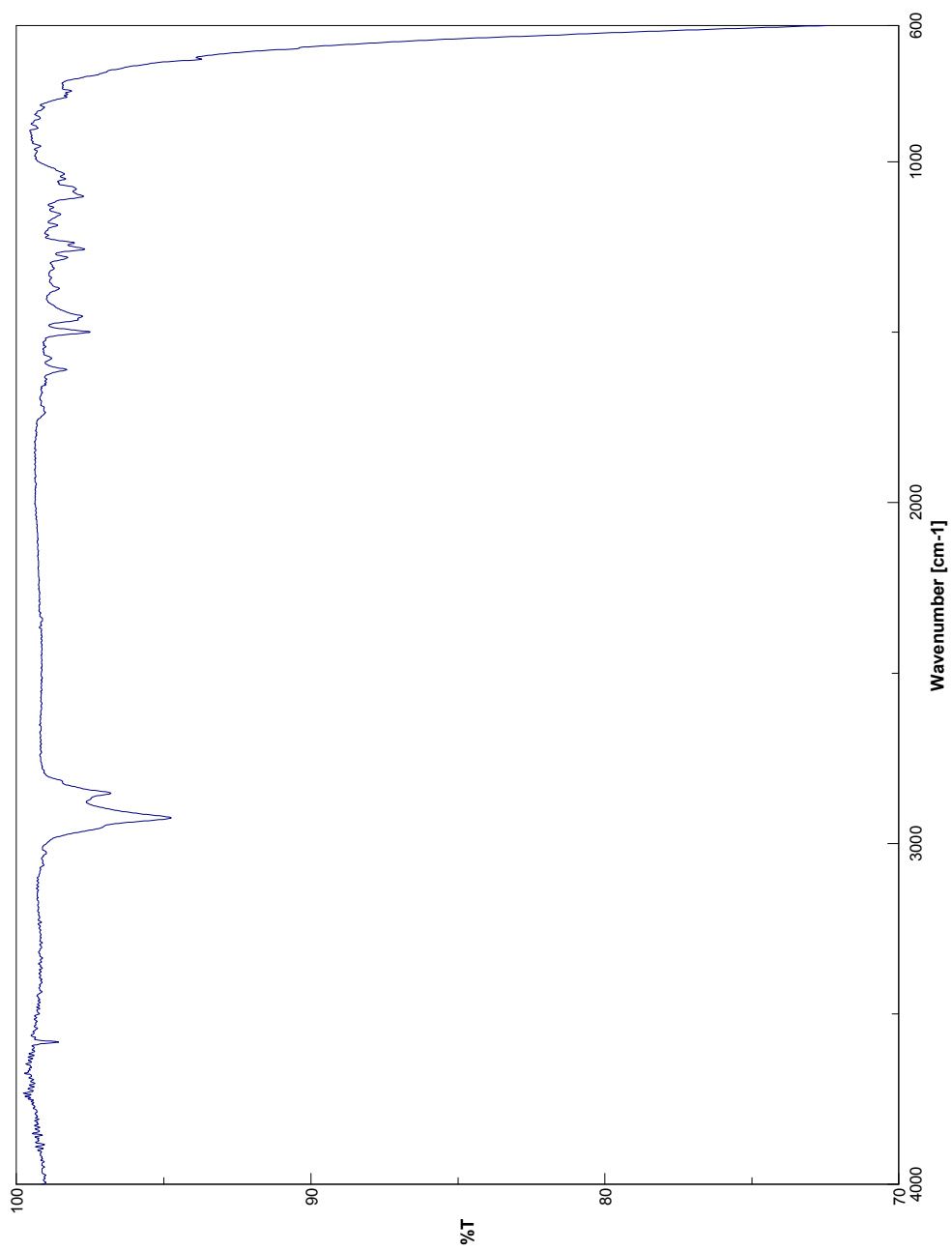
IR Spectrum of Compound 79



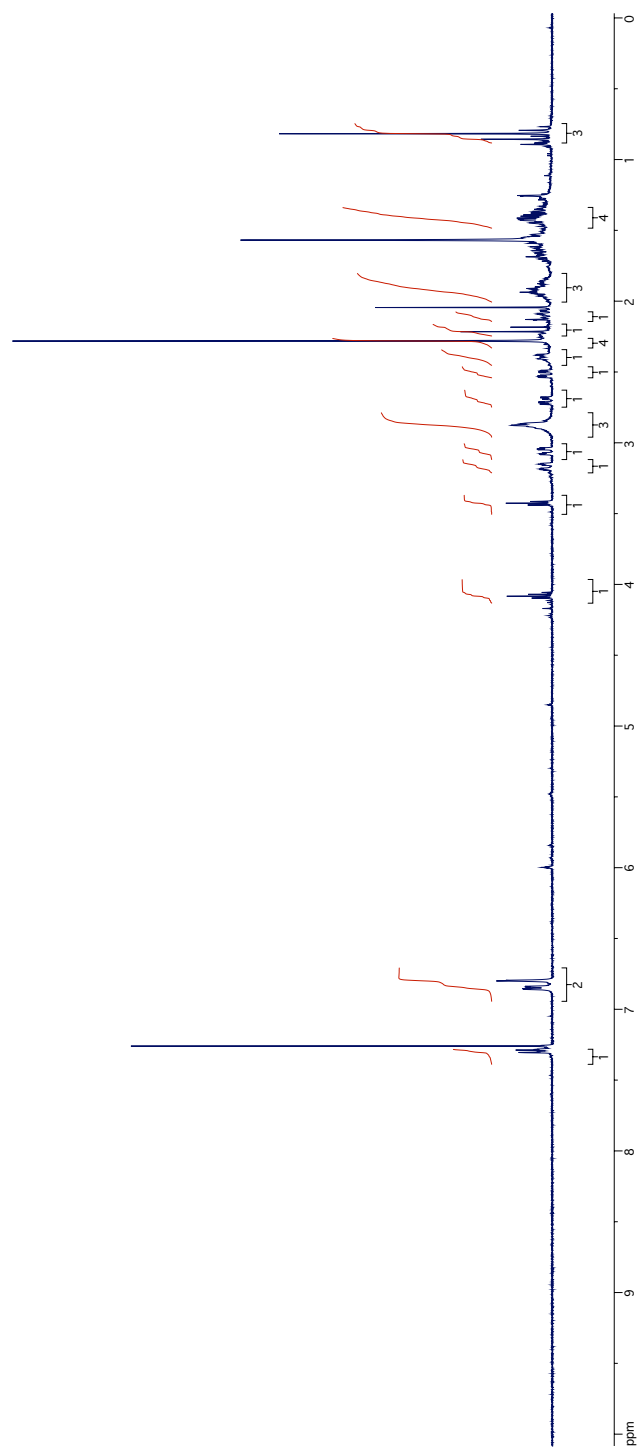
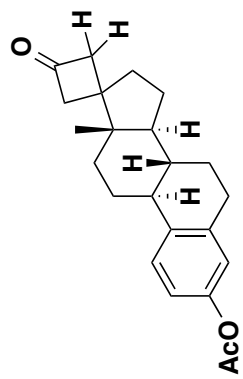
¹H NMR Spectrum of Compound 80



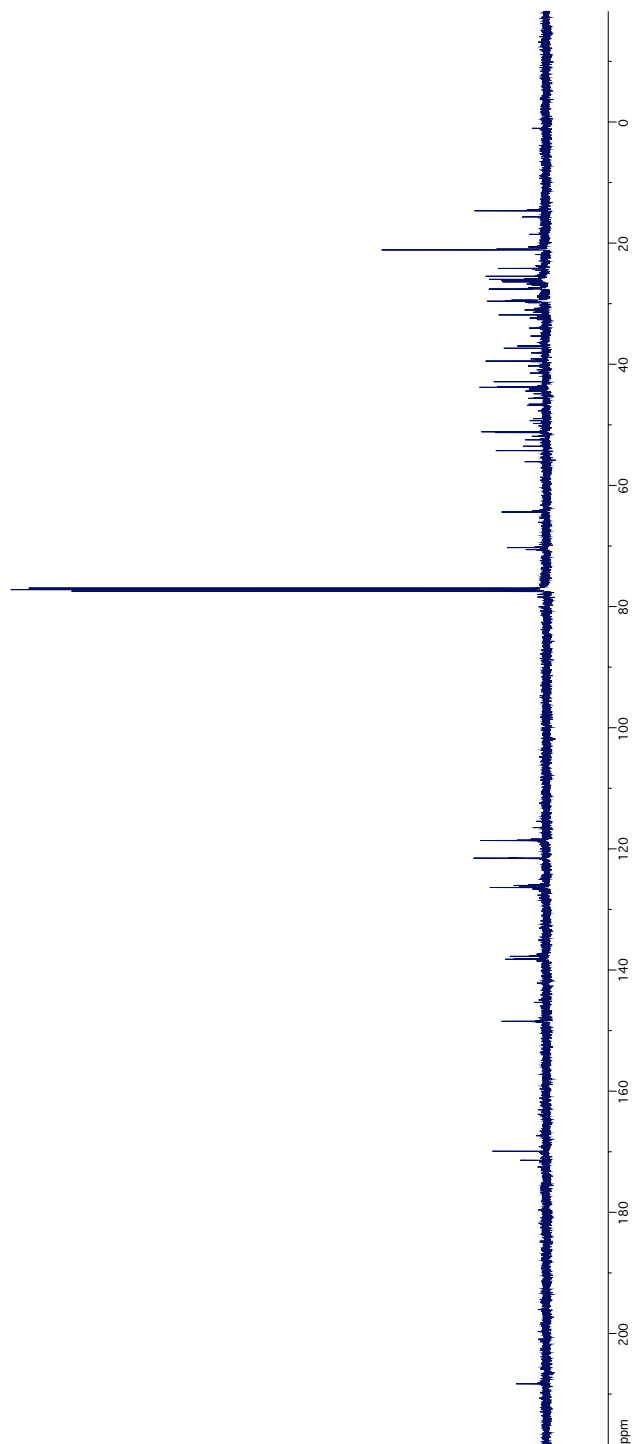
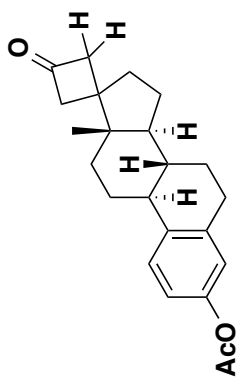
¹³C NMR Spectrum of Compound 80



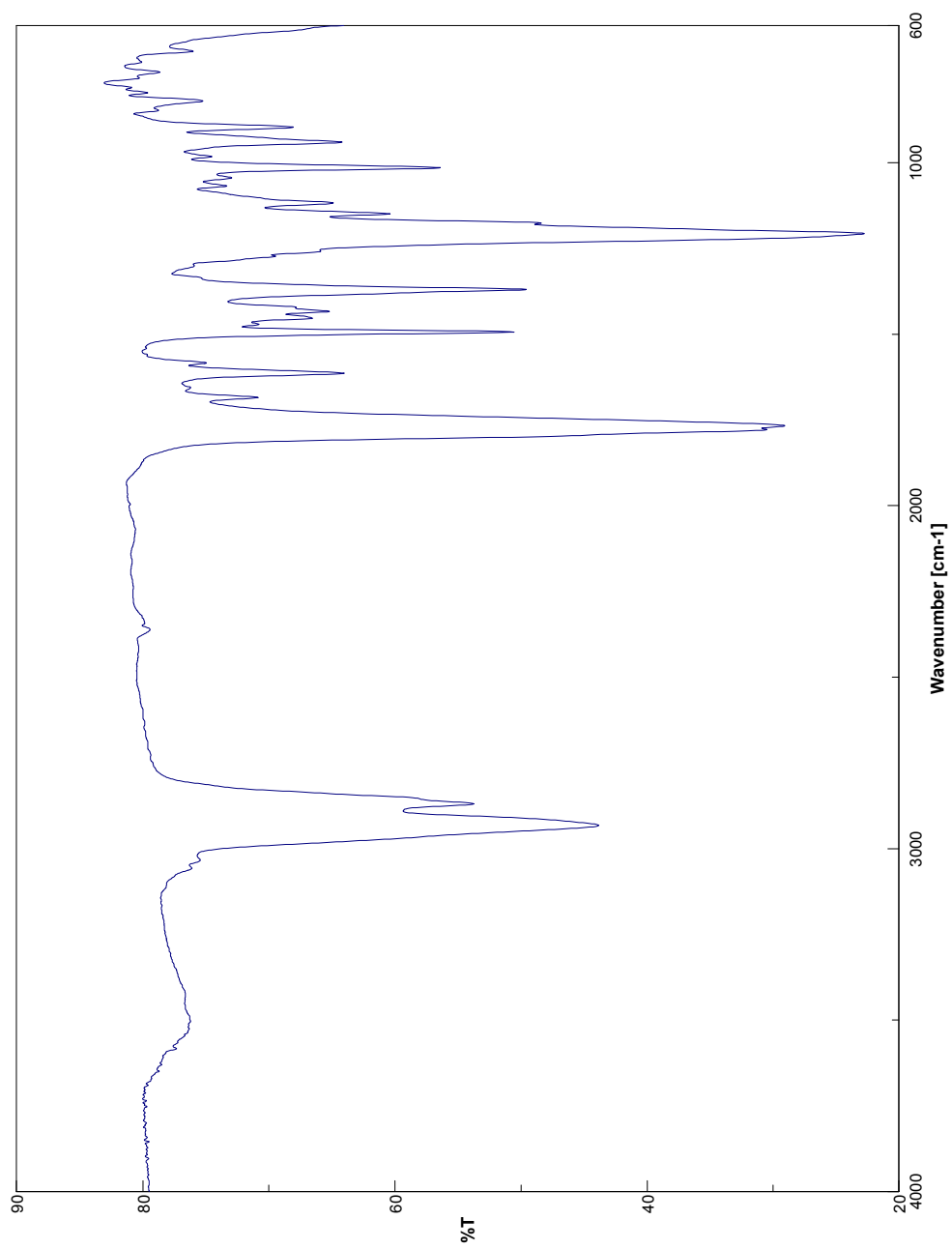
IR Spectrum of Compound **80**



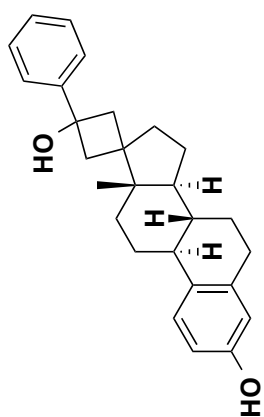
¹H NMR Spectrum of Compound **83**



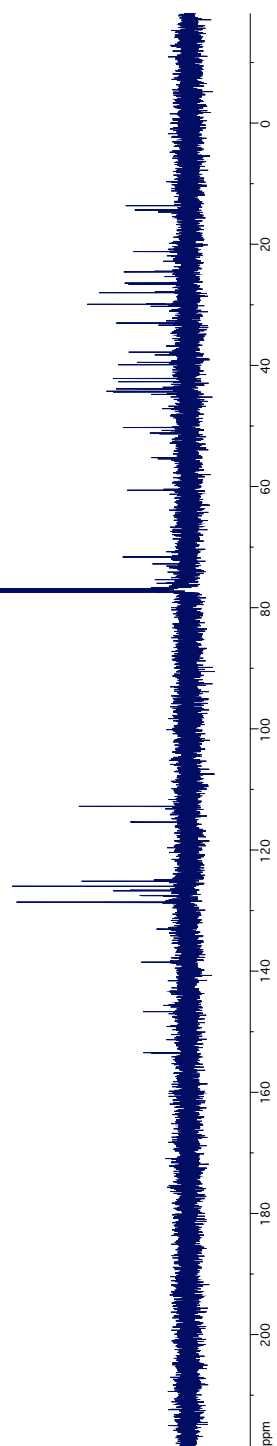
^{13}C NMR Spectrum of Compound 83

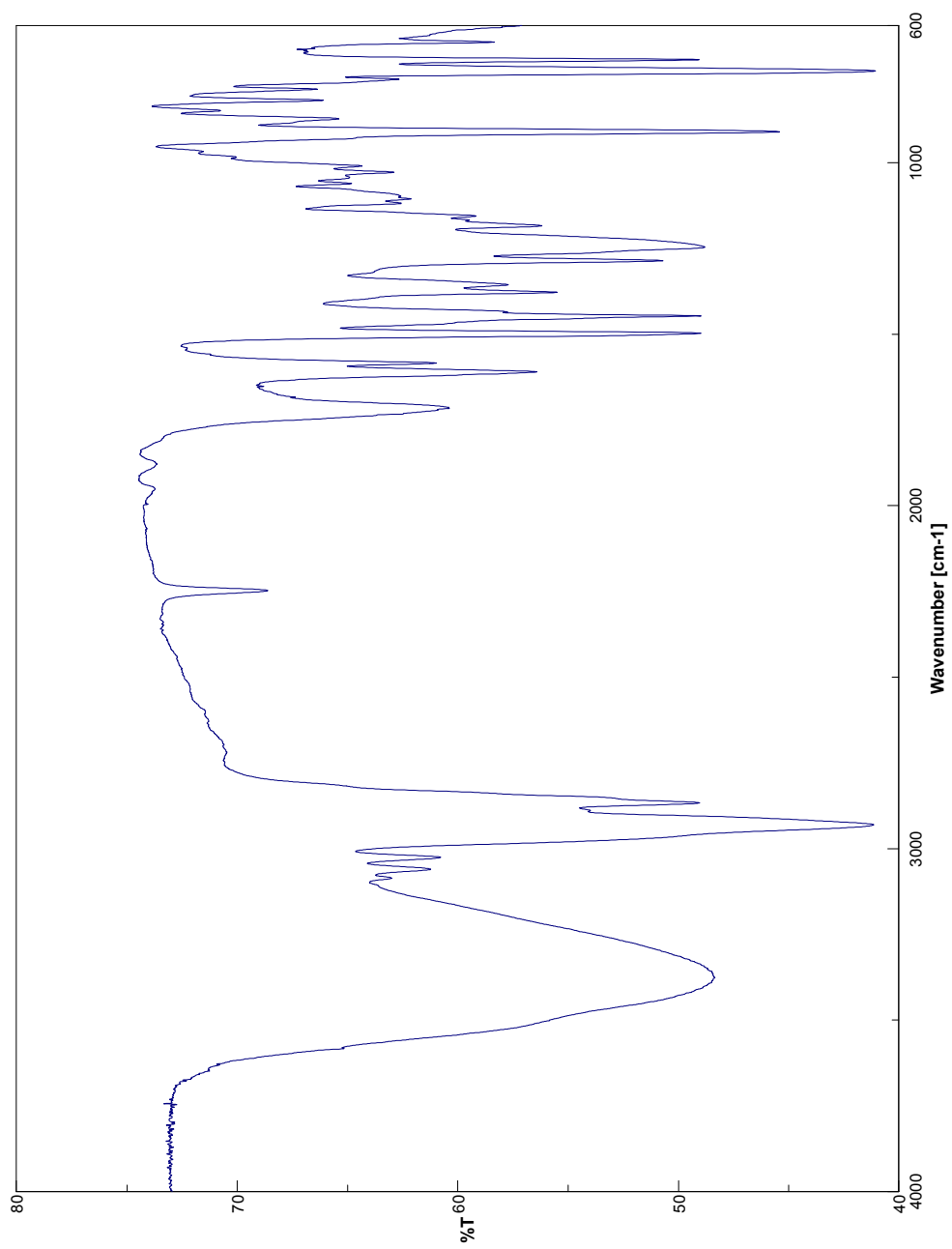


IR Spectrum of Compound **83**

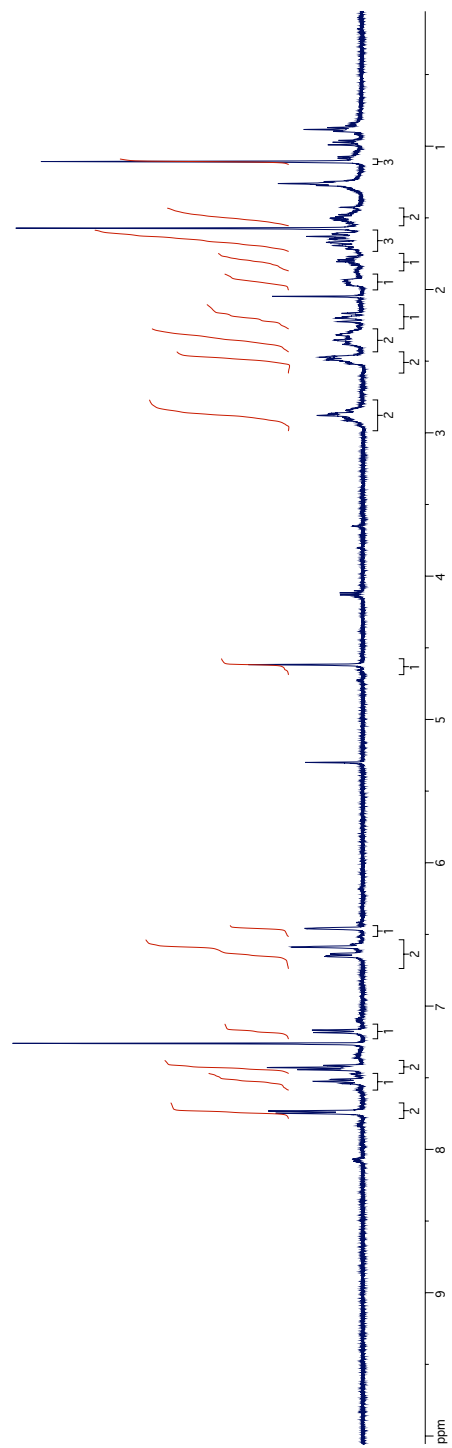
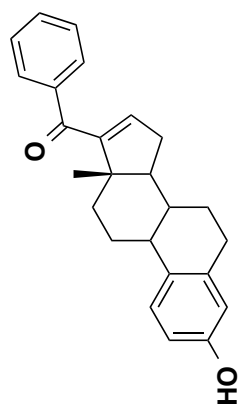


^{13}C NMR Spectrum of Compound 84

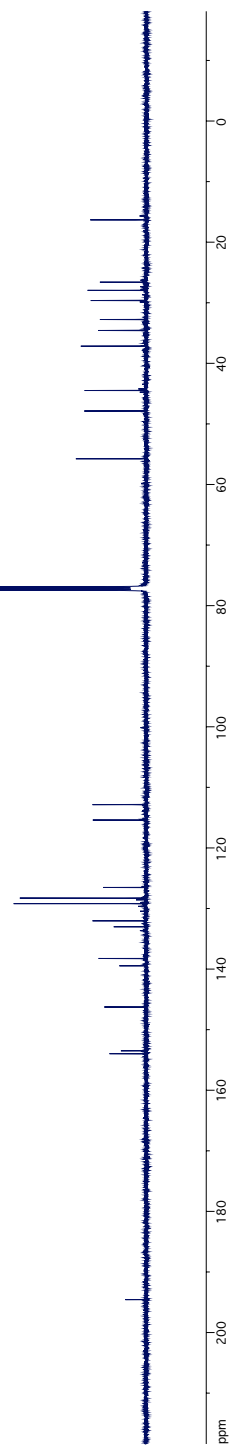
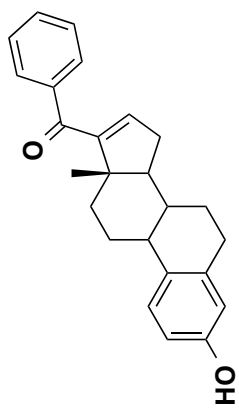




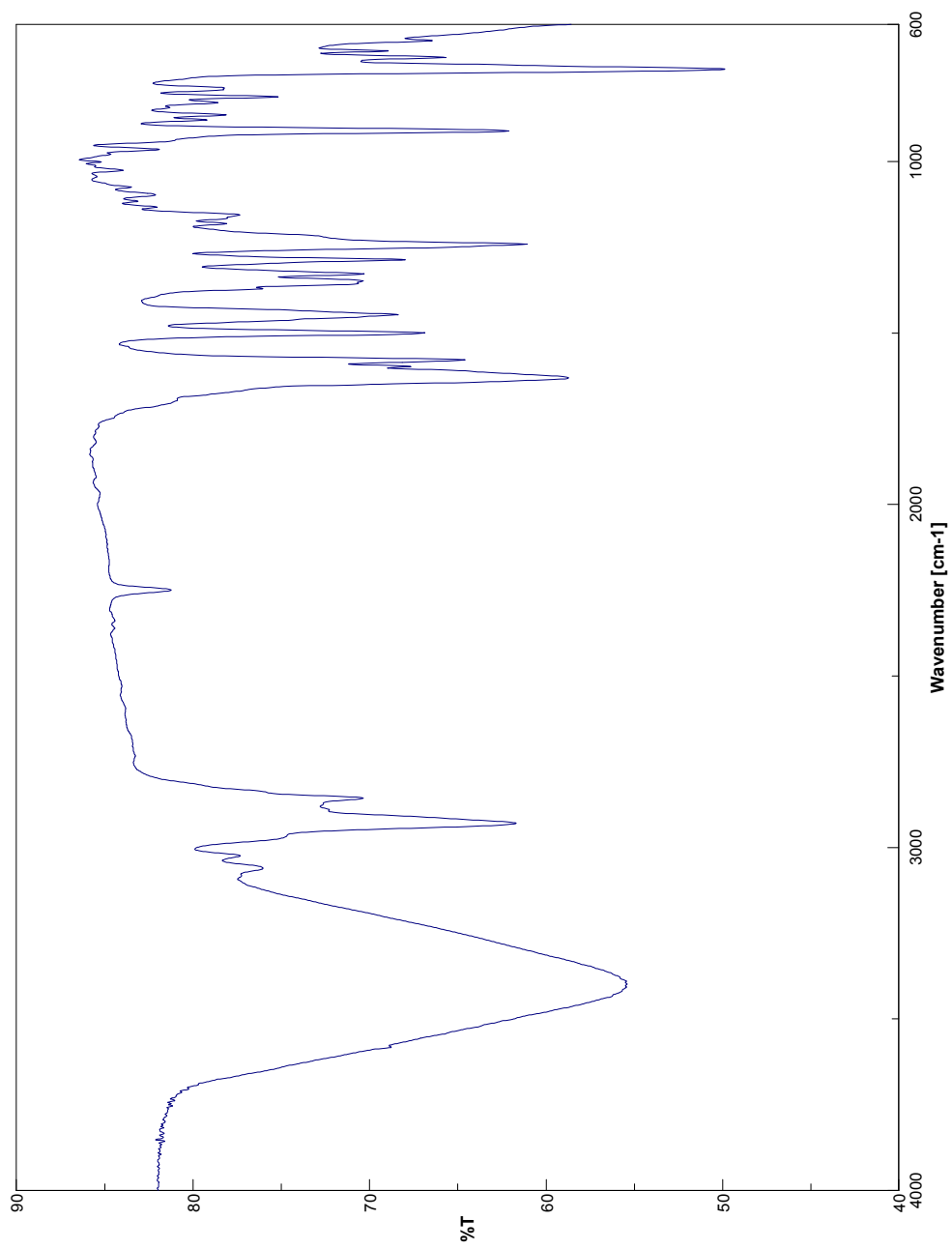
IR Spectrum of Compound **84**



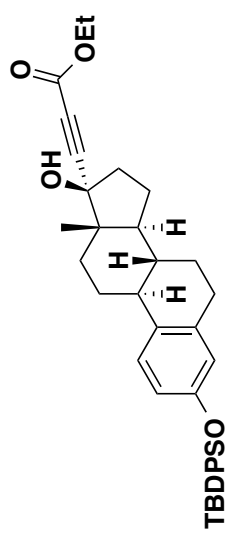
^1H NMR Spectrum of Compound 85



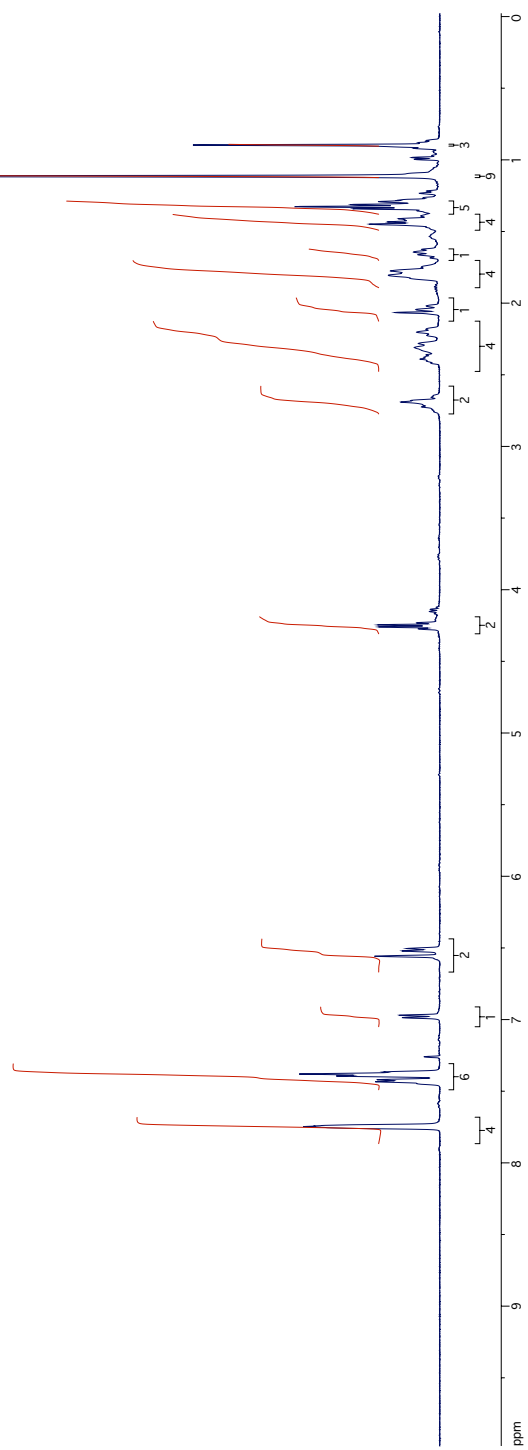
^{13}C NMR Spectrum of Compound 85

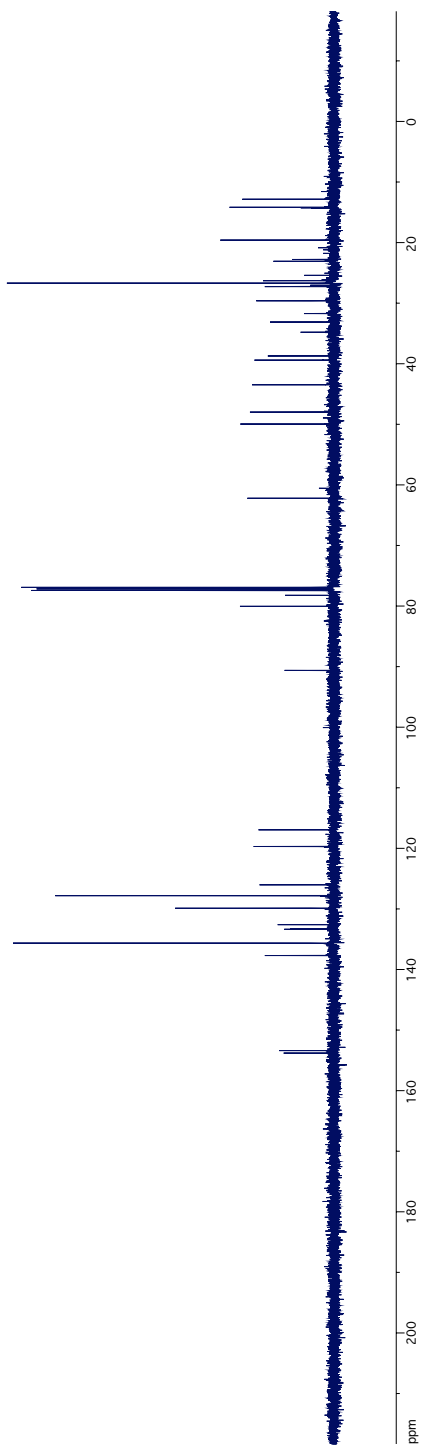
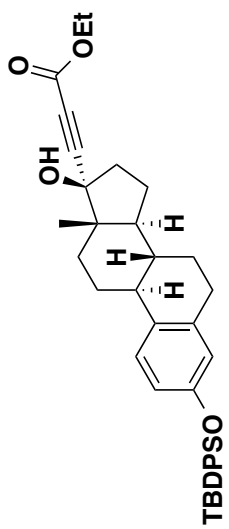


IR Spectrum of Compound **85**

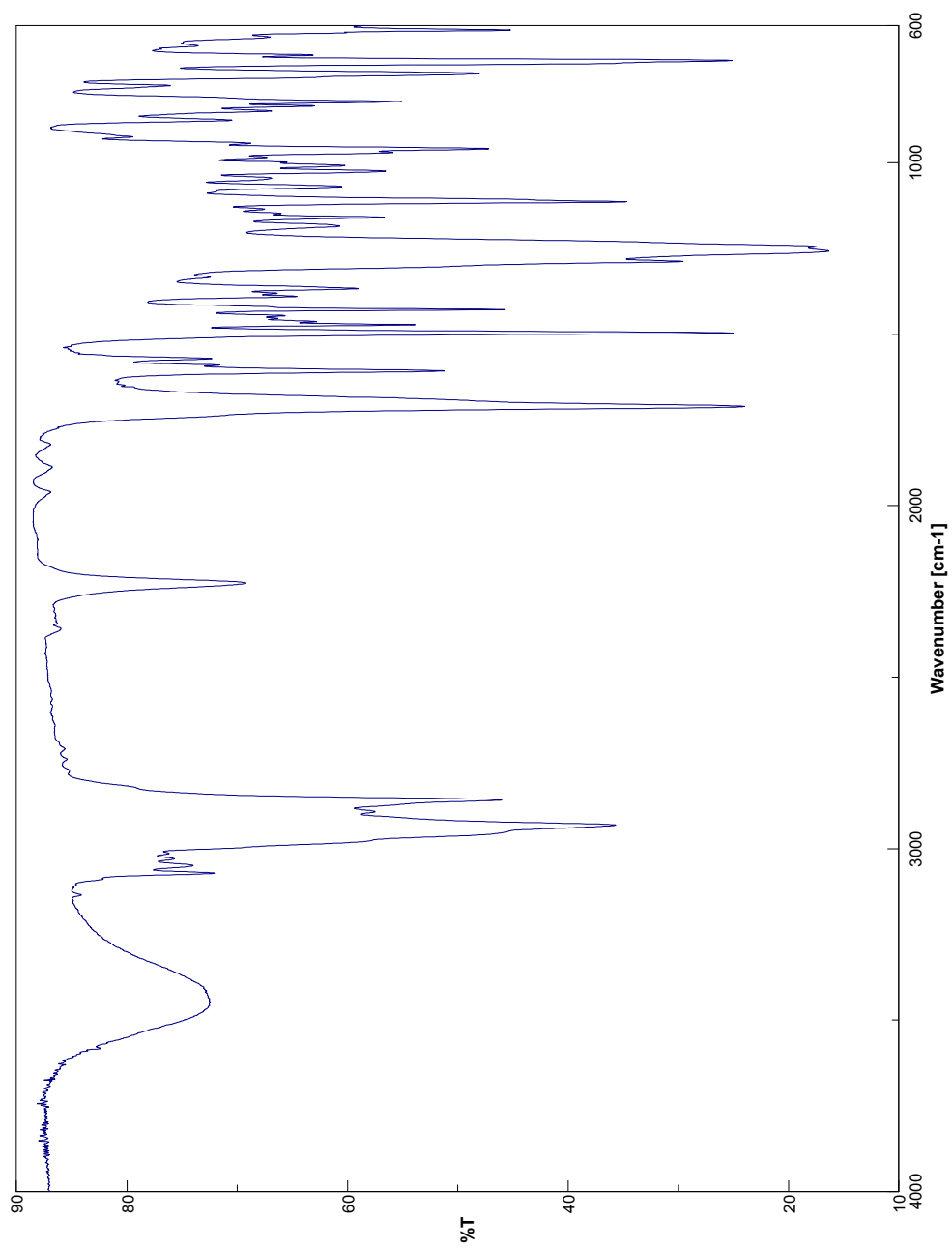


¹H NMR Spectrum of Compound **86**

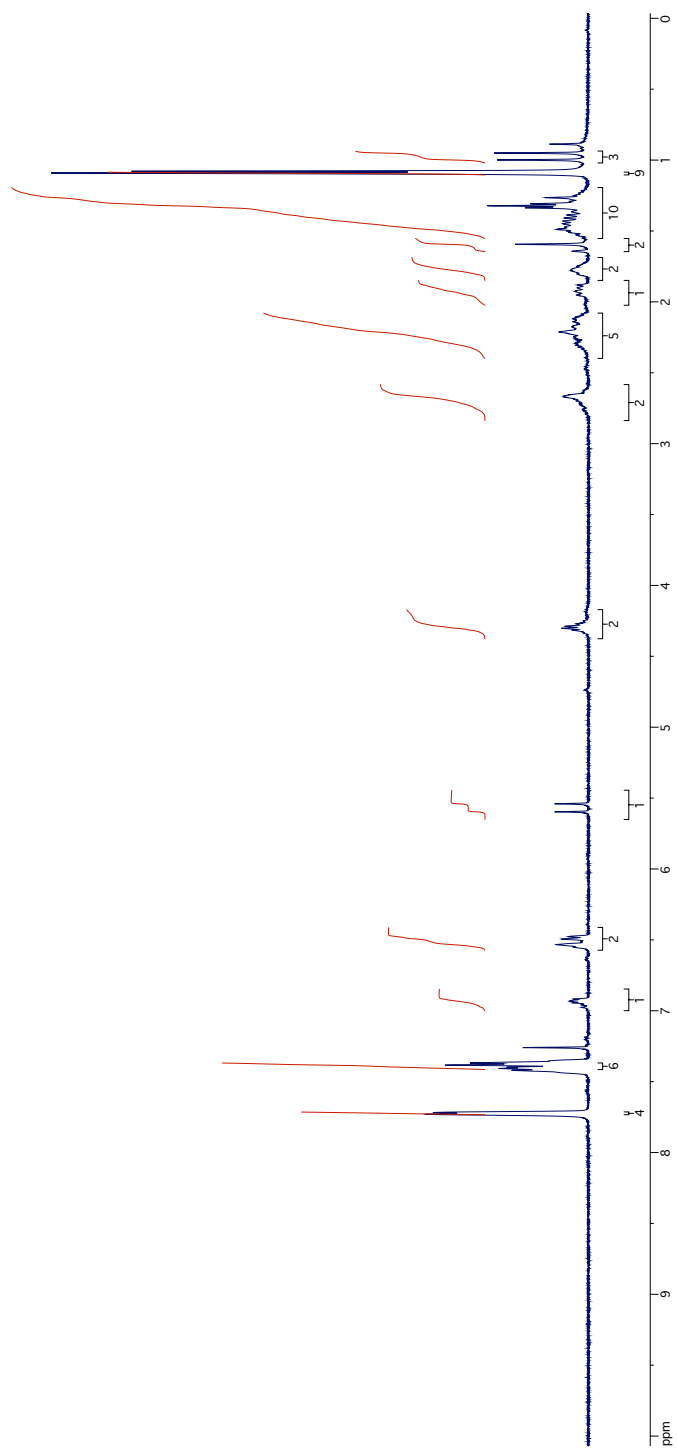
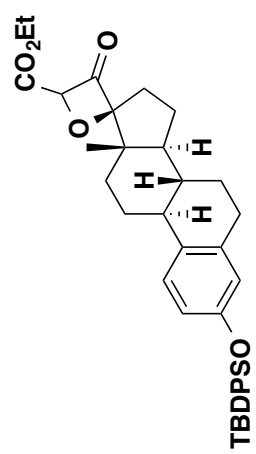




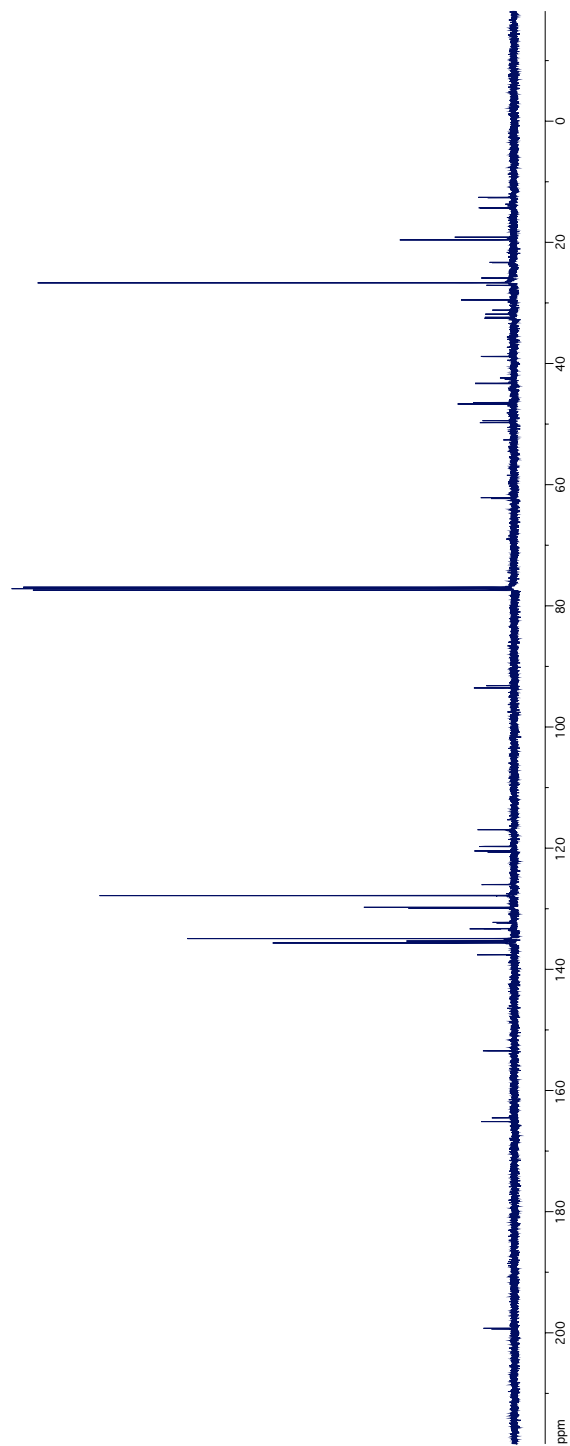
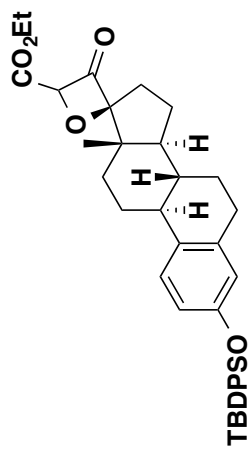
¹³C NMR Spectrum of Compound **86**



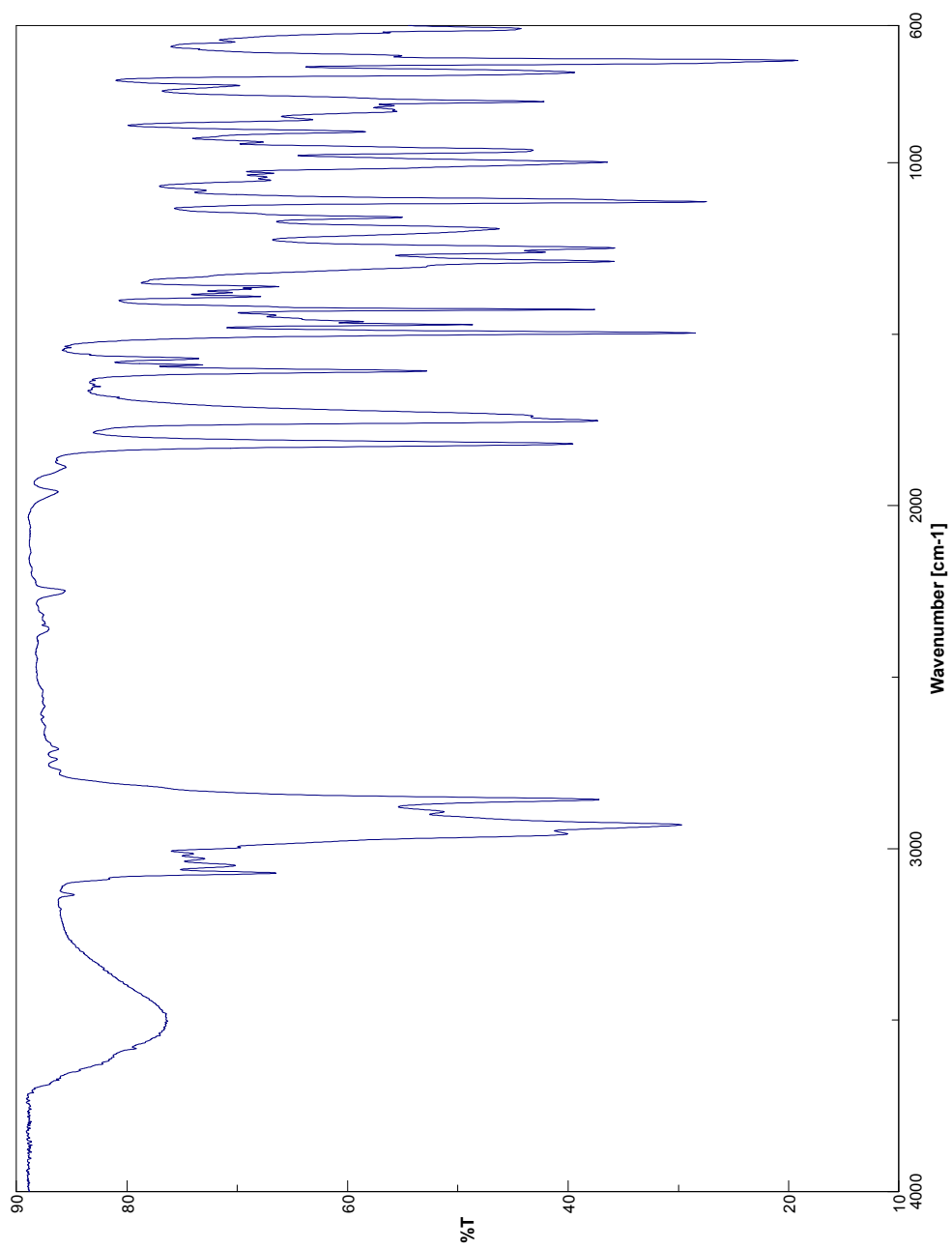
IR Spectrum of Compound **86**



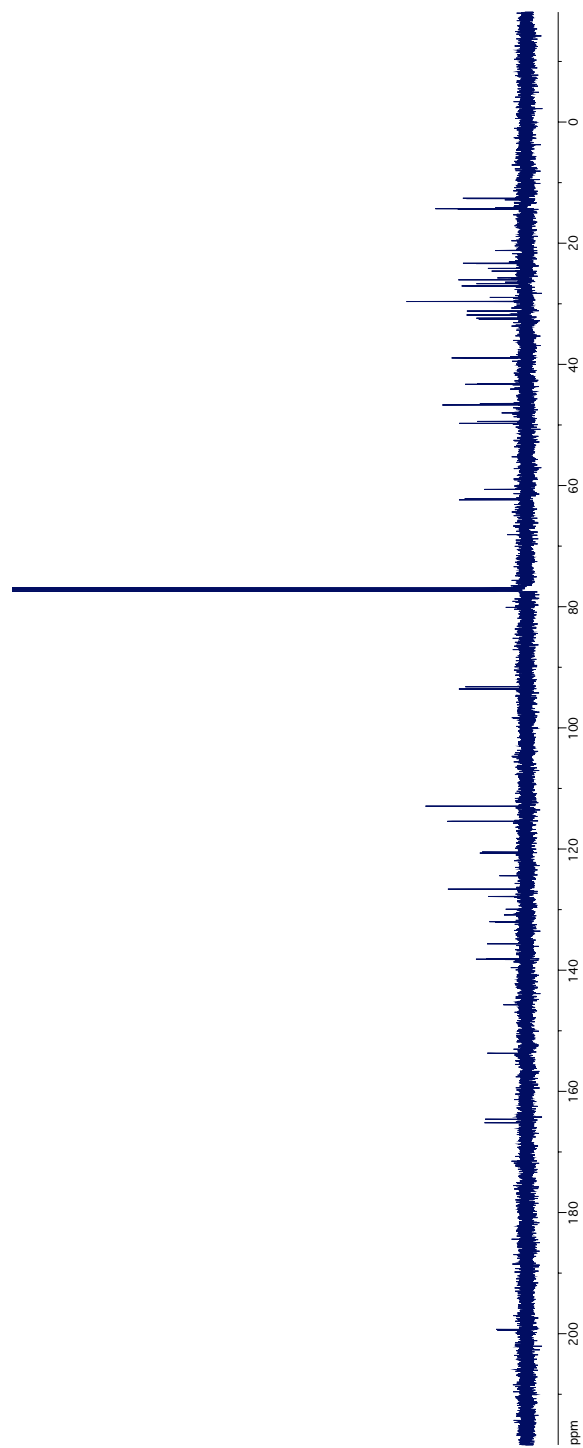
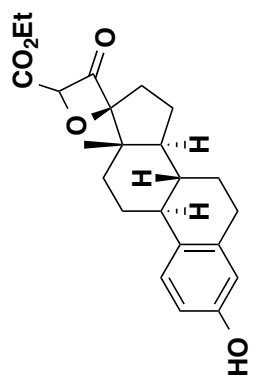
¹H NMR Spectrum of Compound **87**



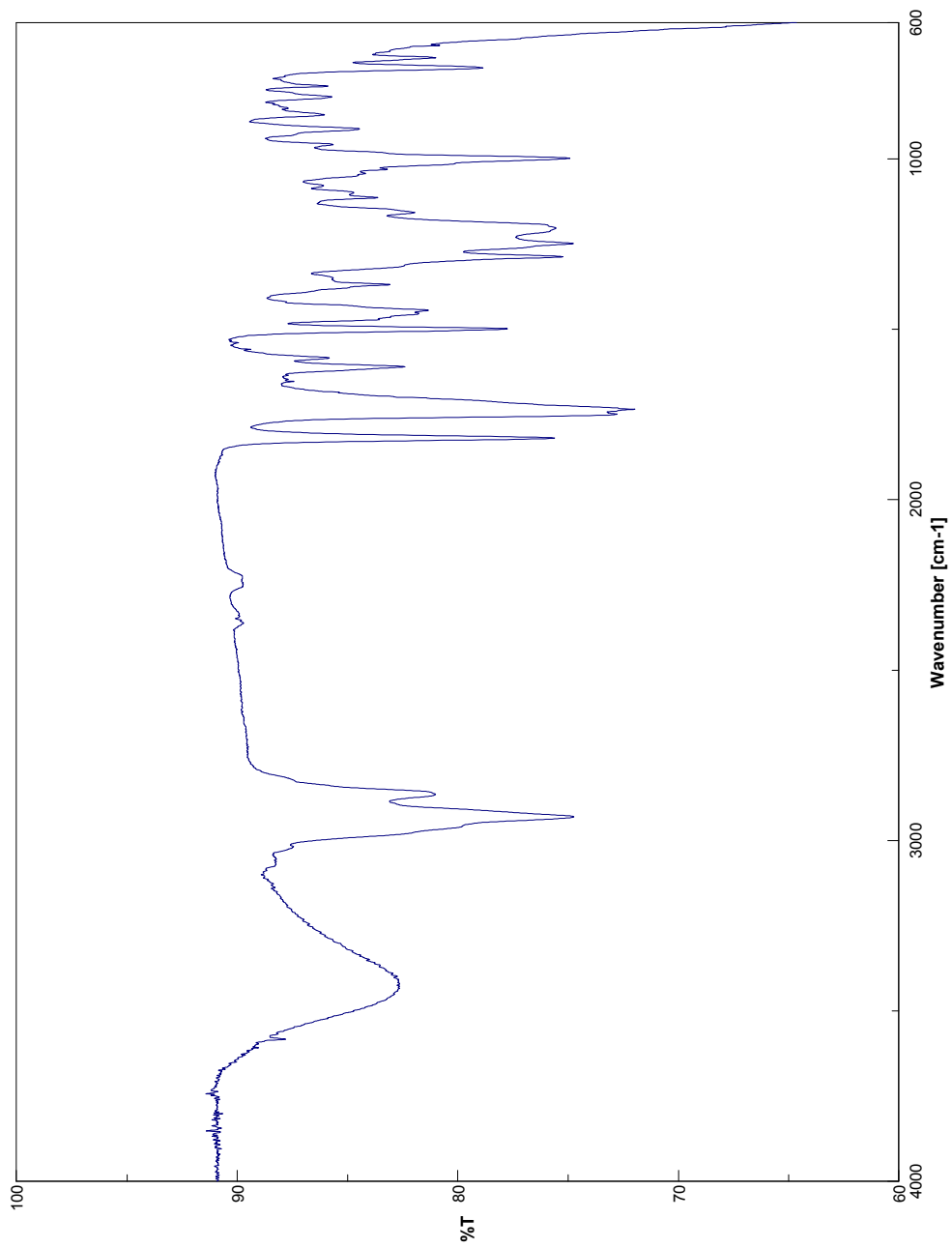
^{13}C NMR Spectrum of Compound **87**



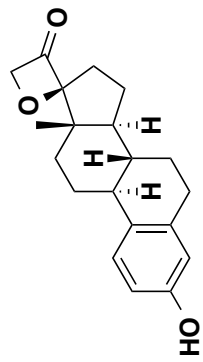
IR Spectrum of Compound 87



¹³C NMR Spectrum of Compound 88

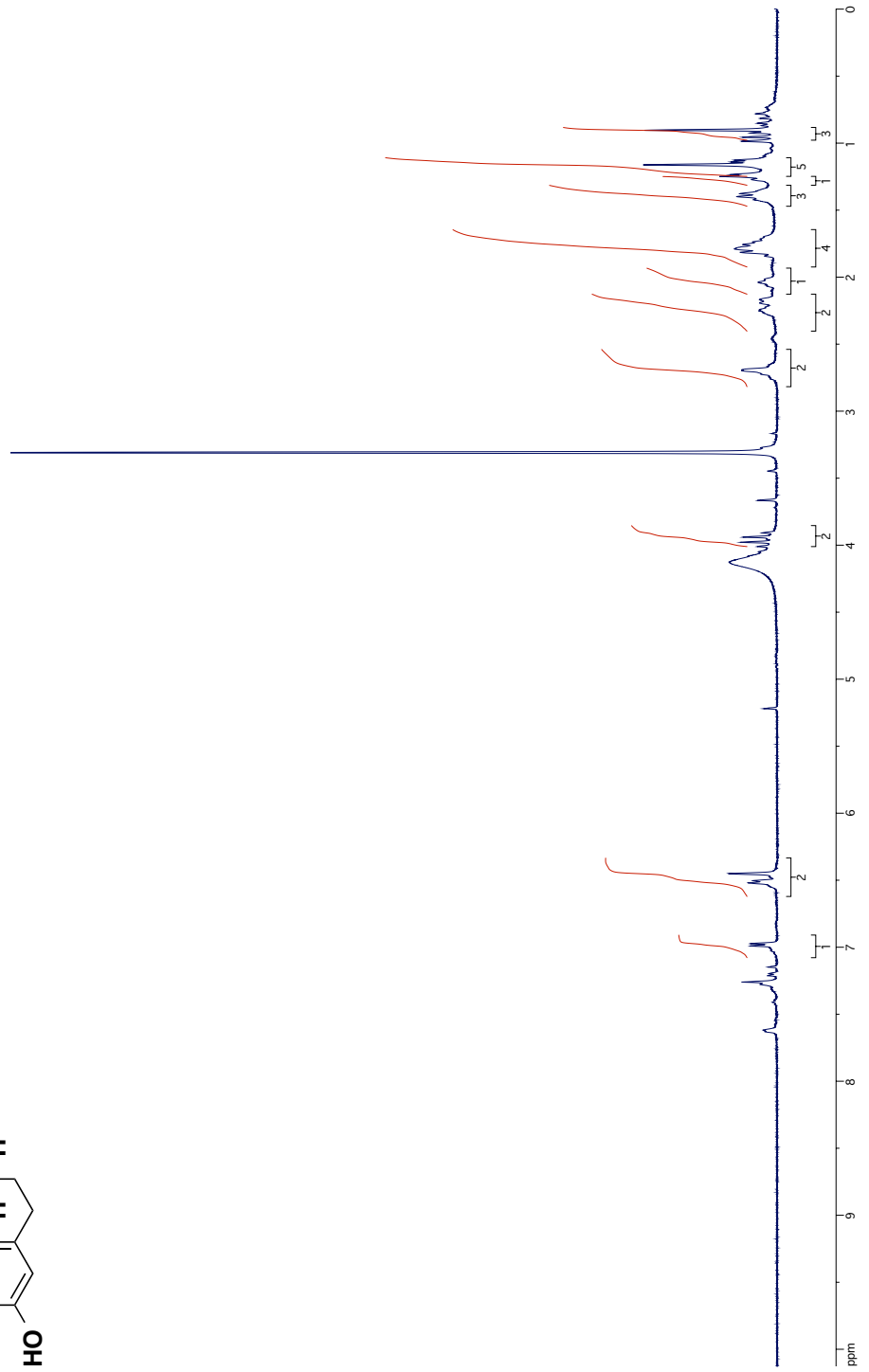


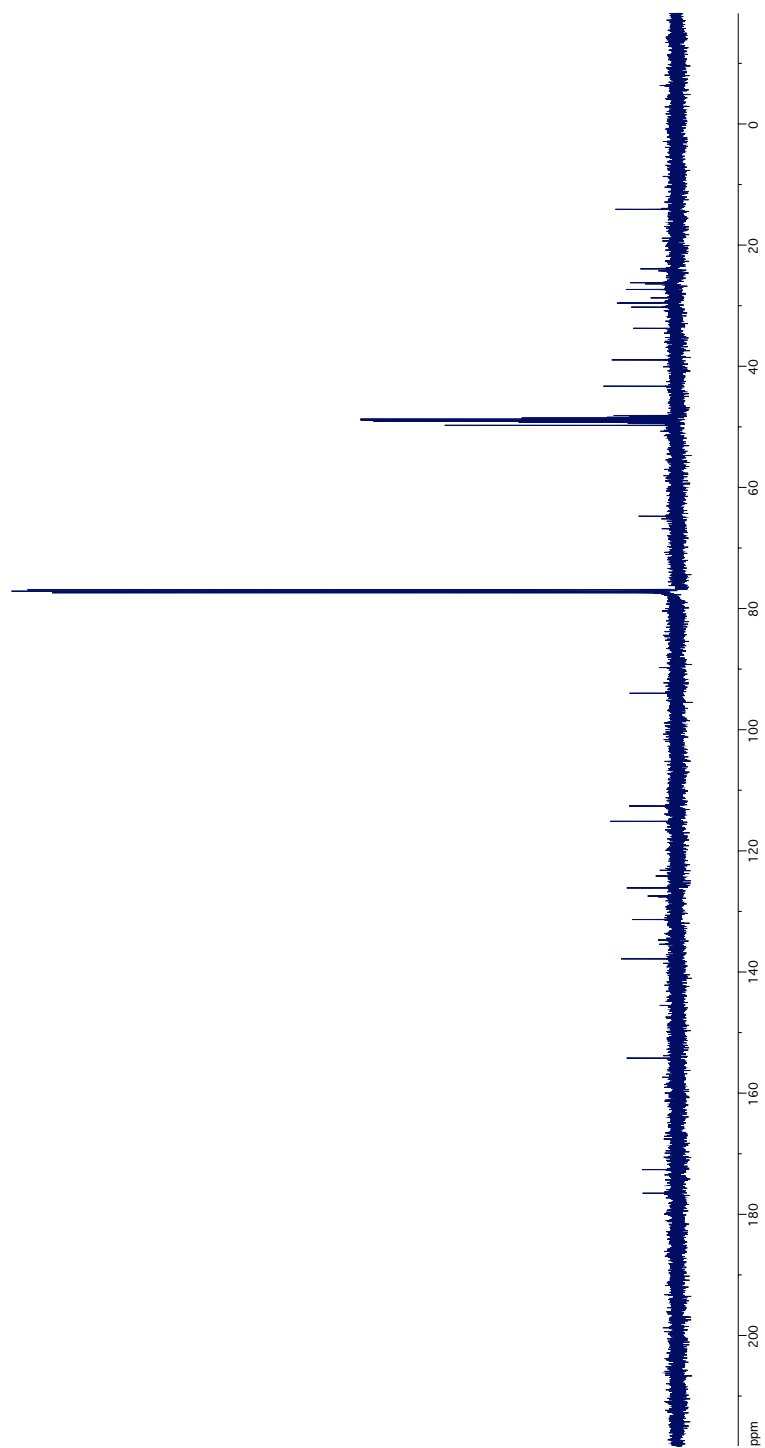
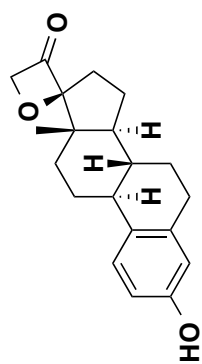
IR Spectrum of Compound **88**



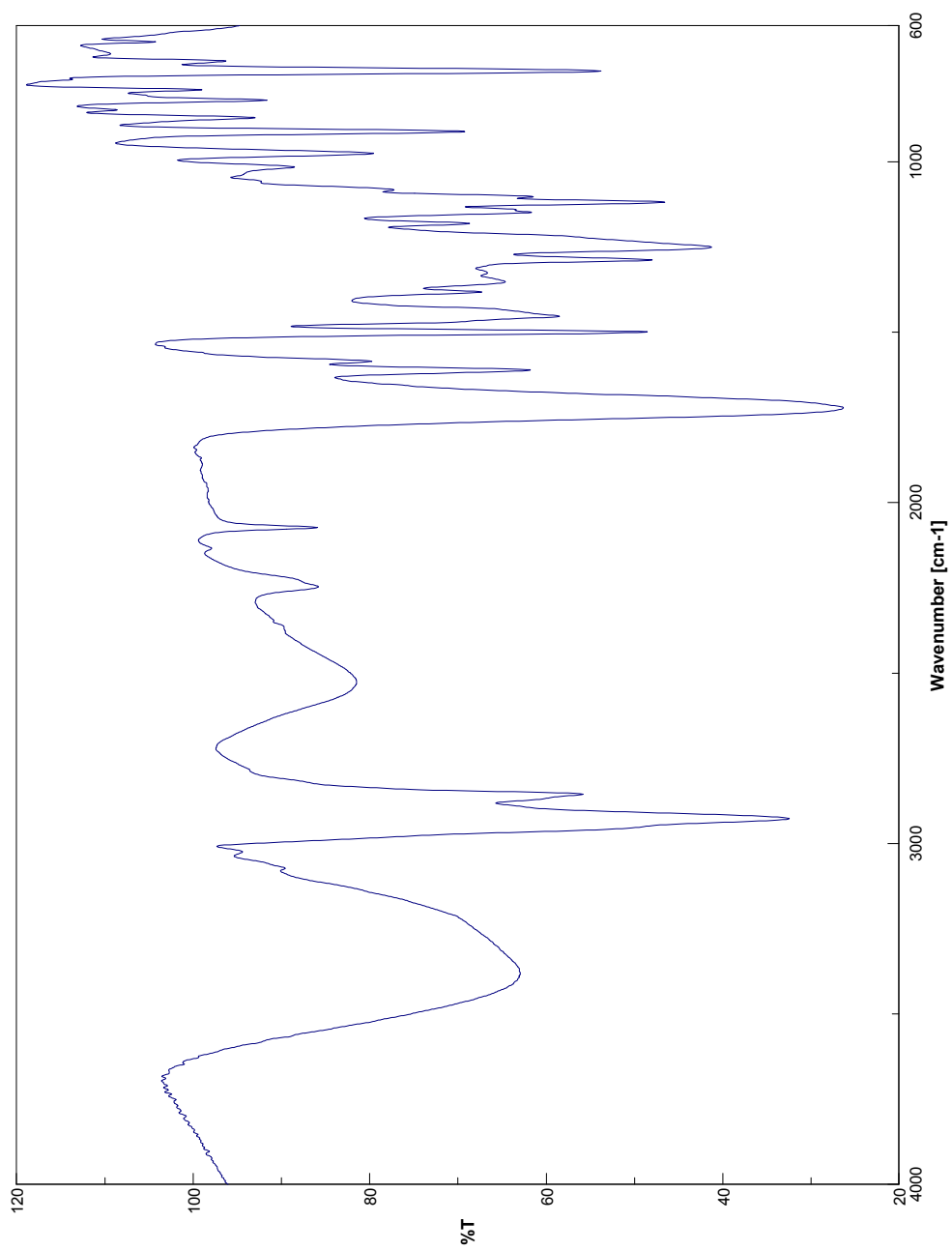
¹H NMR Spectrum of Compound 89

376

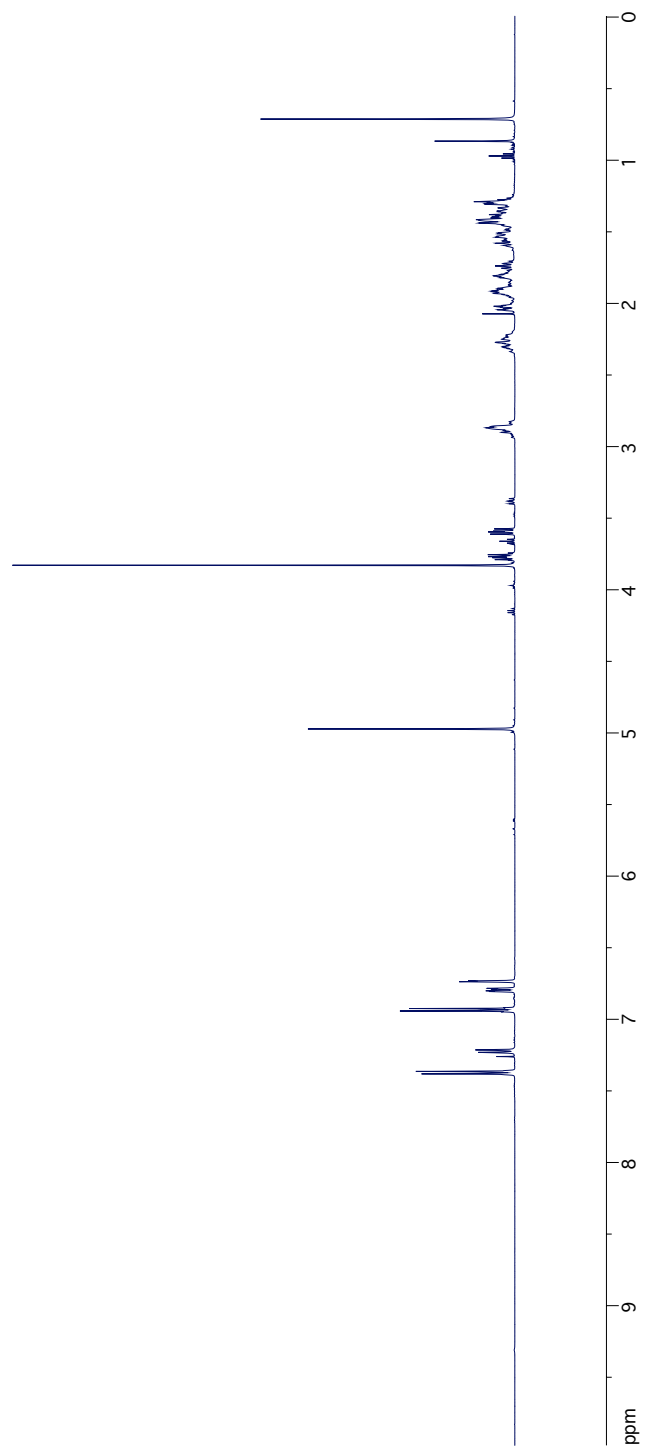
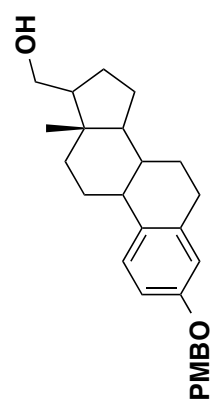




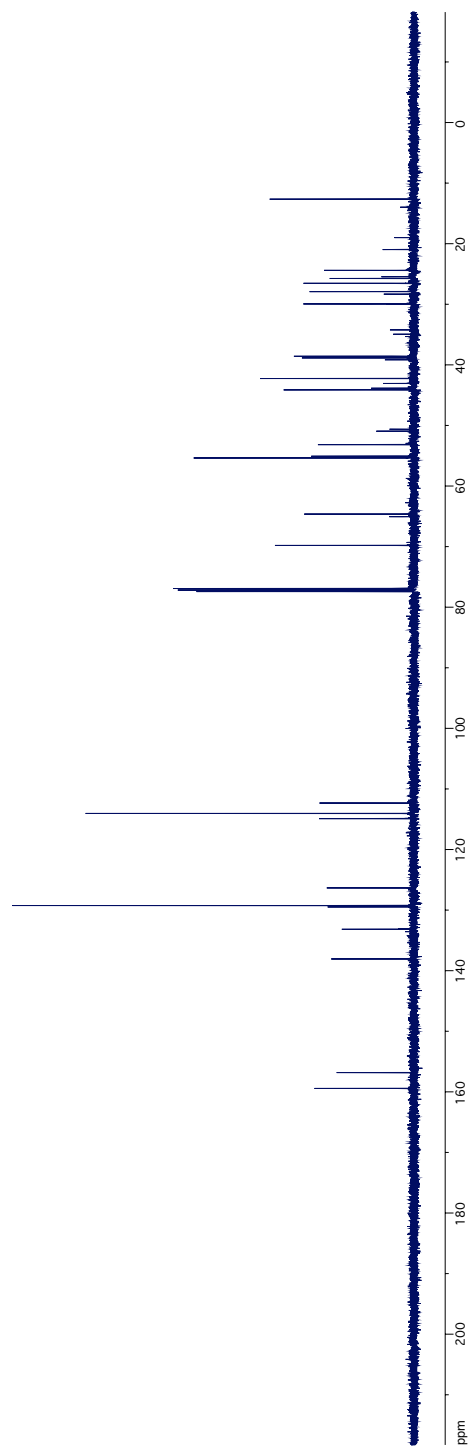
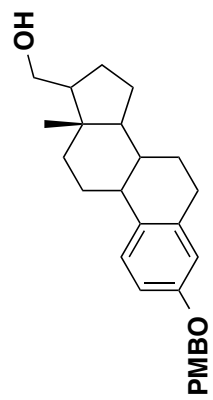
^{13}C NMR Spectrum of Compound 89



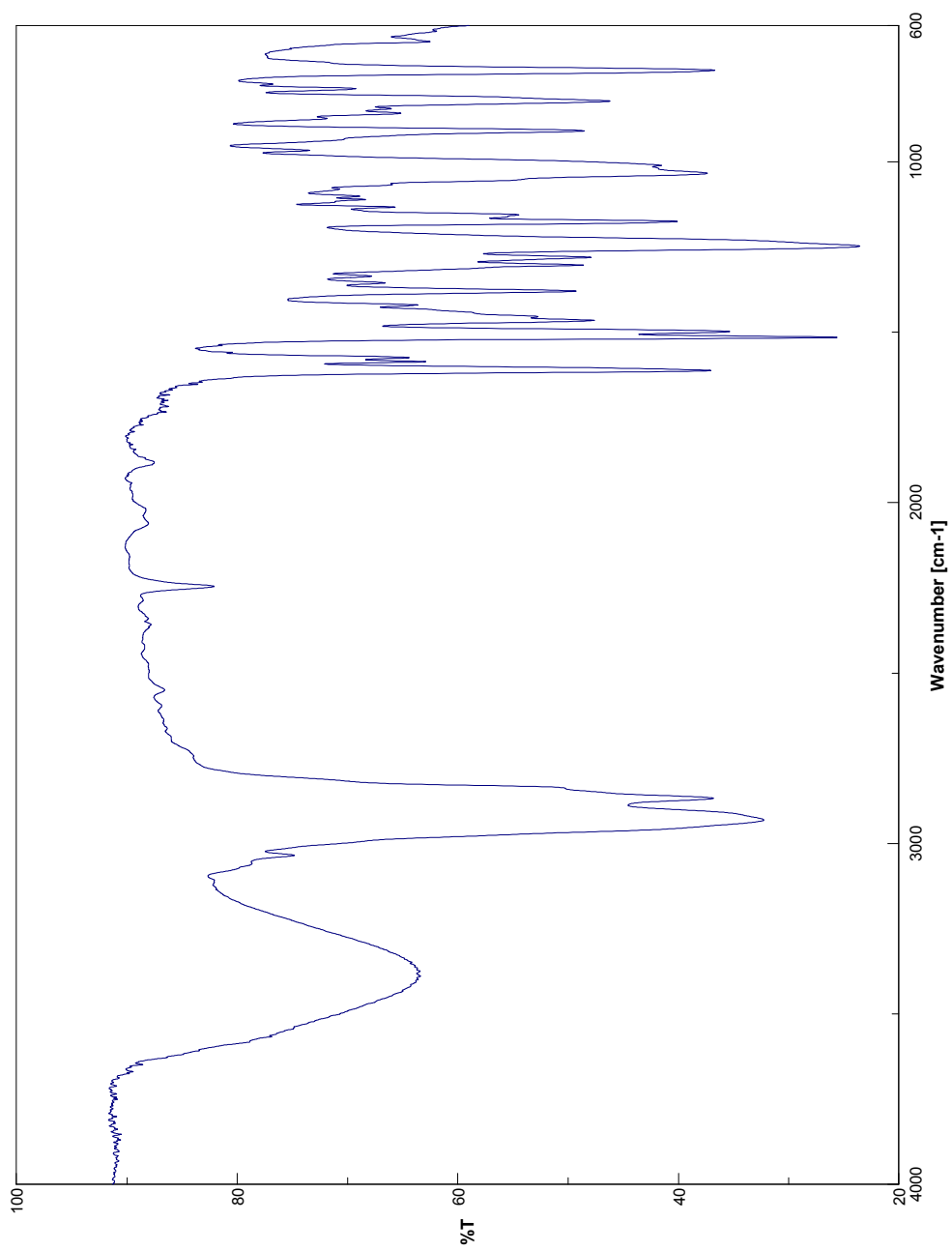
IR Spectrum of Compound **89**



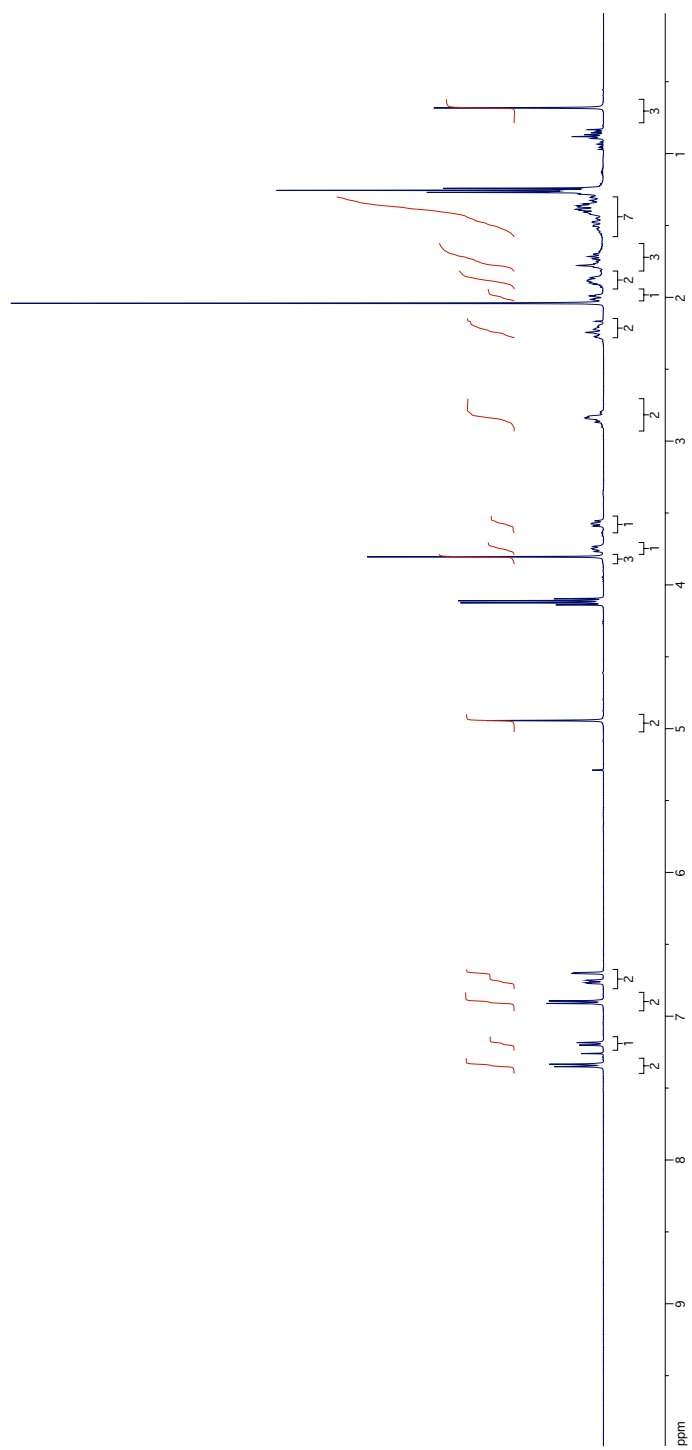
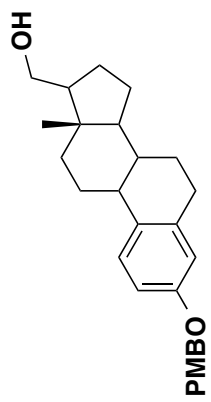
¹H NMR Spectrum of Compound **91**



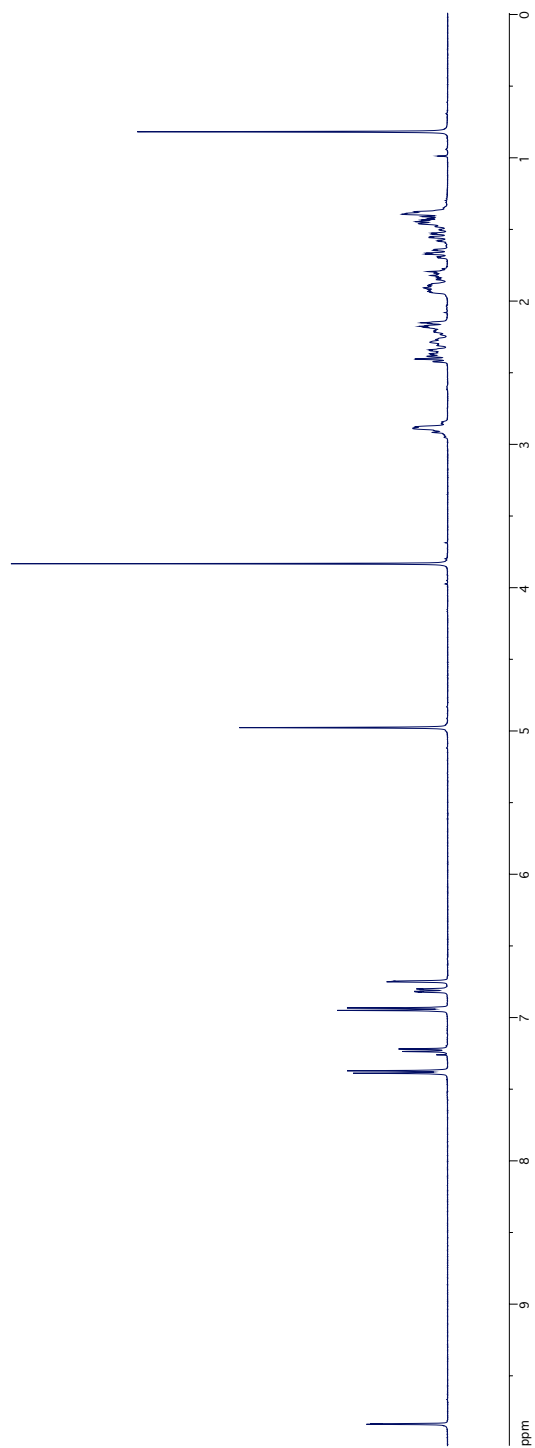
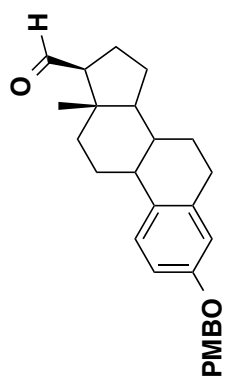
^{13}C NMR Spectrum of Compound **91**



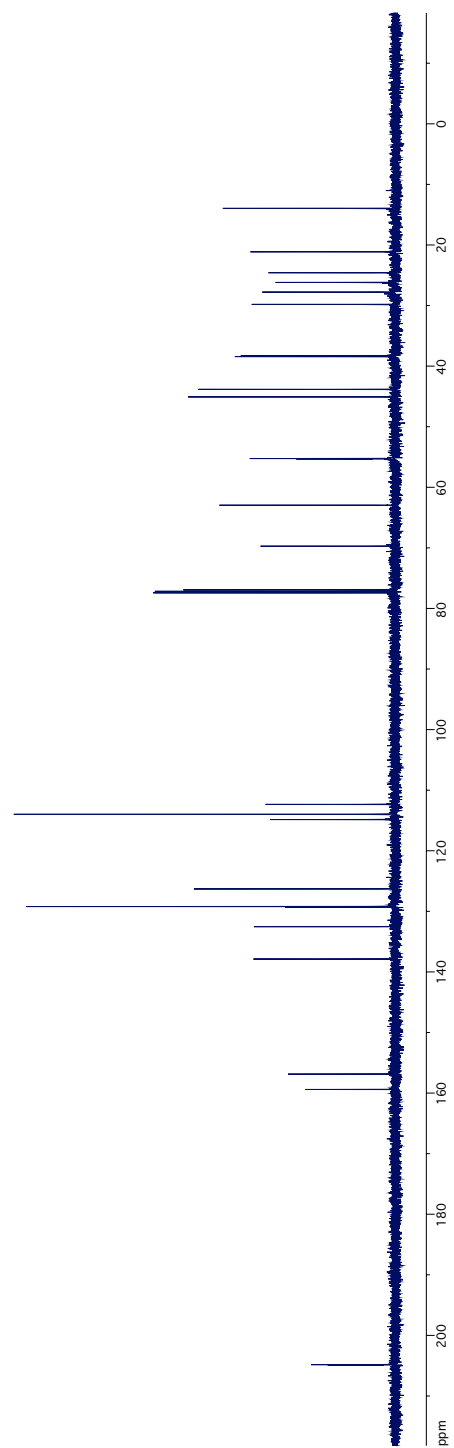
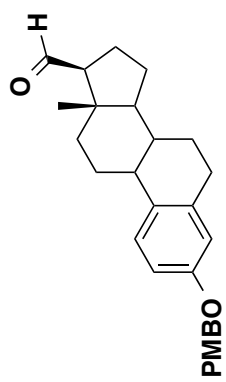
IR Spectrum of Compound **91**



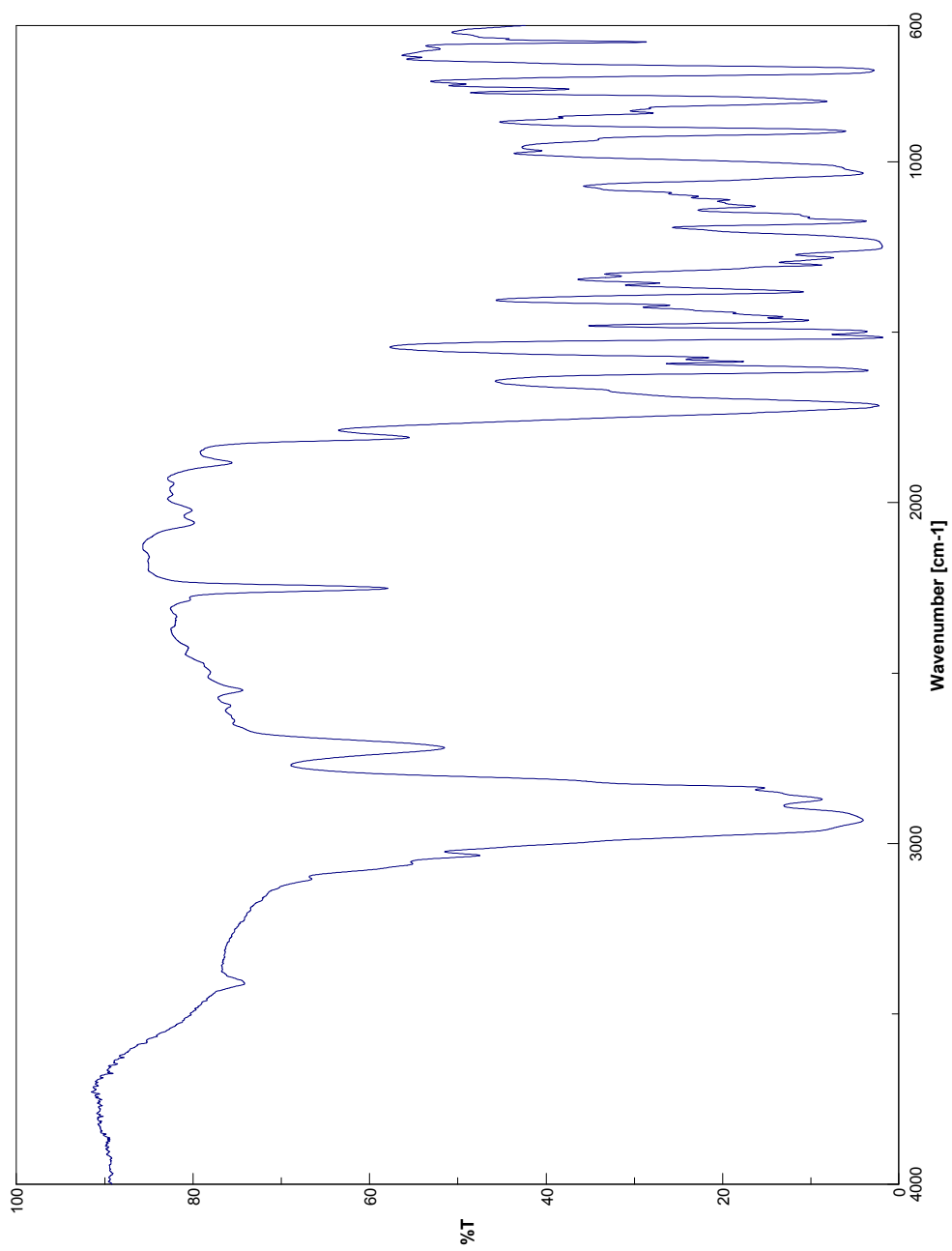
¹H NMR Spectrum of Compound **91: 1 epimer**



^1H NMR Spectrum of Compound **92**

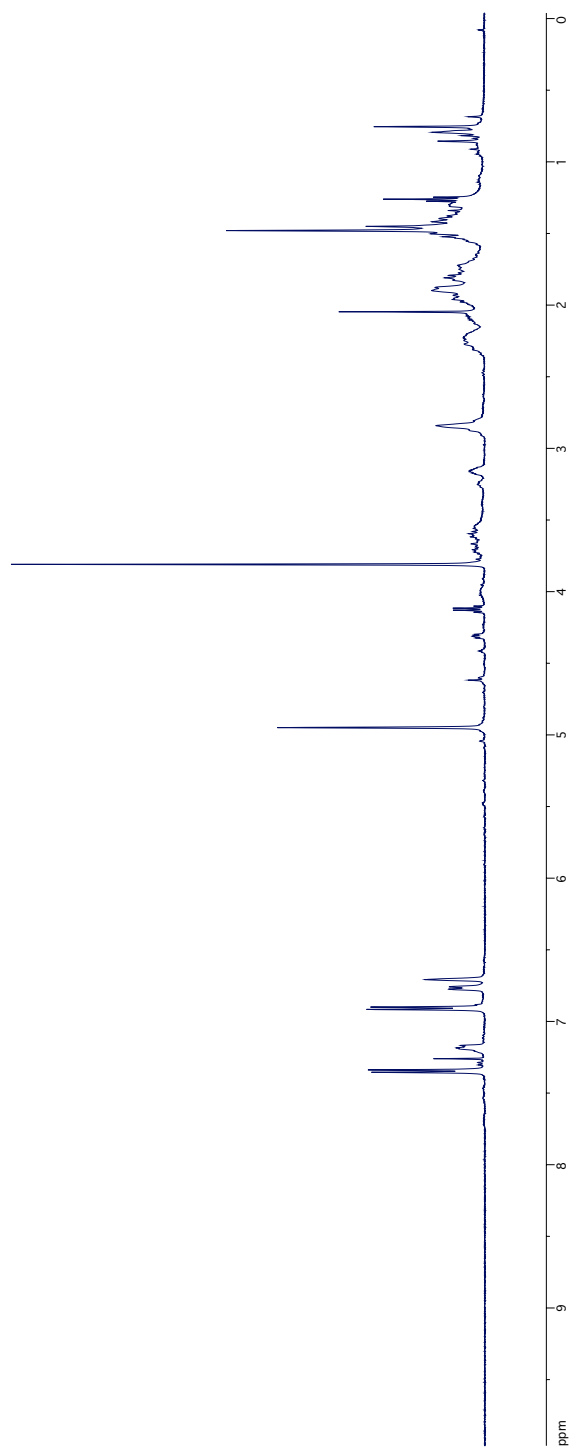
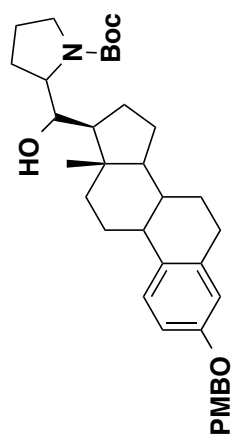


^{13}C NMR Spectrum of Compound **92**

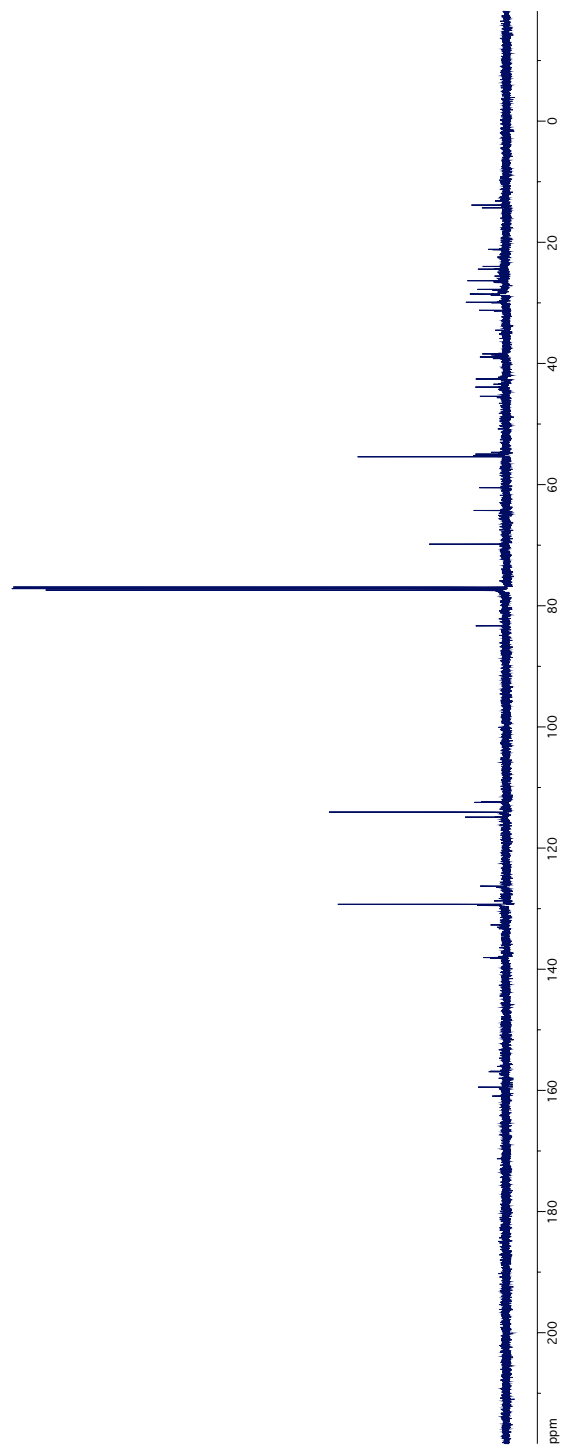
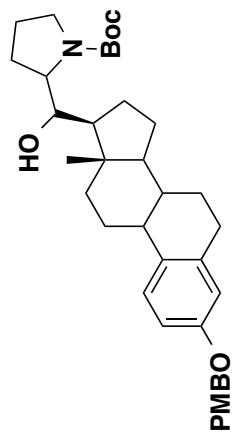


IR Spectrum of Compound **92**

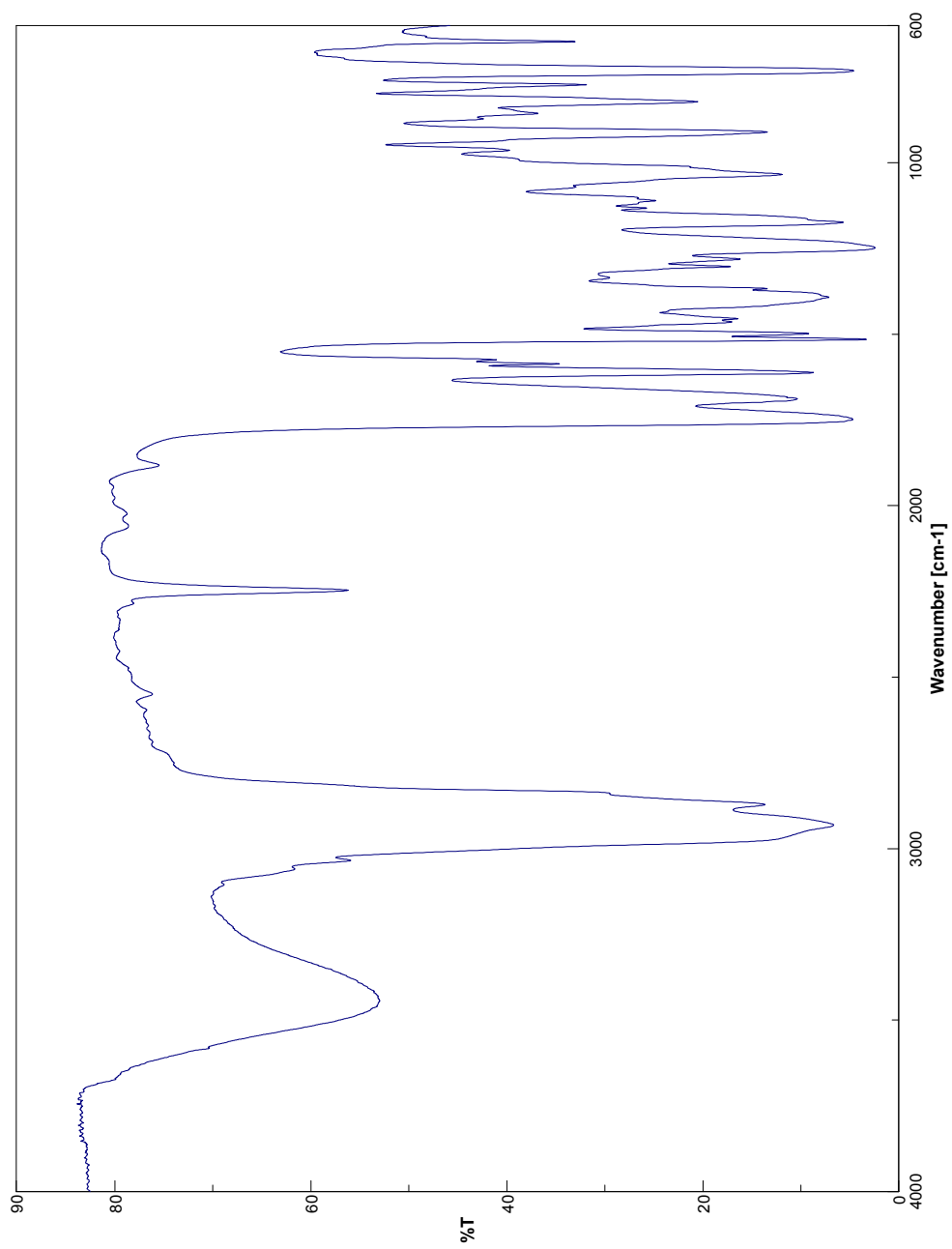
385



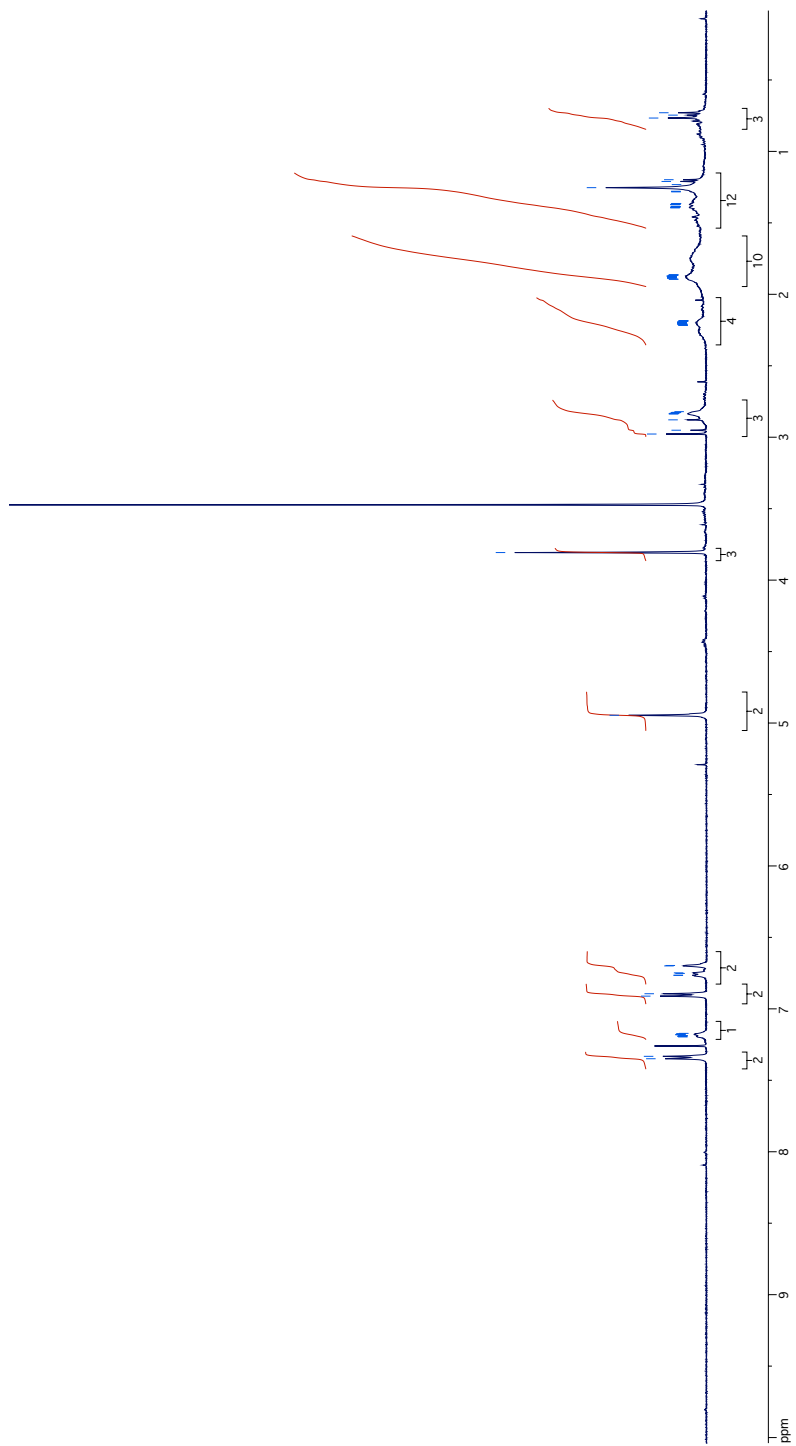
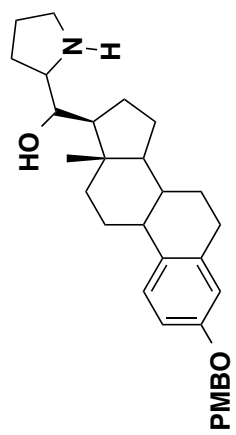
^1H NMR Spectrum of Compound **93**



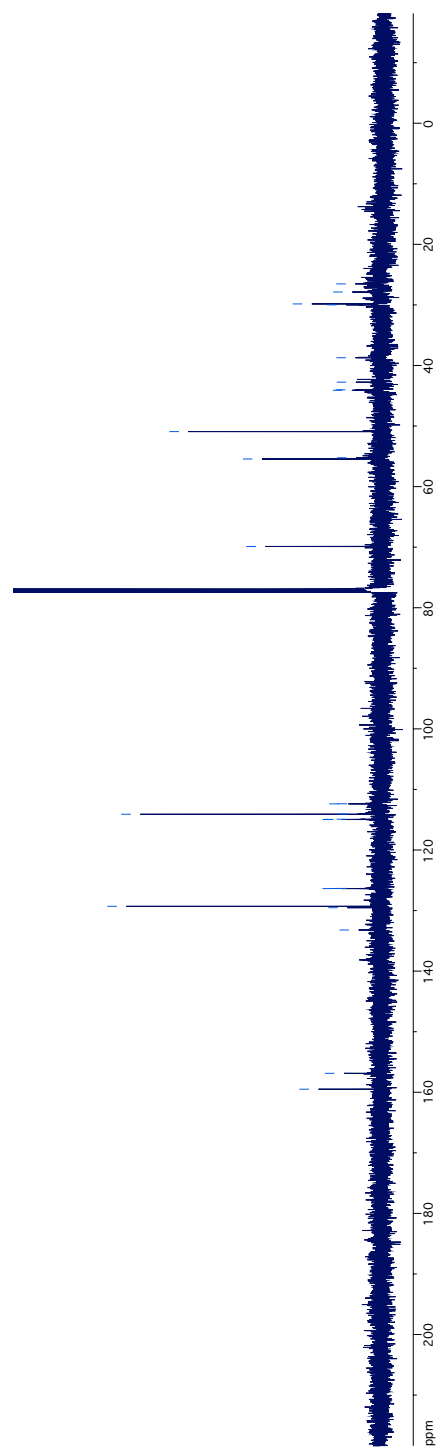
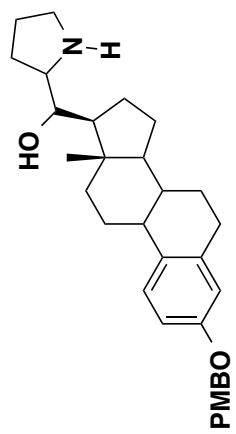
¹³C NMR Spectrum of Compound **93**



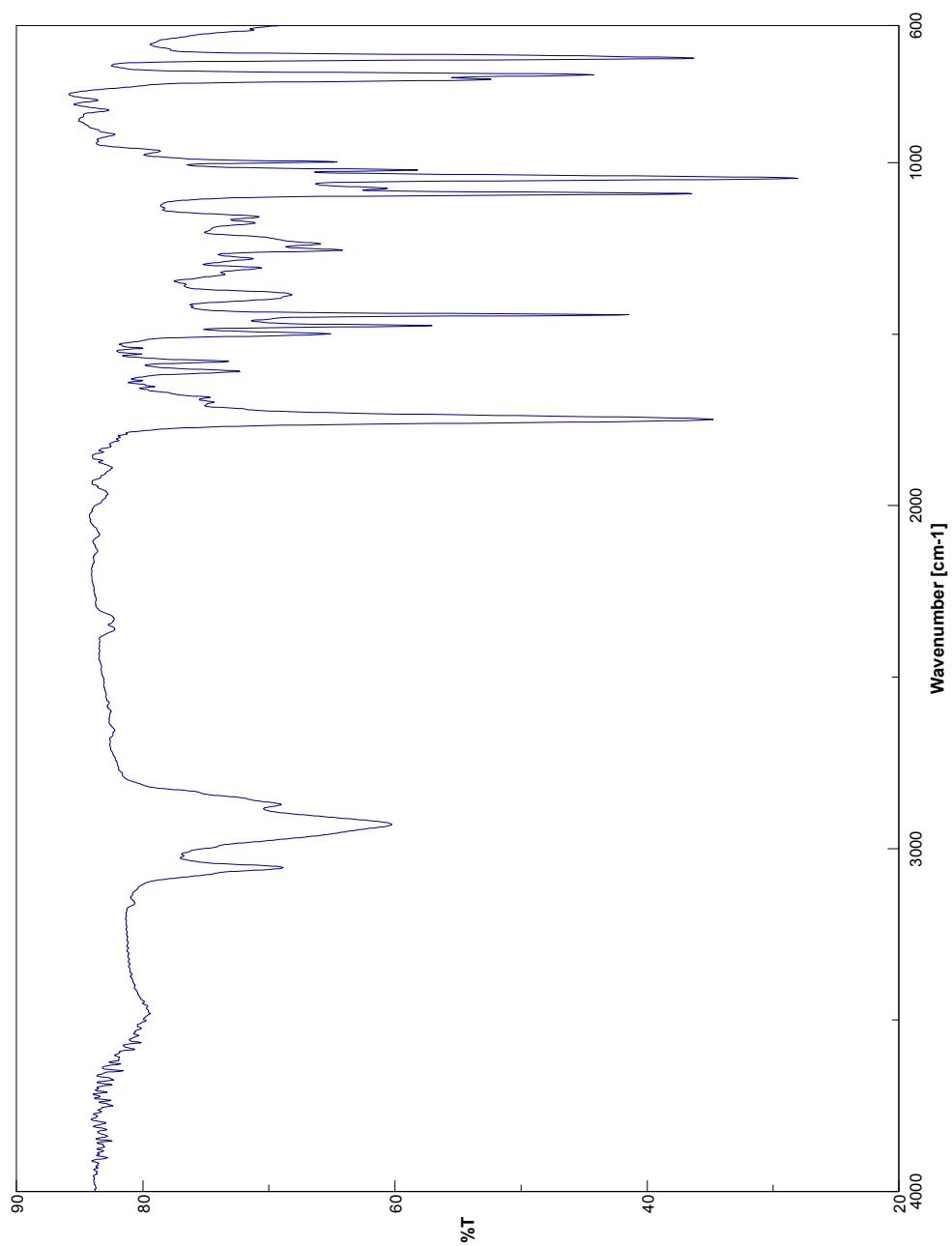
IR Spectrum of Compound **93**



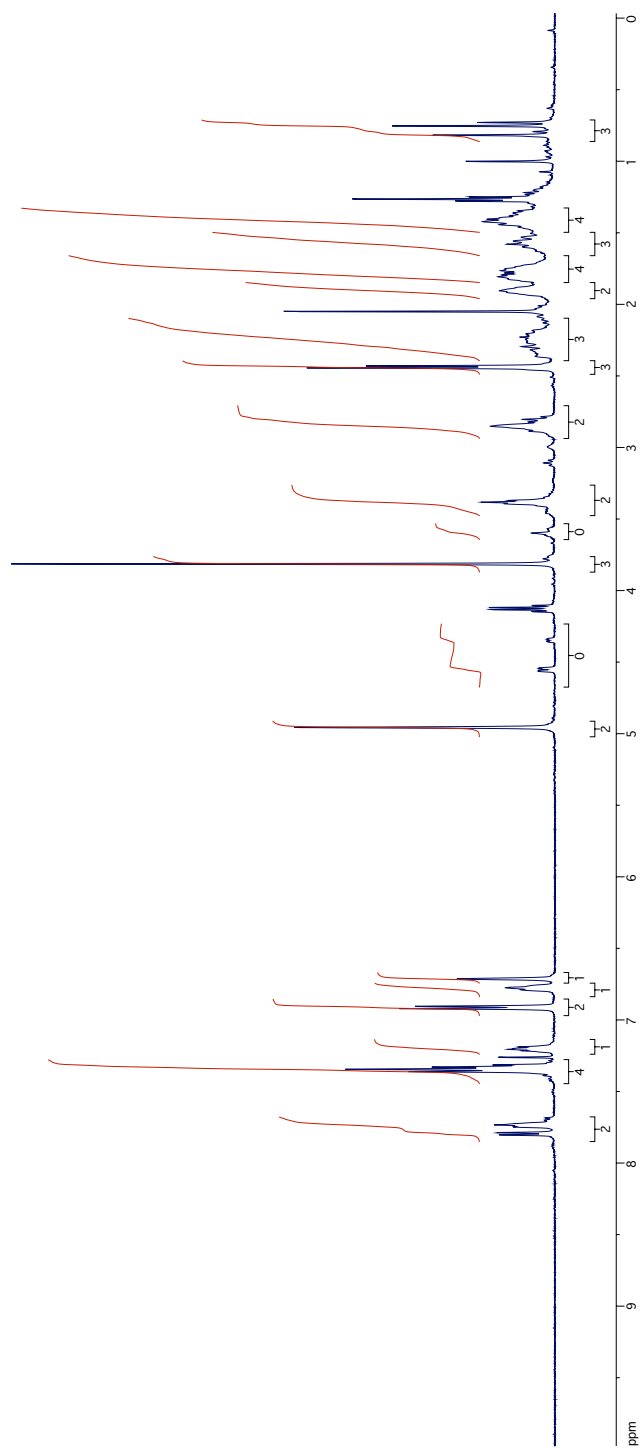
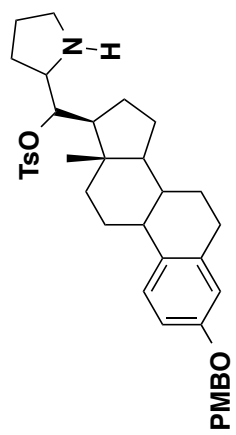
^1H NMR Spectrum of Compound **94**



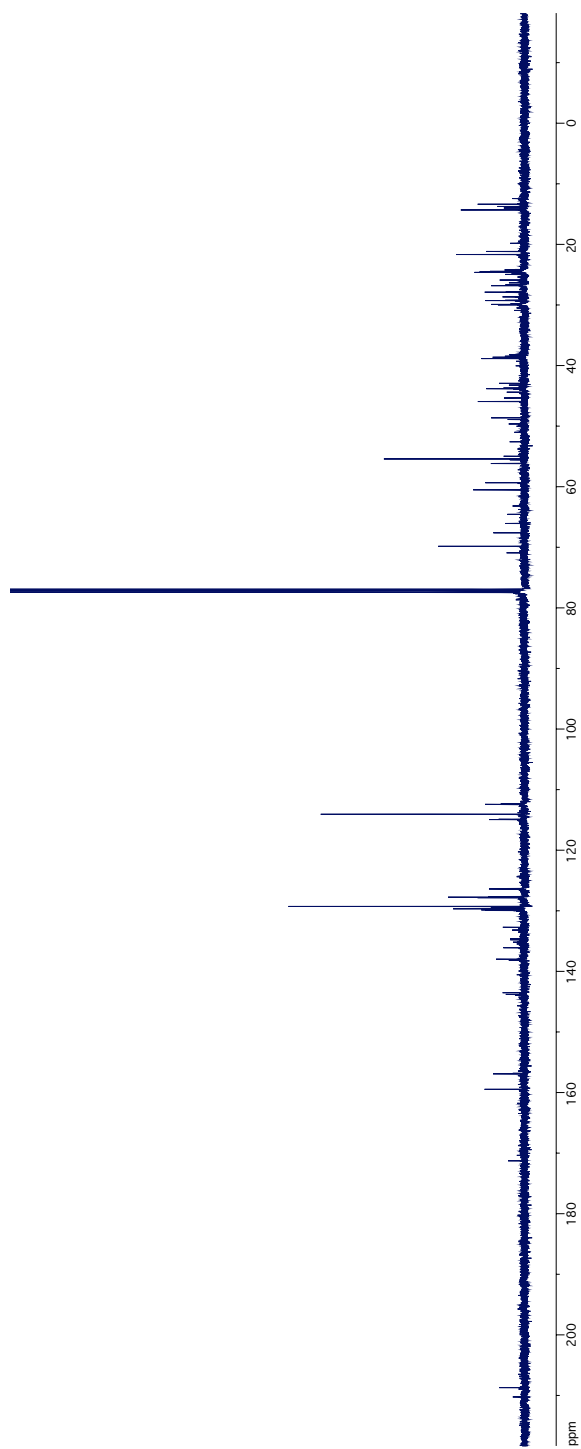
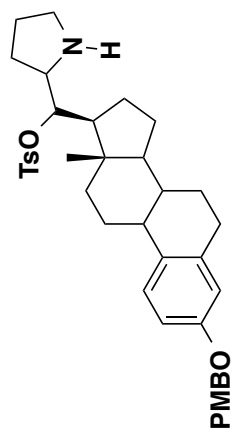
^{13}C NMR Spectrum of Compound **94**



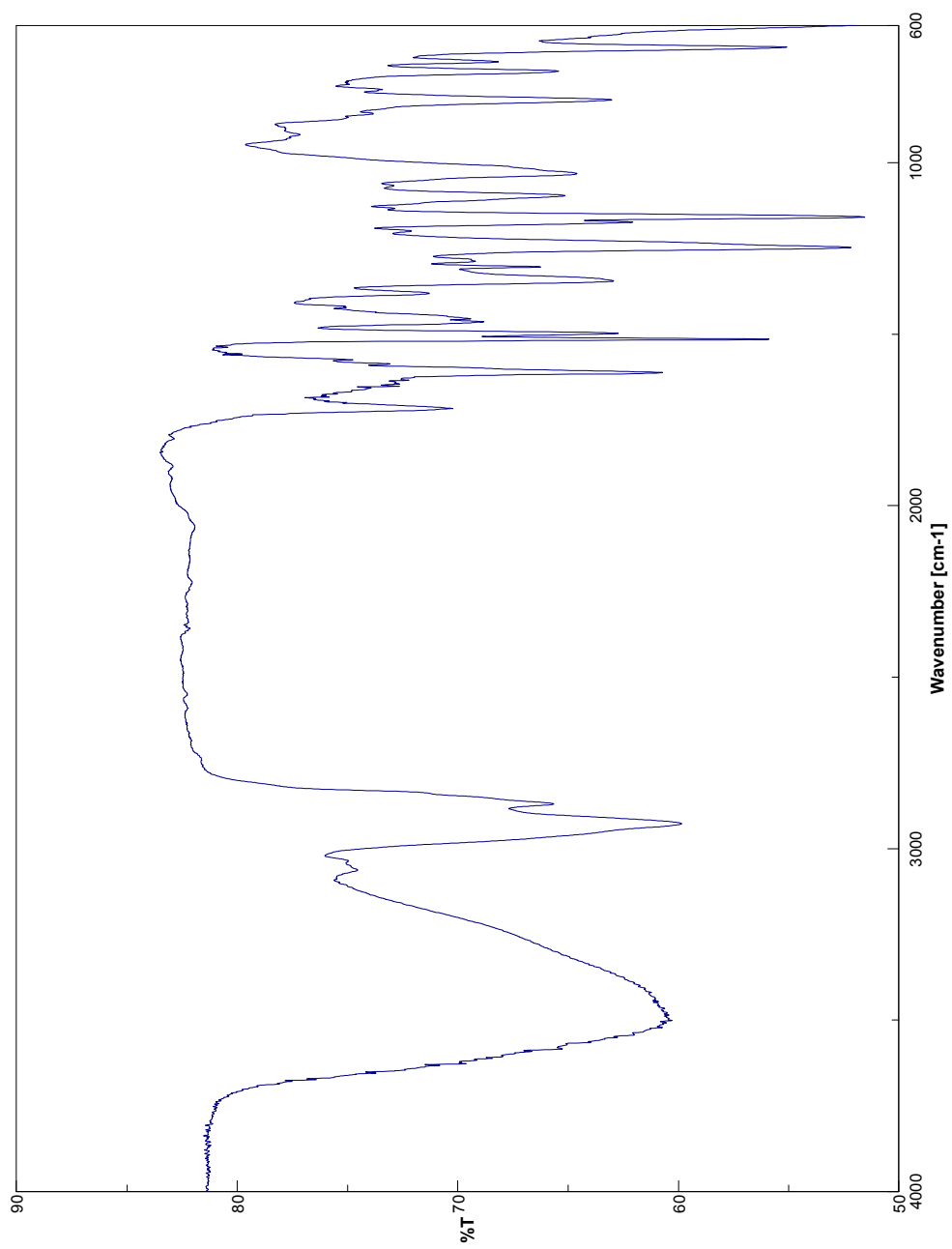
IR Spectrum of Compound **94**



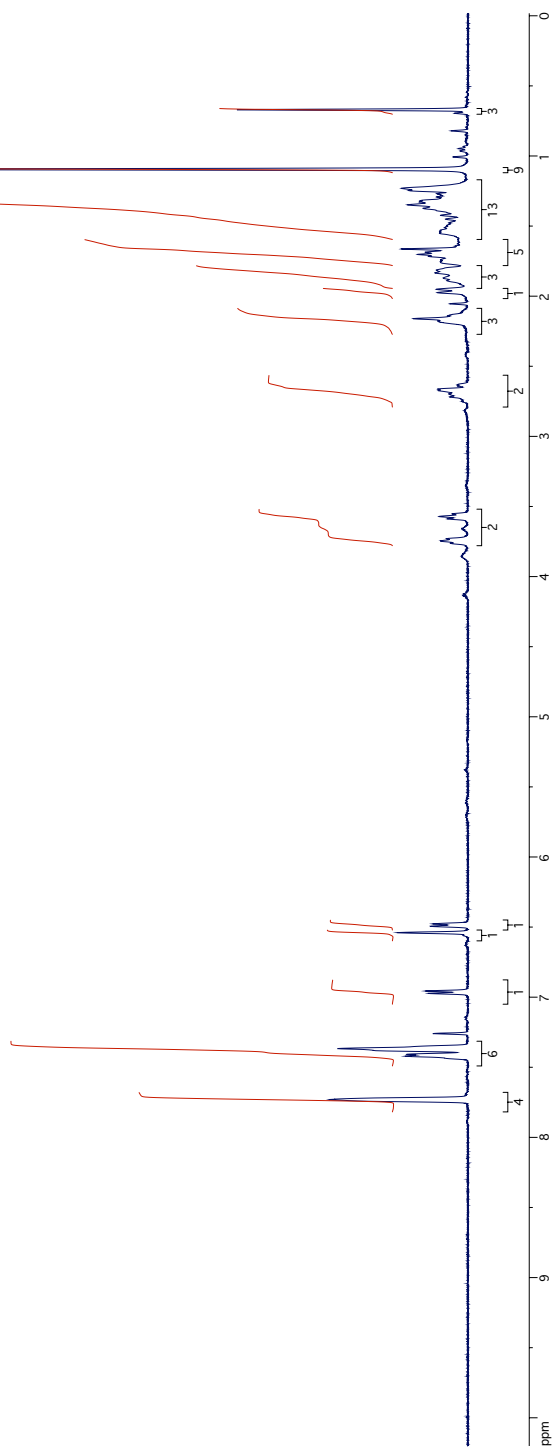
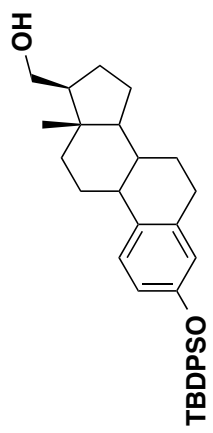
¹H NMR Spectrum of Compound **95**



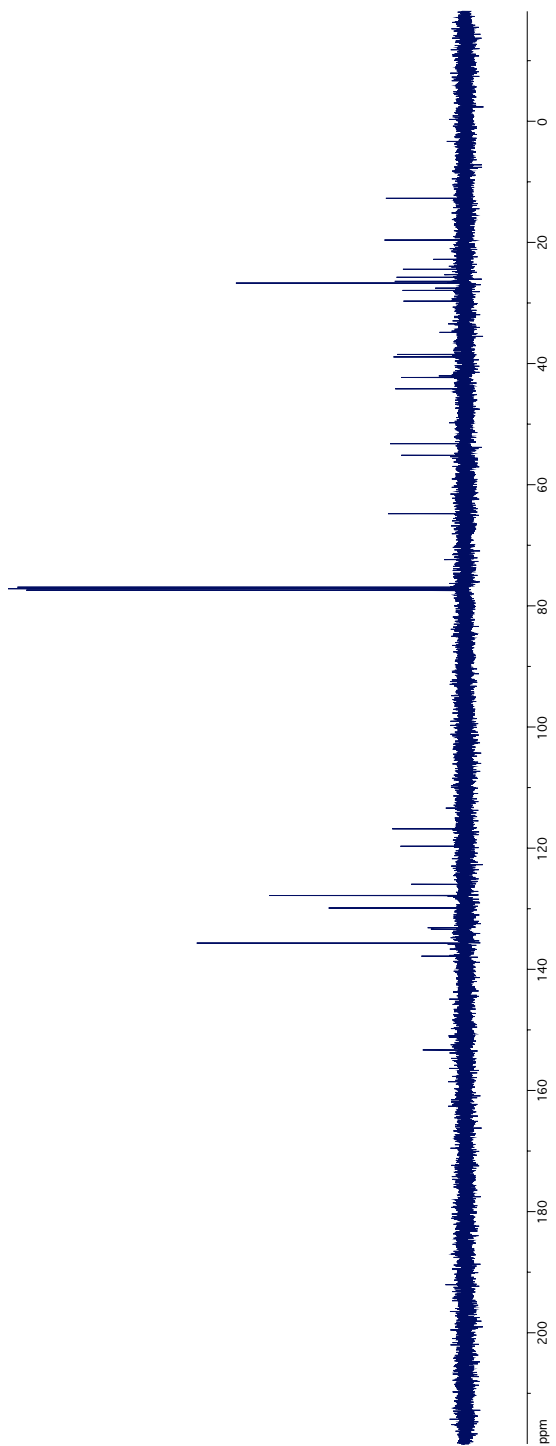
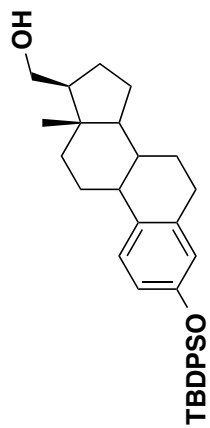
^{13}C NMR Spectrum of Compound **95**



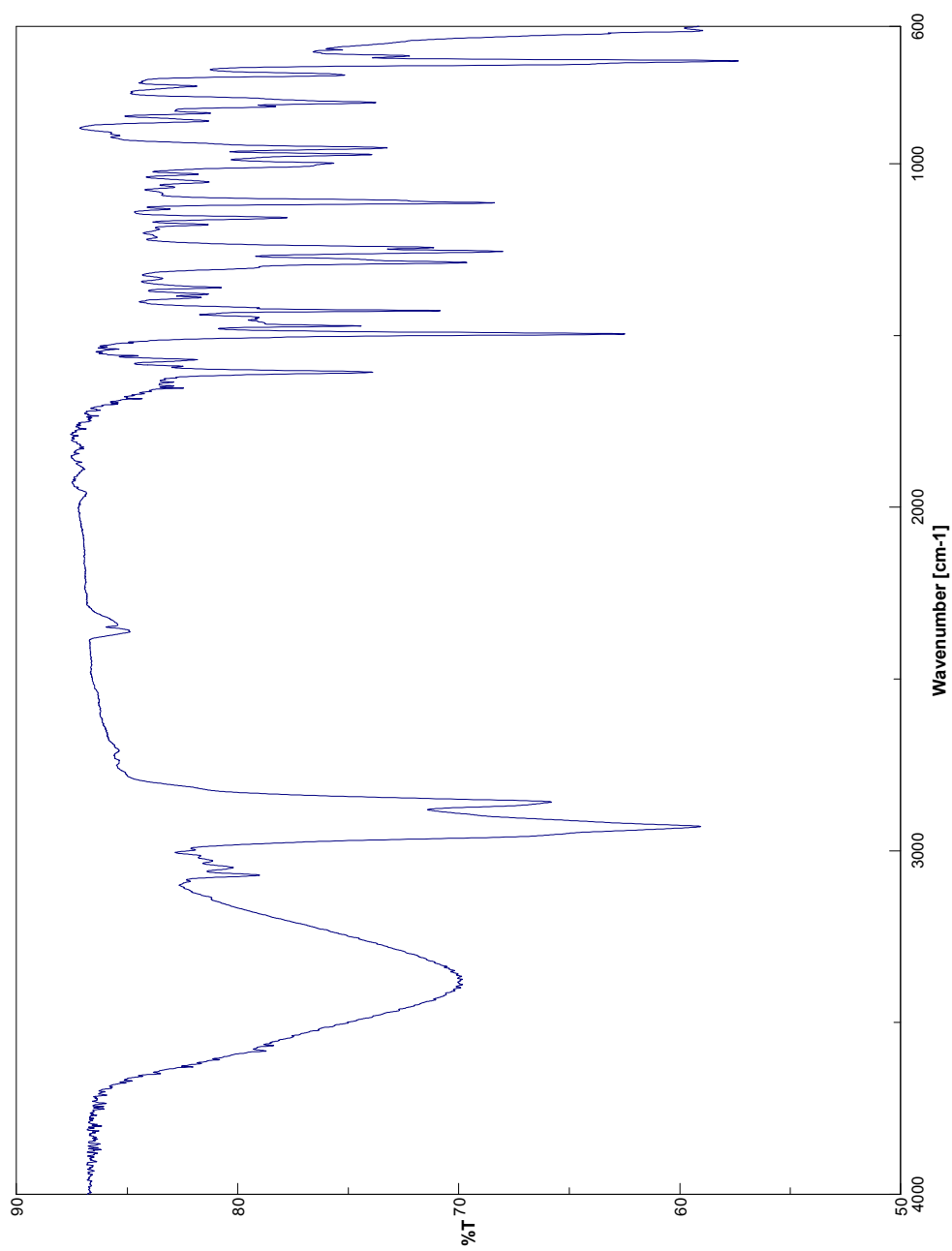
IR Spectrum of Compound **95**



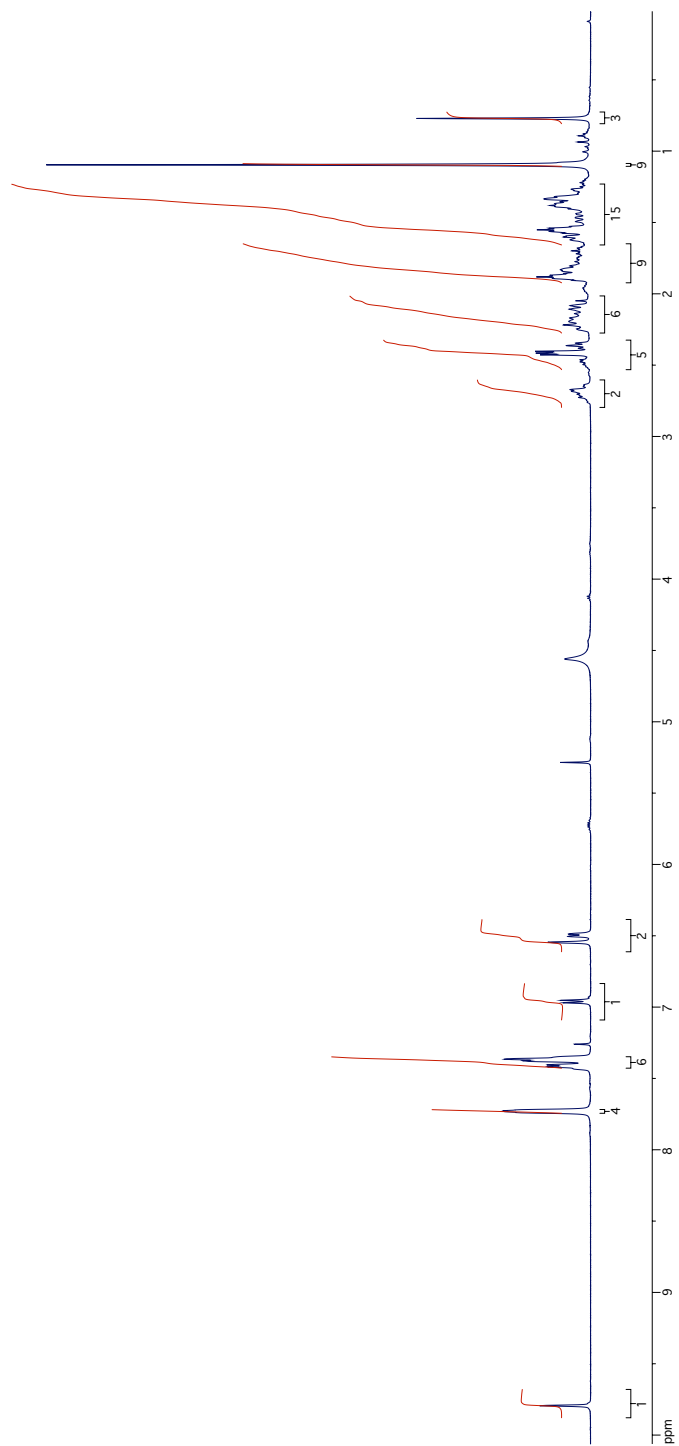
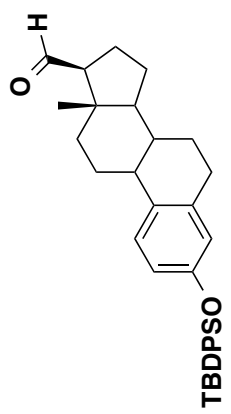
¹H NMR Spectrum of Compound **98**



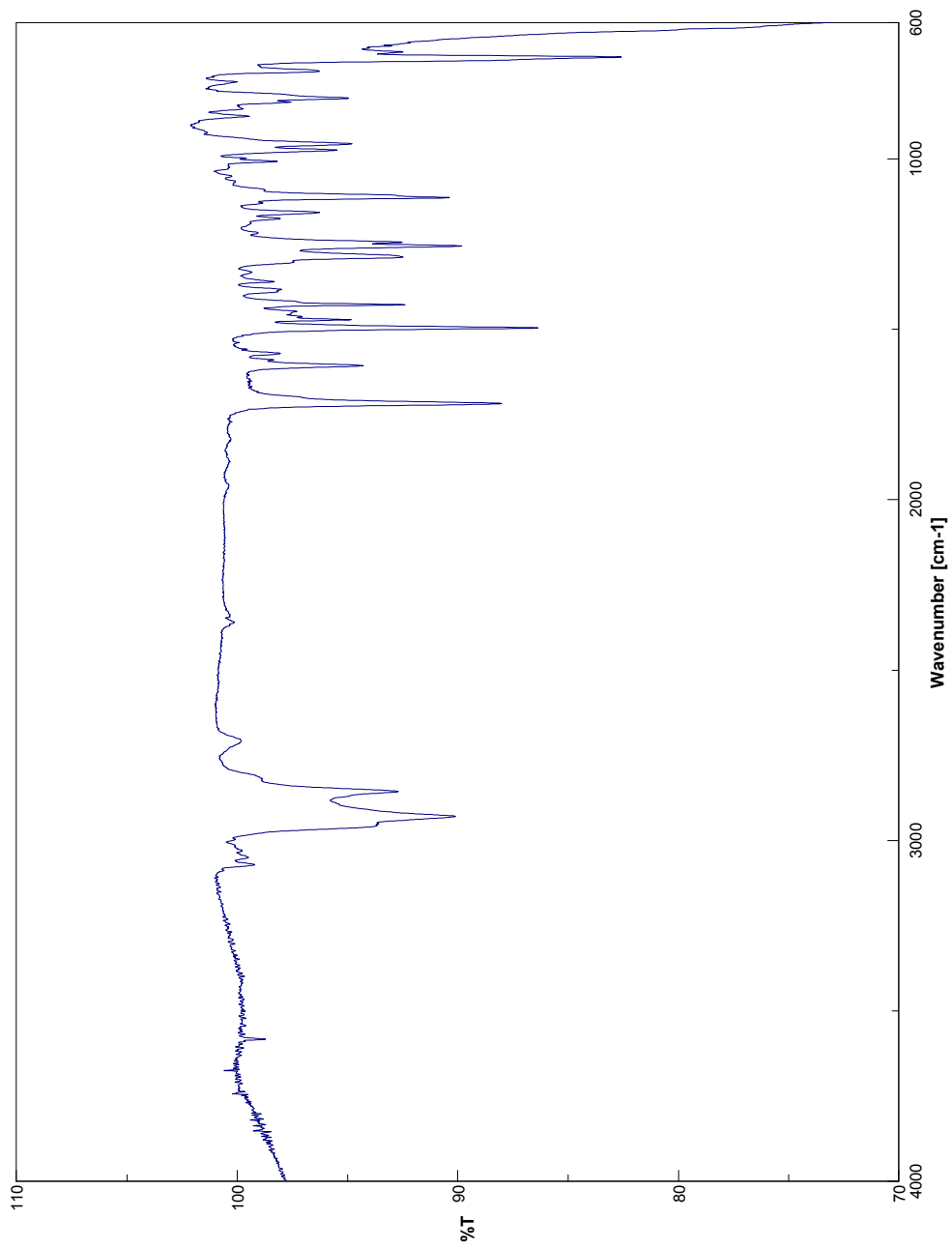
¹³C NMR Spectrum of Compound **98**



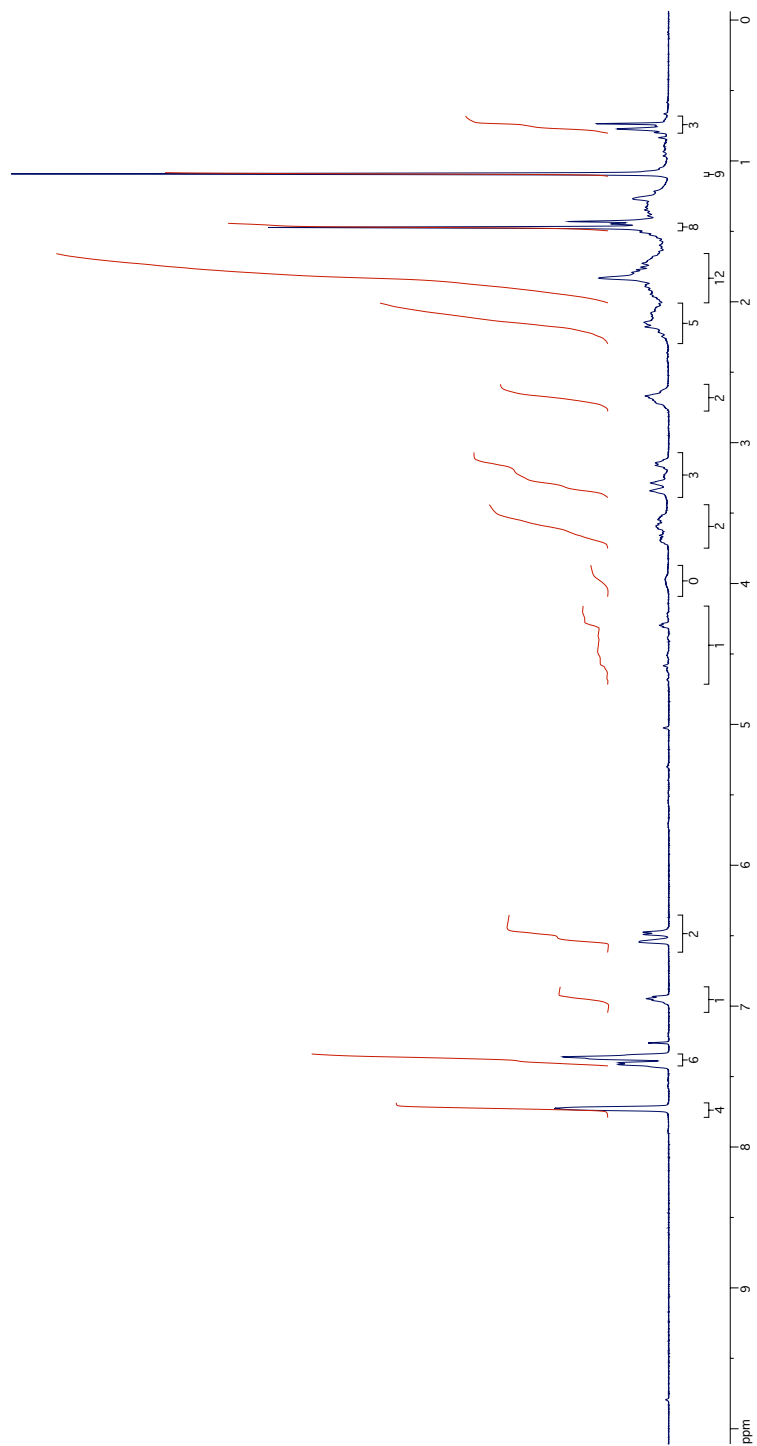
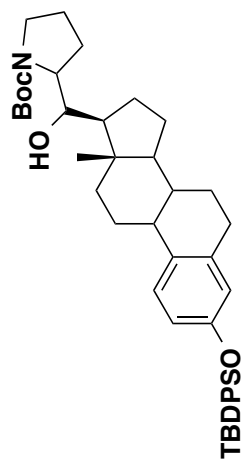
IR Spectrum of Compound **98**



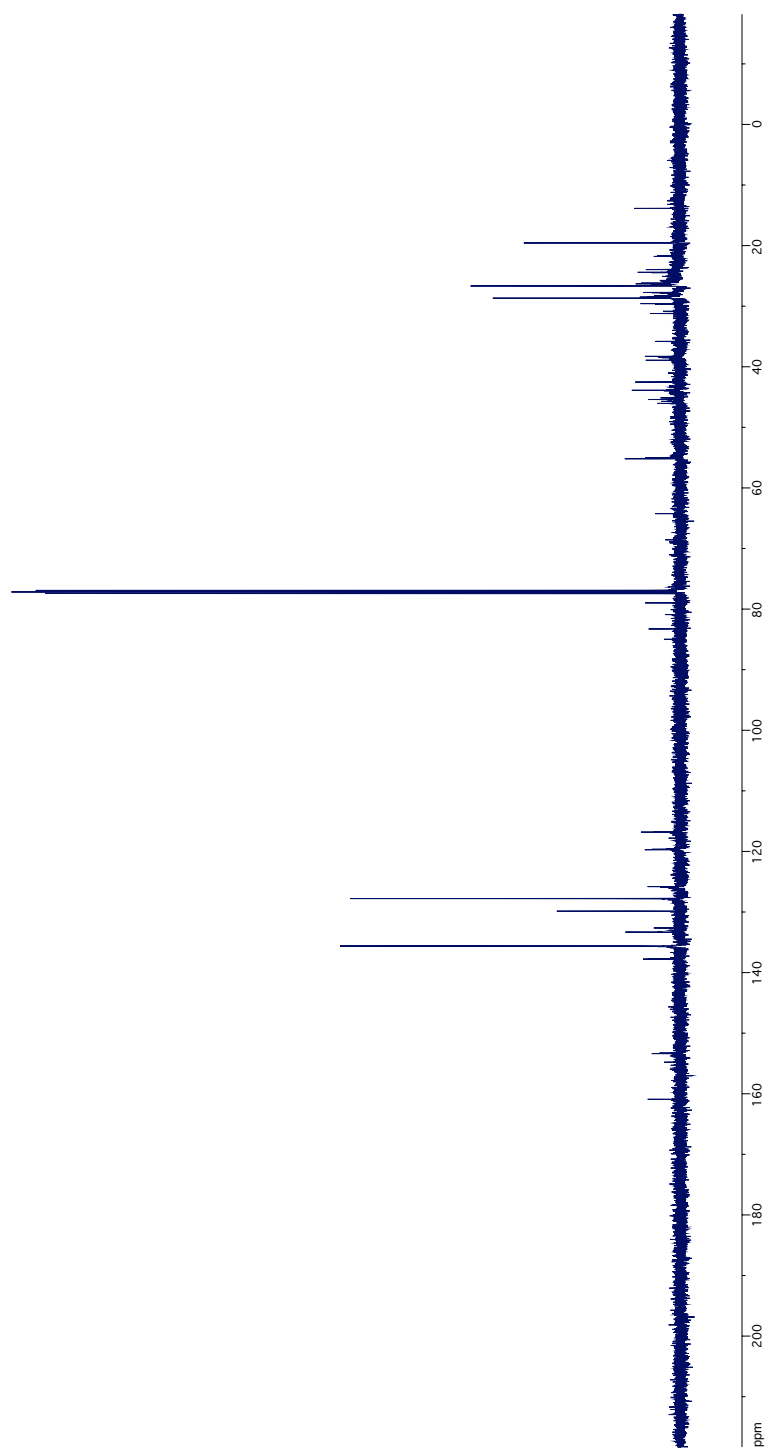
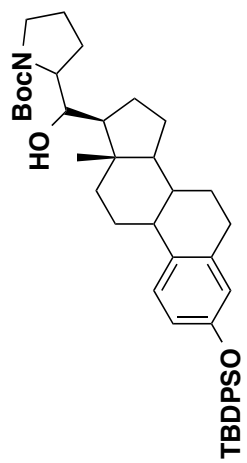
¹H NMR Spectrum of Compound **99**



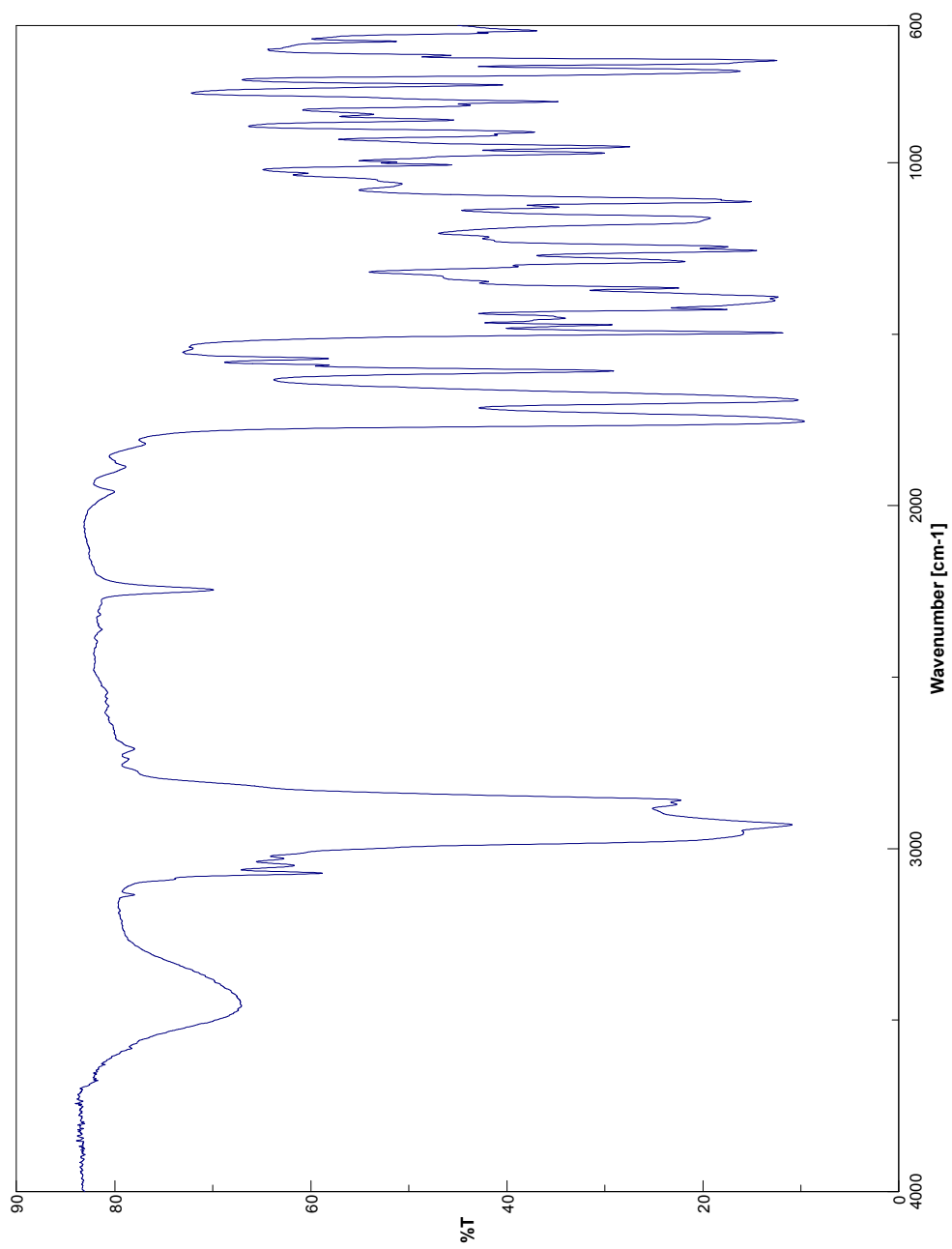
IR Spectrum of Compound **99**



^1H NMR Spectrum of Compound **100**

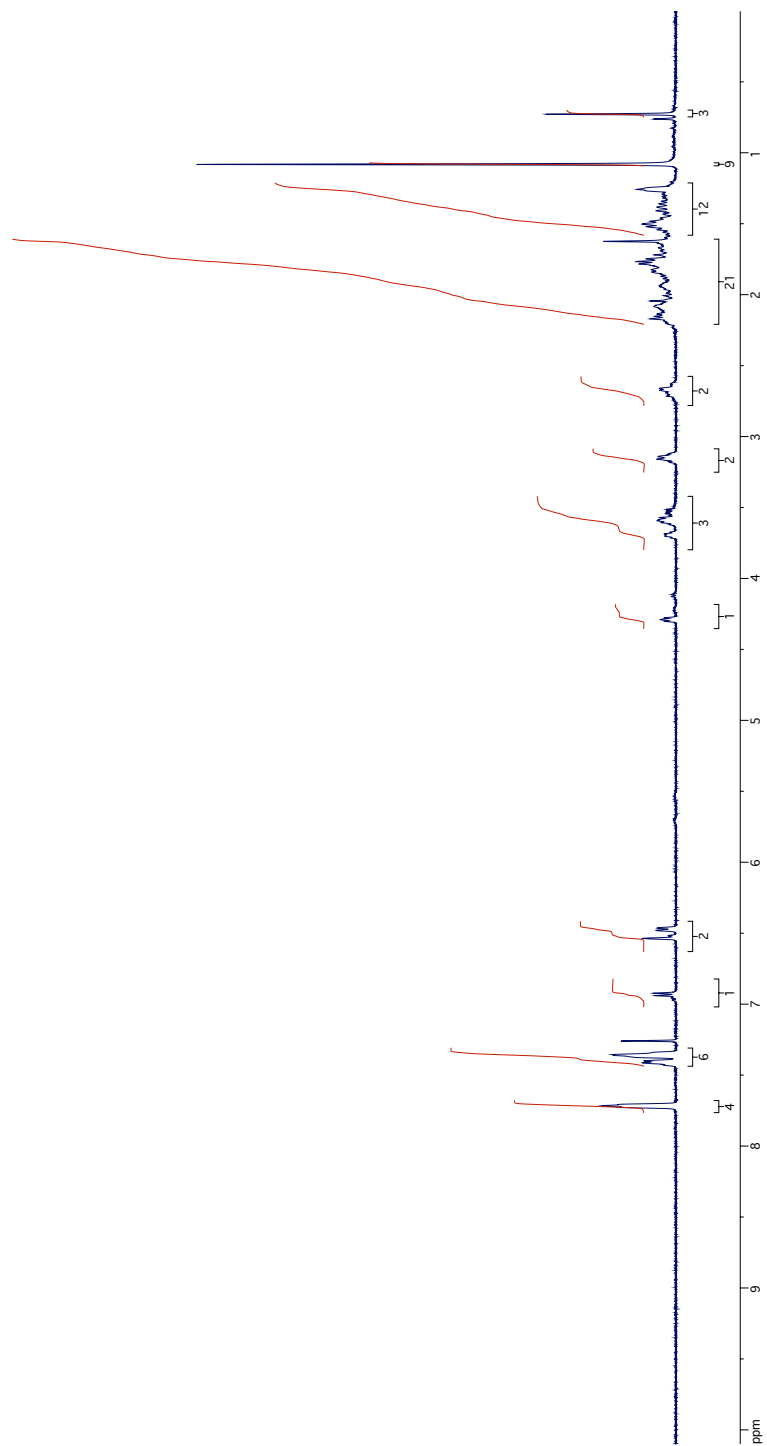
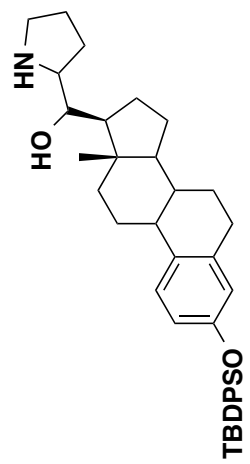


^{13}C NMR Spectrum of Compound 100

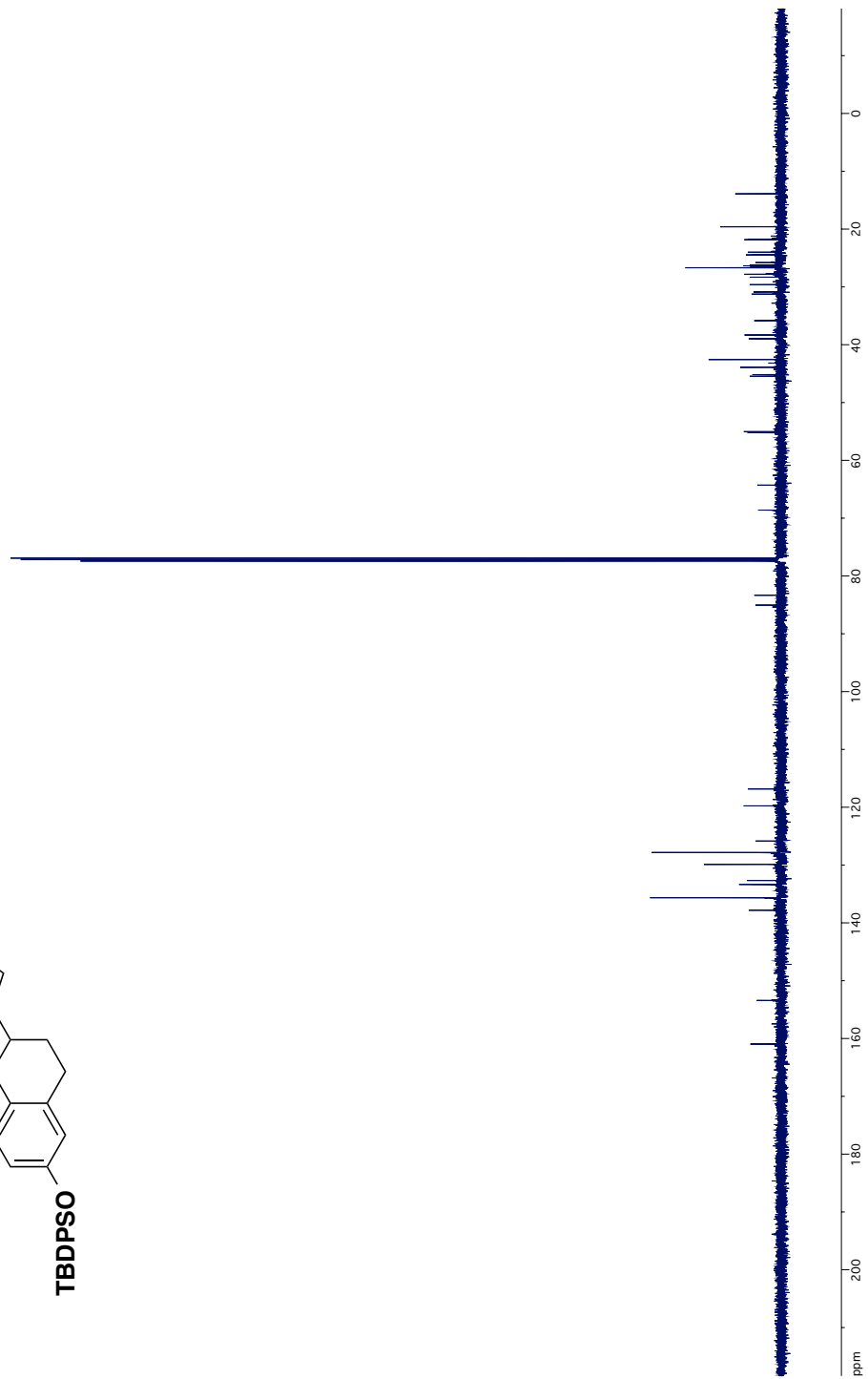
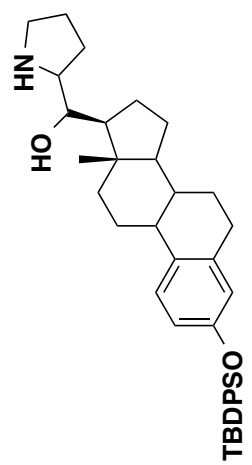


IR Spectrum of Compound **100**

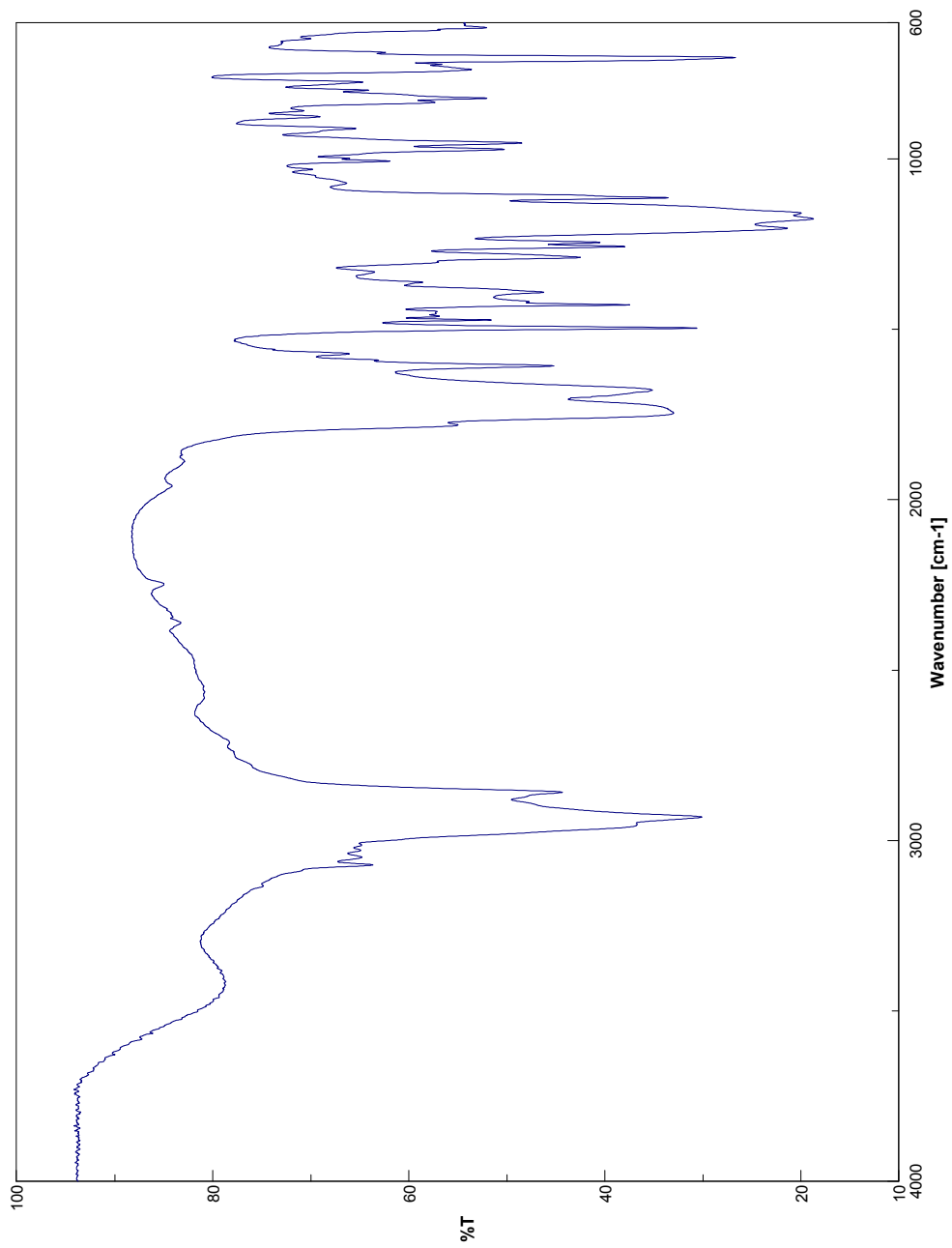
403



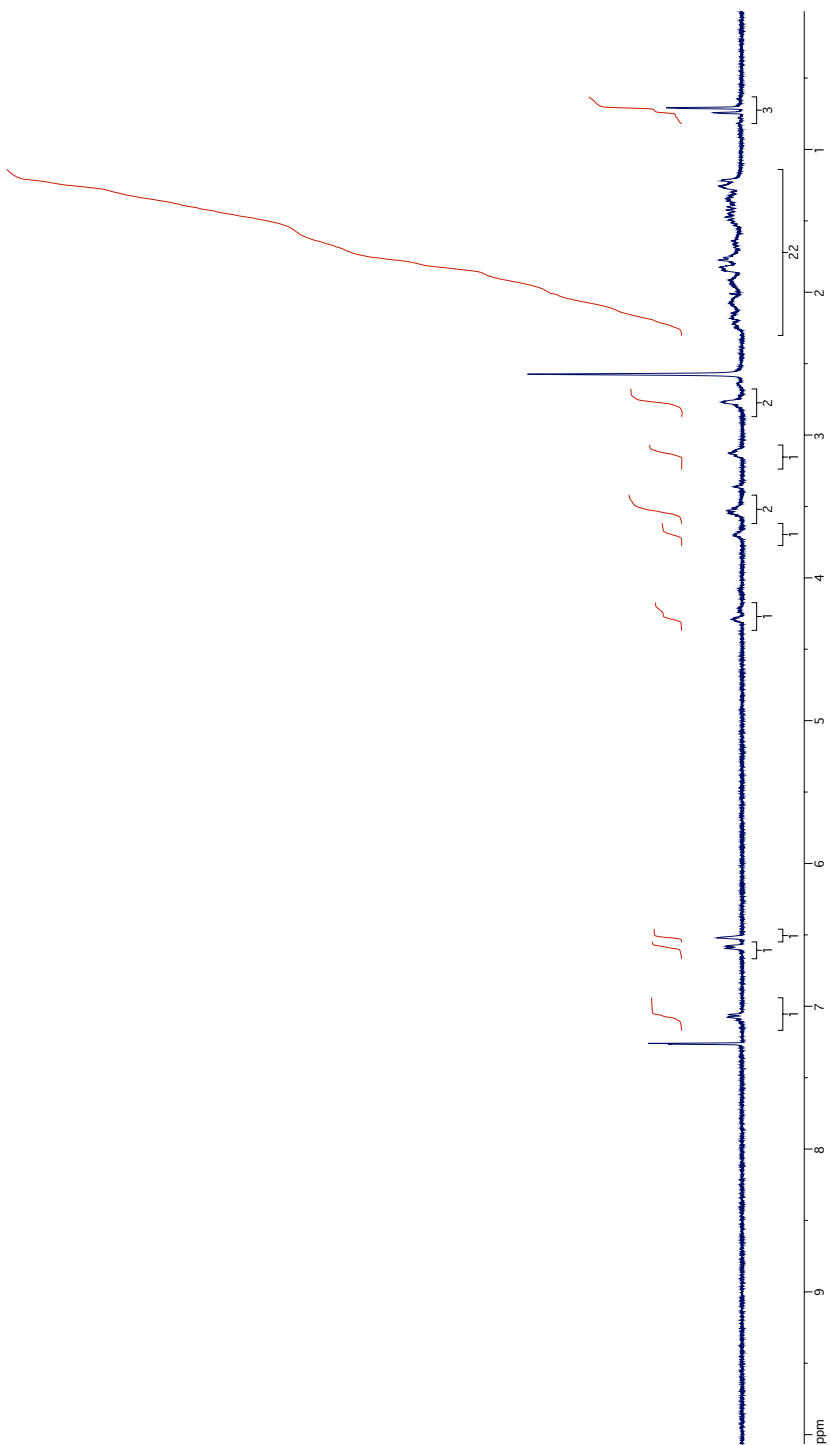
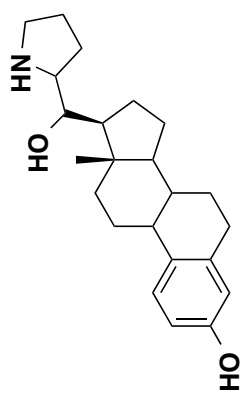
¹H NMR Spectrum of Compound **101**



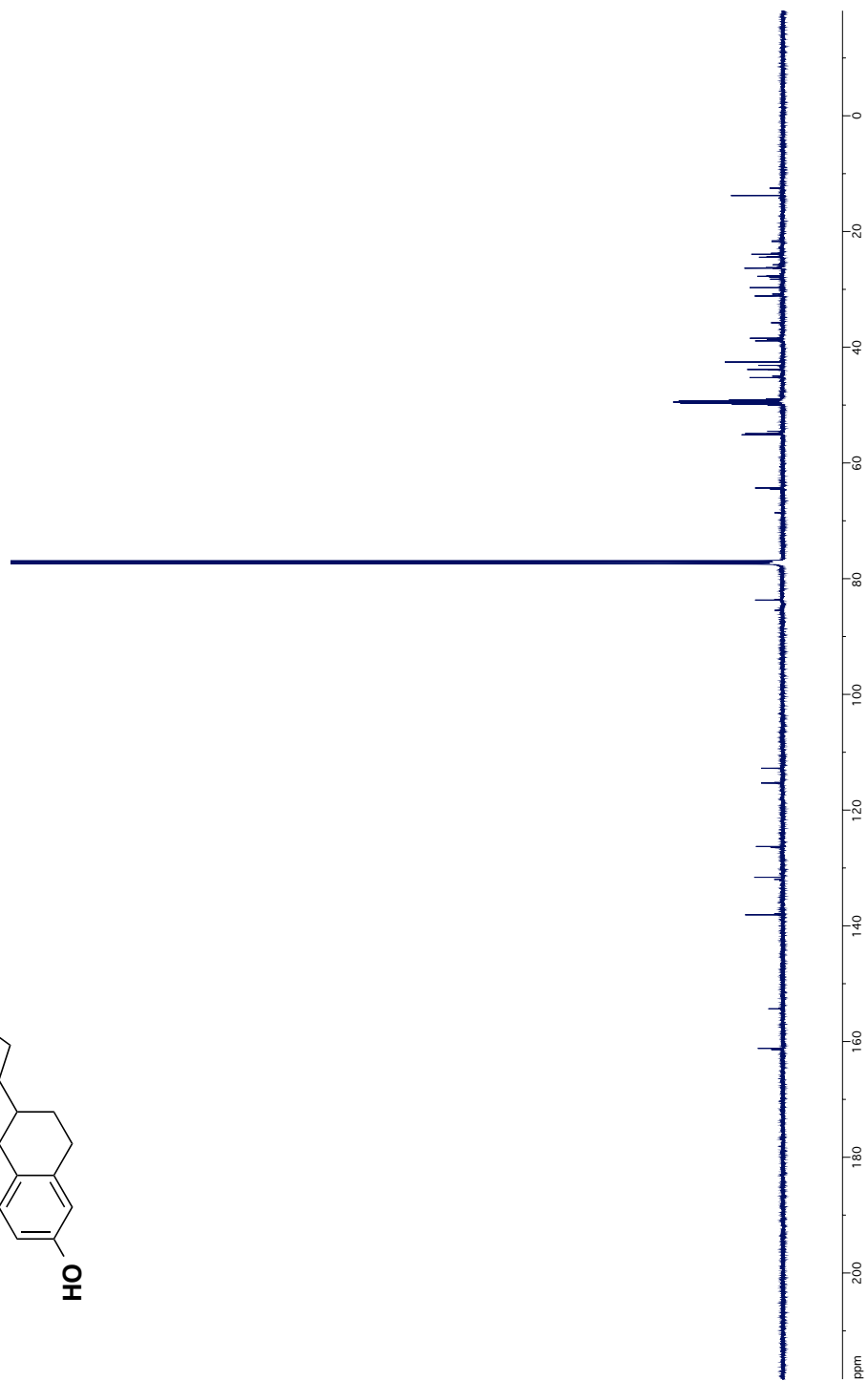
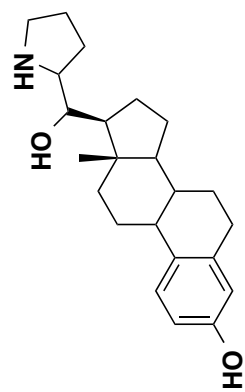
^{13}C NMR Spectrum of Compound **101**



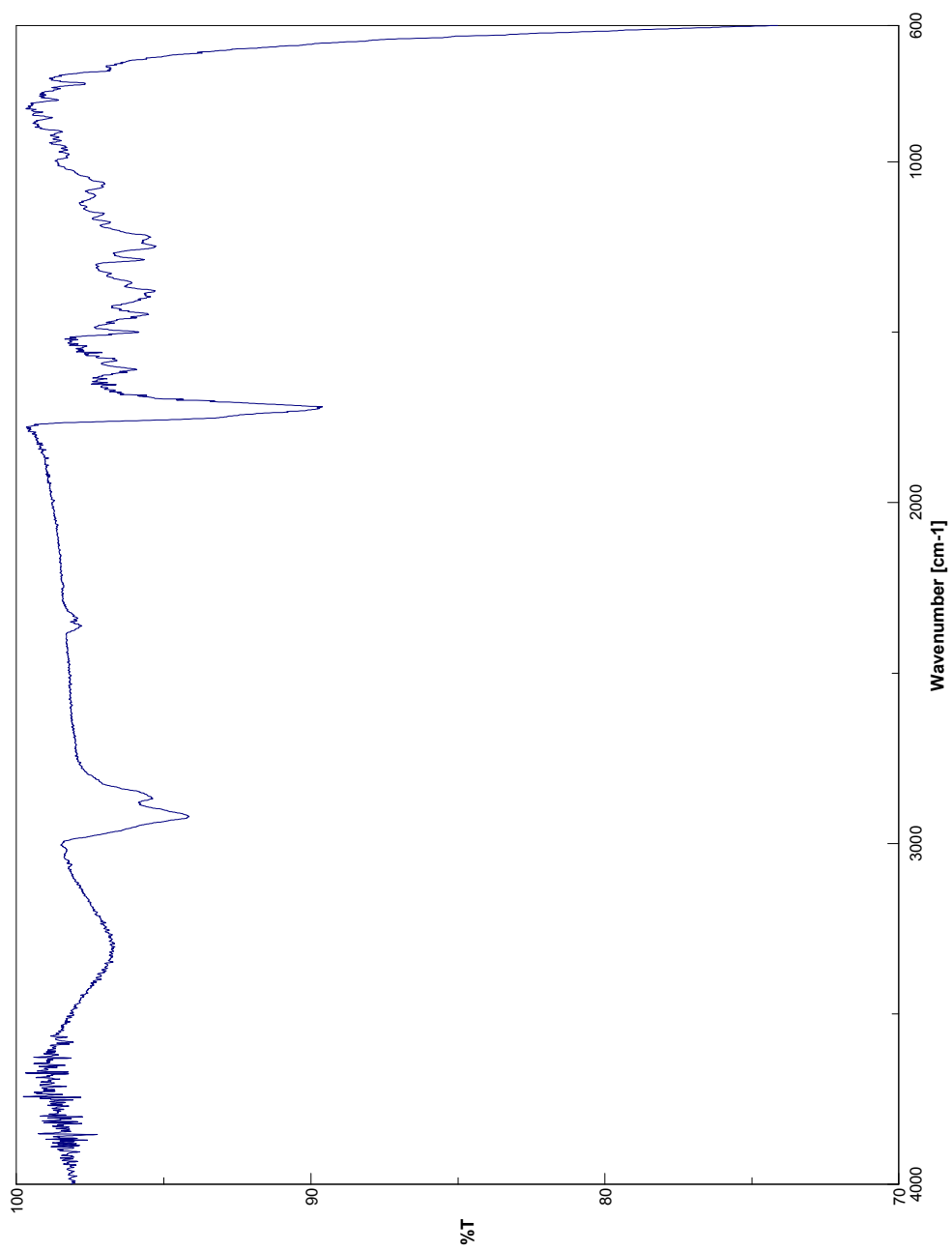
IR Spectrum of Compound **101**



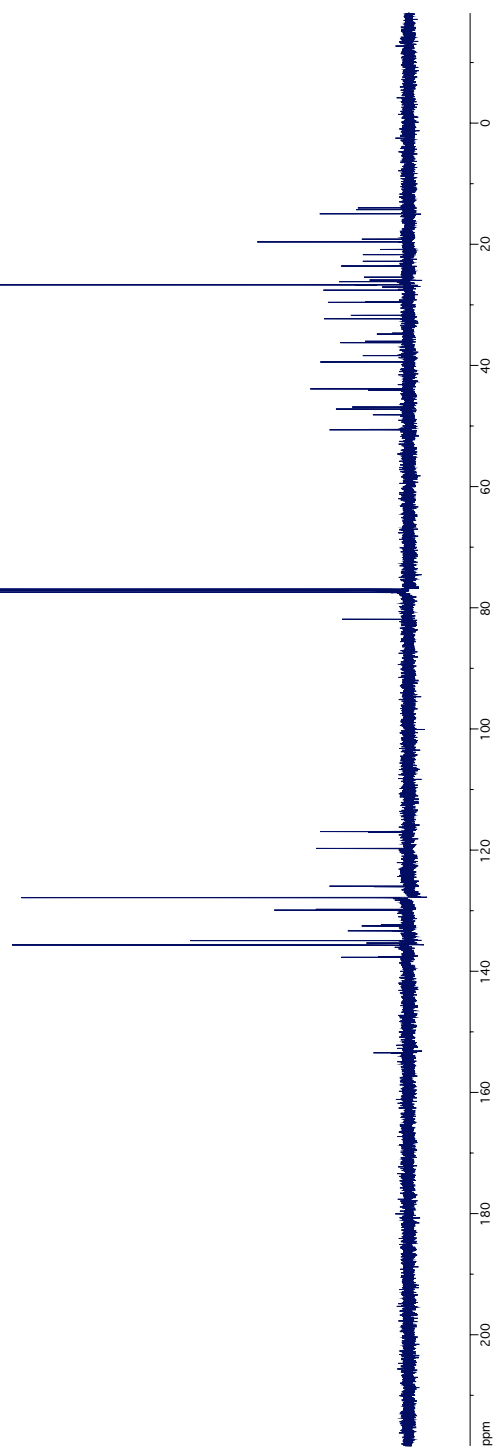
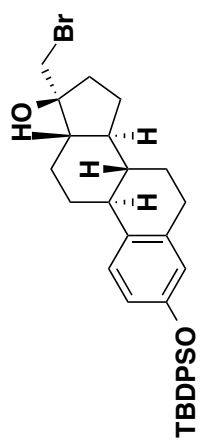
^1H NMR Spectrum of Compound **102**



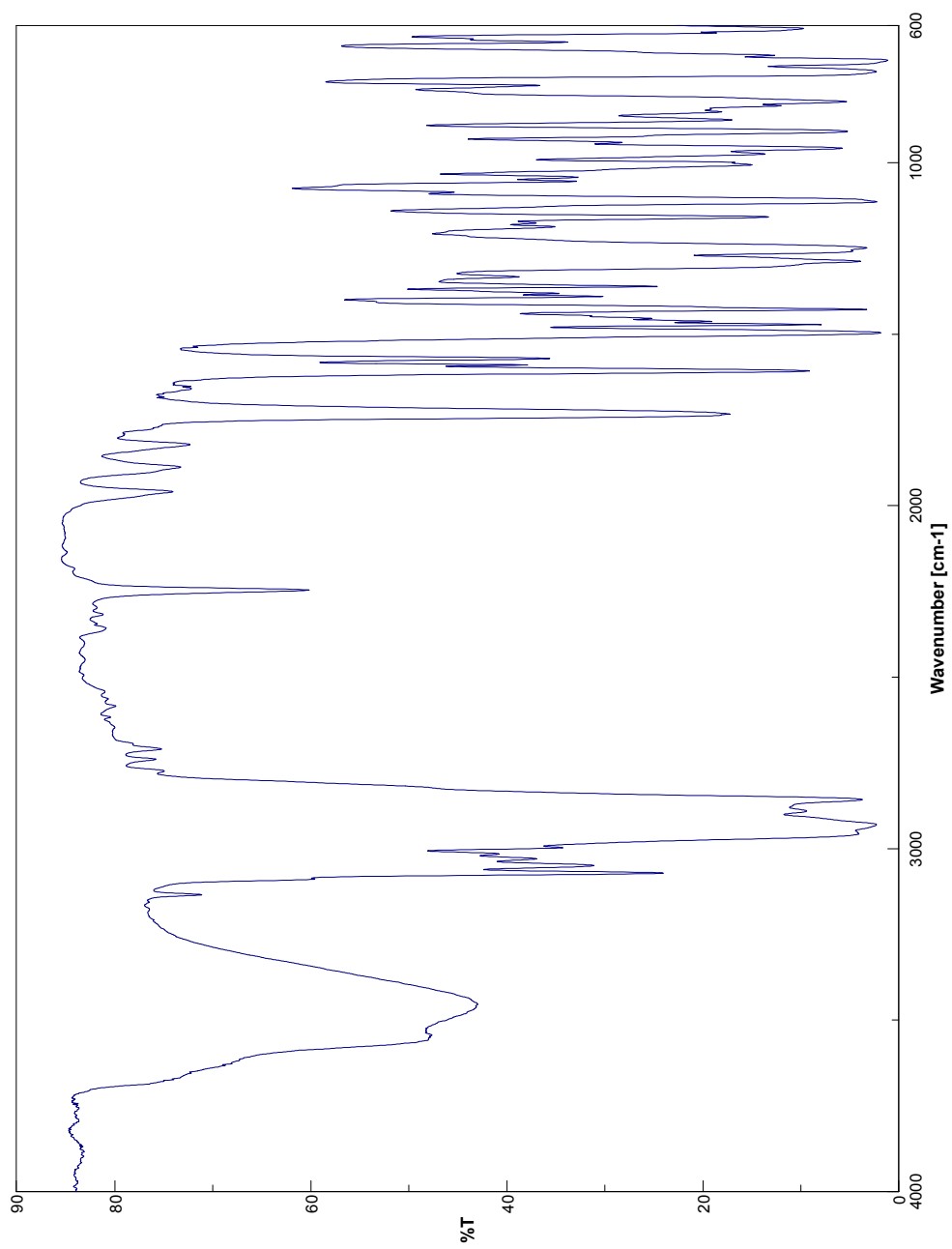
^{13}C NMR Spectrum of Compound **102**



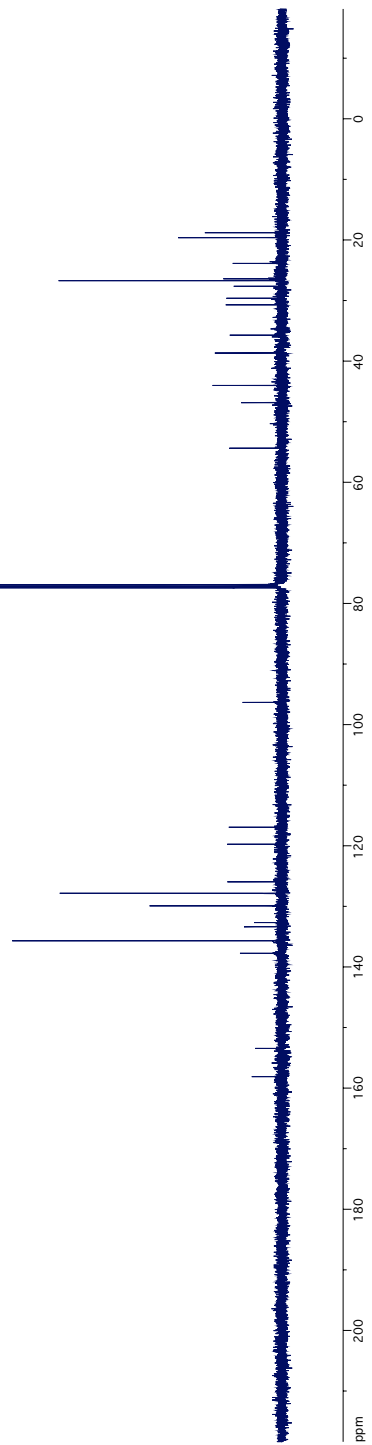
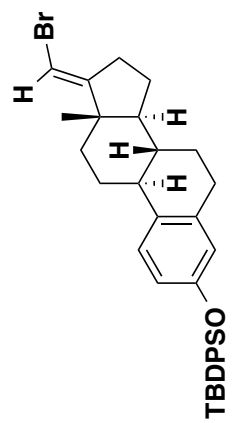
IR Spectrum of Compound **102**



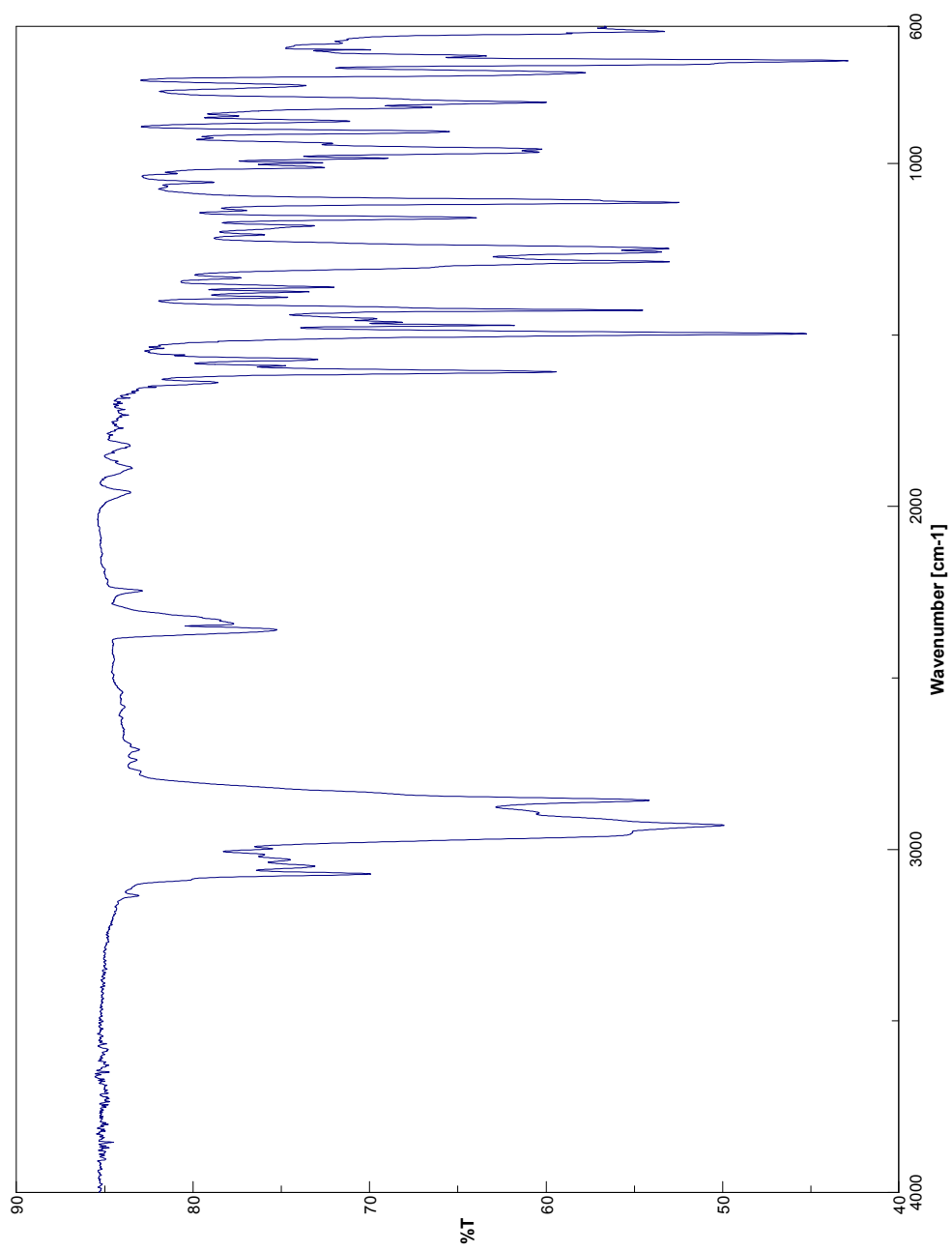
¹³C NMR Spectrum of Compound **104**



IR Spectrum of Compound **104**



¹³ C NMR Spectrum of Compound **105**



IR Spectrum of Compound **105**

BIBLIOGRAPHY

- Auld, D. S.; Southall, N. T.; Jadhav, A.; Johnson, R. L.; Diller, D. J.; Simeonov, A.; Austin, C. P.; Inglese, J. Characterization of Chemical Libraries for Luciferase Inhibitory Activity. *J. Med. Chem.* **2008**, *51*, 2372–2386.
- Berman, D. M.; Karhadkar, S. S.; Hallahan, A. R.; Pritchard, J. I.; Eberhart, C. G.; Watkins, D. N.; Chen, J. K.; Cooper, M. K.; Taipale, J.; Olson, J. M.; et al. Medulloblastoma Growth Inhibition by Hedgehog Pathway Blockade. *Science*. **2002**, *297*, 1559–1561.
- Berthelot, M.; Besseau, F.; Laurence, C. The Hydrogen-Bond Basicity pKHB Scale of Peroxides and Ethers. *Eur. J. Org. Chem.* **1998**, *5*, 925–931.
- Binns, W.; James, L. F.; Keeler, R. F.; Balls, L. D. Effects of Teratogenic Agents in Range Plants. *Cancer Res.* **1968**, *28*, 2323–2326.
- Birladeanu, L.; Andrews, D. W.; Pagnotta, M. Conjugative Interaction in the Orthogonal Enamine, 1-Azabicyclo[3.2.2]non-2-ene. *J. Am. Chem. Soc.* **1985**, *6*, 3813–3817.
- Błaszczuk, K.; Koenig, H.; Paryzek, Z. Cyclobutanone Approach to the Synthesis of Cardenolides. *Eur. J. Org. Chem.* **2005**, 749–754.
- Carpenter, E. P.; Beis, K.; Cameron, A. D.; Iwata, S. Overcoming the Challenges of Membrane Protein Crystallography. *Curr. Opin. Struct. Biol.* **2008**, *18*, 581–586.
- Chen, D.; Xu, C.; Deng, J.; Jiang, C.; Wen, X.; Kong, L.; Zhang, J.; Sun, H. Proton-Exchanged Montmorillonite-Mediated Reactions of Methoxybenzyl Esters and Ethers. *Tetrahedron* **2014**, *70*, 1975–1983.
- Chen, J. K.; Taipale, J.; Cooper, M. K.; Beachy, P. A. Inhibition of Hedgehog Signaling by Direct Binding of Cyclopamine to Smoothed. *Genes Dev.* **2002**, *16*, 2743–2748.
- Chen, J. K.; Taipale, J.; Young, K. E.; Maiti, T.; Beachy, P. a. Small Molecule Modulation of Smoothed Activity. *Proc. Natl. Acad. Sci. U. S. A.* **2002**, *99*, 14071–14076.
- Cooper, M. K.; Porter, J. A.; Young, K. E.; Beachy, P. A. Teratogen-Mediated Inhibition of Target Tissue Response to Shh Signaling. *Science (80-.)*. **1998**, *280*, 1603–1607.
- Cuthbertson, J. D.; Unsworth, W. P.; Moody, C. L.; Taylor, R. J. K. The Total Synthesis of (+)-Elaeokanidine A: Natural Product or Isolation Artefact? *Tetrahedron Lett.* **2015**, *56*, 3123–3126.
- Dahmane, N.; Lee, J.; Robins, P.; Heller, P.; Ruiz i Altaba, A. Activation of the Transcription Factor Gli1 and the Sonic Hedgehog Signalling Pathway in Skin Tumours. *Nature* **1997**, *389*, 876–881.

- Dougherty, D. A. Cation- π Interactions Involving Aromatic Amino Acids. *J. Nutr.* **2007**, *137*, 1504–1508.
- Echelard, Y.; Epstein, D. J.; St-Jacques, B.; Shen, L.; Mohler, J.; McMahon, J. a.; McMahon, a. P. Sonic Hedgehog, a Member of a Family of Putative Signaling Molecules, Is Implicated in the Regulation of CNS Polarity. *Cell* **1993**, *75*, 1417–1430.
- Gaffield, W.; Wong, R. Y.; Lundin, R. E.; Keeler, R. F. Structure of the Steroidal Alkaloid Muldamine and Its Deacetyl Derivative. *Phytochemistry* **1982**, *21*, 2397–2400.
- Giannis, A.; Heretsch, P.; Sarli, V.; Stössel, A. Synthesis of Cyclopamine Using a Biomimetic and Diastereoselective Approach. *Angew. Chem., Int. Ed.* **2009**, *48*, 7911–7914.
- Goodrich, L. V; Milenković, L.; Higgins, K. M.; Scott, M. P. Altered Neural Cell Fates and Medulloblastoma in Mouse Patched Mutants. *Science (80-)*. **1997**, *277*, 1109–1113.
- Gorlin, R. J.; Goltz, R. W. Multiple Nevoid Basal-Cell Epithelioma, Jaw Cysts, and Bifid Rib. *N. Engl. J. Med.* **1960**, *262*, 908–912.
- Heretsch, P.; Tzagkaroulaki, L.; Giannis, A. Cyclopamine and Hedgehog Signaling: Chemistry, Biology, Medical Perspectives. *Angew. Chem., Int. Ed.* **2010**, *49*, 3418–3427.
- Hillisch, A.; Von Langen, J.; Menzenbach, B.; Droescher, P.; Kaufmann, G.; Schneider, B.; Elger, W. The Significance of the 20-Carbonyl Group of Progesterone in Steroid Receptor Binding: A Molecular Dynamics and Structure-Based Ligand Design Study. *Steroids* **2003**, *68*, 869–878.
- Incardona, J. P.; Gaffield, W.; Kapur, R. P.; Roelink, H. The Teratogenic Veratrum Alkaloid Cyclopamine Inhibits Sonic Hedgehog Signal Transduction. *Development* **1998**, *125*, 3553–3562.
- Isaacs, A. K.; Xiang, C.; Baubet, V.; Dahmane, N.; Winkler, J. D. Studies Directed toward the Elucidation of the Pharmacophore of Steroid-Based Sonic Hedgehog Signaling Inhibitors. *Org. Lett.* **2011**, *13*, 5140–5143.
- Jacob, L.; Lum, L. Deconstructing the Hedgehog Pathway in Development and Disease. *Science (80-)*. **2007**, *318*, 66–68.
- Jepsen, T. H.; Kristensen, J. L. In Situ Generation of the Ohira-Bestmann Reagent from Stable Sulfonyl Azide: Scalable Synthesis of Alkynes from Aldehydes. *J. Org. Chem.* **2014**, *79*, 9423–9426.
- Johnson, D. C.; Widlanski, T. S. Cerium (III) Chloride-Mediated Reactions of Sulfonamide Dianions The Sulfonamide Functional Group Has Received Con-. *J. Org. Chem.* **2003**, *68*, 5300–5309.

- Johnson, R. L.; Rothman, a L.; Xie, J.; Goodrich, L. V; Bare, J. W.; Bonifas, J. M.; Quinn, a G.; Myers, R. M.; Cox, D. R.; Epstein, E. H.; et al. Human Homolog of Patched, a Candidate Gene for the Basal Cell Nevus Syndrome. *Science (80-)*. **1996**, *272*, 1668–1671.
- Johnson, W. S.; Cox, J. M.; Graham, D. W.; Whitlock, H. W. The Total Synthesis of 17-Acetyl-5 α -Etiogerv-12,14,16-Trien-3 β -Ol. *J. Am. Chem. Soc.* **1967**, *89*, 4524–4526.
- Keeler, R. F. First Isolation of Veratramine and Alkaloid Q and a Reliable Method for Isolation of Cyclopamine. *Phytochemistry* **1968**, *7*, 303–306.
- Keeler, R. F.; Binns, W. Teratogenic Compounds of *Veratrum Californicum* (Durand). II. Production of Ovine Fetal Cyclopia by Fractions and Alkaloid Preparations. *Can. J. Biochem.* **1966**, *44*, 829–838.
- Khaliullina, H.; Panáková, D.; Eugster, C.; Riedel, F.; Carvalho, M.; Eaton, S. Patched Regulates Smoothed Trafficking Using Lipoprotein-Derived Lipids. *Development* **2009**, *136*, 4111–4121.
- Kouznetsov, V.; Cruz, U. M.; Zubkov, F. I.; Nikitina, E. V. An Efficient Synthesis of 17-Epi-Ethynylestradiol. *Tetrahedron* **2006**, *54*, 4277–4282.
- Kusuma, B. R.; Zhang, L.; Sundstrom, T.; Peterson, L. B.; Dobrowsky, R. T.; Blagg, B. S. J. Synthesis and Evaluation of Novologues as C-Terminal Hsp90 Inhibitors with Cytoprotective Activity against Sensory Neuron Glucotoxicity. *J. Med. Chem.* **2012**, *55*, 5797–5812.
- Lajunen, M.; Koskinen, J.-M. Acid-Catalyzed Hydrolysis of Oxetane. *Acta Chem. Scand.* **1994**, *48*, 788–791.
- Landau, E. M.; Rosenbusch, J. P. Lipidic Cubic Phases: A Novel Concept for the Crystallization of Membrane Proteins. *Proc. Natl. Acad. Sci. U. S. A.* **1996**, *93*, 14532–14535.
- Langer, P.; Shojaei, H.; Greifswald, D.-; E-mail, G. Fragmentation ' Reactions of 1-Azido-2-Hydroxy-4 , 6-Dioxohexanes. *Chem. Comm.* **2003**, 3044–3045.
- Levin, M.; Johnson, R. L.; Stern, C. D.; Kuehn, M.; Tabin, C. A Molecular Pathway Determining Left-Right Asymmetry in Chick Embryogenesis. *Cell* **1995**, *82*, 803–814.
- Liu, P.; Hong, S.; Weinreb, S. M. Total Synthesis of the Securinega Alkaloid (-) - Secu'amamine A. *J. Am. Chem. Soc.* **2008**, *130*, 7562–7563.
- Lum, L.; Beachy, P. a. The Hedgehog Response Network: Sensors, Switches, and Routers. *Science (80-)*. **2004**, *304*, 1755–1759.

- Masamune, T.; Takasugi, M.; Murai, A.; Kobayashi, K. The Synthesis of Jervine and Related Alkaloids. *J. Am. Chem. Soc.* **1967**, *89*, 4521–4523.
- Milić, D.; Veprintsev, D. B. Large-Scale Production and Protein Engineering of G Protein-Coupled Receptors for Structural Studies. *Front. Pharmacol.* **2015**, *6*, 1–24.
- Miller-Moslin, K.; Peukert, S.; Jain, R. K.; McEwan, M. a.; Karki, R.; Llamas, L.; Yusuff, N.; He, F.; Li, Y.; Sun, Y.; et al. 1-Amino-4-Benzylphthalazines as Orally Bioavailable Smoothened Antagonists with Antitumor Activity. *J. Med. Chem.* **2009**, *52*, 3954–3968.
- Muchow, G.; Brunel, J. M. Pd0 -Catalyzed Hydrogenolysis of a Bicyclic Allylic Diacetate. *Eur. J. Org. Chem.* **2013**, *2013*, 6449–6454.
- Murone, M.; Rosenthal, A.; De Sauvage, F. J. Sonic Hedgehog Signaling by the Patched-Smoothened Receptor Complex. *Curr. Biol.* **1999**, *9*, 76–84.
- Niwa, T.; Yorimitsu, H.; Oshima, K. Palladium-Catalyzed 2-Pyridylmethyl Transfer from 2-(2-Pyridyl)ethanol Derivatives to Organic Halides by Chelation-Assisted Cleavage of Unstrained Csp³-Csp³ Bonds. *Angew. Chem., Int. Ed.* **2007**, *46*, 2643–2645.
- Nüsslein-Volhard, C.; Wieschaus, E. Mutations Affecting Segment Number and Polarity in *Drosophila*. *Nature* **1980**, *287*, 795–801.
- Pan, S.; Wu, X.; Jiang, J.; Gao, W.; Wan, Y.; Cheng, D.; Han, D.; Liu, J.; Englund, N. P.; Wang, Y.; et al. Discovery of NVP-LDE225, a Potent and Selective Smoothened Antagonist. *ACS Med. Chem. Lett.* **2010**, *1*, 130–134.
- Panchapakesan, G.; Dhayalan, V.; Dhatchana Moorthy, N.; Saranya, N.; Mohanakrishnan, A. K. Synthesis of 2-Substituted 17 β -hydroxy/17-Methylene Estratrienes and Their in Vitro Cytotoxicity in Human Cancer Cell Cultures. *Steroids* **2011**, *76*, 1491–1504.
- Paryzek, Z.; Blaszczyk, K. Synthesis and Stereochemistry of Steroidal Spirocyclobutanones. *Liebigs. Ann. Chem.* **1990**, 665–670.
- Perrot, S.; Dutertre-Catella, H.; Martin, C.; Warnet, J.-M.; Rat, P. A New Nondestructive Cytometric Assay Based on Resazurin Metabolism and an Organ Culture Model for the Assessment of Corneal Viability. *Cytom. Part A* **2003**, *55*, 7–14.
- Petrova, E.; Rios-Esteves, J.; Ouerfelli, O.; Glickman, J. F.; Resh, M. D. Inhibitors of Hedgehog Acyltransferase Block Sonic Hedgehog Signaling. *Nat. Chem. Bio.* **2013**, *9*, 247–249.

- Peukert, S.; Miller-Moslin, K. Small-Molecule Inhibitors of the Hedgehog Signaling Pathway as Cancer Therapeutics. *ChemMedChem* **2010**, *5*, 500–512.
- Pietruszka, J.; Witt, A. Synthesis of the Bestmann-Ohira Reagent. *Synthesis (Stuttg)*. **2006**, 4266–4268.
- Pritchard, J. G.; Long, F. a. The Kinetics of the Hydrolysis of Trimethylene Oxide in Water, Deuterium Oxide and 40% Aqueous Dioxane 1. *J. Am. Chem. Soc.* **1958**, *80*, 4162–4165.
- Robarge, K. D.; Brunton, S. A.; Castanedo, G. M.; Cui, Y.; Dina, M. S.; Goldsmith, R.; Gould, S. E.; Guichert, O.; Gunzner, J. L.; Halladay, J.; et al. GDC-0449 — A Potent Inhibitor of the Hedgehog Pathway. *Bioorg. Med. Chem. Lett.* **2009**, *19*, 5576–5581.
- Searles, S.; Butler, C. F. Reactions of Alcohols and Phenols with Trimethylene Oxide. *J. Am. Chem. Soc.* **1954**, *76*, 56–58.
- Serino, C.; Stehle, N.; Park, Y. S.; Florio, S.; Beak, P. ChemInform Abstract: Asymmetric Syntheses of N-Boc 2-Substituted Pyrrolidines and Piperidines by Intramolecular Cyclization. *J. Org. Chem.* **1999**, *64*, 1160–1165.
- Taipale, J.; Chen, J. K.; Cooper, M. K.; Wang, B.; Mann, R. K.; Milenkovic, L.; Scott, M. P.; Beachy, P. a. Effects of Oncogenic Mutations in Smoothed and Patched Can Be Reversed by Cyclopamine. *Nature* **2000**, *406*, 1005–1009.
- Tellis, J. C.; Primer, D. N.; Molander, G. a. Single-Electron Transmetalation in Organoboron Cross-Coupling by Photoredox/Nickel Dual Catalysis. *Science (80-)*. **2014**, *345*, 433–436.
- Tremblay, M. R.; Lescarbeau, A.; Grogan, M. J.; Tan, E.; Lin, G.; Austad, B. C.; Yu, L. C.; Behnke, M. L.; Nair, S. J.; Hagel, M.; et al. Discovery of a Potent and Orally Active Hedgehog Pathway Antagonist (IPI-926). *J. Med. Chem.* **2009**, *52*, 4400–4418.
- Tremblay, M. R.; Nevalainen, M.; Nair, S. J.; Porter, J. R.; Castro, A. C.; Behnke, M. L.; Yu, L. C.; Hagel, M.; White, K.; Faia, K.; et al. Semisynthetic Cyclopamine Analogues as Potent and Orally Bioavailable Hedgehog Pathway Antagonists. *J. Med. Chem.* **2008**, *51*, 6646–6649.
- Trott, O.; Olson, A. J. Software News and Update AutoDock Vina : Improving the Speed and Accuracy of Docking with a New Scoring Function , Efficient Optimization , and Multithreading. *J. Comput. Chem.* **2009**, *31*, 455–461.
- Wang, C.; Wu, H.; Evron, T.; Vardy, E.; Han, G. W.; Huang, X.-P.; Hufeisen, S. J.; Mangano, T. J.; Urban, D. J.; Katritch, V.; et al. Structural Basis for Smoothed Receptor Modulation and Chemoresistance to Anticancer Drugs. *Nat. Commun.* **2014**, *5*, 4355–4365.

- Wang, C.; Wu, H.; Katritch, V.; Han, G. W.; Huang, X.-P.; Liu, W.; Siu, F. Y.; Roth, B. L.; Cherezov, V.; Stevens, R. C. Structure of the Human Smoothed Receptor Bound to an Antitumour Agent. *Nature* **2013**, *497*, 338–343.
- Wechsler-Reya, R. J.; Scott, M. P. Control of Neuronal Precursor Proliferation in the Cerebellum by Sonic Hedgehog. *Neuron* **1999**, *22*, 103–114.
- Weierstall, U.; James, D.; Wang, C.; White, T. a; Wang, D.; Liu, W.; Spence, J. C. H.; Bruce Doak, R.; Nelson, G.; Fromme, P.; et al. Lipidic Cubic Phase Injector Facilitates Membrane Protein Serial Femtosecond Crystallography. *Nat. Commun.* **2014**, *5*, 3309–3314.
- Williams, J. a; Guicherit, O. M.; Zaharian, B. I.; Xu, Y.; Chai, L.; Wichterle, H.; Kon, C.; Gatchalian, C.; Porter, J. a; Rubin, L. L.; et al. Identification of a Small Molecule Inhibitor of the Hedgehog Signaling Pathway: Effects on Basal Cell Carcinoma-like Lesions. *Proc. Natl. Acad. Sci. U. S. A.* **2003**, *100*, 4616–4621.
- Winkler, J. D.; Isaacs, A.; Holderbaum, L.; Tatard, V.; Dahmane, N. Design and Synthesis of Inhibitors of Hedgehog Signaling Based on the Alkaloid Cyclopamine. *Org. Lett.* **2009**, *11*, 2824–2827.
- Xie, J.; Murone, M.; Luoh, S.-M.; Ryan, A.; Gu, Q. Activating Smoothed Mutations in Sporadic Basal-Cell Carcinoma. *Nature* **1998**, *391*, 90–92.
- Yauch, R. L.; Dijkgraaf, G. J. P.; Aliche, B.; Januario, T.; Ahn, C. P.; Bazan, J. F.; Kan, Z.; Seshagiri, S.; Hann, C. L. Smoothed Mutation Confers Resistance to a Hedgehog Pathway Inhibitor in Medulloblastoma. *Science (80-.)*. **2009**, *326*, 572–575.
- Ye, L.; He, W.; Zhang, L. Gold-Catalyzed One-Step Practical Synthesis of Oxetan-3-Ones from Readily Available Propargylic Alcohols. *J. Am. Chem. Soc.* **2010**, *132*, 8550–8551.
- Zhang, Z.; Baubet, V.; Ventocilla, C.; Xiang, C.; Dahmane, N.; Winkler, J. D. Stereoselective Synthesis of F-Ring Saturated Estrone-Derived Inhibitors of Hedgehog Signaling Based on Cyclopamine. *Org. Lett.* **2011**, *13*, 4786–4789.
- Zheng, Z.; Perkins, B. L.; Ni, B. Diarylprolinol Silyl Ether Salt as New Eff Water-Soluble & Recyclable Organocat Asymm Michael Addition on Water. *J. Am. Chem. Soc.* **2010**, *132*, 50–51.